Geology and mineralisation at the Cleveland mine western Tasmania

GEOLOGY AND MINERALISATION AT THE CLEVELAND MINE WESTERN TASMANIA

by

Peter L.F. Collins, B.Sc.(Hons)

Lionel Fleury

A thesis submitted in partial fulfilment
of the requirements for the degree of
Doctor of Philosophy

University of Tasmania
HOBART

June, 1983

Except as stated herein this thesis contains no material which has been accepted for the award of any other degree or diploma in any University, and, to the best of my knowledge and belief, this thesis contains no copy or paraphrase of material previously published or written by another person, except when due reference is made in the text of the thesis.

PETER L.F. COLLINS,
University of Tasmania,
Hobart.
June, 1983

CONTENTS

Appendices

LIST OF FIGURES

LIST OF PLATES

LIST OF TABLES

ABSTRACT

The Cleveland tin-copper deposit lies within a sequence of mafic volcanics and clastic sediments with minor limestone, of probable Eocambrian-Early Cambrian age. The north-east trending sequence is near vertical to north-west dipping, and faces north-west. The probable shallow marine volcano-sedimentary succession consists of an older mafic volcanic sequence (the Deep Creek Volcanics) and a predominantly clastic sequence (the Crescent Spur Sandstone) which are separated by a transitional sequence of clastic sediments, mafic volcanics and limestone (the Hall Formation). The Deep Creek Volcanics is dominated by spilitic, tholeiitic basalt with intercalated and interbedded lapilli, litho-vitric and lithic tuff, argillite and volcaniclastic greywacke. The Hall Formation consists of interbedded argillite, limestone and turbiditic greywacke and minor chert, lithic and litho-vitric tuff and spilitic, tholeiitic basalt. It is conformably overlain by the Crescent Spur Sandstone which consists of turbiditic greywacke and interbedded mudstone with argillite, chert, volcaniclastic greywacke and minor spilitic basalt. High-titania, spilitic basalt in the Deep Creek Volcanics and the Hall Formation exhibits geochemical affinities to ocean floor basalt, and has whole rock $\delta^{18}O$ compositions similar to marine, hydrothermally metamorphosed basaltic rock. The volcano-sedimentary sequence is cut by regionally concordant, tectonically emplaced, older(?) low-titania, mafic-ultramafic ophiolitic complexes (*e.g.* the Whyte River complex), and is intruded by pre-mineralisation, high-titania basalt-dolerite dykes which are probably associated with the Deep Creek volcanism.

The Crescent Spur Sandstone is intruded by a near vertical, WNW-ESE trending dyke-like body of topazised quartz porphyry carrying wolframite and cassiterite, which probably is associated with emplacement of the nearby, Late Devonian, peraluminous (S-type) Meredith Granite.

Cassiterite-stannite-chalcopyrite mineralisation occurs as stratiform replacement lenses in limestone interlayered with chert and shale beds within the Hall Formation, and to a minor extent in veins in the host rocks. The near-vertical sulphide lenses have been dislocated by a series of south-east dipping reverse faults that were active prior to and during the mineralisation episode, and caused local overturning of the volcano-sedimentary succession. The paragenetic sequence is divided into five stages with a superimposed mineralogical zonation, as follows:

Stage I: early quartz + fluorite + wolframite + molybdenite + bismuth + bismuthinite + minor cassiterite + minor sulphides occur in stockwork veins in the footwall Crescent Spur Sandstone in the centre of the deposit, and centred on the penecontemporaneous topazised quartz porphyry intrusive.

Stage II: quartz + tourmaline + fluorite + chlorite + pyrrhotite + cassiterite with hornblende + magnetite + minor scheelite at depth and later chalcopyrite + stannite + sphalerite (main stage of mineralisation). The assemblages occur in stratabound lenses with sphalerite and arsenopyrite common at the extremities of the upper sulphide lenses. Quartz veins with sphalerite + arsenopyrite + chalcopyrite + pyrrhotite ± galena surround the deposit and are associated with tourmalinisation of clastic sediments.

Stage III: quartz + arsenopyrite + minor stannite, sulphides and silicates occur as minor vein and vug fillings.

Stage IV: fluorite + carbonates + quartz fill veins and vugs throughout the sulphide lenses and host rocks.

Stage V: late pyrite lining cavities.

An extensive alteration halo in the hanging wall of the sulphide lenses (in the Deep Creek Volcanics) is defined by increased replacement by actinolite of clinopyroxene in spilitic basalt near the ore, accompanied by an increase in K, Rb, Sn and Zn and decrease in Na. However, these changes are not reflected in near constant whole rock $\delta^{18}O$ values.

Fluid inclusion and stable isotope data reveal a systematic trend in depositional temperature but a marked consistency in composition of the hydrothermal fluid. Fluids of Stages I and II were low to moderately saline (8-14% NaCl) but while Stage I fluids were of low CO_2 content, the CO_2 content of Stage II fluids was locally high (up to 15 mole% CO_2). Carbon dioxide in Stage II fluids was probably derived from dissolution of limestone. The salinity of the fluid decreased slightly to 7-11% NaCl and was very low in CO_2 during Stage IV. Fluid temperatures (pressure corrected) are estimated at 480°C for Stage I, 500°C for Stage II, and about 300°C during Stage IV, with an estimated confining pressure of about 150 MPa. The calculated $\delta^{18}O$ composition of water in the hydrothermal fluid remained constant at about +8.7 per mil for Stage I, +10.2 per mil for Stage II, and +9.5 per mil for Stage IV. The $\delta^{34}S$ values of the sulphides are close to 0 per mil (-0.2 to +5.5 per mil) throughout the mineralisation episode, and the calculated $\delta^{34}S_{\Sigma S}$ values average +2.3 per mil for the main tin-bearing fluid. The consistent salinity and the oxygen, hydrogen and sulphur isotopic compositions indicate a magmatic source for the mineralising fluid and a lack of mixing with meteoric water.

Formation of the W-Mo-Bi-Sn stockwork veining (Stage I) took place at about 480°C at low fO_2 ($10^{-23.7}$ to $10^{-24.8}$ atm) and low fS_2 ($10^{-6.8}$ atm). Formation of the sulphide lenses (Stage II) took place at about 500°C at slightly lower fS_2 ($10^{-6.5}$ to $10^{-7.5}$ atm) and low fO_2 ($10^{-22.5}$ to 10^{-24} atm), and low pH. Ore deposition primarily occurred as a result of increase in pH due to dissolution of limestone.

The Cleveland deposit originated from the metasomatic replacement of limestone beds by tin-bearing, low to moderately saline fluids of initially low CO_2 content derived from a granitic source related to the Meredith Granite.

INTRODUCTION

This study of the Cleveland cassiterite-sulphide deposit forms part of a series of research investigations of the geology and genesis of mineral deposits in Tasmania that have been undertaken at the University of Tasmania and supervised by Dr M. Solomon. It is the third major investigation of the cassiterite-sulphide deposits in western Tasmania, with previous studies of the Mt Bischoff deposit and the granitic rocks spatially associated with the tin deposits completed in 1968 by Dr D.I. Groves, and of the Renison tin mine by Dr D.J. Patterson in 1979.

Research into the genesis of the Cleveland deposit began in November, 1975 as a part-time Ph.D. project whilst employed with the Geological Survey Branch of the Tasmania Department of Mines. The work partly follows on from an investigation of the Renison tin deposit by the author for an Honours B.Sc. project in 1972, which generated interest in this type of deposit.

Purpose and scope of study

The purpose of the study has been to establish the geological setting and genesis of the Cleveland cassiterite-sulphide deposit. Historically, this deposit, and similar cassiterite-sulphide deposits at Mt Bischoff and Renison Bell, have been considered to be of a metasomatic replacement origin, associated with the emplacement of a large granitic mass (the Meredith Granite). However, since this study commenced, some authors have proposed a volcanogenic or partial volcanogenic origin.

The thesis begins with a brief discussion of the regional geology of that part of western Tasmania containing the cassiterite-sulphide deposits and the associated granitic rocks; and a review of genetic

features of tin (and tungsten) deposits. This is essential for an understanding of the regional stratigraphic setting of the Cleveland deposit, particularly in relation to other tin deposits in western Tasmania. Discussion of the regional geology includes the results of regional geological mapping carried out by the author in the Mt Cleveland-Mt Bischoff area, and other areas of western Tasmania, and by geologists of the Aberfoyle-Cominco group of companies in the Luina area.

Descriptions of the geology of the Cleveland mine cover the stratigraphy, petrology, structure and geochemistry of the host volcano-sedimentary sequence; the stratigraphic control, paragenesis, mineralogy and zoning of the mineralisation; and the petrology and geochemistry of host-rock alteration. Surface geological mapping in the mine area was undertaken at scales of 1:500 and 1:1000 and later reduced to 1:5000 for compilation of data. Underground mapping carried out on mine section N at a scale of 1:200, and a detailed interpretation of mine section Qa, were undertaken to determine the structural and stratigraphic relationships of the orebodies and their host rock. Discussion of host-rock alteration is limited mainly to the hanging-wall rocks due to sampling restrictions imposed by the orientation and positioning of deep diamond drill holes.

The results of a detailed fluid inclusion study and stable isotope data (S, O, C) are used in discussion of the temperature, composition and origin of the ore fluid and of prevailing physico-chemical conditions.

Details of analytical techniques, together with tables of results, and other descriptive data not essential to the main theme of the thesis, are presented in a series of appendices.

Some of the results of the research have already been published in two papers (Appendices 8 and 9): one on the effect and use of the formation of gas hydrate (clathrate) in CO_2-rich fluid inclusions (Collins, 1979*a*), and a summary paper on aspects of the fluid inclusion and stable isotope studies (Collins, 1981).

Location, access, and field and sampling conditions

The cassiterite-sulphide deposits of the Cleveland tin-copper mine are situated approximately one kilometre south-east of Luina in north-western Tasmania (latitude 41°29'S, longitude 145°23'E; Fig. I.1). The mine is about 15 km west of Mt Bischoff and 35 km north of Renison Bell, where two other major cassiterite-sulphide deposits are located (Fig. I.1). The mine is readily accessible by road, lying just south of the Corinna Road between Savage River and Waratah.

The Luina area has a thick cover of eucalypt and rain forest and exposure of rock is generally less than 5%. In the immediate mine vicinity, the area is crossed by numerous roads and drill access tracks, and elsewhere there are forestry roads and tracks, an old tramway, transmission line and numerous cut grid lines. All rock types and particularly the mafic rocks, are generally deeply weathered, which inhibits surface sampling. The freshest exposures are in creek beds and in road cuttings. In some areas there appears to be a preponderance of chert, but its occurrence may be exaggerated by weathering and erosion.

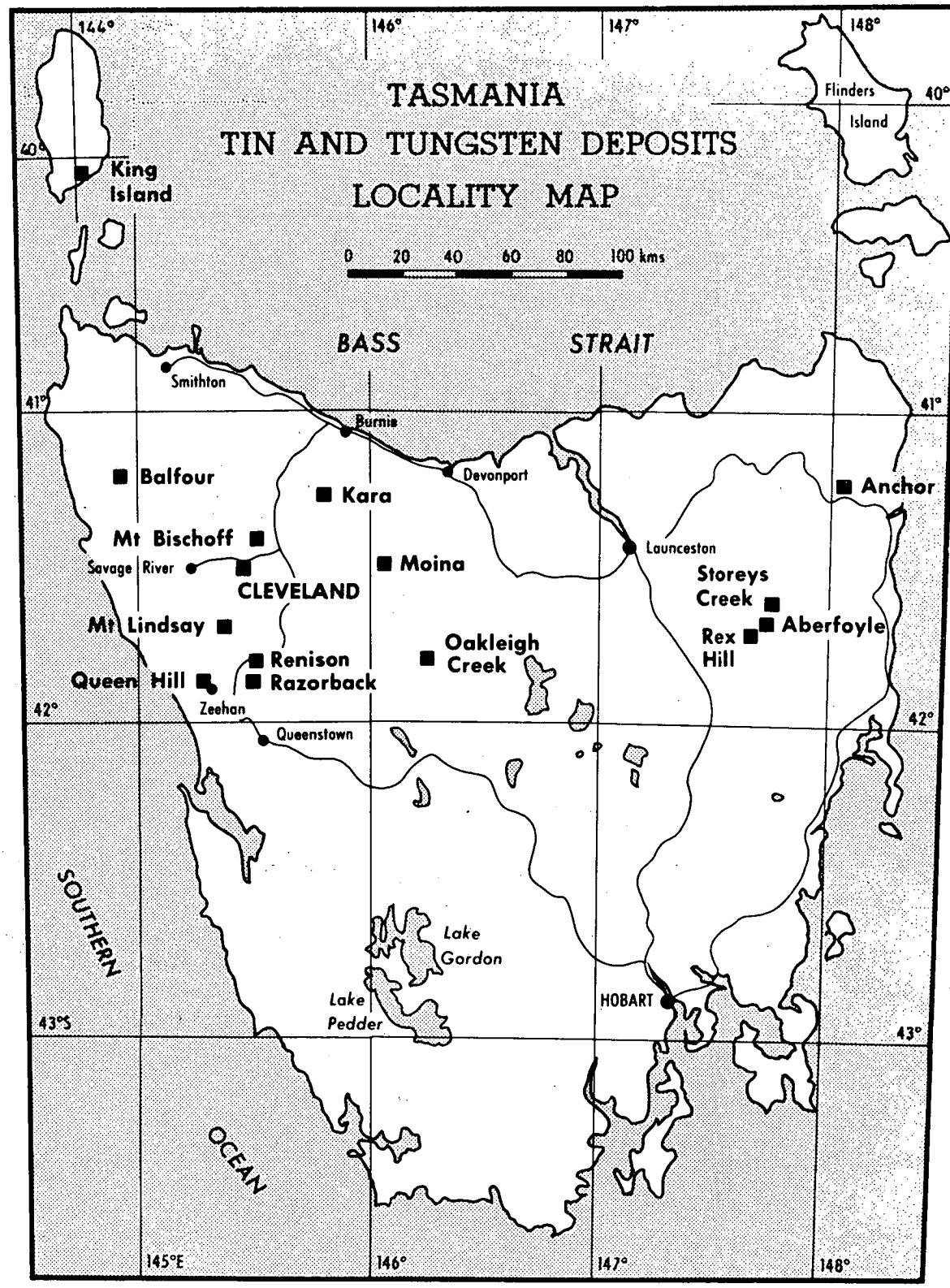

FIG. I.1 Location of the Cleveland mine, and other major tin and tungsten deposits in Tasmania.

The deep weathering and overgrown nature of many outcrops inhibits field determination of sedimentary facing. Although some facings were determined in the field, mainly in cuttings on recent logging roads located to the south and south-east of Cleveland, most facing evidence was obtained by collecting orientated specimens of complete beds of greywacke, including argillaceous beds on either side, and later cutting a flat, clean surface for examination for graded bedding, flame structures, etc. Several specimens were collected from each locality, mainly from road cuttings on the Corinna Road west of Whyte Hill, where there is almost continuous exposure of the Cambrian volcano-sedimentary sequence.

Most specimens have been collected from the underground workings, and from diamond drill core, which provides the most extensive sampling coverage of the ore and hanging-wall rocks but is limited in its coverage of the footwall rocks. Underground, ore sampling and inspection is restricted by development and mining, and is generally from below 12 level. Above this level, most of the ore bodies were mined out at the commencement of the study and hence inaccessible, except for a pillar at mine section N, between mine levels 2 and 11.

Co-ordinates of surface localities referred to in the text are given to either the nearest 10 m (8 numerals) or 100 m (6 numerals) in the 100 km square grid CQ of the Australian Map Grid, Zone SK-55. These co-ordinates are prefixed by CQ (*e.g.* CQ060074). Other co-ordinates are for the Cleveland mine grid. Its relationship to the A.M.G. is shown in Figure 3.3.

Throughout the thesis all bearings (*i.e.* strike of bedding, faults etc.) are given for grid north on the A.M.G.

Specimens and thin/polished sections, and diagrams

All specimens, thin/polished sections and analytical preparations are housed either in the Geology Department, University of Tasmania or with the Geological Survey, Tasmania Department of Mines. Specimens with numbers 48284 to 48356 and 104300 to 104470 are those of the Geology Department, University of Tasmania, and all other specimens (*e.g.* 78-437, 81-21) are housed in the Geological Survey collection. A list of specimens and their locations is given in Appendix 7.

The author has been fortunate in obtaining some of the thin sections (but no polished sections) used by Dr R. Cox in a study of the deposit completed in 1968. These are also held by the Geological Survey.

Original transparencies of all diagrams are housed in the geological cartographic office of the Geological Survey, Department of Mines.

History, production and previous literature

The gossanous outcrops of the Cleveland ore bodies are reported to have been discovered in 1898 (Reid, 1923). Following a period of prospecting and development, the Mt Cleveland Tin Mining Company N.L. exploited gossanous ore during the period 1909-1917 and recovered 349 tonnes of cassiterite from over 36 894 tonnes of ore (*i.e.* a recovery grade of 0.66% Sn). Several attempts were made later to re-open the mine and re-treat old dumps, but during the period 1938-1960 the mine lay dormant except for geological, mineralogical and geophysical investigations by the Tasmania Department of Mines (Henderson, 1937; Carey, 1945; Hughes, 1953, 1954), the C.S.I.R.O. (Stillwell, 1944a, b) and the Bureau of Mineral Resources (Keunecke and Tate, 1954).

In 1961, the Aberfoyle Tin Development Partnership secured the Mineral Leases and initiated an exploration and development programme which culminated in March, 1966 with the announcement of 2 896 000 tonnes of indicated and inferred ore reserves at an average grade of 1.02 mass% Sn and 0.43 mass% Cu. Cleveland Tin N.L. was formed and large-scale exploitation commenced in 1968.

Total production from the Cleveland mine during the period 1968-1982 has been 22 884 tonnes Sn and 8974 tonnes Cu from treatment of 5 097 300 tonnes of ore. This represents an overall recovery grade of 0.45% Sn and 0.18% Cu. Current production is about 350 000 tonnes per year at an ore head grade of about 0.65% Sn and 0.29% Cu. Mineable ore reserves in 1982 were 1 100 000 tonnes at a grade of 0.73% Sn and 0.33% Cu (Aberfoyle Ltd., Annual Report, 1982).

The deposit was first described by Reid (1923) as irregular replacements of chert and tuff. An epigenetic, metasomatic replacement origin for the deposit has been subsequently postulated by numerous authors (*e.g.* Henderson, 1937; Carey, 1945; Hughes, 1953; Cox and Glasson, 1967; Cox, 1968a; Groves, 1968; Cox and Glasson, 1971; Ransom and Hunt, 1975; Palmer, 1976). The possibility of a volcanogenic origin was briefly mentioned by Cox (1968a) and Palmer (1976), and recently, a volcanogenic exhalative origin or partial volcanogenic exhalative origin for the Renison and Cleveland type of mineralisation has been postulated by Hutchinson (1979, 1980) and Plimer (1980).

The work reported by Cox (1968a) was undertaken during exploration and the initial development of the deposit, and included a major investigation of sampling techniques for mineral evaluation of hard-rock tin deposits (*e.g.* Cox, 1968b, c). Groves' (1968) study was undertaken at the same time, but his work at Cleveland was restricted to a few ore samples collected from surface workings. Ransom and Hunt (1975) summarised

the mine geology and presented a re-interpretation of the geological structure. In contrast to a single 'lode bed' sliced up by near vertical faults into a series of *en echelon* segments as postulated by Cox (1968a) and Cox and Glasson (1967, 1971), Ransom and Hunt (1975) and Palmer (1976) described a succession of discrete lenses of mineralisation. The latter interpretation is supported, and has been further developed, by this investigation.

Nomenclature

The term sulphide lens (or lenses) is used in this thesis to define the lenses of stratabound cassiterite-sulphide mineralisation and/or conformable ore bodies within the Hall Formation. The sulphide lenses have been referred to previously as the lode bed (Cox, 1968a; Cox and Glasson, 1967, 1971), sulphide-rich 'bed' (Ransom and Hunt, 1975) and ore lenses (Palmer, 1976).

Geographical nomenclature is as shown on the Tasmap Arthur River 1:100 000 map sheet (7915), except for Deep Creek which is a small rivulet flowing into the Whyte River a few hundred metres downstream from the Cleveland mine. During the course of this investigation the long-standing name Deep Creek has been changed to Washington Creek. However, on all diagrams and in the text of this thesis the rivulet is referred to as Deep Creek.

Acknowledgements

As this project has been undertaken on a part-time basis, numerous people have made significant contributions to the research and preparation that went into the thesis. The work was carried out with the financial assistance of the Tasmania Department of Mines, through study leave granted in 1976 and 1977. The active co-operation and support of the then Director of Mines, J.G. Symons, and his successor, H. Murchie, and I.B. Jennings, Chief Geologist, A.J. Noldart and D.J. Jennings are acknowledged.

The project was initiated and supervised by Dr M. Solomon. I have benefited from discussions with other colleagues at the University of Tasmania and the Geological Survey, particularly A.V. Brown, Dr C.J. Eastoe, Dr J. Foden, Dr D.C. Green, G.R. Green, K.J. Moon, Dr D.J. Patterson, Dr R. Varne, Dr J.L. Walshe, Dr E. Williams and Dr P.R. Williams; and Dr T.A.P. Kwak, La Trobe University, and Dr R.W.T. Wilkins, CSIRO. Acknowledgement is also given for the contributions made by reviewers of papers published during the course of this study: Dr D.I. Groves, Dr P.J. Eadington, Dr R.C. Burruss, Dr D.J. Milton and Drs Solomon and Eastoe. Prof. A.J. Barduhn, Syracuse University, made a significant contribution to a study of gas hydrates in fluid inclusions.

I am indebted to Cleveland Tin Limited, Cominco Exploration Pty Ltd and Aberfoyle Ltd for their continued and generous support. I am grateful to many of their geological staff members for assistance and comment including K.G. Palmer, G. Boyle, C. Young, G. McArthur, P. Ellis and E. Dronsjeka. I am particularly grateful to Tom Tulp for many constructive discussions and for his assistance and generous hospitality during the early years of this study.

Acknowledgement is also given to the Institute of Nuclear Sciences, D.S.I.R., Lower Hutt, New Zealand, and its then Director, Dr T.A. Rafter, for granting permission to utilise the Institute's facilities. The stable isotope research was carried out under the instruction and guidance of Dr P. Blattner and Dr B.W. Robinson and their advice and assistance are gratefully acknowledged. Miss I. Smolnicki and Mrs M.A. Cox offered technical assistance.

The assistance of P. Robinson, R.N. Woolley and B.J. Griffin with X-ray fluorescence and X-ray diffraction analytical techniques and the electronprobe micro-analyser, respectively, is acknowledged. Invaluable assistance with drafting was given by D. Hardy, J.H. Clarke, A.J. Hollick, J.S. Ladaniwskyj, P. Nankivell and Mrs B. Bird at the Department of Mines, particularly with Figures 2.1, 3.1, 3.3, 3.12, 4.1, 4.2 and 4.3. Several whole-rock analyses were carried out at the Department of Mines Assay Laboratories, Launceston, under the supervision of H.K. Wellington. My gratitude is also extended to Mrs A. Taylor and Mrs C. Humphries for typing various sections of the manuscript, to Mrs O. Collins for typing the expansive tables in the appendices, and to Miss A. McGuinness, Mrs D. Purdon, and Mrs V. Smith for additional typing assistance with early drafts of the manuscript.

Final and most sincere thanks are extended to my family. To my wife, Pam, for her support and encouragement throughout the project, and to my sons, Samuel, Tomas and Nicholas, who have missed out on a lot of my time, but whose antics assisted in keeping me sane during completion of this project.

1. GENETIC FEATURES OF PRIMARY TIN DEPOSITS

INTRODUCTION

The Cleveland mine is principally a tin mine, with sub-ordinate copper, having produced some 23 400 t Sn and 9100 t Cu. Tin occurs primarily as cassiterite and minor stannite, and copper as chalcopyrite, in near-vertical stratabound lodes (sulphide lenses). However, there are also significant concentrations of tungsten mineralisation which occurs either as wolframite in quartz-fluorite stockwork veins with sub-ordinate molybdenite, cassiterite, bismuthinite and bismuth, or as scheelite in the deeper portions of the sulphide lenses, in excess of 400 m below the surface. Thus, in reviewing geologic and genetic features of primary tin mineralisation, reference is also made to various features of primary tungsten mineralisation. This is necessary not only because of its occurrence at Cleveland, but also because of the widespread association of tin and tungsten in many hydrothermal mineral deposits.

GENERAL RELATIONSHIPS

Primary tin deposits occur in a wide variety of geological environments, but most are associated with granitoids emplaced in orogenic belts on continental margins (*e.g.* Taylor, 1979) and this is the setting of the Tasmanian deposits. Tin deposits are also associated with emplacement of anorogenic granite in Precambrian shield areas, but these are comparatively rare and are generally smaller than those in orogenic belts. They include the Nigerian tin deposits which occur as greisens or disseminations within circular, albitized granitic intrusive complexes, preceded by rhyolitic extrusives, of Jurassic age (*e.g.* Olade, 1980; Bowden, 1982) and similar greisen and vein deposits in Rondovia, Brazil (*e.g.* Kloosterman,

1970). The tin deposits associated with the Bushveld granites, which occur as sheet-like bodies stratigraphically above layered mafic rock of the complex (*e.g.* Hunter, 1976) appear to be unique in their tectonic setting.

Tin deposits are characteristically associated with silicic igneous rocks, particularly peraluminous or S-type biotite granite (*e.g.* White *et al.*, 1977) and pegmatites. This spatial association is usually interpreted as implying a genetic relationship between granite and tin mineralisation (*e.g.* Hosking, 1968; Stemprok, 1963, 1965), although the associated granite may or may not be anomalous in tin. Numerous attempts have been made to establish criteria for differentiating 'tin granite' from other granite, and the evidence assembled suggests that highly differentiated, and more leucrocratic biotite or biotite-muscovite varieties, emplaced as late or post-tectonic, high-level intrusions are spatially and genetically associated with tin deposits and generally have elevated trace tin concentrations (*e.g.* Barsukov, 1958; Gotman and Rub, 1960; Rattigan, 1963; Durasova, 1967; Klominsky and Groves, 1970; Groves, 1972, 1977; Flinter *et al.*, 1972; Tischendorf, 1977; Blockley, 1980; Olade, 1980; Higgins *et al.*, in prep.). In a review of geochemical and petrographic features of granites associated with tin mineralisation, Tischendorf (1977) established three groups of granites defined as (I) 'tin-specialised' or stannigene granites (30±20 g/t Sn) with which tin mineralisation is spatially and genetically connected; (II) precursors of stannigene granite (10±5 g/t Sn) which are biotite granites occurring in tin-bearing areas and associated with, but older than stannigene granites; and (III) 'normal' granites (<8 g/t Sn). Although most stannigene granites are anomolous in tin (*c.f.* 3-4 g/t Sn average

for granitic rock, Hamaguchi and Kuroda, 1969), not all have a high tin content (Tischendorf, 1977) and tin mineralisation also may occur in close spatial association with biotite granite having very low tin contents (*e.g.* Herberton district, N.E. Queensland: Sheraton and Black, 1973; Olatunji *et al.*, 1977; Cornwall: Hosking, 1968; Blue Tier Batholith, N.E. Tasmania: Groves, 1977; Higgins *et al.*, in prep).

Studies of trace element abundances indicate that all felsic rocks contain minor amounts of tin which in most granites is accommodated in the lattices of minerals such as biotite, amphibole and sphene (Barsukov and Durasova, 1966; Petrova and Legeydo, 1965; Tauson *et al.*, 1968; Groves, 1977) whereas in stannigene granite it occurs in greater concentration in biotite (Rattigan, 1963; Davy, 1972; Groves, 1977) or, if the granite is greisenised, in muscovite and/or cassiterite. In the Blue Tier Batholith, for example, the tin content is much higher in biotite in late-phase, biotite-(muscovite) alkali feldspar granite (150-900 g/t Sn) than in earlier biotite granite/adamellite (<75 g/t Sn) (Groves, 1977), which are comparable to stannigene granite and precursors of stannigene granite of Tischendorf (1977), respectively. In some cases the trace tin content of granite may be related to variations in modal biotite (Rattigan, 1963).

Most primary tin deposits are related to granite emplaced into Palaeozoic, Mesozoic and Tertiary linear orogenic belts (Itsikson, 1960). They occur in a variety of magmatic environments that may be categorised into volcanic, subvolcanic and 'shallow'-'deep' plutonic (Taylor, 1979). The Mexican cassiterite-wood tin deposits associated with Tertiary rhyolitic lavas (Ypma and Simons, 1970; Taylor, 1979) and the Bolivian porphyry tin and tin-silver vein deposits genetically associated with

high level, acid igneous stocks and eruptive complexes of early Tertiary age emplaced in the Andean orogenic belt (*e.g.* Turneaure, 1971; Sillitoe *et al.*, 1975; Grant *et al.*, 1980), are examples of deposits in volcanic-subvolcanic environments.

Although subvolcanic felsic intrusives and/or extrusives may be important hosts to tin mineralisation in restricted areas (*e.g.* Bolivia; Mexico; and Asiatic Russia: Smirnov, 1976), many major primary tin deposits (and most secondary deposits) are genetically associated with granitoids of 'shallow' to 'deep' plutonic character (*e.g.* Taylor, 1979) and occur in both exo-granitic and endo-granitic environments. For example, elongate bodies of stanniferous granite, of Late Cretaceous-Triassic age, emplaced into an orogenic belt extending as an arc from Indonesia north through the spine of the Malay Peninsula are host to a wide diversity of only minor primary tin deposits (pegmatite, skarn, vein and greisen), but from which have been derived extensive alluvial and/or eluvial deposits (*e.g.* Hosking, 1970, 1973). The Cornish vein-tin deposits and the tin-(tungsten) greisen and skarn deposits at Erzgebirge are associated with Permo-Carboniferous granitoids emplaced into folded early Palaeozoic rocks of the Hercynian/Variscan orogeny (*e.g.* Hosking, 1968; Tischendorf, 1973). In eastern Australia, several suites of granitoids ranging in age from Late Devonian to Permo-Triassic have been emplaced along the axis of the Tasman orogenic belt and have associated significant primary tin deposits (*e.g.* Taylor, 1979; Solomon *et al.*, 1972). Most of the deposits are related to S-type granitoids (*e.g.* White *et al.*, 1977; Higgins *et al.*, in prep.) and include vein and greisen deposits in the Herberton district, N. Queensland, the New England district, New South Wales and the Blue Tier and Aberfoyle districts, north-east Tasmania, and cassiterite-sulphide replacement deposits (*e.g.* Renison,

Cleveland, Mt Bischoff) and skarns (*e.g.* St Dizier, Mt Lindsay, Moina) in western Tasmania (*e.g.* Taylor, 1979; Solomon, 1981).

Primary tungsten mineralisation is, like tin, clearly linked to felsic igneous processes, and generally is related to granitoids emplaced into orogenic belts. Although most tungsten deposits are genetically associated with leucocratic granitic rock, particularly vein and greisen deposits, the association is not so obvious in all cases, and some tungsten deposits, particularly scheelite-bearing skarns, are closely associated with more mafic granitic rock (*e.g.* Smirnov, 1976; Shchleglov and Butkevich, 1977; Horsnail, 1979). Tungsten deposits associated with granitoids in orogenic belts may be categorised into: (i) endo-granitic deposits of wolframite/scheelite in pegmatites, and wolframite ± cassiterite in greisens (*e.g.* Erzgebirge: Tischendorf, 1973; U.S.S.R.: Shchlegov and Butkevich, 1977); (ii) wolframite ± cassiterite vein deposits occurring as single or sheeted veins (*e.g.* Pasto Bueno, Peru: Landis and Rye, 1974; Carrock Fell, England; Shepherd *et al.*, 1976; Panasqueira, Portugal: Kelly and Rye, 1979; Tungsten Queen, North Caroline: Foose *et al.*, 1980; Casadevall and Rye, 1980; Aberfoyle, Tasmania: Kingsbury, 1965; Hellsten, 1979) and as stockwork veins (*e.g.* Mount Carbine, Queensland); (iii) disseminated deposits associated with subvolcanic/granitic porphyries (*e.g.* Mount Pleasant, New Brunswick: Dagger, 1972); and (iv) as scheelite-bearing skarns associated generally with more mafic members of the granitic series (*e.g.* King Island, Tasmania: Danielson, 1975; Sangdong, Korea: Yong Won, 1963; Moon, 1983; Fujigatani , Japan: Sato, 1980; U.S.S.R.: Smirnov, 1976, p.156-196; Shchleglov and Butkevich, 1977).

In addition to deposits associated with igneous rocks there are also stratabround scheelite deposits which are believed to be genetically associated with submarine mafic volcanism (*e.g.* Holl *et al.*, 1972;

Maucher, 1976), and recent deposits formed by supergene migration and sedimentation from tungsten-bearing brines (*e.g.* Owens Valley, California: Carpenter and Garrett, 1959). Disseminated scheelite also occurs rarely in metasomatically altered (phlogopite-rich) mafic-ultramafic bodies adjacent to leucogranite-pegmatite intrusives (*e.g.* Tantalite Valley, Africa: Moore, 1980).

TIN (-TUNGSTEN) DEPOSITS IN TASMANIA

Tasmania forms a very small part of the Tasman orogenic belt, of Palaeozoic age, which extends from Antarctica through Eastern Australia (*e.g.* Solomon *et al.*, 1972; Solomon and Griffiths, 1974). All known primary tin and tungsten deposits in Tasmania occur in rocks ranging in age from Late Proterozoic to Late Devonian, and are spatially and genetically associated with emplacement of post-kinematic granites of Late Devonian to Early Carboniferous age (*e.g.* Solomon, 1981).

The various genetic types of tin (-tungsten) deposits in Tasmania are illustrated in Figure 1.1. They occur in two major provinces: north-east Tasmania and north-west Tasmania, each with separate styles of mineralisation. In north-east Tasmania, tin mineralisation occurs predominantly in greisens and, with tungsten, in sheeted vein systems, whereas in north-western Tasmania, there is a paucity of greisen deposits, but an abundance of tin and tungsten replacement and/or skarn mineralisation. Historically, much of the tin produced in Tasmania has been extracted from alluvial deposits derived from greisens and greisenised granite in north-east Tasmania, whereas the currently mined primary tin deposits in western Tasmania (*i.e.* Cleveland and Renison) account for approximately 97% of Tasmania's annual tin production.

The primary tin(-tungsten) deposits in Tasmania may be grouped as follows (Fig. 1.1):

(A) Disseminated cassiterite, with minor wolframite and molybdenite, in altered, layered, greisenised biotite-

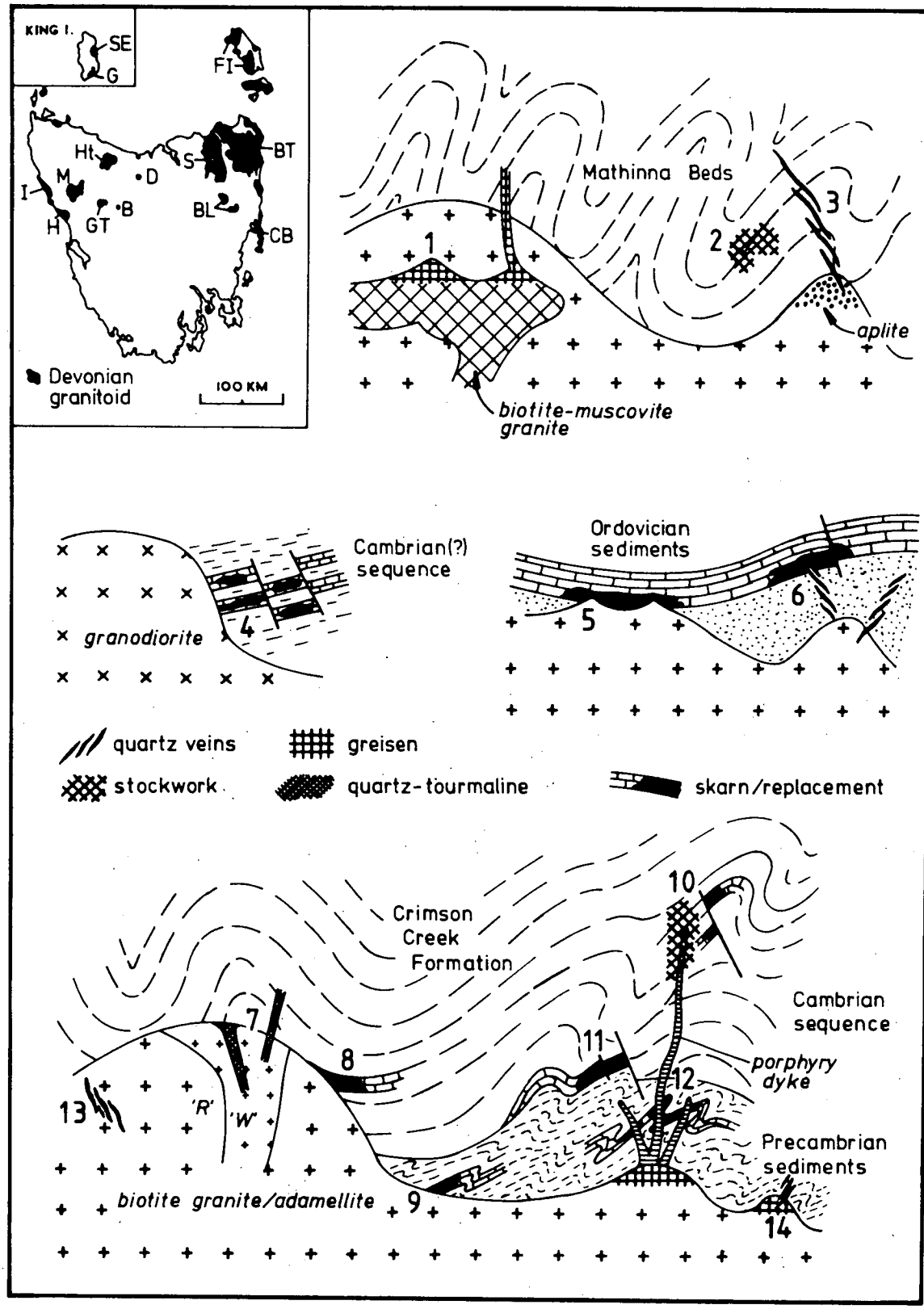

FIG. 1.1 Sketches illustrating genetic types of tin and tungsten deposits in Tasmania (modified after Solomon, 1981), and the location of major Devonian granitoids. Legend: see over.

FIG. 1.1 continued

1. Anchor mine (closed): cassiterite in greisen; 2. Great Pyramid mine (closed): cassiterite in quartz vein stockwork; 3. Aberfoyle, Lutwyche and Storeys Creek mines (closed): cassiterite and wolframite in quartz veins; 4. King Island Scheelite mine: scheelite in skarn; 5. Kara mine: scheelite in skarn; 6. Shepherd and Murphy mine (closed): cassiterite, wolframite, molybdenite and bismuthinite in quartz veins; and Moina prospect: fluorite and minor cassiterite and scheelite in skarn; 7. Federation mines, Maynes mine, south Heemskirk (closed): cassiterite in quartz-tourmaline-topaz alteration veins, pipes and breccias (R = 'Red' Granite, W = 'White' Granite); 8. Mt Lindsay prospect: cassiterite and Sn-bearing silicates in skarn; 9. St Dizier prospect: tin in skarn; 10. Cleveland mine: cassiterite, stannite and chalcopyrite in replacement lenses; and wolframite, molybdenite, cassiterite and fluorite in quartz vein stockwork; 11. Renison mine: cassiterite in carbonate replacement bodies and fracture zones; 12. Mt Bischoff (closed): cassiterite in replacement bodies and altered porphyry dykes; 13. Interview River mine (closed): wolframite and scheelite in quartz-greisen veins; 14. Oakleigh Creek mine (closed): wolframite in quartz veins.

Inset The locations of major Devonian granitoids: B = Birthday Granite, BL = Ben Lomond Granite, BT = Blue Tier Batholith, CB = Coles Bay Granite, D = Dolcoath Granite, FI = Flinders Island Granites, G = Grassy Granodiorite, GT = Granite Tor granite, H = Heemskirk Granite, Ht = Housetop Granite, I = Interview River Granite, M = Meredith Granite, S = Scottsdale Batholith, SE = Sea Elephant Granite.

(muscovite) alkali feldspar granite which was emplaced into earlier and much larger bodies of biotite granite/adamellite and granodiorite. In the Blue Tier Batholith in north-east Tasmania, the greisenised granite and greisen are generally confined to irregularities in the upper surfaces of the alkali feldspar granite, adjacent to overlying impervious biotite granite/adamellite, and have an autometasomatic rather than post-magmatic origin (*e.g.* Anchor mine, Blue Tier district: Groves and Taylor, 1973; Groves, 1977).

In the Heemskirk Granite in western Tasmania an older, layered, medium to coarse-grained biotite granite ('red' granite) apparently has been intruded by a sill-like body of more alkaline, medium-grained biotite-muscovite granite ('white' granite) (Klominsky, 1972; Wells, 1978). Tin mineralisation is associated with the 'white' granite and occurs as disseminated cassiterite in greisen veins, pipes and irregular zones of quartz-topaz-tourmaline alteration in argillised granite (*e.g.* Federation mine: Wells, 1978). At the Central Federation mine, breccias developed in some of the larger veins contain exotic fragments (*e.g.* hornfels), indicating close proximity to the top of the granitoid.

(B) Quartz-cassiterite-wolframite veins either penetrating country rock overlying granitic cupolas, occurring as discrete veins or sheeted-vein systems (*e.g.* Aberfoyle, Lutwyche and Storeys Creek: Kingsbury, 1965; Hellsten, 1979; Moina district: Collins, 1979*b*; and Oakleigh Creek: Kuys, 1981) and as stockwork deposits (*e.g.* Great Pyramid: Groves, 1972*b*); or as discrete veins within granite (*e.g.* Interview River: Henderson, 1943).

(C) Cassiterite-sulphide replacement deposits occurring mainly as

stratabound lenses derived from replacement of carbonate beds, and associated small and/or large scale fissure lodes (*e.g.* Renison: Patterson *et al.*, 1981; Mt Bischoff: Groves *et al.*, 1972; Queen Hill: Lutley, 1975; and Cleveland), and also from replacement of carbonate derived from serpentinisation of an ultramafic complex (*e.g.* Razorback: Blissett and Gulline, 1961). Although these deposits are all somewhat remote (up to 1 km) from their associated granite, altered quartz porphyry and orthoclase-quartz porphyry dykes are present at Mt Bischoff, Cleveland and Renison.

(D) Tin and tungsten-bearing skarns either adjacent to, or very close to granite and/or granodiorite. They may be divided into (i) scheelite-bearing skarn with nil or trace tin (*e.g.* King Island: Danielson, 1975; Kwak and Tan, 1981; and at Kara); and (ii) low-grade (<0.5% Sn) tin-bearing skarns in which much of the tin occurs in minerals other than cassiterite (*e.g.* Moina: Kwak and Askins, 1981; and St Dizier and Mt Lindsay).

The deposit types (A) to (D) have characteristics consistent with group 1(d) of Taylor (1979), involving granitoids of plutonic character emplaced in association with major periods of orogeny, though predominantly post major folding. Deposit type (C) and the greisen veins and pipes in the Heemskirk Granite are difficult to categorise, but are probably transitional between Taylor's (1979) groups 1(c) and 1(d) as, for example, the Heemskirk Granite has a high-level plutonic character but lacks subvolcanic complexes, and the cassiterite-sulphide deposits are associated with medium to high-level granite but may occur at shallower depths.

Type (A) deposits are similar to the 'tin-bearing greisens of the intrusive zone' of Materikov (1977), and type (B) deposits are comparable to the 'hydrothermal quartz-cassiterite-wolframite deposits' of Shchleglov and Butkevich (1977), though the Interview River quartz-wolframite-scheelite deposits are more like their 'hydrothermal quartz-wolframite type'.

SPECIFIC ASPECTS OF TIN (-TUNGSTEN) MINERALISATION

Mineralogy and zoning

Primary tin deposits may be broadly divided into two types of tin-bearing assemblages (Patterson *et al*, 1981): cassiterite-silicate and cassiterite-sulphide, based on S.S. Smirnov's original classification of tin deposits (in Magak'yan, 1968).

Cassiterite-silicate deposits are extensively developed in most stanniferous provinces occurring mainly as veins, stockworks, breccias and greisens. They are characterised by early development of cassiterite with quartz and variable muscovite, tourmaline, topaz, fluorite, and commonly with minor associated wolframite, molybdenite and bismuthinite, and later(?) development of arsenopyrite and base-metal sulphides.

Cassiterite-sulphide deposits are less widely recognised, but are significantly developed in Asiatic USSR (*e.g.* Smirnov, 1976; Materikov, 1977) and also occur in Malaysia (Hosking, 1970, 1973) and China (Hsieh, 1963). They are characterised by the presence of cassiterite with arsenopyrite, pyrrhotite, pyrite and base-metal sulphides in a gangue of quartz, tourmaline and various ferruginous silicates (tremolite-actinolite, phlogopite, iron-rich chlorite). The cassiterite-sulphide deposits in western Tasmania (*i.e.* Mt Bischoff, Cleveland, Renison, Queen Hill, Razorback) show close affinities with this type of deposit.

Although most deposits fall within these two assemblages, some hydrothermal tin deposits show a transition from cassiterite-quartz (-silicate) to peripheral cassiterite-sulphide mineralisation (*e.g.* Erzgebirge: Tischendorf, 1973; USSR: Smirnov, 1976, p.283), confirming their common genesis.

Many hydrothermal deposits are markedly zoned (*e.g.* Cornwall: Hosking, 1968) and in most zoned areas tin (-tungsten) deposits form the

central part of a mineral field with an outer zone of lead-zinc-sulphide mineralisation (*e.g.* Zeehan field: Both and Williams, 1968; Both *et al*, 1969; Solomon, 1981). A similar pattern occurs at Mt Bischoff, where several lead-zinc vein deposits are peripheral to the area of cassiterite-sulphide mineralisation (Groves, 1968; Groves *et al*, 1972). The Mt Pleasant, New Brunswick deposit also is apparently zoned with a central tungsten-bismuth zone, with minor tin zones, which is enclosed by a copper-lead-zinc sulphide zone (Dagger, 1972; Parrish and Tully, 1978).

Alteration environments

During formation of tin deposits, the hydrothermal fluid reacts with the enclosing rocks to produce wall-rock alteration haloes occurring as a wide variety of mineralogical assemblages and geochemical patterns (*e.g.* Smirnov, 1976, p.291-295; Taylor, 1979, p.173-212). Wall-rock alteration has been best defined for hydrothermal vein deposits in exo- and endo-granitic environments, in which case the alteration is relatively restricted and rarely exceeds 5 m in thickness, and for broad-scale greisen, feldspathic, argillic and tourmaline alteration in granitic rocks in apo-granitic environments.

There are very few mineralogical or geochemical data on wall-rock alteration to calc-silicate and/or magnetite-rich or sulphide-rich skarns (equivalent to exoskarns of Smirnov, 1976) and lower temperature carbonate replacement deposits (equivalent to endoskarns) (*e.g.* Taylor, 1979). Although hydrothermal effects generally are superimposed on meta-morphism, contact (or thermal) metamorphic effects of adjacent granitoids may reduce the effects of wall-rock hydrothermal alteration associated with exoskarns. However, carbonate replacement deposits that are peripheral to the contact metamorphic aureole (*e.g.* Renison: Patterson *et al*. 1981) should show broad-scale hydrothermal alteration effects, such as a sericite alteration halo to the Cleveland deposit (Cox, 1968a; Cox and Glasson, 1971).

Temperature

Temperature data derived from homogenisation temperatures of fluid inclusions (pressure corrected) and from stable isotope fractionation indicate that crystallisation of primary cassiterite generally occurs above 300°C, and in most deposits is within the range 350° to 550°C (*e.g.* Little, 1960; Groves *et al*, 1970; Kelly and Turneaure, 1970; Haapala and Kinnunen, 1979; Grant *et al*, 1980; Kwak and Askins, 1981; Wilkins and Ewald, 1982). However, in some vein deposits, cassiterite and wolframite appear to have crystallised at lower temperatures, in the range 250° to 300°C (*e.g.* Carrock Fell: Shepherd, *et al.*, 1976), whereas in some skarn deposits scheelite and/or cassiterite appear to have formed at temperatures up to 600°C or higher (*e.g.* Fujigatani: Sato, 1980; King Island: Tan and Kwak, 1979; Kwak and Tan, 1981).

The cassiterite-sulphide deposits in western Tasmania fall within the general temperature range of tin deposition, with 300° - 350°C for the main tin-bearing stages at Renison (Patterson *et al*, 1981) and 300° - 450°C, but up to 580°C at Mt Bischoff (Groves and Solomon, 1969; Little, 1960).

Many hydrothermal tin (-tungsten) deposits exhibit well-defined spatial and/or temporal variations in temperature, with the latter stages of mineralisation generally in the range 150° to 300°C (*e.g.* Mt Bischoff: Groves and Solomon, 1969; and Bolivia: Kelly and Turneaure, 1970; Grant *et al*, 1980).

Boiling of the hydrothermal fluid is not a characteristic of tin and tungsten deposits, although in some deposits which formed at relatively shallow depths the occurrence of co-existing gas-rich and aqueous (and salt-rich) inclusions indicate intermittent boiling of the ore fluid (*e.g.* Bolivia: Grant *et al*, 1980; Moina: Kwak and Askins, 1981; Sangdong: Moon, 1983; Aberfoyle: Halley, 1982) and

the ultrasaline fluids of Bolivia and King Island could only result from two-phase systems. Kelly and Turneaure (1970) proposed that boiling of the ore fluid caused deposition of cassiterite and wolframite in the Bolivian deposits.

Fluid composition

Analyses of inclusion fluids from different types of tin deposits indicate that the hydrothermal fluids are essentially Na-K-Cl brines with variable but minor amounts of Ca, Mg, Fe, HCO_3^- and F (*e.g.* Groves and Solomon, 1969; Kelly and Turneaure, 1970; Barsukov and Suschevskaya, 1973; Charoy and Weisbrod, 1975; Kelly and Rye, 1979; Haapala and Kinnunen, 1979; Patterson *et al*, 1981).

The carbon contents are variable, with liquid CO_2 inclusions being reported in cassiterite from several deposits (*e.g.* Little, 1960; Kelly and Turneaure, 1970) and CO_2 enriched aqueous inclusions occurring in the gangue minerals of numerous deposits (*e.g.* Groves and Solomon, 1969; Kelly and Turneaure, 1970; Kelly and Rye, 1979; Wilkins and Ewald, 1982). Methane is reported less often, but has been detected in bulk fluid inclusion extracts (*e.g.* Patterson *et al*, 1981) and may be more common than previously suspected. For example, many workers (*e.g.* Kelly and Turneaure, 1970; Kelly and Rye, 1979) have reported CO_2-hydrate decomposition at temperatures above 10°C (its critical decomposition temperature) which indicates the presence of gas phases other than CO_2, principally CH_4 (Collins, 1979*a*).

The salinities of inclusion fluids vary from equivalent NaCl concentrations of less than 2 mass% to greater than 50 mass%, although most deposits appear to have formed from moderately saline fluids of 5-20% NaCl (*e.g.* Groves and Solomon, 1969; Kelly and Turneaure, 1970; Landis and Rye, 1974; Kelly and Rye, 1979; Haapala and Kinnunen, 1979). Highly saline inclusion fluids are found in some deposits formed at shallow depths (*e.g.* Bolivia: Kelly and Turneaure, 1970; Grant *et al*, 1980). The rare occurrence of inclusions containing halite and sylvite

at Mt Bischoff and at Renison (Collins, 1972) has been attributed to localised boiling, and such high salinity fluids are considered not representative of the original hydrothermal fluid (Groves and Solomon, 1969). In deposits which show a wide range of salinities there is an approximate linear relationship between salinity and the homogenisation temperature of inclusions (*e.g.* Mt Bischoff: Groves and Solomon, 1969), the lower salinities corresponding to lower temperatures, consistent with phase relationships of the $NaCl-H_2O$ system. This temporal variation in temperature and salinity is apparent in many deposits (*e.g.* Grant *et al*, 1980; Kelly and Rye, 1979; Kelly and Turneaure, 1970).

Stable isotope geochemistry

Few published data are available regarding stable isotope geochemistry of tin and tin-tungsten deposits.

Sulphide $\delta^{34}S$ values of replacement sulphides at Mt Bischoff (Rafter and Solomon, 1967; Groves, 1968), of sulphides in vein deposits at Panasqueira (Kelly and Rye; 1979) and Tungsten Queen (Casadevall and Rye, 1980), and in a greisen pipe at Rex Hill (Groves *et al*, 1970) are close to 0±5 per mil which indicates that the sulphur involved in the formation of these deposits is most likely of an igneous or deep-seated origin (Ohmoto and Rye, 1979). At Renison, sulphides associated with the tin mineralisation are heavier (average of 6.3±2.5 per mil; Rafter and Solomon, 1967; Patterson *et al*, 1981), but in relation to primary(?) sulphide $\delta^{34}S$ values of about 4 per mil in the spatially associated granite, are believed consistent with granitic rock being the major or sole source of sulphur for the fluids (Patterson *et al*, 1981). A similar situation occurs at Moina, where sulphides have $\delta^{34}S$ values of 8.4-9.3 per mil in skarn and 8.9 per mil in greisenised granite (Kwak and Askins, 1981).

Limited available oxygen and hydrogen isotope data for minerals and inclusion fluids in and associated with tin deposits indicate con-

siderable variation in the magmatic fluid component of ore-forming fluids. In some deposits magmatic fluid is the sole or major source of mineralising hydrothermal fluids (*e.g.* Renison: Patterson *et al*, 1981; Bolivia: Grant *et al*, 1980) whereas in others there is supposedly a dominance of meteoric water in the hydrothermal fluid, in which the role of magmatic water has been difficult to assess (*e.g.* Cornubian Batholith: Sheppard, 1977). Conversely, in several hydrothermal tin and tungsten vein deposits, isotopic evidence indicates that the hydrothermal fluid originated from mixing of meteoric water and a magmatic or deep-seated component (*e.g.* Pasta Bueno: Landis and Rye, 1974; Carrock Fell: Shepherd *et al*, 1976; Panasqueria: Kelly and Rye, 1979; Tungsten Queen: Casadevall and Rye, 1980).

A few measurements have been made of the $\delta^{18}O$ value of cassiterites, which all fall within the range 0-7 per mil (*e.g.* Wolf and Espozo, 1972; Borshchevskiy *et al*, 1979; Kelly and Rye, 1979; Patterson *et al*, 1981) and of wolframites and scheelites which have a range of 1-6 per mil (Landis and Rye, 1974; Kelly and Rye, 1979; Higgins, 1980), but few conclusions can be drawn from these isolated measurements, particularly in the absence of experimental mineral-water fractionations.

Transport and deposition of tin

As most tin deposits appear to have formed at temperatures above 350°C, few thermodynamic calculations on depositional conditions (fO_2, fS_2, pH, etc.) have been carried out. Patterson *et al*. (1981) have demonstrated that formation of the cassiterite bearing stages at the Renison tin mine took place at 350°C at relatively low fO_2, low fS_2 and low pH and that an increase in pH due to dolomite replacement was the dominant control on ore deposition. Conditions of formation of higher temperature skarns vary from relatively high pH and fO_2 as inferred for andraditic skarn at King Island (Solomon, 1981) to relatively low fO_2 and fS_2 for hedenbergitic skarn at Fujigatani (Sato, 1980).

Mechanisms of tin transport are extremely varied (*e.g.* Taylor, 1979, Ch. 11), but recent data (Eadington and Giblin, 1979; Patterson *et al.*, 1981) indicates transport of tin as Sn(II)-chloride complexes occurs at low pH and low fO_2 conditions, and as Sn(IV) complexes at high pH and/or high fO_2. An increase in pH and/or fO_2 or fall in temperature will cause precipitation of cassiterite from stannous chloride solutions.

2. REGIONAL GEOLOGICAL SETTING

INTRODUCTION

The purpose of this chapter is to set the regional geological framework within which the geology of the Cleveland deposit can be described, and particularly its stratigraphic setting in relation to other cassiterite-sulphide and tin deposits in Tasmania. More detailed reviews of the pre-Carboniferous geology and metallic ore deposits of western Tasmania, and from which this summary is mainly compiled, are given by Williams *et al* (1975), Solomon *et al* (1976), Corbett *et al* (1977) and Williams (1979), and a summary by Solomon (1981).

The geology of central western Tasmania is illustrated in Figure 2.1, and the relationships of the major rock units and the principal types of ore deposits are shown diagrammatically in Figure 2.2.

PRECAMBRIAN ROCK

Rocks of late Precambrian age crop out mainly in two regions, the Tyennan and Rocky Cape regions, which are isolated from each other by a meridional belt of rocks of Cambrian age and younger (Fig. 2.1). The Tyennan region consists predominantly of quartzite-phyllite assemblages and mica and garnet schist-quartzite assemblages which were probably derived from successions of interbedded siltstone and orthoquartzite (Gee *et al*, 1970). The metamorphic rocks are the product of two periods of metamorphism, with the earlier period attaining upper greenschist facies, and of two widespread phases of deformation (*e.g.* Gee *et al*, 1970; Spry, 1964; Raheim, 1977). The metamorphism and much of the deformation of this region are attributed to the upper Proterozoic Frenchman Orogeny (Spry *in* Spry and Banks, 1962).

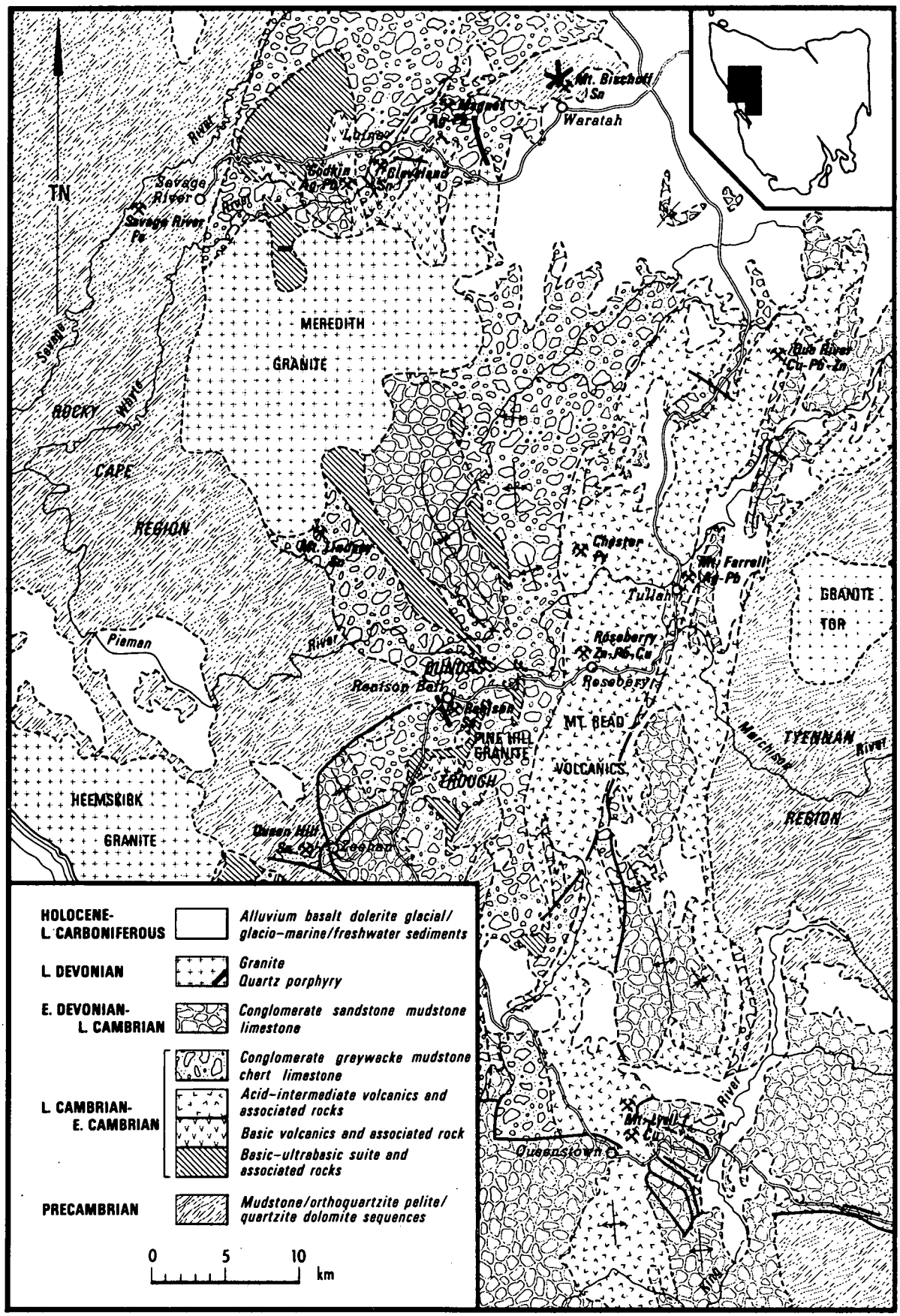

FIG. 2.1 Generalised geological map of central western Tasmania, showing major mineral deposits (modified after Williams and Turner, 1974; Corbett and Brown, 1976).

FIG. 2.2 Diagrammatic representation of the pre-Carboniferous geology and principal types of ore deposits and their relationships, in north-western Tasmania (after Collins, 1978)

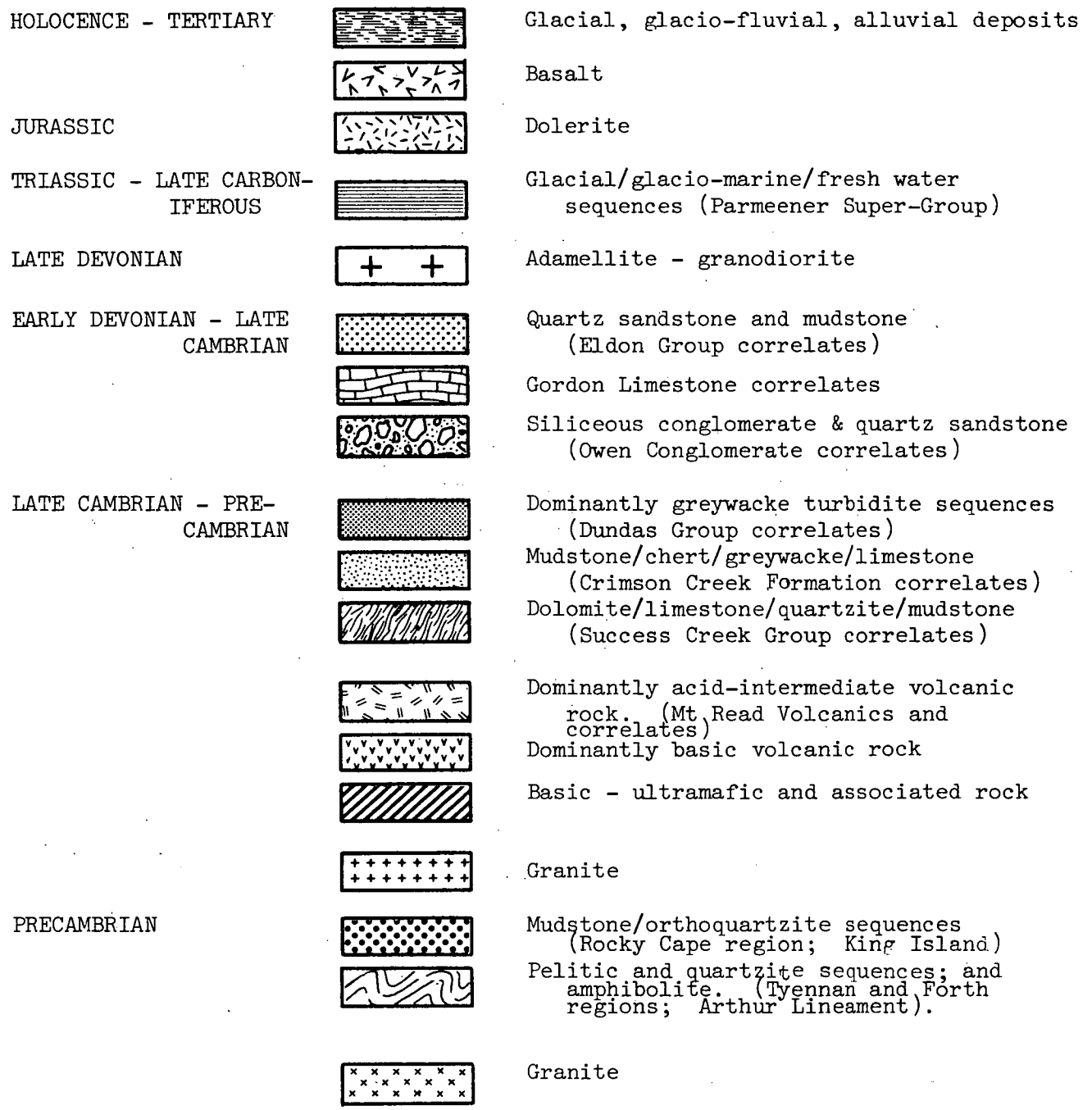

FIG. 2.2 continued

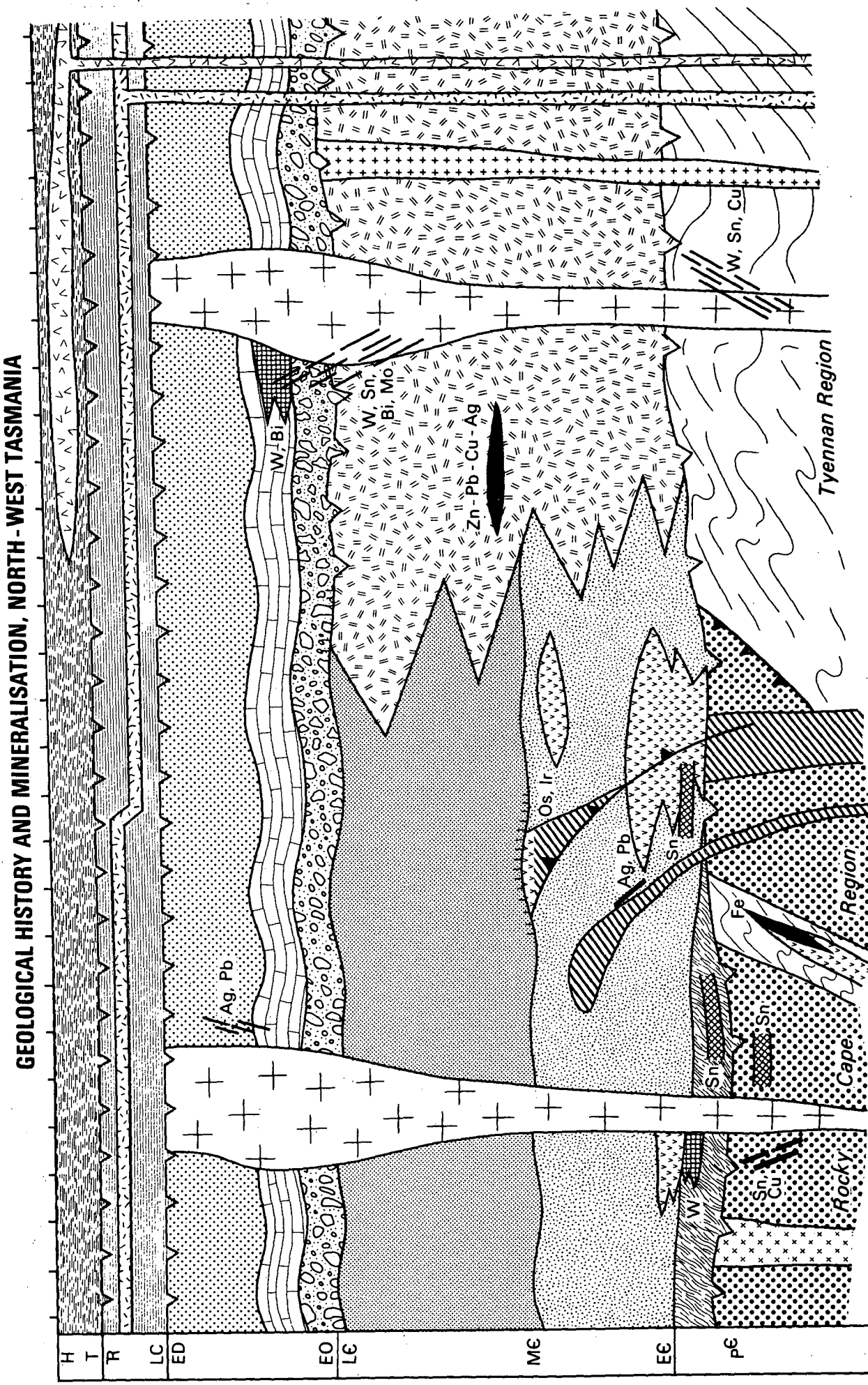

The Rocky Cape region in the west is underlain predominantly by unmetamorphosed laminated mudstone and super-mature orthoquartzite sequences with minor turbiditic greywacke and rare occurrences of basaltic lava and mafic tuff. Along its eastern margin there is an 8-15 km wide belt of low-grade metamorphic pelitic schist and amphibolite (the Arthur lineament, Gee, 1967; Fig. 2.2) which extends from the west coast, north of the Heemskirk Granite, northwards along the western flank of the Meredith Granite (see Figure 1 of Solomon, 1981). Within the metamorphic belt, in the Savage River area, apparently stratiform, but disrupted lenses of magnetite-pyrite mineralisation (*e.g.* Savage River mine, Fig. 2.1, 2.2) occur within a suite of metamorphosed tholeiitic basalt, andesitic tuff and gabbroic intrusives (Coleman, 1975).

East and south-east of the Arthur lineament is a complexly folded sequence of interbedded slaty mudstone, siltstone, quartzite and turbiditic quartzwacke which is apparently younger than the mudstone-orthoquartzite sequence to the west (Gee, 1967; Spry, 1964). The younger rocks include a shale and quartzite sequence with minor dolomite at Mt Bischoff, which is isolated by surrounding Cambrian rock (Groves *et al*, 1972; Fig. 2.1). The Mt Bischoff sequence has been deformed by at least two phases of Precambrian deformation, the first of which resulted in overturning of a large part of the succession, as part of a south-facing recumbent or reclined anticline (Williams, 1982).

The folding, and the development of the metamorphic belt in the Rocky Cape region are attributed to the Penguin Orogeny (Spry *in* Spry and Banks, 1962; Gee, 1979), which is regarded as younger than the Frenchman Orogeny (Spry, 1964; Williams, 1979). The age of the Penguin Orogeny is estimated to be less than 725 m.y. on the basis of radiometric age determination of probable syn-sedimentary dolerite dykes which intrude

the younger sequence on the north coast (Crook, 1980).

EOCAMBRIAN-CAMBRIAN SYSTEM

The Tyennan and Rocky Cape regions flank a meridional belt of Eocambrian and Cambrian rock (Dundas Trough and associated igneous rocks; Fig. 2.1) within which five major stratigraphic-lithologic groups may be distinguished (Fig. 2.2): (i) a probable Late Precambrian (or Eocambrian) orthoquartzite-shale sequence with minor dolomite (Success Creek Group); (ii) mudstone-greywacke sequences with basaltic volcanic rock and minor chert and limestone (Crimson Creek Formation); (iii) ultramafic and mafic complexes; (iv) fossiliferous, Middle to Late Cambrian mudstone-greywacke-conglomerate sequences (Dundas Group); and (v) dominantly acid to intermediate volcanic rocks with felsic intrusives (Mt Read Volcanics). The sedimentary and mafic volcanic rocks dominate the western portion of the belt (the Dundas Trough) and the Mt Read Volcanics dominate the eastern portion (Fig. 2.1).

Success Creek Group

The earliest Eocambrian-Cambrian sediments, the Success Creek Group (Taylor, 1954), consist of up to 800 m of massive, coarse-grained quartz sandstone, interbedded with laminated, fine-grained quartz sandstone with minor shale, breccia, tuff and basal mixtite. At the stratigraphic top, at Renison Bell, the quartz sandstone grades into a shale sequence up to 150 m thick, with interbedded dolomite and hematitic chert, mudstone and conglomerate deposited in a shallow water environment (Collins, 1972; Brown, 1980). The boundary relationship between the Success Creek Group and underlying Precambrian rock of the Rocky Cape region has been interpreted as an angular or transgressive landscape unconformity (Williams, 1979; Brown, 1980). The Success Creek Group is restricted in its occurrence to the Renison Bell area, and is not known to occur north of the Meredith Granite.

Crimson Creek Formation and correlates

Conformably overlying the Success Creek Group is a 2440-3040 m thick sequence of unfossiliferous, red-purple and green laminated argillite and siltstone, volcaniclastic greywacke and basaltic lava with minor carbonate horizons of the Crimson Creek Formation (Blissett, 1962 after Taylor, 1954; Brown, 1980). Successions lithologically similar to the Crimson Creek Formation occur in the Mt Lindsay area, on the southern boundary of the Meredith Granite (Fig. 2.1) where tholeiitic basalt flows and carbonate horizons are abundant (Brown, 1980), and also abut the eastern flank of the Meredith Granite where the mudstone-greywacke sequence again contains abundant mafic volcanics (Fig. 2.1).

North of the Meredith Granite, in the Waratah-Luina area, there occurs an unfossiliferous sequence of indeterminate thickness, which consists of greywacke, mudstone, shale, chert and minor limestone with abundant intercalated spilitic volcanic rocks and discordant and concordant intrusive bodies of dolerite and gabbro (Groves *et al*, 1972; Collins, this study). These rocks constitute the Arthur River sequence (Groves, 1968; Groves and Solomon, 1964) and are correlated with the Crimson Creek Formation (*e.g.* Groves *et al*, 1972; Williams, 1979). The correlation is supported by rare earth element data (Brown and Waldron, 1982) for spilitic tholeiitic basalt in the Arthur River sequence (Deep Creek Volcanics) which are almost identical to basalt in the Crimson Creek Formation in the Mt Lindsay-Renison Bell area. At Waratah, the Arthur River sequence overlies the Precambrian Mt Bischoff sequence with a degree of regional conformity, but on the south flank of Mt Bischoff the relationship between the two formations is believed to be a fault zone that was active during deposition of the overlying basal

Eocambrian-Cambrian sequence, and into which slumped large blocks of deformed Precambrian rock (Groves, 1971).

Ultramafic-mafic complexes

Large ultramafic-mafic ophiolitic(?) complexes have been tectonically emplaced within the Crimson Creek Formation, generally along the western margin of the Dundas Trough (Fig. 2.1). They represent oceanic basaltic crust and mantle which probably developed in rift structures during an early phase of extension of pre-existing crust, and during later movement (pre-Dundas Group) were dismembered and thrust into sediments of the trough and locally eroded (Brown *et al*, 1980; Rubenach, 1974; Solomon, 1981). The ophiolitic masses locally contain nickel sulphides (*e.g.* Lord Brassey mine, Fig. 4.1) but are noted for osmiridium recovered from alluvial deposits (*e.g.* Ford, 1981).

The largest complex, the Heazlewood River Complex, located west of Luina, consists of orthopyroxenite, peridotite and dunite which occur in association with basaltic and dacitic volcanic rocks (Rubenach, 1973). The mafic volcanic rocks in the complex are chemically unlike those in the Arthur River sequence to the east (Crenaune, 1980; Brown and Waldron, 1982).

Also within the Arthur River sequence are regionally concordant, but tectonically emplaced linear belts of altered ultramafic rock, dolerite and spilitic basalt (Rubenach, 1973; Groves *et al*, 1972). They include the Magnet 'Dyke' (Scott, 1954; Groves and Solomon, 1964) which occurs along the northern and western boundary of the Mt Bischoff sequence, and the Whyte River complex (Rubenach, 1973) which occurs in the valley of the Whyte River at Luina (Fig. 2.1).

Dundas Group and correlates

The Crimson Creek Formation is succeeded with structural conformity by the fossiliferous Dundas Group (Elliston, 1954; Blissett, 1962). Following deposition of the Eocambrian Crimson Creek Formation and emplacement of the ophiolitic(?) complexes there occurred a period of erosion during the Early to early-Middle Cambrian, prior to the onset of Dundas Group sedimentation in the middle-Middle Cambrian (Brown, 1980), which then continued through to the middle-Late Cambrian (Jago, 1979). The Group consists of about 2600 m of interbedded mudstone, turbiditic lithicwacke, chert-breccia, conglomerate, paraconglomerate and minor felsic volcanic tuff (Blissett, 1962; Jago, 1979). Biostratigraphic correlates of the Dundas Group occur north of the Pieman River (*e.g.* Huskisson Group of Taylor, 1954) but are not known to occur north of the Meredith Granite.

Mt Read Volcanics

East of the dominantly sedimentary and mafic volcanic sequences of the Dundas Trough is a considerable pile of rhyolitic to dacitic volcanic rocks with andesitic and basaltic volcanics which constitute the Mt Read Volcanics (*e.g.* Corbett, 1981; Figure 2.1). The sequence includes flow-banded and auto-brecciated lava, ash-fall and ash-flow tuff and breccia, sub-aqueous pyroclastic flows, felsic to mafic intrusive bodies (including granitic bodies) and lenses of mudstone and sandstone (*e.g.* Corbett, 1979, 1981; Collins, *et al*, 1981). The volcanic rocks are calc-alkaline and are comparable to Andean, rather than island arc volcanic suites (*e.g.* Solomon and Griffiths, 1974). Several stratiform, volcanogenic massive sulphide deposits occur within the Mt Read Volcanics, including the Zn-Pb-Cu deposits at Rosebery (Green *et al*, 1981) and Que River (Webster and Skey, 1979; Duggan, 1980), the massive pyrite deposit at Chester (Collins *et al*, 1981) and the disseminated copper ore bodies at Mt Lyell (Cox, 1981; Walshe and

Solomon, 1981) (Fig. 2.1).

The bulk of the Mt Read volcanism appears to have occurred during Dundas Group time, *i.e.* Middle and Late Cambrian (Corbett, 1981). The age of the earliest volcanism has not been determined, but it is probably younger than abyssal tholeiitic volcanism in the Crimson Creek Formation (Williams, 1979). Along the western margin, the volcanic rocks interfinger with or are faulted against sediments of the Dundas Trough while to the east they are either faulted against or unconformably overly the Precambrian Tyennan region.

In the Queenstown area, an angular unconformity separates the bulk of the pyroclastic and lava sequence that contains the Mt Lyell copper ore bodies from a younger sequence of tuff and agglomerate, with minor lava and sedimentary rock (Tyndall Group) of late-Middle or early-Late Cambrian age (Jago *et al*, 1972; Corbett, 1979, 1981). Above this unconformity the sequence is regionally conformable and continues through the Ordovician and Silurian periods to the Early Devonian.

LATE CAMBRIAN - EARLY DEVONIAN SEQUENCES

The eugeosynclinal-type sedimentation that characterised much of the Eocambrian-Cambrian period, terminated in the Late Cambrian and was replaced by deposition of siliceous conglomerate and sandstone, with most of the detritus derived from the uplifted Precambrian Tyennan region. The main siliceous clastic unit is the Owen Conglomerate which consists of up to 1200 m of terrestrial fans of siliceous, pebble to boulder conglomerate, and shallow-marine conglomerate and quartz sandstone (Wade and Solomon, 1958; Banks *in* Spry and Banks, 1962). The Owen Conglomerate is underlain by a locally-derived volcaniclastic conglomerate (Jukes Conglomerate) which in some areas conformably overlies the Tyndall Group (Corbett, *et al*, 1974). Elsewhere, the Owen Conglomerate rests unconformably on underlying Cambrian rock. The siliceous clastic sequence is followed conformably by up to several

hundred metres of shallow-marine, Middle to Late Ordovician Gordon Limestone (Banks *in* Spry and Banks, 1962; Blissett, 1962). North of Zeehan, on the western margin of the Dundas Trough, correlates of the Owen Conglomerate thin rapidly and are absent north of the Meredith Granite. The Gordon Limestone also thins to the north of Zeehan, and is either absent or occurs discontinuously beneath Silurian rock in the Heazlewood-Godkin Area, west of Luina (Groves, 1966).

The Gordon Limestone is succeeded conformably by the Silurian to Early Devonian Eldon Group which consists of shallow-marine, interbedded mudstone and quartz sandstone that attained a maximum thickness of 1800 m in the Zeehan area (Blissett, 1962). The Eldon Group is incomplete in the Heazlewood-Godkin area, where it consists of thickly bedded saccharoidal sandstones interbedded with quartzite and conglomerate (Groves, 1966). In general, accumulation of the Early Ordovician to Early Devonian sedimentary sequences of shelf-type sedimentation represents a tectonically quiescent period, although minor uplift of the source area probably occurred prior to Eldon Group sedimentation (Groves *et al*, 1972; Williams, 1979).

DEVONIAN DEFORMATION

Between the Early Devonian and late-Middle Devonian there occurred a widespread, major period of deformation (the Tabberabberan Orogeny) which affected all Early Palaeozoic rock in Tasmania and, to a lesser extent, rocks of the Rocky Cape and Tyennan regions (Williams *et al*, 1975; Williams, 1978, 1979).

In western Tasmania, the Tabberabberan Orogeny exaggerated probable earlier Cambrian folds, and includes two main phases of folding: early-formed major broad, open folds which rejuvenated major faults, and later small-scale folds and faults which are superimposed on, and interfere with, the major structures (*e.g.* Solomon,

1965; Williams, 1979). The early folds trend north to north-northwest in the Queenstown-Zeehan area but have north-east to north-northeast trends in the Que River area to the north (Fig. 2.1). At Mt Bischoff, an easterly trending major antiformal flexure of the Mt Bischoff sequence and co-axial folds in the Cambrian sequence to the north are inferred to be the earliest Devonian folds in this area, and mesoscopic, north-northwest trending folds represent a second Devonian deformation event (Williams, 1982).

LATE DEVONIAN GRANITOIDS AND ASSOCIATED MINERALISATION

During the Late Devonian there occurred a major period of emplacement of post-tectonic granitoid intrusions (*e.g.* Heemskirk Granite, Meredith Granite and Granite Tor mass; Fig. 2.1, 2.2), probably representing the final phase of the Tabberabberan Orogeny. The granitic rocks of western Tasmania have minimum isotopic ages ranging from 340 to 375 m.y. (McDougall and Leggo, 1965; Brooks and Compston, 1965; Brooks, 1966).

The granitoid plutons appear to have been emplaced at relatively shallow depths (pressures below 200 MPa; *e.g.* Solomon, 1981) and are essentially post-kinematic, in that they truncate fold structures of the surrounding rock (*e.g.* Williams, 1979; Fig. 2.1). Gravity data (Leaman *et al*, 1980) indicate that all granitoids in western Tasmania are linked at relatively shallow depth as a single large mass. The largest exposed granitoid is the markedly discordant Meredith Granite (Fig. 2.1) which underlies an area of about 300 km^2, and is composed predominantly of biotite granite/adamellite (*e.g.* Groves *et al*, 1972). The stratigraphic position and structure of the country rocks to the north and south of the Meredith Granite are similar and suggest continuity prior to intrusion (Fig. 2.1). The smaller Heemskirk Granite, at the west coast (Fig. 2.1) was emplaced as a stock-like body of biotite and biotite-muscovite granite/adamellite (Brooks and Compston,

1965; Klominsky, 1972). The dominance of peraluminous (or S-type) biotite granite/adamellite is characteristic of western Tasmanian granitoids, although hornblende-biotite granodiorite crops out at Grassy, King Island (*e.g.* Solomon, 1981).

Numerous tin and tungsten deposits and associated(?) silver-lead-zinc mineralisation, occur near or within the Devonian granitoids, and include the cassiterite-sulphide deposits at the Renison and Cleveland mines and at Mt Bischoff, and the scheelite-bearing skarn at Grassy, King Island (Fig. 1.1, 2.2). Exo-granitic tin-tungsten deposits are hosted by rocks ranging in age from Precambrian to Ordovician. Those occurring in Precambrian rocks include the Mt Bischoff deposit where cassiterite occurs in stratabound lenses of massive pyrrhotite within the Mt Bischoff sequence, adjacent to cassiterite-bearing, altered Devonian quartz-feldspar porphyry dykes (*e.g.* Groves *et al*, 1972). At St Dizier, stanniferous magnetite skarn occurs adjacent to the northern contact of the Heemskirk Granite, and stanniferous quartz-tourmaline stockwork veins and breccias penetrate orthoquartzite at Maynes mine, adjacent to its southern margin (Fig. 1.1).

Deposits in Eocambrian-Cambrian rock are numerous and widespread, but skarn and/or replacement-type deposits are restricted to the Success Creek Group and the Crimson Creek Formation and correlates, reflecting the high incidence of carbonate in the older sequences. They include the large stratabound cassiterite-sulphide deposits at Renison Bell, which occur in the Success Creek Group (*e.g.* Patterson *et al*, 1981), and a similar deposit at the Cleveland mine occurring in the Arthur River sequence, a correlate of the Crimson Creek Formation (*e.g.* Cox and Glasson, 1971; Collins, 1981, this study). Marginal to the Meredith

Granite are several tin and/or tungsten-bearing skarn deposits, also occurring in Crimson Creek Formation correlates (*e.g.* Mt Lindsay: Edwards, 1951; and recent discoveries at Mt Ramsay and Mt Youngbuck, 14 km SSE and 10 km WSW of Cleveland, respectively).

Several tin-tungsten deposits have haloes of argentiferous lead and zinc sulphide mineralisation (*e.g.* Zeehan field, Both and Williams, 1968; and Mt Bischoff, Groves *et al*, 1972). The quartz-galena-sphalerite-pyrite-siderite veins of the main part of the Zeehan field are centred on the Queen Hill-Oonah stannite-cassiterite-sulphide deposits (*e.g.* Solomon, 1981), and the Magnet silver-lead-zinc deposit (Cox, 1975) occurs in the outer zone of mineralisation at Mt Bischoff (Fig. 4.1).

The only significant endo-granitic tin deposits are irregular, linear zones and pipes of quartz-tourmaline-topaz-cassiterite mineralisation at the south Heemskirk tin field (*e.g.* Federation mine, Klominsky, 1972; Wells, 1978). Minor deposits in the Meredith Granite include a small, pipe-like greisen body at the Cundy mine (Reid, 1923) and quartz-greisen veins at the South Bischoff mine (Jack and Groves, 1965).

In summary, there is a clear spatial association between granitic rock and cassiterite-sulphide and other exo-granitic tin (-tungsten) deposits in western Tasmania (see also Solomon, 1980, 1981), regardless of the age of the host rocks which are generally older than the Mt Read volcanism. Thus, stratigraphic relationships of the sequence hosting cassiterite-sulphide mineralisation support an epigenetic origin, rather than a syngenetic volcanogenic origin for this type of deposit.

LATE CARBONIFEROUS-HOLOCENE ROCKS

Emplacement of the Late Devonian granitoids was followed by a prolonged period of erosion, which ended with the accumulation of glacial, glacio-marine, and fresh-water sequences of the Parmeener Super-Group of Late Carboniferous to Triassic age (Banks, 1973). These sequences, and Precambrian and Palaeozoic rock are locally intruded by Jurassic dolerite. Tertiary basalt, and glacial and glacio-fluvial deposits associated with Pleistocene glaciation blanket vast areas of Mesozoic, Palaeozoic and Precambrian rock, and Holocene alluvial deposits are present in most major river valleys.

3. GEOLOGY OF THE CLEVELAND MINE AREA

INTRODUCTION

The Cleveland mine is located within a near vertical to steep north-west dipping, NE-SW trending sequence of unfossiliferous sedimentary and mafic volcanic rock, occurring between two regionally concordant, fault-bounded slices of mixed, partially serpentinised basalt, dolerite, gabbro and peridotite/pyroxenite (Figs. 3.1, 3.2). The fault-bounded mafic-ultramafic bodies (*e.g.* Whyte River complex at Luina) were tectonically emplaced into the volcano-sedimentary sequence (Rubenach, 1973), and thus are probably the oldest rocks in the Cleveland area, being at least of probable pre-Middle Cambrian age (Rubenach, 1973).

The sedimentary and mafic volcanic sequence forms part of the Arthur River sequence of Groves and Solomon (1964) and Groves (1968), which disconformably or unconformably overlies Precambrian rock at Waratah (Groves, 1971). The author agrees with Groves and Solomon (1964), Groves *et al*, (1972) and Rubenach (1973) that the Arthur River sequence is lithologically similar to and correlated with the Eocambrian Crimson Creek Formation (Blissett, 1962), and is unlike the Middle to Late Cambrian sequences (*i.e.* Dundas Group). In the Cleveland area, the correlate of the Crimson Creek Formation is intruded by masses of dolerite-gabbro which also are of probable Eocambrian-Early Cambrian age. Unconformably overlying the volcano-sedimentary sequence is an Ordovician(?) to Early Devonian succession of limestone, sandstone, quartzite and conglomerate (Eldon Group correlates; Groves, 1966; Groves *et al*, 1972). The Eocambrian to Early Devonian rocks have been intruded by the Late Devonian Meredith Granite. East of the Meredith Granite, the Palaeozoic rocks are blanketed by Tertiary basalt (Figs. 3.1, 4.1).

The Cambrian stratigraphy in the Cleveland area (Table 3.1;

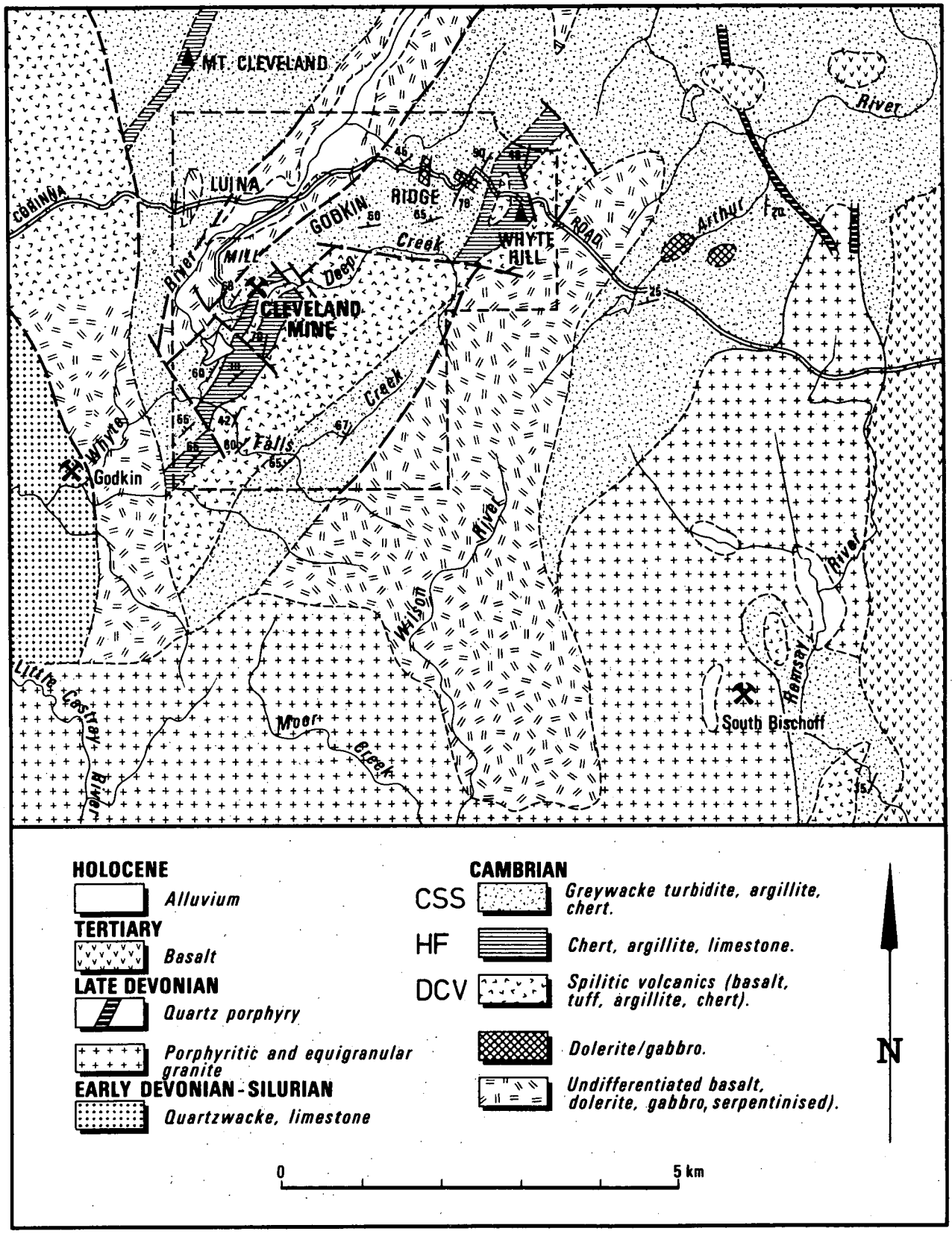

FIG. 3.1 Geological map of the Mt Cleveland area. The dashed outline indicates the area shown in Figure 3.3.
CSS = Crescent Spur Sandstone, HF = Hall Formation, DCV = Deep Creek Volcanics, in the vicinity of the Cleveland mine.

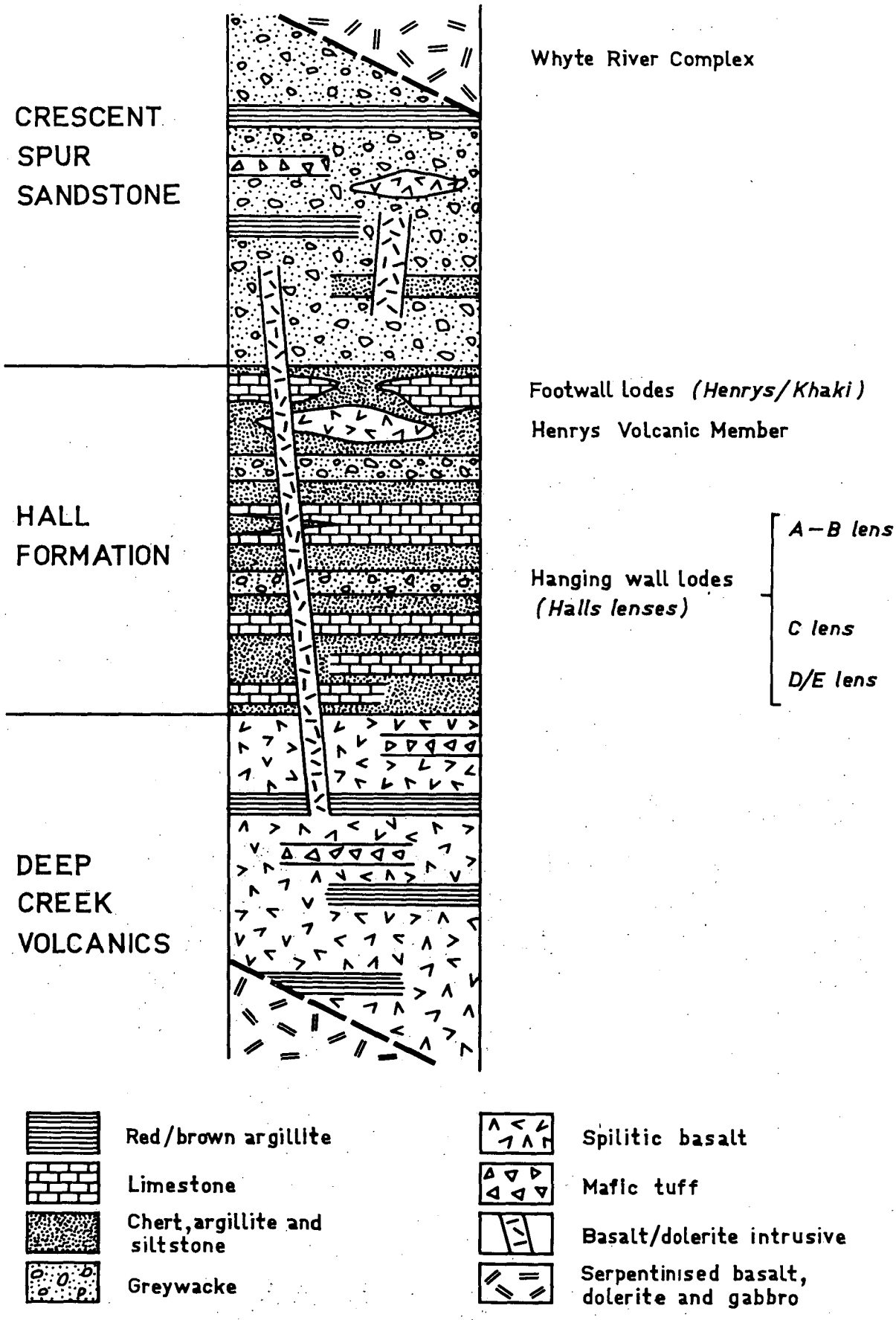

FIG. 3.2 Schematic representation of the Cambrian stratigraphic succession in the Cleveland mine area, showing the relative positions of the sulphide lenses within the Hall Formation.

TABLE 3.1. Stratigraphic succession in the Mt Cleveland area.

Age	Stratigraphic unit	Thickness (m)	Lithology
Holocene		0-10+	River gravel and alluvium.
Tertiary		0-100+	Olivine basalt; gravel, conglomerate and alluvium.
E. Devonian-Silurian	Eldon Group correlate	50+	Quartz sandstone, quartzite, siltstone, thin conglomerate beds.
Ordovician	Gordon Limestone correlate	20+	Limestone.
Cambrian-Eocambrian	Arthur River sequence: Crescent Spur Sandstone	350+	Grey, micaceous greywacke and interbedded siltstone and mudstone, with red-brown argillite, volcaniclastic greywacke, and minor grey chert and mafic green spilitic basalt.
	Hall Formation	50-150	Light-dark grey and purple argillite with grey limestone, chert, greywacke and litho-vitric tuff, and mafic green spilitic basalt and tuff (Henrys Volcanic Member).
	Deep Creek Volcanics	350-600+	Massive and locally pillowed spilitic basalt with intercalated/interbedded red-brown argillite, litho-vitric and lapilli tuff, volcaniclastic greywacke and red-grey chert.

Fig. 3.2) has been assigned a variety of descriptive terms and formation names, but this is clarified and defined in Appendix 1. The three main stratigraphic units in the Cleveland mine area were described by Cox (1968a) and Cox and Glasson (1967, 1971) as comprising the Crescent Spur Group, but they are here considered as part of the wider-based Arthur River sequence of Groves and Solomon (1964) and Groves (1968). The Luina Beds of Rubenach (1973), which abut the Heazlewood River Complex to the west of Luina, also form part of the Arthur River sequence.

The Cambrian succession at the Cleveland mine has been previously considered to be east facing with the Crescent Spur Sandstone the oldest unit (*e.g.* Glasson and Hopwood, 1962; Cox and Glasson, 1967, 1971; Cox, 1968a), although Cox (1968a) reported that cross-bedding and graded bedding had not been observed in beds of turbiditic greywacke. Later, Palmer (1976) described the eastern limit of the Crescent Spur Sandstone as irregularly and locally unconformably overlain by the Hall Formation. However, evidence gathered in this study (*e.g.* sedimentary structures in the Crescent Spur Sandstone) indicate a conformable, west facing sequence with the Deep Creek Volcanics the oldest unit. Hughes (1953) also recognised the 'lavas' as being the oldest rocks, and the 'tuffs' (equivalent to the Crescent Spur Sandstone) as the youngest.

MAFIC-ULTRAMAFIC COMPLEXES

The oldest(?) rocks in the Cleveland area occur in mafic-ultramafic complexes cropping out in the Whyte River valley (the Whyte River complex of Rubenach, 1973), and on the high ground to the south and east of Whyte Hill (Fig. 3.1). The complexes are composed of peridotite, gabbro, dolerite and basalt that was tectonically re-emplaced into the volcano-sedimentary succession of the Arthur River sequence (Rubenach, 1973). They are generally serpentinised and sheared, and contain lenses or slivers of chert, siltstone and argillite (Fig. 3.3) which probably are

tectonic inclusions (Rubenach, 1973).

The complex to the east and south of Whyte Hill has not been previously described, and is generally poorly exposed, though fresh outcrop occurs in the headwaters of Deep Creek (Fig. 3.3). The complex consists of massive, equigranular-subporphyritic, vesicular, olivine(?)-bearing basalt and serpentinised ultramafic rock (78-436). It is extensively sheared and in places contains post-deformation quartz-carbonate veins (*e.g.* at CQ690074) with associated quartz and carbonate alteration of the host rock (78-432). Basalt in this complex is composed of interlocking feldspar laths and pyroxene plates generally less than 0.1 mm across with interstitial chlorite and accessory sphene and opaques, and chlorite/calcite-filled vesicles. The sub-porphyritic variety (78-434) contains phenocrysts and glomerocrysts of cloudy feldspar laths up to 0.5 mm in length. The olivine(?)-bearing basalt (78-437) contains subrounded grains, up to 1.5 mm in diameter, which are composed of pleochroic pale yellow-green serpentine and chlorite with internal, red hematitic boxworks. These grains comprise 10-15% of the rock and are probably olivine pseudomorphs.

Whyte River complex

The Whyte River complex is a regionally concordant, NE-SW trending sill-like body, up to 1 km in width, which underlies the floor of the Whyte River valley (Figs. 3.1, 3.3). The complex has been briefly described by Nye (1923), Cox (1968a), Groves and Solomon (1964), Groves (1966) and Rubenach (1973); and geochemical data are given in Foden (1973) and Creenaune (1980).

The complex consists of dark green serpentinised ultramafic rock, gabbro, albite dolerite and spilitic basalt, as well as slivers and lenses of sedimentary rock (Fig. 3.3). The ultramafic rock was probably originally peridotite and plagioclase pyroxenite (Cox, 1968a; Rubenach, 1973; Foden, 1973). The gabbro (81-23; Groves and Solomon,

1964) is composed of interlocking laths of cloudy plagioclase (albite-oligoclase) and pleochroic green-brown, fibrous hornblende crystals (actinolite), with minor chlorite, sericite and opaques. The rock is equigranular, with crystals generally 0.5-1 mm in length, and exhibits an ophitic-granitic texture. Some hornblende plates contain cores of remanent augite.

Spilitic basalt (48335, 48336) is generally fine grained, equigranular (less than 0.5 mm) to subporphyritic, and is texturally and mineralogically similar to spilitic basalt in the Arthur River sequence. It is composed of altered, cloudy plagioclase laths (albite-oligoclase) and clinopyroxene in a sub-ophitic texture, with interstitial chlorite, calcite, sericite, sphene and opaques. Thin shear zones traversing the rock are filled with quartz, chlorite and calcite. A subporphyritic variant (81-22) contains phenocrysts of feldspar and augite, up to 1 mm in length.

Chemical compositions of spilitic basalt, dolerite and ultramafic rock from the Whyte River complex are given in Appendix 2, Table A2.7, and include two analyses of spilitic basalt on the eastern margin of the complex, at the Cleveland mine, three analyses of serpentinised ultramafic rock cropping out at Luina and south of the mill, and analyses of dolerite and peridotite from Foden (1973) and Creenaune (1980). The rocks in the complex are characterised by low titanium values with 0.18-0.41 mass% TiO_2 in the basalt/dolerite and 0.07-0.11 mass% TiO_2 in the ultramafic rocks. Basalt, dolerite and ultramafic rock in the Heazlewood River complex also have low titanium values (Rubenach, 1973; Creenaune, 1980). Hence the origin of the Whyte River complex probably is petrogenetically allied to formation and emplacement of the ophiolitic Heazlewood River Complex (Brown *et al*, 1980). The ultramafic rocks have characteristically high Cr values (2415-3239 g/t), high Ni values (1120-1550 g/t) and a high magnesium content (25.4-31.0 mass%

MgO). High Rb values (54 and 63 g/t) in spilitic basalt on the eastern edge of the complex at the mine (48335, 48336), reflect hydrothermal alteration associated with the mineralisation (see Chapter 5).

DEEP CREEK VOLCANICS

The Deep Creek Volcanics is the oldest unit of the Cambrian volcano-sedimentary sequence in the Cleveland mine area. It is 350-600 m in thickness and crops out on the high ground to the south-east of the Cleveland mine, predominantly between Deep Creek and Falls Creek and on Whyte Hill (CQ688080) (Figs. 3.1, 3.3). Mafic green basalt also crops out south-west of the Cleveland mine, on the west bank of the Whyte River near the Washington Hay silver-lead mine (Fig. 3.3), but its stratigraphic position has not been determined. The Deep Creek Volcanics is characterised by a predominance of mafic green, spilitic tholeiitic basalt with intercalated and interbedded green to green-grey lithovitric and lapilli tuff, red-brown argillite and minor chert, mafic green volcaniclastic greywacke and red-brown volcaniclastic conglomerate. The basalt generally is deeply weathered to either yellow-brown decomposed rock or red-brown soil. Cox (1968a) also described pyroclastic rocks (volcanic breccias and agglomerates) interbedded with basaltic lava flows. The agglomerates are described as consisting of accumulations of bombs, up to 150 mm in length, and breccias as accumulations of lava blocks, up to 150 mm across, embedded in a fine grained matrix. The breccias are most likely due to localised autobrecciation of lava flows (*e.g.* 48306).
Bomb-like ejecta have not been observed during this investigation, but their origin is probably allied to that of the coarse lapilli tuffs which occur sporadically throughout the volcanic pile.

FIG 3.3 Geology of the Cleveland mine area (map in pocket). Compiled from original geological mapping by P.L.F. Collins, supplemented with some additional mapping by mine geologists. The area of the map is outlined in Figure 3.1.

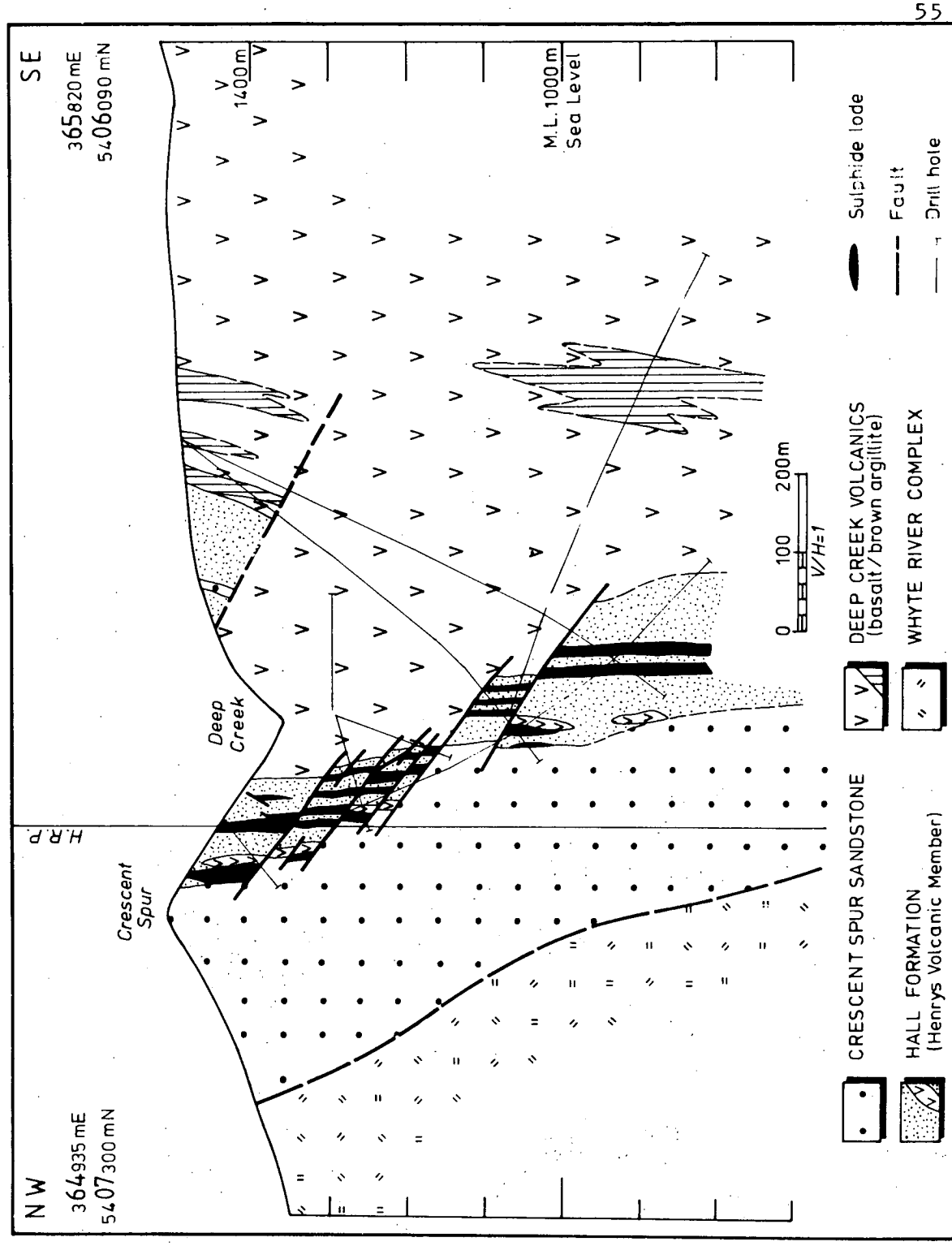

FIG. 3.4 Geological cross-section, Cleveland mine area, based on mine section Qa. Coordinates of end points are for the AMG (see Fig. 3.3).
H.R.P. = Halls reference plane.

Spilitic Basalt

Basalt occurs predominantly as massive lava flows, though pillow structures have been recognised at several locations (*e.g.* CQ65650625, and in Three Falls Creek at CQ64900475). Triangular cusps between pillows are filled with pale green chert, and vesicles are common within pillows. The best exposure of pillowed lava (albeit weathered) is in a cutting on the Corinna Road at the summit of Whyte Hill (Plate 3.1B; CQ68800795).

Massive lava flows are generally equigranular, though sub-porphyritic and porphyritic variants occur, with feldspar phenocrysts up to 5 mm in length. The basalt also contains chlorite-carbonate and sulphide filled vesicles (Plate 3.1D). Auto-brecciation(?) textures have been observed in massive flows (in drill core) occurring as angular to subrounded basalt fragments, in a relatively close-packed arrangement, with a dark green-black interstitial aphanitic matrix. Chlorite, calcite, quartz and minor epidote commonly occur in veins which range from a few millimetres to in excess of 50 mm in thickness (*e.g.* 48300; Plate 3.1E, F). Adjacent to the sulphide lenses, the basalt has been hydrothermally altered, as described in Chapter 5.

The basalt (*e.g.* 48299, 48300, 48302, 48309) consists of inter-grown equigranular clinopyroxene and subhedral plagioclase laths, exhibiting a basaltic to sub-ophitic texture (Plate 3.1E, F), with a groundmass of fine-grained clinopyroxene, actinolite, chlorite, sphene, epidote, calcite and opaques (magnetite, ilmenite(?) and sulphides). Olivine and primary quartz have not been observed in the basalt, although serpentinite/chlorite pseudomorphs after euhedral olivine occur in basalts in the mafic-ultramafic complexes (78-437; Cox, 1968a; Groves and Solomon, 1964).

Porphyritic varieties (48323, 81-31) contain cloudy plagioclase phenocrysts comprising up to 10% of the rock, and occurring either as

tabular subhedral laths up to 3 mm in length, or as glomerocrysts up to 5 mm across consisting of several interlocking laths.

Autobrecciated basalt (48305, 48306) consists of subrounded fragments of fine-grained, equigranular basalt in a translucent to opaque glassy matrix with very fine crystals of plagioclase, clinopyroxene and chlorite, and fine basalt grains (Plate 3.1C). This texture probably results from autobrecciation of either the top or base of basalt flows.

In thin section, plagioclase occurs as laths, 0.2-0.6 mm in length, and is variably altered to sericite, quartz, chlorite and epidote. Sericite alteration of feldspar is more intense near the Cleveland mine where it is regarded as a product of wall-rock alteration. The plagioclase generally has the composition albite-oligoclase (about An_{10}) as determined by electron probe microanalyses (Table 3.2; specimen 48307) and from maximum symmetrical extinction angles. However, in specimen 48299, a more calcic plagioclase is indicated for laths enclosed within unaltered pyroxene grains, and has been confirmed by electron probe micro-analysis (Table 3.2). This plagioclase has a labradorite composition (An_{67}, An_{30}, Or_3) and indicates a parental, more calcic feldspar. Clinopyroxene occurs as subhedral grains (0.2-0.5 mm across) commonly intergrown with plagioclase (Plate 3.1G, H), and exhibiting green-yellow pleochroism. The clinopyroxene is dominantly augite, with minor, co-existing sub-calcic augite or pigeonite (Foden, 1973). Some pyroxene grains exhibit alteration to green-brown pleochroic actinolite. Electron probe micro-analysis of clinopyroxene in specimen 48299 (Table 3.2) confirms the augite composition, and also show that the rims of augite grains are depleted in Mg and Ca, and enriched in Fe and Mn relative to the core.

TABLE 3.2 Composition of minerals in spilitic basalt, Deep Creek Volcanics (summarised from Table A4.1).

Mineral	CPX	CPX	CPX	CPX	PLAG	PLAG	ACT	SPH	CAL	CHL
Specimen	48299	48299	48299	48307	48299	48307	48307	48299	48299	48299
Anal.	Range (16)	Core (2)	Rim (2)	(4)	(4)	(4)	(3)	(4)	(2)	(5)
Mass % oxide										
SiO_2	47.15-51.70	49.66	48.27	50.60	52.76	68.55	49.61	31.38	0.54	26.82
TiO_2	0.55- 1.42	0.82	1.15	0.93	0.29	0.13	0.61	29.46	-	0.09
Al_2O_3	2.20- 4.70	4.54	3.16	2.10	27.39	20.71	5.87	4.41	0.29	17.21
FeO	8.45-17.20	8.90	14.90	16.75	1.53	0.34	21.59	3.99	0.76	36.20
MnO	0.15- 0.38	-	0.17	0.49	-	-	0.27	-	-	0.45
MgO	11.37-15.69	14.92	11.88	11.81	0.47	-	9.03	-	-	8.21
CaO	12.90-21.72	20.90	19.98	17.65	11.85	1.00	14.47	28.21	58.42	0.52
Na_2O	-	-	-	0.55	5.09	9.95	0.82	-	-	-
K_2O	-	-	-	-	0.41	0.15	0.27	-	-	0.06
Cr_2O_3	0.19- 0.39	0.31	0.24	0.31	0.20	0.17	0.30	-	-	0.19
TOTAL		100.04	99.74	101.19	99.99	101.00	102.84	97.45	60.01	89.75
Atomic proportions										
O ions	6	6	6	6	8	8	23	20	6	28
Si	1.834-1.912	1.850	1.859	1.923	2.419	2.962	7.176	4.228	0.050	5.870
Ti	0.015-0.041	0.023	0.033	0.027	0.010	0.004	0.065	2.986	-	0.014
Al	0.096-0.204	0.199	0.144	0.094	1.480	1.055	1.012	0.700	0.031	4.440
Fe	0.262-0.545	0.278	0.479	0.534	0.059	0.012	2.637	0.451	0.059	6.629
Mn	0.005-0.012	-	0.005	0.012	-	-	0.032	-	-	0.085
Mg	0.655-0.865	0.829	0.682	0.668	0.032	-	2.012	-	-	2.678
Ca	0.750-0.867	0.835	0.824	0.718	0.582	0.047	2.149	4.073	5.794	0.122
Na	-	-	-	0.041	0.453	0.833	0.231	-	-	-
K	-	-	-	-	0.024	0.008	0.050	-	-	0.024
Cr	0.006-0.012	0.009	0.007	0.009	0.007	0.006	0.034	-	-	0.033
TOTAL	4.020-4.041	4.022	4.033	4.026	5.066	4.927	15.394	12.438	5.934	19.895
Ca:Mg:Fe	-	43:43:14	42:34:24	37:35:28	-	-	31:30:39	-	-	2:28:70
Ca:Na:K	-	-	-	-	55:43:2	5:94:1	-	-	-	-

CPX = clinopyroxene, PLAG = plagioclase, ACT = actinolite, SPH = sphene, CAL = calcite, CHL = chlorite.
Anal. = number of analyses from which the analysis is taken.

PLATE 3.1 Pillowed basalt, Whyte Hill and photomicrographs of autobrecciated, vesicular and equigranular basalt, Deep Creek Volcanics.

A: Basalt pillows, Henrys Volcanic Member, Whyte Hill (CQ68370794).

B: Weathered pillowed basalt, Deep Creek Volcanics, Corinna Road, Whyte Hill (CQ68830795).

C: Autobrecciated basalt, Deep Creek Volcanics (48306). Basalt fragments in a glassy matrix, and late quartz-chlorite-calcite vein. Scale bar = 1 mm, plane pol. light.

D: Vesicular basalt, Deep Creek Volcanics (81-27), with augite phenocryst (left centre). Scale bar = 1 mm, plane pol. light.

E: Equigranular basalt, Deep Creek Volcanics (48302), with quartz-calcite-chlorite veins. Scale bar = 1 mm, plane pol. light.

F: As above, X nicols.

G: Intergrown plagioclase laths and augite in spilitic basalt, Deep Creek Volcanics (48302). Scale bar = 100μm, plane pol. light.

H: As above, X nicols.

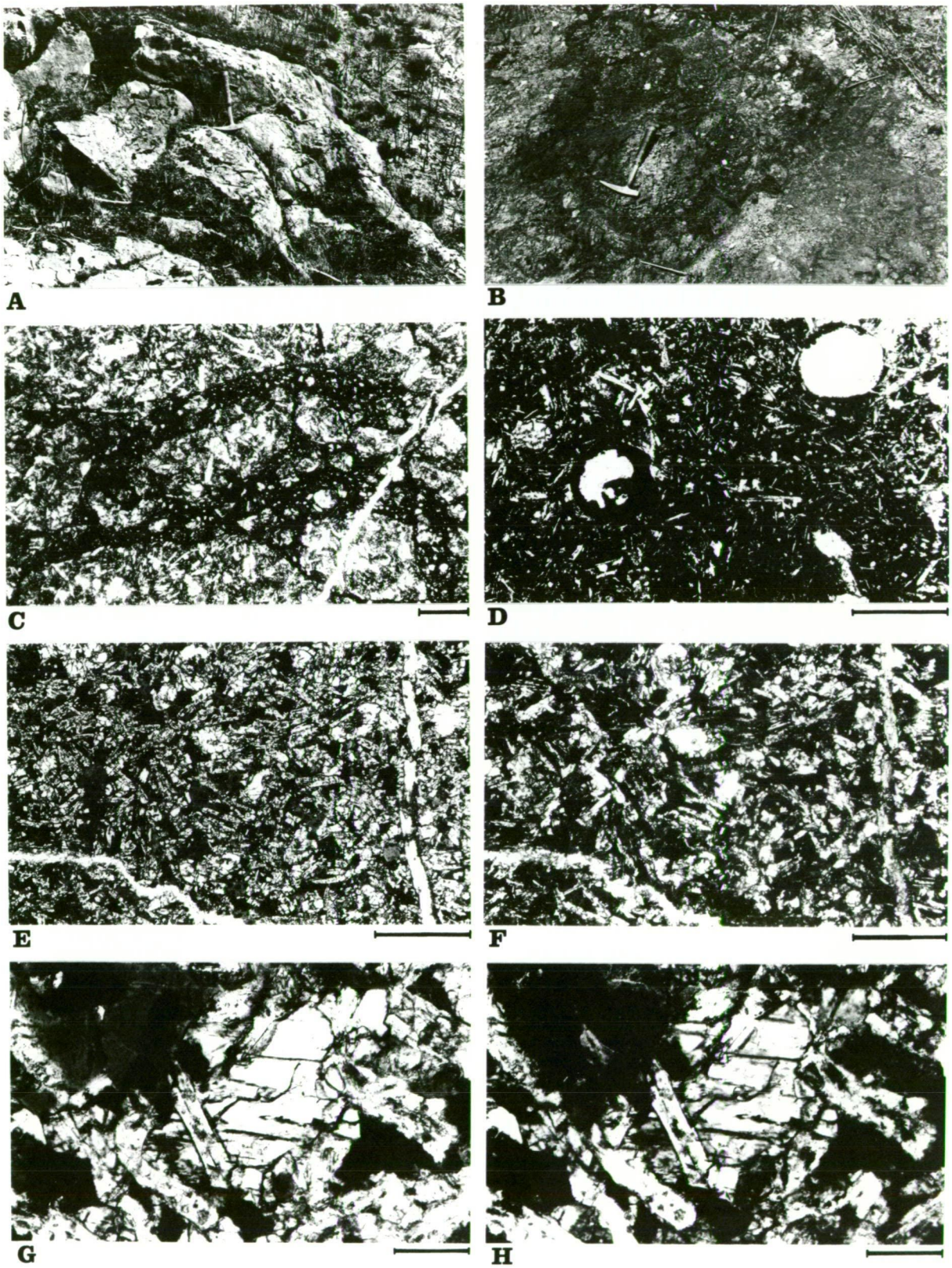

PLATE 3·1

The groundmass consists of small, anhedral grains of augite, plagioclase laths, composite grains of very fine grained sphene, and fine grained chlorite, epidote, calcite, actinolite and opaques. Analysis of the sphene (Table 3.2) indicates high Fe and Al contents, substituting for Ti. Chlorite occurs interstitially with feldspar laths and pyroxene grains, and shows very pale green pleochroism. The chlorite is enriched in Fe (Table 3.2) and has the composition brünsvigite. Calcite occurs as fine aggregates, and is almost pure $CaCO_3$, with only very minor Fe, and nil(?) Mn and Mg (Table 3.2). Opaques are dominantly magnetite and minor sulphides (pyrrhotite, chalcopyrite) occurring as anhedral grains.

The basalt has been subjected to greenschist facies metamorphism as evidenced by chlorite, sericite, actinolite and epidote as products of alteration of clinopyroxene, plagioclase and the groundmass, and calcite and chlorite in veins and vesicles. It has a typical spilitic assemblage with abundant sodic-plagioclase in addition to other alteration minerals, but neither greenschist facies metamorphism nor spilitisation developed to an advanced stage as evidenced by the occurrence of relic primary labradorite and the high proportion of unaltered clinopyroxene. Thus the basalt is best described as spilitic basalt rather than spilite. More intense hydrothermal alteration is associated with the mineralisation (Chapter 5).

Tuffaceous Units

Tuffs occur sporadically throughout the Deep Creek Volcanics, as beds or units, up to 0.5 m in thickness, intercalated or interbedded with basalt flows and red-brown argillite. They are generally grey-green to green and rarely pink in colour and range from lapilli tuff to coarse grained lithic and litho-vitric tuff and to fine to medium grained, equigranular vitric tuff. Grading of fragments is commonly developed in coarse grained tuffs, but there is no preferred orientation

of grading with conflicting apparent facing directions, even in adjoining tuff beds in the same length of drill core.

Vitric tuffs (48304, 48311) are laminated to thinly bedded ash beds which, in thin section, consist of a felted mass of microcrystalline quartz, chlorite, carbonate and sericite with minor sphene and opaques. Under low-power magnification (1 x objective) the tuffs clearly consist of devitrified mafic glass shards, generally 0.1-0.2 mm but up to 0.5 mm in length, with a pronounced foliation parallel to bedding. Lithic and litho-vitric tuffs (48304, 104383, 77-634) consist of varying proportions of lithic fragments in an equigranular vitric tuff matrix. Fragments are generally lenticular to elongate, sub-rounded and 0.5-8 mm in length, and consist of laminated argillite and siltstone, and rarely of quartzite (Plate 3.2B). The lithic fragments are mostly locally derived.

Lapilli tuffs (*e.g.* 48310, 48311) consist predominantly of mafic volcanic fragments (40-50%) embedded in a groundmass of equigranular vitric tuff (50-60%), which is green or pink in colour. Lithic fragments (argillite, siltstone, quartzite) comprise up to 5% of the tuff. Angular to subrounded detrital quartz grains, up to 0.5 mm in diameter, feldspar laths, up to 0.5 mm long, and pyroxene grains occur as minor components in the tuff. The volcanic fragments are elongate, up to 10 mm in length (Plate 3.2A), and occur as angular to rounded, commonly embayed fragments of finely crystalline basalt, which consists of an interlocking mass of chlorite, carbonate, sericite, feldspar laths and clinopyroxene. Some fragments are relatively coarse grained (*i.e.* larger feldspar laths), and some are porphyritic, with microphenocrysts of feldspar. The vitric tuff groundmass has a pronounced foliation defined by parallelism of shard-like structures and of small fragments. The foliation bends around the larger fragments, with equant deviation (Plate 3.2A). The fragmental material in all lithic and lapilli tuffs

has an open framework (*e.g.* Plates 3.2A, B) and rarely exceeds 50% of the tuff.

Volcaniclastic greywacke/conglomerate

Fine grained, equigranular volcaniclastic greywacke (81-32, 81-34) crops out on Whyte Hill (at CQ68630796) on the boundary between the Deep Creek Volcanics and the Hall Formation. It consists of angular to sub-rounded, close-packed grains, generally 0.2-0.4 mm in diameter, of finely crystalline basalt (interlocking pyroxene and feldspar laths), devitrified mafic glass fragments and glass shards, augite crystals and plagioclase laths, and minor quartz and quartzite grains and mica flakes with interstitial chlorite, clays, quartz, sericite and finely disseminated opaques. It is similar to volcaniclastic greywacke in the Crescent Spur Sandstone.

Poorly-sorted volcaniclastic conglomeratic units (77-620, 77-622, 77-629) occur interbedded with tuffs and chocolate-brown argillite. They consist of varying proportions of basalt, argillite and volcaniclastic greywacke occurring as rounded to elongate fragments up to 3 mm across, flattened glass shards up to 2 mm in length, and minor rounded quartz grains, 0.2-0.5 mm in diameter, in an argillaceous matrix with quartz, chlorite and calcite. In some sections (*e.g.* 77-622, 77-629) fragments are extensively altered by calcite, occurring as coarse recrystallised calcite, which may comprise up to 50% of the rock.

Argillite and chert

Laminated red-brown to chocolate-brown argillite with minor chert crops out as discontinuous lenticular units intercalated with spilitic basalt lava (Fig. 3.3). The argillite is dominantly finely laminated, but commonly grades into thinly bedded siltstone and tuffaceous siltstone, with beds up to 100 mm thick. In thin section (78-771, 77-620), the argillite consists of clay-size material with minor carbonate, chlorite and sericite, and rare angular detrital(?) quartz grains (less

PLATE 3.2 Photomicrographs of tuff, chert, argillite and limestone in the Deep Creek Volcanics and the Hall Formation.

A: Lapilli tuff, Deep Creek Volcanics (48310). Volcanic fragments (white) in a foliated glassy matrix with rare lithic fragments (dark grey). Scale bar = 1 mm, plane pol. light.

B: Litho-vitric tuff, Deep Creek Volcanics (48304). Lithic fragments in a fine grained matrix of quartz, lithic fragments and glass shards. Scale bar = 1 mm, plane pol. light.

C: Interbedded litho-vitric tuff, argillite and chert in 'chert' interlayered with ore, Hall Formation (48287). Note 'bleaching' adjacent to quartz-chlorite-carbonate veinlets. Scale bar = 1 mm, plane pol. light.

D: Interbedded chert, tuffaceous siltstone and litho-vitric tuff in 'chert' in ore, Hall Formation (48287); with syn-depositional micro-faulting. Scale bar = 1 mm, plane pol. light.

E: Calcite lenticles in laminated calcareous argillite in 'chert' in ore, Hall Formation (48292). Scale bar = 1 mm, X nicols, stained section.

F: Limestone, Hall Formation (48298). Finely recrystallised calcite (grey) with interstitial chert, chlorite, quartz and dolomite (white). Worm-like wisps of dolomite define original grainsize. Scale bar = 100μm, plane pol. light, stained section.

G: Recrystallised limestone, Hall Formation (48294). Coarse recrystallised calcite (grey) with remanent interstitial dolomite, at right; and finely recrystallised calcite as in F above, at left. Scale bar = 1 mm, plane pol. light, stained section.

H: Stylolitic limestone, Hall Formation (48296). Black carbonaceous material, chert and quartz in irregular stylolitic structure in calcisiltite; partially recrystallised at right. Scale bar = 1 mm, plane pol. light, stained section.

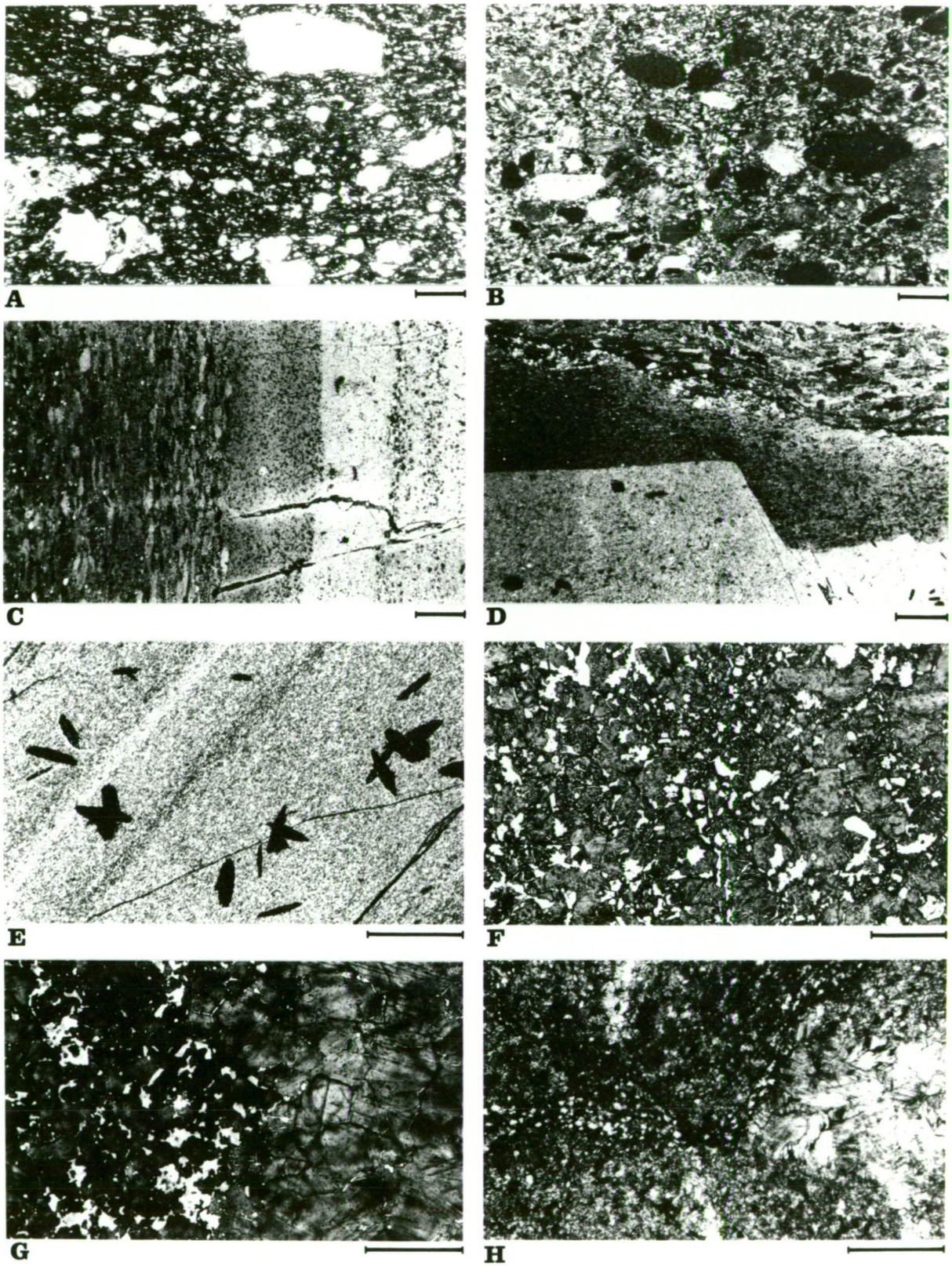

PLATE 3·2

than 0.01 mm in diameter). Tuffaceous units commonly contain fine grained (0.1-0.5 mm) chloritic volcanic detritus and minor quartz disseminated throughout red-brown to chocolate-brown argillite. They rarely contain rounded basalt fragments, up to 3 mm in diameter (77-629), and relic, flattened glass shards, up to 1 mm in length (77-620).

Reduction spots are locally developed within thick argillite units (*e.g.* at CQ64750705), occurring as cream coloured ovoid spots, generally 1 mm to 20 mm in length (78-771). In places the spots have been so intensively developed that they have amalgamated into elongate zones parallel to bedding, and give the appearance of cream coloured argillite/chert interbedded with red-brown argillite (*e.g.* at CQ65800695). Assuming an original spherical shape, the reduction spots have been deformed, with the long axes of flattened spots co-planar with cleavage which is also parallel to near vertical bedding.

Chert occurs either thinly interbedded with argillite, where it is orange-red to chocolate-brown in colour and probably of authigenic origin; or it is intercalated or interbedded with basalt and/or lithic to vitric tuff where it is green to green-grey in colour and most likely is derived from deposition of very fine ash (*e.g.* 81-29).

HALL FORMATION

The Hall Formation is 50-150 m thick and is dominated by light-dark grey and purple argillite with greywacke, limestone, chert, tuff and mafic green spilitic, tholeiitic basalt (Fig. 3.2). It forms a transitional sequence between a dominantly basaltic lava sequence (Deep Creek Volcanics) to the east, and a dominantly turbiditic greywacke sequence (Crescent Spur Sandstone) to the west (Fig. 3.1, 3.4). The Hall Formation is characterised by the occurrence of limestone which is not known to occur in the other formations.

The Hall Formation crops out on Whyte Hill (CQ685080) and at the Cleveland mine where limestone beds within the sequence have been replaced

by cassiterite-sulphide mineralisation. Eleven lenses of mineralisation have been recognised within the Hall Formation (Palmer, 1976) and they are conveniently divided into two groups of lodes (the footwall lodes and hanging wall lodes) by lenses of spilitic basalt known as Henrys Volcanic Member (Fig. 3.2).

South east of the Cleveland mine is a similar, subparallel sequence of red-grey argillite, orange, red and grey chert, greywacke and limestone occurring within the Deep Creek Volcanics (Fig. 3.3, 3.4). This sequence is considered to be equivalent to the Hall Formation having been faulted into its present position and is known locally as the 'eastern sediments'.

Argillite, Chert and Tuff

Argillite and chert (48284, 48285, 48286) are generally thinly interbedded (Plate 3.2C), though laminated argillite also occurs thickly interbedded with micaceous greywacke. The argillite consists of very fine grained (0.01 mm) quartz, sericite, chlorite, calcite and sulphides with minor angular to subrounded quartz grains up to 0.1 mm in diameter, and rare muscovite flakes up to 0.1 mm in length. Chert consists of cryptocrystalline quartz with minor chlorite, sericite and carbonate, and variable amounts of sulphides. Calcite is a major component of much of the argillite at the Cleveland mine, comprising up to 30% of the rock. It occurs as finely disseminated grains interstitial with quartz, chlorite and sericite, as irregular clots up to 0.5 mm across, and as interlocking lenticular masses, up to 0.6 mm x 0.1 mm (Plate 3.2E).

Fine grained lithic and litho-vitric tuff commonly are thinly interbedded with argillite and chert, occurring as beds generally 5-10 mm, but up to 50 mm in thickness. The tuff (48287) consists of elongate to lenticular argillaceous fragments and sub-rounded detrital quartz grains, 0.2-0.4 mm in diameter, in a devitrified glass shard matrix. The lithic fragments are generally 0.5-1 mm and up to 2 mm in length, and exhibit a

pronounced lineation (Plate 3.2C, D).

Limestone

Unfossiliferous limestone occurs in the Hall Formation at the north-eastern end of the mine, where it is stratigraphically equivalent to the sulphide lenses, and also occurs in the faulted block of the Hall Formation located to the south-east of the mine (Fig. 3.4). It crops out in a gully at CQ65050618, and on the south bank of Deep Creek at CQ65030646, where it occurs as grey-dark grey, soft, weathered material with euhedral pyrite occurring along bedding planes (48344).

The limestone is a massive laminated, micritic limestone or calcisiltite, which is recrystallised and locally stylolitic. The calcisiltite is composed of finely crystalline calcite occurring as angular, interlocking grains, 0.01-0.05 mm across, with minor interstitial dolomite, authigenic quartz, chert, chlorite and sulphides, and minor allogenic quartz occurring as angular grains up to 0.1 mm across. The non-carbonate fraction comprises 10-15% of the rock. Recrystallised calcisiltite (48294) consists of angular and irregularly interlocking calcite grains, generally less than 0.1 mm across, but with irregular patches of relatively coarse recrystallised calcite as grains up to 1 mm across (Plate 3.2F, G). Stylolitic structures (48296) consist of angular silt-grade quartz and opaque carbonaceous material concentrated in irregular, wispy bands less than 1 mm thick (Plate 3.2H).

X-ray diffraction analysis and staining of thin sections has confirmed calcite as the dominant carbonate mineral. Dolomite was not detected by X-ray diffraction, but staining reveals interstitial dolomite in calcisiltite and worm-like wisps, possibly defining original grain boundaries, in recrystallised calcisiltite (Plate 3.2F, G).

Sulphides comprise less than 2% of the limestone, and are mainly pyrrhotite with minor sphalerite, chalcopyrite and pyrite, and rare galena.

Pyrrhotite occurs as anhedral grains up to 0.4 mm across and may be either intergrown with or contain inclusions of sphalerite and chalcopyrite. Sphalerite also occurs as individual grains, and contains inclusions of pyrrhotite, pyrite and rarely galena. Pyrite in 48295 occurs as spherical grains up to 1.2 mm in diameter. The sulphides are commonly concentrated and aligned along bedding planes and may be authigenic.

Limestone in the 'eastern sediments' is typically grey-dark grey, laminated and massive calcisiltite, with thinly interbedded light grey chert. The calcisiltite (48312) is composed of finely crystalline calcite occurring as interlocking grains up to 0.1 mm diameter, and is partially recrystallised. The calcisiltite grades into chert beds which, in thin section, are 5-10 mm thick and contain clots (0.2-0.3 mm in diameter) of finely crystalline calcite. Authigenic sulphides (dominantly pyrite, with minor chalcopyrite and pyrrhotite) are concentrated in cherty or carbonaceous beds, but also occur as disseminated euhedral pyrite (0.01-0.05 mm) in the calcisiltite. Pyrite most commonly occurs as bands of euhedral crystals, up to 1 mm in diameter, in chert.

Chemical analyses of the limestone (Appendix 2, Table A2.9) indicate that it is composed almost entirely of calcite and quartz (and chert) with only minor amounts of iron, magnesium and manganese. This contrasts with the dolomite host rock at Renison and Mt Bischoff (Fig. 3.5, and Patterson, 1982) both of which are in stratigraphically older sequences. The relative proportions of equivalent calcite and quartz in the limestone vary between 40-80% and 10-42%, respectively, and tend to fall into two groups: relatively pure limestone (48291, 48293, 48295, 48296, 48298) characterised by high calcite (74-85%) and low quartz (10-16%), and impure limestone (48301, 48355, 48356) with less calcite (40-66%), higher quartz (21-42%) and higher Al_2O_3, Ba and

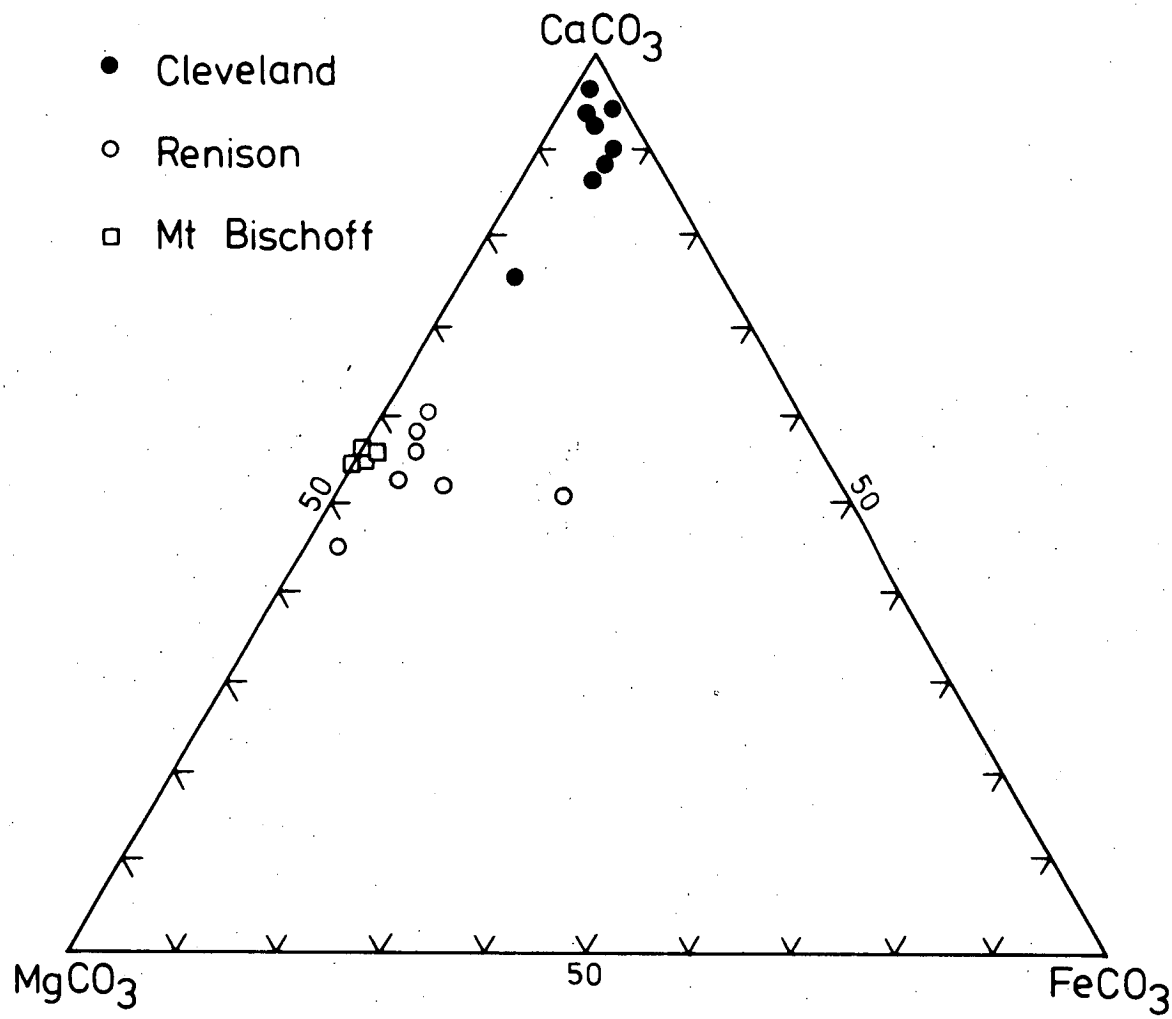

FIG. 3.5 Triangular plot of $CaCO_3$-$MgCO_3$-$FeCO_3$ of limestone in the Hall Formation. Equivalent carbonate has been calculated from analytical data in Table A2.9. The composition of host dolomitic rocks at Renison and Mt Bischoff are plotted for comparison (data from Groves, 1968; Collins, 1972).

Rb (Table A2.9).

High Cu and Zn, particularly in 48298, may be due to veins and replacement mineralisation within the limestone, and in which sphalerite is a dominant mineral. Only one specimen (48295) has a tin content in excess of 10 g/t and four have less than 2 g/t Sn.

Henrys Volcanic Member

Henrys Volcanic Member is the local term for lenses of mafic volcanics occurring at the same stratigraphic level towards the top of the Hall Formation (Fig. 3.2, Appendix 1). The member is significant in that at Cleveland it separates the lenses of mineralisation into the footwall lodes (Henrys, Khaki, Lucks) to the north-west, and the hanging wall lodes (Halls lenses) to the south-east (Fig. 3.2, 4.2). Henrys Volcanic Member consists predominantly of mafic green, fine grained, equigranular to subporphyritic basalt, though porphyritic varieties also occur and is similar to the spilitic basalt of the Deep Creek Volcanics. Palmer (1976) shows minor mafic green tuff occurring stratigraphically above the basalt.

Henrys Volcanic Member crops out approximately 200 m west of the summit of Whyte Hill (Fig. 3.3), where it occurs as massive, equigranular basalt in well-defined pillow structures (Plate 3.1A) with light green inter-pillow chert. The fine grained, equigranular basalt (81-36) consists of interlocking augite and plagioclase laths (albite-oligoclase) with interstitial chlorite, sericite, sphene and opaques. Autobrecciated basalt (81-37) occurring within the pillowed basalt, consists of rounded fragments of very fine grained (less than 0.1 mm) subporphyritic basalt, containing augite phenocrysts up to 0.5 mm across, in an opaque glassy to translucent felted mass of chlorite, plagioclase and pyroxene, and small basalt fragments. Calcite occurs as irregular patches in the basalt fragments and in the matrix, and irregular veins

of chalcedonic quartz and calcite traverse the rock. An analysis by Foden (1973) of the basalt cropping out on the Corinna Road is reproduced in Table A2.5 (analysis 41045).

At the Cleveland mine, equigranular basalt (48316, 48319, 48320, 48324) is extensively altered and consists of pleochroic green to brownish green actinolite (after pyroxene), plagioclase, quartz, sericite, chlorite, calcite, sphene and opaques. Although relict pyroxene has not been observed, twinning has been preserved in some grains, and in some larger actinolite grains pleochroic green cores are surrounded by pleochroic colourless-pale green rims which probably reflect chemical variation similar to that observed in augite in spilitic basalt of the Deep Creek Volcanics. Plagioclase laths are almost completely altered to a very fine grained felted mass of quartz, chlorite and sericite. Chlorite, sphene and opaques occur interstitially with actinolite grains and feldspar laths, and rare amygdules, up to 0.5 mm diameter, are filled with chlorite and calcite. The grain size of the equigranular basalt is generally 0.1-0.2 mm, though rare larger actinolite grains and feldspar laths up to 0.5 mm impart a subporphyritic texture. Porphyritic basalt (48318) consists of altered feldspar phenocrysts up to 5 mm in length and comprising 10-20% of the rock, in a fine grained groundmass of altered feldspar, actinolite, chlorite and sphene similar to but finer grained than equigranular basalt.

Greywacke

Massive to thinly bedded, micaceous greywacke within the Hall Formation closely resembles that in the overlying Crescent Spur Sandstone. It commonly occurs interbedded with argillite between the sulphide lenses (Figs. 3.12, 4.3) but has not been observed within the lenses. The greywacke (48313, 81-33) is poorly sorted and consists of angular to sub-rounded grains and fragments, generally 0.05-0.2 mm but up to 1 mm in diameter, of quartz, quartzite, schist and siltstone/

mudstone in a matrix of fine grained quartz, chlorite, sericite and clay. Plagioclase occurs as laths, up to 0.1 mm in length, and muscovite and minor biotite occur as flakes up to 2 mm in length. Quartzite and much of the quartz exhibit undulose extinction, indicative of derivation from deformed Precambrian rock.

CRESCENT SPUR SANDSTONE

The Crescent Spur Sandstone conformably overlies the Hall Formation, cropping out on Godkin Ridge and on Crescent Spur, but is terminated to the west by the Whyte River complex (Figs. 3.1, 3.3, 3.4). Similar rocks crop out west of the Whyte River complex and east of the Deep Creek Volcanics in the headwaters of Falls Creek (Figs 3.1, 3.3).

The Crescent Spur Sandstone typically is a turbiditic sequence, at least 350 m thick, and composed predominantly of a monotonous sequence of grey to dark green-grey, fine to medium grained micaceous greywacke and interbedded siltstone and mudstone. Also, within the turbiditic sequence are thick units of red-brown to chocolate-brown argillite, light to dark grey banded chert, and volcaniclastic greywacke, and minor mafic green spilitic basalt (Fig. 3.2). Throughout the formation are semi-concordant to discordant intrusive bodies of basalt, dolerite and gabbro (Fig. 3.3).

Red-brown argillite is similar to the chocolate-brown argillite in the Deep Creek Volcanics, though lacking tuffaceous horizons, and occurs either thinly interbedded with turbiditic greywacke, or as massive to finely laminated units up to 30 m in thickness. Equigranular, fine grained spilitic basalt cropping out on the Corinna Road (CQ67450830), is similar to spilitic basalt elsewhere in the sequence, consisting of interlocking subhedral clinopyroxene grains and altered plagioclase laths in a groundmass of pyroxene, plagioclase, chlorite, sphene and opaques. The basalt (81-45) also contains rare glomerocrysts, up to 5 mm across, of ophitic clinopyroxene and plagioclase.

Grey-dark grey chert occurs interbedded with the turbiditic greywacke as lenticular bedded units up to 10 m in thickness (*e.g.* CQ36750850). Individual chert beds are generally 100-250 mm thick, and commonly exhibit very fine lamination or banding parallel to bedding. Cox (1968a) also describes spherical structures, up to 0.2 mm in diameter, of indeterminate origin, within darker bands, and syn-sedimentary microfaulting and folding of the fine lamellae.

Turbiditic greywacke

Micaceous greywacke occurs typically as a turbiditic sequence consisting of greywacke beds, ranging from 50 mm to in excess of 2 m in thickness, but generally 100-250 mm thick, which are thinly interbedded with laminated argillite and siltstone. Exposures generally are deeply weathered and the greywacke/argillite is cream to light brown to dark brown in colour, but where fresh (*i.e.* drill core) it is light-dark grey to pale brown in colour. In surface outcrops, the thicker greywacke beds typically show spheroidal weathering.

The greywacke beds commonly are graded and indicate a predominantly west to north-west facing sequence. Basal contacts with underlying argillite and siltstone are generally very sharp and rarely exhibit scouring. Water-escape structures such as flame structures of argillite penetrating the greywacke have been observed, and convolution of the underlying laminated argillite is rare. The upper one quarter to one third of greywacke beds are distinctly finer grained than in the lower part, and at this level elongate, subrounded rafts of laminated argillite are common. The shale rafts are up to 100 mm in length and are parallel to bedding. At the top, the greywacke passes relatively abruptly into overlying laminated siltstone and argillite. Most of these sedimentary features have been either observed or confirmed by observation of flat, cut surfaces of complete bedded units.

In thin section (*e.g.* 48314, 48348, 48349, 81-39, 81-40), the greywacke is texturally and compositionally immature. It is poorly sorted and consists of angular to subrounded grains of quartz, quartzite, quartz-muscovite-sericite schist, quartz-chlorite schist, chert and siltstone/argillite, generally 0.1-0.4 mm in diameter but up to 2.5 mm in length (*e.g.* 48314), and muscovite and minor biotite flakes up to 0.05 x 0.5 mm, all in a semi-open framework (Plate 3.3A, B). Plagioclase occurs rarely as laths up to 0.2 mm in length (*e.g.* 81-39). Accessory minerals include sphene, zircon, topaz and tourmaline (Cox, 1968a), and rare detrital garnet (Cox and Glasson, 1967). The quartz grains generally are angular and either exhibit undulose extinction similar to undulose extinction in quartz in the quartzite grains, indicative of a Precambrian provenance, or it contains lines of aqueous inclusions and has straight extinction, indicative of undeformed vein quartz. The schist grains and muscovite also have a probable Precambrian provenance, but the biotite may be either primary detrital flakes or a product of burial metamorphism. Some muscovite flakes show marginal alteration to biotite. The matrix consists of quartz grains (up to 0.01 mm in diameter) and minor chlorite, muscovite/sericite and carbonate, with finely disseminated opaques as anhedral and euhedral grains (cubes, rhombs) up to 0.1 mm in diameter and fine biotite platelets (up to 0.02 mm in diameter). The lithic fragments and quartz grains comprise about 70% of the greywacke, mica flakes 10-15%, and the matrix 10-20%.

Volcaniclastic greywacke/lithic tuff

Volcaniclastic greywacke and lithic tuff crop out on the Corinna Road, north of Godkin Ridge (between CQ67130832 and CQ67430830; Fig. 3.3), as a thick unit (50-100 m) within and at a relatively high level in the Crescent Spur Sandstone. Absence of the volcanogenic rocks at the Cleveland mine and on Crescent Spur is probably due to truncation of that

PLATE 3.3 Photomicrographs of greywacke and volcaniclastic greywacke in Crescent Spur Sandstone, porphyritic basalt/dolerite dyke, and quartz-feldspar porphyry.

A: Micaceous greywacke, Crescent Spur Sandstone (48315). Scale bar = 1 mm, plane pol. light.

B: As above, X nicols, highlighting lithic fragments.

C: Volcaniclastic greywacke, Crescent Spur Sandstone (81-46), showing different texture to turbiditic greywacke in A/B above. Scale bar = 1 mm, plane pol. light.

D: Clinopyroxene crystal (cpx) and shard-like structures in volcaniclastic greywacke, Crescent Spur Sandstone (81-47). Scale bar = 100µm, plane pol. light.

E: Basalt/dolerite dyke (48328), showing igneous texture defined by plagioclase laths, augite microphenocrysts (Ag), quartz glomerocryst (white) and vesicle (black). Scale bar = 1 mm, plane pol. light.

F: Hydrothermally altered basalt/dolerite dyke in ore (48288), showing remanent igneous texture (*cf.* E above) and vesicles, and quartz glomerocrysts (white). Scale bar = 1 mm, plane pol. light.

G: Quartz-feldspar porphyry (48347) showing partially altered feldspar phenocrysts and biotite flakes (dark grey) in fine grained felted groundmass. Scale bar = 1 mm, plane pol. light.

H: As above, showing zoning in plagioclase phenocrysts, X nicols.

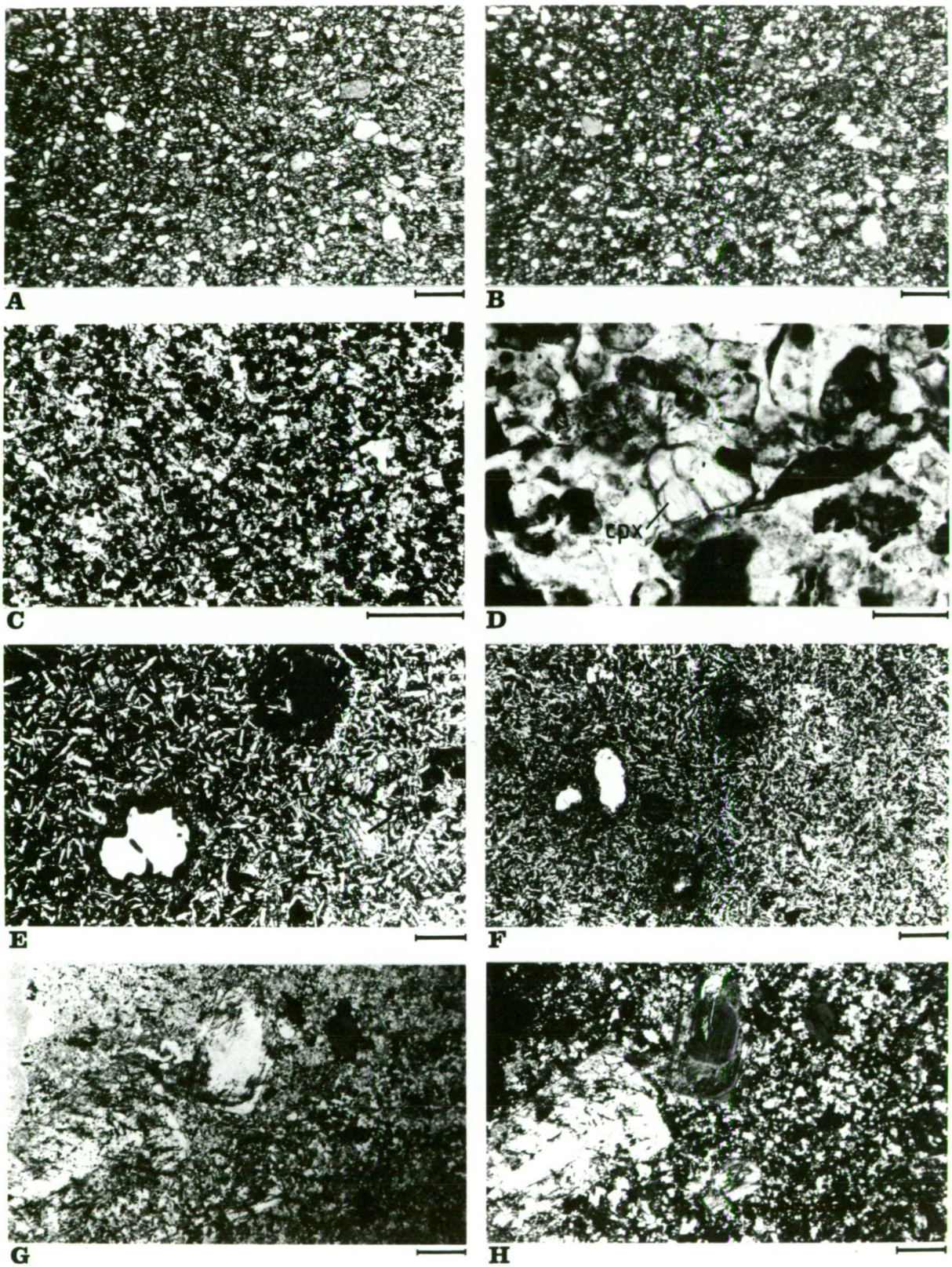

PLATE 3·3

part of the sequence during emplacement of the Whyte River complex.

The mafic green volcaniclastic greywacke and lithic tuff occur as massive beds generally 250 mm to 1 m in thickness, with interbedded red-brown to chocolate brown siliceous argillite (81-47). Water escape structures of argillite penetrating the volcaniclastic greywacke are common, and indicate a west facing sequence. In thin section (81-46, 81-47, 81-50, 81-51), volcaniclastic greywacke consists of angular to sub-angular grains of quartz, pyroxene, feldspar, quartzite, argillite and chlorite in a green chloritic and calcareous matrix which exhibits shard-like outlines under low magnification (Plate 3.3B, C). Lithic fragments and crystal grains are generally 0.1-0.4 mm in diameter, and the proportions of fragments, grains and glass-shard(?) matrix varies considerably. Specimens with a high shard-like component grade into litho-vitric and vitric tuffs (*e.g.* 81-48, 81-49, 81-52, 81-53).

The provenance of the volcaniclastic greywacke and lithic tuff appears to have been two-fold. The high proportion of mafic volcanic detritus is locally derived, possibly from scouring of underlying basalt and unconsolidated tuff, whereas many of the lithic fragments probably have a Precambrian provenance. The volcanogenic rocks occur stratigraphically above a thin unit of spilitic basalt (Fig. 3.3), and thus most likely are related to local instability and uplift associated with a brief period of rejuvenation of mafic volcanism.

GEOCHEMISTRY OF CAMBRIAN BASALT

Twenty-five specimens of spilitic basalt from the Deep Creek Volcanics and six specimens of Henrys Volcanic Member from within the Hall Formation have been analysed for ten major elements and fifteen trace elements (Ag, Ba, Co, Cr, Cu, Nb, Ni, Pb, Rb, Sn, Sr, V, Y, Zn, Zr). Sampling and analytical techniques are described in Appendix 2, and analytical data are listed in Table A2.4 and summarised in Table 3.3. Additional analytical data from Foden (1973) are listed in Table A2.5.

TABLE 3.3. Range and average composition of spilitic basalt in the Cleveland mine area[1]

	Deep Creek Volcanics[2]			Henrys Volcanic Member[3]	
	Range (30)	Range* (6)	Mean* (6)	Range (5)	Mean (1)
Major elements (mass%)					
SiO_2	43.90-50.56	45.35-49.80	47.62	47.37-50.06	48.40
TiO_2	1.57- 3.95	1.57- 3.76	2.27	1.17- 2.65	1.59
Al_2O_3	11.80-15.10	12.64-14.47	13.34	12.84-14.86	13.56
Fe_2O_3	0.60- 6.60	0.60- 4.83	3.10	1.82- 2.68	15.24
FeO	7.50-16.28	9.95-12.70	11.39	10.07-13.48	-
MnO	0.17- 0.92	0.20- 0.38	0.28	0.48- 0.80	0.25
MgO	4.54- 7.50	5.53- 6.99	6.32	5.63- 6.64	5.13
CaO	1.75-11.27	8.22-10.58	9.53	7.87- 9.23	9.17
Na_2O	0.03- 3.93	2.63- 3.92	3.09	0.45- 2.69	3.69
K_2O	0.08- 4.71	0.20- 0.61	0.38	0.45- 2.45	0.84
P_2O_5	0.13- 0.82	0.17- 0.78	0.34	0.14- 0.34	0.20
LOI	1.02- 4.50	1.82- 4.05	2.60	1.87- 3.25	2.34
TOTAL			100.26		100.41
Trace elements (g/t)					
Ba	35-442	35-147	107	120-482	-
Co	41-57	-	-	-	-
Cr	36-133	48-92	63	53-142	70
Cu	14-398	36-301	248	9-308	-
Nb	<5-24	7-21	12	6-15	-
Ni	27-103	28-65	55	58-67	45
Pb	<3-11	<3-7	6	3-14	-
Rb	4-1116	7-48	29	63-609	25
Sr	95-620	141-620	312	99-306	305
Sn	<2-582	<2	<2	73-493	-
V	317-685	317-473	419	312-483	371
Y	3-76	27-76	42	15-47	43
Zr	26-220	85-187	129	63-161	115
Zn	31-445	80-136	111	206-453	-

(1) Compiled from data in Tables A2.4 and A2.5.

(2) Range is for all data (30 analyses). Range* and Mean* are for six unaltered spilitic basalt analyses, 48302, 48305, 48306, 48325, 48326, 48333 only.

(3) Range is for altered spilitic basalt (5 analyses) at the Cleveland mine. Mean is for one analysis of unaltered spilitic basalt (41045, Table A2.5).

Sampling and analysis of spilitic basalt was undertaken to determine the chemical composition and hence the nature and genetic character of the parent magma, and also to ascertain whether there exists a chemical alteration halo to the cassiterite-sulphide mineralisation, which is apparent in basalt petrology. This latter aspect of the chemical composition of the spilitic basalt is discussed in Chapter 5.

Because of the hydrothermal alteration associated with the mineralisation, the analytical data are subdivided into two groups: spilitic basalt which has been hydrothermally altered, and that which has not been hydrothermally altered (Figs. 3.6 to 3.10). Of thirty-one specimens of spilitic basalt analysed, only eight analyses of the Deep Creek Volcanics are considered to be remote from, and not to have undergone hydrothermal alteration. These analyses (48302, 48305, 48306, 48325, 48326, 48333, 781011, 781012; Table A2.4) form the basis for discussion of spilitic basalt geochemistry and all are in excess of 250 m distant from the lenses of cassiterite-sulphide mineralisation. All analyses of Henrys Volcanic Member exhibit characteristics of hydrothermal alteration of the spilitic basalt. Only one of the analyses by Foden (1973) is considered remote from the alteration (41042, Table A2.5), but use of this data is limited by a lack of details of sample locations.

The spilitic basalt is generally uniform in chemical composition, with little variation in most major elements, particularly calcium, iron (FeO), magnesium and manganese (Table 3.3). When altered spilitic basalt is taken into consideration these elements display a much wider, but unsystematic variation. For example, calcium has a range of 8.22-10.58% CaO in spilitic basalt increasing to 1.75-11.27% CaO in altered spilitic basalt, and iron has a range of 9.95-12.70% FeO increasing to 7.5-16.28% FeO (Table 3.3). Henrys Volcanic Member has a wide range in composition,

consistent with the wide variation in altered spilitic basalt in the Deep Creek Volcanics. The silica content has a range of 43.9-50.56% SiO_2, though most analyses are within the range 46-50% SiO_2 (Fig. 3.6), and is well below the maximum of 53% SiO_2 for basalt (Branch, 1968). The spilitic basalts have a variable normative composition, but generally unaltered spilitic basalt is olivine normative and hydrothermally altered spilitic basalt is quartz normative (Table A2.8).

The titanium content is variable and relatively high, with values of 1.57-3.95% TiO_2 in the Deep Creek Volcanics and 1.17-2.65% TiO_2 in Henrys Volcanic Member, but is comparable with Cambrian spilitic basalt in the Crimson Creek Formation elsewhere in western Tasmania (*e.g.* Foden, 1973; Brown and Waldron, 1982). Titanium is, however, much higher than in basalt and related rocks in the Whyte River complex, which have 0.07-0.41% TiO_2 (Table A2.7), and in low-titania basalt in the Heazlewood River Complex (Rubenach, 1973; Brown *et al*, 1980; Creenaune, 1980). This indicates that spilitic basalt in the Arthur River sequence (*i.e.* Deep Creek Volcanics and Henrys Volcanic Member) petrogenetically is not associated with the tectonically emplaced mafic-ultramafic complexes (Creenaune, 1980; Brown and Waldron, 1982).

The only major elements to show any significant variation are sodium and potassium which have a systematic inverse relationship spatially associated with the sulphide lenses (see Chapter 5). Despite this variation, the total alkali content ($Na_2O + K_2O$) of all spilitic basalt is relatively consistent (Table 3.3; Fig. 3.6).

Most trace elements exhibit little variation in the spilitic basalt, but the variation is broadened when altered spilitic basalt is taken into consideration. Elements which vary least are the 'immobile' elements Cr, Nb, Ni, V, Y and Zr, and Pb, Co and Ag (all less than 3 g/t

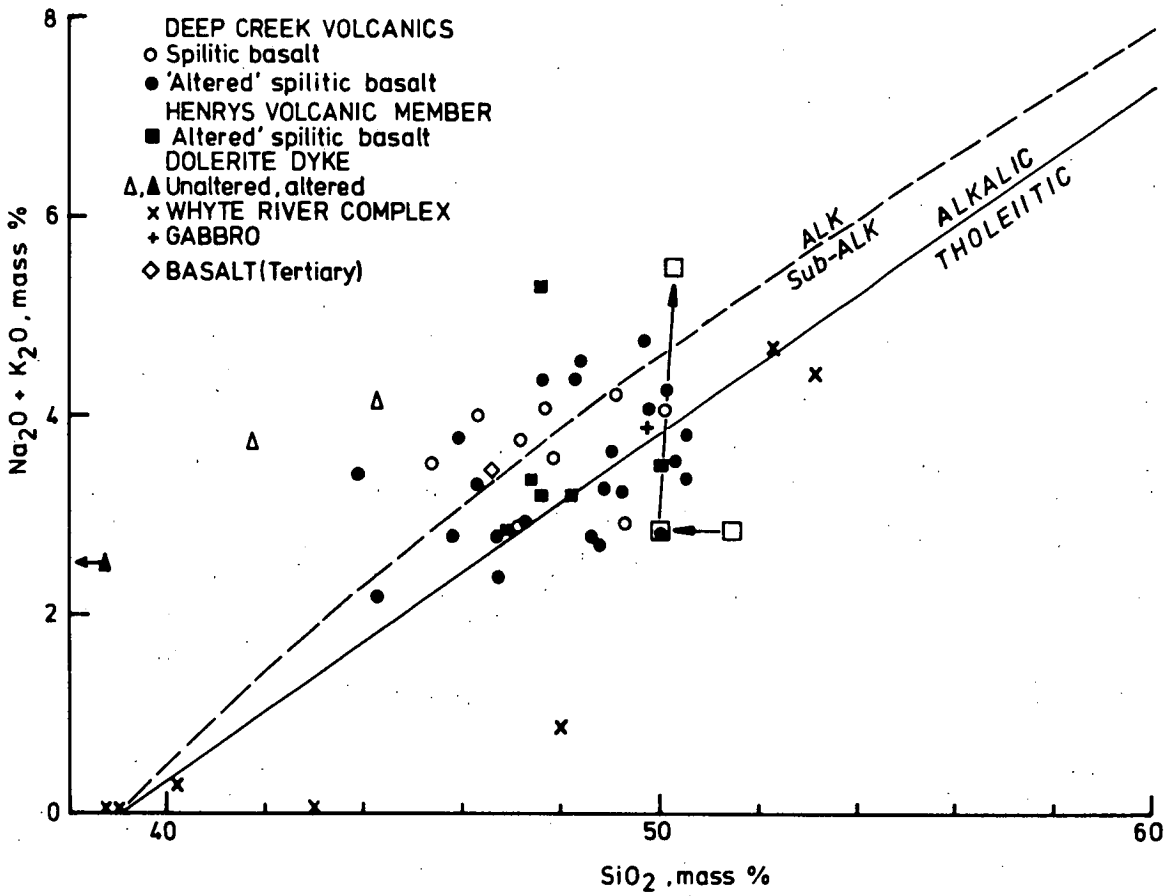

FIG. 3.6 $Na_2O + K_2O$ versus SiO_2 diagram for basalts, dolerite, gabbro and mafic-ultramafic rock in the Cleveland mine area. Alkalic-tholeiitic line is from MacDonald and Katsura (1964) and the dashed line is the alkaline-sub-alkaline discriminator of Irvine and Barager (1971). Open squares connected by arrows show the direction of spilitic degredation of basalt (from Coleman, 1977).

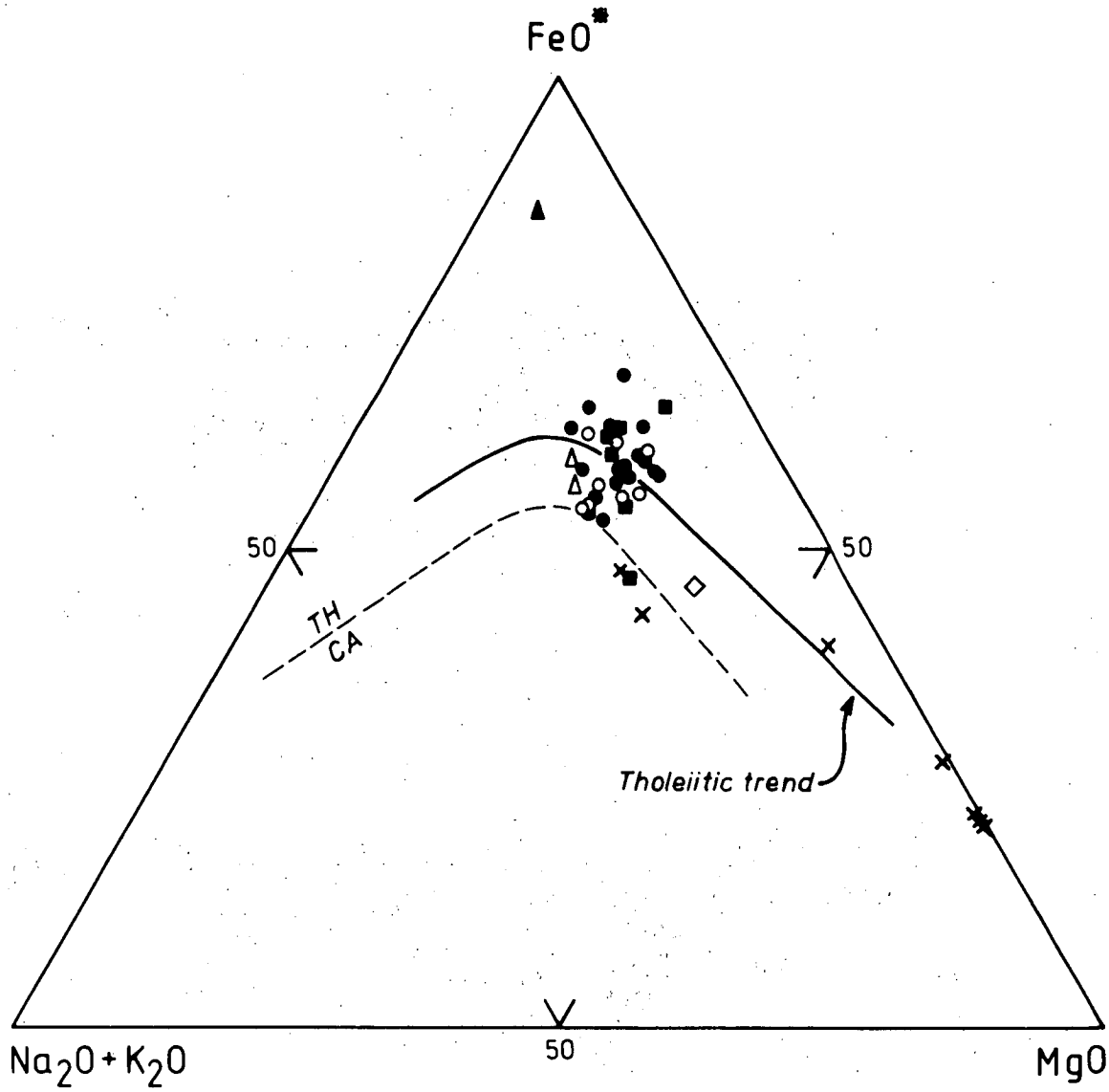

FIG. 3.7 AFM diagram for basalts, dolerite, gabbro and mafic-ultramafic rock in the Cleveland mine area. Symbols as in Figure 3.6, FeO* = total Fe as FeO. The solid line is the tholeiitic trend based on Thingmulli, and the dashed line is a tholeiitic (TH)-calc-alkaline (CA) discriminator, from Irvine and Barager (1971).

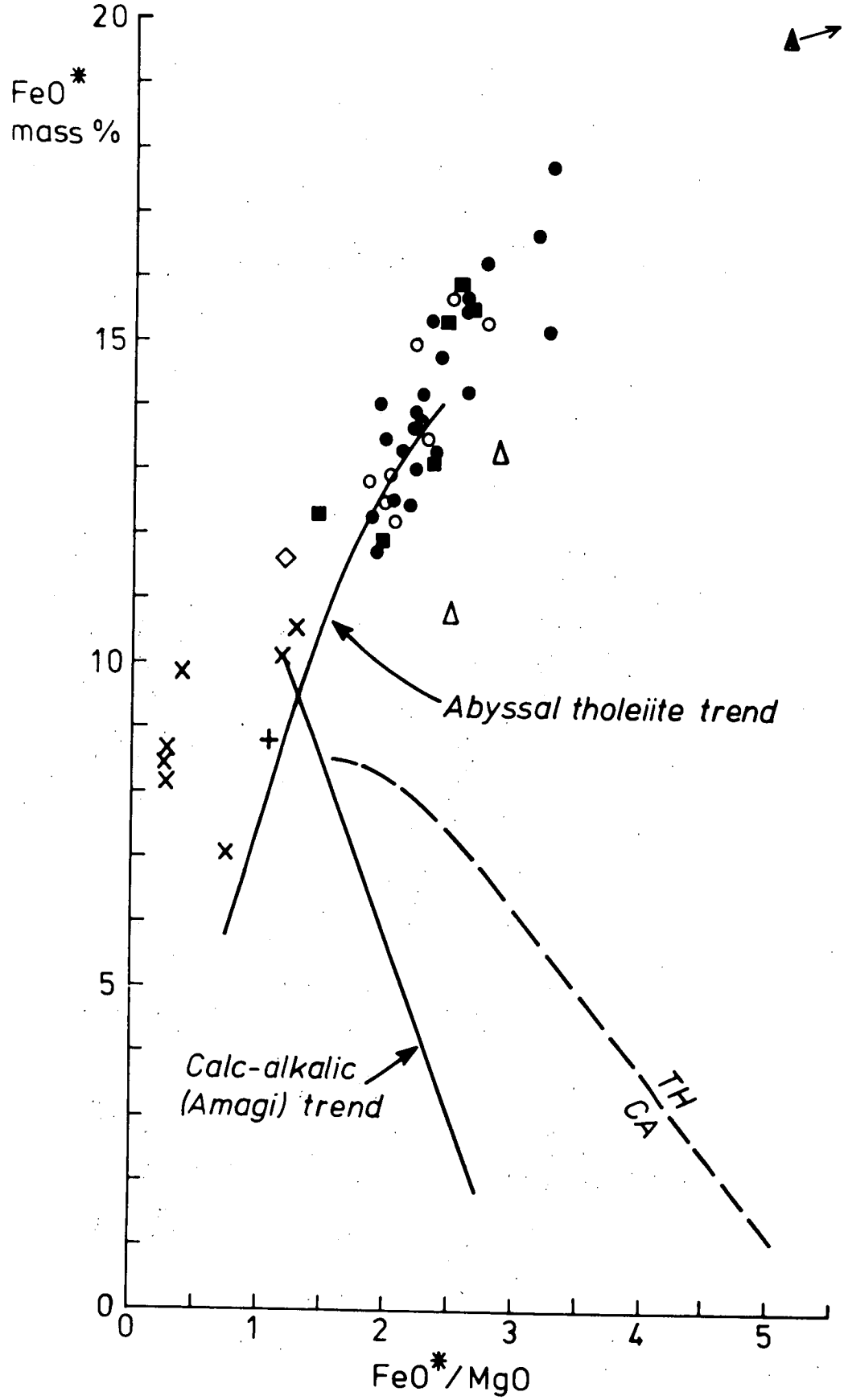

FIG. 3.8 FeO* versus FeO*/MgO diagram for basalts, dolerite, gabbro and mafic-ultramafic rock in the Cleveland mine area. Symbols as in Figure 3.6, FeO* = total Fe as FeO. Dashed line is the distinction between tholeiitic (TH) and calc-alkalic (CA) series (Miyashiro, 1975). Abyssal tholeiite (mid-oceanic ridge) and calc-alkalic (exemplified by the Amagi Volcano) trends after Miyashiro (1975).

where determined) (Table 3.3). Some trace elements such as Ba, Cu, and Sr exhibit a broad but unsystematic variation, which for Sr and Ba(?) is most likely due to interaction of hot basalt with sea water (*i.e.* spilitisation, Cann 1969). Rb, Sn and Zn have limited compositional ranges in spilitic basalt (Table 3.3) but exhibit a systematic spatial variation in hydrothermally altered spilitic basalt, relative to the sulphide lenses (See Chapter 5). The tin content of spilitic basalt is less than 2 g/t, which is consistent with the very low values of tin generally in mafic volcanic rocks (Hamaguchi & Kuroda, 1969).

The tholeiitic character of the spilitic basalt is confirmed by the iron enrichment, and plotting on the tholeiitic trend line in an AFM diagram, $(Na_2O + K_2O)$ - FeO* (=FeO + Fe_2O_3 x 0.8998) - MgO (Fig. 3.7). Although there is considerable variation in Na_2O and K_2O, all analyses of spilitic basalt plot as a small group in the AFM diagram (Fig. 3.7). This is due to the inverse relationship of Na_2O/K_2O variation in altered spilitic basalt which maintains the total alkali content at a relatively constant level (*i.e.* 2.5-4.5% $Na_2O + K_2O$, Fig. 3.6). A plot of FeO* versus FeO*/MgO also demonstrates the tholeiitic nature of the spilitic basalt with most analyses plotting at the iron enriched end of the abyssal tholeiite trend (Fig. 3.8). However, in an $Na_2O + K_2O$ versus SiO_2 diagram most analyses plot in the alkali basalt field (Fig. 3.6). This is accounted for by the mobility of Na and Si during spilitic degradation which can effectively modify the original composition of tholeiitic basalt so that the altered rock assumes the composition of an alkali basalt (Fig. 3.6; Vallance, 1974).

A number of workers (*e.g.* Cann, 1970; Pearce and Cann, 1971, 1973) have suggested that some trace elements such as Ti, Zr, Y, Ni, Cr, V, Nb are immobile during spilitic alteration and greenschist facies meta-

morphism, and that they may be used as genetic discriminants for distinguishing the parentage of mafic volcanics from different tectonic settings. Foden (1973) suggested that spilitic basalt from the Cleveland area exhibits a close geochemical affinity to ocean-floor basalt. The additional analytical data available from this investigation confirm the oceanic basalt affinity, but the use of petro-genetic discrimination diagrams is not entirely satisfactory for interpretation of the tectonic setting of extrusion of high-Ti spilitic basalt in the Cleveland area.

In Pearce and Cann's (1973) Ti versus Zr diagram, most analyses plot outside the fields for ocean-floor basalt, calc-alkaline basalt and low potassium tholeiite due to their high titanium content (Fig. 3.9). Some analyses plot in the ocean-floor basalt field, but none plot in the other two fields. The analyses display a positive linear trend and are concentrated into three distinct groups corresponding approximately to 1, 1.5 and 2% Ti and 100, 150 and 200 g/t Zr, respectively. The reason for this is not known, but it is unrelated to stratigraphic position in the volcanic pile and hydrothermal alteration. Similar linear or curvilinear relationships have been noted in other less titanium-enriched basalt suites where they are considered to be of primary magmatic origin (*e.g.* Abbotts, 1981). The same three groupings occur in a Ti versus Y diagram, but there is less definition of the linear trend due to increasing variation in Y with increasing Ti (Fig. 3.9).

In ternary discrimination diagrams, plots of analyses are similarly inconclusive, though there is a tendency towards ocean-floor basalt affinity. In a K_2O-TiO_2-P_2O_5 diagram (Fig. 3.10B), spilitic basalt plots within the field of ocean floor basalt, but hydrothermally altered spilitic basalt exhibits a distinct linear trend out of the ocean-floor basalt field towards the K_2O apex, reflecting an increase in K_2O nearer to the sulphide lenses. A screening requirement for use of this diagram is that analyses plot below the 20% iso-alkaline line in an AFM diagram,

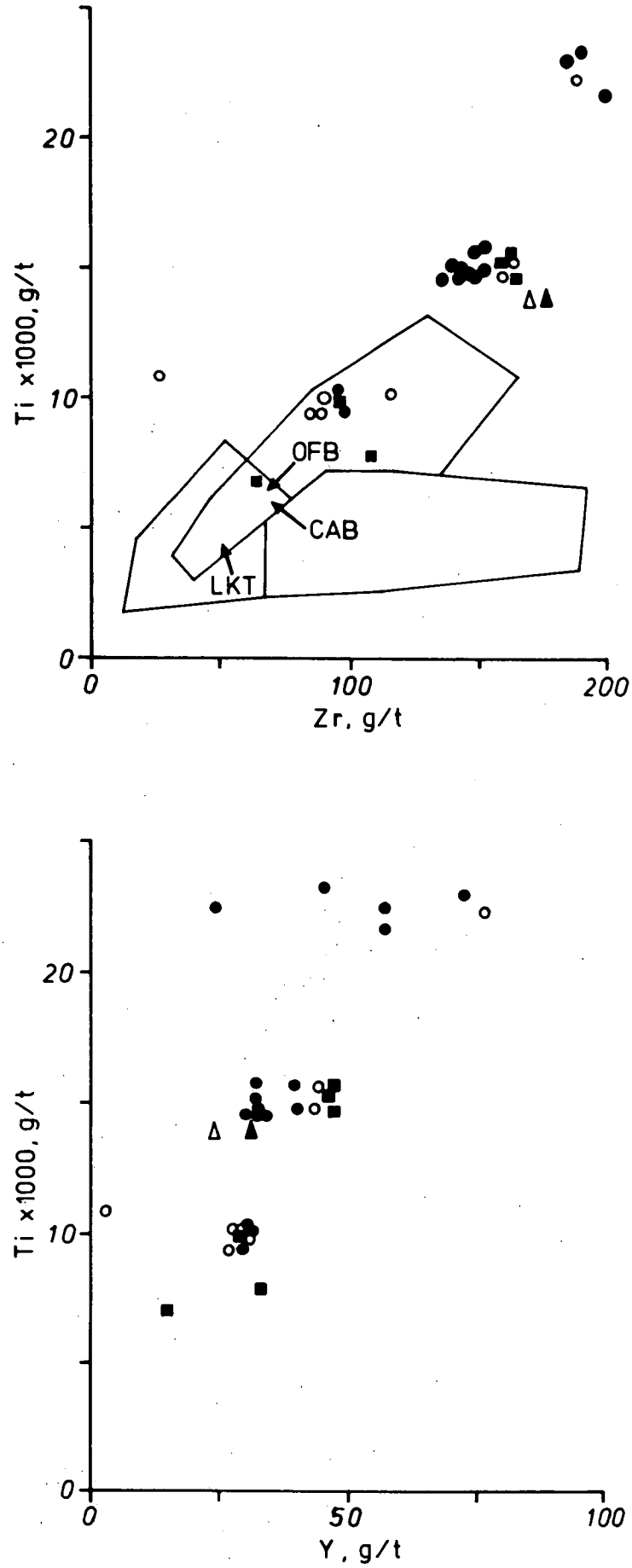

FIG. 3.9 Ti vs Zr discrimination diagram (after Pearce and Cann, 1973) and Ti vs Y diagram for Cambrian spilitic basalt and basalt/dolerite dyke, Cleveland mine area. Symbols as in Figure 3.6, and petrogenetic fields as in Figure 3.10.

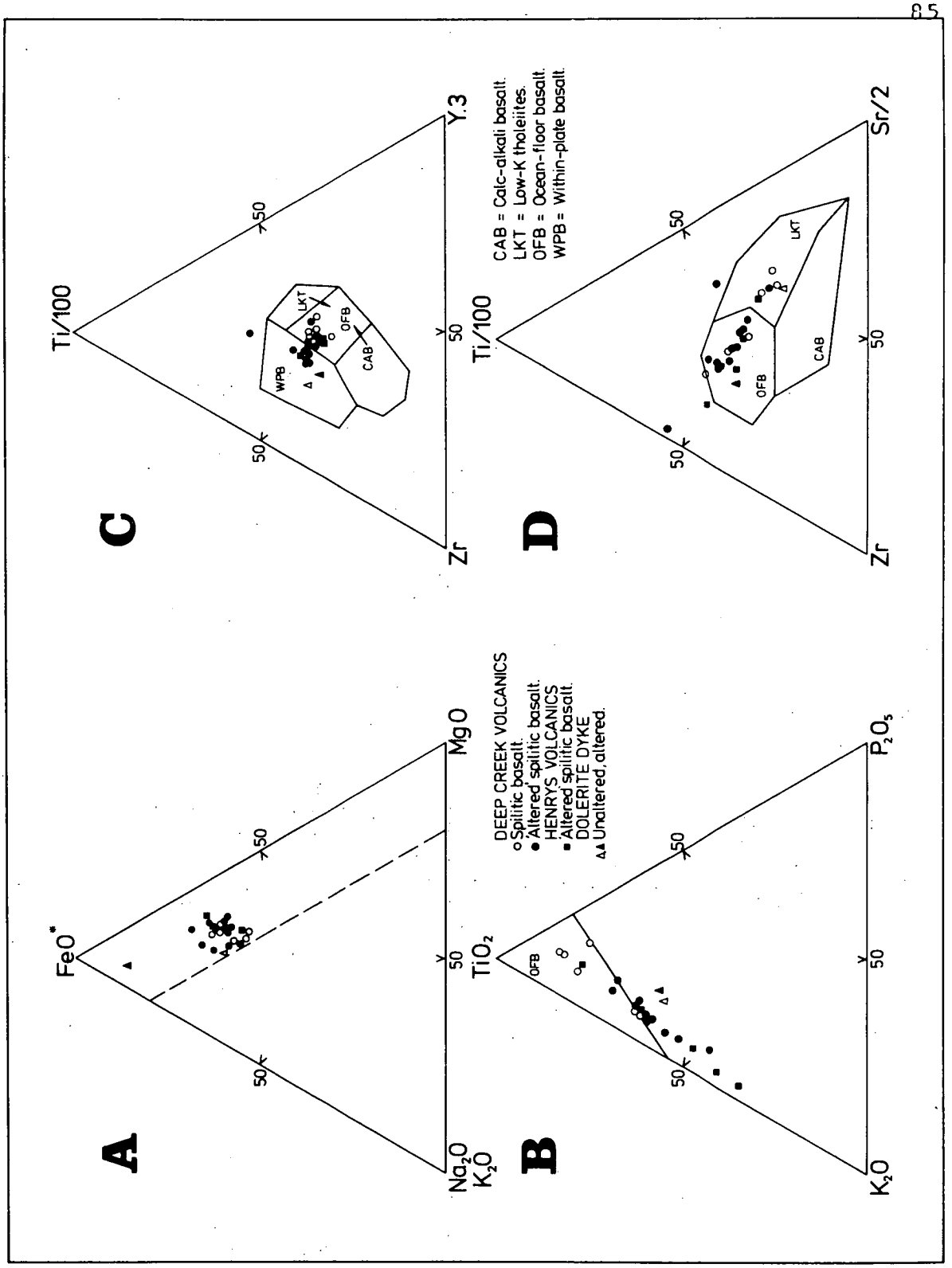

FIG. 3.10 Spilitic basalt and basalt/dolerite dyke at the Cleveland mine plotted on ternary, petrogenetic discrimination diagrams. Spilitic basalt data are for samples from mine section Qa only.
A: AFM diagram (FeO* = total Fe as FeO). Dashed line is the 20% isoalkaline line, a screening limit for Figure 3.10B.
B: K_2O-TiO_2-P_2O_5 diagram of Pearce *et al.*(1975).
C: Zr-Ti/100-Y.3 diagram of Pearce and Cann (1973).
D: Zr-Ti/100-Sr/2 diagram of Pearce and Cann (1973).

a condition satisfied by the Cleveland data (Fig. 3.10A).

In the Zr-Ti/100-Y.3 diagram of Pearce and Cann (1973), analyses straddle the ocean-floor basalt and within-plate basalt fields (Fig. 3.10C), though most spilitic basalt plot in the OFB field. In their Zr-Ti/100-Sr/2 diagram (Fig. 3.10D) most analyses plot along a median linear zone passing through the Sr/2 apex. There is no systematic variation attributable to a hydrothermal alteration process which could account for this trend and it is concluded that this enrichment and depletion in Sr is due to pre-mineralisation alteration of the basalt and probably that associated with spilitisation of the basalt. Numerous other petrogenetic discrimination diagrams have been devised, and all indicate a tendency toward ocean-floor basalt, similar to that derived from the diagrams in Figures 3.9 and 3.10.

In summary, spilitic basalt in the Cleveland area is relatively uniform in chemical composition, the only significant variation being in basalt subject to hydrothermal alteration associated with the mineralisation episode. The high-titania basalt is tholeiitic in character and exhibits a geochemical affinity to ocean-floor basalt.

GEOLOGICAL ENVIRONMENT OF ACCUMULATION OF THE CAMBRIAN SEQUENCE

Interpretations of the origin of the meridional, Eocambrian-Cambrian Dundas Trough in terms of plate tectonics and subduction as either a collision zone (*e.g.* Solomon and Griffiths, 1974; Corbett *et al.*, 1972; Crook, 1980), or as a back-arc basin or marginal sea (*e.g.* Corbett *et al.*, 1972; Solomon, 1977) have relied heavily on the similarity of the Mt Read volcanism to Andean-type continental margin volcanicity, and interpretation of the ophiolitic ultramafic complexes as ancient oceanic crust.

Arguments in favour of a collisional event may be countered by evidence for an initial origin by rifting, such as matching of Precambrian basement on either side of (and within) the trough, and the apparent absence of complex folding and high pressure metamorphism commonly associated with subduction and continental collision (Williams, 1978, 1979). Brown *et al.* (1980) have interpreted the ophiolitic and mafic-ultramafic complexes as oceanic crust formed in ruptures in an aborted continental rift setting, though this seems incompatible with the continental margin-style Mt Read volcanism.

The high-titania, spilitic, tholeiitic basalts in the Deep Creek Volcanics and Henrys Volcanic Member, although showing some geochemical resemblance to ocean-floor basalt, are compositionally unlike and petrogenetically not associated with the low-titania mafic volcanics in the ophiolitic, mafic-ultramafic complexes. They are geochemically similar to Cambrian high-titania, tholeiitic basalt elsewhere in the Dundas Trough, which Brown *et al.* (1980) have assigned to an aborted continental rift environment, with eruption through thinned Precambrian basement into shallow water being partly contemporaneous with the low-titania ophiolitic complexes. Pillow lavas within the Deep Creek Volcanics and Henrys Volcanic Member are consistent with eruption into an aqueous environment (Solomon, 1969; Moore, 1975), as too is an enrichment in the whole-rock ^{18}O content of the spilitic basalt (Chapter 7). The occurrence of laminated argillite and thinly bedded tuffs intercalated with the basalt also indicate an aqueous environment, but the relatively high proportions of glass shard material and lapilli tuffs are inconsistent with an

ocean-floor environment as sediments interlayered with ocean-floor basalt are almost invariably pelagic, and rarely contain tuffaceous and explosive material (Berger, 1974; Coleman, 1977). The overlying turbiditic sequence (Crescent Spur Sandstone) is dominated by terrigenous material derived from Precambrian basement rocks, with minor admixed, locally-derived volcaniclastic material. Similar sediments elsewhere in the Dundas Trough are considered to have been deposited in a subsiding shelf environment (Brown and Waldron, 1982). The Hall Formation may thus form a transitional sequence between an initial phase of basaltic volcanism in a subaqueous, shallow marine environment (Deep Creek Volcanics) and later subsidence and deeper marine sedimentation (Crescent Spur Sandstone).

Further evidence of a shallow marine environment may be derived from the oxygen isotopic composition of calcite in limestone in the Hall Formation (Chapter 7). The calcite has $\delta^{18}O$ values at the lower end and beyond the range of Eocambrian-Cambrian marine limestone (*cf.* Keith and Weber, 1964; Veizer and Hoefs, 1976). Although alternative origins are possible, the isotopically light calcite is best explained by precipitation from water depleted in ^{18}O due to influx of isotopically light oxygen from continental sources (Keith and Weber, 1964) into an enclosed(?) shallow marine or near-shore aqueous environment.

In conclusion, the results of this investigation are consistent with previous interpretations of crustal extension or rifting for initial development of the Dundas Trough, though not necessarily 'continental rifting', with deposition of mafic volcanic and sedimentary rocks of the Arthur River sequence in an enclosed(?), subsiding, shallow marine environment.

CAMBRIAN IGNEOUS ROCKS

Intruding the Cambrian volcano-sedimentary sequence are several basalt-dolerite dykes and semi-concordant sills, 0.2-20 m in thickness, and much larger gabbroic masses of undefined shape (*e.g.* in the Arthur River, Fig. 3.1, at CQ705073 and CQ712072).

The basalt-dolerite intrusive bodies are well exposed, though deeply weathered, in cuttings on the Corinna Road west of Whyte Hill (Fig. 3.3), where they have a similar mineralogy to the spilitic basalt lava, but are coarser grained. Thin sections of less weathered remanent cores (81-54 to 81-59) indicate a medium grained igneous rock composed of anhedral-subhedral pyroxene crystals up to 2 mm across and altered plagioclase laths up to 4 mm in length, in an ophitic-subophitic texture, with interstitial chlorite, sphene and opaques.

The larger dolerite-gabbro masses crop out as boulders of green, medium-grained, equigranular igneous rock with a thin, yellow-brown weathered crust. Sulphides (pyrite and chalcopyrite) occur as fine disseminated grains and in small (<5 mm) cavities. In thin section (78-415), the dolerite-gabbro is a medium-grained, equigranular rock composed of anhedral-subhedral clinopyroxene (augite) and minor orthopyroxene crystals, generally 1-2 mm in diameter and partially altered to actinolite, and altered plagioclase laths up to 2 mm in length. Twinning in plagioclase enclosed within pyroxene grains indicates an albite-oligoclase composition. The pyroxene and plagioclase exhibit an ophitic texture, with an interstitial groundmass consisting of a felted mass of fine-grained chlorite, sericite, altered feldspar and opaques (mainly sulphides). An analysis of dolerite-gabbro cropping out in the Arthur River (780999, Table A2.10) indicates a similar composition to Cambrian gabbro elsewhere in western Tasmania (Table 3.4), but the low titanium content (0.43% TiO_2) is more like the low-titania rocks in the tectonically emplaced mafic-ultramafic complexes (*i.e.* Whyte River complex) than the

basaltic volcanics and basalt-dolerite intrusives of the Arthur River sequence (Table 3.4). Thus the dolerite-gabbro masses are probably genetically associated with the mafic-ultramafic complexes and are not associated with the basaltic volcanism of the Deep Creek Volcanics.

Porphyritic basalt-dolerite dyke

At the southern end of the Cleveland mine there is a porphyritic basalt-dolerite dyke, 0.2-1 m in thickness, striking 120°-130° and dipping 90°-85°S. The dyke intrudes the three stratigraphic units (Fig. 3.2) and crops out at the surface and in underground workings, and in drill core intersections.

The dyke (76-671, 76-673, 48-328) consists of glomerocrysts, up to 2 mm across, of subhedral-euhedral augite crystals up to 1 mm in length, in a fine grained, felted groundmass of plagioclase (andesine-labradorite), augite, calcite, chlorite, opaques and minor biotite. Augite is partially altered to actinolite and chlorite. The dyke characteristically contains irregular glomerocrysts, up to 5 mm across, of clear to smoky quartz, and minor vesicles up to 1.5 mm in diameter, filled with carbonate, clay and chlorite (Plate 3.3E). The quartz glomerocrysts are rimmed by fine grained sericite and augite, and the subhedral quartz crystals making up the glomerocrysts contain planes of minute, two-phase aqueous inclusions that terminate at grain boundaries, which indicates that the quartz glomerocrysts are probably allogenic to the dyke.

On mine levels 14 and 17, in drives at the south end of the mine, the dyke has been completed altered to a siderite-quartz-clay rock where it intersected limestone beds (sulphide lenses). Cross-jointing and banding parallel to the contacts are preserved in the altered dyke (Plate 3.4A, B), which on 14 level is one metre thick and also contains the characteristic quartz glomerocrysts. In thin section (48288), the dyke exhibits an igneous texture in plane polarised light (Plate 3.3F) similar to its unaltered equivalent, and is composed of siderite, clay and quartz with

TABLE 3.4 Average major element compositions of Cambrian gabbro, dolerite and basalt, Cleveland area.

	1	2	3	4	5
SiO_2	49.7	48.37	52.17	47.62	43.00
TiO_2	0.43	1.03	0.31	2.27	2.27
Al_2O_3	15.3	17.96	13.53	13.34	13.49
Fe_2O_3	2.2	4.52	10.72*	3.10	1.14
FeO	6.8	7.21	-	11.39	10.95
MnO	0.20	0.17	0.20	0.28	0.21
MgO	8.0	5.72	7.72	6.32	4.49
CaO	10.5	8.16	9.92	9.53	10.29
Na_2O	3.3	3.06	3.17	3.09	2.62
K_2O	0.45	0.84	0.23	0.38	1.29
P_2O_5	0.21	0.22	0.04	0.34	0.55
L.O.I.	2.5	2.84	3.09	2.60	8.89
	99.59	100.10	101.12	100.26	99.19

1. Gabbro, Arthur River (780999, Table A2.10)

2. Cambrian gabbro (average of 5 analyses from Solomon, 1964 and Collins, 1972)

3. Basalt/dolerite, Whyte River complex (average of 4 analyses, Table A2.7)

4. Spilitic basalt, Deep Creek Volcanics (average of 6 analyses, Table A2.6)

5. Porphyritic basalt/dolerite dyke (average of 2 analyses, Table A2.6)

* Total iron as Fe_2O_3

PLATE 3.4 Altered basalt/dolerite dyke and folds preserved in ore, Cleveland mine.

A: Altered basalt/dolerite dyke (d) intersecting B South lens, east wall, 14 level south exploration drive (dyke at 10678 m E, 15219 m N), showing cooling cross-joints. Scale bar = 250 mm.

B: Split in altered basalt/dolerite dyke (d) intersecting B South lens, west wall, 14 level south exploration drive (dyke at 10672 m E, 15222 m N). Arrows indicate banding in ore.

C: Tectonic(?) fold with near-vertical axial surface preserved in ore, Khaki lens, 8 level. Scale bar = 250 mm.

D: Sedimentary(?) fold preserved in ore, Halls Blens north, 14 level (see also Plate 4.1). Scale bar = 250 mm.

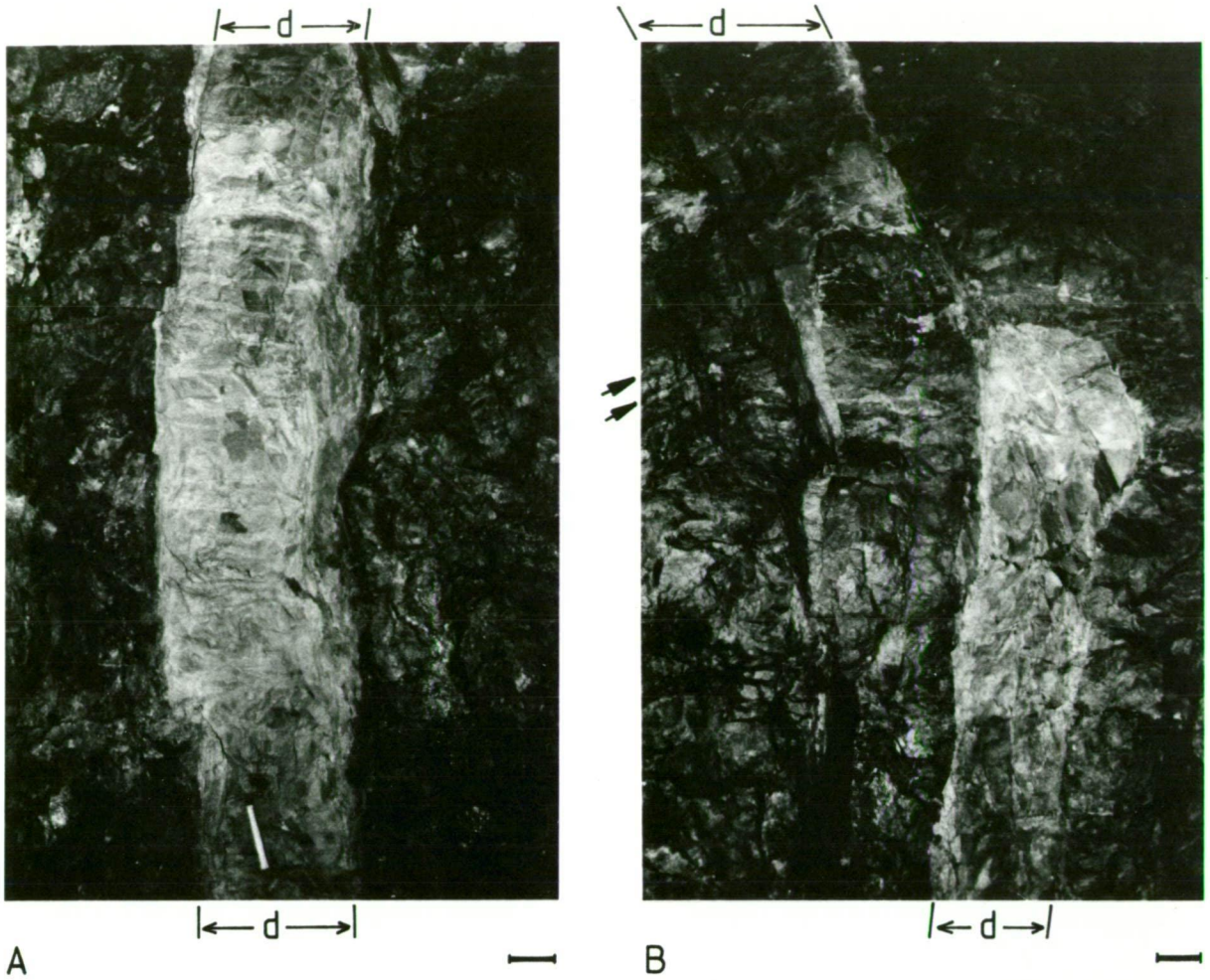

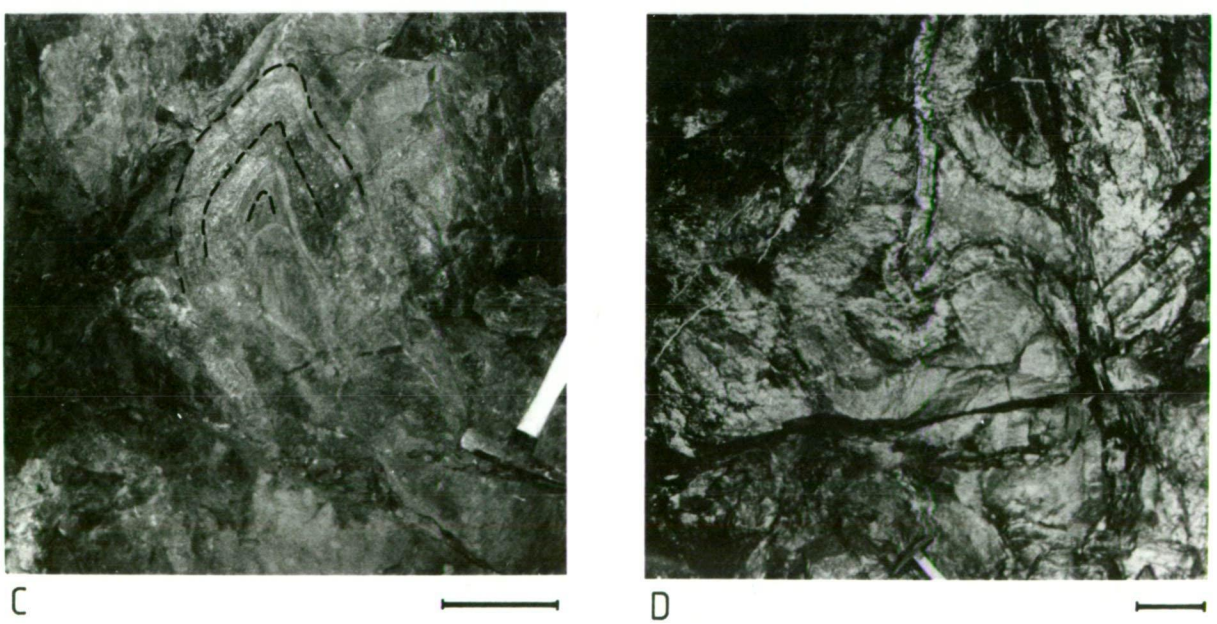

PLATE 3.4

poorly preserved plagioclase laths and minor biotite. Diamond drill core intersections (*e.g.* D.D.H. C274 933'9"-963'11") indicate that the alteration extends for only a short distance along the strike of the dyke from where it intersects the sulphide lenses, and thus is a result of hydrothermal alteration associated with the mineralisation.

In surface outcrop (CQ64800665), the 230 mm thick dyke is decomposed to clay, in which occur irregular quartz glomerocrysts up to 5 mm across. A similar decomposed dyke with quartz glomerocrysts crops out east of Deep Creek (CQ65180633), where it intrudes argillite and chert in the fault-emplaced block of the Hall Formation (Fig. 3.3).

The dyke is chemically similar to spilitic basalt of the Deep Creek Volcanics (Tables 3.4, A2.6), particularly its TiO_2 content. The altered dyke on 14 level (48288) has many element concentrations, particularly the 'immobile' elements (*e.g.* TiO_2, Nb, Ni, V, Y, Zr), similar to the unaltered dyke and to the spilitic basalt (Table A2.6). High FeO in the altered dyke is due to siderite. Despite the intense alteration, the tin content of the altered dyke has not changed.

The presence of vesicles in the dyke indicates near-surface intrusion, and its mineralogical and chemical similarity to spilitic basalt of the Deep Creek Volcanics, indicate that it is genetically associated with, though a late phase of the mafic volcanism.

ORDOVICIAN-EARLY DEVONIAN

West of the Cleveland mine, between the Godkin mines and Mt Stewart (Fig. 4.1) is a NW-SE trending synclinal structure of Ordovician to Early Devonian sedimentary rock. The sequence consists predominantly of white, thickly bedded, medium-grained, saccharoidal quartz sandstone, with medium grained quartzite, siltstone, mudstone and rare conglomerate, and stylolitic limestone (Groves, 1966, 1968). The siliceous sediments are correlated with the Eldon Group (Silurian-Early Devonian), but the limestone contains fossils of Ordovician age and may be correlated with the

Gordon Limestone (Groves *et al*, 1972). The limestone is apparently discontinuous around the base of the Eldon Group, though this may be the result of intersecting faults (Groves, 1966, 1968). The sequence unconformably overlies Cambrian volcanic and sedimentary rocks and the Heazlewood River Complex to the west and is faulted against similar rocks to the east (Groves, 1968, Rubenach, 1973).

STRUCTURE OF THE CAMBRIAN SEQUENCE

Regional geologic structure

Cox (1968a) and Cox and Glasson (1967, 1971) considered that the Cleveland mine is situated on the overturned south-east limb of a south-west plunging anticline, with dips showing considerable variation from north-west (overturned) to steep south-east. However, mapping during this investigation, including numerous determinations of sedimentary facings, and subsequent structural analysis has shown that the deposit is located on the north-west limb of a NE-SW trending anticline.

Bedding in the Cambrian sequence hosting the Cleveland deposit has a regional north-northeast to north-east trend, dipping generally 40°-80° W-NW. Tectonically emplaced mafic-ultramafic bodies (*e.g.* Whyte River complex) parallel this regional trend (Fig. 3.1). A stereographic plot of poles to bedding (all measurements) reveals that there is a dominant trend which strikes 035° and dips 60°-70° NW (Fig. 3.11A). There are also two subsidiary trends, both near-vertical, and striking 045° and 075° (Fig. 3.11A). The 075° trend is contributed mainly by an easterly swing in bedding strike close to, and north of the major interpreted fault along the transmission line in Deep Creek (Fig. 3.3), and may be related to dextral movement on this fault. The near-vertical, 045° trend is contributed mainly by steeper bedding at the Cleveland mine (cf. Figs. 3.11A and B).

Facings in greywacke beds (*e.g.* graded bedding, flame structures)

indicate a dominant west to north-west facing sequence (*e.g.* Corinna Road west of Whyte Hill, Fig. 3.3). Rare south-east facings (*e.g.* at CQ67750818, Fig. 3.3) are probably due to minor folding of the sequence.

Thus the Cleveland deposit is situated on the probable north-west limb of a major NE-SW trending anticline, with an axial surface to the south-east of Cleveland. This interpretation is consistent with a previously postulated north-east trending anticlinal zone located to the south-east of Cleveland and passing through Mt Bischoff (*e.g.* Solomon, 1965).

Despite a relative paucity of fold closures in the Cambrian sequence, two contrasting sets of minor folds (half wave lengths less than 10 m) have been recognised. The dominant set has steep, north-east trending axial surfaces, sub-paralleling the regional bedding trend, and dipping generally steeper than 70° NW or SE (Fig. 3.11C). The second set has north-west trending axial surfaces which dip 70°-75° NE (Fig. 3.11C). The dominant north-east trending folds have relatively flat fold axes, generally plunging less than 35° NE or SW, whereas the north-west trending folds have steeper plunges, generally in excess of 50° SE or NW (Fig. 3.11D).

Folding of the Cambrian sequence resulted from either late Cambrian deformation or Middle Devonian deformation associated with the Tabberabberan Orogeny. In contrast to the dominant north-east trending folds in the Cambrian succession, the Eldon Group (Silurian-Early Devonian) sedimentary rocks to the west of Luina, and unconformably overlying Cambrian rock, form an open north-west trending syncline (Figs. 2.1, 4.1) which is almost certainly of Tabberabberan age. The minor north-west trending folds in the Cambrian succession are probably a reflection of this structure. Thus two phases of deformation of the Cambrian sequence can be distinguished. An earlier phase (f1) is a regional folding about near-horizontal north-east to north-northeast trending axes, while a second

phase (f2) produced north-west trending folds with steeper axes. The first phase (f1) resulted in the major north-northeast trending anticlinal structure with small-scale, north-east trending parasitic folds on its north-western limb. The second phase (f2) produced smaller, superimposed north-west trending folds in the Cambrian succession and the open north-west trending synclinal structure in the Eldon Group sequence at Heazlewood. The age of the earlier phase (f1) has not been resolved. It may represent a period of Cambrian deformation, or alternatively, all of the deformation may have taken place during the Tabberabberan Orogeny. The second alternative is preferred as the style of folding in the Cleveland area is similar to inferred Devonian deformation of Precambrian-Cambrian rock at nearby Mt Bischoff (Groves, 1968; Williams, 1982). Whatever the cause, the bulk of the deformation of the Cambrian succession is certainly of Tabberabberan age or older, because the Meredith Granite margin cuts across the Tabberabberan structures, and there has been no major post-Tabberabberan deformation in western Tasmania.

The Cambrian succession has been dislocated by several major, interpreted north-west trending faults, and the Cleveland deposit is located between two such faults (Figs. 3.1, 3.3). These faults also apparently truncate and dislocate the north-east trending faulted margins of mafic-ultramafic complexes (Figs. 3.1, 3.3). The major easterly trending fault dislocation of the Deep Creek Volcanics along the HEC transmission line in Deep Creek (Fig. 3.3) may be a series of parallel, north-west trending faults, rather than a single fault as shown.

A stereographic plot (Fig. 3.11E) of poles to fault surfaces indicate that although there is no obvious preferred orientation, contouring suggests that there are two main sets. One set trends north-east and parallels the dominant regional bedding and fold trends, and the other has a north-northwest trend, sub-parallel to the minor fold trend.

FIG. 3.11 Structural elements of Cambrian sequences in the Cleveland mine area (equal area stereographic projections, lower hemisphere).

A: Bedding orientation (all surface measurements, total area in Figure 3.3). Contours of poles to bedding at 1, 2, 3, 4, and 5% per 1% area.

B: Bedding orientation, Cleveland mine sub-area (surface measurements). Contours of poles to bedding at 2, 4, 6, 8 and 10% per 1% area.

C: Poles to axial surfaces of folds (total area).

D: Plunge of fold axes (total area).

E: Orientation of surface faults (total area). Poles to fault surfaces, and contours at 3 and 5% per 1% area. Dashed lines are fields of poles to EN and Ratchet faults.

F: Sub-surface bedding and fault orientation (poles plotted), Cleveland mine, underground levels 2 - 11, mine section N (see Fig. 3.12). Open circles are plots of major faults: EN = EN fault, R = Ratchet fault, enclosed by dashed lines.

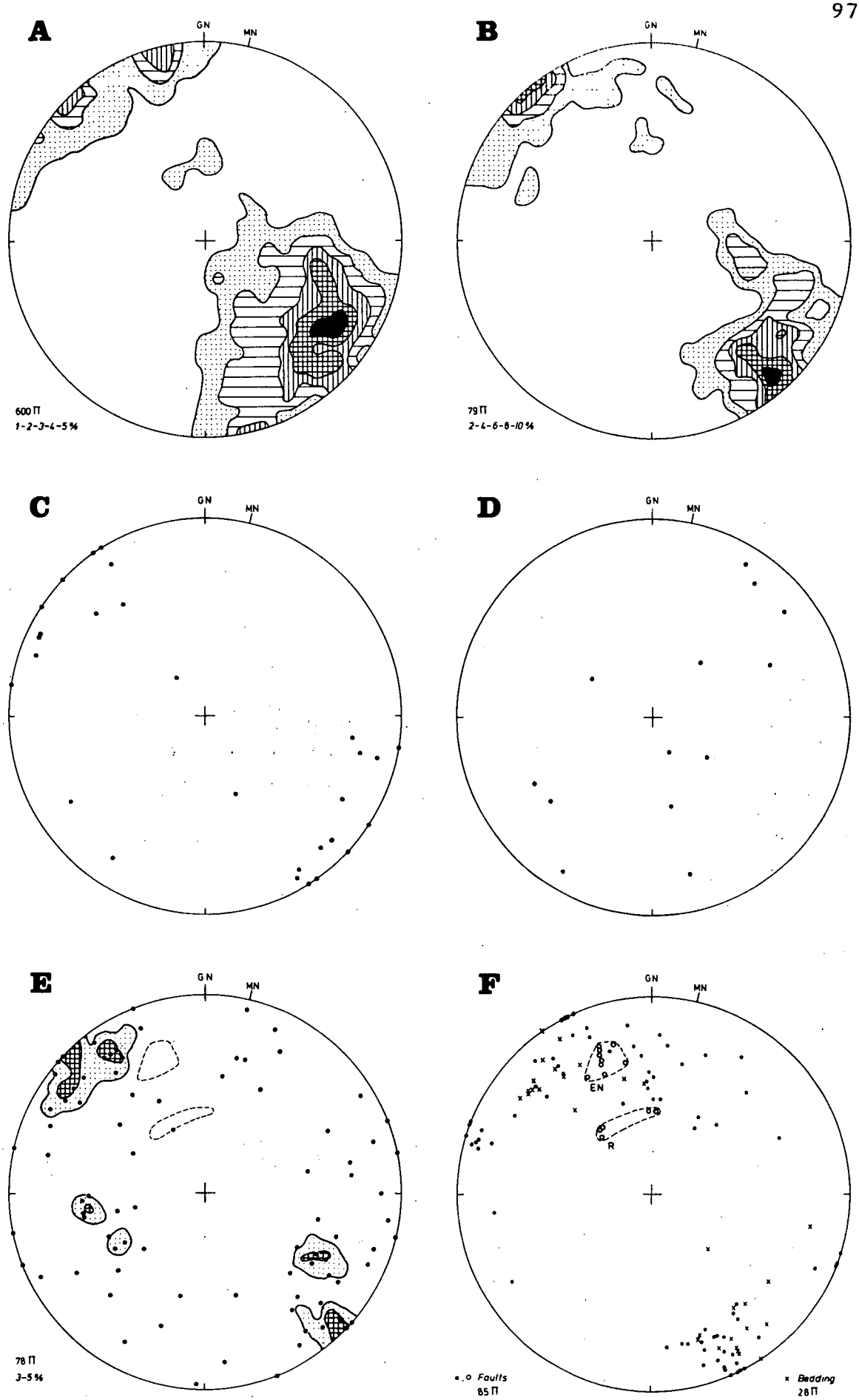
A
GN
MN
600 Π
1-2-3-4-5 %
B
GN
MN
79 Π
2-4-6-8-10 %
C
GN
MN
D
GN
MN
E
GN
MN
78 Π
3-5 %
F
GN
MN
EN
R
• , o Faults
85 Π
× Bedding
28 Π

FIGURE 3.11

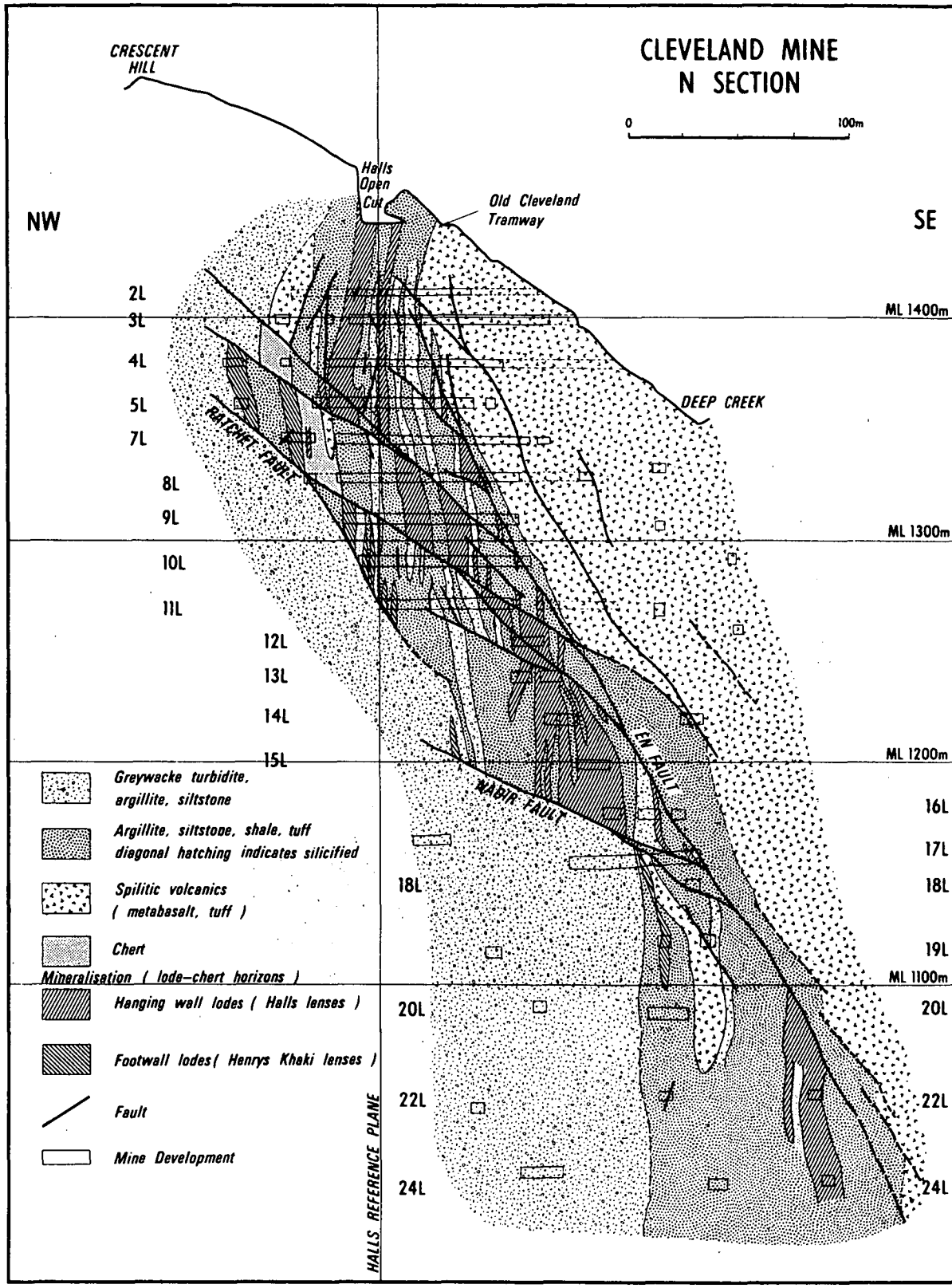

FIG. 3.12 Geological section of the Cleveland mine, on mine section N. Geological interpretation by P.L.F. Collins from original mapping on N section cross-cut drives (2 - 11 levels) and compilation of data from development mapping and drilling.

Geologic structure at the mine

Cox (1968a) and Cox and Glasson (1967, 1971) postulated a single 'lode bed' sliced up into a series of near vertical, *en echelon* segments by steep, west dipping, north-east trending normal faults. A much simpler interpretation by Ransom (1972), Ransom and Hunt (1975) and Palmer (1976) proposed a succession of discrete lenses of mineralisation within a steep, south-east dipping sequence dissected by a single reverse fault.

The present structural interpretation (Fig. 3.12) is similar to the three later interpretations, but with a greater dissection of the host sequence by reverse faults. The structural interpretations illustrated in the cross-sections in Figures 3.12 and 4.3 have been developed from mapping of the upper levels on mine section N (Fig. 3.12) and compilation of stratigraphic and structural data from diamond drilling, cross cuts, drives and mine level plans (mine section Qa and below 11 level on N section).

Although the regional bedding trend is for a dip of 60°-70° to the north-west, at the Cleveland mine the volcano-sedimentary sequence generally has a much steeper dip and more easterly strike than the regional trend (cf. Figs. 3.11A and B). The bedding poles used to construct Figure 3.11B are derived from an area bounded by Deep Creek, Crescent Spur and the two major interpreted faults to the north-east and south-west of the mine (Fig. 3.3).

Underground, there is distinct dip reversal with depth, from a steep north-west dip at the surface to a vertical to steep south-east dip below 4/5 level (Figs. 3.11F, 3.12). This change in dip direction is most likely due to drag associated with a series of sub-parallel reverse faults trending east-northeast and dipping 30°-45° SE (Fig. 3.12). Two of these faults (Nadir and Ratchet faults) have caused significant displacements of the sulphide lenses (Figs. 3.12, 4.3). Movement occurred prior to, and again during the mineralisation episode. For example,

open fractures in Nadir fault are filled with quartz veins bearing cassiterite (Plate 3.5), but later movement has caused localised intense deformation and shearing of the quartz. In addition to the low-angle reverse faults there are numerous north-west trending, post mineralisation (?) faults (*e.g.* Qa fault, Fig. 4.2) and several vertical to steep north-west dipping normal and reverse faults, particularly evident in the upper levels of the mine (Figs. 3.12, 4.3).

The only other major fault is a steep south-east dipping fracture (EN fault) located within the Hall Formation adjacent to the structurally overlying Deep Creek Volcanics (Figs. 3.12). The flatter reverse faults feather into this fracture and on N section do not appear to penetrate into the Deep Creek Volcanics as originally interpreted to occur on Qa section (cf. Figs. 3.12 and 4.3). Within the Deep Creek Volcanics there are several other steep south-east dipping faults which parallel EN fault (Fig. 3.12).

A stereographic plot (Fig. 3.11F) of poles to fault surfaces mapped on mine section N, levels 2-11, indicate three main sets of faults. One set has a north-east to easterly trend, dipping generally 30°-70° SE-S, and includes the low angle reverse faults and the steeper EN fault (dip 60°S), both striking 070° (Fig. 3.11F). Although dominant underground, the style of faulting represented by the low-angle reverse faults (*e.g.* Ratchet fault) and EN fault generally is not evident in surface faults (cf. Figs. 3.11E and F). This may be due to fanning out and weakening of these structures up dip (*i.e.* entirely sub-surface structures) or it may be due to erosional effects since the slope of the ground surface at the mine sub-parallels Ratchet and Nadir faults (Figs. 3.12, 4.3). There are only two mapped surface faults with this orientation, one of which crops out in a tributary of Deep Creek near W prospect (CQ367070) and strikes 065°, dip 44°S (Fig. 3.3).

A second set of faults also strike 060° but dip 90°-65°N. These

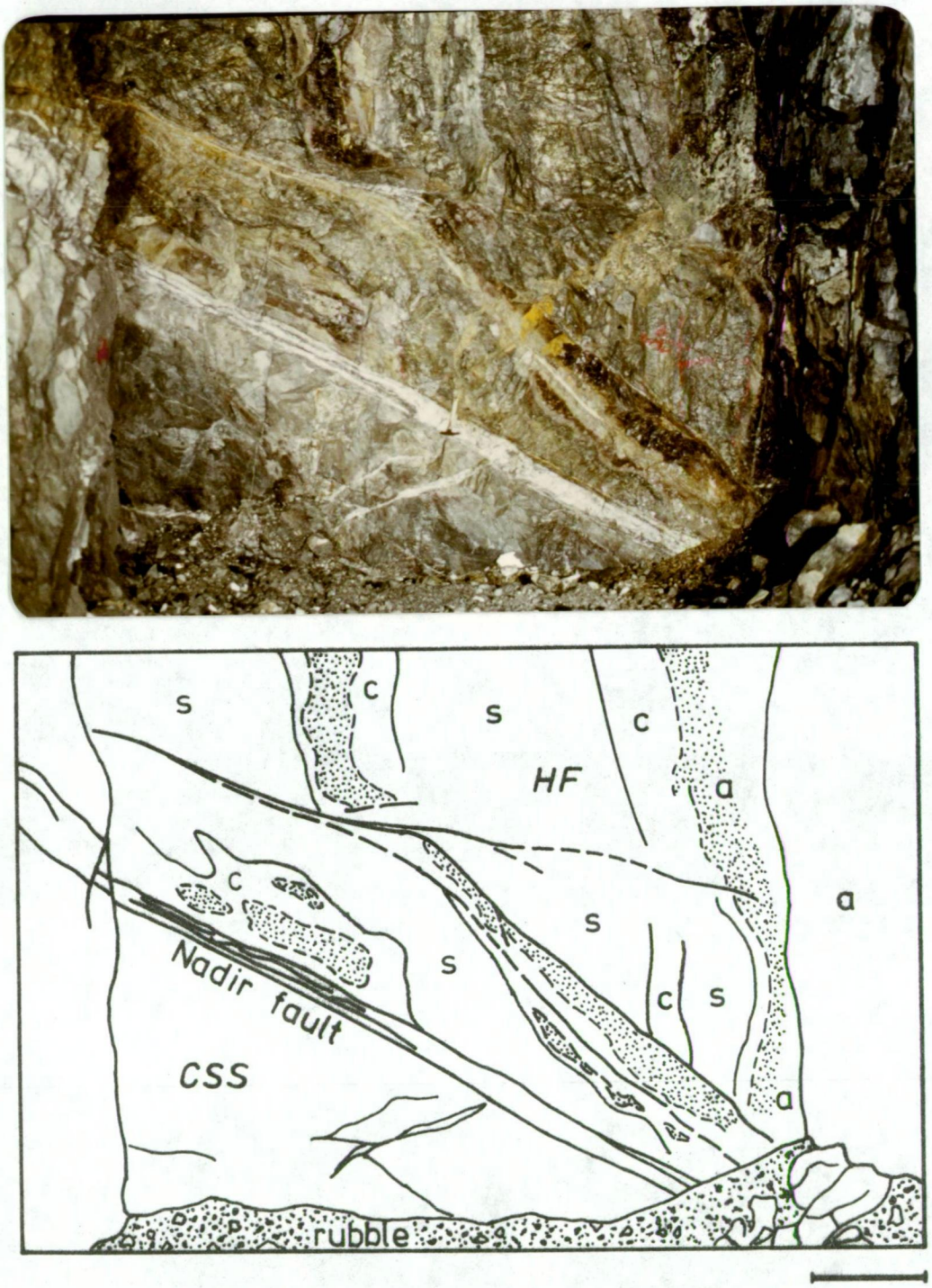

PLATE 3.5 Nadir fault (white quartz) and associated fractures with Halls A/B lens (HF) above (banded brassy yellow pyrrhotite and 'chert') and the Crescent Spur Sandstone (CSS) below. Bedding in the sulphide lens is near-vertical at top of photograph but is sub-parallel to the fault surface immediately above the Nadir fault (*e.g.* to right of hammer) due to drag associated with sinistral movement. Note bleaching (c) of brown argillite (a, stippled) parallel to fractures (*e.g.* to right of hammer) and adjacent to mineralised units (s). Face in B lens north, development drive, 16 sub-level, looking north-east. Scale bar = 1 m.

faults are most apparent in the upper levels of the mine (*i.e.* 2-7 level) and probably correspond to the steep north-west dipping normal faults described by Cox (1968a) and Cox and Glasson (1971), and to which they attribute segmentation of the 'lode bed'. A third set of faults striking 020° and dipping 90°-75°E, are probably associated with the major anticlinal structure.

Small scale folds (*i.e.* half wavelength less than 2 m) are locally preserved in the sulphide lenses. Some are related to post-Cambrian deformation, with axial surfaces parallel to the regional trend (Plate 3.4C), whereas others have features such as confinement between mineralised layers (Plate 3.4D), suggestive of preserved sedimentary slump structures.

The major effect of the dominant north-east trending folding and associated reverse (or thrust) faulting at the mine has been to dislocate the host sequence into a number of segments, thus imparting an apparent overall south-easterly dip to the Cambrian sequence. Localisation of the reverse faults (*e.g.* Ratchet, Nadir, EN faults) at the mine has undoubtedly played a major role in ore deposition, as such a fracture system, demonstrably active during the mineralisation episode, would provide suitable channels for rising hydrothermal solutions.

DEVONIAN IGNEOUS ROCK

The northern margin of the Meredith Granite occurs 4-5 km to the south and east of the Cleveland mine (Figs. 3.1, 4.1). It has been dated by both K-Ar and Rb-Sr methods to be about 350 m.y. (McDougall and Leggo, 1965; Brooks, 1966). Reid (1923, p. 152, Plate III) reported two north-northeast trending, narrow, severely altered quartz porphyry 'protrusions' on the south-east flank of Crescent Spur, in the vicinity of the mine. However, these protrusions have not been found during subsequent investigations (*e.g.* Hughes, 1954; Mason, 1965), and Groves (1968, p. 45, P.B. Nye, pers. comm.) reported that the rocks probably were misidentified. Later,

Cox and Glasson (1967, 1971) and Cox (1968a) described a thin (230 mm wide), highly decomposed quartz porphyry dyke (striking 105° M and dipping steeply north) intruding greywacke-sandstone within 180 m of the tin mineralisation. This dyke was believed to be an acid igneous intrusive associated with the Meredith Granite, but it is now known to be the extremely weathered surface expression of a porphyritic basalt/dolerite dyke at the southern end of the Cleveland mine.

Recent drilling of stockwork vein mineralisation in the footwall rocks of the sulphide lenses has intersected a probable near-vertical, west-northwest trending, dyke-like intrusive body of altered quartz porphyry. It is laced with veins similar to those in the host rocks, and drilling of this mineralised zone is continuing.

Meredith Granite

The Meredith Granite is a large stock-like body that crops out over about 300 km^2. It has been described by numerous workers (*e.g.* Reid, 1923; Jack and Groves, 1965; Groves, 1966), with petrographic and geochemical investigations by Groves (1966, 1968), Groves *et al*, (1972) and Stockley (1972). Regional mapping of the northern end of the granitoid, supplemented with thin section examinations and some additional geochemical data (Appendix 3, Table A3.1), during this study, confirm the results of previous investigations.

The Meredith Granite is composed predominantly of two main textural types: an equigranular, fine-medium grained, grey biotite adamellite and a porphyritic biotite granite/adamellite. Minor granitic types include sodaclase microgranite, alaskite aplite, pegmatite, quartz-feldspar and granite porphyry, and cassiterite-bearing greisen and quartz-tourmaline veins (Groves, 1968; Groves *et al*, 1972; Stockley, 1972). Emanating from the northern margin of the granitoid are quartz-feldspar porphyry dykes (Figs. 3.1, 4.1).

The two main granitic types have similar petrographic and geochemical characteristics. The equigranular adamellite (78-441) consists of quartz, K-feldspar and plagioclase (andesine) occurring as anhedral grains 0.5-1 mm across with subordinate biotite as flakes 0.2-0.5 mm in length, and minor muscovite. Other accessory minerals include hornblende, apatite, tourmaline, zircon, rutile and sphene (Groves, 1968). Large K-feldspar phenocrysts, up to 30 mm in length, and radial tourmaline clots, up to 20 mm in diameter, occur rarely. The porphyritic adamellite (78-442, 78-443) is characterised by large euhedral K-feldspar phenocrysts, up to 60 mm in length, with subordinate phenocrysts of quartz, biotite and plagioclase in a fine to medium grained groundmass, slightly coarser than the equigranular adamellite. Biotite-rich mafic segregations (78-444) occur sporadically within the porphyritic adamellite, and joints are commonly coated with splashes of molybdenite.

The relationship between the two texturally different adamellites is not known (*e.g.* Waterhouse, 1914; Reid, 1923; Groves, 1968), with the only exposed contact (at CQ729058) containing 'rafts' of hornfelsed sedimentary rock (Groves, 1968). However, in the upper reaches of the Ramsay River the porphyritic adamellite appears to be marginal to the equigranular adamellite.

Quartz-feldspar porphyry and granite porphyry (*e.g.* Mt Stewart) occur within and protrude outward as dykes from the Meredith Granite (Waterhouse, 1914; Groves, 1968; Fig. 3.1). An example of a quartz-feldspar porphyry crops out on Butlers Road (CQ725074) and in the Arthur River (Fig. 3.1). It consists of bi-pyramidal to rounded quartz phenocrysts up to 10 mm in diameter and lath-shaped phenocrysts of feldspar (plagioclase and K-feldspar), 10-15 mm in length, in a light grey, fine grained groundmass containing biotite and disseminated pyrrhotite. In thin section (78-417), the quartz phenocrysts are

generally 3-5 mm in diameter, being well-rounded, and consist of several quartz grains with sharp internal margins but irregular outer margins, probably the result of interaction with the groundmass. The plagioclase phenocrysts (Plate 3.3G, H) exhibit fine twinning superimposed upon concentric zoning, and are partially altered around the margins and adjacent to fractures. Microphenocrysts of biotite (Plate 3.3G, H) occur as dark-light brown pleochroic flakes generally 0.5-1 mm in length, but up to 2 mm. The groundmass has a felted texture, consisting of a fine (0.05-0.2 mm) intergrowth of quartz (about 50%), feldspar (35%) and biotite (15%) with minor opaques (pyrrhotite), chlorite, apatite and zircon. Biotite is commonly partially altered to green chlorite, and rarely is poikolitically enclosed in feldspar phenocrysts. Petrographically, the porphyry is dissimilar to the Mt Bischoff porphyry which is characterised by abundant by-pyramidal quartz phenocrysts, minor muscovite, and absence of plagioclase (Groves *et al*, 1972).

A contact aureole to the Meredith Granite is composed predominantly of the albite-epidote hornfels and hornblende hornfels facies and locally of the pyroxene hornfels facies (Groves, 1968; Groves *et al*, 1972). Magnetite is also finely disseminated throughout the contact aureole around the northern margin of the Granite, particularly in the more pelitic rocks (*e.g.* 78-413). Estimates of lithostatic load at the time of granite emplacement vary from 100-250 MPa, and the minimum initial contact temperature is estimated at 650°C (Groves *et al*, 1972). The aureole extends up to 2.5 km in plan from the contact (Groves, 1968), but this may be exaggerated by the attitude of the upper granite surface which, between the Arthur and Wilson Rivers (Fig. 3.1), appears to have a shallow, north-westerly dip.

TABLE 3.5. Average compositions of granitic rocks from the Meredith Granite and at Mt Bischoff[1].

	1	2	3	4	5	6
Major elements (mass%)						
SiO_2	71.93	72.17	74.30	74.90	69.90	75.30
TiO_2	0.37	0.33	0.15	0.10	0.58	0.02
Al_2O_3	13.95	13.60	13.23	12.20	13.70	14.25
FeO[2]	2.04	2.34	1.79	1.45	3.15	1.95
MnO	0.03	0.05	0.02	0.04	0.06	0.06
MgO	0.80	0.70	0.65	0.10	0.99	0.60
CaO	0.98	1.13	0.32	0.46	1.10	0.20
Na_2O	3.05	3.17	3.37	3.90	3.00	0.14
K_2O	4.88	4.73	4.53	4.60	4.90	4.90
P_2O_5	0.08	0.12	0.03	0.03	0.14	0.09
LOI[3]	1.28	0.98	1.07	0.52	2.03	1.85
TOTAL	99.39	99.32	99.46	98.30	99.61	99.36
Trace elements (g/t)						
Ba	542	474	121	-	682	149
Cu	8	7	5	4	41	4
Li	48	43	38	66	47	93
Mo	8	10	11	-	6	-
Pb	21	18?	17	-	11	32
Rb	231	237	298	245	230	906
Sr	92	79	28	12	137	3
Sn	<3?	6?	8	3	17	72
Th	24	23	22	18	35	11
U	10	10?	17	3	<11	13
W	<11	<11	14	-	17	-
Zn	47	33	19	15	46	122
Ratios						
A/CNK[4]	1.16	1.10	1.20	1.00	1.12	2.4
K/Rb	211	200	152	188	213	54
Rb/Sr	2.5	3	11	20	2	302
U/Th	0.42	0.42(?)	0.77	0.17	<0.31	1.18
K_2O/Na_2O	1.60	1.49	1.34	1.18	1.63	35

MEREDITH GRANITE

1. equigranular biotite adamellite (average of 4 analyses).
2. porphyritic biotite adamellite (average of 7 analyses).
3. Microgranite (average of 3 analyses).
4. porphyritic granite/adamellite dyke (1 analysis).
5. quartz-feldspar porphyry (1 analysis).

MT BISCHOFF PORPHYRY

6. quartz-feldspar porphyry (average of 5 analyses).

Notes:

(1) Average compositions from analytical data in Table A3.1 and data from Groves *et al*, (1972, Tables 14 and 17; summarised in Table A3.2).
(2) Total iron as FeO.
(3) Loss on ignition includes H_2O and SO_2 where applicable.
(4) Molecular proportions $Al_2O_3/(CaO+Na_2O+K_2O)$.

Geochemistry of granitic rock of the Meredith Granite

The geochemistry of granitoids associated with cassiterite-sulphide and other tin deposits in western Tasmania has been studied by Groves (1968; summarised in Groves *et al.*, 1972) and Klominsky and Groves (1970) with additional work on the Meredith Granite by Stockley (1972), and its possible southern extension to the Pine Hill Granite by Patterson (1979) and Ward (1981). The earlier work on the Meredith Granite (*e.g.* Table A3.2) has been supplemented here by additional chemical data reported in Appendix 3 (Table A3.1). The analytical data in Table A3.1 are consistent with previous data on the same granitic rock types from the Meredith Granite (*e.g.* Groves, 1968; Stockley, 1972), though there are no comparable data for some elements (*e.g.* Nb, Mo, Y, W, Zr). Average compositions of granitic rocks of the Meredith Granite and of the Mt Bischoff porphyry are listed in Table 3.5.

The porphyritic biotite adamellite, equigranular biotite adamellite and biotite microgranite of the Meredith Granite are chemically similar (Groves, 1968; Groves *et al.*, 1972; Stockley, 1972). They all have a restricted range of silica contents (68.9-77.4% SiO_2) and show patterns of regular chemical variation on Harker diagrams (Fig. 3.13). For most elements there is an approximate linear or curvilinear relationship between SiO_2 and other elements indicating that the granitic rocks of the Meredith Granite belong to the same chemical suite. A biotite-rich mafic segregation in porphyritic adamellite (781010, Table A3.1) is slightly depleted in silica (67.9% SiO_2) but is enriched in lime, magnesia and iron (Fig. 3.13), and thus may be the least differentiated granitic rock of the suite.

The high proportion of alkalis relative to lime, magnesia and iron in differentiated granite, due to smaller amounts of iron-magnesium minerals and more alkali feldspar, is reflected in a ternary plot of $CaO - (FeO + MgO) - (Na_2O + K_2O)$ (Fig. 3.14), on which most granites plot on a curved line trending towards the alkalis apex with increased

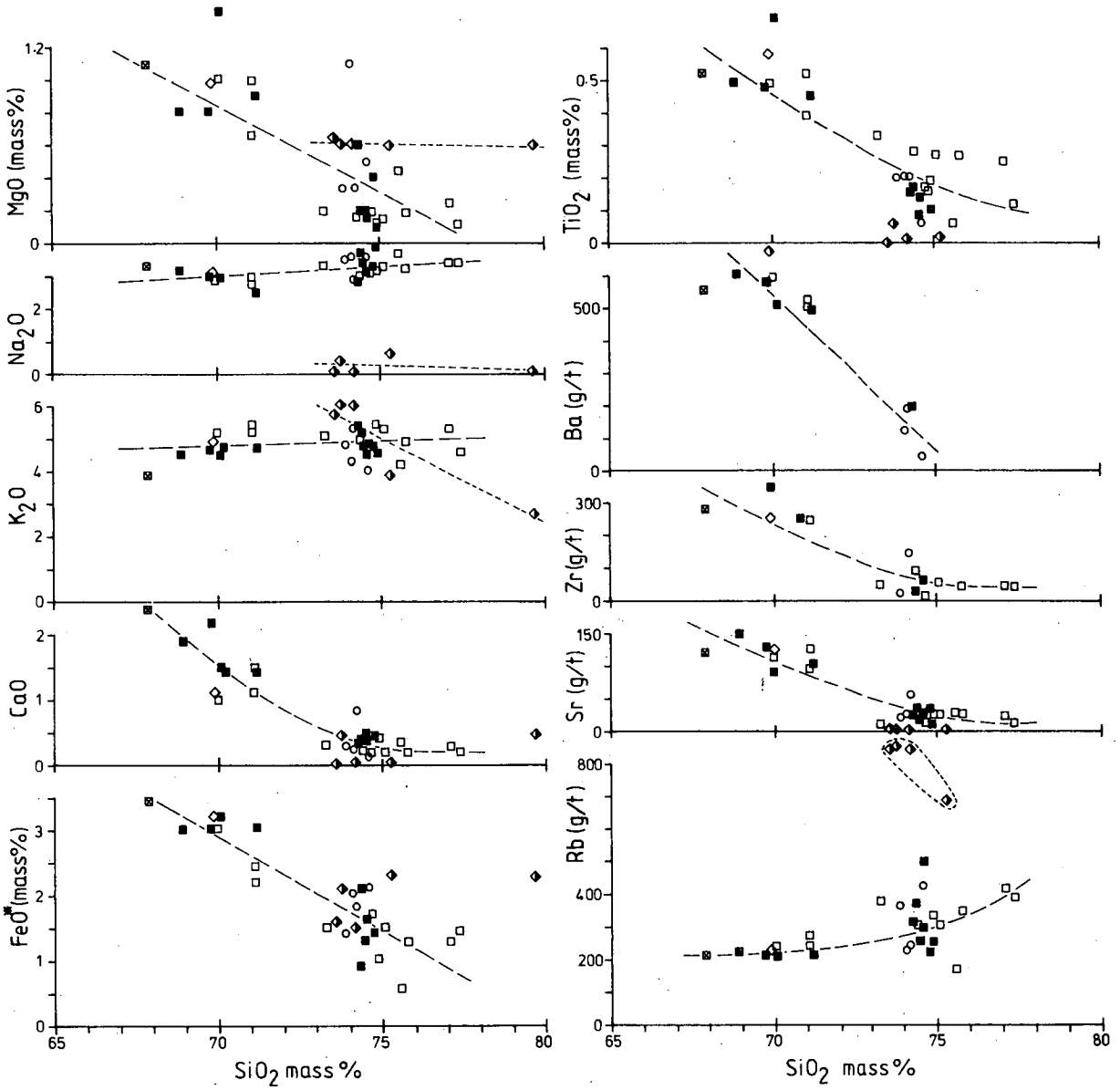

FIG. 3.13 Harker diagrams for various oxides and trace elements in the Meredith Granite and Mt Bischoff porphyry. Symbols as in Fig. 3.14. Compiled from data in Table A3.1 and analytical data listed in Groves *et al.* (1972) and Stockley (1972). Long dash lines are trends for the Meredith Granite and short dash lines for Mt Bischoff porphyry.

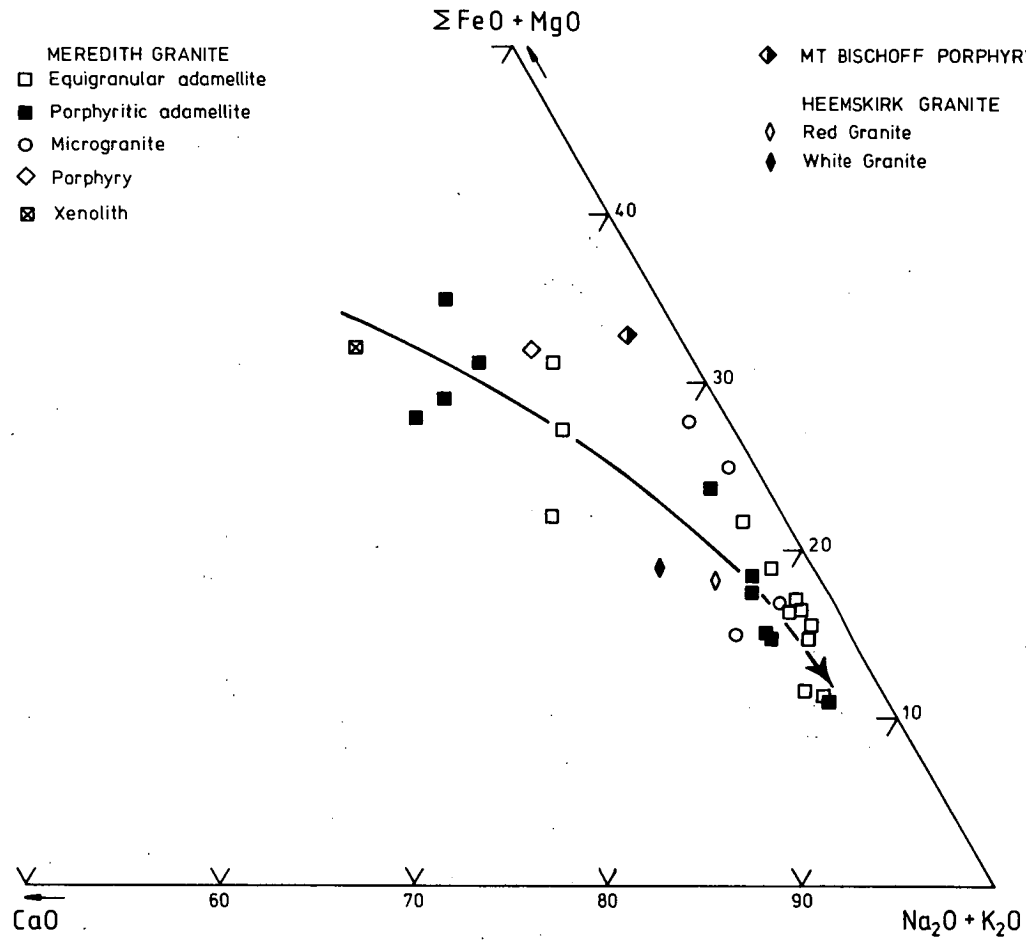

FIG. 3.14 Triangular plot of CaO-(ΣFeO + MgO) - ($Na_2O + K_2O$) for granitic rock from the Meredith Granite. Arrow indicates trend of increasing SiO_2 content. Average values for the Heemskirk Granite and Mt Bischoff porphyry are plotted for comparison. Compiled from data listed in Tables A3.1 and A3.2 and in Groves *et al.* (1972) and Stockley (1972).

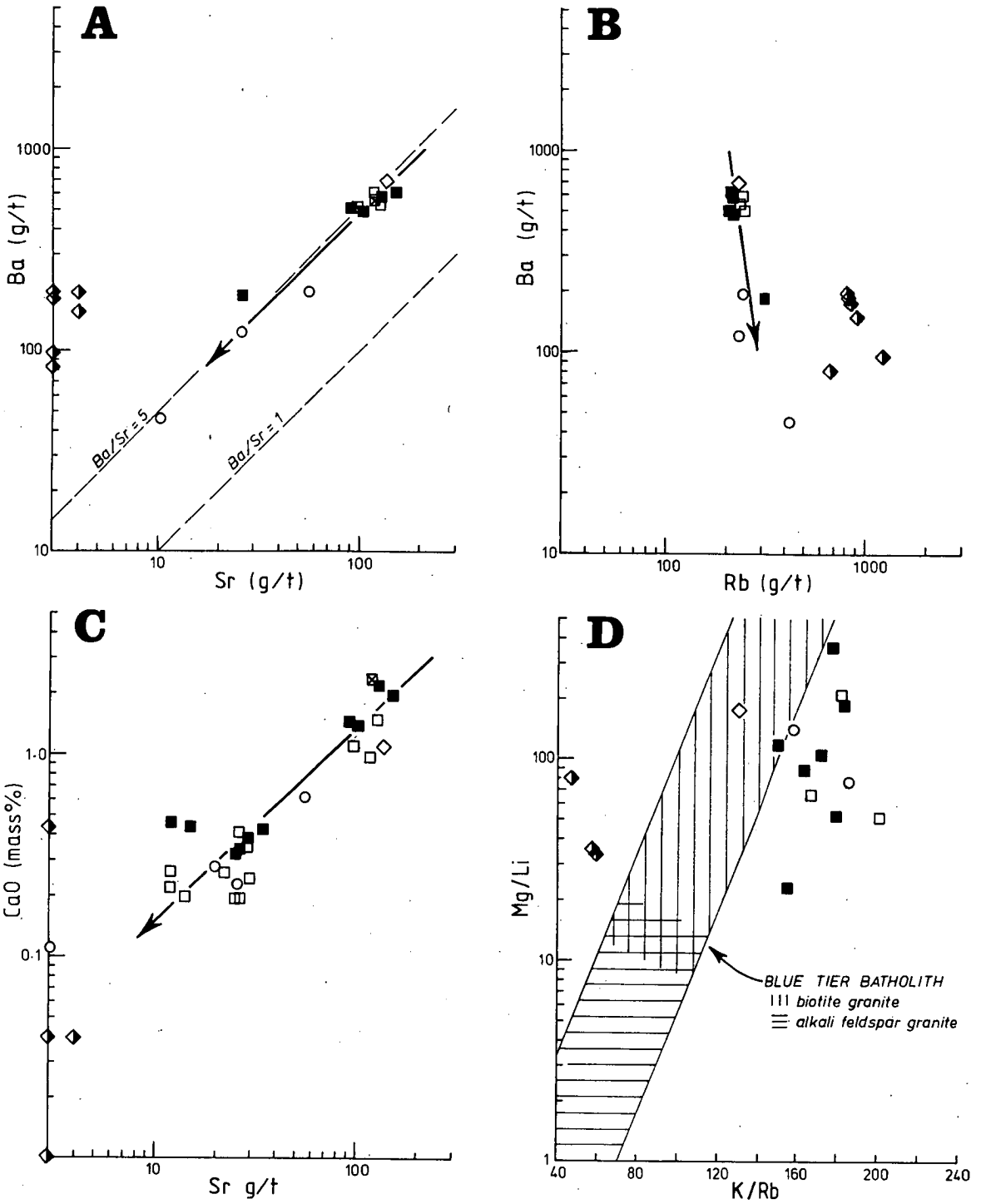

FIG. 3.15 Selected major and trace element variation diagrams illustrating geochemical variation within the Meredith Granite, and dissimilarity of the Mt Bischoff porphyry. Symbols as in Fig. 3.14. Arrows indicate trends of increasing SiO_2 contents. Compiled from data listed in Table A3.1 and in Groves *et al.* (1972) and Stockley (1972). Trends in diagrams A and B, and the Ba/Sr = 5 are almost identical to variation in biotite granite/adamellite in the Blue Tier Batholith (*e.g.* Higgins *et al.*, in prep.). The fields of biotite granite/adamellite and later alkali feldspar granite in the Blue Tier Batholith (after Groves, 1977) are plotted on the Mg/Li-K/Rb diagram for comparison with the Meredith Granite data.

differentiation (*e.g.* Blockley, 1980). Analyses of the Meredith Granite parallel this trend, with an increase in alkali content coincident with increasing SiO_2 content (Fig. 3.14) indicating a relatively advanced stage of differentiation, similar to the nearby high-level Heemskirk Granite (Fig. 3.14).

The trace element compositions of equigranular adamellite, porphyritic adamellite and microgranite are similar, and also show patterns of regular chemical variation on Harker diagrams (Fig. 3.13). The Ba-Sr, Ba-Rb, Ca-Sr, Mg-Li and K-Rb relationships (Fig. 3.15) provide further evidence indicating a single genetically related geochemical series in which the microgranite may be a slightly more advanced differentiate than the adamellites (*e.g.* Ba-Sr, Ba-Rb variation, Fig. 3.15). The inter-element relationships and trends on variation diagrams (Figs. 3.13, 3.15) are similar to trends observed for early formed biotite granite/adamellite in the Blue Tier Batholith (*e.g.* McClenaghan *et al.*, 1982; McClenaghan and Williams, 1982; Higgins *et al.*, in prep.) and are consistent with fractional crystallisation being a dominant process of differentiation of the granitic magma (*c.f.* Higgins *et al.*, in prep.), but late-phase differentiates (*i.e.* alkali feldspar granite) are not known to occur in the Meredith Granite (*e.g.* Fig. 3.15D).

The composition of the Meredith Granite follows the general calc-alkaline trend (Irvine and Baragar, 1971) of granitoids in orogenic belts, but as it lacks basic end members and contemporary volcanics, the Meredith Granite (and other granitoids in western Tasmania) correspond to the 'compositionally restricted' calc-alkaline type of Pitcher (1979). The Meredith Granite is relatively enriched in potassium (4.2-5.5% K_2O), and is peraluminous with $Al_2O_3/(CaO + Na_2O + K_2O)$ molar ratios greater than one (*i.e.* A/CNK >1) (Clarke, 1981; Table 3.5). It has geochemical

(and petrographic) features consistent with the genetically classified S-type granite (*e.g.* A/CNK >1.1, high SiO_2, high K/Na ratio, corundum normative; *e.g.* Chappell and White, 1974; Hine *et al.*, 1978).

The granitic rocks of the Meredith Granite contain more than 80% normative quartz + albite + orthoclase, generally <3% anorthite, and are corundum normative. The normative quartz:albite:orthoclase ratios and albite:anorthite:orthoclase ratios of adamellites and microgranite plot as a neat group at the 'minimum melt' composition (Winkler, 1979), close to the temperature minimum for 100 MPa water pressure (Fig. 3.16). The average values of equigranular adamellite and porphyritic adamellite fall on the 100 MPa cotectic line, close to its ternary minimum.

The quartz-feldspar porphyry at Butlers Road has a silica content of 69.9% SiO_2 which is much lower than quartz-feldspar porphyry at Mt Bischoff (73.6-79.7% SiO_2) and has a much higher titania content (0.58% compared with 0.02% TiO_2 at Mt Bischoff). It falls on the trend lines on variation diagrams (Figs. 3.13, 3.14, 3.15), thus indicating that the porphyry is a relatively early differentiate, which was emplaced with the main Meredith Granite mass.

The Mt Bischoff porphyry tends to plot well away from trends defined by the Meredith Granite (Fig. 3.13, 3.15), and for some elements (*e.g.* Na_2O, K_2O, MgO, and Rb) a separate suite may be defined on Harker diagrams (Fig. 3.13), thus substantiating the dissimilarity of the Mt Bischoff and Butlers Road porphyries. The Mt Bischoff porphyry is probably a later and/or more highly differentiated

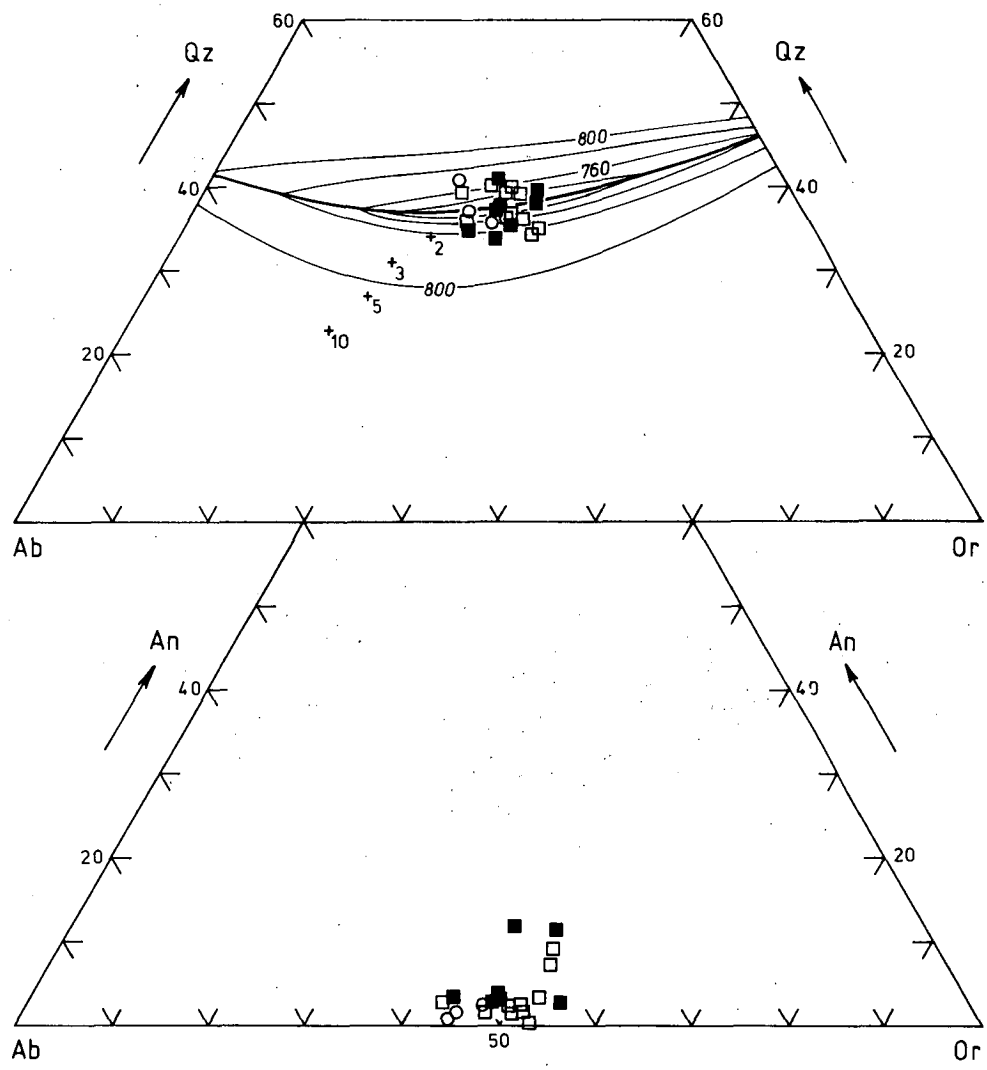

FIG. 3.16 Normative Qz-Ab-Or and An-Ab-Or composition of the Meredith Granite (compiled from data in Appendix 3; Groves *et al.*, 1972; Stockley, 1972). Symbols as in Fig. 3.14. On the Qz-Ab-Or diagram, thin lines are isotherms (*e.g.* 800°C) and the thick line is the cotectic line at 100 MPa P_{H_2O} (after Winkler, 1979). The ternary minima for 200 and 300 MPa and eutectic points at 500 and 1000 MPa P_{H_2O} are shown as crosses labelled 2, 3, 5 and 10, respectively (Winkler, 1979).

derivative of the Meredith Granite (Groves, 1968), though some of the chemical variation (*e.g.* enhanced Rb, reduced Sr and Na_2O, Fig. 3.13) is probably due to alteration.

U/Th ratios of the Meredith Granite are generally less than 0.5, with higher ratios for the microgranite (average 0.77) and Mt Bischoff porphyry (average 1.18; Table 3.5). High U/Th ratios (*i.e.* >0.5) characteristically are associated with tin-bearing, late phase, highly differentiated granitic rock (Collins *et al.*, 1981), and the relatively high ratios in the microgranite are consistent with it being a slightly more advanced differentiate than the adamellites.

Of the economically important metals, copper is consistently low (<16 g/t), except for the Butlers Road porphyry which has 41 g/t Cu, much higher than the Mt Bischoff porphyry (<3-6 g/t Cu). Lead ranges up to 33 g/t and zinc has a wider range of 10-81 g/t. These values are similar to average abundances in granitic rock (*e.g.* Levinson, 1974) with the metals probably occurring as disseminated minute sulphide grains (Groves, 1968). Molybdenum and tungsten are remarkably consistent with 10-14 g/t and less than 14 g/t, respectively in adamellites and microgranite, but with less molybdenum (6 g/t) and slightly more tungsten (17 g/t) in the Butlers Road porphyry (Table A3.1). The molybdenum content is higher than that in average granitic rock (2 g/t Mo; Levinson, 1974) and in most stannigene granites (4±2 g/t Mo; Tischendorf, 1977), reflecting the occurrence of molybdenite on joint surfaces.

Tin values in equigranular and porphyritic adamellite (<3-13 g/t Sn), and in microgranite (<3-17 g/t Sn) are similar to the average concentration in granitoids considered as precursors of stannigene granites (10±5 g/t Sn; Tischendorf, 1977) and to early-formed biotite granite/adamellite in the Blue Tier Batholith (*e.g.* Groves, 1977; McClenaghan *et al.*, 1982). Most tin in the Meredith Granite occurs in biotite, which has a range of 22-40 g/t Sn (Groves, 1968). This is similar to biotites in biotite granite/adamellite in the Blue Tier Batholith which contain up to 160 g/t Sn (generally <75 g/t Sn) and contrasts with 140-865 g/t Sn in biotites in late-phase biotite-(muscovite) alkali feldspar granite (Groves, 1977). The quartz-feldspar porphyry at Butlers Road contains 17 g/t Sn, much less than the Mt Bischoff porphyry (30-144 g/t Sn, Groves *et al.*, 1972).

In summary, geochemical data indicate that the S-type biotite adamellites and microgranite of the Meredith Granite are relatively advanced differentiates of a single granitic magma (see also Groves, 1968; Groves *et al.*, 1972). The Meredith Granite is similar to early-phase biotite granite/adamellite plutons of the Blue Tier Batholith and has many features of the precursors of tin-specialised or stannigene granites of Tischendorf (1977), but later-phase, highly differentiated granite (such as the alkali feldspar granite that hosts stanniferous greisens at Lottah and Blue Tier) is either not present or not exposed in the main Meredith Granite mass. Late-phase differentiates (or stannigene granites) may occur beneath the Cleveland mine and Mt Bischoff, though deep drilling at the Renison mine has intersected granitic rock similar to the Meredith Granite (Patterson *et al.*, 1981).

Altered quartz porphyry

The only felsic igneous rock in the vicinity of the Cleveland mine is an altered quartz porphyry dyke discovered during recent drilling of the W-Mo-Sn-F stockwork vein system, (Foleys zone) in the footwall of the sulphide lenses. The dyke trends 110°-120° and dips 80°-85°N, approximately perpendicular to the general trend of the sulphide lenses. The lateral extent of the dyke has not been defined, and it is possible that it intersects sulphide lenses at its south-eastern end. The top of the dyke is at about 1000 m M.L. (*i.e.* sea level) or about 400 m below the surface, having been intersected in the decline at 25/26 level (Figs. 4.6, 7.2). It is about 30 m thick at 600 m M.L. and tapers to less than 5 m at the top.

The porphyry consists essentially of quartz phenocrysts up to 10 mm in diameter in a fine-grained groundmass of quartz, topaz, fluorite, carbonate, sericite and sulphides. No evidence of feldspar has been observed in either hand specimen or thin section. The quartz phenocrysts are generally rounded, anhedral-subhedral grains occurring either as single crystals or as composites of several crystals (Plate 4.3A, B). The outer margins of most phenocrysts are diffuse and corroded. Minute solid inclusions, probably topaz and zircon, are present in some crystals that also contain rows of two-phase, aqueous fluid inclusions. Lath-shaped muscovite occurs along the boundaries between quartz crystals in some composite phenocrysts, and biotite occurs rarely as flakes, up to 0.05 mm long, within quartz crystals. The biotite and quartz phenocrysts probably are remnants of the original porphyry.

Alteration of the groundmass has been so extensive, that its original texture and composition has been obliterated. It consists of a fine-grained (0.05-0.1 mm) mosaic of topaz and quartz, with interstitial

fluorite, carbonate, sericite, cassiterite and sulphides. Topaz has been confirmed by X-ray diffraction, and occurs as clear anhedral grains, generally less than 0.05 mm across, and displays slight pleochroism of a faint brown tint in some grains. Sericite occurs in lath-shaped aggregates and stringers up to 0.3 mm in length (Plate 4.3C, D). Fluorite occurs interstitially with the quartz and topaz and as irregular patches up to 2 mm across with inclusions of quartz, topaz, carbonate and wolframite. The fluorite is generally clear but commonly contains centres of purple colouration. It is also a common coating on joint surfaces where it is generally a deep purple colour. Siderite occurs as large irregular patches with intermixed sericite, and as smaller grains interstitial with quartz and topaz. Carbonate also occurs as a reaction or replacement rim around sulphides similar to late carbonate in the sulphide lenses.

Cassiterite is present in most sections as granular, anhedral-euhedral crystals up to 0.6 mm in diameter, occurring either interstitially with quartz and topaz or as single crystals or clusters associated with patches of carbonate and fluorite (Plate 4.3C, D, E). In thin section it is translucent red-brown to pale brown in colour, commonly twinned (Plate 4.3D), and some grains display light/dark colour banding. Wolframite is disseminated through the porphyry as bladed crystals up to 0.5 mm in length, and in one section (48353) occurs as a patch of sub-radiating bladed crystals, generally 0.4 x 0.05 mm, but up to 1.2 x 0.2 mm, associated with coarse-grained quartz, fluorite and carbonate (Plate 4.3A, B). Sulphides (dominantly pyrrhotite with minor chalcopyrite) occur as anhedral grains in irregular masses up to 2 mm across, and comprise less than 5% of the rock (*e.g.* 48352). Pyrite occurs rarely as isolated grains up to 0.1 mm across (49354).

The porphyry is dissected by several sets of quartz veins carry-

ing fluorite, wolframite, molybdenite, cassiterite, bismuthinite and bismuth and other sulphides, which are part of the Foleys zone of stockwork vein mineralisation. The margins of the veins are poorly defined and diffuse into the host altered porphyry, indicating that veining and alteration of the porphyry are contemporaneous. The mineralogy of the veins is described in Chapter 4.

Alteration of the quartz porphyry at Cleveland is very similar to the alteration of quartz-feldspar porphyry dykes at Mt Bischoff, adjacent to the massive pyrrhotite-cassiterite mineralisation. The altered porphyries at Mt Bischoff contain abundant topaz and sulphides, minor amounts of fluorite, carbonate, muscovite, cassiterite and wolframite, and insignificant porportions of original feldspar (Groves, 1968; Groves *et al*, 1972).

TERTIARY

An alkali olivine basalt sheet, at least 50 m thick, blankets the area to the east of the Ramsay River, and relicts of basalt flows cap many of the hills (Figs. 3.1, 4.1). The basalt is underlain by poorly cemented coarse gravel with bands of clay and lignite (Finucane and Blake, 1933; Jack and Groves, 1965). The gravel, which contains pebbles of quartz, quartz-tourmaline, granite, slate and greywacke, was probably widespread over the area, but has since been largely removed and reworked by stream erosion (Jack and Groves, 1965).

The basalt (78-440) consists of fine intergrowths of labradorite laths up to 0.3 mm in length and anhedral augite grains, up to 0.5 mm across with interstitial opaque to translucent, dark green glass and very fine opaques. Olivine occurs as rounded grains up to 0.5 mm in diameter with translucent brown iron-oxide lining internal fractures. Magnetite is the only opaque mineral, occurring as interstitial very fine grains and long needles up to 0.2 mm long. Groves and Solomon

(1964) recorded olivine crystals up to 2 mm in diameter, and also describe the basalt as extremely vesicular and/or scoriaceous in places.

An analysis of basalt cropping out in a quarry on the Corinna Road (CQ742063) is given in Appendix 2, Table A2.10. It is chemically similar to Tertiary basalt elsewhere in Tasmania.

QUATERNARY-RECENT

Late Tertiary and/or Quaternary alluvium was deposited as higher alluvial terraces along the courses of present streams, as a result of reworking of the older Tertiary alluvium, and also occurs filling old stream valleys (Jack and Groves, 1965) and as alluvial fans at the base of some streams. Some old stream valleys are exposed in road cuttings on the Corinna Road between Whyte Hill and the Whyte River (Fig. 3.3). The material in these valleys is usually locally derived; for example, a small in-filled gully near the summit of Whyte Hill (Fig. 3.3; at CQ688080) contains boulders, up to 250 mm in diameter, of the underlying weathered gabbro. Recent deposits of river gravel and sand occur in the beds and flood plains of the present streams. Much of this material is probably derived from reworking of the older alluvial material, particularly the extensive deposits in the Whyte River valley (Fig. 3.3).

4. MINERALISATION AT THE CLEVELAND MINE

INTRODUCTION

The ore bodies at the Cleveland mine (CQ650070) lie within a broad, east-northeast trending zone of Ag-Pb-Zn, Sn-Cu(-W) and Cu mineralisation which parallels the northern margin of the Meredith Granite, extending from Mt Stewart in the west to Mt Bischoff (Fig. 4.1; Solomon, 1977, 1981). Two major tin deposits within the zone (Cleveland and Mt Bischoff) are each surrounded by a halo of small Ag-Pb-Zn vein deposits (*e.g.* Groves, 1968; Groves *et al.*, 1972; Solomon, 1981). Major Ag-Pb-Zn deposits occur at the Magnet mine (CQ705110; Cox, 1975), approximately equidistant from Cleveland and Mt Bischoff, and at the Godkin mines (CQ628050; Nye, 1923), located 2 km south-west of Cleveland (Fig. 4.1). Osmiridium and nickel sulphide deposits in the Caudrys Hill and Mt Stewart areas are associated with Cambrian ultramafic complexes (Groves, 1966; Ford, 1981).

Primary tin mineralisation occurs within the Meredith Granite at the abandoned South Bischoff and Cundy mines, located approximately 8 km south-east and east-southeast of Cleveland, respectively (Fig. 4.1). At the South Bischoff mine (CQ713017), cassiterite occurs in narrow quartz-tourmaline-muscovite veins (Jack and Groves 1965), and at the Cundy mine (CQ728047) cassiterite occurs in a short lens-shaped body of green, fluorine-bearing mica with arsenopyrite, pyrite, sphalerite, chalcopyrite and molybdenite (Reid, 1923). Alluvial and eluvial cassiterite occurs in recent sediments overlying granite in low-lying areas and creek beds in the headwaters of the Ramsay River (*e.g.* Wombat Flat, Summer Creek deposits; Fig. 4.1).

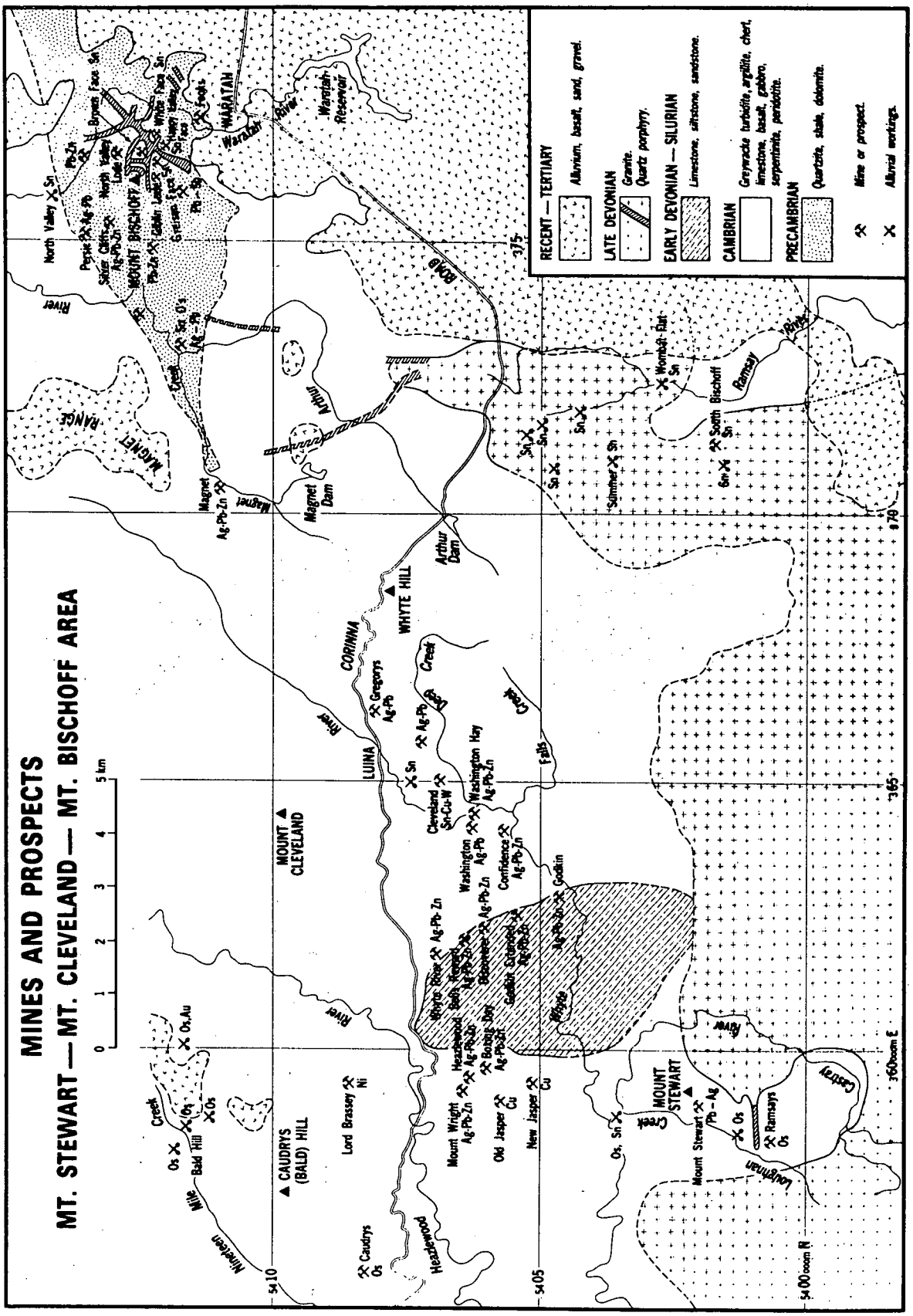

FIG. 4.1 Mines and prospects in the Mt Stewart-Mt Cleveland-Mt Bischoff area.

DISTRIBUTION AND STYLE OF MINERALISATION

At Cleveland, the tin-copper mineralisation is restricted to a north-east trending, narrow zone approximately 800 m in length and up to 150 m wide. It occurs as a series of sub-parallel, near-vertical lenses within the Hall Formation (Figs. 4.2, 4.3). The orebodies consist of variable amounts of fine to medium-grained quartz, tourmaline, fluorite, chlorite, siderite, hornblende and pyrrhotite with minor amounts of cassiterite, chalcopyrite, stannite, arsenopyrite and sphalerite, and other sulphides and gangue minerals.

Eleven lenses of mineralisation are recognised, and are divided into two groups (Ransom and Hunt, 1975; Palmer, 1976): the footwall lodes and hanging wall lodes, which are separated by a micaceous greywacke unit and an overlying mafic volcanic unit (Henrys Volcanic Member) (Fig. 4.2). The footwall lodes include three short, but relatively thick lenses (Henrys, Lucks and Khaki) which have strike lengths of less than 200 m, but are up to 40 m thick. The hanging wall lodes (or Halls lenses) are composed of five main lenses designated, from north-west to south-east, as A, B, C, D and E lens. The hanging wall lodes are of much greater strike length and stratigraphic continuity than the footwall lodes, attaining a maximum thickness of about 30 m and a maximum strike length of about 600 m (Fig. 4.2; Ransom and Hunt, 1975; Palmer, 1976). The A and B lenses locally combine as a single lens, and these are separated from the other Halls lenses by a micaceous greywacke unit up to 10 m thick (Fig. 4.3).

The sulphide lenses have been offset by a series of sub-parallel, south-east dipping reverse faults (Figs. 3.12, 4.3). Most of the movement on these faults occurred prior to the mineralisation episode, with some later movement subsequent to the formation of the sulphide lenses. In some instances, different sulphide lenses have been

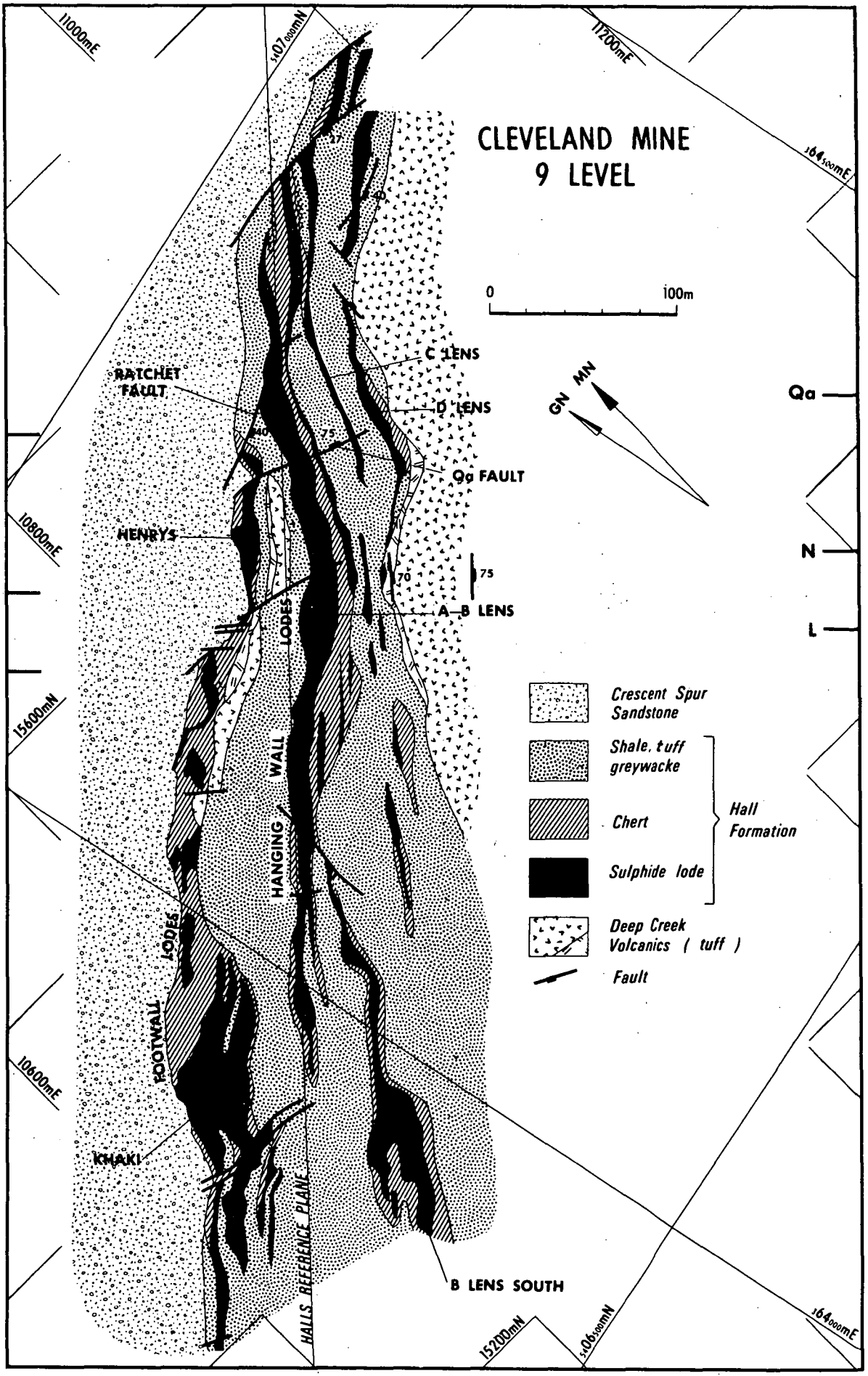

FIG. 4.2 Geological plan of 9 level, Cleveland mine (see Figs. 3.12, 4.3), modified after Palmer (1976).

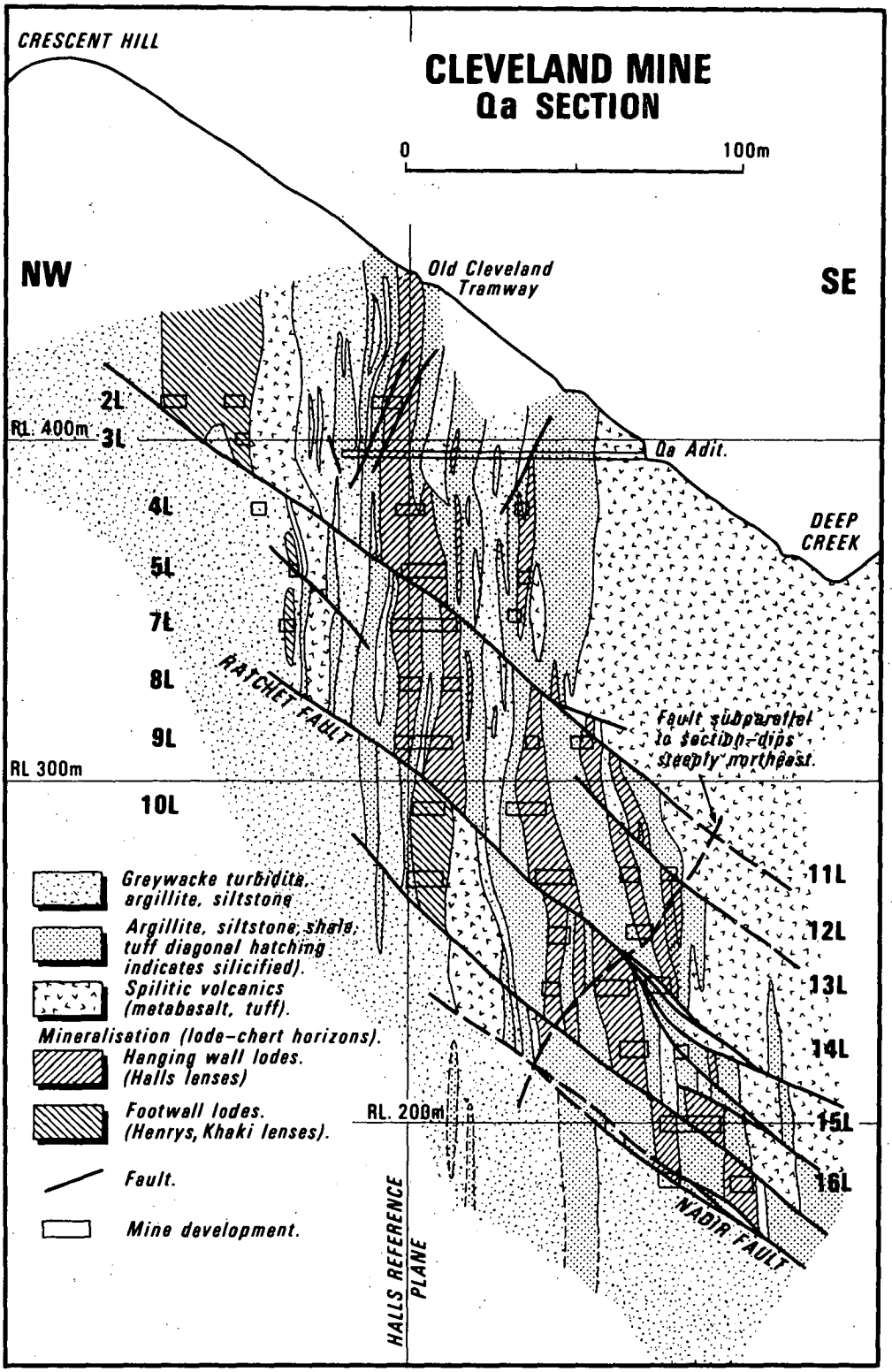

FIG. 4.3 Geological cross-section of the Cleveland mine, on mine section Qa (see Fig. 4.2). The steep, north-east dipping fault, sub-parallel to the section is Qa fault (Fig. 4.2).

faulted into juxtaposition. For example, towards the northern end of the mine, movement on the Ratchet fault has brought A-B lens directly above Henrys lens, and C lens above A lens (Fig. 4.3). Another reverse fault, the Nadir fault (Plate 3.5) has caused sufficient offset and separation of the sulphide lenses for them to be considered as two separate ore bodies, designated as the 'upper ore' and 'lower ore' depending on whether they occur above or below this fault (Figs. 3.12, 4.3).

Stratigraphic control of the sulphide lenses

The sulphide lenses are conformable with bedding in the host rocks (Figs. 4.3, 3.12) as first described by Carey (1945) and subsequently by Cox (1968a), Cox and Glasson (1971), Ransom and Hunt (1975) and Palmer (1976). They are stratabound in the sense of Canavan (1973), occurring within limestone horizons in the Hall Formation, but may also be considered stratiform as each lens is composed of several interlayered 'chert' beds and mineralised units, generally 0.2 - 1 m but up to 10 m thick and 100 m in strike length (Palmer, 1976; Plate 4.1). 'Chert' is here considered as interbedded chert and silicified shale and tuff. Contacts between interlayered 'chert' beds and mineralised units, as well as the outer walls of the sulphide lenses, are normally very sharp, with only negligible amounts of marginal disseminated mineralisation and narrow veins in the adjacent 'chert' wall-rocks.

The mineralised units commonly exhibit a fine compositional banding which is generally parallel to bedding in adjacent 'chert' (Plate 4.2) and has been interpreted as representing primary bedding preserved during replacement (Cox, 1968a; Palmer, 1976). The bands range from 0.05 mm - 100 mm in thickness but are generally 2 - 5 mm thick. Macroscopically, the banding is defined by concentrations of either pyrrhotite or mafic gangue minerals occurring alternately with light coloured ore. In thin section (*e.g.* 104334, 104405, 104409),

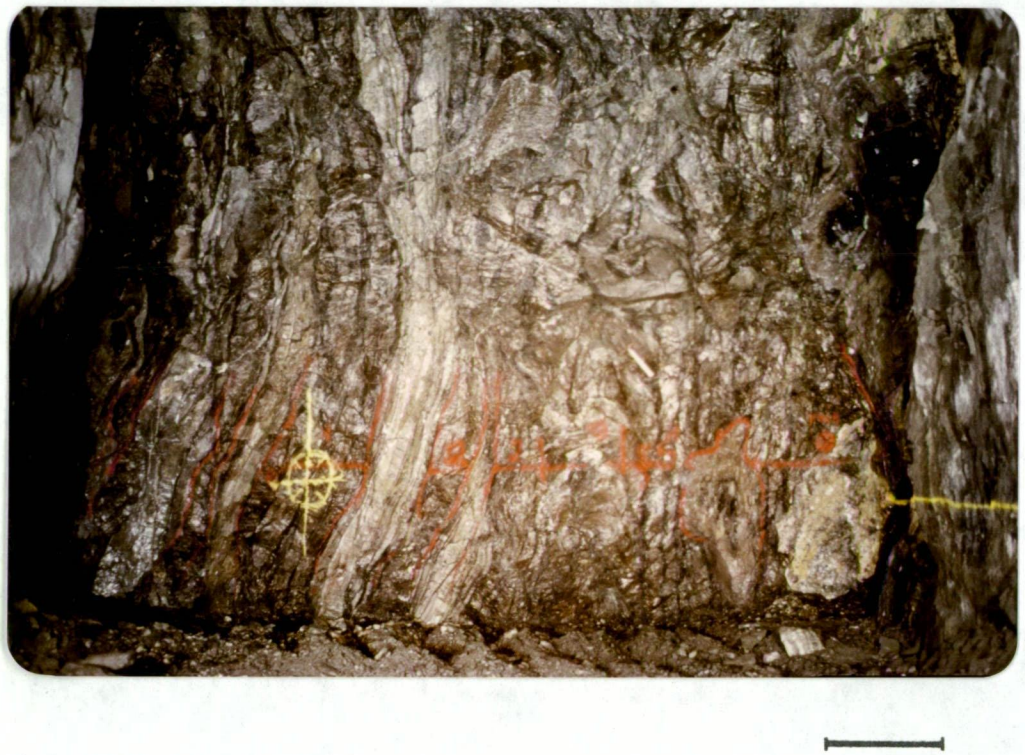

PLATE 4.1 Interlayered 'chert' and sulphide mineralisation in Halls B lens, showing bedding in 'chert' and banding in the ore. Within the thick mineralised unit at right is a premineralisation, intraformational sedimentary fold (above hammer to the right of centre) preserved during replacement (*cf.* Plate 3.4D). Specimen 48287 (Plate 3.2C, D) is from the 'chert' bed to the right of the yellow circle. Red markings indicate the mineralised units. Face in B lens north, development drive, 14 level, looking north-east. Scale bar = 1 m

PLATE 4.2 Finely banded mineralisation in sulphide lens. Dark bands are tourmaline rich and lighter bands are pyrrhotite and/or quartz-chlorite rich. The banding is parallel to bedding in adjacent 'chert'. Face in B lens, north development drive, 15 level, looking north-east. Scale bar = 100 mm.

non-sulphide banding is defined by concentration of tourmaline and/or chlorite in darker bands and fluorite, quartz and siderite in pale bands. Cassiterite is erratically distributed throughout the ore, and does not show preference for any mineral assemblage, though Cox (1968a) suggested concentration of cassiterite in quartz-rich bands.

GENERALISED PARAGENESIS AND ZONING

The mineralisation episode at Cleveland may be divided into at least five stages, with a complex micro-paragenesis in the main stage of the mineralisation episode. Complementing the paragenetic sequence is a distinct spatial distribution of the various stages, and a mineral (and metal) zonation within the first two stages. The generalised paragenetic scheme based on geometric features, such as vein-ore relationships observed in underground exposures and in drill core, and from microscopic evidence is shown in Figure 4.4. The mineralogical zonation for Stages I and II is schematically illustrated in Figures 4.5 and 4.6. Within the Stage II mineralisation there is a complex sequence of replacement and precipitation of hydrothermal minerals, and delineation of this sequence is complicated by a superimposed mineralogical zonation which may in itself be temporally controlled.

Stage I

The first stage of mineralisation consists predominantly of quartz, fluorite, wolframite and molybdenite occurring in veins, generally 10 - 100 mm thick, with minor bismuth, bismuthinite, pyrite, arsenopyrite, chalcopyrite, pyrrhotite, cassiterite, ilmenite and trace hematite. Base-metal sulphides occur either as intergranular grains or as inclusions in quartz, fluorite and wolframite; and molybdenite commonly occurs as a selvege along vein margins.

The quartz-wolframite-molybdenite veins occur as a stockwork system (known as Foleys zone), predominantly within the footwall

Crescent Spur Sandstone, but extending into the Hall Formation at the top. The stockwork system occurs as a steep-sided, vertical, cone-shaped body located in the centre of the sulphide lenses, with the nose of the cone extending into a low-grade zone in the upper ore-bodies (*cf.* Figs. 4.5 and 4.6). The central part of the cone consists of quartz veins bearing wolframite, molybdenite, bismuth and bismuthinite, and this is surrounded by an envelope in which molybdenite, bismuth and bismuthinite are minor to absent. Vein-ore relationships above the Nadir fault indicate that the quartz-wolframite veins are pre- (low-grade) ore (104333). The veins in this area contain abundant coarse cassiterite crystals, 2 - 3 mm in diameter, in addition to wolframite, with fluorite also appearing to be more abundant towards the nose or top of the cone.

The conical shape of the stockwork system appears to be centred on the altered quartz porphyry intrusive body which also is mineralised and penetrated by stockwork veins (Chapter 3). Further drilling of the Foleys zone will most likely show the stockwork veining to be concentric about the porphyry intrusive. The grade (in mass %) of mineralisation in the Foley zone is indicated in the following diamond drill hole intersections (from Aberfoyle Limited, Interim Directors Report, 1981):

D.D.H.	Intersection (m)	WO_3	MoS_2	Sn	Fluorite
C1485	165	0.30	0.03	0.06	-
C1608	125	0.26	0.04	0.04	5.9
C1611	162.5	0.30	0.03	0.04	-

Stage II

The second, and main stage of mineralisation includes the sulphide lenses and is conveniently divided into three types (Fig. 4.4): mineralisation occurring in reverse faults (*i.e.*, Nadir fault), as sulphide lenses (ore), and in veins in the surrounding host rocks.

FIG. 4.4 Mineralogy and paragenesis of the mineralisation episode at the Cleveland mine. Line thickness indicates relative abundance, dashed line = trace. Stage II mineralisation: Flt = mineralisation in reverse faults; Ls = limestone in the Hall Formation; Ore = sulphide lenses; Vein = veins in wall rocks. Paragenesis in the sulphide lenses is indicated by the relative length of lines and variation in line thickness indicates relative abundance.

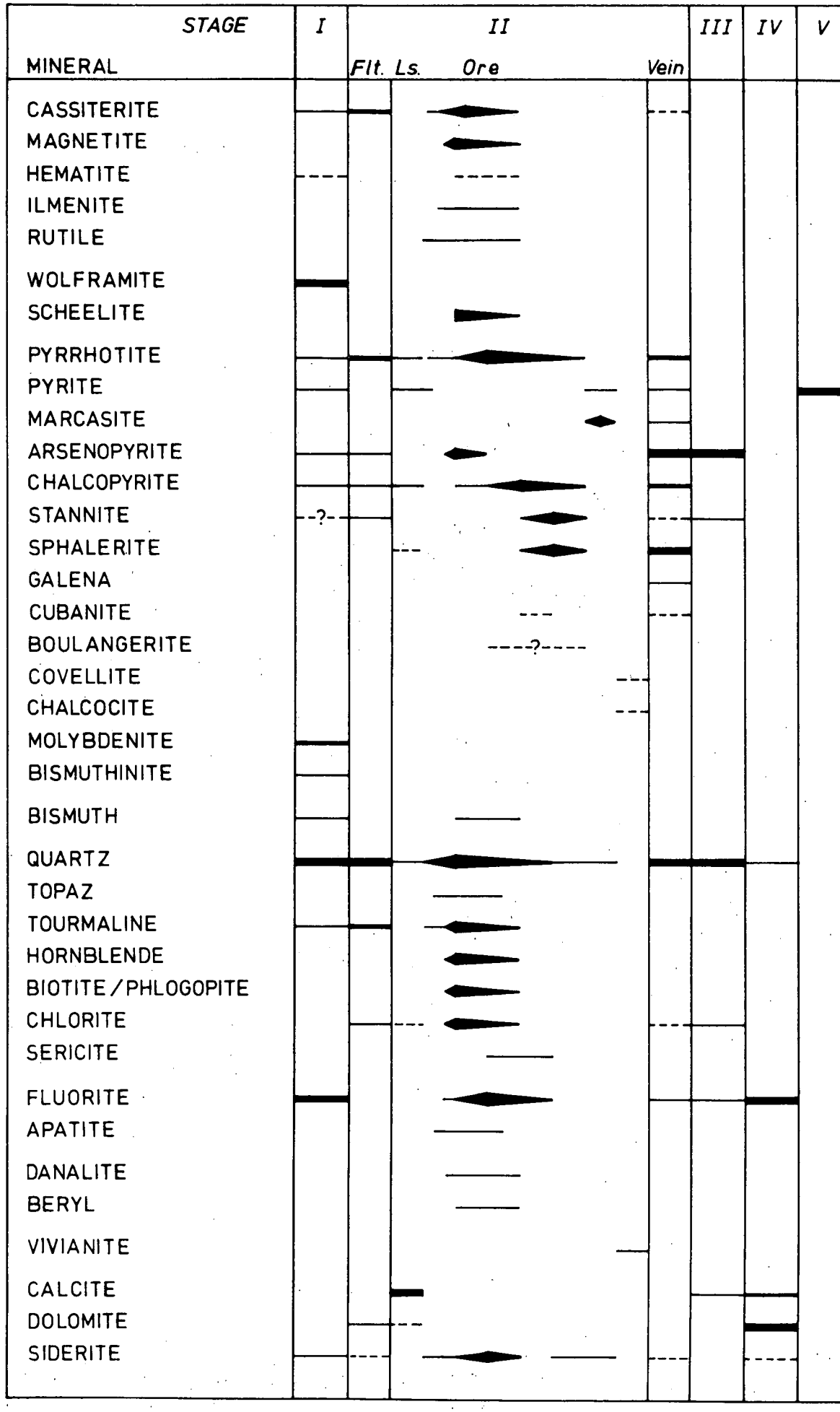
STAGE
MINERAL
I
II
III
IV
V
Flt.
Ls.
Ore
Vein
CASSITERITE
MAGNETITE
HEMATITE
ILMENITE
RUTILE
WOLFRAMITE
SCHEELITE
PYRRHOTITE
PYRITE
MARCASITE
ARSENOPYRITE
CHALCOPYRITE
STANNITE
?
SPHALERITE
GALENA
CUBANITE
BOULANGERITE
?
COVELLITE
CHALCOCITE
MOLYBDENITE
BISMUTHINITE
BISMUTH
QUARTZ
TOPAZ
TOURMALINE
HORNBLENDE
BIOTITE / PHLOGOPITE
CHLORITE
SERICITE
FLUORITE
APATITE
DANALITE
BERYL
VIVIANITE
CALCITE
DOLOMITE
SIDERITE

FIGURE 4.4

The mineralisation occurring in the south-east dipping reverse faults probably represents the initial phase of Stage II mineralisation and consists predominantly of white quartz which has been locally fractured and brecciated by post-stage II and pre-stage IV movement on the faults. In addition to quartz, the faults also contain varying amounts of tourmaline, chlorite, colourless fluorite, relatively coarse grained cassiterite, dolomite, arsenopyrite, pyrrhotite, stannite and chalcopyrite.

The sulphide lenses comprise about 90% of the total mineralisation and are composed of a complex combination of the minerals shown in Figure 4.4. Sulphides normally comprise 20 - 30% by volume of the sulphide lenses, occurring as disseminated grains and massive, irregular aggregates within and defining compositional layers. The main sulphide minerals are pyrrhotite (which may be altered to pyrite or marcasite), chalcopyrite and sphalerite with minor arsenopyrite, pyrite, stannite and trace galena. Chalcocite and covellite (Cox, 1968a), cubanite (Farrand, 1963) and native bismuth (Stillwell, 1944; Edwards, 1951) have also been reported in the ore. Cassiterite is the main tin mineral. The main gangue minerals are quartz, tourmaline, chlorite, hornblende, colourless fluorite and siderite with minor apatite, topaz, green biotite, sericite and beryl. In deep drill hole intersections of the lower ore, magnetite, coexisting with pyrrhotite, is prominent in the sulphide lenses, and in the lower levels of the mine , below 22 level (*i.e.* below about 1050 m M.L.), the sulphide lenses contain disseminated scheelite and danalite.

A zonal pattern in the mineralogy of the sulphide lenses was proposed by Cox (1968a) and further developed by Jessup (1970), Ransom and Hunt (1975) and Palmer (1976). Concentric zones have been defined above the Nadir fault, and are centred about the top of the quartz-wolframite-molybdenite stockwork vein system.

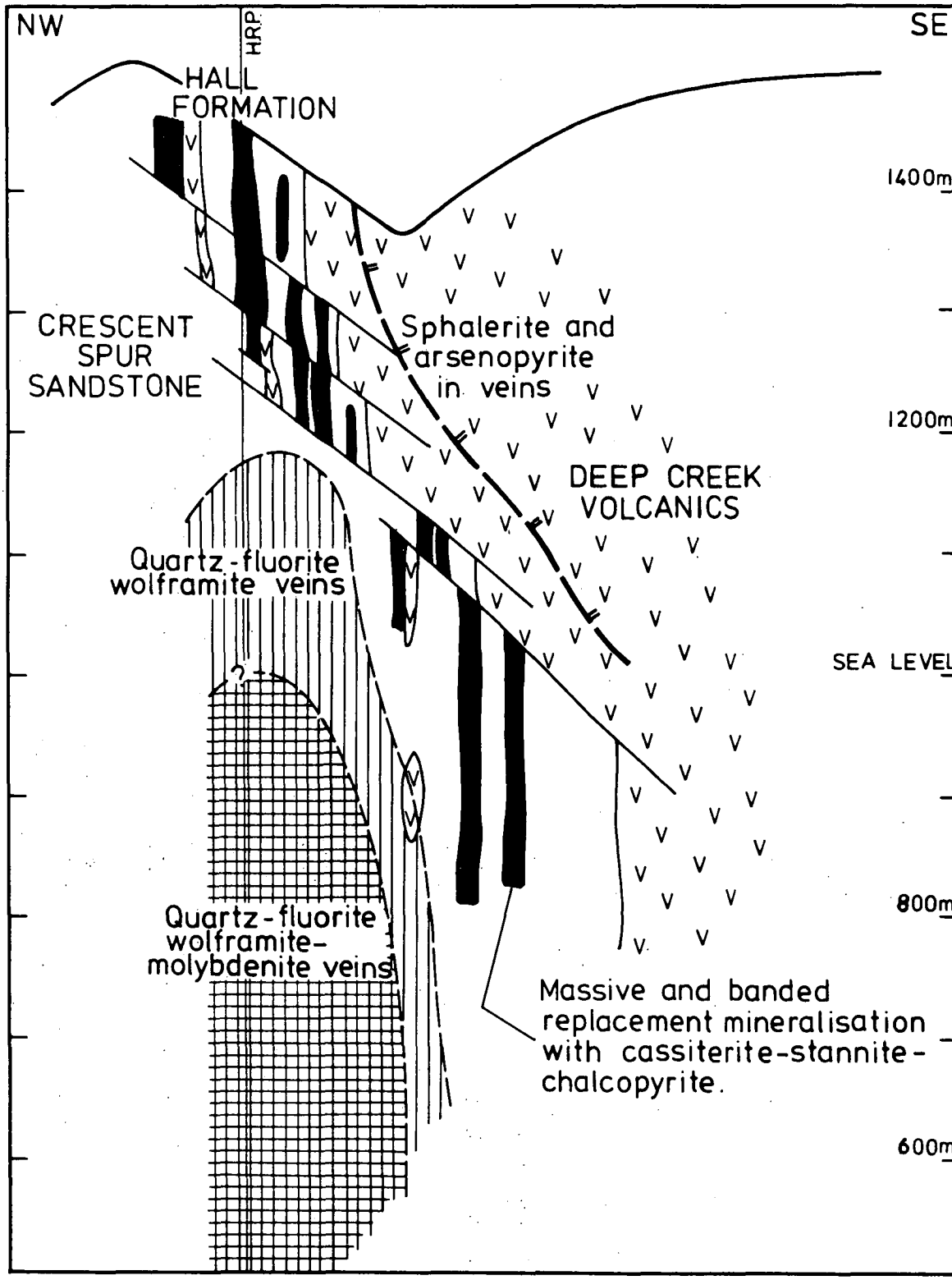

FIG. 4.5 Schematic geological section of the Cleveland mine (based on mine sections G, L and Qa, Fig. 4.6) illustrating the mineral zonation, and the position of the stage I stockwork veins in relation to the sulphide lenses (stage II).

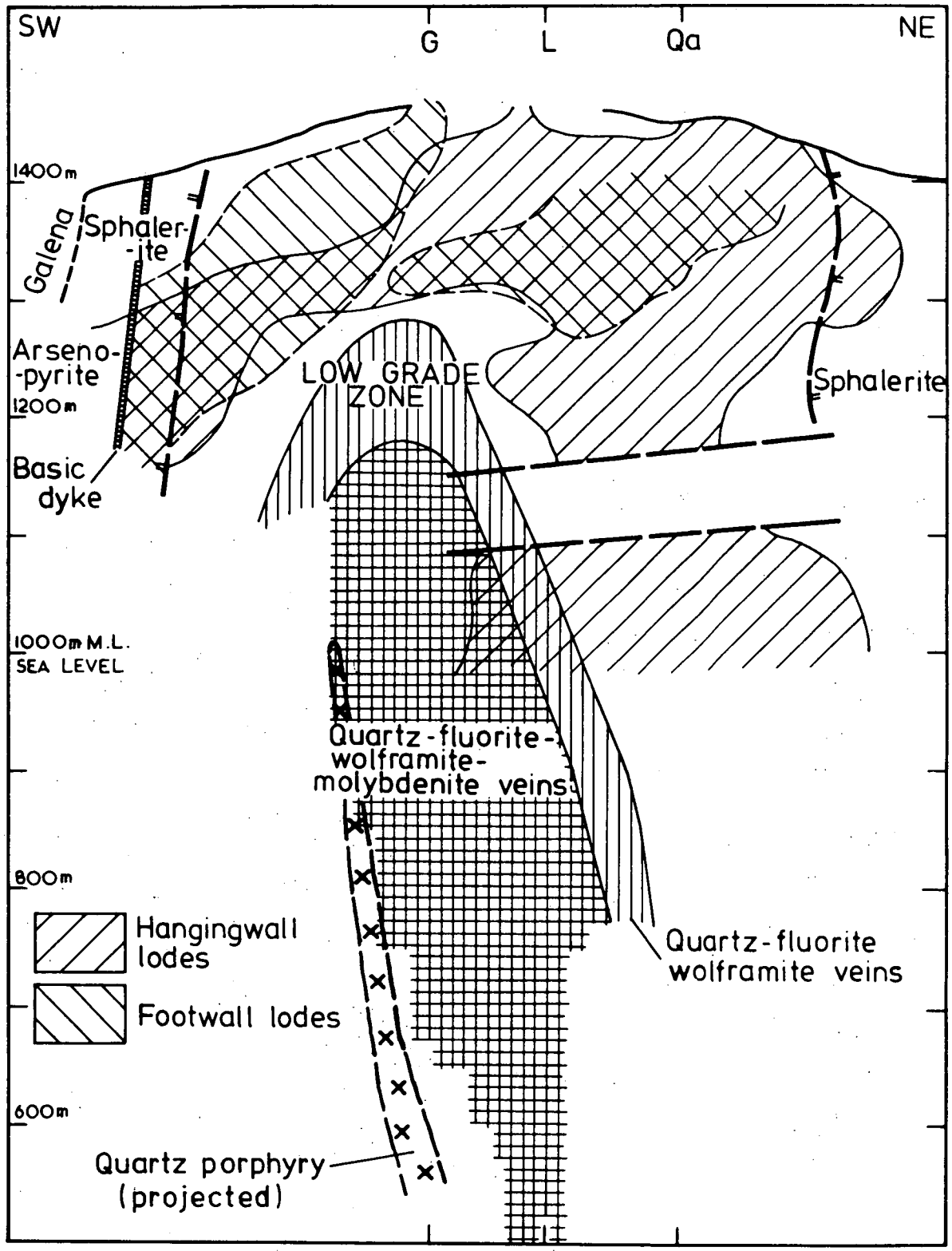

FIG. 4.6 Schematic longitudinal section of the Cleveland mine showing the location of the quartz-wolframite-molybdenite stockwork veins (stage I) in relation to the 'low-grade zone' and surrounding 'ore-grade' zones of the sulphide lenses (stage II) (see also Fig. 7.2), the mineralogical zoning in the two stages, and the projected position of a quartz porphyry intrusive.

The zones overlap and grade into one another, but are defined primarily by their cassiterite and sphalerite content. The central low-grade zone (Fig. 4.6), containing only trace tin, is surrounded by the ore zone containing 0.5 - 1% Sn, of which 5 - 15% occurs in stannite and the remainder in cassiterite (Palmer, 1976). The ore zones may be subdivided into two zones with the southern ore zone (mainly 'B South' lens) containing less chlorite, more tourmaline and more hypogene pyrite/marcasite alteration than in the northern ore zone. Surrounding the ore zone is a second low grade zone containing less than 0.1% Sn and increasing proportions of sphalerite and arsenopyrite. A fourth ore zone may be defined below Nadir fault, and is characterised by scheelite, magnetite and hornblende increasing in prominence with increased depth.

In addition to the observed variations in mineralogy of the sulphide lenses, as defined mainly for the upper levels of the mine, there is also a consistent decrease in their tin and copper content with depth. This is demonstrated in values of tin and copper ore grades for both ore mined and in ore reserves (Fig. 4.7). Although these values fluctuate because of variation in input of ore from various parts of the mine, there is a steady decrease in ore grades with time, and hence depth, beginning at 1.02% Sn and 0.43% Cu for the initial reserves in 1968 and decreasing to about 0.5% Sn and 0.22% Cu in 1981 (Fig. 4.7). Despite this variation in grade, the Cu:Sn ratio has remained constant at 0.40 ± 0.05, throughout the life of the mine. Although there are no analytical data available for tungsten, the decrease in tin and copper grade with depth is accompanied by the occurrence of visible scheelite below the Nadir fault.

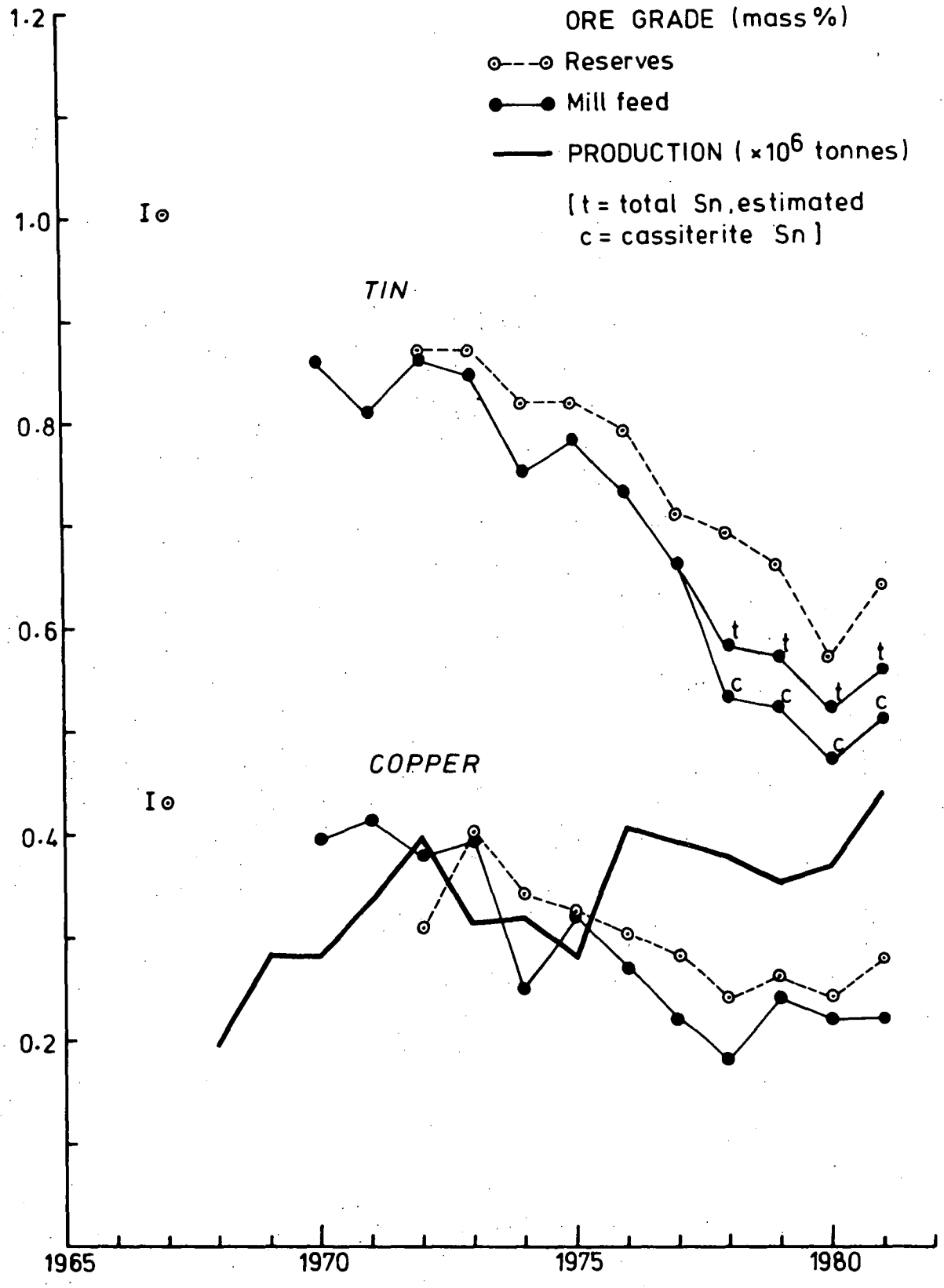

FIG. 4.7 Grade of Cleveland ore (mill head grade and reserve grade) in relation to year of production (or published reserves) and hence increased depth of mining. Production is total ore milled, I = initial 'starting up' reserves. Since 1978, mill feed head grade is quoted as cassiterite tin (c), and total tin (t) is estimated assuming 10% Sn as stannite. Source: Annual Reports of Director of Mines and Aberfoyle Ltd.

In the host rocks surrounding the deposit there are abundant quartz-sulphide veins containing minor amounts of chlorite, fluorite and carbonates. The sulphide minerals in these veins (pyrrhotite, pyrite, marcasite, chalcopyrite, sphalerite, arsenopyrite, stannite and galena) exhibit a distinct spatial distribution. Veins in limestone at the northern end of the deposit are dominated by sphalerite, pyrrhotite and arsenopyrite, which is consistent with the abundance of sphalerite and arsenopyrite at the extremities of the sulphide lenses (Fig. 4.6). In the hanging wall Deep Creek Volcanics, the veins contain predominantly pyrrhotite and chalcopyrite near the sulphide lenses, with sphalerite, arsenopyrite and minor galena appearing 50 - 60 m from the lenses (Fig. 4.5) and increasing in relative abundance away from the ore. A similar pattern occurs in the footwall Crescent Spur Sandstone at the southern end of the mine, but with increased abundance of galena.

Quartz-cassiterite-sulphide mineralisation also is locally developed in lithic and lapilli tuff beds within the Deep Creek Volcanics, close to the sulphide lenses (Palmer, 1976), and is correlated with Stage II mineralisation.

Stage III

This minor stage of the mineralisation episode consists of quartz, arsenopyrite, chlorite, green fluorite and minor stannite, sphalerite, chalcopyrite and carbonates occurring in veins, up to 10 mm thick, in the sulphide lenses and in cavities in the Nadir fault. The mineral composition of Stage III is similar to the Stage II quartz-sulphide veins which penetrate the host rocks, but is designated as a separate stage as it is clearly later than the sulphide lenses where it occurs as cross-cutting veins in banded ore, and in the Nadir fault, Stage III quartz is undeformed whereas earlier quartz is commonly fractured and brecciated.

Stage IV

Green fluorite, dolomite, calcite and quartz occurring in veins and lining vugs and cavities in faults and open joints is locally developed throughout the deposit and is the last major phase of the mineralisation episode.

Fluorite veins, up to 0.5 m in thickness, have been intersected in deep drill holes (*e.g.* 104429-31, 104457) at 520-550 m M.L. The green fluorite veins dissect Stage I veins (104454), and are correlated with Stage IV mineralisation in the mine.

Stage V

The final stage of the mineralisation episode consists simply of pyrite occurring as a coating on minerals lining vugs in the sulphide lenses and lining cavities in open veins, joints and faults.

Silver-lead-zinc deposits

Isolated, small Ag-Pb-Zn vein deposits occur throughout the Cleveland area (Fig. 4.1). The mineralisation is confined to thin quartz-carbonate-sulphide veins, the majority of which are structurally controlled by geologic contacts (Groves, 1966). To the west of Cleveland, the Godkin lodes (Godkin, Godkin Extended, Discover, Bells Reward and Whyte River mines; Fig. 4.1) occur along a north-northeast trending faulted contact between an Ordovician-Silurian sedimentary sequence and Cambrian mafic igneous rocks (Groves, 1966).

Closer to Cleveland, the Washington, Washington Hay, Confidence and Gregory lodes to the south-west of the mine and the W prospect to the north-east (at CQ658072; Fig. 4.1), may represent more remote parts of the Stage II mineralisation. The lodes to the south-west of Cleveland occur on faulted contacts within or between mafic igneous rocks of the Whyte River Complex and Cambrian volcano-sedimentary rocks. At the Washington Hay mine sphalerite and argentiferous galena are irregularly interbanded with quartz and siderite (Stage II(?) equivalent), with later clear quartz crystals (Stage IV(?)) and anhedral pyrite (Stage V(?))

lining vugs (104470). At the W prospect, quartz, arsenopyrite, sphalerite and chalcopyrite occur in veins, up to 50 mm thick (*e.g.* 78-453), dispersed throughout the Crescent Spur Sandstone and may correspond to the Stage II quartz-sulphide veins.

MINERALOGY OF THE WOLFRAMITE, MOLYBDENITE, CASSITERITE AND BISMUTH-BEARING VEINS (STAGE I)

The Stage I vein mineralisation has a simple mineralogy, dominated by quartz and fluorite with wolframite and minor sulphides (molybdenite, arsenopyrite, pyrrhotite, chalcopyrite and bismuthinite), native bismuth, cassiterite and other oxides, silicates and carbonates. The mineralogy of the veins is described below, and the mineralogy of the contemporaneously altered quartz porphyry has been previously described (Chapter 3).

Quartz is overwhelmingly the most abundant mineral in Stage I veins, occurring as milky-white, anhedral interlocking grains, intergrown with most other minerals. It contains inclusions of topaz, tourmaline, fluorite, wolframite, cassiterite and sulphides.

Fluorite is the next most abundant mineral occurring either as coarse aggregates in the central parts of some veins or intergrown with fine-grained quartz, tourmaline, wolframite and sulphides (104379). The fluorite is generally colourless, with a slight purple-brown tint, but commonly contains deep purple coloured, radial centres, 0.5 - 1 mm in diameter (104427, 104455). Coarse grained aggregates contain inclusions of (or interstitial) wolframite, molybdenite, native bismuth and bismuthinite.

Tourmaline occurs as fine needles up to 2 mm in length intergrown with quartz and fluorite and generally occurring near vein margins. Topaz occurs interstitially with quartz as anhedral grains

up to 0.5 mm in diameter, and as euhedral inclusions in quartz and fluorite. Carbonate (siderite) occurs interstitially with quartz and fluorite, but carbonates more commonly occur as rim replacements of pyrrhotite and arsenopyrite, and filling fractures in quartz and wolframite. Rutile is disseminated throughout the veins as needles, up to 0.5 mm in length, and hematite occurs rarely as red coloured flakes in fluid inclusions in fluorite (104455).

Wolframite is the dominant metallic mineral in the veins, occurring as bladed crystals intergrown with quartz, fluorite, cassiterite, molybdenite, bismith and bismuthinite. X-ray diffraction analysis (Appendix 4) shows it is the iron-rich variety ferberite, with about 10-20 mole% $MnWO_4$. It occurs either as randomly orientated, interlocking crystals (104382, 104432) or as radial clusters centred on vein margins. Wolframite blades are up to 50 mm in length, but most are less than 20 mm, and are generally 5 - 10 mm long (Plate 4.3F). It also occurs as irregular aggregates and as single bladed crystals (less than 3 mm long) disseminated throughout the veins (104380). The wolframite is distinctly anisotropic, and is characteristically twinned, with a single twin-plane parallel to the prominent bladed cleavage. Solid inclusions in wolframite are uncommon, but irregular inclusions (less than 0.1 mm across) of bismuth and bismuthinite, molybdenite flakes, rounded inclusions of arsenopyrite, and subhedral pyrite have been observed (104436, 104437). In specimen 104432, cassiterite occurs rarely as rounded inclusions 0.1 mm in diameter. Arsenopyrite and chalcopyrite also occur as impregnations along wolframite blade margins. Wolframite also occurs rarely as bladed crystals up to 0.05 mm long in arsenopyrite (104432).

Cassiterite is a minor component of the veins, occurring as anhedral to euhedral grains, up to 3 mm in diameter, and is intergrown with quartz, fluorite and wolframite (Plate 4.3F). It appears to be more abundant and coarser grained towards the top of the stockwork

PLATE 4.3 Photomicrographs of topazised quartz porphyry and Stage I mineralisation.

A: Altered quartz porphyry (48353) showing quartz phenocrysts and at right, a mesh of fine blades of wolframite. Scale bar = 1 mm, plane pol. light.

B: As above, X nicols, showing corroded margins of quartz in phenocrysts.

C: Cassiterite crystal with quartz and siderite in groundmass of altered quartz porphyry (48353). Scale bar = 100μm, plane pol. light.

D: As above, showing twinned cassiterite, X nicols.

E: Cassiterite (cs) intergrown with pyrrhotite (black) and silicates, fluorite etc. in groundmass of altered quartz porphyry (48352). Scale bar = 1 mm, plane pol. light.

F: Zoned cassiterite (cs) and wolframite blade (wo) intergrown with euhedral quartz (qz) and fluorite (fl) in Stage I vein (104333). Scale bar = 1 mm, plane pol. light.

G: Molybdenite platelets (mo) in native bismuth (bi) with minor bismuthinite (bis), adjacent to large wolframite blade (wo), Stage I (104436). Scale bar = 100μm, reflected light.

H: Intergrowth of arsenopyrite (as), bismuthinite (bis) and kinked and bent flakes of molybdenite (mo), Stage I (104432). Scale bar = 200μm, reflected light.

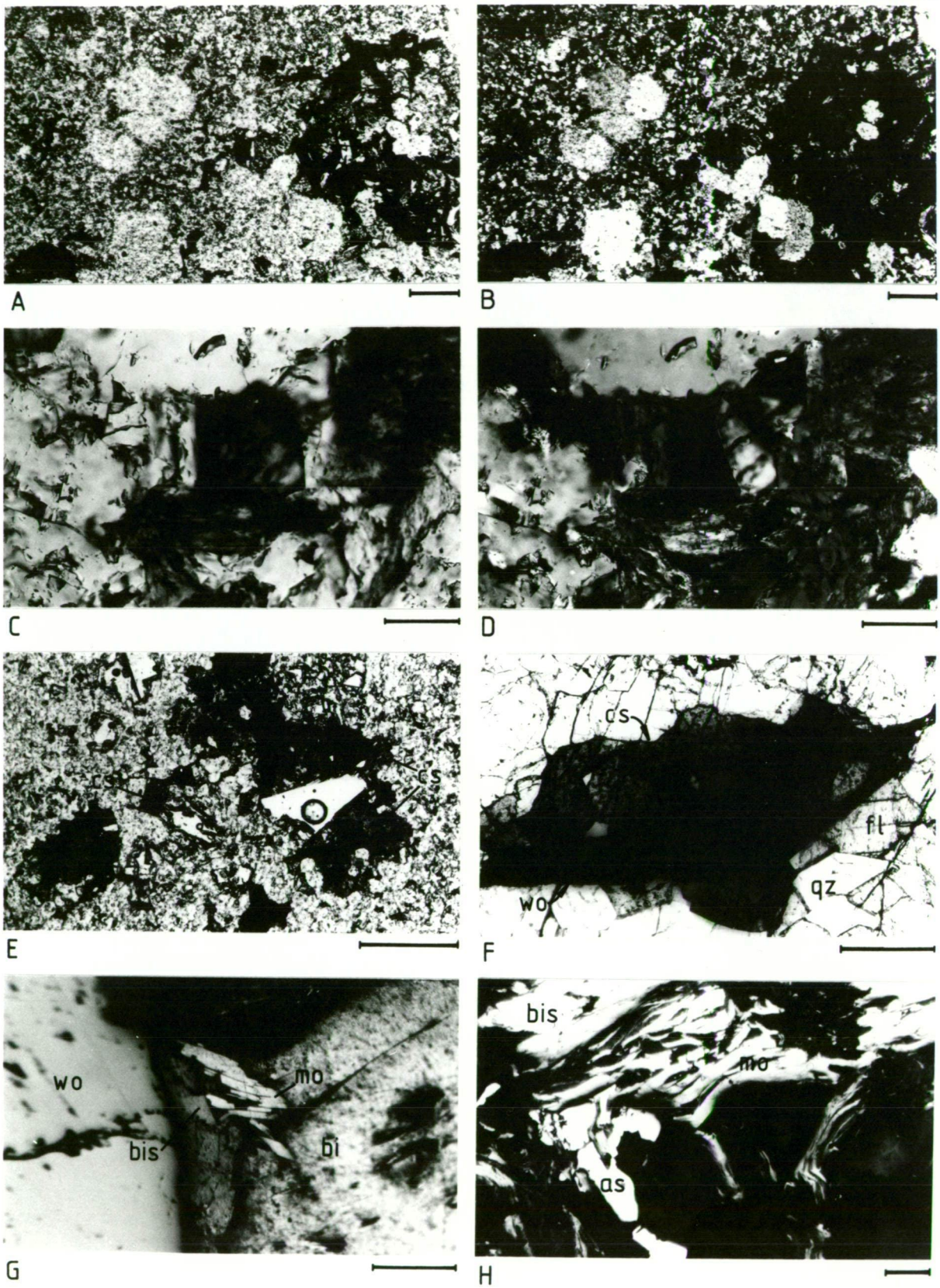

PLATE 4.3

vein system, and in the topazised quartz porphyry intrusive. Macroscopically, the cassiterite is dark brown to black in colour, but in thin section (104333) it is light to dark brown and commonly concentrically banded or zoned with alternating light and dark brown bands (Plate 4.3F). Solid inclusions have not been observed.

Molybdenite is concentrated in the central part of the stockwork zone (Fig. 4.5) occurring either as a selvege (2 - 3 mm thick) along the vein/host rock interface (*e.g.* 104378), or as flakes and books (1 - 5 mm long) disseminated throughout the veins (*e.g.* 104432). Flakes are commonly bent or kinked, and are intergrown with quartz, fluorite, wolframite, arsenopyrite, pyrrhotite, bismuth and bismuthinite (Plate 4.3G, H). It also occurs as inclusions in bismuthinite.

Native bismuth and bismuthinite occur as disseminated, irregular aggregates intergrown with quartz, fluorite, wolframite, arsenopyrite and molybdenite (Plate 4.3G, H), and as inclusions in quartz and wolframite. The occurrence of both native bismuth and bismuthinite has been confirmed by X-ray diffraction. They commonly occur as irregular and lamellar inclusions in each other, and as anhedral inclusions (up to 0.1 mm across) in wolframite and arsenopyrite (104432, 104437).

Arsenopyrite occurs throughout the veins as interstitial, disseminated anhedral grains and as subhedral-euhedral rhombs, up to 0.5 mm in length, and as rounded aggregates up to 4 mm in diameter (104432). It contains inclusions of wolframite and bismuth, and occurs as inclusions in bismuthinite and wolframite, and is intergrown with molybdenite (Plate 4.3H).

Pyrrhotite is the dominant iron sulphide, occurring sporadically throughout the veins as fine disseminatiions and as coarse aggregates, 2 - 3 mm across. It occurs interstitially with quartz, fluorite and tourmaline, and in specimen 104379 is marginal to euhedral quartz grains. Pyrrhotite also exhibits mutual boundary relationships with

molybdenite and bismuthinite (104380).

Chalcopyrite occurs as interstitial, finely disseminated anhedral grains, as irregular masses associated with the larger pyrrhotite aggregates, and occurs rarely in quartz as rounded inclusions, about 0.05 mm in diameter. An isotropic, olive-brown coloured mineral occurs rarely in association with chalcopyrite and carbonate in specimen 104379, but its identification as either stannite or tetrahedrite-tennanite has not been ascertained.

Pyrite occurs as euhedral crystals, commonly fractured and healed with carbonate, in late carbonate veins intersecting the quartz veins. Pyrite/marcasite also occurs as fine grained aggregates marginal to, and replacing pyrrhotite.

MINERALOGY OF THE CASSITERITE-CHALCOPYRITE-STANNITE MINERALISATION (STAGE II)

The tin and copper-bearing stratiform replacement sulphide lenses and associated fault-filling and vein mineralisation at Cleveland have a relatively simple mineralogy with a limited number of metallic sulphides (principally pyrrhotite, chalcopyrite, sphalerite and stannite) and oxides (magnetite, cassiterite and rutile), and silicates (quartz, tourmaline, chlorite, hornblende and biotite/phlogopite), fluorite and carbonates. Macroscopically, the ore consists predominantly of pyrrhotite with minor chalcopyrite, and quartz, chlorite, tourmaline, siderite and hornblende. Cassiterite is generally too fine grained to be visible macroscopically, though clusters of coarse (> 1 mm) cassiterite crystals are relatively common in early fault fillings and associated veins such as the Nadir fault (Plate 3.5). Chalcopyrite commonly occurs as coarse aggregates with massive pyrrhotite, but stannite is rarely visible.

Previous mineragraphic and mineralogic examinations by Stillwell (1944a, b), Edwards (1951), Farrand (1963), Everard (1964), Cox (1968a) and Groves (1968) were undertaken on specimens collected from old surface workings and from the upper parts of the sulphide lenses, prior to the present large scale development. They provide valuable information on the mineralogy of the uppermost parts of the deposit, much of which is now inaccessible. Of particular importance is the apparent abundance of arsenopyrite and sphalerite, which from this investigation are shown to be most abundant at the lateral extremities of the sulphide lenses. This suggests that the present ground surface is close to the top or upper limit of the sulphide lenses, a conclusion which is supported by the geometry of the ore (Figs. 4.6, 7.2).

Cassiterite-sulphide mineralisation also occurs in lithic tuff beds, adjacent to faults and/or veins, within the Deep Creek Volcanics, in close proximity to the sulphide lenses. The mineralised lithic tuff (104383) is similar to lithic tuff elsewhere in the host sequence, consisting of elongate-rounded lithic fragments, 0.5 - 30 mm in length (generally 2 - 6 mm), in a matrix dominated by wispy, chloritic, devitrified glass shards with angular quartz grains, up to 0.05 mm in diameter, clays, calcite and chlorite (Plate 4.4A). The tuff is veined by numerous quartz stringers with minor carbonate, sulphides, chlorite and cassiterite; and is replaced by quartz and sulphides occurring in radial aggregates with nucleii of fine grained quartz, chlorite, carbonate and sulphides (Plate 4.4A). Quartz in the radial aggregates occurs as interlocking grains, 0.2 - 0.3 mm in diameter, with minor interstitial topaz occurring as euhedral crystals up to 0.05 mm in diameter. Cassiterite is relatively common in the radial aggregates occurring as anhedral to euhedral grains, 0.1 - 0.2 mm in diameter,

and up to 0.7 mm in length (Plate 4.4A). Sulphides are dominantly sphalerite and chalcopyrite, occurring as irregular masses intergrown with quartz, and exhibit mutual boundary relationships, and contain small inclusions and exsolution bodies of each other. Pyrrhotite occurs as exsolution bodies or inclusions in sphalerite, commonly as composites with chalcopyrite. Galena occurs at sphalerite-chalcopyrite boundaries and rarely as inclusions in sphalerite and chalcopyrite. The irregular masses of sphalerite and chalcopyrite are generally marginal to the radial aggregates and thus probably later than the quartz and cassiterite.

The mineralogy and paragenesis of Stage II mineralisation as determined by this investigation and supplemented with data from previous examinations, is shown in Figure 4.4. Detailed descriptions of the minerals are given below in the same order and groups as in Figure 4.4 (*i.e.* oxides, tungstates, sulphides, silicates, halides etc.). Descriptions generally refer to the sulphide lenses unless specified otherwise. The occurrence of wollastonite and cordierite in Cleveland ore recorded by Everard (1964) has not been confirmed by this investigation, and their occurrence was also neither confirmed by Groves (1968) nor recorded by Cox (1968a).

Cassiterite

Cassiterite is the dominant tin mineral in Cleveland ore. It occurs throughout the sulphide lenses as anhedral-euhedral (idioblastic) twinned crystals (Plate 4.4 B-E). Grain sizes typically are less than 0.1 mm in diameter and most are within the range of 0.01 - 0.05 mm. A grain size analysis of cassiterite in the upper levels of the mine (Manson *et al.*, 1963), indicated that only 16% of grains are greater than 0.15 mm; 27% greater than 0.1 mm and 35% passed 0.04 mm. The maximum dimensions of idioblastic crystals

in the thin and polished sections examined are about 1 mm in diameter in cross-section and about 3 mm in length. The coarsest cassiterite occurs as columnar or acicular crystals in quartz veins in reverse faults (*e.g.* Nadir fault; 104368, 104438; Plate 4.4B). In the sulphide lenses, the coarsest cassiterite is in silicate rich bands (*e.g.* 104323) and in fluorite masses and veinlets (*e.g.* 104329), where it may be up to 1 mm in largest dimension. Cassiterite occurs as a minor component of Stage II veins surrounding the deposit, in close proximity to the sulphide lenses.

Cassiterite occurs either disseminated as single grains throughout the ore, or in clusters up to 4 mm in diameter, commonly in a silicate and/or fluorite rich gangue. Cox (1968a) and Cox and Glasson (1971) suggest that although cassiterite distribution is unrelated to sulphides, it is concentrated in quartz and/or carbonate rich laminae and depleted in chlorite and/or mica-rich laminae.

Macroscopically, the coarsest cassiterite is red-brown to pale brown (honey) in colour, which contrasts with the dark brown-black cassiterite in Stage I veins. In thin section, cassiterite is colourless to pale brown, and typically shows fine internal banding (Plate 4.4E), with alternating colourless and pale brown, or pale and dark brown laminae. Cassiterite grains generally have dark coloured cores and pale coloured rims, but this observation is not universally applicable. Rare grains of green coloured cassiterite with green and green-brown colour banding occur in specimen 104304. This cassiterite also contains rutile inclusions, which suggests that the green colouration may be due to titanium substitution.

Solid inclusions in cassiterite are rare, but tourmaline, rutile, topaz, hornblende, magnetite, pyrrhotite and chalcopyrite have been observed. In some sections (104323, 104353, 104391), the core of cassiterite grains contain numerous, minute acicular inclusions, similar to an early generation of 'dirty' quartz (Plate 4.4D).

PLATE 4.4 Photomicrographs of mineralised lithic tuff and of cassiterite mineralisation, Stage II.

A: Mineralised lithic tuff, Deep Creek Volcanics (104383), showing quartz veining (lower right) and a cluster of radiating quartz crystals, replacing lithic fragments, and centred on a nucleus of fine grained quartz and chlorite. A large cassiterite crystal (cs) is intergrown with quartz. Scale bar = 1 mm, plane pol. light.

B: Idiomorphic cassiterite crystals in quartz (white) and a mass of fine needles of tourmaline (grey), Nadir fault (104368). Cassiterite crystal at lower left shows rim replacement by stannite. Scale bar = 1 mm, plane pol. light.

C: Twinned cassiterite crystal with inclusions of fine tourmaline needles, in sulphide lens (104358). Scale bar = 100µm, X nicols.

D: Acicular inclusions in 'dirty' cassiterite intergrown with 'dirty' quartz, sulphide lens (104358). Scale bar = 100µm, plane pol. light.

E: Zoned cassiterite in quartz, Nadir fault (104368). Scale bar = 100µm, plane pol. light.

F: Arsenopyrite rhomb (as) intergrown with cassiterite (cs), Nadir fault (104438). Scale bar = 100µm, reflected light.

G: Pyrrhotite (po) and magnetite (mt) intergrowth in sulphide lens (104451). Scale bar = 100µm, reflected light.

H: Magnetite (mt) intergrown with and as inclusions in cassiterite (cs), in sulphide lens (104451). Scale bar = 100µm, reflected light.

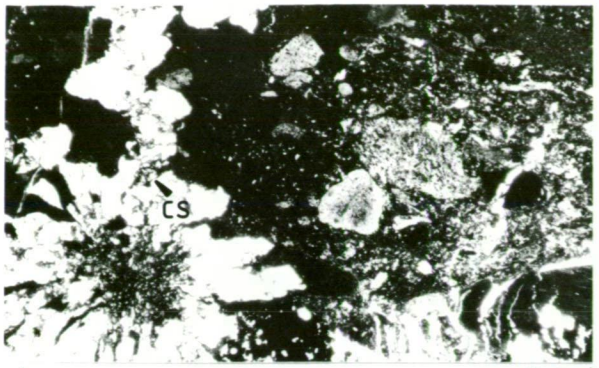

A

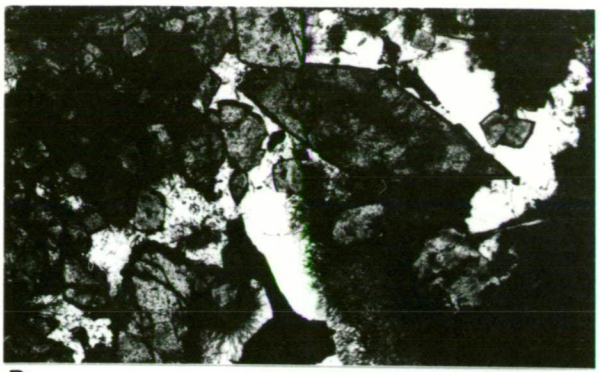

B

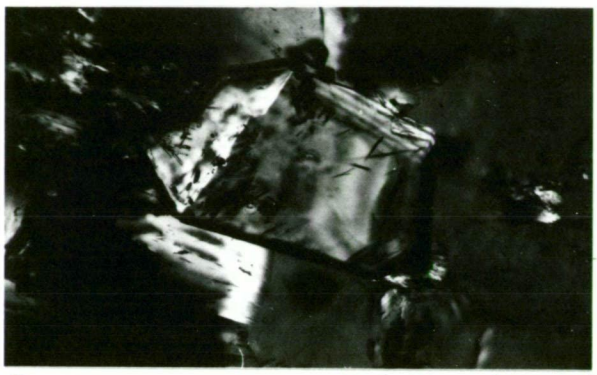

C

D

E

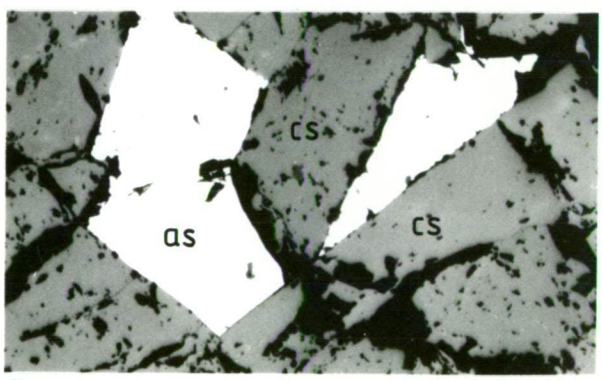

F

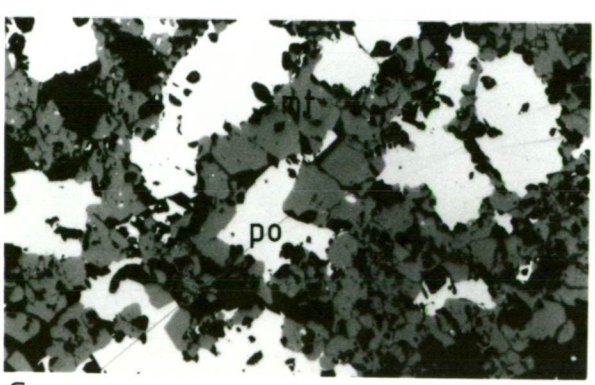

G

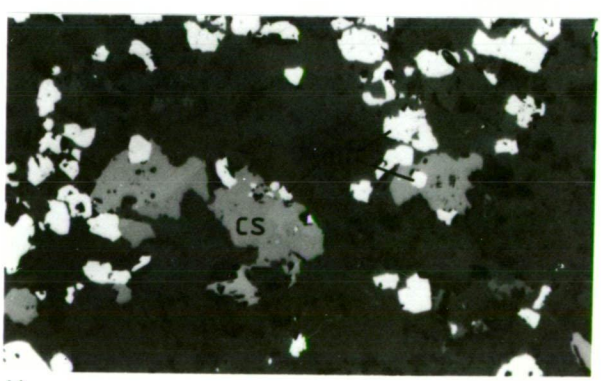

H

PLATE 4.4

Cassiterite occurs as anhedral to irregular grains intergrown with quartz, tourmaline, hornblende and chlorite, and as idioblastic crystals in pyrrhotite, quartz, carbonate and fluorite. In tourmaline-rich zones in Nadir fault (*e.g.* 104368), cassiterite grain boundaries are pierced by fine tourmaline needles. Cassiterite is one of the earliest minerals deposited, but is extensively replaced by stannite, occurring either as rims around or as veinlets in and dissecting cassiterite grains (Plate 4.7H). Stannite replacement commonly occurs where cassiterite is associated with sulphides, carbonate and fluorite and is generally absent where cassiterite is enclosed in quartz, tourmaline and hornblende. Cassiterite grains enclosed in pyrrhotite masses, commonly have narrow rims of stannite, and some grains have been almost totally replaced (*e.g.* 104441). Cox (1968a) recorded fractures in cassiterite filled with quartz and wolframite, but this has not been confirmed by this study.

Magnetite

Magnetite is restricted in its occurrence to the lower ore, and is apparently more abundant with increased depth. It occurs in deep diamond drill core intersections of the sulphide lenses in excess of 400 m below surface (*i.e.* below sea level).

Magnetite occurs as bands of massive, polycrystalline aggregates and as fine disseminated grains (104451, 104452). The aggregates consist of anhedral to euhedral (cubic) grains generally 0.02 - 0.1 mm, but up to 0.3 mm in diameter. Some of the larger grains exhibit a faint concentric zoning defined by slight variations in colour (in reflected light). Magnetite also occurs as short acicular inclusions (0.05 mm long) in hornblende, and as rounded inclusions in pyrrhotite and cassiterite (Plate 4.4H), and also contains rounded inclusions of pyrrhotite (Plate 4.4G). It is replaced rarely by late siderite (*e.g.* 104459).

Farrand (1963) also recorded small magnetite inclusions in amorphous pyrite, but this is probably associated with later alteration of pyrrhotite.

Hematite

Hematite occurs rarely as minute red coloured flakes trapped as accidental minerals in fluid inclusions in fluorite in deep drill core sections of the sulphide lenses (*e.g.* 104423; Plate 5.1 S). Groves (1968) described small irregular patches of hematite associated with quartz and partially replaced by sulphides.

The presence of hematite associated with a pyrrhotite dominated assemblage, clearly is anomalous and its origin is enigmatic. Its occurrence in fluid inclusions indicates it may have been transported in fluid from much greater depths. *In situ* deposition in the sulphide lenses is highly unlikely, as this would have required dramatic changes in oxygen fugacity (3 to 4 log fO_2 units).

Ilmenite

Ilmenite is a minor component of the sulphide lenses commonly associated with rutile, and finely disseminated as platey-bladed crystals up to 0.2 mm in length (*e.g.* 104340).

Rutile

Rutile (and/or anatase) is a relatively common accessory mineral being widely distributed throughout the sulphide lenses, and occurring rarely as inclusions in cassiterite (*e.g.* 104304). It is intergrown with or earlier than most silicates, sulphides, fluorite and carbonate. Stillwell (1944a) describes lath-like crystals of rutile along cleavage planes in chlorite as a possible alteration product of conversion of mica to chlorite.

Rutile occurs as translucent brown, short prismatic crystals generally 0.01 - 0.02 mm in length which occur sporadically as fine disseminations in the ore, but more commonly as 'needles' up to 2 mm in length. The rutile 'needles' are made up of numerous short,

interlocking, geniculated euhedra, commonly with intergrown ilmenite.

Wolframite

Wolframite has been previously described as occurring as rare discrete bladed crystals, up to 0.5 mm in length associated with, and replaced by quartz (Cox 1968a; Groves 1968). It has also been described as occurring as prismatic crystals, up to 0.05 - 0.3 mm, commonly orientated parallel to 'bedding' in chlorite-rich laminae and randomly orientated and enclosed by later sulphide in sulphide-rich laminae (Cox and Glasson, 1971). Also, Farrand (1963) described small ragged rods of wolframite dispersed in the 'country' rock or with sulphides. The occurrence of wolframite in the sulphide lenses has not been confirmed by this investigation.

Scheelite

Scheelite has been only recently detected in the sulphide lenses, in the lower ore in development drives below 20 level. It is disseminated through the ore as anhedral, granular aggregates, up to 5 mm in diameter but generally less than 1 mm, and is intergrown with quartz, hornblende, pyrrhotite and chalcopyrite (104302).

Pyrrhotite

Pyrrhotite is the dominant sulphide mineral in the sulphide lenses, but is subordinate to sphalerite and arsenopyrite in quartz veins surrounding the deposit.

In the sulphide lenses, pyrrhotite occurs as anhedral grains which either occur as fine disseminations or form large, irregular, interlocking masses. The grain size (visible under cross polarised light) varies considerably from about 0.05 - 0.2 mm in diameter where it occurs as fine interstitial disseminations and in thin bands (104324), to coarse (> 5 mm in diameter) anhedral interlocking grains in large polycrystalline pyrrhotite masses (104316, 104340). Coarse grained pyrrhotite exhibits lamellar growth and/or transformation twinning, and exhibits minor kinking or deformation of the twin planes.

Pyrrhotite exhibits local preferred orientation (Falvey, 1966; Ransom and Hunt, 1975), possibly associated with post-Stage II movement on the reverse faults. It has a monoclinic symmetry, although etching has indicated the presence of minor blebs of hexagonal pyrrhotite (Groves, 1968). Pyrrhotite in the sulphide lenses contains 59.86 - 61.02 (average 60.45) mass % Fe and 37.77 - 40.14 (39.19) mass % S (Table A4.2), which is equivalent to 46.12 - 48.12 (average 46.96) atomic % Fe. Minor copper in the pyrrhotite (0.18 - 0.42 mass % Cu) is probably present as minutely exsolved chalcopyrite.

Pyrrhotite is either intergrown with, or occurs interstitially with most non-sulphide gangue minerals (*i.e.* quartz, chlorite, tourmaline, amphibole, fluorite, siderite, etc.) and with cassiterite and scheelite. It replaces and invades fractures in pyrite and rarely arsenopyrite, and is replaced by chalcopyrite, stannite and sphalerite, and by a second generation of pyrite and/or marcasite. Replacement by late carbonate is widely developed throughout the sulphide lenses, generally occurring as narrow rims (0.05 - 0.2 mm thick), and as veins in pyrrhotite masses. In some cases, pyrrhotite has been almost completely replaced, leaving only tiny remanent grains in a fine grained carbonate mass. Replacement by second generation pyrite/marcasite is evident generally in the upper ore, and in veins surrounding the deposit. In the sulphide lenses it occurs around the margins of pyrrhotite masses and along fracture margins, and commonly is associated with late carbonate alteration.

In deep drill hole intersections (104451, 104452, 104459), pyrrhotite co-exists with magnetite, occurring as interstitial grains in magnetite rich bands, and as irregular pyrrhotite rich masses and bands of interlocking anhedral grains (0.02 - 0.05 mm) with interstitial anhedral to euhedral magnetite (Plate 4.4G). It also occurs as minute inclusions in magnetite.

Pyrrhotite also occurs as spherical (oolitic) structures, 2 - 8 mm in diameter, sporadically developed within more massive equigranular bands in the sulphide lenses. Cox (1968a) described these structures as commonly having an internal concentric structure with a core of quartz ± pyrrhotite surrounded by a rim of pyrrhotite and quartz. Others consist entirely of an intergrowth of pyrrhotite and quartz, with no apparent internal structure. Similar spherical structures in 104441 consist of fine grained pyrrhotite concentrated in a circular mass about 5 mm in diameter, with no apparent internal structure and a margin that is gradational to disseminated pyrrhotite in the surrounding ore. The origin of these structures is enigmatic, as any original texture was most likely destroyed during ore formation and recrystallisation, though Cox (1968a) favoured formation from a gel during a later phase of the mineralisation episode.

A second generation of pyrrhotite in the sulphide lenses occurs as exsolution bodies and interstitial inclusions and as veinlets in sphalerite and chalcopyrite (*e.g.* 104352).

In ore and veins (?) at the northern end of the sulphide lenses (104370, 104371), pyrrhotite occurs as irregular masses, as fine (< 0.05 mm) disseminations, and as small rounded inclusions and/or exsolution bodies in arsenopyrite, but is most common as inclusions and exsolution bodies in sphalerite where it occurs as rounded blebs of either pyrrhotite or composites of pyrrhotite and chalcopyrite, and as needle-like exsolution bodies. In some sphalerite, pyrrhotite inclusions are so dense that it has a leopard spot appearance (*e.g.* 104371).

In the veins surrounding the sulphide lenses, pyrrhotite occurs either as large irregular masses intergrown with and/or interstitial to quartz and other sulphides, or as inclusions or exsolution blebs in sphalerite and less commonly in chalcopyrite and rarely in arsenopyrite and pyrite. Much of the pyrrhotite in the veins has been

replaced by porous masses of finely granular pyrite/marcasite with interstitial carbonate and quartz, leaving only irregularly shaped remanent cores of pyrrhotite (Plates 4.5E and 4.5F). Pyrrhotite occurs in sphalerite either as rounded inclusions, or as rounded, ovoid, needle-like and highly irregular exsolution blebs occurring either as monomineralic bodies or as composite bodies with chalcopyrite. Exsolution textures are discussed in more detail in descriptions of sphalerite.

Pyrite and marcasite

Pyrite occurs in trace to minor amounts in the sulphide lenses, but is relatively common in the surrounding veins. In the sulphide lenses, pyrite occurs rarely as discrete grains or in bands of subhedral-euhedral grains, 0.5 - 1 mm across (104375). It contains rare inclusions of pyrrhotite and chalcopyrite. The pyrite crystallised prior to the majority of the pyrrhotite and other sulphides which commonly have replaced it around grain margins and invaded it as small veinlets, and it is replaced by a late generation of carbonate. The pyrite euhedra may represent an early phase of pyrite deposition prior to, or contemporaneous with pyrrhotite. Alternatively, it may represent relicts of pyrite occurring in the original limestone. Similar pyrite euhedra occur in limestone at the northern end of the mine (48295) and in the 'eastern sediments' (48312).

A second generation of pyrite, probably resulting from hypogene alteration of pyrrhotite, is widespread as a minor component of the sulphide lenses but a significant component of veins surrounding the deposit. It typically occurs as porous masses of minutely granular pyrite and/or marcasite, with interstitial carbonate and/or quartz. In the sulphide lenses, this pyrite has developed as a replacement of pyrrhotite either at the margins of large masses or within pyrrhotite adjacent to carbonate ± quartz veinlets (104375).

Much of the pyrrhotite in veins surrounding the sulphide lenses has been replaced by second generation pyrite/marcasite, typically occurring as very fine grained, banded, porous masses, commonly containing remnants of pyrrhotite (Plate 4.5F). 'Birds-eye' textures are commonly developed, occurring as lenticular remnants of pyrrhotite surrounded by concentrically banded pyrite (Plate 4.5E). Alteration and replacement of pyrrhotite initially occurred along fracture margins and then spreading along fronts through the pyrrhotite (Plate 4.5F). Other sulphides (*i.e.* sphalerite, chalcopyrite, arsenopyrite) are unaffected by this alteration (Plate 4.5F). In places, the finely granular pyrite/marcasite masses appear to have recrystallised to form medium to large euhedral pyrite crystals (cubes, rhombs and blades) with interstitial carbonate and quartz (Plate 4.5H). Similar textures have been observed in the Mt Bischoff ore, where euhedral pyrite is also attributed to recrystallisation of fine grained masses of pyrite and marcasite (Groves *et al.*, 1972).

An hypogene origin for second generation pyrite and/or marcasite is indicated by the absence of any control over its distribution by the present land surface and its common association with a late generation carbonate.

Arsenopyrite

Arsenopyrite is a relatively minor component of the ore, but is relatively abundant towards the extremities of the sulphide lenses, and in quartz veins in faults (*i.e.* Nadir fault). It is one of the earliest minerals to be deposited, occurring as rhombs intergrown with quartz and cassiterite (Plate 4.4F), and as anhedral grains intergrown with cassiterite and tourmaline (104438). Inclusions in arsenopyrite are rare, generally occurring as small rounded blebs of pyrrhotite, chalcopyrite (?), cassiterite (< 0.02 mm) and small quartz grains. It is replaced by pyrrhotite, sphalerite and carbonate.

PLATE 4.5 Photomicrographs of Stage II sulphide lenses and veins.

A: Pyrrhotite (po) replaced by chalcopyrite (cp) and stannite (st), sulphide lens (104310). Scale bar = 100μm, reflected light.

B: Chalcopyrite (cp) replaced by stannite (st), sulphide lens (104310). Scale bar = 100μm, reflected light.

C: Cassiterite (cs) showing rim replacement by stannite (st), sulphide lens (104310). Scale bar = 100μm, reflected light.

D: Arsenopyrite (as) replaced(?) by sphalerite (sp) containing inclusions of pyrrhotite and chalcopyrite (cp). Sphalerite and arsenopyrite replaced(?) by galena (gn). Vein in Crescent Spur Sandstone (104392). Scale bar = 100μm, reflected light.

E: 'Bird's eye' texture of concentric bands in second generation pyrite/marcasite, about remanent pyrrhotite. Vein in Crescent Spur Sandstone (104468). Scale bar = 200μm, reflected light.

F: Granular mass of second generation pyrite/marcasite from hypogene alteration of pyrrhotite (po). Sphalerite (sp) is unaffected by the alteration which appears to have been controlled by fractures in pyrrhotite. Vein in Crescent Spur Sandstone (104468). Scale bar = 200 μm.

G: Fractures in arsenopyrite (as) and in sphalerite (sp) healed with chalcopyrite (arrowed in arsenopyrite). Vein in Hall Formation (104453). Scale bar = 100μm, reflected light.

H: Recrystallised second generation pyrite (py) enclosing galena (gn), and segregation of pyrite and carbonate (dark grey). Vein in Deep Creek Volcanics (104467). Scale bar = 100μm, reflected light.

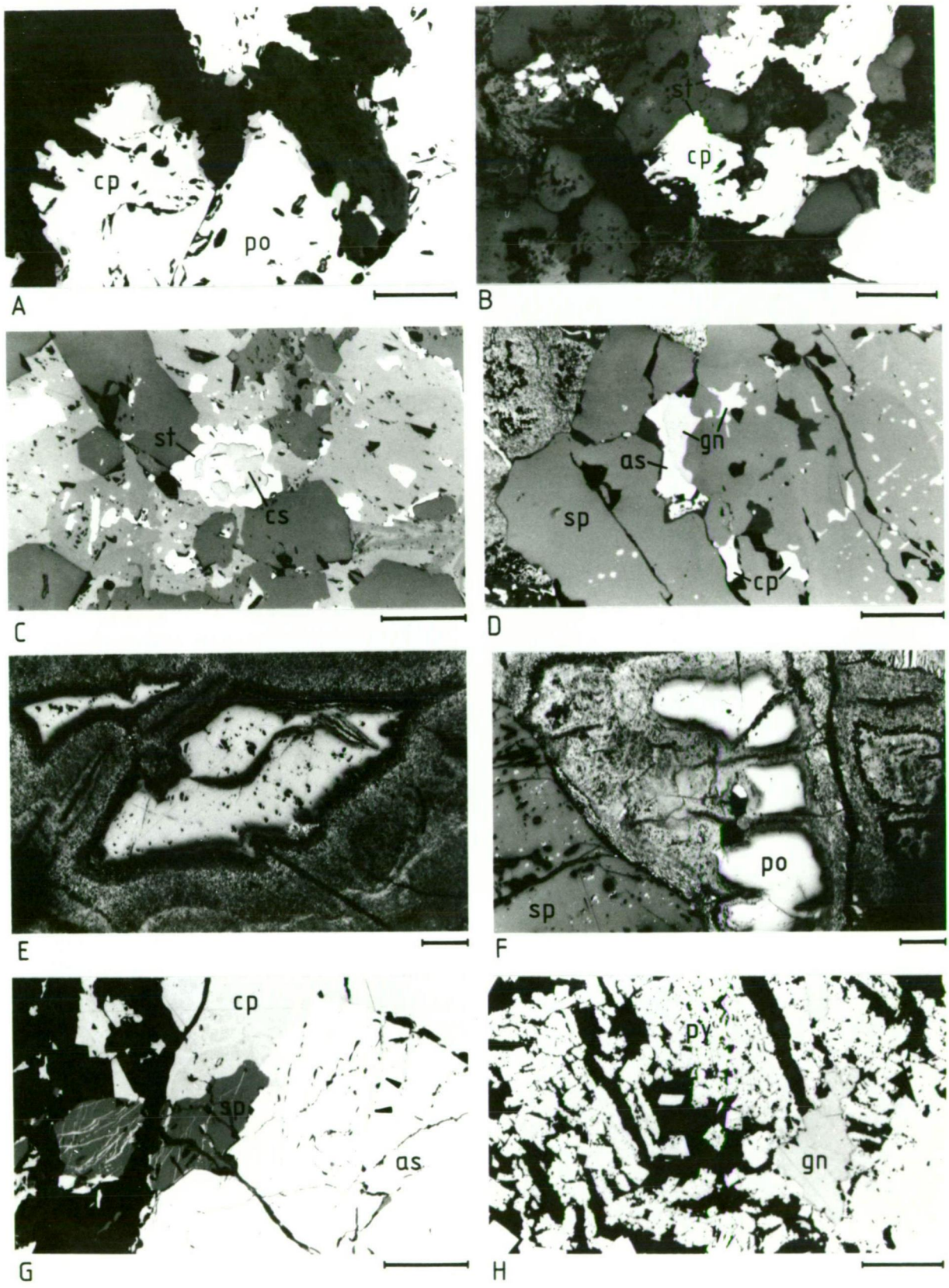

PLATE 4.5

TABLE 4.1. Compositions of arsenopyrite from the Cleveland mine (full details given in Appendix 4, Table A4.3).

Sample no.	Description*	As (atomic %)
Stage II		
104366	Nadir fault (po, cp)	34.6
104438	Nadir fault (po)	33.6
104370	Ore/vein in limestone (po, cp)	32.9, 32.7
104435	Vein, Deep Creek Vol. (sp, cp, po)	34.0
104465	Vein, Deep Creek Vol. (sp, cp, gn)	31.8
104466	Vein, Deep Creek Vol. (sp, cp, po, gn)	33.9
104469	Vein, Crescent Spur Sst. (sp, po, cp, gn)	33.3
Stage III		
104366	Vug in Nadir fault (st)	32.5
104368	Vug in Nadir fault (st)	32.7, 32.6
104376	Vein in ore	33.3
104449	Vein in ore (sp, cp)	33.1

* Other co-existing (?) sulphides in brackets : cp = chalcopyrite, gn = galena, po = pyrrhotite, sp = sphalerite, st = stannite.

At the extremities of the sulphide lenses, arsenopyrite occurs as large idioblastic crystals, generally 3 - 5 mm in length, with square, rectangular and diamond-shaped outlines (104370). It is commonly fractured, and is healed with either sphalerite, chalcopyrite and stannite or with carbonate. It is replaced by sphalerite and chalcopyrite.

Arsenopyrite is abundant in quartz-sulphide veins surrounding the sulphide lenses occurring as large idioblastic crystals and as large anhedral-subhedral polycrystalline aggregates. It is intergrown with quartz, and is generally free of solid inclusions, with only rare pyrrhotite and galena. Boundaries with sphalerite are either plain crystal faces or gently cuspate and apparently replacive. Arsenopyrite in the veins commonly exhibits deformation and brecciation by brittle fracture, with at least two discernible deformation events. Fractures developed during the first deformation are healed with either chalcopyrite alone (Plate 4.5G) or chalcopyrite and minor pyrrhotite, sphalerite, pyrite (after pyrrhotite) and carbonate. Fractures developed during a second deformation event are healed with carbonate, and commonly cut across earlier chalcopyrite veins (104453). The fracturing of arsenopyrite is the most intensive deformation texture observed in hydrothermal minerals at Cleveland, and is most likely associated with movement on reverse faults during the mineralisation episode.

Compositions of arsenopyrite were determined by using the X-ray diffraction method of Kretschmar and Scott (1976; Appendix 4), assuming that trace element concentrations (particularly cobalt) are low. Stage II arsenopyrite (7 samples) has a wide range in composition with 31.8 - 34.6 atomic %As, though most are more arsenic rich (Table 4.1). There appears to be a real, albeit tentative, trend with spatial distribution, with more arsenic rich arsenopyrite in the Nadir fault (33.6, 34.6 atomic %As) and decreasing away from the ore body with

the lowest arsenic concentrations (31.8 atomic %As in 104465) in veins at least 200 m from the sulphide lenses at their southern extremity. This difference between Stage II fault and vein mineralisation is most likely due to variation in temperature and/or sulphur fugacity during the mineralisation episode.

Chalcopyrite

Chalcopyrite is the dominant copper mineral and probably the second most abundant sulphide, being widely distributed throughout the sulphide lenses, and is a major component of the surrounding veins. In the sulphide lenses, it commonly occurs as thin bands or large irregular masses around the margins of, and replacing pyrrhotite masses. It also occurs as fine disseminations (0.05 - 0.2 mm) interstitial with pyrrhotite and non-sulphide gangue minerals, and commonly has associated sphalerite and stannite. Chalcopyrite also occurs as veinlets in pyrrhotite and replacing pyrrhotite along fracture margins. With stannite, it invades fractures in cassiterite (104325), and Cox (1968a) described chalcopyrite replacing cassiterite. In the pyrrhotite-magnetite ore (*e.g.* 104451) irregular masses of chalcopyrite enclose euhedral magnetite crystals and rounded pyrrhotite inclusions and/or remanent grains, but it does not occur as inclusions in magnetite. Chalcopyrite in the sulphide lenses contains 34.69 mass % Cu, 30.55% Fe and 34.76% S (Table A4.2), which is almost stoichiometric chalcopyrite with a Cu:Fe:S molar ratio of 1.002:1.004:0.995.

Most chalcopyrite is later than pyrrhotite, though the occurrence of interstitial grains and rare exsolution bodies in pyrrhotite indicate that some chalcopyrite is contemporaneous with pyrrhotite. Chalcopyrite contains exsolution bodies and/or inclusions of stannite, sphalerite, and pyrrhotite, and is exsolved in sphalerite, commonly as composite grains with pyrrhotite, and in stannite. It is replaced by stannite and rarely by sphalerite, and also by late carbonate similar to the marginal carbonate alteration of pyrrhotite.

Chalcopyrite is a major component of veins in the host rocks surrounding the deposit, occurring either as large irregular masses or granular aggregates, or as exsolution bodies and interstitial grains in sphalerite, with which it is penecontemporaneous. It replaces arsenopyrite and is veined by late carbonate, but is unaffected by hypogene alteration of pyrrhotite to pyrite/marcasite. A second (?) generation of chalcopyrite occurs as veinlets healing brittle fractures in arsenopyrite and in adjoining sphalerite (Plate 4.5G; 104453). In some instances, these veinlets originate from or merge into large irregular masses of chalcopyrite. The veinlets are dissected, and in arsenopyrite commonly are offset by later carbonate veins, also filling fractures.

Stannite

Stannite is the second most abundant tin or copper bearing mineral, occurring in most sections of the sulphide lenses, and the following mineral associations are commonly developed:

stannite

stannite - cassiterite

stannite - cassiterite - chalcopyrite

stannite - chalcopyrite ± sphalerite

stannite - pyrrhotite

stannite - pyrrhotite - chalcopyrite ± sphalerite

stannite - sphalerite

A common occurrence of stannite is as rims enclosing and replacing cassiterite (Plate 4.5C), and as thin bands around the margins of, and replacing pyrrhotite (Plate 4.5A). It may occur alone, as irregular, interstitial masses, but generally is associated with chalcopyrite (Plate 4.5B) and less commonly sphalerite, and exhibits mutual boundary relationships with both sulphides. Stannite occurs rarely as inclusions in pyrrhotite (*e.g.* 104391). Large masses of stannite up to 0.2 x 0.5 mm (104327) commonly contain

exsolution bodies of chalcopyrite and inclusions of pyrrhotite, sphalerite and chalcopyrite. In 104324, it occurs with sphalerite as a vein cutting intergrown chalcopyrite and siderite, and the chalcopyrite and siderite have been replaced by stannite around their margins.

Stannite appears to show a preference for sulphides in its distribution in the sulphide lenses. It is depleted in silicate-rich, sulphide-poor bands in the ore, but is common in pyrrhotite-rich bands (*e.g.* 104323). Also, where pyrrhotite is present, stannite appears to selectively replace pyrrhotite in preference to cassiterite.

The stannite is olive-green to olive-brown in colour and is isotropic in polished sections. It has been confirmed by X-ray diffraction analysis by the author and by Groves (1968). Cox (1968a) suggested that the stannite at Cleveland is the cubic variety, isostannite (Claringbull and Hey, 1955), but X-ray diffraction confirms it is the tetragonal variety. The composition of stannite in the sulphide lenses averages 30.4 mass % Cu, 13.1 - 18.1 (average 14.5) % Fe, 21.7 - 26.9 (average 25.05) % Sn and 30.1 % S (Table A4.2). This is close to its stoichiometric composition with a Cu : (Fe + Sn) : S molar ratio of 1.029 : 0.974 : 1.009. The variation in the Fe : Sn ratio with some stannite enriched in iron, may reflect its origin, with stannite derived from replacement of pyrrhotite having a higher iron content.

At the northern extremity of the sulphide lenses, stannite occurs interstitially with arsenopyrite and sphalerite, as small rounded inclusions in sphalerite and filling fractures in arsenopyrite (104370). In veins surrounding the sulphide lenses, stannite occurs rarely as rounded inclusions in sphalerite (104466).

Sphalerite

Sphalerite occurs sporadically throughout the ore-grade sulphide lenses and increases in abundance towards the periphery of the lenses where it may comprise 30 - 50% of the rock (104352). It appears to be penecontemporaneous with stannite and slightly later than most chalcopyrite. In the ore, sphalerite occurs as marginal replacement of chalcopyrite, as composite grains with stannite and/or chalcopyrite, and as disseminated irregular interstitial grains. In 104324, sphalerite and stannite occur as veinlets in chalcopyrite and siderite, and in 104356 it occurs as a marginal replacement (?) of cassiterite. A minor earlier generation of sphalerite is represented by exsolution(?) bodies in chalcopyrite (104356, 104410). At the extremities of the sulphide lenses, sphalerite is a dominant mineral occurring as granular, interlocking aggregates interstitial with and replacing arsenopyrite, pyrrhotite and chalcopyrite, and is veined and replaced by carbonate, similar to the carbonate replacement of pyrrhotite.

In veins surrounding the depost, sphalerite commonly is the dominant sulphide occurring as coarse, granular aggregates, as interstitial masses and veins in and replacing arsenopyrite, and as remnants in pyrite/marcasite ± pyrrhotite masses. The hypogene alteration of pyrrhotite to pyrite/marcasite has not affected the sphalerite (Plate 4.5G), and neither has it affected pyrrhotite included in sphalerite. Sphalerite is replaced by galena (Plate 4.5D) and late carbonate, and is veined by chalcopyrite and/or pyrrhotite in healed fractures.

Sphalerite contains abundant exsolution bodies, interstitial inclusions and grain boundary films of pyrrhotite and chalcopyrite, and less commonly of galena and stannite. Exsolution bodies generally have an ovoid-spheroidal shape, commonly 0.005 - 0.02 mm but up to 0.05 mm in diameter, whereas interstitial inclusions have more anhedral

to euhedral (square) outlines. Pyrrhotite also occurs as parallel needles, developed along twin planes, and exsolved galena occurs in cuspate forms. Exsolution blebs generally are monomineralic (pyrrhotite or chalcopyrite or galena or stannite) but composite blebs of pyrrhotite and chalcopyrite are common, and rarely of pyrrhotite and galena (104392, 104453). Groves (1968) recorded composite chalcopyrite and stannite exsolution blebs in a sphalerite host and composite chalcopyrite and sphalerite blebs in a stannite host. The exsolution bodies generally are randomly distributed throughout sphalerite, but may also occur as lines of blebs. Pyrrhotite-healed fractures cutting across lines of exsolution blebs have not affected continuity of the lines, indicating that the fractures are filled with later pyrrhotite (and/or chalcopyrite) and did not form by 'draining' of pyrrhotite from adjacent sphalerite.

Sphalerite in the sulphide lenses (Henry's lode) contains 14.7 - 19.7 (± 1.6) mole% FeS (Groves, 1968), and 18.8 mole% FeS in a vein on 7 level (Cox, 1968*a*), but the lack of contemporaneous iron sulphides precludes its use as a geobarometer.

Galena

Galena occurs rarely in the sulphide lenses as minute rounded inclusions or exsolution blebs in sphalerite and pyrrhotite (104343, 104352), though it appears to be more abundant towards the periphery of the lenses (104371).

Galena is a minor component of the veins surrounding the ore, and clearly increases in abundance away from the sulphide lenses. The galena commonly occurs in interstices between arsenopyrite euhedra and as veinlets (with carbonate) filling fractures in arsenopyrite and rarely in pyrrhotite (*e.g.*104465, 104466). It also occurs as irregular masses within or marginal to sphalerite masses (Plate 4.5D; 104392, 104467), as rounded to elongate inclusions, up to 0.05 mm in length (104465), and as narrow veinlets in

in sphalerite (104467). The irregular masses interstitial with arsenopyrite commonly contain rows of triangular voids occurring either in straight lines or in slightly curved lines indicative of mild deformation.

Other Sulphides

Groves (1968) tentatively identified boulangerite in Cleveland ore, occurring in small irregular patches at sphalerite grain boundaries. Cubanite is described by Farrand (1963) as occurring at the margins of some chalcopyrite grains, and probably exsolved from it, and occurring in veins with pyrrhotite, chalcopyrite, sphalerite and arsenopyrite. Cox and Glasson (1967) and Cox (1968a) reported that chalcocite and covellite are locally developed from chalcopyrite, but generally the Cleveland ore is free of secondary copper minerals.

Native Bismuth

Traces of native bismuth occur sporadically in the sulphide lenses as fine disseminations, up to 0.02 mm in diameter, occurring interstitially with pyrrhotite and/or non-sulphide gangue minerals (104349, 104451, 104452). Stillwell (1944a) and Edwards (1951) also recorded sporadic blebs (up to 0.02 x 0.06 mm) or groups of blebs in pyrrhotite masses. Bismuthinite has not been observed in the sulphide lenses.

Quartz

Quartz is the most abundant non-sulphide component of stage II mineralisation, occurring in all crystalline forms ranging from subrounded grains, to highly irregular interlocking crystals to idiomorphic crystals, and with considerable variation in grainsize ranging from < 0.01 mm to > 10 mm. The coarsest and more idiomorphic crystals occur in quartz-sulphide veins surrounding the sulphide lenses, where it is generally milky white in colour, with fine grained quartz on the vein margins and coarser, more idiomorphic

PLATE 4.6 Photomicrographs of replacement textures, and silicates in the sulphide lenses and Nadir fault, Stage II.

A: Aggregates of minute acicular inclusions in early-formed 'dirty' quartz, sulphide lens (104315). Scale bar = 100 μm, plane pol. light.

B: As above, showing later, clear quartz overgrowths on 'dirty' quartz, X nicols.

C: Pyrrhotite intergrown with massive 'dirty' quartz in sulphide lens (104358). Scale bar = 100 μm, plane pol. light.

D: As above, X nicols, showing recrystallisation of early 'dirty' quartz into large irregularly interlocking quartz grains. Pyrrhotite grains define the original grainsize.

E: Interlocking tourmaline lenticles in quartz-tourmaline rich sulphide lens (104354). Compare the texture with calcite lenticles in Plate 3.2E. Scale bar = 1 mm, plane pol. light.

F: Cassiterite crystal marginally pierced by fine needles of tourmaline, Nadir fault (104368). The cassiterite grain is embedded in a very fine mesh of tourmaline with interstitial quartz. Scale bar = 100 μm, plane pol. light.

G: Cassiterite crystal (CS) in quartz (white) pierced by acicular hornblende crystals in sulphide lens (104389). Hornblende and quartz are intergrown with pyrrhotite (black). Scale bar = 100 μm, plane pol. light.

H: As above, X nicols, showing twinning in cassiterite and characteristic diamond shape of hornblende rods.

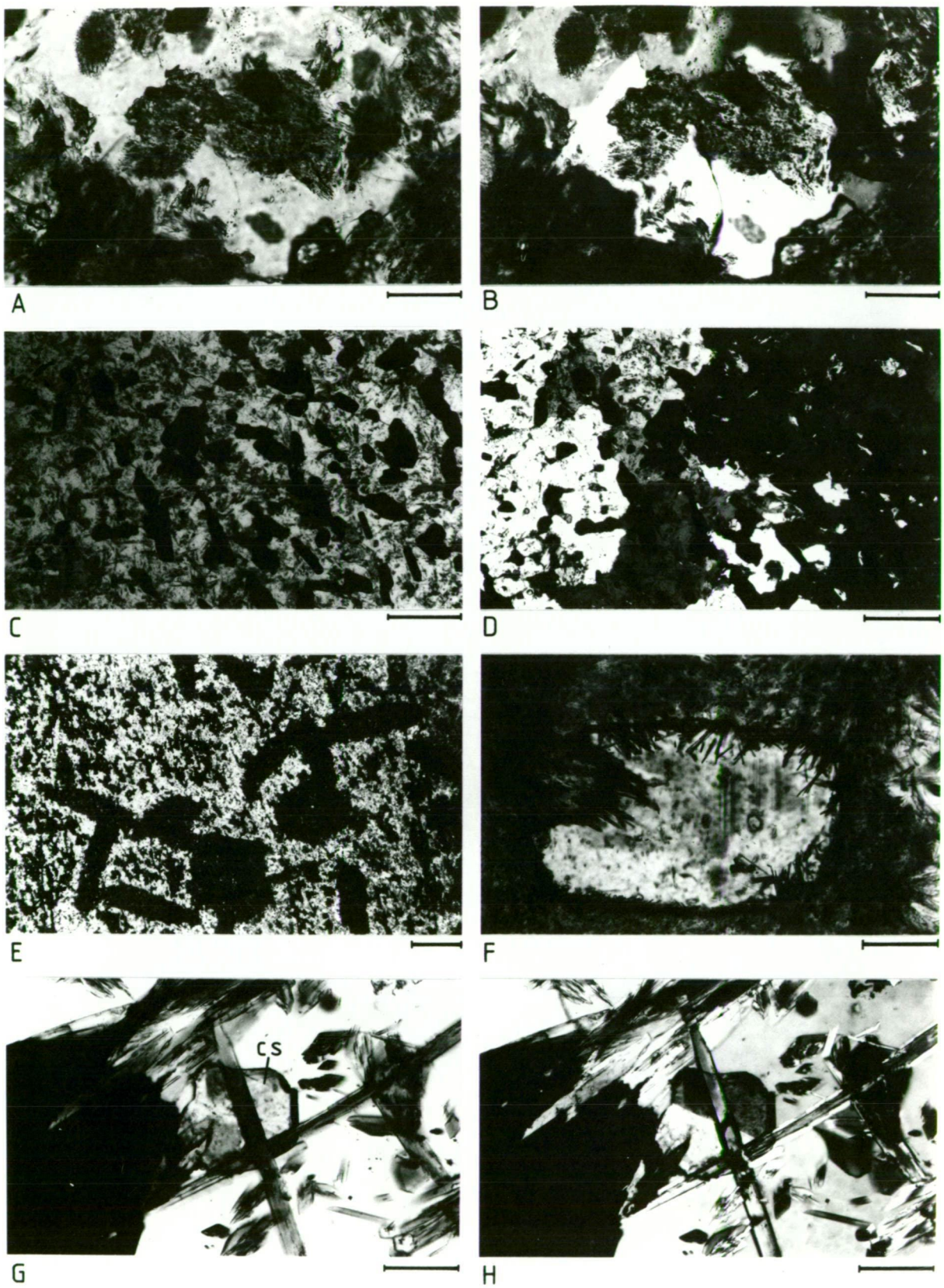

PLATE 4.6

quartz in the central parts of veins.

In the sulphide lenses, three generations of quartz are recognised. The first generation occurs as small aggregates or masses of sub-rounded, drusy grains with undulose extinction (104323), and represent remnants of an original calcareous clastic sediment rarely preserved within sulphide lenses. Groves (1968) describes similar clastic undulose quartz grains in partially replaced rock.

A second generation of non-undulose, 'dirty' quartz typically occurs intergrown with silicates (*e.g.* tourmaline, chlorite) and is enclosed within larger, and later, clear quartz overgrowths (Plate 4.6A, B). 'Dirty' quartz is equigranular, 0.1 - 0.3 mm in diameter, and characteristically is crowded with a network of minute solid inclusions (principally carbonate). The inclusions commonly are acicular, with a parallel alignment, but in adjoining patches of 'dirty' quartz have different orientations. Similar acicular inclusions occur rarely in cassiterite (*e.g.* Plate 4.4D). The quartz overgrowth is in optical continuity with 'dirty' quartz, it is generally free of minute inclusions, and has regular boundaries with other quartz overgrowths (Plate 4.6A, B). The 'dirty' quartz probably represents initial replacement and recrystallisation, but not total replacement, of original carbonate rock with later recrystallisation and replacement during quartz regrowth. The origin of the aligned acicular inclusions in 'dirty' quartz is enigmatic, though it may reflect cleavage planes in original carbonate.

A third generation of 'clear' hydrothermal quartz occurs as large, irregular poikilitic grains generally devoid of minute, solid acicular inclusions, but commonly containing inclusions of other hydrothermal minerals (*e.g.* tourmaline, chlorite, amphibole, cassiterite, fluorite, and pyrrhotite) and inclusions of 'dirty' quartz. This quartz probably is derived from recrystallization of second generation quartz into irregular masses, generally 1 - 4 mm

across, within highly irregular, interlocking boundaries with other third generation quartz. Originally, the quartz was equigranular and similar in grain size to the non-quartz inclusions (Plate 4.6C. D). In sections of the lower ore, almost all third generation quartz occurs as irregular, poikilitic crystals with no evidence of second generation quartz, indicating that recrystallization is more intense in the lower ore.

Tourmaline

Tourmaline (*var.* schorl) is present in most sections of the sulphide lenses, but is most abundant in the southern parts of the upper ore, where locally it may comprise 50 - 80% of the ore (104334, 104340). It is one of the first minerals to form, and is the only boron mineral. In thin section, tourmaline occurs as small idioblastic crystals generally 0.2 - 0.5 mm in length, but up to 1 mm, and 0.05 - 0.2 mm in diameter in cross-section. Crystals typically are zoned in cross-section with slate blue cores and brown to green-brown rims, and exhibit strong pale green and green-brown pleochroism in crystals cut parallel to their long axis. Inclusions in tourmaline have not been observed, but it commonly occurs as idiomorphic inclusions in quartz, fluorite, carbonate and sulphides (mainly pyrrhotite).

In the Nadir fault, tourmaline occurs as masses of interlocking fine needles, less than 0.01 mm in diameter in cross-section, with pale yellow-green and green pleochroism, and commonly are intimately intergrown with cassiterite. The outer margins of cassiterite crystals are pierced by fine tourmaline needles (Plate 4.6F).

In the sulphide lenses, tourmaline occurs as disseminated crystals, as masses of interlocking needles and as radial aggregates; and is intergrown with quartz, chlorite, cassiterite, fluorite and sulphides. In some sections it is concentrated in bands (dark bands), with fluorite concentrated in adjacent lighter coloured bands (*e.g.* 104334). In 104354 from Halls south lens, tourmaline occurs

as lenticular shaped masses of fine needles with minor intergrown quartz and carbonate (Plate 4.6E). The lenses commonly are intergrown, and the texture resembles calcite-filled lenticles in calcareous siltstone at the northern end of the mine (*cf.* Plate 4.6E and Plate 3.2E).

Hornblende

Hornblende (*var.* hastingsite - ferrohastingsite) is a significant, and in places a major component of the sulphide lenses in the deeper mine levels and in deep drill hole intersections, occurring as idioblastic to acicular crystals intimately intergrown with clear hydrothermal quartz, cassiterite and pyrrhotite (Plate 4.6G, H). It occurs either as isolated crystals or as masses of very fine parallel needles with interstitial quartz (Plate 4.7A, B). Adjacent masses of needles may have different orientations, which gives the ore the appearance macroscopically, of a coarse granular texture (*e.g.* 104302, 104389).

In thin section, the hornblende occurs as acicular needles generally 0.5 - 1 mm in length, but up to 4 mm, and up to 0.05 mm across characteristically diamond shaped cross sections (Plate 4.6G, H). Hornblende also occurs as coarser grains up to 0.5 mm in diameter, with prominent cleavages, but it is unclear whether these are single crystals or masses of closely packed needles. Acicular crystals cut parallel to their long axis have low extinction angles and exhibit strong olive-green to yellow-green and dark olive-green to blue-green pleochroism.

Hornblende is one of the earliest minerals deposited, occurring as inclusions in quartz, fluorite, cassiterite and pyrrhotite, but inclusions rarely have been observed in hornblende crystals.

PLATE 4.7 Photomicrographs of silicates, carbonates and sulphides in Stage II mineralisation.

A: Intergrown hornblende 'grains' composed of parallel needles in quartz, in sulphide lens (104302). Scale bar = 1 mm, plane pol. light.

B: As above, X nicols, showing hornblende grains intergrown with larger irregular recrystallised (?) quartz grains.

C: Intergrowth of chlorite (grey), siderite (light grey) and cassiterite (dark grey) in sulphide lens (104323). Scale bar = 100 µm, plane pol. light.

D: As above, X nicols.

E: Siderite rhombs intergrown with pyrrhotite (black) and cassiterite (cs), in sulphide lens (104323). Scale bar = 1 mm, plane pol. light.

F: Euhedral siderite (sid) intergrown with pyrrhotite (black), quartz (qz), fluorite (fl) and chlorite (ch) in sulphide lens (104391). Scale bar = 100 µm, plane pol. light.

G: Danalite (dan) intergrown with pyrrhotite (black), quartz, fluorite and siderite in sulphide lens (104391). Scale bar = 100 µm, plane pol. light.

H: Rim replacement of cassiterite (cs) by stannite (st) in Nadir fault (104368). Scale bar = 100 µm, reflected light.

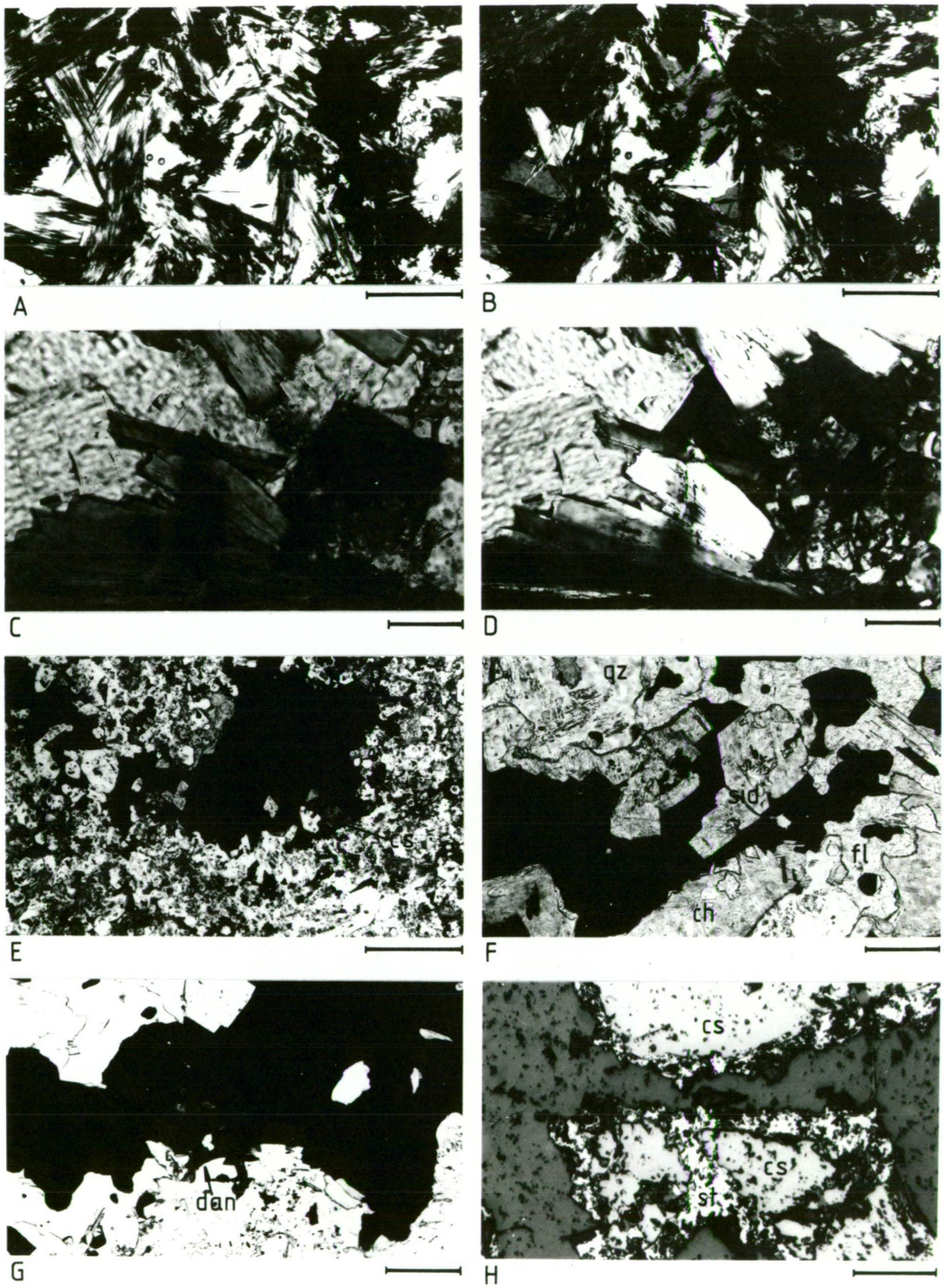

PLATE 4.7

Biotite/phlogopite

Mica (biotite and/or phlogopite) is widely distributed throughout the sulphide lenses where it is intergrown with quartz, fluorite, chlorite, tourmaline, hornblende, sulphides etc. Biotite generally occurs in the lower ore as flakes or plates, up to 1 mm in length, and exhibiting green to pale brown-green pleochroism, and commonly is concentrated in bands (104409). It also commonly occurs as inclusions in quartz and fluorite, occurring as randomly oriented hexagonal platelets 0.01 - 0.1 mm in diameter (Plate 6.1F). In 104409 biotite contains rare cassiterite inclusions, up to 0.05 mm in diameter. Biotite in the sulphide lenses has been replaced by carbonate along cleavage traces (*e.g.* 104406, 104410).

Phlogopite is relatively common in the upper ore, particularly in the southern lenses, where it occurs as colourless to pale yellow-brown to brown pleochroic flakes and sheafs intergrown with quartz, tourmaline, chlorite, siderite, cassiterite and sulphides. It is extensively replaced along cleavage traces by a later generation of finely crystalline carbonate (104353). This replacement leaves a brown iron-oxide staining of the carbonate and of adjacent phlogopite, particularly where it is intergrown with pyrrhotite.

Chlorite

Chlorite is most common in the northern lenses of the upper ore, where it is either disseminated throughout the ore or concentrated into bands, and occurs sporadically in the southern lenses and in the lower ore. In some sections of the northern sulphide lenses, chlorite comprises up to 50% of the non-opaque minerals (*e.g.* 104327). It also occurs as a minor component of veins surrounding the deposit.

Chlorite occurs as discrete flakes, as sheaves or books, and as radial clusters of flakes or rosettes, and is intergrown (and penecontemporaneous) with quartz, sulphides, tourmaline, fluorite, siderite, cassiterite, etc. (Plate 4.7C. D). The flakes and sheaves

are generally 0.2 - 0.3 mm, but up to 0.5 mm in length, and the chlorite is pleochroic colourless to pale green or yellow-green. Cox and Glasson (1967) and Cox (1968a) recorded preferred orientation of chlorite fibres parallel to compositional banding in some chlorite-rich laminae. In the Nadir fault, chlorite commonly occurs as rosettes, up to 2 mm diameter, of fine chlorite fibres as well as flakes and sheaves intergrown with quartz, tourmaline, cassiterite, fluorite and arsenopyrite (104368).

Chlorite in the sulphide lenses commonly is replaced by a late generation of finely crystalline carbonate, with brown iron-oxide staining of carbonate and chlorite (104323, 104356), similar to alteration of phlogopite. In quartz-rich masses, chlorite generally is free of carbonate replacement.

Sericite

Sericite occurs in the sulphide lenses in trace amounts, generally as platelets intergrown and/or interstitially with quartz and chlorite. It also occurs as small rosettes of radial fibres (up to 0.05 mm in diameter) and as a marginal alteration of chlorite (104325).

Topaz

Trace amounts of topaz occur in the sulphide lenses as small idiomorphic crystal inclusions, up to 0.05 mm in diameter, in quartz and fluorite and rarely in biotite, and also interstitially with quartz and biotite (104328, 104389, 104409).

Fluorite

Fluorite, which is generally colourless but with a faint mauve-blue tint, occurs throughout the sulphide lenses as large irregular masses or pods, as narrow veinlets, and as finely disseminated interstitial grains. It is present in most sections of the ore, and textural relationships indicate that fluorite ranges from pene-contemporaneous to post silicate, cassiterite and pyrrhotite, but

appears to be earlier than stannite, chalcopyrite and sphalerite (as evidenced by the absence of these sulphides as inclusions). It is replaced along fractures by late carbonate.

In the Nadir Fault, fluorite occurs as irregular, colourless masses, 1 - 2 mm across, with inclusions of idioblastic quartz, cassiterite, tourmaline and apatite, and fills interstices in cassiterite-rich clusters (104368).

In the sulphide lenses, fluorite has three modes of occurrence. Firstly, it occurs in poorly defined, irregular veins intergrown with chlorite, quartz, tourmaline and relatively coarse cassiterite (104352). These veins probably represent the initial veining and replacement of the host limestone as third generation hydrothermal quartz in massive ore blends with or transects these veins, commonly disguising their occurrence. Secondly, fluorite occurs as fine disseminations, intergrown and/or interstitial with quartz, tourmaline, chlorite, mica and pyrrhotite. Thirdly, it occurs as relatively large (1 - 5 mm), irregular masses or pods with inclusions of idiomorphic quartz (early 'dirty' quartz and later hydrothermal quartz), tourmaline, biotite, cassiterite, chlorite and apatite, and anhedral pyrrhotite (104315, 104328, 104340, 104410). Fluorite in the irregular masses is generally colourless, but commonly contains small radial centres of dark purple colouration (104405).

Trace element analyses, including rare earth elements (REE), of five fluorites from Stages II and IV have been undertaken by Prof. H-J. Schneider of the Freie Universität, Berlin (Appendix 4, Table A4.4). It has been previously demonstrated (Schneider *et al.*, 1975; 1977; Möller *et al.*, 1976) that REE fractionation during crystallisation and/or recrystallisation is an effective geochemical discriminator of fluorite genesis. The magnitude of the Tb/Ca atomic ratio relative to that of Tb/La (*i.e.* ratio of heavy/light REEs)

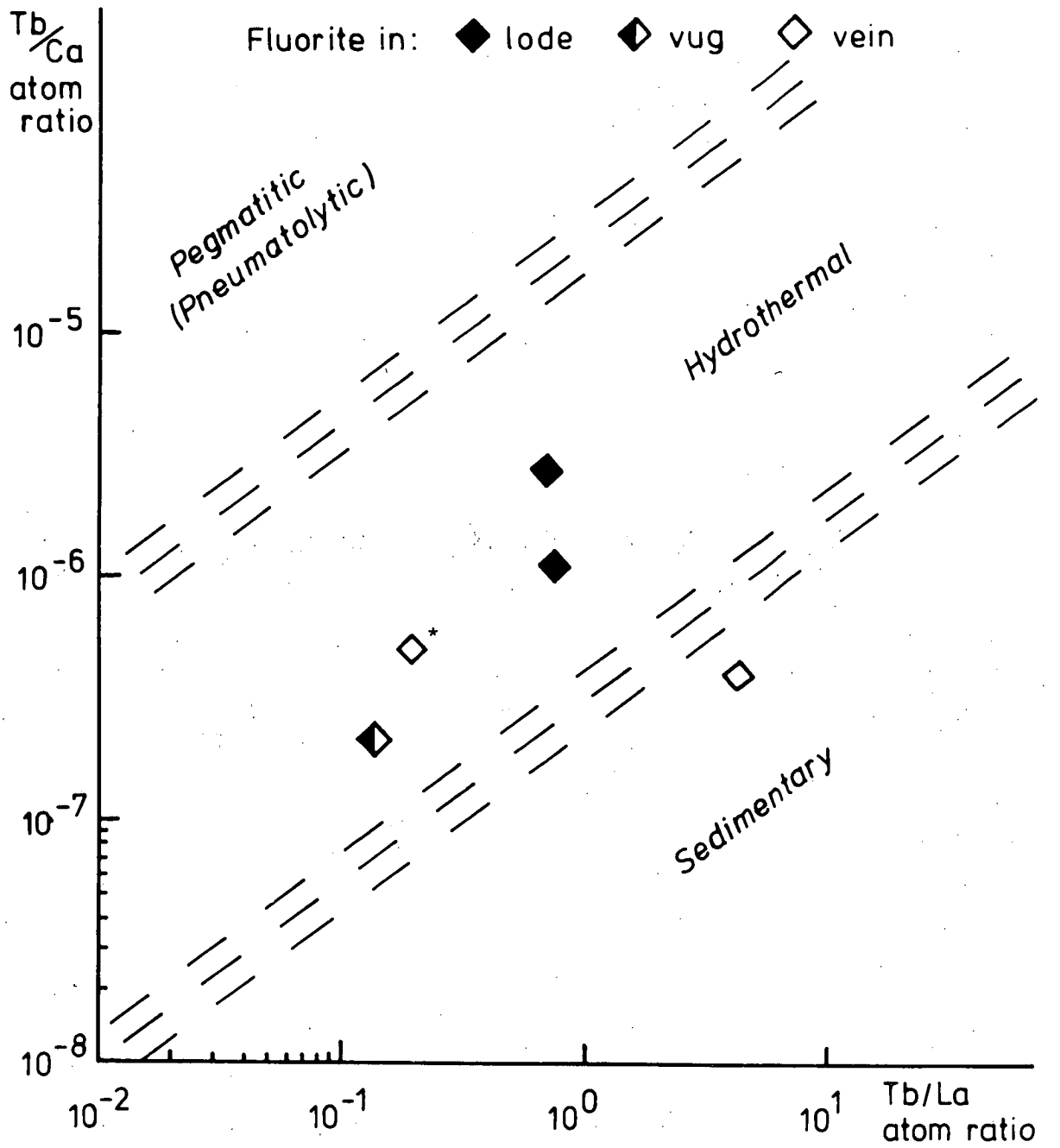

FIG. 4.8 Tb/Ca - Tb/La relationship in fluorite from the Cleveland mine, in relation to three different genetic groups (after Schneider *et al.*, 1975, 1977; Möller *et al.*, 1976). Stage IV fluorite is indicated by an asterisk (*).

define three broad genetic groups : 'pegmatitic' (or pneumatolytic), 'hydrothermal' and 'sedimentary' (synsedimentary or diagenetic) (Fig. 4.8). Two samples of fluorite in the sulphide lenses and one of fluorite lining a vug in ore (all Stage II), and a sample of Stage IV vein fluorite plot within the 'hydrothermal' field (Fig. 4.8), indicative of a hydrothermal origin for Cleveland fluorite. However, one sample of vein fluorite (analysis 2, Table A4.4) plots within the 'sedimentary' field. This is most likely due to assimilation of calcium from the host limestone by the hydrothermal fluid. Such assimilation tends to diminish the Tb/Ca ratio to the extent that fluorite generated in this way exhibits a Tb/Ca ratio characteristic of 'sedimentary' instead of 'hydrothermal' fluorite (Möller *et al.*, 1976).

Apatite

Apatite is a ubiquitous, minor to trace component of the sulphide lenses, occurring as subhedral to euhedral, colourless crystals, generally 0.01 - 0.1 mm across, intergrown with and as inclusions in quartz, fluorite (Plate 6.1I), tourmaline, chlorite, biotite, hornblende, cassiterite, etc.

Danalite

Danalite has been observed only in the lower ore, occurring as red-pink coloured, finely crystalline aggregates, up to 5 mm across, distributed sporadically throughout the ore, and as fine disseminations intergrown with quartz, fluorite, carbonate and pyrrhotite (Plate 4.7G). The occurrence of danalite in the Cleveland ore has been confirmed by X-ray diffraction analysis of crystalline aggregates. In thin section (104391), it occurs as anhedral translucent brown to red-brown, isotropic grains, generally less than 0.2 mm in diameter.

Danalite typically occurs in contact metamorphosed rocks and in skarns (*e.g.* Deer *et al.*, 1966), and in Tasmania its only other known occurrence is in bismuth-bearing garnet-magnetite-amphibole skarn at Mt Ramsay (Department of Mines, 1970, p. 38), on the east flank of the Meredith Granite. Groves (1968) described idioblastic crystals of garnet in one section of Mt Bischoff ore (Greisen Face), but as garnet and danalite have similar optical and physical properties, then the garnet recorded at Greisen Face may be danalite.

Beryl

Beryl has been observed only in hand specimens of the ore, from above the Nadir fault, occurring as pale blue-green acicular crystals in parallel aggregates, up to 5 mm in length, distributed sporadically through the northern parts of the sulphide lenses. Its occurrence has been confirmed by X-ray diffraction.

Vivianite

Vivianite occurs commonly as coatings on joint surfaces in the sulphide lenses. It occurs as radial aggregates of bladed crystals, commonly several centimetres in length. It is unrelated to the mineralisation episode.

Carbonates

Siderite is a significant component of the replacement ore, but dolomite is the dominant carbonate in the reverse faults. Calcite(?) is preserved in early 'dirty' quartz and rarely is preserved in the ore (104326).

In the sulphide lenses, siderite occurs as irregular grains intergrown with quartz, chlorite, tourmaline, cassiterite, etc. (Plate 4.7C, D) and as rhombs and polyhedral grains intergrown with pyrrhotite, chalcopyrite, fluorite and silicates (Plate 4.7E. F). It is abundant in the upper ore, particularly in the southern lenses, but is rare in the lower ore and has not been observed in magnetite bearing ore. Minor siderite also occurs in veinlets carrying

sulphides.

A late generation of siderite, possibly of hypogene origin, is a ubiquitous but minor component of Stage II mineralisation, occurring in the reverse faults, in the sulphide lenses and in veins in the host rocks. It commonly occurs as very fine grained crystalline aggregates forming a reaction and/or replacement rim around pyrrhotite and rarely chalcopyrite and magnetite. In some sections, replacement of pyrrhotite is almost complete with only minute remanent sulphide grains within an irregular mass of finely crystalline siderite. Late siderite also has replaced chlorite and biotite in the upper ore, commonly where it is intergrown with or adjacent to pyrrhotite (*e.g.* 104323, 104330, 104356).

Summary of the depositional sequence and zoning

The interpreted microparagenetic sequence in the sulphide lenses is schematically illustrated in Figure 4.4, beginning with the composition of the original limestone and proceeding through to secondary copper and phosphate minerals. The earliest phase of crystallisation was apparently sulphide deficient, and consisted primarily of quartz, tourmaline, cassiterite and minor siderite, sulphides (arsenopyrite and minor pyrrhotite) and oxides. This was followed by apparently contemporaneous deposition of most of the pyrrhotite, cassiterite, siderite, fluorite and silicates. In the lower ore, deposition of hornblende, magnetite, scheelite and danalite are attributed to this phase, but the sequence here is complicated by partial recrystallisation. Chalcopyrite is a minor component of the main phase of deposition but is more prominent in the final phases. The last phase of hydrothermal mineralisation is characterised by deposition of stannite, replacing earlier formed cassiterite and pyrrhotite, accompanied by sphalerite, chalcopyrite and pyrrhotite. Subsequent to formation of the sulphide lenses, sulphides and silicates

have been subjected to extensive hypogene replacement by pyrite/marcasite and siderite. Similar, but incomplete sequences of deposition occur in the reverse faults and in veins in the host rocks. Apart from stannite, late phase minerals are absent from the reverse faults, and apart from arsenopyrite, early formed minerals are absent from the veins. The distribution of arsenopyrite is inconsistent with its paragenetic position. It occurs in the reverse faults and as a minor phase in ore grade sulphide lenses where it is intergrown with early-formed minerals, but is most abundant at the extremities of the sulphide lenses and in veins in the host rocks where it is earlier than but associated with late-phase minerals. This indicates that arsenopyrite was probably deposited at the 'front' of replacement of limestone, but was replaced by later-formed sulphides (principally pyrrhotite). Concentration of late phase copper-zinc minerals at the extremities of the deposit probably reflects the unreceptiveness of most early-formed minerals to reaction with later fluids, and hence their migration to the outer margins of the deposit.

The mineralogical zoning in Stages I and II also corresponds to the paragenetic sequence, with three main zones defined by the occurrence of wolframite ± molybdenite, cassiterite and sphalerite ± galena. An early-formed central zone in the footwall Crescent Spur Sandstone and altered quartz porphyry with abundant wolframite ± molybdenite, bismuth/bismuthinite and minor cassiterite (Foleys zone) passes into a zone of abundant cassiterite with pyrrhotite and silicates (sulphide lenses) and an outer and later zone of sphalerite ± galena at the extremities of the sulphide lenses and in veins peripheral to the deposit. Chalcopyrite spans the two latter zones in both temporal and spatial distribution, but stannite is restricted mainly to the pyrrhotite rich sulphide lenses. The generalised

paragenesis and zoning at Cleveland, particularly the Stage I mineralisation and associated quartz porphyry dyke, is strikingly similar to the Fire Tower Zone at the Mt Pleasant, New Brunswick porphyry W-Mo-Bi-Sn deposit, where disseminated wolframite + molybdenite + bismuth + cassiterite mineralisation in a pene-contemporaneous, sub-volcanic plug of quartz-feldspar porphyry is surrounded by a later base-metal sulphides (+ stannite) zone which occurs near the contacts of the plug and as irregular replacements in the altered host felsic volcanics (Dagger, 1972; Parrish and Tully, 1978).

The mineralogy of the sulphide lenses changes with increased depth from assemblages typical of cassiterite-sulphide (Renison and Mt Bischoff-type) mineralisation to mineral assemblages more typical of high temperature skarns, with calc-silicates (*e.g.* hastingsite), danalite, magnetite and scheelite. Thus Cleveland may be a transitional deposit, intermediate between sulphide dominant Renison-type carbonate replacement tin deposits relatively remote from their associated granite, and stanniferous skarns at or close to the contact of granitic plutons. At greater depths (*i.e.* in excess of 600 m below the surface), more exotic tin minerals such as malayaite (*e.g.* Burt, 1978) and stanniferous amphiboles, garnets, etc. may occur within the 'sulphide' lenses.

MINERALOGY OF THE FINAL STAGES OF THE MINERALISATION EPISODE

The mineral composition of Stage III veins is dominated by coarse-grained, anhedral arsenopyrite, green fluorite and quartz with lesser amounts of chlorite and calcite and rare sphalerite and chalcopyrite intergrown with the arsenopyrite (104376, 104449). In a cavity in the Nadir fault, arsenopyrite occurs as rhombohedral crystals, up to 6 mm across, intergrown with euhedral quartz crystals, up to 20 mm in length, which are speckled with fine-grained (<1 mm diameter) dark blue/grey

stannite (104368). Stage III arsenopyrites have a narrow range of composition with 32.5-32.7 at % As in the Nadir fault and 33.1-33.3 at % As in veins in the sulphide lenses (Table 4.1), but the lack of other sulphides limits their effectiveness in defining temperature and fS_2 conditions (Kretschmar and Scott, 1976). Stage III arsenopyrites fall within the compositional range of Stage II arsenopyrites (31.8-34.6 at % As), though there are apparent differences at individual localities (*e.g.* in Nadir fault, Stage III arsenopyrites have a lower As content than Stage II; Table 4.1).

Stage IV mineralisation (Fig. 4.4) is widespread throughout the Cleveland deposit but the complete mineral assemblage generally is not present at each locality. It occurs as veins in the sulphide lenses and host rocks (*e.g.* 104359, 104429-31), lining vugs in the sulphide lenses (104301), and lining cavities in faults (104361) and open joints (104351). Fluorite is the dominant mineral and is apparently slightly earlier than most carbonates and quartz. It is characteristically pale green to pale blue, which contrasts with the colourless to purple and brown tinted fluorite in Stages I and II, and has a trace element constitution consistent with an hydrothermal origin (Fig. 4.8). The fluorite generally occurs either as irregular clear to cloudy masses on cavity walls and blanketed by later carbonates, or as clear cubic crystals, up to 30 mm across, lining open veins and joints and with only minor contemporaneous quartz and carbonates (*e.g.* 104351). The fluorite veins intersected in deep drill holes at about 540 m M.L. consist almost entirely of massive, milky green to clear fluorite (104429-31) which has fluid inclusion homogenisation temperatures similar to Stage IV fluorite in the mine (Chapter 6). Cream to pale pink rhombohedral dolomite with minor intergrown calcite commonly occurs as a coating (2-4 mm thick) on earlier Stage IV fluorite in cavities in faults and open veins (*e.g.* 104361).

Stage IV(?) calcite also occurs as clear to milky euhedral platelets coating Stage II fluorite lining a vug in the sulphide lenses (*e.g.* 104301).

Throughout the deposit, all exposed previous minerals lining vugs and cavities in open veins and joints are coated with pyrite occurring as (a) a dusting of very fine-grained euhedral pyrite (104351); (b) an encrustation (1-3 mm thick) of intergrown pyritohedral crystals (0.5-2 mm across) (104361); and (c) as scattered semi-spherical masses (up to 2 mm in diameter) and typically with an irridescent tarnish. This pyrite represents the final stage of the mineralisation episode (Stage V), and sulphur isotope data (Chapter 7) indicate that it is unrelated to the ubiquitous marcasite/pyrite alteration of pyrrhotite in mineralisation Stages I and II.

The timing of the hypogene marcasite/pyrite alteration is unknown, but it is probably later than the mineralisation episode, and so too is the formation of vivianite on joints in the sulphide lenses and of supergene chalcocite and covellite.

5. WALL-ROCK ALTERATION

INTRODUCTION

Wall-rock alteration is well developed around the Cleveland deposit, and shows a distinct spatial relationship to the sulphide lenses and major geological structures. In the hanging wall Deep Creek Volcanics, there is a well-defined mineralogical and geochemical alteration halo to the mineralisation with the intensity of alteration decreasing away from the sulphide lenses. A similar style of alteration occurs in Henrys Volcanic Member within the Hall Formation. In the footwall Crescent Spur Sandstone, there is extensive veining and alteration of greywacke, but it is uncertain whether this is an alteration zone or halo to the mineralisation, because of limitations imposed by the orientation and depth of drilling. The footwall alteration may form a halo associated with either the sulphide lenses or the Stage I vein mineralisation, it may represent a contact aureole associated with the quartz porphyry body or with the Meredith Granite, or alternatively it may be a combination of all of these.

Previous investigations

Cox (1968a) and Cox and Glasson (1971) described an elliptical zone (in plan) of sericitisation of the host rocks, defined by alteration to sericite of the detrital feldspars in greywacke in the Crescent Spur Sandstone and of plagioclase in basalt in the Deep Creek Volcanics, with the degree of alteration decreasing away from the ore. This zone is described as 1000 m long and 500 m wide, with the long axis parallel to the regional strike and centred on the ore body. However, Ransom and Hunt (1975) suggested that sericitisation is more widespread, and attributed this alteration to regional metamorphism. Palmer (1976) observed little alteration

obviously related to the mineralisation, but suggested there is some evidence that chloritisation of mafic volcanics is more intense close to ore.

Everard (1964) considered that the chert interlayered with mineralised units represents the product of wallrock alteration (*i.e.* silicification of shale), but Farrand (1963), Cox (1968a) and Cox and Glasson (1971) proposed that the chert beds are primary chemical precipitates.

ALTERATION IN THE DEEP CREEK VOLCANICS

An alteration zone within the Deep Creek Volcanics, adjacent to the sulphide lenses in the Hall Formation, has been defined on mine section Qa, which is located in the centre of the northern ore-bodies (Figs. 4.2 and 4.6). The alteration has been defined by petrologic examination and chemical analysis of a series of drill core specimens collected from diamond drill holes on Qa section. Sampling extends vertically over a distance of 600 m, and up to 400 m laterally from the sulphide lenses (Fig. 5.1).

Mineralogy

Mineralogically, the alteration halo is defined by alteration to actinolite of clinopyroxene in the spilitic basalt (compare Plates 3.1 G, H; 5.1 A-F). The degree of alteration of the pyroxene decreases away from the mineralisation, extending 80 - 100 m into the Deep Creek Volcanics (Fig. 5.1). On the edge of the alteration zone the outer edges of clinopyroxene plates are altered to pleochroic green-light green/brown actinolite exhibiting a prominent cleavage (*e.g.* 48308, 48330; Plate 5.1 A, B). Further away from the sulphide lenses, the clinopyroxene appears fresh and there is no evidence of actinolite development (*e.g.* 48331, 48332). Nearer to the sulphide lenses, replacement of clinopyroxene by pleochroic

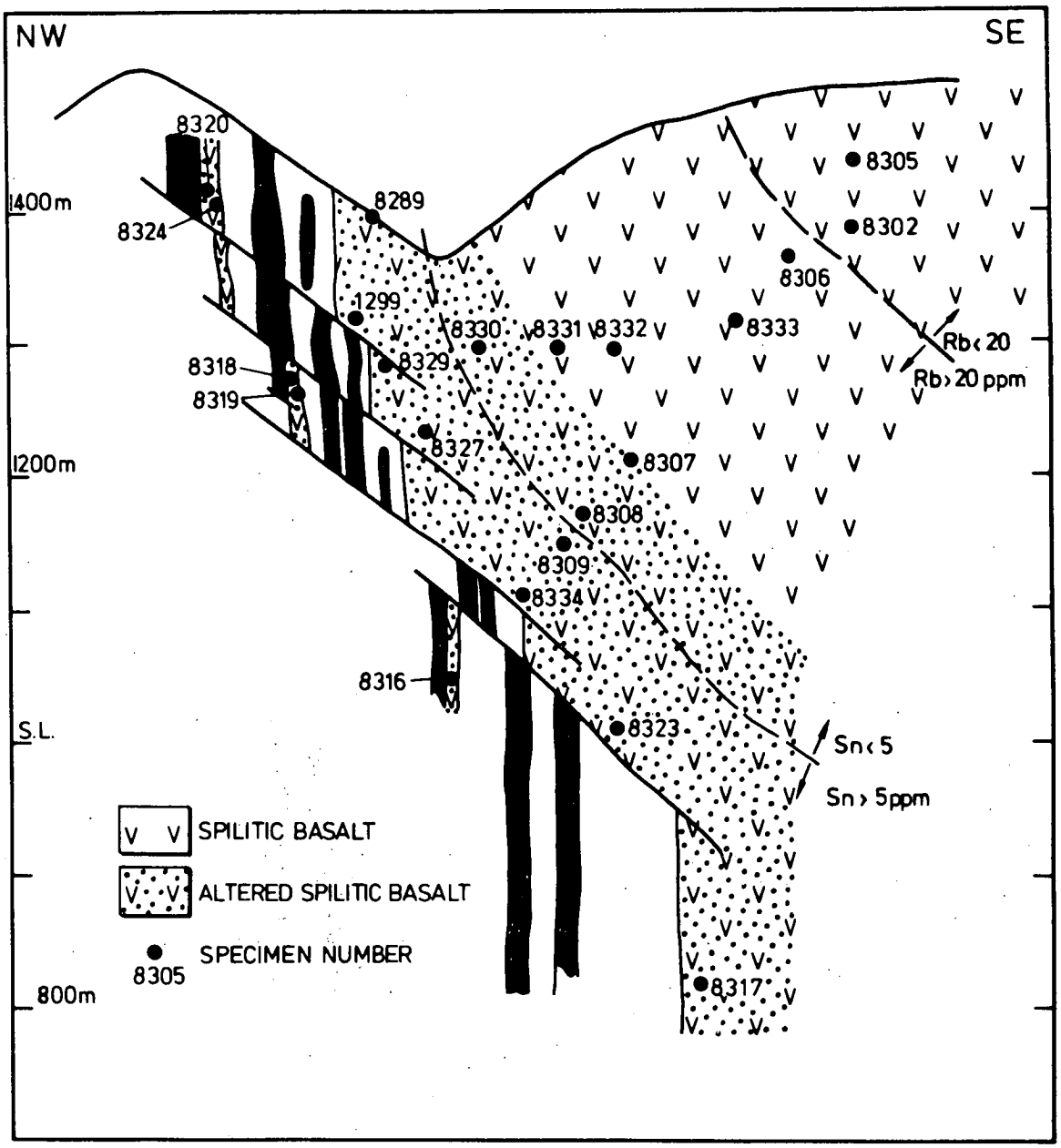

FIG. 5.1 Schematic section (based on mine section Qa, see Figs. 4.3 and 4.5) illustrating the alteration of the Deep Creek Volcanics, and the limits of high Sn, and high Rb in spilitic basalt. Altered spilitic basalt is defined in the text. Specimen numbers refer to analyses in Table A2.4 and should be prefixed with 4 (*i.e.* 8305 = 48305); number 1299 is analysis 781299 in Table A2.4.

green/brown-green actinolite is more extensive, and adjacent to the ore there is total replacement of clinopyroxene (*e.g.* 48334, 48329), with actinolite occurring as ragged, broad tabular grains, up to 1 mm across (Plate 5.1 D), which have an extinction angle of 10° - 15°, and are strongly pleochroic brownish green-pale green. Foden (1973) described similar textures in a specimen from 7L adit portal (specimen 41036), close to the Battery lens (Fig. 3.3).

Alteration of clinopyroxene to actinolite is essentially a hydration reaction:

$$5Ca(Mg,Fe)Si_2O_6 + H_2O = Ca_2(Mg,Fe)_5Si_8O_{22}(OH)_2 + 2SiO_2 + 3Ca^{2+}$$

In the presence of carbon dioxide (liberated by dissolution of limestone), the excess calcium in the above reaction, is precipitated as calcite, which occurs as inclusions in some actinolite grains (48329, 41036). Analyses of actinolite replacing augite on the edge of the alteration zone (48307) indicate an iron enrichment and a depletion in calcium and magnesium in actinolite, relative to the replaced augite (Table 3.2). The actinolite has an 100 Mg : (Mg + Fe + Mn) ratio of 43 which is in the middle range of actinolite composition (Deer *et al.*, 1966).

In the following discussion, hydrothermally altered spilitic basalt is defined as basalt in which clinopyroxene exhibits replacement by actinolite, and in 'unaltered' spilitic basalt (referred to as spilitic basalt) there is no observed replacement of clinopyroxene by actinolite. At its extreme development, altered spilitic basalt less than 20 m from ore contains biotite which occurs as minute platelets disseminated throughout replaced plagioclase laths and groundmass (48329; Plate 5.1 F).

PLATE 5.1 Photomicrographs of hydrothermally altered basalt, Deep Creek Volcanics and tourmalinised greywacke.

A: Sub-ophitic clinopyroxene showing marginal alteration by actinolite (*e.g.* darker grain left of centre) at the outer edge of the alteration halo in the Deep Creek Volcanics (48302). Scale bar = 100 μm, plane pol. light.

B: As above, X nicols, showing alteration of plagioclase laths.

C: Altered spilitic basalt (70 m from ore) showing remanent feldspar phenocrysts and igneous texture (not visible under X nicols) (48290). Scale bar = 1 mm, plane pol. light.

D: Irregular, bladed crystals of actinolite in altered spilitic basalt (40 m from ore), no remanent pyroxene (48289). Scale bar = 100 μm, plane pol. light.

E: Remanent igneous texture (microphenocrysts of feldspar) in intensely altered spilitic basalt (10 m from ore) (48329). Scale bar = 1 mm, plane pol. light.

F: Finely grained texture of intensely altered spilitic basalt (48329), showing minute biotite platelets (light grey) in feldspar lath at left. Scale bar = 100 μm, plane pol. light.

G: Alteration of greywacke adjacent to a vein in the Hall Formation (104317). A quartz + fluorite + sulphides + tourmaline (light grey mass at right) vein, at right, separated from greywacke, at left, by tourmaline + quartz alteration. Intensity of alteration decreases away from the vein, with remanent quartz grains in the greywacke visible only at the outer edge of alteration. Nearer the vein, the clastic texture has been destroyed. Scale bar = 1 mm, plane pol. light.

H: As above, X nicols.

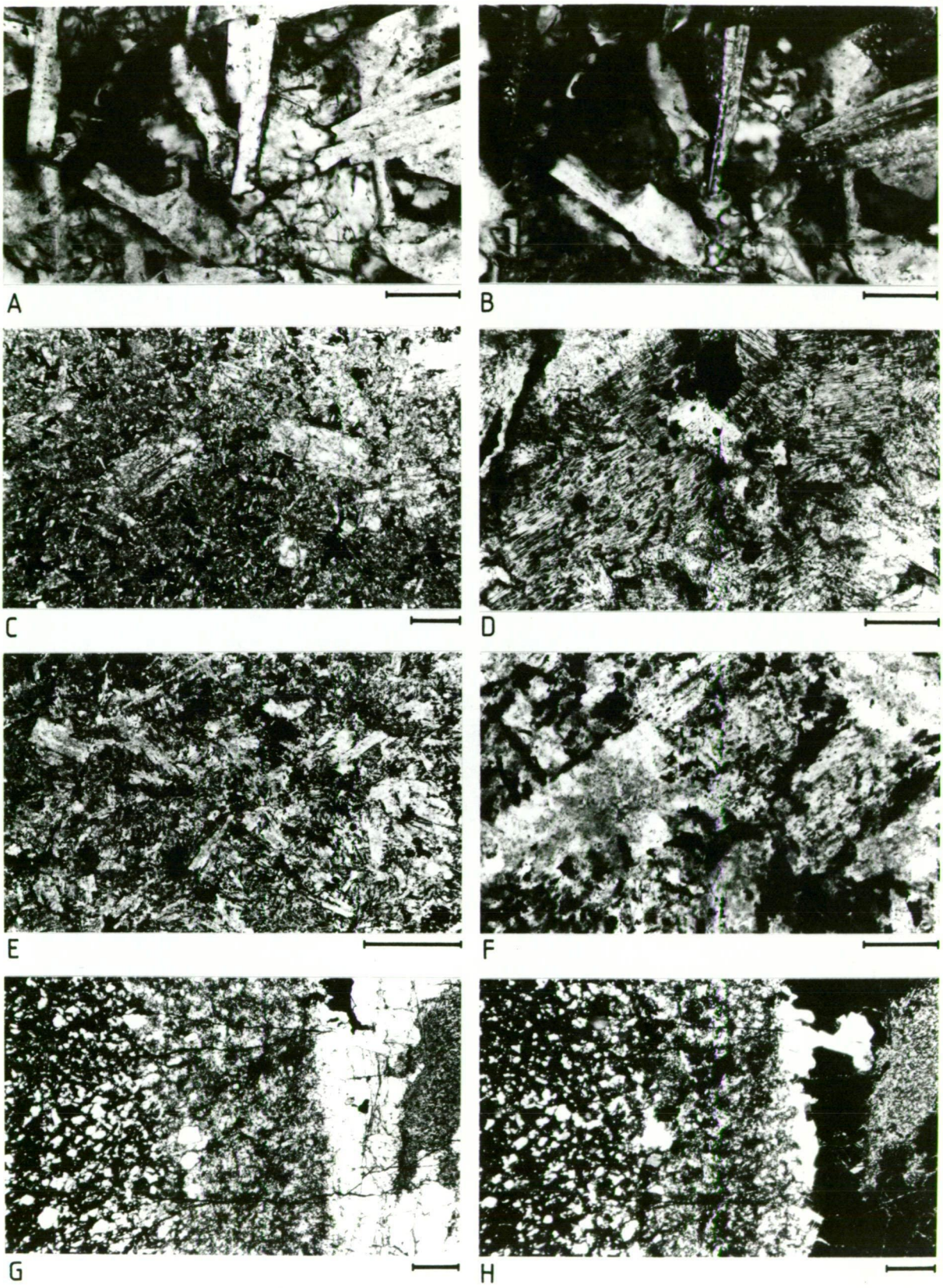

PLATE 5·1

Widespread development of sericite throughout the Cambrian sequence may partially be due to regional metamorphism, as proposed by Ransom and Hunt (1975), but there is also an apparent sericite alteration halo to the Cleveland mineralisation within the Deep Creek Volcanics. Sericite alteration of plagioclase is prevalent within the actinolite alteration zone, but also extends erratically into spilitic basalt. Near the sulphide lenses, the original albitised plagioclase laths have completely broken down to a felted mass of very fine grained quartz, sericite, chlorite and minor biotite. The original outline of the laths is only discernible under plane polarised light (Plate 5.1 C, E). The intensity of alteration of the plagioclase laths appears to decrease away from the mineralisation, extending 200 - 300 m into the Deep Creek Volcanics, before 'unaltered' albitised plagioclase is observed in thin section (*e.g.* 48302, 48305). The width of this sericite alteration is similar to that previously described by Cox (1968a) and Cox and Glasson (1971).

Chemistry of the alteration

To investigate whether there is any spatial variation in the chemical composition of basalt in the Deep Creek Volcanics, seventeen specimens were collected on Qa section from the positions shown in Figure 5.1. Analytical data are listed in Table A2.4, which also gives the distance of the sample from the sulphide lenses. Sampling and analytical procedures are described in Appendix 2.

Before attempting to define any variations in the chemical composition of basalt in the Deep Creek Volcanics, which may be due to hydrothermal alteration, it is essential to show that prior to the mineralisation episode there existed a body of uniform chemical composition. This is particularly relevant to the Cleveland deposit, because of the strong stratigraphic control of the mineralisation, and subsequently of any alteration halo.

The majority of the ten major and 15 trace elements analysed (Table A2.4) show very little variation, and certainly no systematic spatial variation. For example, elements such as Ca, Fe, Mg, Cr, Ni which may reflect differentiation within the magma from which the lava was derived, exhibit a uniform composition throughout the volcanic pile. This uniformity is illustrated in Fig. 5.2 for CaO, FeO* (total iron as FeO) and MgO. Except for the CaO content of one specimen (48329), these elements exhibit limited variation, and any irregularity is probably attributable to spilitisation of the basalt, which may also be implied from the extreme and irregular variation in Sr concentrations (Chapter 3). Hence, it is concluded that the Deep Creek Volcanics are composed of spilitic basalt of uniform chemical composition and that any spatial variations in the chemistry of the basalt must be associated with post-depositional hydrothermal activity.

Five of the elements analysed (Na, K, Rb, Sn, and Zn), however, exhibit a systematic variation in composition which is related to distance of the sample from the sulphide lenses. Steep increases in the concentrations of Rb, Sn and Zn, and a marked reversal in Na_2O and K_2O are recorded for the altered spilitic basalt compared with spilitic basalt. These variations are illustrated in Figures 5.2 and 5.4, in which element concentration (mass % oxide and g/t metal) is plotted against distance of the sample from the sulphide lenses, and in Figures 5.3 and 3.10 B.

Potassium increases gradually from less than 0.5 mass % K_2O in spilitic basalt to approximately 2 mass % near the sulphide lenses, with one specimen (48329) containing 4.7 mass % K_2O (Fig. 5.2). In contrast, sodium decreases from 3 - 4 mass % Na_2O in spilitic basalt, to less than 0.5 mass % Na_2O in altered spilitic basalt near the sulphide lenses (Fig. 5.2). The decrease in Na_2O begins at

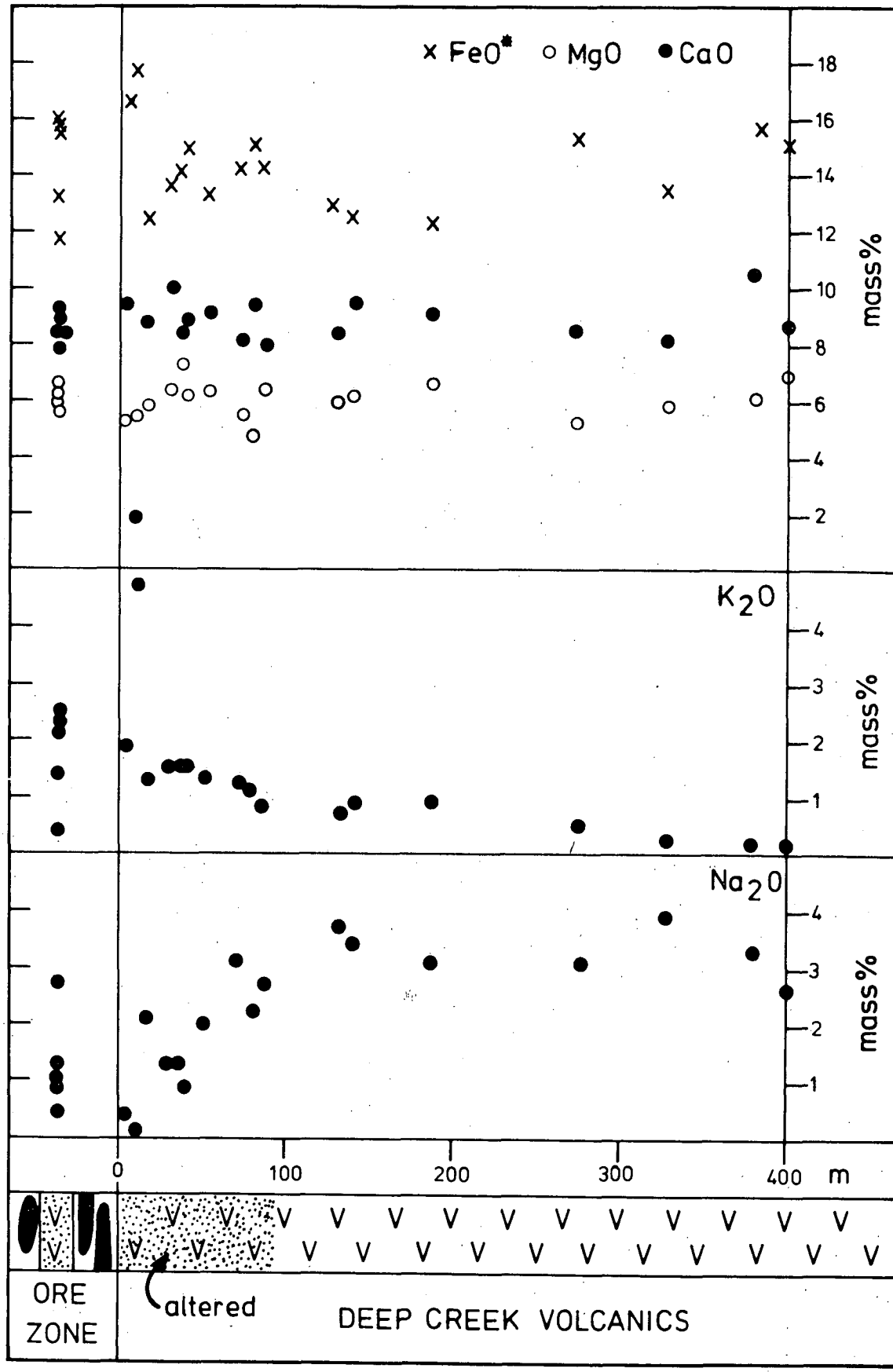

FIG. 5.2 Schematic representation of the Na_2O, K_2O, FeO* (total Fe as FeO), MgO and CaO content of unaltered and altered spilitic basalt in the Deep Creek Volcanics and Henrys Volcanic Member, relative to distance from the sulphide lenses. Specimen locations are shown in Figure 5.1, and analyses are given in Table A2.4. The length scale indicates the distance of the specimen from the nearest sulphide lens (see Table A2.4).

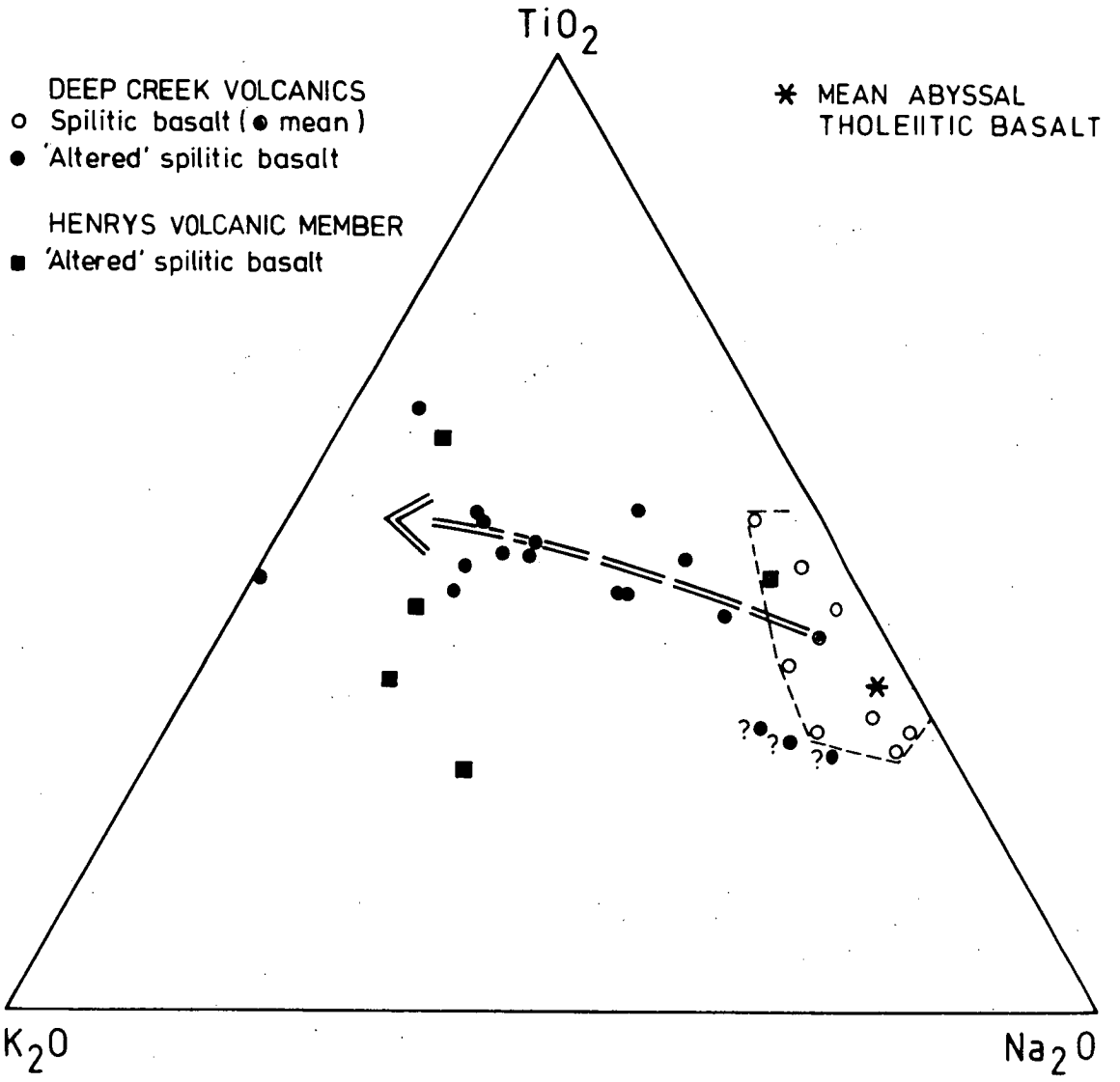

FIG. 5.3 Triangular plot of K_2O-TiO_2-Na_2O showing the trend in hydrothermally altered spilitic basalt, Cleveland mine. The dashed line outlines the compositional range of unaltered spilitic basalt. The large arrow indicates the trend of increasing potassic alteration with closer proximity to the sulphide lenses.

about 100 m from the ore lenses, which is a similar distance to the limit of development of actinolite.

The inverse relationship between Na_2O and K_2O reflects increased alteration of plagioclase by quartz, sericite and biotite nearer to the sulphide lenses. The potassic alteration is illustrated in Figure 5.3, in which the proportions of K_2O and Na_2O are combined in a ternary diagram with an 'immobile' element (TiO_2) of similar concentration. Spilitic basalt in the Deep Creek Volcanics plots close to the TiO_2-Na_2O join with ratios similar to average abyssal tholeiitic basalt (Fig. 5.3). Altered spilitic basalt plots outside the field of spilitic basalt and shows a broad curvilinear trend toward the TiO_2-K_2O join with closer proximity to the ore. The potassic alteration is also reflected in the K_2O-TiO_2-P_2O_5 discrimination diagram of Pearce *et al.* (1975), in which altered spilitic basalt shows a distinct linear trend from the ocean floor basalt field toward the K_2O apex, with increased alteration (Fig. 3.10 B).

Rubidium, like potassium, increases gradually from less than 10 g/t in spilitic basalt to about 300 g/t near the sulphide lenses, with one specimen (48329) containing an anomolously high 1120 g/t Rb (Fig. 5.4).

Tin shows a steep increase within 50 - 60 m of the sulphide lenses from less than 10 g/t (most samples less than 2 g/t) to about 300 g/t adjacent to the ore lenses, with 582 g/t Sn in specimen 48329 (Fig. 5.4). However, one specimen (48317) located 85 m from the sulphide lenses contains 191 g/t Sn (Fig. 5.4), but is close to the projected position of the steep reverse fault (EN fault) adjacent to the boundary between the Hall Formation and the Deep Creek Volcanics, as defined on mine section 'N' (Fig. 3.12). If it was a feeder channel for rising hydrothermal solutions, then proximity to this fracture would explain the high tin value.

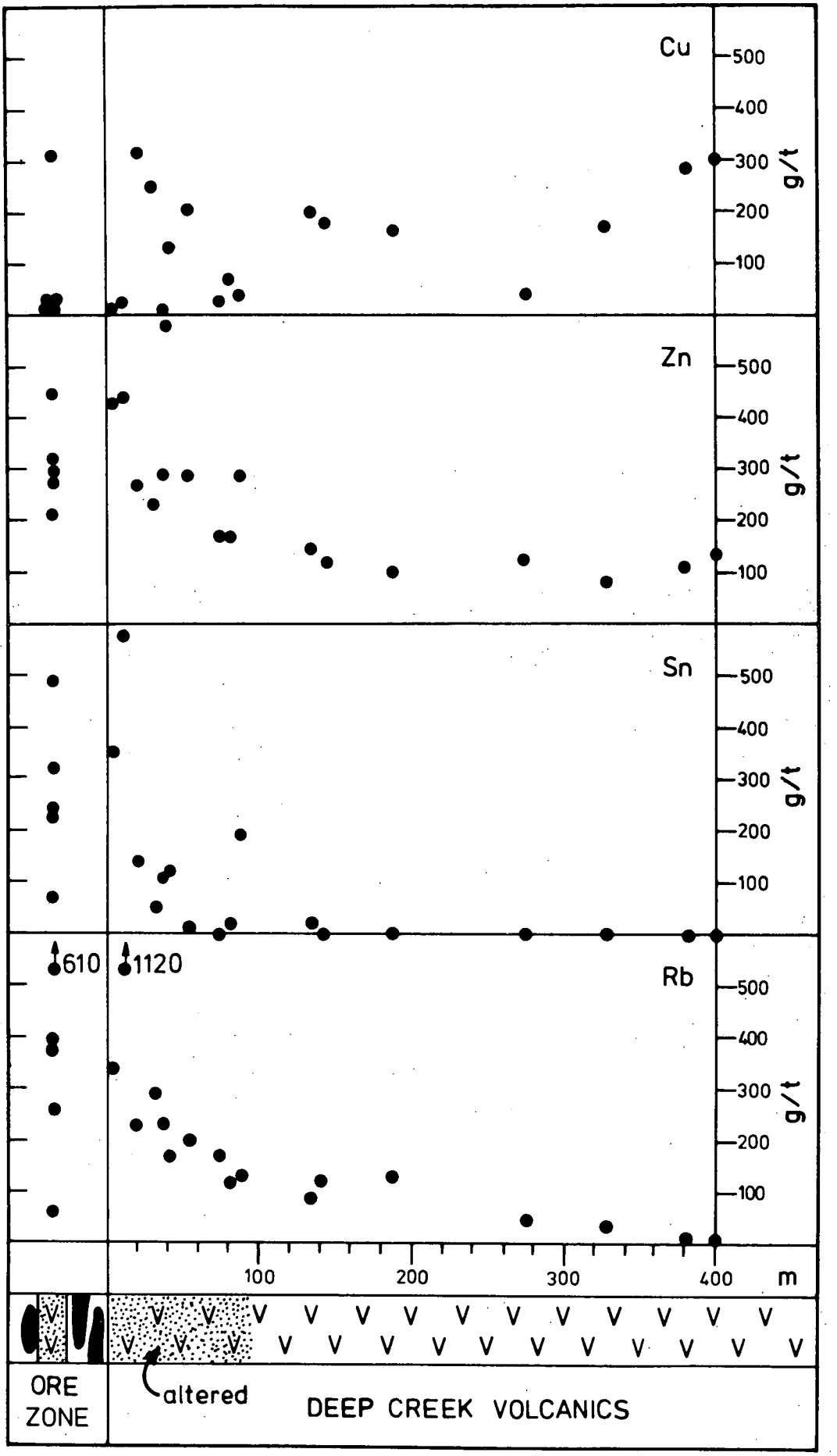

FIG. 5.4 Schematic representation of the Cu, Zn, Sn and Rb content of unaltered and altered spilitic basalt. See Figure 5.2 for explanation.

Zinc increases within about 100 m of the sulphide lenses, from 80 - 150 g/t in spilitic basalt to about 400 g/t in altered spilitic basalt adjacent to the ore (Fig. 5.4). This increase contrasts with the observed mineralogical zonation in which sphalerite is not present in Stage II quartz veins in the Deep Creek Volcanics within 50 - 60 m of the ore. Thus, as the zinc content of the altered spilitic basalt decreases, sphalerite in quartz veins increases. Copper is very erratic and does not show any systematic spatial variation (Fig. 5.4), though there is a tentative inverse relationship between copper and tin, with many high tin samples depleted in copper.

The hydrothermal alteration is also reflected in normative compositions of unaltered and altered spilitic basalt. Most spilitic basalt is olivine normative and has a high normative Ab : Or ratio, whereas most altered spilitic basalt is quartz normative and has normative Or > Ab (Table A2.8).

Summary of alteration in the Deep Creek Volcanics

The Deep Creek Volcanics is composed of spilitic basalt of uniform chemical composition, which has undergone post-depositional hydrothermal alteration. There exists within the Deep Creek Volcanics, structurally above the sulphide lenses, an alteration halo to the mineralisation which is defined by increasing replacement of clinopyroxene by actinolite, increasing K_2O, Rb, Sn and Zn, and decreasing Na_2O approaching the ore. The various elements comprising the alteration halo have varying ranges of effect (Fig. 5.1). Approaching the sulphide lenses, K_2O and Rb begin a gradual increase from about 250 m, which is similar to the limit of sericitisation of plagioclase in the basalt. Na_2O decreases from about 100 m, which is similar to the limit of replacement of clinopyroxene by actinolite. Tin increases steeply from about 50 m, and zinc increases from 100 - 120 m.

In addition to the above trends there is also an apparent, though less well defined, angular discordance of about 30° between the alteration halo and the sulphide lenses. The various zones of the alteration halo have an apparent steep south-east dip, sub-parallel to the EN fault which forms a structural boundary between the Deep Creek Volcanics and the Hall Formation, whereas the sulphide lenses within the Hall Formation are vertical (*cf.* Figs. 5.1 and 3.12).

ALTERATION IN THE HALL FORMATION

In addition to alteration and replacement of limestone, which may be considered a form of host-rock alteration (*e.g.* Taylor, 1979) and as such is described in Chapter 4, there also has been extensive silicification and bleaching of argillite, chert and tuff inter-layered with mineralised units in the sulphide lenses, silicification and tourmalinisation of clastic sediments adjacent to veins, and alteration of basalt in the Henrys Volcanic Member similar to the Deep Creek Volcanics.

Alteration of sedimentary rocks

The stratabound, replacement orebodies at the Renison mine are rimmed by a continuous zone, 10 cm to 100 m wide, of coarsely crystalline siderite which formed a 'front' between massive pyrrhotite and unaltered dolostone (Patterson *et al.*, 1981). The sulphide lenses at Cleveland do not appear to be enclosed by such a zone of recrystallised carbonate, but limestone in advance of the mineralisation, along strike, is cut by transverse, Stage II quartz + sulphide ± calcite veins with associated wall-rock alteration. The limestone is also penetrated by numerous calcite ± quartz veinlets, up to 10 mm thick (48295), and commonly is coarsely recrystallised in irregular veins and patches (48294; Plate 3.2 G). It is uncertain whether this calcite veining and recrystallisation formed during diagenesis or is associated with the mineralisation. Adjacent to

the quartz-sulphide veins, the limestone is altered to a fine intergrowth of quartz, chlorite and tourmaline which is separated from limestone by a zone of recrystallised calcite and chlorite (48295). In the tourmalinised zone, green-blue tourmaline occurs as needles, up to 0.5 mm in length, intergrown with quartz occurring as anhedral grains, generally 0.1 - 0.2 mm but to 0.4 mm in diameter, and interstitial pleochroic green to light green chlorite. The proportion of tourmaline decreases away from the veins, commensurate with declining intensity of alteration.

The sedimentary units interlayered with the mineralisation are described locally as 'chert', but previously there has been no uniform agreement as to their origin. Everard (1964) considered that the 'chert' represented the product of wall-rock alteration (*i.e.* silicification of argillite) associated with pneumatolytic hydrothermal replacement. Conversely, Farrand (1963), Cox (1968a) and Cox and Glasson (1971) proposed that the 'chert' beds are primary chemical precipitates and are not the product of wall-rock alteration. The results of this study indicate that although primary chert occurs within the Hall Formation, most of the 'chert' at the mine is the result of silicification and bleaching of originally brown to purple coloured argillite and fine grained tuff (Plate 3.2 C, D; 48284 - 48287). At the extremities of the sulphide lenses, particularly at the northern end of the mine, cores of unbleached argillite are preserved within pale grey to cream coloured 'chert' (Plate 5.2). Bleaching and silicification of argillite may either parallel bedding, particularly near the walls of sulphide lenses, or it is transverse to bedding (Plate 5.2; see also Plate 3.5). Within the sulphide lenses, there is complete bleaching of the sedimentary units (Plate 4.1).

PLATE 5.2 Alteration of chocolate-brown argillite and tuff interlayered mineralised units. Pyrrhotite-rich mineralised unit (under hammer) between beds of partially altered 'chert'. At left, bleaching is parallel to bedding and at right, is transverse to bedding with remanent cores of unbleached 'chert'. Banding in the mineralised unit parallels bedding in adjacent 'chert'. Face in Halls lode (B lens north), development drive, 14 level, looking north-east. Scale bar = 1 m.

Alteration of the argillite and chert is restricted to the immediate mine area, and is not as extensive as alteration of the Deep Creek Volcanics. This is probably due to the interbedded limestone which would have been more receptive to reaction with a hydrothermal fluid than the finer grained and less permeable argillite and chert.

Greywacke within the Hall Formation generally is not in contact with the sulphide lenses and appears unaffected by hydrothermal fluids, having been protected from the mineralisation by enclosing argillite and chert. However, greywacke penetrated by Stage II veins is intensely tourmalinised adjacent to the veins (*e.g.* 104317; Plate 5.1 G, H). The alteration consists of finely intergrown tourmaline and quartz with interstitial fluorite, chlorite and minor sulphides (pyrrhotite, chalcopyrite, stannite, arsenopyrite). The zoned, pleochroic slate blue to brown tourmaline occurs as needles, generally 0.1 - 0.2 mm long, but up to 0.5 mm long adjacent to vein margins, and is similar to tourmaline in the sulphide lenses. Alteration of greywacke has completely destroyed the clastic texture near veins, but decreases in intensity away from the vein with remanent quartz grains preserved only at the outer edge of alteration (Plate 5.1 G. H).

Henrys Volcanic Member

Potassic alteration of basalt in the Henrys Volcanic Member is petrologically and chemically similar to alteration of spilitic basalt in the Deep Creek Volcanics. Clinopyroxene is replaced by pleochroic green-brownish green actinolite, with twinning and zoning of original pyroxene preserved in some sections (*e.g.* 48320). Plagioclase laths are altered to a fine grained felted mass of quartz, sericite and chlorite.

Chemically, the altered spilitic basalt has the same relative high concentrations of K_2O, Rb, Sn and Zn and low Na_2O as that determined for altered spilitic basalt in the Deep Creek Volcanics (Figs. 5.2, 5.3, 5.4), but the variation in element concentration is greater than that expected for a single unit at a constant relative stratigraphic and structural position within the sequence. Most of the variation is due to specimen 48320 which has K_2O, Na_2O, Rb and Sn values similar to altered spilitic basalt on the outer edge of the alteration halo in the Deep Creek Volcanics. This specimen highlights a tentative trend of an increase in K_2O, Rb, Sn and Zn and decrease in Na_2O (*i.e.* greater degree of alteration) with increased depth, as exemplified by rubidium which has values of 63, 257, 393, 381 and 609 g/t down dip. A similar trend is not apparent in the Deep Creek Volcanics. Also, specimens close to the reverse faults (48324 and 48318) exhibit a higher degree of alteration than specimens further displaced from the faults (48320, 48319; Fig. 5.1), which probably indicates fluid migration away from the reverse faults. For example, specimen 48324 contains more K_2O, Rb (257 g/t) and Sn (493 g/t) and less Na_2O than specimen 48320 (*e.g.* 63 g/t Rb, 73 g/t Sn).

ALTERATION IN THE CRESCENT SPUR SANDSTONE

Alteration in the Crescent Spur Sandstone occurs in the form of tourmalinisation of greywacke adjacent to veins, and an apparent increase in alteration of muscovite and chlorite in greywacke to biotite with increased depth.

Biotite is a minor component of greywacke in surface outcrops, occurring as detrital flakes, but at the mine it is apparently more abundant with increased depth, where it occurs as marginal alteration

of muscovite and chlorite and disseminated as minute platelets in the matrix (81-69, 81-70, 81-72). As the biotite alteration increases with depth, it may be part of a contact metamorhpic aureole to the Meredith Granite. However, deep sampling is necessarily restricted to drill holes within the Foley zone of mineralisation, hence the biotite alteration also may be associated with the altered quartz porphyry.

Tourmalinisation of greywacke adjacent to veins is similar to that in the Hall Formation, with obliteration of the original clastic texture close to the vein wall and intensity of alteration declining away from veins. The tourmaline alteration commonly is disproportionately extensive in relation to the width of veins as, for example, alteration may extend 100+ mm on either side of veins less than 10 mm thick. The brown to blue-green tourmaline occurs as rods or needles intergrown with quartz, fluorite, chlorite (altered by late carbonate), minor biotite and rare cassiterite (81-67, 81-68, 81-71).

ALTERATION OF CAMBRIAN IGNEOUS ROCK

Alteration of the porphyritic basalt/dolerite dyke which intrudes the Hall Formation at the southern end of the mine, is described in Chapter 3. Chemically, the altered dyke is depleted in silica, magnesia, lime and strontium and enriched in iron (due to siderite) relative to the unaltered dyke (Table A2.6), but has none of the characteristics of alteration of spilitic basalt in the Deep Creek Volcanics and Henrys Volcanic Member.

The Whyte River complex is relatively remote from, and apparently unaffected by the mineralisation, though basalt on the eastern edge of the complex at the mine is enriched in rubidium (63 and 54 g/t; Table A2.7) relative to tholeiitic basalt elsewhere in the Cleveland area, and is most likely due to alteration associated with the mineralisation.

6. FLUID INCLUSION GEOTHERMOMETRY, GEOBAROMETRY AND COMPOSITION

INTRODUCTION

A fluid inclusion study was undertaken to determine the temperature and composition of the hydrothermal fluid and to ascertain whether there was any spatial or temporal variation in termperature and fluid composition in the various generations of vein and massive mineralisation.

Over 1000 fluid inclusions in hydrothermal minerals from mineralisation Stages I, II and IV have been analysed by microthermometric techniques (*i.e.* freezing and heating of selected samples and observation of the temperatures of phase changes in individual inclusions). Most heating, and all freezing measurements were made on a Chaixmeca apparatus, and a small number of heating measurements were made on a heating stage previously constructed at the University of Tasmania. Details of the experimental technique and calibration of the heating/freezing apparatus are given in Appendix 5, and all heating and freezing experimental results and observations are listed in Tables A5.1 and A5.2

Heating measurements are reported directly as homogenisation temperatures, uncorrected for pressure, and freezing measurements have been converted to, and reported in the text as mass% equivalent NaCl, abbreviated to % NaCl. For the Chaixmeca apparatus, temperature measurement is accurate to ±0.2°C below 35°C, and the error increases gradually to ±3°C at 500°C, whereas the University of Tasmania stage is accurate to ±3°C at 200°C, increasing to ±5°C at 400°C (Appendix 5). Freezing data have been converted to salinity using salt-depressed freezing curves for the systems H_2O-CO_2-NaCl (Collins, 1979) and H_2O-NaCl (Potter *et al*, 1978).

The theory and assumptions involved in fluid inclusion studies, and the criteria for differentiating inclusion origins have been discussed at length by Yermakov (1965) and Roedder (1972, 1976, 1979, 1981). At Cleveland, most specimens contain aggregates or intergrowths of several minerals, but even so it has been possible to differentiate primary and pseudosecondary inclusions from secondary inclusions. Crystals of fluorite collected from vugs and some vein fluorite contain crystal growth zones defined by colour banding with associated, easily recognisable primary inclusions (*e.g.* Plate 6.1J).

GAS HYDRATES IN FLUID INCLUSIONS

During this investigation, a study was undertaken of the occurrence of gas hydrates (or clathrates) in fluid inclusions and their application to fluid inclusion microthermometry. The results of this study have been previously published (Collins, 1979), and are reproduced in Appendix 8.

The main conclusions drawn from the study are that gas hydrates such as the carbon dioxide hydrate ($CO_2.5.75H_2O$), freeze out in fluid inclusions prior to freezing of the remaining aqueous solution to ice. When crystallised in aqueous solutions, gas hydrates form pure compounds of the hydrating agent and H_2O molecules and exclude from the hydrate lattice any salts or ions in solution. Hence the residual aqueous solution, after clathration, is more saline than the original aqueous solution, and measurement of salinity using depression of the fusion temperature of ice by salt will indicate a higher apparent salinity of the aqueous solution. Therefore, the formation of the CO_2 hydrate in CO_2-bearing fluid inclusions, or any gas hydrates in fluid inclusions, invalidates the use of depression of the fusion temperature of ice for estimation of the salinity of an aqueous solution.

However, the temperature of decomposition of the CO_2 hydrate is depressed by saline solutions, similar to the depression of the fusion temperature of ice. In water, the critical decomposition temperature

(melting point) of the CO_2 hydrate is 10.0°C and this decreases with increasing salinity to a minimum temperature of -9.8°C at a salinity of 24.2 mass% NaCl. Therefore, the temperature of decomposition of CO_2 hydrate may be used as a reliable measure of salinity in fluid inclusions consisting of an aqueous phase, a CO_2-rich liquid phase and a CO_2-H_2O gas phase, and in which other gases have not been detected (*e.g.* methane, which forms mixed CO_2-CH_4 hydrates, counteracts the depression by NaCl of the decomposition temperature of the CO_2 hydrate).

Melting (or decomposition) of the CO_2 hydrate (*e.g.* plate 6.1W) has been used during this investigation to measure the salinity of the aqueous phase of CO_2-enriched fluid inclusions (Table A5.1), assuming that methane and other volatiles are not present in the inclusion.

NATURE OF THE INCLUSIONS

The minerals examined for fluid inclusions were mostly quartz and fluorite, but inclusions in siderite and apatite have also been analysed. Most other minerals are too fine grained or opaque to be useful for fluid inclusion study. For example, the average grain size of cassiterite at Cleveland is about 75μm (Mason, 1965), and sphalerite, although coarse grained, is too opaque.

Fluid inclusions in hydrothermal minerals from Cleveland are classified as follows:

Type 1: two-phase aqueous inclusions of low to moderate salinity, commonly with minute solid phases;

Type 2: multi-phase aqueous inclusions bearing non-halide(?) accidental(?) minerals; and

Type 3: three-phase CO_2-bearing inclusions.

Inclusion fluids saturated in NaCl or KCl have not been observed at Cleveland but have been found in fluorite at the Renison tin mine (Collins, 1972) and in fluorite and cassiterite from Mt Bischoff (Little,

1960; Groves and Solomon, 1969). The presence of halite and sylvite as daughter minerals in these inclusions is not considered indicative of an ultrasaline hydrothermal fluid, but rather the result of either localised boiling or 'necking down' of the inclusions (Groves, 1968; Groves and Solomon, 1969). Rare, gas-rich inclusions, co-existing with type 1 inclusions, at Mt Bischoff are also attributed to localised boiling (Groves, 1968; Groves and Solomon, 1969).

Type 1 inclusions

Type 1 inclusions are found in all hydrothermal minerals, occurring as primary, pseudosecondary and secondary fluid inclusions. The cavities of primary and pseudosecondary inclusions are generally regular in shape, varying from faceted ovoid to euhedral in form, and are generally less than 50μm in diameter, but are up to 500μm (Plate 6.1A to N). In Stage IV fluorite, inclusions generally are well faceted, and negative crystal inclusions are common (*e.g.* Plate 6.1K). In Stage I and Stage II minerals, inclusions are less regular in shape, and many are attached to solid phases included in the host mineral (*e.g.* Plate 6.1E to H).

Most type 1 inclusions consist of an aqueous liquid and a vapour bubble which occupies 10%-50% of the cavity volume (c.f. Plate 6.1D, M and N). Daughter(?) minerals in type 1 inclusions in Stage I and Stage II minerals are common and are usually less than 2μm in diameter, or less than 1% of the inclusion volume (Plate 6.1C, H). Type 1 inclusions commonly contain two to four different minerals, and up to seven have been observed in a single inclusion. They may be opaque, isotropic or anisotropic, and do not dissolve on heating to over 500°C*, which is 100°C above the highest homogenisation temperature recorded. Daughter(?) minerals occur rarely in inclusions in Stage IV fluorite.

---

* Maintained at 510°-520°C for approximately one hour.

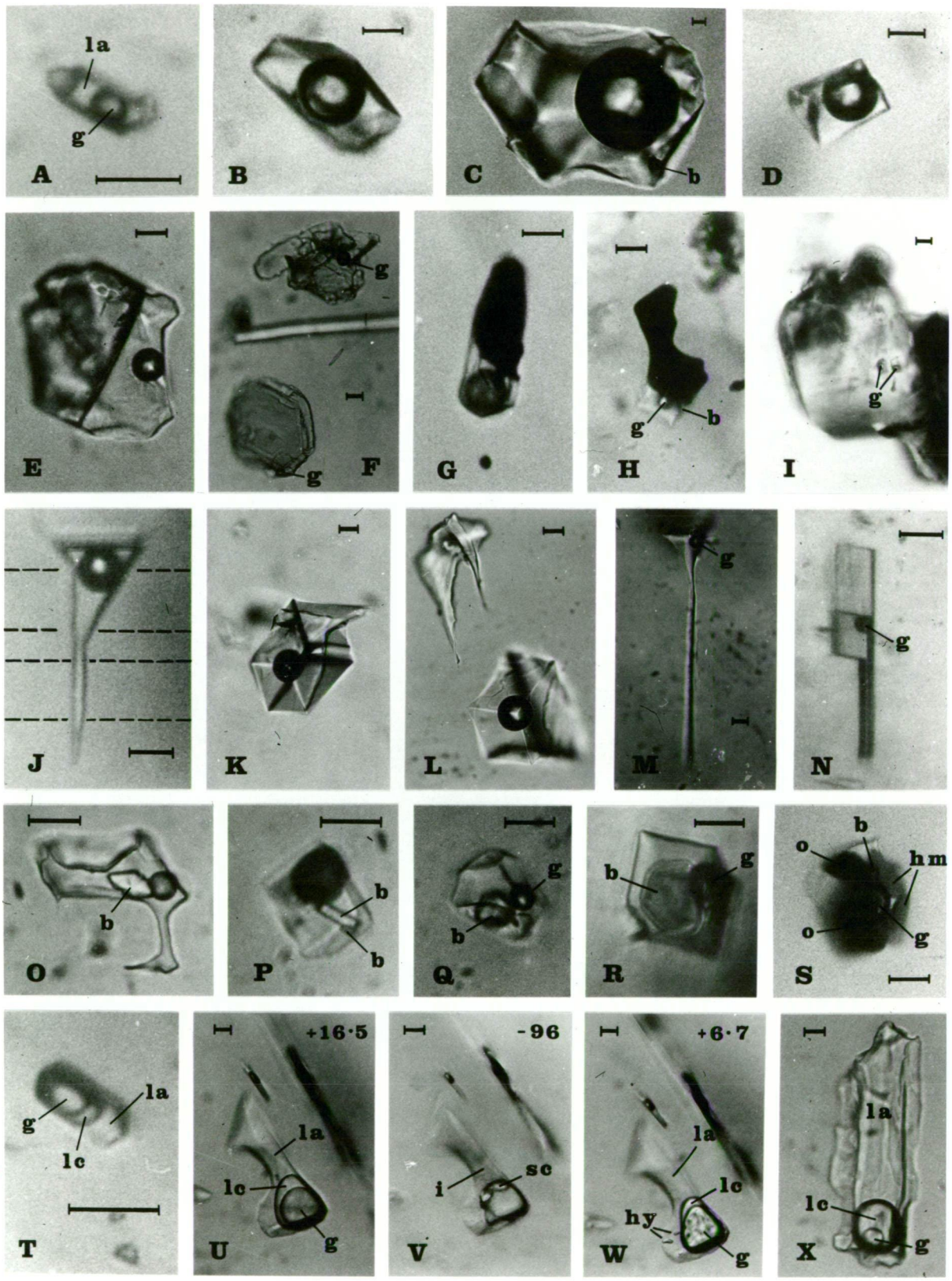

PLATE 6.1 Photomicrographs of primary fluid inclusions in quartz, fluorite, apatite, and siderite from the Cleveland mine, mineralisation stages I, II and IV.
Legend: see over. Scale bar = 10μm.

Plate 6.1 continued

Photomicrographs A-D: Type 1 inclusions in quartz and fluorite, Stages I and II; E-H: Type 1 inclusions attached to solid phases in quartz and fluorite, Stage II; I: Type 1 inclusions in apatite, Stage II; J-N: Type 1 inclusions in fluorite, Stage IV; O-S: Type 2 inclusions in quartz and fluorite, Stage II; T-X: Type 3 inclusions in fluorite, Stages I and II. Symbols: g = gas bubble, la = aqueous liquid, i = ice, lc = CO_2-rich liquid, b = birefringent salt, o = opaque phase, hm = hematite, hy = CO_2 hydrate, sc = CO_2-rich solid phase. All photomicrographs are at room temperature (18-20°C) unless otherwise indicated (i.e. U, V and W). Details of each photomicrograph are listed below, and experimental data for individual inclusions are given in Appendix 5, Table A5.1.

A. Type 1 in quartz, stage I, specimen 104427, inclusion 25.

B. Type 1 in quartz, stage II, specimen 104301, inclusion 61.

C. Type 1 in fluorite, stage II, specimen 104301.

D. Type 1 in fluorite, stage II, specimen 104301, inclusion 52 (Table A5.2). The inclusion has a large vapour/liquid ratio.

E. Type 1 in fluorite, stage II, specimen 104423, inclusion 42. The inclusion has developed adjacent to a solid phase.

F. Type 1 in fluorite, stage II, specimen 104419. Inclusions have developed adjacent to biotite flakes.

G. Type 1 in fluorite, stage II, specimen 104413. The inclusion has developed adjacent to an opaque phase (pyrrhotite?).

H. Type 1 in quartz, stage II, specimen 104346, inclusion 15. The inclusion has developed adjacent to an opaque phase (pyrrhotite?).

I. Type 1 in apatite, stage II, specimen 104423, inclusions 49 and 50. The apatite crystal is a solid inclusion in fluorite.

J. Type 1 in fluorite, stage IV, specimen 104307 inclusion 52. Dashed lines indicate colour banding.

K. Type 1 in fluorite, stage IV, specimen 104351, inclusion 8. A negative crystal inclusion.

L. Type 1 in fluorite, stage IV, specimen 104351. A necked primary inclusion.

M. Type 1 in fluorite, stage IV, specimen 104431, inclusion 2. A needle-shaped primary inclusion.

N. Type 1 in siderite, stage IV, specimen 104395, inclusion 18.

Plate 6.1 continued

O. Type 2 in fluorite, stage II, specimen 104419. The inclusion contains a pale green, birefringent mineral.

P. Type 2 in fluorite, stage II, specimen 104419. The inclusion contains a columnar or needle-like birefringent mineral, exhibiting parallel extinction.

Q. Type 2 in fluorite, stage II, specimen 104388, inclusion 2. The inclusion contains a green, birefringent mineral exhibiting parallel extinction.

R. Type 2 in fluorite, stage II, specimen 104388. The inclusion contains a large, green, hexagonal(?), plate-like mineral.

S. Type 2 in fluorite, stage II, specimen 104423. The inclusion contains two red plates of hematite(?), at least one birefringent mineral, and two opaque phases.

T. Type 3 in fluorite, stage I, specimen 104455, inclusion 28. The inclusion exhibits critical homogenisation of the CO_2-rich and H_2O-rich phases.

U. Type 3 in fluorite, stage II, specimen 104307, inclusion 5. (Photomicrograph at + 16.5°C).

V. Same as U. Showing CO_2-rich solid phase (- 96°C).

W. Same as U. Showing CO_2 hydrate crystals in the aqueous phase (+ 6.7°C).

X. Type 3 in fluorite, stage II, specimen 104423, inclusion 3. The inclusion has a large liquid/gas ratio in the CO_2-rich phases.

Minor amounts of gas or volatile liquid (probably CO_2) have been detected in some type 1 inclusions during freezing runs, using techniques listed by Collins (1979). These are recorded in Table A5.1.

Type 2 inclusions

Type 2 inclusions are only found in minerals from the second stage of mineralisation. They consist of an aqueous phase, a vapour bubble (10-40% of the inclusion volume), and relatively large accidental crystals (Plate 6.1O to S). Common forms of these unidentified non-opaque minerals are rhombs, needles and plates (Plate 6.1O, P and R, respectively). They are green to colourless, birefringent and do not dissolve on heating. Needles commonly exhibit parallel extinction, and may be tourmaline. Some green plates have hexagonal outlines (*e.g.* Plate 6.1R) and may be biotite. An attempt was made to identify the minerals using an electron micro-probe, by scanning a broken mineral surface, but type 2 inclusion cavities were not located. Most of the daughter minerals are large relative to the inclusion cavity (*e.g.* Plate 6.1R) and were probably trapped as a solid phase within a developing crystal cavity.

In specimens 104423 and 104455 there are a few inclusions containing red, hexagonal flakes which darken on heating, but do not dissolve, and are probably hematite. Rare inclusions in fluorite in specimen 104423 contain opaque and birefringent minerals in addition to one or two hematite flakes (Plate 6.1S). These inclusions probably formed by the trapping of fluid about a mineral or group of minerals (including hematite) attached to the surface of a growing fluorite crystal.

Type 3 inclusions

Type 3 inclusions are found rarely in Stage 1 quartz-wolframite-molybdenite veins and commonly in the main phase of mineralisation (Stage II). Primary type 3 inclusions are generally less than 30μm in

diameter, and up to 200μm, occurring in regular to rounded cavities (Plate 6.1T, U), but generally with irregular and embayed cavity walls (Plate 6.1X). These inclusions consist of an aqueous phase, a CO_2-rich liquid phase and a CO_2-rich gas bubble. Many type 3 inclusions also contain minute non-halide(?) daughter(?) minerals similar to those occurring in type 1 inclusions, though not as common.

The composition of the non-aqueous phase is considered to be predominantly carbon dioxide with only minor amounts of other gases or volatile liquids. This is deduced from the observation of critical point behaviour at homogenisation of the CO_2-rich liquid and CO_2-rich vapour phases at the CO_2 critical temperature (+31.1°C), and from melting of gas hydrate crystals, formed during freezing runs, below 10°C which is the critical decomposition temperature of the CO_2 hydrate (Collins, 1979; Appendix 8).

The mole fraction of CO_2 (X_{CO_2}) in type 3 inclusions has been estimated using the volumetric method described by Burruss (1981) and results are reported in Table A5.1. The relative volume % of CO_2-rich and H_2O-rich phases in the two phase region (CO_2 liquid and CO_2 gas have homogenised) have been estimated from photomicrographs assuming that areal ratios are proportional to volume ratios. Roedder (1979) has demonstrated the difficulty in translating accurately areal proportions to 3-d volume proportions in irregularly shaped inclusions, and the estimated volume % aqueous phase is probably slightly over-estimated with resultant underestimation of X_{CO_2}. Also, for inclusions that homogenise at or near the critical point of CO_2 a slight error in estimated internal pressure will cause a relatively large error in estimated fluid density (*i.e.* in the range 70-90 bars in Fig. 11 of Burruss, 1981*b*) thereby reducing the accuracy of X_{CO_2} in such inclusions. Taking into consideration the uncertainties and inaccuracies involved in the determination (see also Burruss, 1981; Hendel and Hollister, 1981) type 3 inclusions in Stage II minerals have an estimated X_{CO_2}=

0.08 - 0.12 (Appendix 5, Table A5.1; Fig. 6.5). All type 3 inclusions in Stage II contain approximately the same proportions of CO_2 and H_2O as the inclusions for which X_{CO_2} has been determined, and there are no inclusions with more than about 15 mole% CO_2 (*i.e.* no CO_2-rich inclusions). In a sample of Stage I fluorite (104455) a single inclusion in a planar group of type 3 inclusions that contain the same proportions of CO_2 and H_2O phases and which exhibit critical point behaviour has an estimated $X_{CO_2} = 0.3$. These are the only primary(?) type 3 inclusions observed in Stage I minerals.

Several inclusions in Stage II fluorite (104321, 104345, 104397) exhibit critical point behaviour at homogenisation of the CO_2-rich phases in the range +27.1 to +28.5°C (Fig. 6.1) which may indicate the presence of small amounts of methane (*e.g.* Burruss, 1981). Melting of the CO_2 solid phase was measured at -60.5° and -59.5°C in a single inclusion in Stage I quartz (104455, inclusion 30) and in Stage II fluorite (104307, inclusion 5), respectively (Fig. 6.1). Carbon dioxide melting below -56.6°C indicates the presence of other volatiles, in particular methane (*e.g.* Burruss, 1981). Depression of CO_2 melting by 3 to 4°C may indicate up to 12-15 mole% CH_4 in the non-aqueous phase, but CO_2 melting alone does not uniquely define the CH_4 composition (Burruss, 1981*b*). In view of the limited data, and problems encountered in calibration and use of the Chaixmeca apparatus at these temperatures (Appendix 5), the CO_2 liquid/CO_2 gas homogenisation temperature data are considered more reliable. Therefore, the non-aqueous phase in type 3 inclusions is composed predominantly of carbon dioxide with minor to trace amounts of methane and possibly some other volatile compounds. The mole fraction of methane in the CO_2-rich phases is certainly less than 0.15 and is most likely to be about 0.02 or less. Methane does not occur in all type 3 inclusions, as indicated by homogenisation of the CO_2-rich phases at, or very close to the critical temperature of pure CO_2 (*i.e.* 31.1°C) (Fig. 6.1).

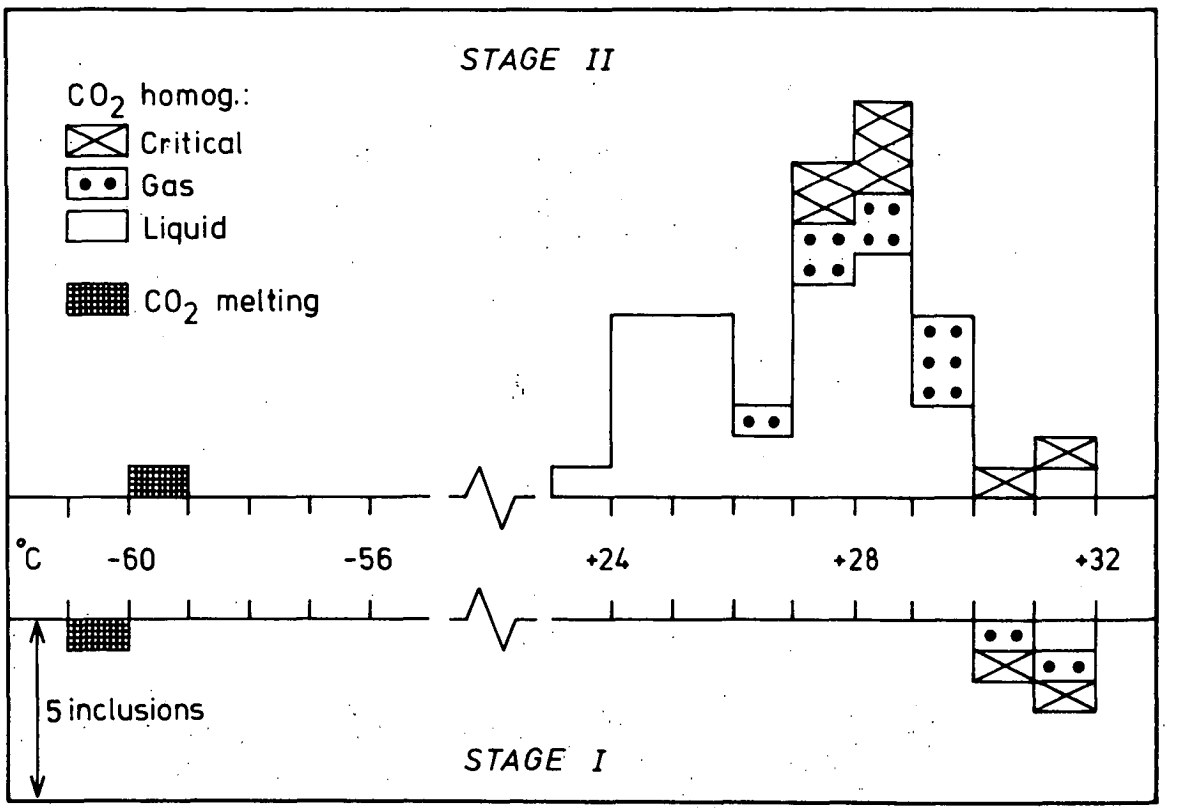

FIG. 6.1 Frequency distribution of melting and homogenisation temperatures of CO_2-rich phases in type 3 inclusions. Data are for primary inclusions in specimens 104307, 104321, 104345, 104396, 104397, 104402, 104422, 104423 and 104455 (Table A5.1).

Type 3 inclusions commonly are associated with type 1 inclusions. In the early quartz-wolframite-molybdenite veins, type 3 inclusions occur within the same grains as type 1 inclusions, but co-existing type 1 and type 3 inclusions have not been observed. In Stage II mineralisation, co-existing(?) type 1 and type 3 inclusions have been observed, but generally occur as separate groups of each inclusion type.

Composition of the aqueous phase

The overall composition of the aqueous phase may be deduced from measurements of phase changes induced in fluid inclusions at low temperatures (*i.e.* freezing experiments). The principal dissolved components and their relative proportions in the aqueous phase may be inferred from the temperature of initial melting (*e.g.* Crawford, 1981). Although looked for, eutectic melting was not observed in inclusions in samples from Cleveland, but this is not uncommon in low salinity inclusions due to the very small volumes of melt generated at the eutectic (*e.g.* Crawford, 1981) and the difficulty in observation of phase changes in small inclusions. The only accurate measurements on Cleveland samples are final melting temperatures of ice and gas hydrate (reported in Table A5.1) which indicate total salinities of 7-15% NaCl in type 1 and 2 inclusions and 2-7% NaCl in the aqueous phase in type 3 inclusions.

The salinity of type 1 (and 2) inclusions is similar to the salinity of aqueous inclusions at Mt Bischoff (5-15% NaCl; Groves and Solomon, 1969) and to calculated fluid salinities of cassiterite-bearing stages at the Renison mine (10.5% NaCl; Patterson *et al.*, 1981). Bulk fluid inclusion analyses of ore and mineral samples from Mt Bischoff and Renison indicate that the extracted inclusion fluids are Na-K-Ca-Mg chloride brines and that NaCl is the dominant dissolved salt with Na/K ratios of 1.1-4.0 and >5.5, respectively (Groves and Solomon, 1969; Patterson *et al.*, 1981). Type 1 (and 2) inclusions at Cleveland probably have a composition similar to that at Mt Bischoff and Renison, though the

potassic alteration halo in the Deep Creek Volcanics indicates KCl may be a more significant component of the hydrothermal fluid at Cleveland. However, in the absence of more accurate data it is assumed that NaCl is the dominant dissolved salt, and in following discussions fluid inclusions are considered in terms of the systems H_2O-NaCl and CO_2-H_2O-NaCl.

TEMPERATURE AND SALINITY DATA

Inclusions in quartz-wolframite veins (Stage I)

Quartz and fluorite in the Stage I quartz-fluorite-wolframite-molybdenite veins (104379, 104380, 104381, 104382, 104427, 104455) contain predominantly type 1 inclusions and rarely type 3 inclusions. Type 1 inclusions containing minute daughter minerals are rare but when such inclusions occur, they contain up to three daughter minerals, including hematite(?). Type 2 inclusions are absent. Quartz and fluorite in these veins are intergrown, and formed contemporaneously with wolframite, molybdenite, bismuth and bismuthinite.

Only a few type 1 inclusions were large enough for freezing experiments, the results of which are plotted in Figure 6.2. Quartz and fluorite from deep vein intersections (104427, 104455) contain fluids of 8-11% NaCl which is marginally less than inclusions in specimens from shallower intersections (104379-104382) with 9.5-13% NaCl (Fig. 6.2). This difference is probably due to the smaller number of inclusions measured in the deep specimens, and the salinity is essentially consistent at 9-12% NaCl.

Homogenisation temperatures of type 1 inclusions show very little variation in temperature (Fig. 6.2), but there is an indication of slightly higher homogenisation temperatures in two deep specimens of quartz-fluorite-wolframite veins (104427, 104455 at M.L.s 620 m and 535 m, respectively) compared with four samples near the upper ore-

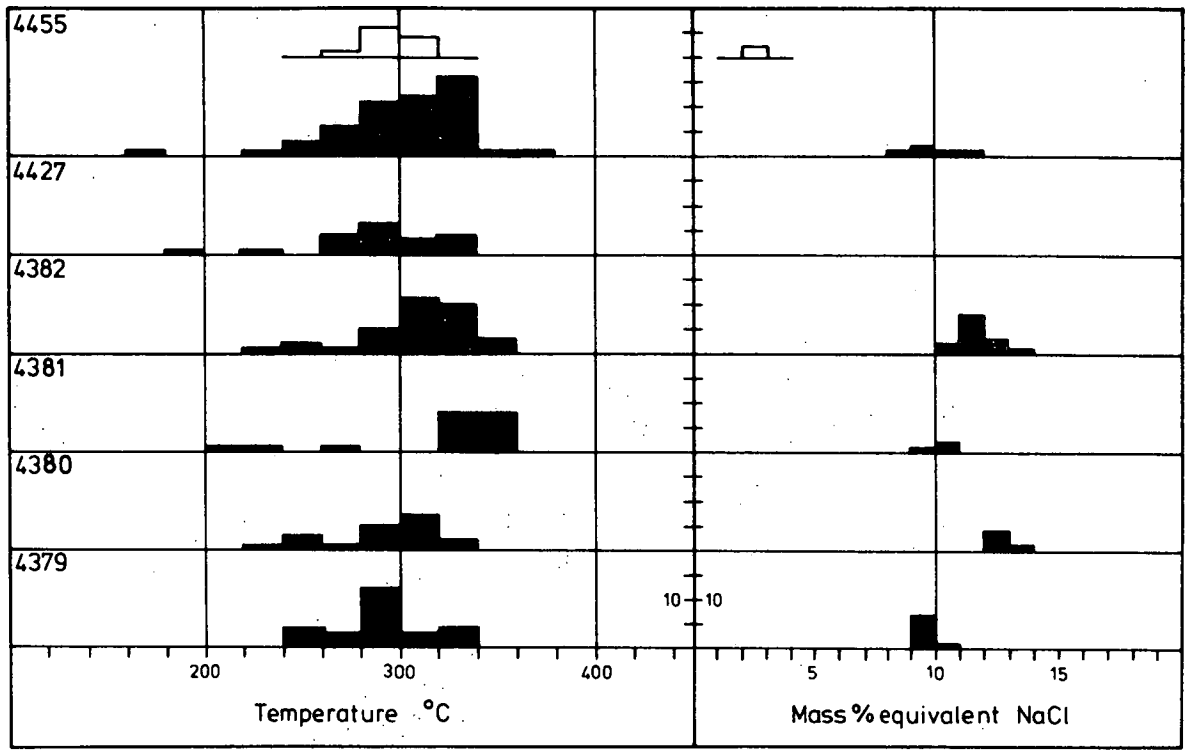

FIG. 6.2 Frequency distribution of homogenisation temperatures and salinity data for type 1 inclusions (black histograms) and type 3 inclusions (white histograms) in stage I quartz and fluorite. Specimen numbers are prefixed by 10 (*i.e.* 4455 = 104455).

SAMPLE DETAILS:

Specimen no.	*Depth (m, M.L.)*	*Mineral(s)*
104379	980	Fluorite
104380	970	Fluorite, quartz
104381	905	Fluorite, quartz
104382	905	Fluorite, quartz
104427	620	Fluorite, quartz
104455	535	Fluorite

bodies (104379-382 at 905 m to 980 m M.L.). This trend is reinforced when differences in lithostatic (or hydrostatic) pressure between the two sample groups are taken into consideration. If lithostatic pressure prevailed during vein emplacement, the resulting pressure difference of 8-10 MPa (27 MPa/km depth) represents a positive temperature difference of about 20°C for the deep specimens.

In fluorite from specimen 104455 a planar group of type 3 inclusions, up to 15μm long, have relatively large CO_2 contents (X_{CO_2} = 0.3; *e.g.* Plate 6.1T), and exhibit homogenisation phenomena consistent with critical point behaviour. Homogenisation of the CO_2 liquid and CO_2 gas phases in five of these inclusions occurred within the range 30.6°-31.2°C with two exhibiting abrupt fading of the meniscus at 30.7° and 31.2°C at slow heating rates (<0.5°C/min). The other three homogenised in the liquid or gas phase (Fig. 6.1). Only one inclusion was large enough to observe freezing behaviour, for which CO_2 melting occurred at -60.5°C and gas hydrate melting was measured at +8.9°C, equivalent to 2.3% NaCl. Homogenisation of the CO_2-rich and aqueous phases in 10 of these inclusions occurred within the range 295°-311°C (nine homogenised between 295° and 303°C). Seven of the ten inclusions exhibited critical point behaviour at homogenisation, whilst the others homogenised rapidly to either an H_2O dominant or CO_2 dominant phase.

Main phase of mineralisation (Stage II)

Specimens from the main phase of mineralisation contain primary and pseudosecondary fluid inclusions of types 1, 2, and 3 (Plate 6.1). Type 1 is the most common, usually containing several minute, unidentified, accidental and/or daughter minerals. Type 3 inclusions also may contain minute solid phases, and are more common than type 2.

During freezing runs temperatures of CO_2 melting, CO_2 hydrate decomposition and ice melting were measured in sufficiently large inclusions. During heating, homogenisation of the CO_2-rich phases and of the CO_2-rich and aqueous phases were recorded (Appendix 5).

As CO_2 is a common phase in fluid inclusions in minerals from this stage of mineralisation all inclusions were checked for the formation of gas hydrate during freezing runs. Ice melting temperatures for inclusions in which gas hydrate formation was detected have been recorded, but not used in discussion of salinity.

Salinity estimates obtained from freezing data (Fig. 6.3) are divided into two distinct groups corresponding to their classification as type 1 (and 2) and type 3 inclusions. In type 1 and 2 inclusions there is a predominance of ice melting within the range -5° to -10°C corresponding to salinities of 8-14% NaCl. In type 3 inclusions, CO_2 hydrate decomposition occurs within the range +8.9° to +7°C corresponding to a salinity of 2-6% NaCl in the aqueous phase. The salinities of inclusion types 1 and 2 and type 3 are consistent throughout the spatial distribution and mode of occurrence (vein, vug, ore) of the specimens, indicating a uniform composition of the ore fluid. The maximum inclusion salinity measured is 14.5% NaCl (ice melting at -10.4°C).

Although no distinct pattern of salinity distribution has emerged from the study there is a semblance of a spatial and distinct temporal variation in the distribution of homogenisation temperatures.

Homogenisation temperatures of type 1 (and 2) inclusions fall into two groups, depending upon their association with type 3 inclusions. Type 1 inclusions associated with type 3 inclusions generally homogenise below 320°C with the majority falling within the range 270°-310°C. In many of these type 1 inclusions, the formation of gas hydrates was detected

during freezing studies, indicating the presence of minor amounts of CO_2(?) in the gaseous phase. All of these type 1 inclusions homogenised in the liquid phase. The associated type 3 inclusions generally homogenise in the liquid phase below 310°C, with the majority falling within the temperature range 250°-310°C. Thus the CO_2-enriched type 3 inclusions and associated aqueous (or CO_2 depleted) type 1 inclusions have very similar homogenisation temperatures (*e.g.* in specimen 104307 coexisting(?) type 1 and type 3 inclusions have been observed, with a limited range in homogenisation temperatures of the two inclusion types, Fig. 6.3). The association of these two inclusion types with similar homogenisation temperatures is discussed below (Chapter 8).

Type 1 (and 2) inclusions not associated with type 3 inclusions homogenise in the liquid phase at temperatures up to 370°C with the majority homogenising within the range 280°C-360°C. In addition, three inclusions in specimen 104395 exhibited critical point behaviour at 395°-415°C. There is a semblance of a spatial temperature variation within these samples, which also corresponds with the tin content of the ore. The highest temperatures recorded occur in specimens 104395 and 104345 which come from within or close to the low grade zone in the centre of the upper ore bodies (Fig. 4.6). Homogenisation temperatures of these specimens range from 320°C to 415°C with a mode at 340-360°C. Homogenisation temperatures of specimens from the ore grade mineralisation, fall within the range 300°C to 380°C with a mode at 320°-340°C. This suggests there is a slightly higher temperature region in the central part of the upper ore bodies which corresponds to the low grade zone and also with the nose of the cone-shaped, Stage I quartz-fluorite-wolframite±molybdenite stockwork vein mineralisation (Fig. 4.6).

FIG. 6.3 Homogenisation temperatures and salinity data for primary (?) fluid inclusions in stage II quartz, fluorite and apatite. Specimen numbers are prefixed with 10 (*i.e.* 4301 = 104301). Black histograms are for type 1 inclusions, and white histograms for type 3 inclusions. Hatched histograms for specimen 104423 are data for type 1 inclusions in apatite (*e.g.* Plate 6.1 I). Histograms A, B and C for specimen 104301 are for different generations of stage II quartz and fluorite, younging from A to C (A = quartz and fluorite in ore; B = the base of a large fluorite crystal (30 - 40 mm in length); and C = the outer edge of the same fluorite crystal).

SAMPLE DETAILS:

Specimen no.	*Depth (m, M.L.)*	*Minerals*
104301	1220	Fluorite, quartz
104307	1240	Fluorite
104320	1190	Fluorite, quartz
104345	1195	Fluorite, quartz
104346	1195	Quartz, fluorite
104351	1185	Quartz, fluorite
104395	1225	Quartz
104396	1215	Fluorite, quartz
104397	1205	Fluorite, quartz
104401	885	Fluorite
104402	880	Fluorite
104413	865	Fluorite
104422	860	Fluorite
104423	850	Fluorite, apatite
104450	875	Fluorite

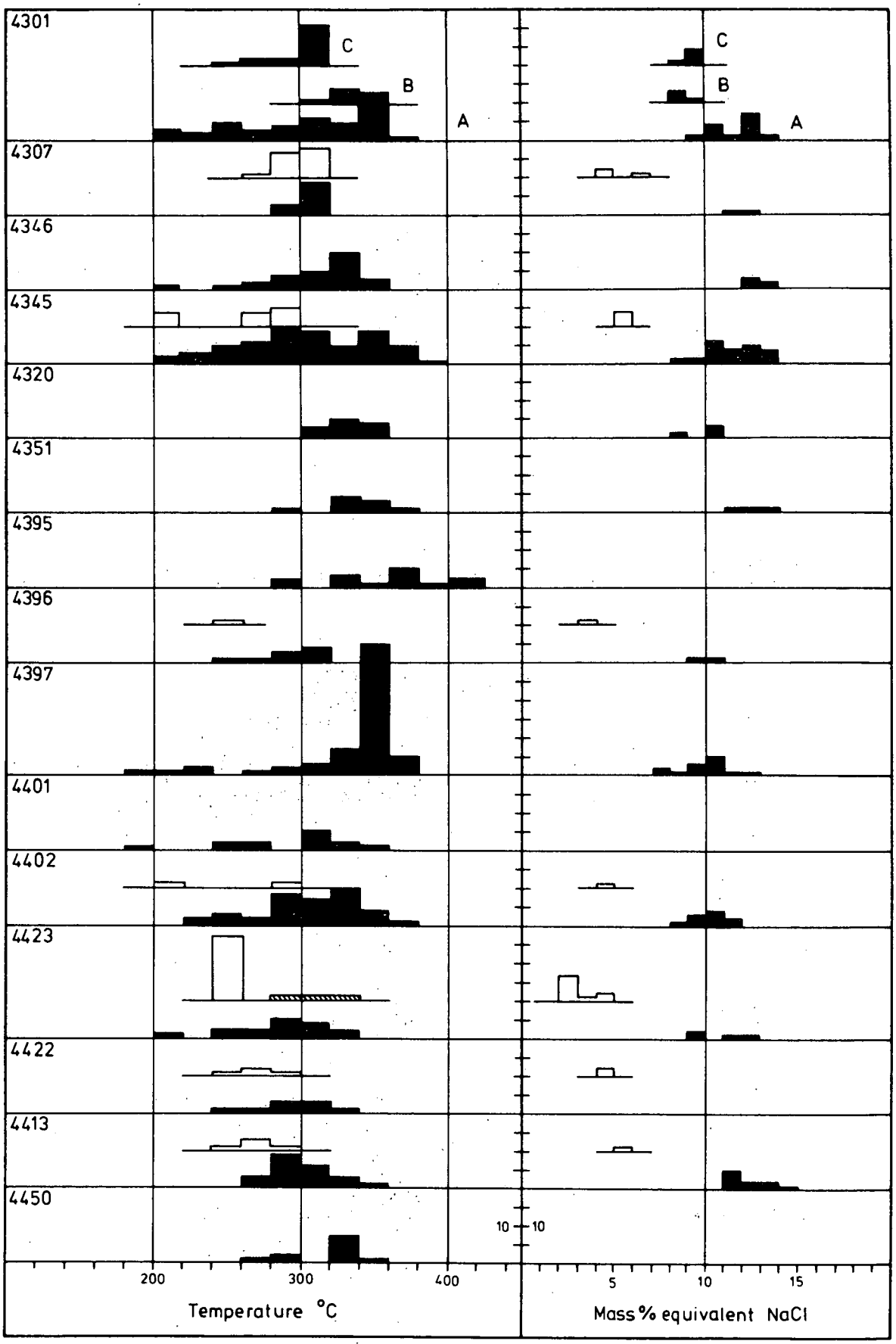
4301
C
B
A
4307
4346
4345
4320
4351
4395
4396
4397
4401
4402
4423
4422
4413
4450
10
200
300
400
Temperature °C
C
B
A
10
5
10
15
Mass % equivalent NaCl

FIGURE 6.3

A further decrease in temperature towards the end of the Stage II mineralisation is indicated by homogenisation temperatures of type 1 inclusions in fluorite and quartz in specimen 104301, as illustrated in histograms A, B, and C in Figure 6.3. The specimen consists of massive replacement mineralisation and slightly later pale blue-colourless fluorite crystals lining a vug within one of the sulphide lenses. The fluorite is blanketed with later (Stage IV?) calcite and Stage V pyrite. Histogram A is of homogenisation temperatures and salinities of inclusions in fluorite and quartz of the sulphide lens, histogram B of inclusions from the base of a fluorite crystal, and C of inclusions from the top or outer part of the same crystal. The histograms indicate a gradual decrease in temperature from 340°-360°C for the massive ore (histogram A) to 300°-320°C for crystallisation of the last portion of the fluorite crystal. A similar trend is apparent for the salinity of the fluids but instead of a gradual decrease there is a marked step from 13-14% NaCl in the massive ore to 8-10% NaCl for inclusions in the fluorite crystal (Fig. 6.3).

In specimen 104423, three type 1 inclusions (less than 10μm long) in euhedral apatite crystals occurring as solid inclusions in fluorite (Plate 6.1I), homogenise at 286°, 312°, and 321°C, which is within the temperature range of the type 1 inclusions in the host fluorite (Fig. 6.3).

Homogenisation temperatures of the CO_2-rich phases in the type 3 inclusions range between 22.5° and 31.1°C with a mode at 27° to 29°C (Fig. 6.1). Several of these inclusions exhibit critical point behaviour in the range 27.1° to 31.1°C with a mode at 28° to 29°C. Homogenisation of the CO_2-rich phases occurred in both the liquid and gaseous phases indicating variation in the CO_2 content and density of the fluid trapped in individual inclusions. Critical homogenisation

close to and at 31.1°C, the critical temperature of CO_2, occurred in two inclusions (104422, 104423) indicating CO_2 is the dominant component of the CO_2-rich phases.

Inclusions in late fluorite (Stage IV) and late siderite

Fluorite from Stage IV mineralisation (104307, 104351, 104429-31) contains only type 1 inclusions, commonly occurring as negative crystals (Plate 6.1K) and as regular faceted cavities associated with growth zones in fluorite (Plate 6.1J). In deep specimens of fluorite (104429-31), needle-shaped inclusions wedged at one end are common (Plate 6.1M). Primary inclusions are readily recognised and so too are features such as 'necking down' of inclusions (Plate 6.1L) which may give erroneous results. The inclusions range from less than 20μm to about 500μm largest dimension. Freezing and heating data are plotted in Figure 6.4. Daughter(?) minerals are rare in these inclusions, and the formation of gas hydrate was not detected during freezing experiments.

Type 1 inclusions in fluorite contain waters ranging from 6-20% NaCl with a mode at 8-10% NaCl (Fig. 6.4), which represents a slight decrease in salinity compared with the earlier stages of mineralisation. Inclusions in specimens 104429-31 from about 540 m M.L., approximately 700 m vertically below the other two specimens (104307, 104351), also have the greatest, unexplained variation in salinity of all the specimens examined.

A metastability effect was suspected in some primary type 1 inclusions in fluorite specimens 104429-31 when the final melting of ice was accompanied by a sudden reappearance of the gas bubble. Ice melting temperatures for such inclusions could not be reproduced. This was most prevalent in small (less than 20μm) inclusions with very low (100°-130°C) homogenisation temperatures.

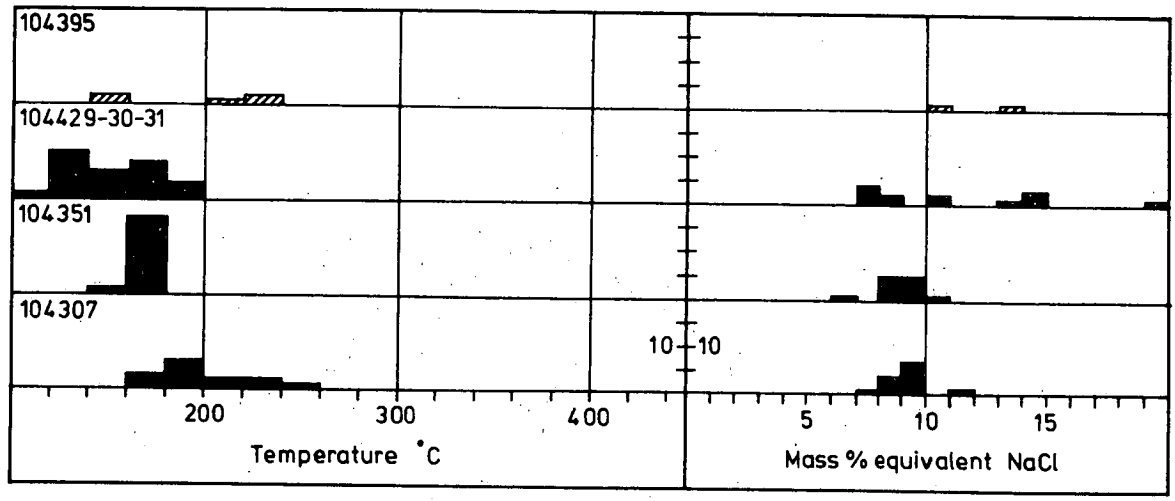

FIG. 6.4 Homogenisation temperatures and salinity data for type 1 inclusions in stage IV fluorite (black histograms) and in siderite (hatching).

SAMPLE DETAILS:

Specimen no.	*Depth (m, M.L.)*	*Mineral*
104307	1240	Fluorite
104351	1185	Fluorite
104395	1225	Siderite
104429	550	Fluorite
104430	540	Fluorite
104431	540	Fluorite

The range of homogenisation temperatures of type 1 inclusions in Stage IV fluorite is quite large, 100°-260°C (Fig. 6.4) but in individual specimens the range may be narrow. The deep specimens (104429-31) have the widest range, and also the lowest homogenisation temperatures, but deposition temperatures show less contrast with shallow specimens because a positive correction must be made for the relative differences in pressure. All but one of the inclusions in specimen 104351, of fluorite lining a cavity in an open vein, homogenise within the very limited range 164°-177°C. Secondary inclusions in Stage II quartz and fluorite from this specimen also homogenise within the range 144°-191°C, and have salinities of 7.5-13.7% NaCl, similar to the Stage IV fluorite.

In specimen 104395, siderite occurs interstitially with earlier formed quartz. Negative crystal type 1 inclusions (Plate 6.1N) in the siderite homogenise at 214°-222°C and contain waters of 10.4 and 13.2% NaCl. This is a slightly higher temperature and more saline solution than the majority of inclusions in Stage IV fluorite (Fig. 6.4).

GEOBAROMETRY

Geological considerations

An estimate of pressure may be obtained by calculating the maximum thickness of overburden above the deposit at the time of mineralisation. This estimate is only an approximation because of difficulties in applying an accurate geological reconstruction (*e.g.* stratigraphic correlation, structural complications), and uncertainty as to whether lithostatic or hydrostatic loads are applicable.

Groves (1968) estimated a maximum overburden thickness of 5790 m above the Hall Formation by the end of the Early Devonian. This was calculated by assuming that 1520 m of a possible 2440 m of Crimson Creek Formation correlates are below the Hall Formation. However, the thickness of the Deep Creek Volcanics is estimated to be about 500 m,

and on regional trends, this sequence passes close to the northern margin of the Precambrian outlier at Mt Bischoff. Hence there is probably not more than 1000 m of Cambrian rock below the Hall Formation, and the maximum thickness of rocks which could have been deposited above the Hall Formation is estimated as follows:

Siluro-Devonian	1800 m
Ordovician	30 m
Cambrian	
Dundas Group	2605 m
Crimson Creek Formation	1500 m
Total	5935 m

The stratigraphic thickness of approximately 5935 m is probably too high as the Cambrian sequence may be considerably reduced in the Cleveland area (*e.g.* Dundas Group correlates have not been found north of the Meredith Granite). Also, mid-Devonian folding and uplift (associated with the Tabberabberan Orogeny) which preceded emplacement of the late-Devonian granitoids was accompanied by severe erosion which would have reduced the overburden thickness (*e.g.* Solomon *in* Spry and Banks, 1962). In contrast, the tectonically emplaced mafic-ultramafic complexes (*e.g.* Whyte River Complex) may have had a positive effect on overburden thickness, but this too is unknown.

The estimated maximum overburden thickness of 5935 m is equivalent to a lithostatic load of 160 MPa and a hydrostatic load of 60 MPa.

Further constraints on pressure may be derived from the level of emplacement of the late-Devonian granitoids, which appear to have been emplaced at relatively shallow depths at confining pressures below 200 MPa (Solomon, 1981). An estimate of pressure may be derived from liquidus phase relationships for the system quartz-albite-orthoclase-

anorthite-water (Fig. 3.16). For the Meredith Granite, the normative quartz:albite:orthoclase ratios of equigranular and porphyritic biotite adamellite plot as 'minimum melts' (Winkler, 1979) on the 100 MPa quartz-feldspar cotectic boundary, close to the minimum liquidus temperature in a fluorine-free system (Fig. 3.16). The presence of fluorine in a granitic melt deflects the quartz-feldspar boundary away from the quartz apex (Manning, 1981), but in this situation it is not considered to have been influential as the fluorine content of granitic rock from the Meredith Granite is very low (less than 0.2%F, Groves *et al.*, 1972).

In summary, geological considerations (*i.e.* overburden thickness and granite composition) indicate a confining pressure of 100-160 MPa at the time of emplacement of the Meredith Granite.

Fluid inclusion data

An estimate of confining pressure at the time of ore formation may be deduced from the nature and composition of fluid inclusions and from critical point behaviour in some type 1 and type 3 inclusions.

As there is no evidence of boiling during trapping of inclusions in the samples studied (*e.g.* no highly saline or gas-rich inclusions), then the inclusions must have formed from an homogeneous fluid at a pressure and temperature above the solvus of the hydrothermal fluid. The absence of evidence for boiling indicates a hydrostatic column depth of at least 1800 m for a 10% NaCl solution at 350°C, corresponding to a minimum pressure of 18 MPa (Hass, 1971). However, the fluid temperature was probably much higher than 350°C, (the mode of homogenisation temperatures of type 1 inclusions) and extrapolation of Hass' (1971) boiling point curve for a 10% NaCl solution indicates hydrostatic column depths in excess of 2.5 km at temperatures above 400°C and in excess of 3.5 km above 450°C, corresponding to minimum pressures of about 25 MPa and 35 MPa, respectively.

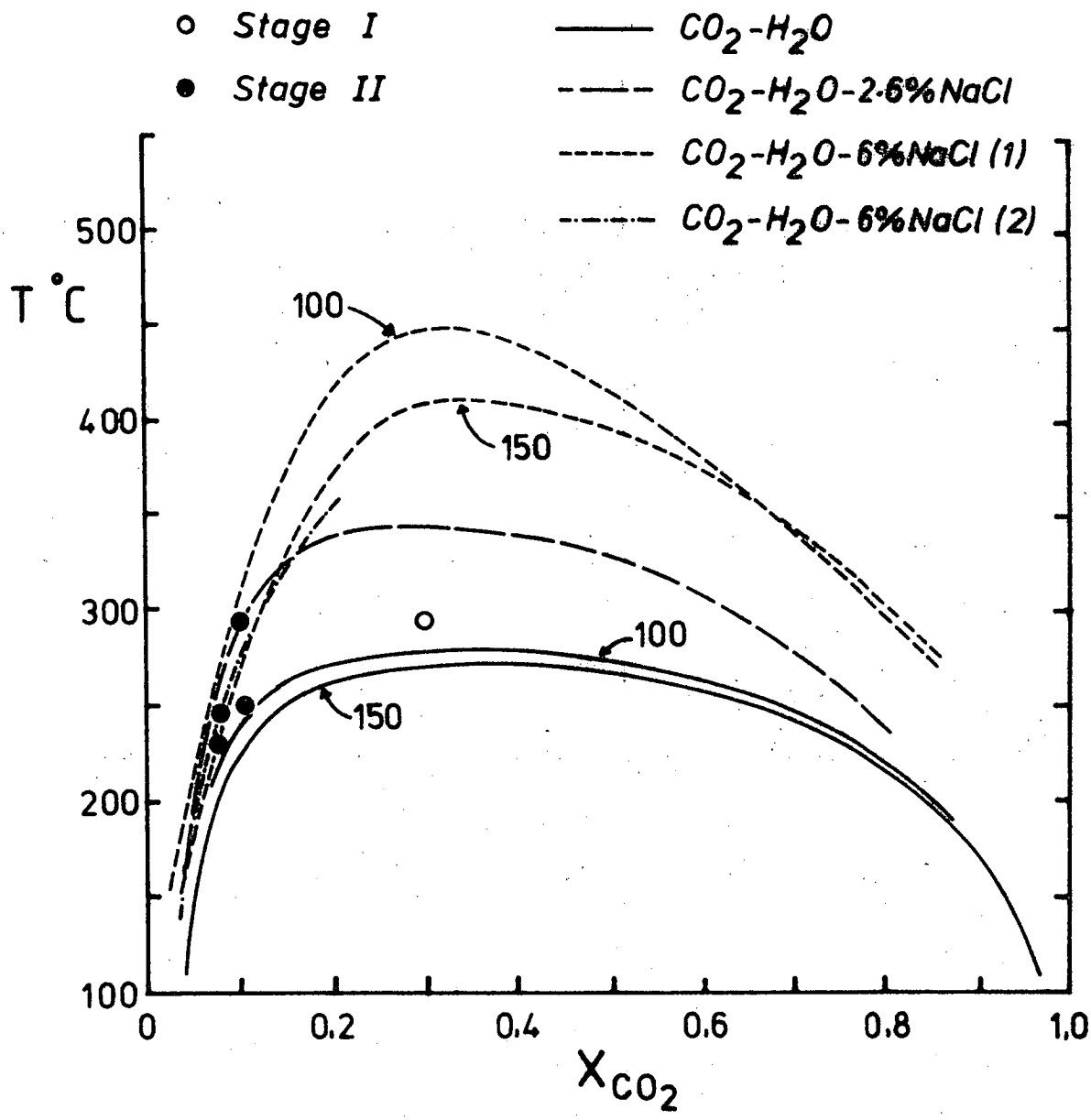

FIG. 6.5 Homogenisation temperature and CO_2 content (X_{CO_2} = mole fraction CO_2) of type 3 inclusions. Lines are solvi for the CO_2-H_2O system (Todheide and Franck, 1963), CO_2-H_2O-2.6% NaCl system (Hendel and Hollister, 1981) and CO_2-H_2O-NaCl system (after Gehrig *et al.*, 1979(1); Takenouchi and Kennedy, 1965(2)). Numbers on lines indicate experimental data at either 100 or 150 MPa. The CO_2-H_2O-2.6% NaCl line is an empirical solvus at 100 to 200 MPa.

In a sample of Stage I quartz-wolframite veins (104455) a planar group of type 3 inclusions containing about 30 mole% CO_2 exhibit critical point behaviour at homogenisation of the CO_2-rich and H_2O-rich phases. The temperature and pressure at the time of trapping of these inclusions must have been equal to, or slightly greater than, the critical temperature and pressure of the fluid. These inclusions homogenise in the range 295° to 311°C (mode 300°C) and have a salinity of 2.3% NaCl in the aqueous phase. Thus the CO_2-H_2O-2.5% NaCl system (Hendel and Hollister, 1981) is a good approximation of these inclusions. On a T-X_{CO_2} diagram (Fig. 6.5) type 3 inclusions in Stage I plot on the high pressure side of an empirical solvus at 100-200 MPa for a 2.5% NaCl fluid, close to an interpolated position of the critical curve. This could mean a minimum trapping pressure well in excess of 200 MPa and/or a salinity slightly less than 2.3% NaCl, though the effect on the solvus of salts other than NaCl is not known. The estimated salinity of the aqueous phase is considered to be reasonably accurate, and it is unlikely that the confining pressure which prevailed during trapping of these inclusions exceeded 200 MPa (most tin deposits formed at confining pressures in the range 30-200 MPa). Thus type 3 inclusions in Stage I probably were trapped at a temperature slightly above 300°C and at a confining pressure close to, but below, 200 MPa.

Further constraints on the minimum pressure of ore formation are imposed by the composition of type 3 inclusions in Stage II, the CO_2 content of which are generally consistent at 8-12 mole% CO_2. The majority of type 3 inclusions homogenise at 250°-300°C and contain 4-7% NaCl in the aqueous phase (Fig. 6.3). Hence the CO_2-H_2O-6% NaCl system (Takenouchi and Kennedy, 1965; Gehrig *et al.*, 1979) is a reasonable approximation of type 3 inclusions. On a T-X_{CO_2} diagram, type 3 inclusions in Stage II

plot in a region of steep pressure gradients and over-lapping isobars (Fig. 6.5) but tend to plot along the 150 MPa solvus for a 6% NaCl solution. Type 3 inclusions containing 10 mole% CO_2 and 6% NaCl that homogenise at 300°C would have a minimum trapping pressure of about 120 MPa and inclusions that homogenise at 250°C indicate pressures in excess of 160 MPa (Takenouchi and Kennedy, 1965; Gehrig *et al.*, 1979). Obviously the temperature of the hydrothermal fluid was higher than the homogenisation temperature, but even so, type 3 inclusions trapped from a homogeneous fluid indicate confining pressures of at least 100 MPa.

In specimen 104395 (Stage II ore), three very small type 1 inclusions exhibited apparent critical point behaviour at homogenisation at temperatures of 395°-415°C (mode 410°C). In the system H_2O-NaCl (Sourirajan and Kennedy, 1962) this corresponds to a minimum pressure of about 31 MPa and a 3.6% NaCl solution. Type 1 inclusions, however, have salinities of 7-14% NaCl (mode about 10% NaCl), for which the critical temperature and pressure is much higher (*e.g.* for a 10% NaCl solution, Tc = 480°C and Pc = 53 MPa; Sourirajan and Kennedy, 1962). This discrepancy may be due to others salts (*e.g.* KCl) in the aqueous phase in addition to NaCl, but nevertheless indicates a minimum pressure of the order of 30-50 MPa, considerably lower than that indicated by type 3 inclusions.

In summary, fluid inclusion data indicate a confining pressure in the range 30 MPa to about 200 MPa, though the most reliable estimates from type 3 inclusions indicate a pressure of 100-200 MPa, and probably at the high pressure end of this range.

Pressure-salinity corrections

As there is no evidence of boiling of the hydrothermal fluid at Cleveland, pressure and salinity corrections must be applied to the

homogenisation temperature data to obtain an estimate of the temperature of trapping. Geological considerations and fluid inclusion data indicate a confining pressure between 100 and 200 MPa, though critical point behaviour in some type 3 inclusions indicate pressures toward the high pressure end of this range. Thus the confining pressure at Cleveland is estimated to be about 150 MPa and in following discussions, this is assumed to be the pressure during the mineralisation episode.

A confining pressure of 150 MPa is consistent with pressure estimates at the Renison mine and at Mt Bischoff. Groves and Solomon (1969) used fluid inclusion data to obtain an estimated pressure of about 75 MPa at Mt Bischoff (later revised to 75-100 MPa*). At Renison, Patterson *et al*, (1981) estimated maximum fluid pressures of about 100-200 MPa, though the inferred fluid temperature indicates pressures closer to 200 MPa. Deep drilling at Renison and Mt Bischoff has revealed that these deposits are 600-700 m and at least 800 m above granite, respectively, whereas skarn-type mineral assemblages in the deeper levels at Cleveland indicate a much closer proximity to granite. Thus fluid pressures of about 150 MPa are reasonable for the mineralisation episode at Cleveland.

For the range of salinities encountered in type 1 (and 2) inclusions (an overall mode of 10% NaCl), the pressure corrections (Potter, 1977) for a formation pressure of 150 MPa are: 130°C for homogenisation temperatures up to 300°C, and 150°C for homogenisation temperatures in the range 300°-400°C.

The mode of homogenisation temperatures of type 1 inclusions in Stage I is 320°-340°C and in Stage II is 340°-360°C (Fig. 6.6) which correspond to formation temperatures of about 480°C and 500°C, respectively.

---

* Trans.Inst.Min.Metall., *81*:B181, 1972.

The maximum homogenisation temperature in Stage I is 372°C (104455) and in Stage II is 397°C (104345) which indicate maximum formation temperatures of 520°C and 550°C, respectively. Type 1 inclusions in Stage IV have a mode at 160-180°C (Fig. 6.6) and a maximum homogenisation temperature of 268°C (104307) which correspond to formation temperatures of about 300°C and a maximum of 400°C.

Therefore, in following discussions, the temperature of the hydrothermal fluid during ore formation is assumed to be 480°C and 500°C for mineralisation Stages I and II, respectively, and 300°C for Stage IV. These estimates may be as much as 20°-40°C too low for Stages I and II, and 100°C too low for Stage IV.

VARIATION IN FLUID TEMPERATURE AND COMPOSITION

During the mineralisation episode, significant variations in the temperature and composition of the hydrothermal fluid are recorded by fluid inclusions, both between stages of mineralisation and also within a single stage of mineralisation. All fluid inclusion homogenisation temperature and salinity data are summarised in the histograms in Figure 6.6, and inclusions with combined heating and freezing (salinity) data are plotted in Figure 6.7.

Homogenisation temperatures of type 1 inclusions in Stages I and II have similar ranges (most data between 220°-380°C) but the mode and maximum for Stage II is 20°-40°C higher than Stage I (Fig. 6.6). Homogenisation temperatures for Stage IV exhibit a wide range from 100° to 270°C with most data within 120°-200°C, and hence are 150°-200°C cooler than Stage II. This indicates a sharp decrease in temperature of the hydrothermal fluid during the waning stages of the mineralisation episode. The freezing data indicate a uniform composition of the hydrothermal fluid ranging from 9 to 13% NaCl in Stage I, 8 to 14% NaCl in Stage II and decreasing slightly to 7-11% NaCl during Stage IV (Fig. 6.6).

Data for Stage II are divided into two groups corresponding to the

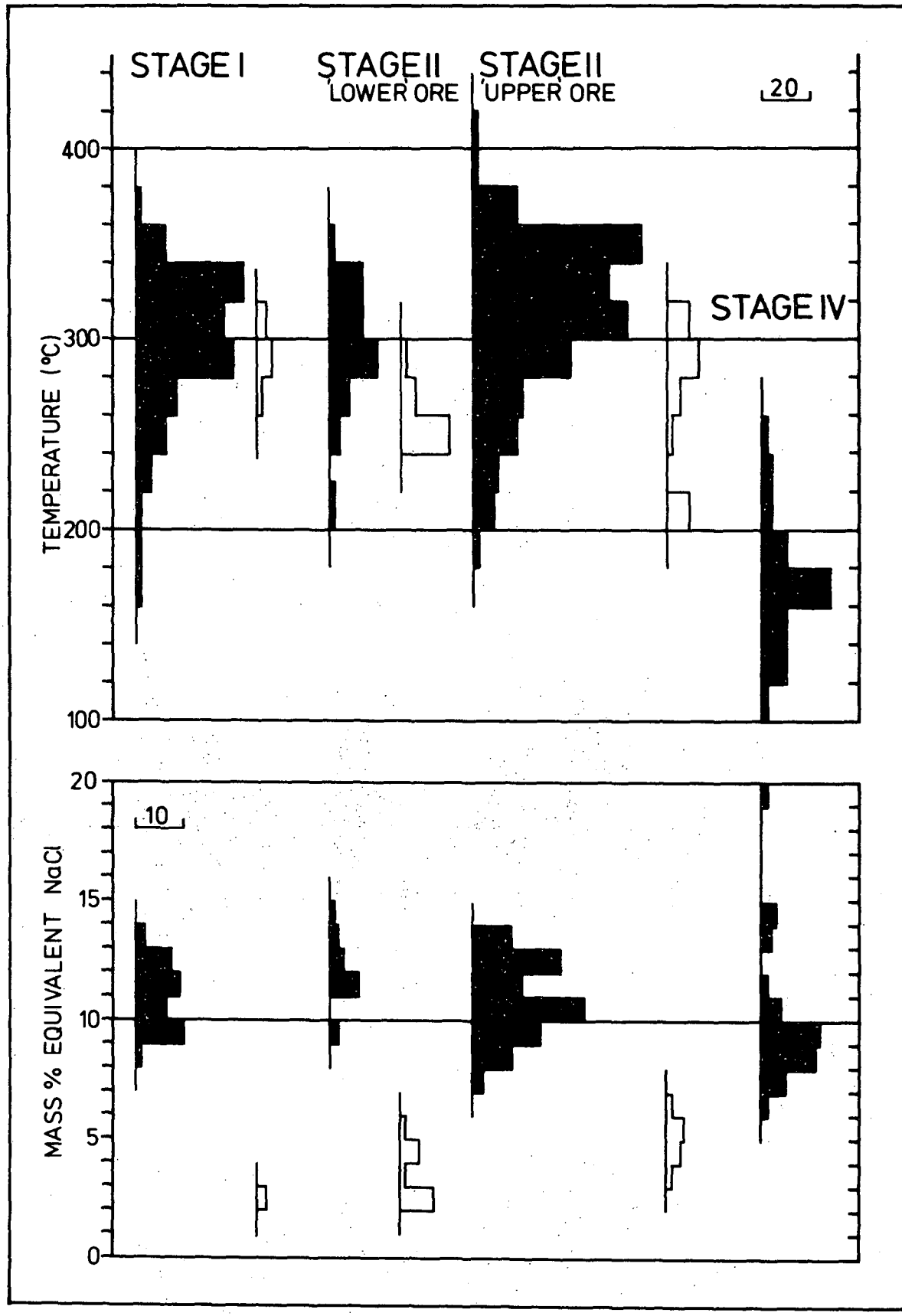

FIG. 6.6 Summary of fluid inclusion homogenisation temperatures (uncorrected) and salinity data for stages I, II and IV of the mineralisation episode at the Cleveland mine. Black histograms are for type 1 inclusions, and white histograms are for type 3 inclusions. 'Lower' ore and 'Upper' ore refer to sulphide lenses situated below or above the Nadir fault, respectively.

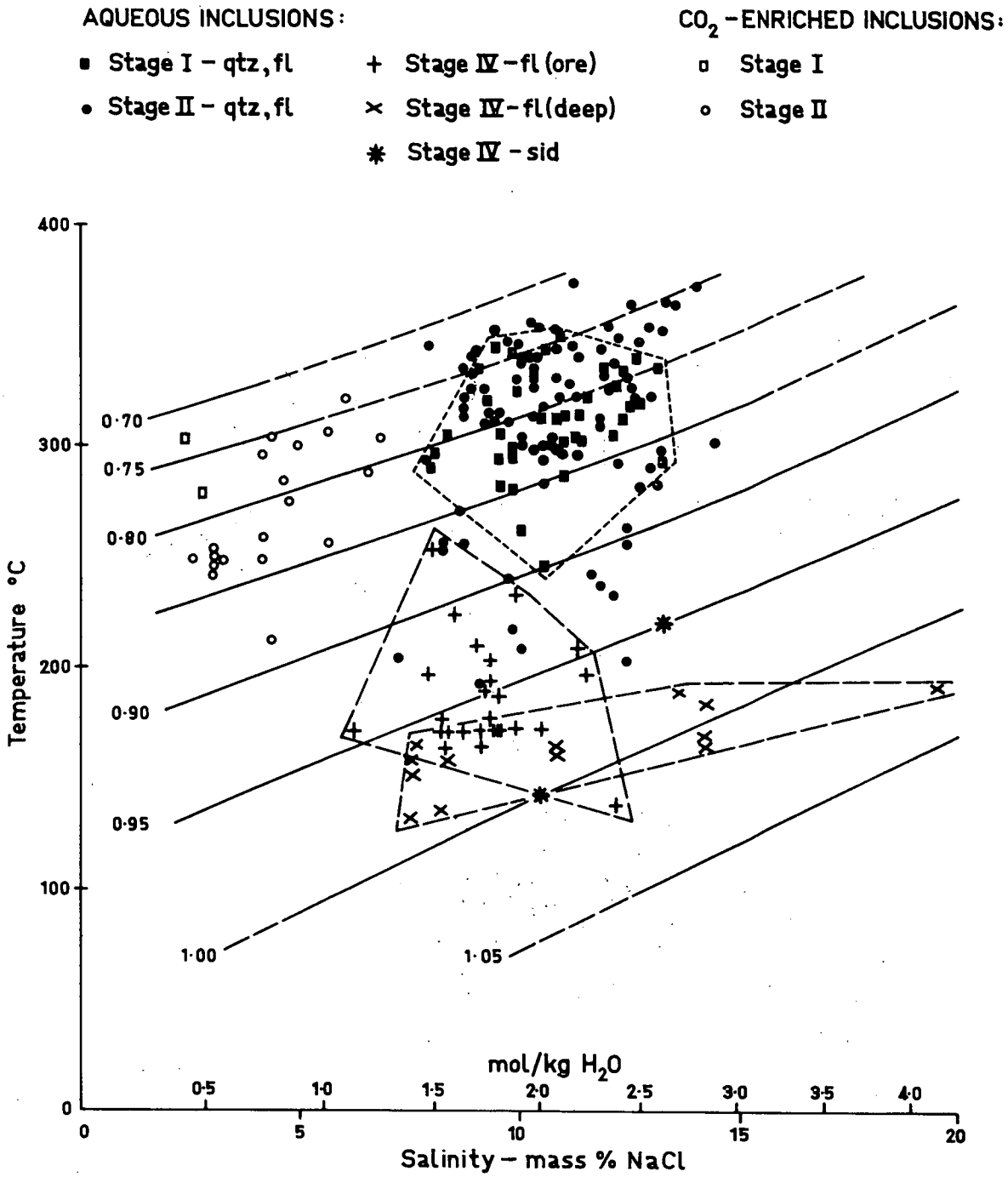

FIG. 6.7 Salinity (expressed as equivalent mass % NaCl and as moles NaCl/kg H_2O) versus temperature of homogenisation of aqueous inclusions. Data for CO_2-rich inclusions are included for comparison. Diagonal lines are isodensity curves and give fluid densities (g/cm^3) in the system H_2O-NaCl (data from Haas, 1976). The field of inclusions in stage I quartz and fluorite is enclosed by short-dash lines, and the fields of inclusions in stage IV fluorite from the mine levels (ore) and from deep drill hole intersections (deep) are enclosed by long-dash lines.

'upper' and 'lower' ore bodies (Fig. 6.6). Homogenisation temperatures of type I inclusions in the 'lower' ore occur within the range of the 'upper' ore, but high homogenisation temperatures (*i.e.* >350°C) are only recorded in specimens from within or close to the low-grade zone above Nadir Fault. Conversely, type 1 inclusions from the 'lower' ore appear to be slightly more saline than from the 'upper' ore (Fig. 6.6).

In a salinity versus homogenisation temperature diagram (Fig. 6.7), type 1 inclusions from Stages I and II generally plot in overlapping fields, indicating fluids of similar density. Taking into consideration the paucity of high homogenisation temperature data (greater than 350°C) then the fluid density for Stages I and II is estimated to be about 0.75 g/cm^3 (possibly as low as 0.7 g/cm^3) based on the NaCl-H_2O system (Fig. 6.7). Type 1 inclusions in Stage IV plot as two partially overlapping fields, depending on their relative sample locations (*i.e.* deep intersections or upper ore; Fig. 6.7), and indicate a more dense fluid (0.9-1.0 g/cm^3) than in Stages I and II. The deep specimens plot as a linear zone, sub-parallel to the 1.0 g/cm^3 iso-density curve. Thus, although there is considerable variation in salinity for deep Stage IV fluorite the fluid density remains constant.

The CO_2-bearing type 3 inclusions are a minor component in Stage I minerals, are relatively common in Stage II minerals, and are absent from Stage IV fluorite. Hence, there was considerable variation in the CO_2 content of the ore fluid during the mineralisation episode. Homogenisation temperatures of CO_2-rich inclusions in Stages I and II are similar (250-310°C), but the Stage II 'lower' ore appears to be at a lower temperature than the 'upper' ore (Fig. 6.6). The salinity of the aqueous phase of type 3 inclusions from the 'upper' ore is also slightly greater than the 'lower' ore (Fig. 6.6). This slight variation cannot be explained by differences in prevailing pressure.

In addition to temperature and salinity variation during the

mineralisation episode, there are variations in fluid temperature and composition within Stage II mineralisation. Firstly, there is a slight temperature gradient within the 'upper' ore, with temperatures decreasing away from the low-grade zone. The highest homogenisation temperatures are from fluid inclusions in specimens from within or close to the low-grade zone. CO_2-bearing inclusions are also absent from these specimens. Secondly, there are two sets of homogenisation temperature data for type 1 inclusions. These are: (1) inclusions with homogenisation temperatures greater than 320°C; and (2) inclusions with homogenisation temperatures in the range 250°-310°C and which are commonly associated with CO_2-bearing type 3 inclusions exhibiting a similar range of homogenisation temperatures. The association and/or co-existence(?) of type 1 and type 3 inclusions in the same specimen cannot be explained by boiling of a CO_2-enriched fluid, as there is no evidence of boiling of the Stage II hydrothermal fluid (*i.e.* no highly saline, gas-rich or CO_2-rich inclusions). Type 3 inclusions are best explained by either formation of a CO_2-enriched fluid during dissolution of limestone, or periodic injections of primary CO_2-enriched fluid (further discussion in Chapter 8).

7. STABLE ISOTOPE GEOCHEMISTRY

INTRODUCTION

A stable isotope study was undertaken to determine the isotopic composition of the mineralising fluid and to ascertain whether there was any temporal or spatial variation in its isotopic composition as an aid to establishing the source of the fluid. Also, the oxygen isotopic composition of the host rock was determined to see whether it reflects the geochemical alteration halo defined in the hanging wall Deep Creek Volcanics.

Most mineral phases and several of the host rocks were analysed for their relevant oxygen, sulphur and carbon isotopic compositions, and two samples of fluid inclusion water were analysed for their hydrogen isotopic composition. Details of sample preparation and analytical technique and precision are given in Appendix 6, and analytical results are listed in Tables A6.1 to A6.3. All results are reported in per mil deviation from the standards: S.M.O.W. for oxygen and hydrogen, Canón Diablo Troilite (C.D.T.) for sulphur, and P.D.B. for carbon.

SULPHUR ISOTOPIC COMPOSITION OF HYDROTHERMAL MINERALS

The sulphur isotopic composition of the main sulphide minerals was analysed to ascertain the sulphur isotopic composition of the mineralising fluid and whether there is any temporal or spatial variation in the $\delta^{34}S$ values which may indicate direction of fluid movement. The $\delta^{34}S$ values of the analysed sulphide minerals are listed in Table A6.2 and are summarised in Table 7.1 and Figure 7.1.

The $\delta^{34}S$ values of the sulphide minerals from all stages of the mineralisation episode except Stage V have a narrow range of -0.2 to +5.5 per mil. Molybdenite in Stage I has $\delta^{34}S$ values of +3.7 to +5.5, which are higher than most other sulphides (Fig. 7.1).

TABLE 7:1 Average oxygen and sulphur isotopic composition of hydrothermal minerals, Cleveland mine (summarised from Table A6.2)

Mineral (Replication)	$\delta^{18}O_{SMOW}$, per mil		$\delta^{34}S_{CDT}$, per mil	
	Range	Mean	Range	Mean
Stage I				
Quartz (6)	+11.7 - +12.6	+12.3		
Wolframite (3)	+ 5.5 - + 5.6	+ 5.5		
Molybdenite (3)			+3.7 - +5.5	+4.5
Stage II, Nadir fault				
Quartz (2)	+14.4	+14.4		
Cassiterite (1)	+ 5.3	+ 5.3		
Pyrrhotite (1)			+2.4	+2.4
Chalcopyrite (1)			+2.5	+2.5
Stage II, 'upper' ore, Halls lenses, north				
Quartz (1)	+13.5	+13.5		
Pyrrhotite (7)			+1.9 - +3.7	+2.6
Chalcopyrite (2)			+2.3 - +2.5	+2.4
Sphalerite (2)			+2.6 - +2.7	+2.6
Stage II, 'upper' ore, Halls lens, south and Khaki lode				
Quartz (1)	+13.4	+13.4		
Cassiterite (1)	+ 6.6	+ 6.6		
Pyrrhotite (6)			+1.8 - +3.2	+2.4
Chalcopyrite (2)			+2.0 - +3.3	+2.6
Sphalerite (2)			+1.5 - +2.2	+1.8
Marcasite/pyrite (1)			+2.7	+2.7
Stage II, 'lower' ore, Halls lenses, north				
Pyrrhotite (9)			+1.6 - +3.9	+2.5
Stage II, veins at periphery of sulphide lenses				
Quartz (2)	+13.4 - +15.4	+14.4		
Pyrrhotite (1)			+2.1	+2.1
Chalcopyrite (2)			+1.8 - +2.4	+2.1
Sphalerite (1)			+2.2	+2.2
Arsenopyrite (1)			+3.3	+3.3
Stage II, veins surrounding sulphide lenses				
Quartz (4)	+14.0 - +15.7	+14.9		
Pyrrhotite (4)			+0.5 - +1.9	+1.4
Chalcopyrite (3)			+0.2 - +1.7	+1.1
Sphalerite (7)			-0.2 - +1.9	+1.3
Arsenopyrite (2)			+2.6 - +2.7	+2.7
Galena (1)			+0.5	+0.5
Pyrite (1)			+0.7	+0.7
Stage III				
Quartz(?) (1)	+14.9	+14.9		
Arsenopyrite (2)			+3.0 - +4.4	+3.7
Stannite (1)			+3.2	+3.2
Stage IV				
Quartz (2)	+12.7 - +14.3	+13.5		
Stage V				
Pyrite (1)			+22.1	+22.1

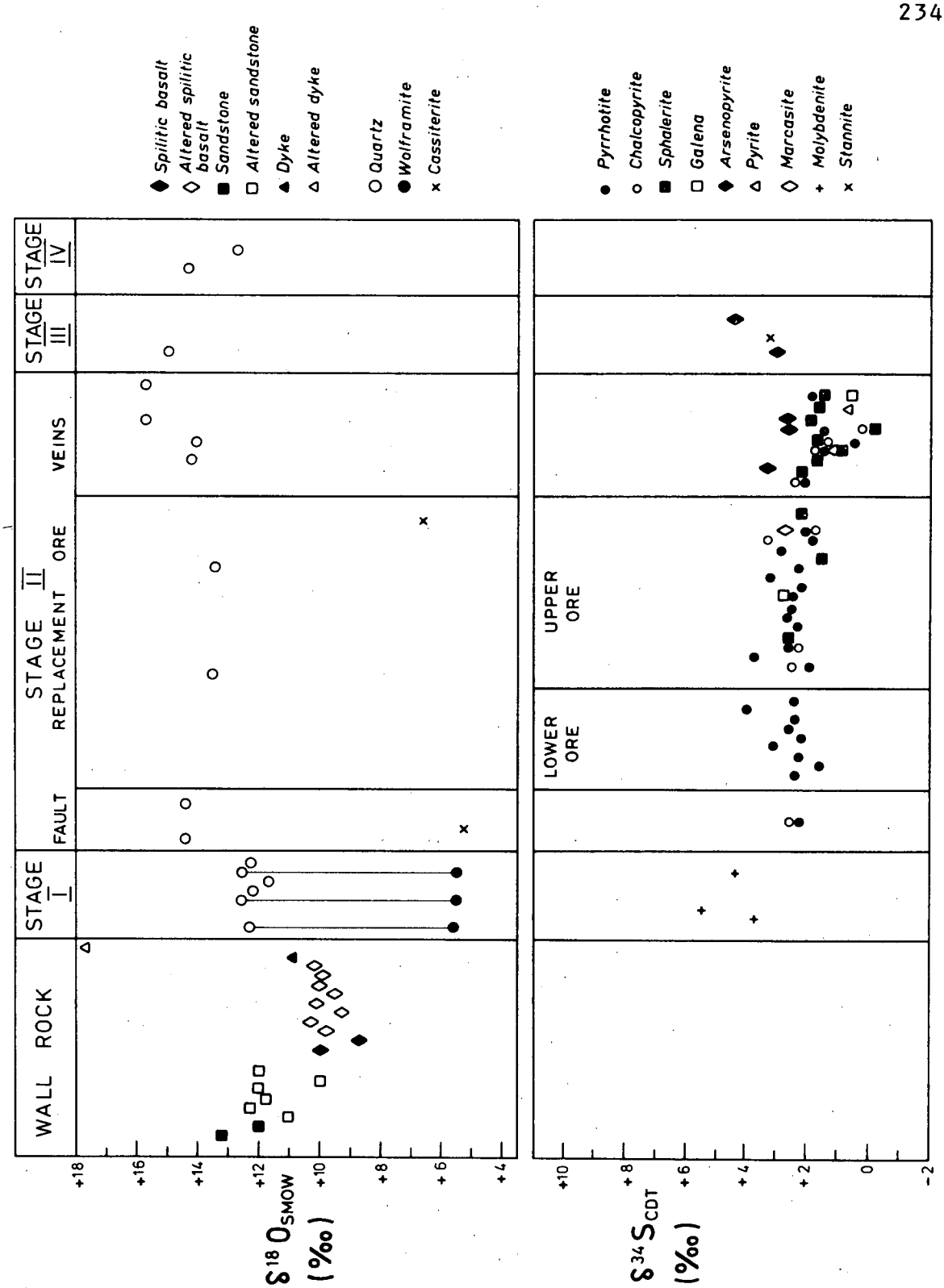

FIG. 7.1 Oxygen and sulphur isotopic data for wall rocks and for hydrothermal minerals in mineralisation stages I-IV, Cleveland mine.

In Stage II, the $\delta^{34}S$ values of sulphides have a limited range of -0.2 to +3.9 per mil, though there is a slight variation between the sulphide lenses and veins in the host rocks. The $\delta^{34}S$ values of sulphides in the sulphide lenses have an extremely limited range, and do not exhibit any systematic spatial variation (Fig. 7.2). Pyrrhotite, for example, has the widest range from +1.6 to +3.9 per mil (mean value of +2.5 per mil), with $\delta^{34}S$ values for deep diamond drill hole intersections (about M.L. 850 m) the same as the upper levels of the mine, some 450 m above (Fig. 7.2). Chalcopyrite and sphalerite have even narrower ranges than pyrrhotite (Table 7.1). The $\delta^{34}S$ value of pyrrhotite and chalcopyrite in the Nadir fault are the same as in the sulphide lenses, but sulphides in veins in the host rock tend to have slightly lower $\delta^{34}S$ values (Fig. 7.1). This depletion may be the result of either decreased fluid temperature, or increased fO_2 and/or pH from interaction of the hydrothermal fluid with the host rock (*e.g.* Ohmoto and Rye, 1979). Arsenopyrite and stannite in Stage III have similar, though slightly higher, $\delta^{34}S$ values than Stage II sulphides (Fig. 7.1).

The single Stage V pyrite sampled analysed is anomalously enriched in ^{34}S ($\delta^{34}S$ = +22.7 per mil) and most likely formed by reduction of sulphate (*e.g.* Ohmoto and Rye, 1979). The pyrite is unrelated to the hypogene marcasite/pyrite that ubiquitously replaced Stage I and Stage II pyrrhotite. A single marcasite sample analysed has a $\delta^{34}S$ value of +2.7 per mil which, as expected, is essentially identical to Stage II pyrrhotite (Table 7.1).

The only other exceptions to the narrow range of $\delta^{34}S$ values are galena (+5.9 per mil) and pyrite (+11.8 per mil) from the Washington Hay mine, located about 0.5 km south of the Cleveland deposit (Fig. 3.3). As mineralisation at the Washington Hay mine is probably part of the same mineralisation episode as Cleveland, then the higher $\delta^{34}S$ values may be a reflection of increased distance from the main centre of mineralisation,

as has been previously observed at Mt Bischoff (Rafter and Solomon, 1967).

There is a lack of sulphide pairs suitable for temperature estimates using sulphur isotope fractionation. The inconsistency of Δ values for co-existing pyrrhotite and chalcopyrite in Stage II (Table A6.1, Fig. 7.1) is due to the non-contemporaneity of the two phases (*e.g.* chalcopyrite generally is later than and replaces pyrrhotite) and is not necessarily due to isotopic disequilibrium. A single sphalerite-galena pair(?) in a Stage II vein (104444) gave a fractionation of 1.1 per mil which indicates a temperature of 537°C (±30°C), using the calibration curve of Ohmoto and Rye (1979).

A narrow $\delta^{34}S$ range near to zero per mil is relatively common for hydrothermal vein and replacement deposits formed in the temperature range 150°-400°C (Rye and Ohmoto, 1974), although this is a lower temperature range than at Cleveland. Comparison with sulphur isotope data from other sulphide-cassiterite deposits, shows that the $\delta^{34}S$ values at Cleveland are intermediate between Mt Bischoff and Renison (Fig. 7.3). It has been previously suggested (Rafter and Solomon, 1967) that increasing distance from the source correlates with an increase in $\delta^{34}S$ values, which implies that the distance of Cleveland from its source is intermediate between Mt Bischoff and Renison, with Mt Bischoff closer to its source. However, at Renison, the higher $\delta^{34}S$ values are probably due to magmatic sulphur slightly enriched in ^{34}S (Patterson *et al.*, 1981). Thus the variation in $\delta^{34}S$ values of sulphides in the massive replacement bodies most likely reflects differences in the ^{34}S content of the fluid, and is not due to varying distances from their source.

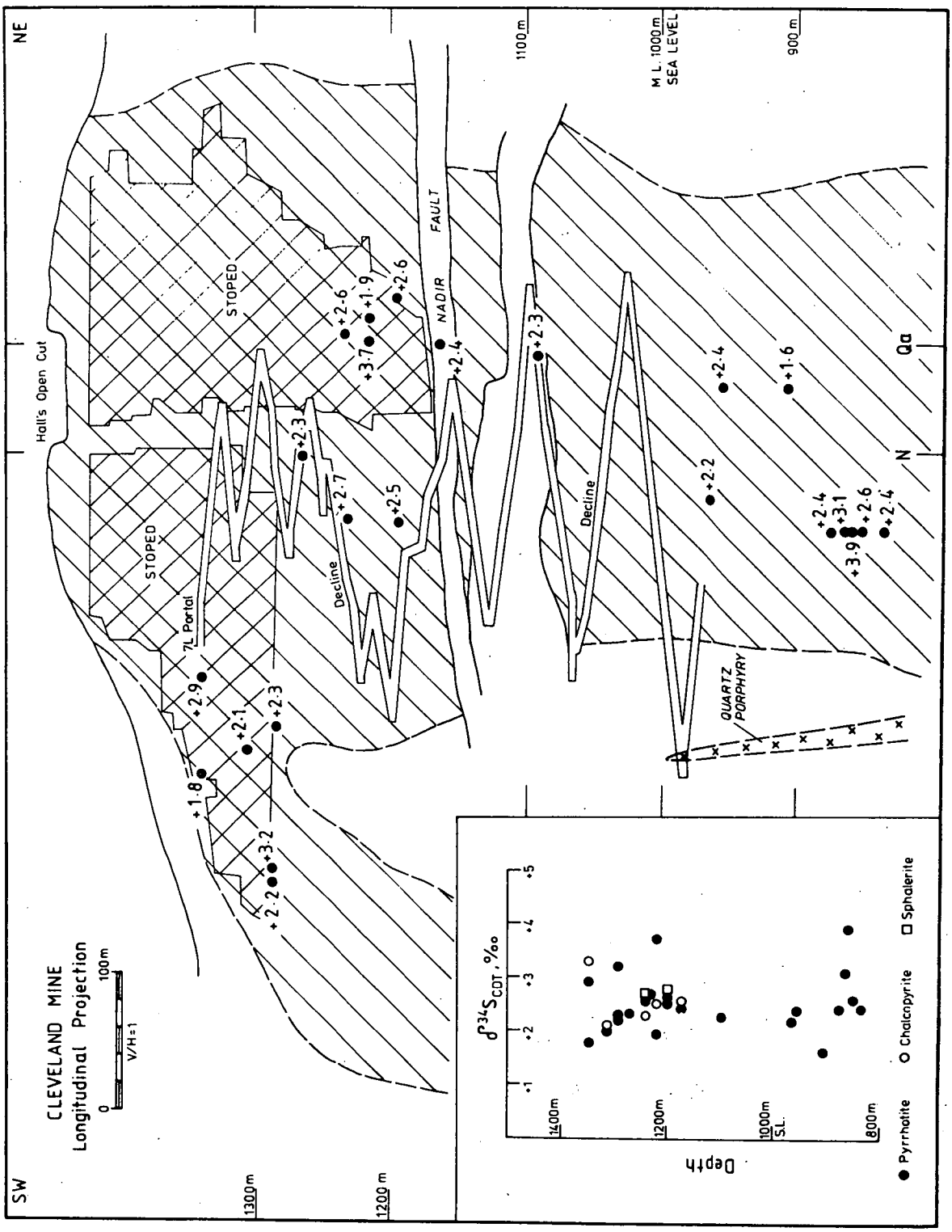

FIG. 7.2 Longitudinal projection of the Cleveland mine showing the sulphur isotopic composition of pyrrhotite in the sulphide lenses. Diagonal hatching is approximate extent of Halls A/B lenses, cross hatching is stoped ore. Inset shows $\delta^{34}S$ values plotted against depth.

FIG. 7.3 Sulphur isotopic composition of sulphides in massive and banded replacement ore (sulphide lenses, stage II) at the Cleveland mine, shown in relation to the equivalent stage of massive pyrrhotite replacement ore at Mt Bischoff and Renison Bell. Data for Mt Bischoff are from Rafter and Solomon (1967) and Groves (1968), and for Renison are from Rafter and Solomon (1967), Groves (1968) and Patterson *et al*. (1981).

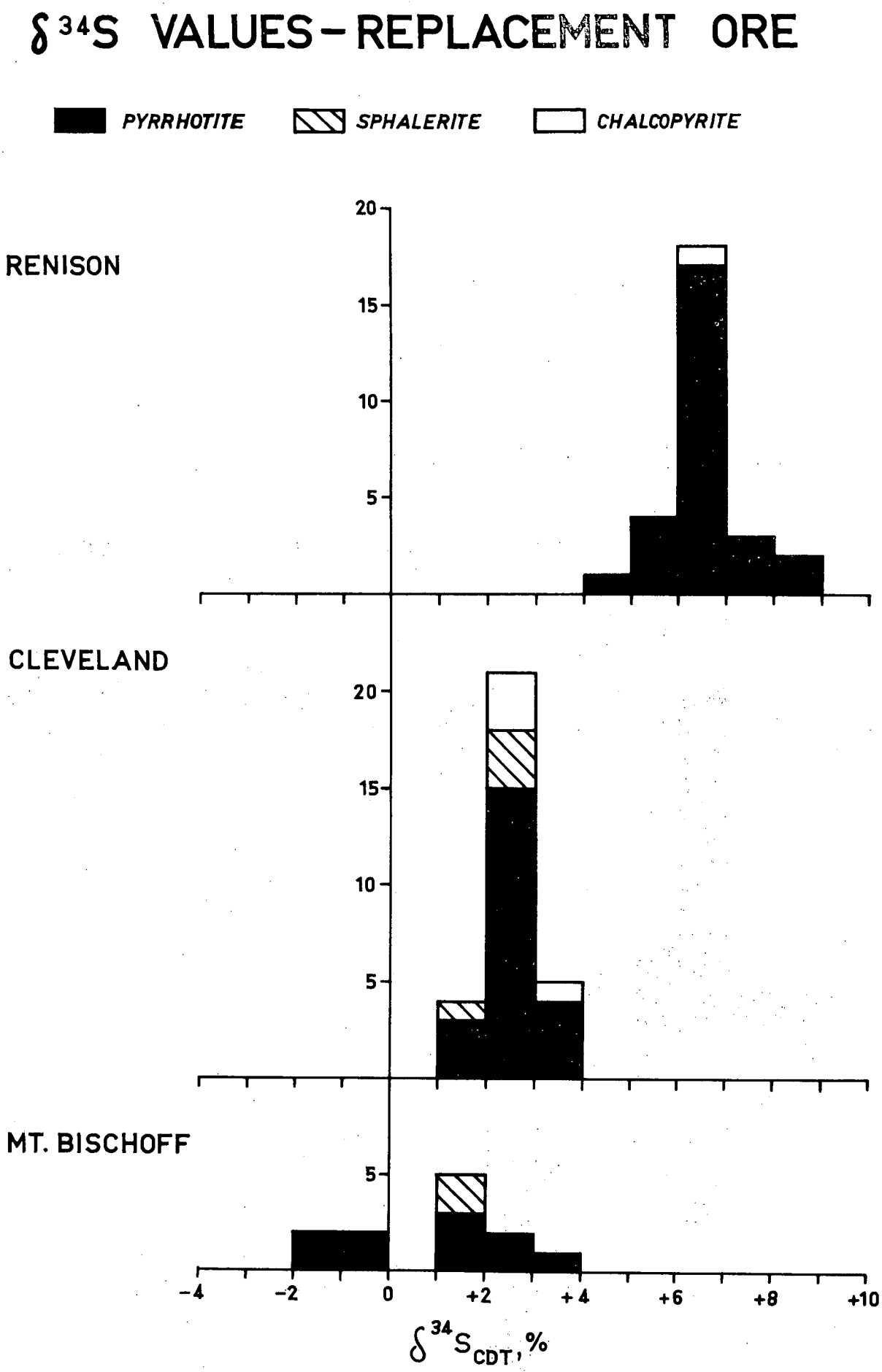
δ 34S VALUES – REPLACEMENT ORE
PYRRHOTITE
SPHALERITE
CHALCOPYRITE
RENISON
CLEVELAND
MT. BISCHOFF
20
15
10
5
-4
-2
0
+2
+4
+6
+8
+10
δ 34S CDT, %

FIGURE 7.3

OXYGEN ISOTOPIC COMPOSITION OF HYDROTHERMAL MINERALS

The ^{18}O composition of oxide minerals are relatively uniform throughout the mineralisation episode (Tables 7.1, A6.2; Fig. 7.1), though there are minor variations.

The $\delta^{18}O$ values of Stage I quartz have a uniform range of +11.7 to +12.6 per mil, which are lighter than Stage II and Stage III quartz which ranges from +13.4 to +15.7 per mil (Fig. 7.1). Quartz in Stage IV(?) has $\delta^{18}O$ values of +12.7 and +14.3 per mil.

Wolframites in Stage I also are very uniform with $\delta^{18}O$ values of +5.5 and +5.6 per mil, and so too are the Δ values (+6.7, +7.1 and +7.1 per mil) of co-existing quartz and wolframite (Fig. 7.1). Cassiterites in Stage II have $\delta^{18}O$ values of +5.3 in the Nadir fault and +6.6 in the sulphide lenses (Khaki lode).

In Stage II, there is a slight variation in the $\delta^{18}O$ values of quartz, with early(?) quartz in Nadir Fault having a $\delta^{18}O$ value of +14.6 per mil, decreasing to +13.5 per mil in the sulphide lenses, but increasing to +14.0 to +15.7 per mil in veins surrounding the deposit. If the $\delta^{18}O$ value for the hydrothermal fluid is constant, then the ^{18}O enrichment in quartz in the veins probably reflects a decrease in fluid temperature away from the sulphide lenses.

CARBON AND OXYGEN ISOTOPIC COMPOSITION OF CARBONATES

The ^{13}C and ^{18}O compositions were determined for sedimentary calcite in limestone, and for hydrothermal calcite, dolomite and siderite. Results are listed in Table A6.3, and illustrated in Figure 7.4.

The $\delta^{13}C$ values of calcite in limestone from the Hall Formation, of which three specimens (48291, 48293 and 48298) are stratigraphically equivalent to the sulphide lenses, show a range of -2.3 to -1.5 per mil. These values are within the range of most marine limestones, which have $\delta^{13}C$ values of 0±4 per mil, regardless of the age of the formation

(Keith and Weber, 1964; Schwarz, 1969; Hudson, 1977).

The $\delta^{18}O$ values of calcite in the limestone range from +12.1 to +13.7 per mil which are much lighter than most marine limestone (Keith and Weber, 1964; Garlick, 1966), and about 7 per mil lighter than Cambrian marine limestone (Fig. 7.4). This depletion in ^{18}O of the limestone relative to normal marine limestone, may reflect a near-shore or transitional marine depositional environment in which deposition of calcareous sediments may have been affected by isotopically light oxygen from continental sources (Keith and Weber, 1964). Alternatively, the $\delta^{18}O$ values may have been adjusted by equilibration with metamorphic water either during the Tabberabberan Orogeny (M. Solomon, pers. comm.), or during spilitisation of basalt within the host sequence.

Calcite occurring in stringer veins within the Whyte River complex, has $\delta^{18}O$ values (+12.4, +12.5 per mil) similar to limestone in the Hall Formation, but is markedly depleted in ^{13}C with δ values of -9.8 and -10.3 per mil (Table A6.3). This calcite most likely is associated with serpentinisation of the mafic-ultramafic complex, and thus is earlier than and unrelated to the mineralisation episode.

Hydrothermal siderite from Stage II has $\delta^{18}O$ values of +16.6 and +16.7 per mil, which are heavier than Stage IV dolomite with $\delta^{18}O$ values of +14.9 to +16.2 per mil (Fig. 7.4). A single calcite sample, tentatively assigned to Stage IV, but may be Stage III, has a $\delta^{18}O$ value of +11.2 which is lighter than all other carbonates at Cleveland (Fig. 7.4).

The $\delta^{13}C$ values of Stage II siderite are -5.1 and -7.0 per mil, and are significantly lighter than the Stage IV dolomite and calcite which have $\delta^{13}C$ values ranging from -3.0 to -1.8 per mil (Fig. 7.4). The values are similar to the $\delta^{13}C$ values normally observed in hydro-

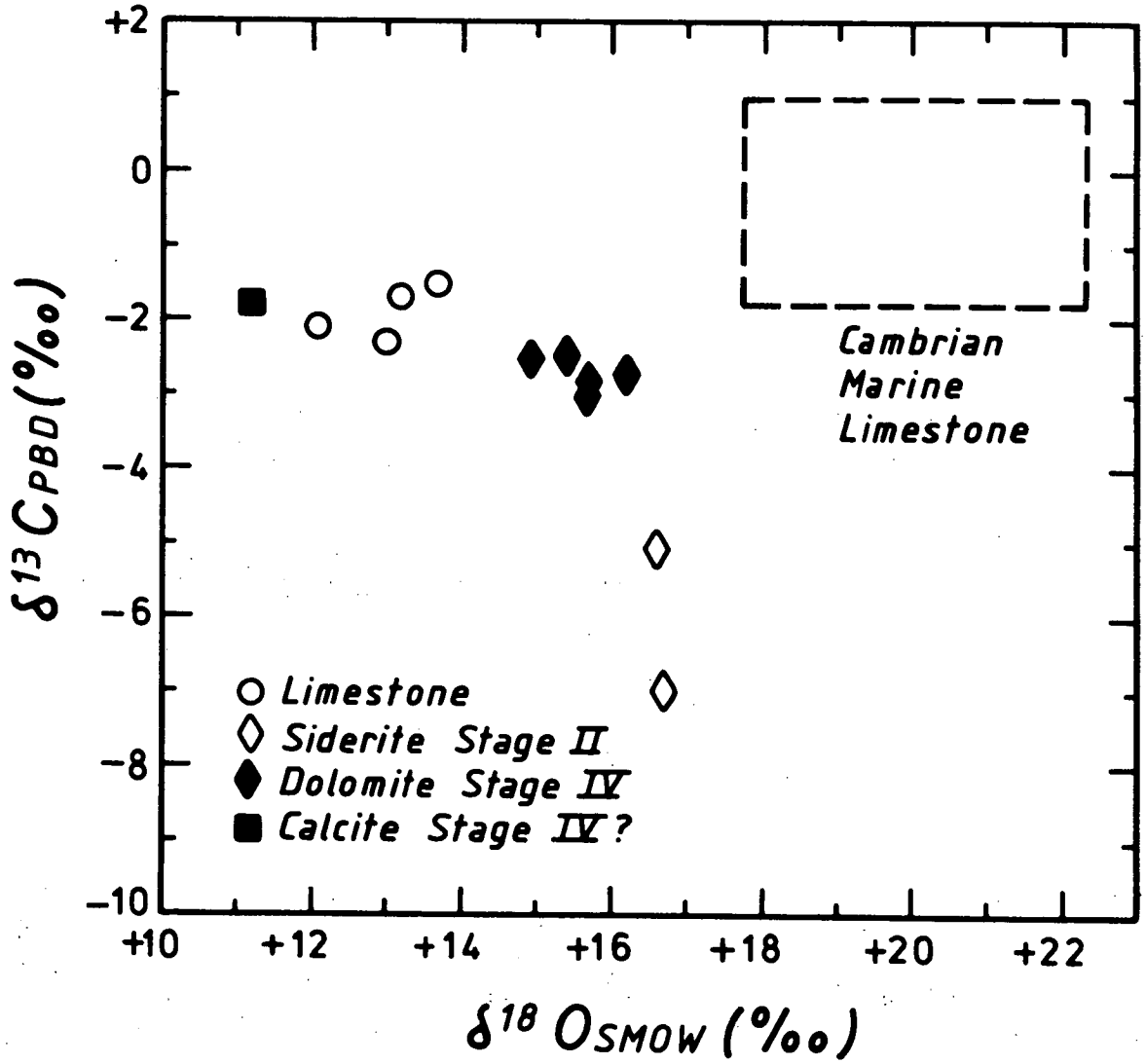

FIG. 7.4 Carbon and oxygen isotopic data for host limestone in the Hall Formation and hydrothermal carbonates, Cleveland mine. The field of Cambrian marine limestone is based on Keith and Weber (1964).

thermal mineral deposits (*c.f.* Rye and Ohmoto, 1974; Ohmoto and Rye, 1979).

The increase of 3-4 per mil in $\delta^{13}C$ of hydrothermal carbonate between Stage II and Stage IV (Fig. 7.4) is similar to a trend of increased $\delta^{13}C$ of late-stage carbonate minerals observed in a number of hydrothermal ore deposits (Rye and Ohmoto, 1974; Ohmoto and Rye, 1979). The low $\delta^{13}C$ values in Stage II siderite also reflect the variation indicated by a single specimen of siderite at Renison (Patterson *et al*, 1981). It has been suggested (Ohmoto and Rye, 1979; Patterson *et al*, 1981) that these trends reflect some contribution of relatively light 'magmatic' carbon, and varying temperature and CO_2/CH_4 ratio in the hydrothermal fluid. At Cleveland, the low $\delta^{13}C$ values in Stage II siderite may also be due to contribution of isotopically light carbon from dissolution of the ^{13}C depleted calcite in the Whyte River complex, or similar complexes at greater depth; and the increase in $\delta^{13}C$ values of late-stage carbonates may also reflect addition of isotopically heavier carbon from dissolution of limestone.

OXYGEN ISOTOPIC COMPOSITION OF THE HOST ROCK

The whole-rock $\delta^{18}O$ values of the analysed mafic rocks and sedimentary rocks that host the Cleveland deposit are listed in Table A6.1, and illustrated in Figures 7.5, 7.6 and 7.7.

Deep Creek Volcanics and Henrys Volcanic Member

Two specimens of spilitic basalt (48299, 48302) from the Deep Creek Volcanics have whole-rock $\delta^{18}O$ values of +8.7 and +10.0 per mil (mean +9.3 per mil). This corresponds to a positive isotopic shift of 2.2 and 3.5 per mil (mean 2.8 per mil) of the spilitic basalt relative to a $\delta^{18}O$ value of +6.5±1 per mil for unmodified oceanic basalt (Heaton

and Sheppard, 1977; Taylor, 1979; Fig. 7.5). This enrichment is similar to, but not as large as most enrichments observed in low to medium grade, sub-seafloor, hydrothermally metamorphosed basaltic rocks (*e.g.* Muehlenbachs and Clayton, 1972; Spooner *et al*, 1974; Heaton and Sheppard, 1977; Munha and Kerrick, 1980), and contrasts with the ^{18}O depletion observed in basalts that have undergone high-temperature (>400°C) marine hydrothermal alteration, and in continental basalts which have been hydrothermally altered or metamorphosed by interaction with isotopically light meteoric water (*e.g.* Taylor and Forester, 1971; Forester and Taylor, 1976; Fig. 7.5). Hence the oxygen isotopic data for spilitic basalt at Cleveland are consistent with the interpretation that it is ocean floor basalt which has reacted with sea water.

The whole-rock $\delta^{18}O$ values of spilitic basalt which has been hydrothermally altered by interaction with the ore fluid range from +9.3 to +10.3 per mil (Table A6.1; Figs. 7.5, 7.6). Analysed samples extend from the edge of the alteration zone to within a few metres of ore, and include one sample of Henrys Volcanic Member (HV) (Figs. 7.6, 7.7). Although there is possibly a slight enrichment of ^{18}O in the 'altered' spilitic basalt (mean $\delta^{18}O$ value of +9.9 per mil) compared with the unaltered spilitic basalt (mean +9.3 per mil) there is no conclusive evidence for any variation of the $^{18}O/^{16}O$ ratios of the spilitic basalt nearer to the sulphide lenses.

The uniformity in $\delta^{18}O$ values of the unaltered and 'altered' spilitic basalt may be because the temperature range of the ore fluid (about 350°-500°C for Stage II mineralisation) was sufficiently high for rock-water fractionation to be negligible. Spilite-water fractionation is essentially represented by silicate-water fractionations occurring within the range spanned by quartz and chlorite (see Taylor, 1979, Figure 6.1; Bottinga and Javoy, 1975), and in the range 400°-600°C the

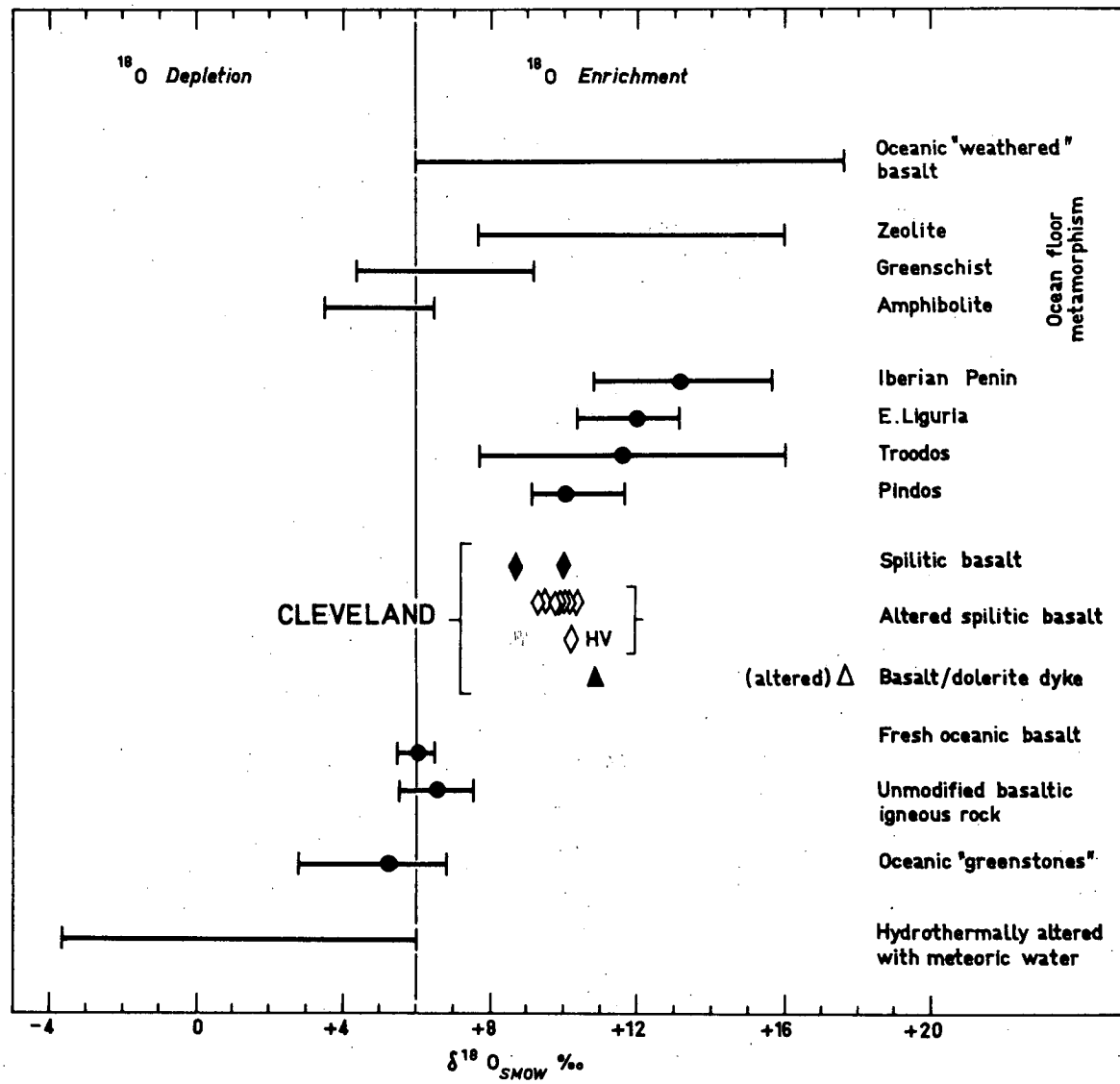

FIG. 7.5 Whole-rock oxygen isotope ratios of ^{18}O enriched metabasic rocks from the Cleveland mine. For comparison, data are included for fresh oceanic basalt (Heaton and Sheppard, 1977); unmodified basaltic igneous rock (Taylor, 1979); oceanic 'greenstones' (Muehlenbachs and Clayton, 1972b); terrestrial hydrothermally altered basalt (Taylor and Forester, 1971; Forester and Taylor, 1976); spilitic and metabasic rocks from Pindos, Greece (Spooner *et al.*, 1974), Troodos, Cyprus (Spooner *et al.*, 1974; Heaton and Sheppard, 1977), East Liguria, Italy (Spooner *et al.*, 1974) and the Iberian Pyrite Belt (Munha and Kerrich, 1980); ocean floor metamorphic facies (Heaton and Sheppard, 1977); and oceanic 'weathered' basalt (Garlick and Dymond, 1970; Muehlenbachs and Clayton, 1972a).

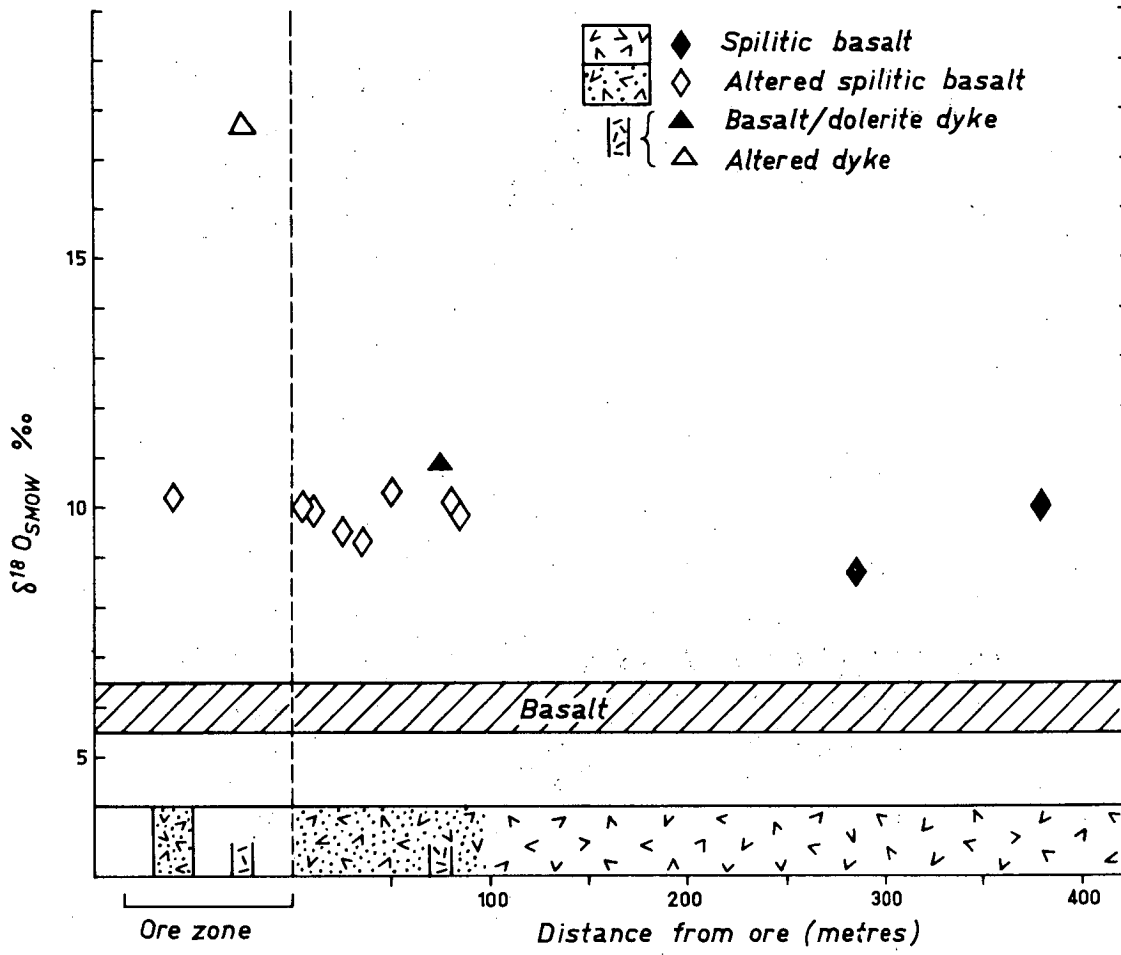

FIG. 7.6 Whole-rock oxygen isotopic composition of metabasic rocks versus distance from the sulphide lenses (*cf.* Fig. 7.7). Basalt range is from Heaton and Sheppard (1977) and Taylor (1979).

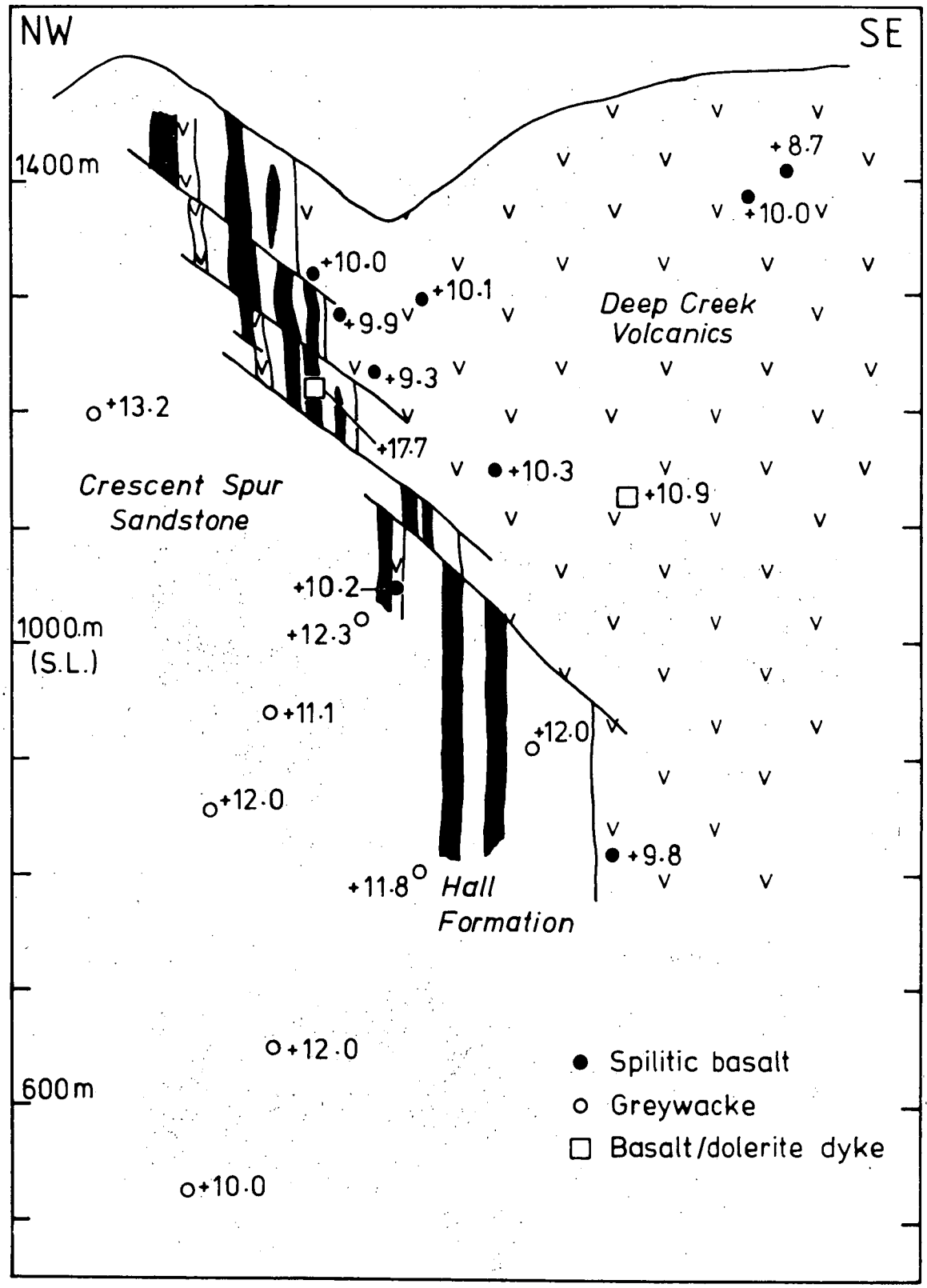

FIG. 7.7 Whole-rock oxygen isotopic data for spilitic basalt (Deep Creek Volcanics, Henrys Volcanic Member), greywacke (Crescent Spur Sandstone), and basalt/dolerite dyke.

silicate-water fractionations are relatively insensitive.

Crescent Spur Sandstone and Hall Formation

The whole-rock $\delta^{18}O$ values of greywacke in the footwall Crescent Spur Sandstone range from +10.0 to +13.2 per mil. A single sample of greywacke in the hanging wall, in the Hall Formation (48313), has a $\delta^{18}O$ value of +12.0 per mil (Fig. 7.7). Samples of chocolate-brown shale and of bleached, altered(?) shale/chert in a sulphide lens have $\delta^{18}O$ values of +13.1 and +13.7 per mil, respectively. These values are similar to the ^{18}O composition of Cambrian siliceous clastic sediments in the upper levels of the Renison mine (Patterson, 1979; Patterson *et al*, 1981).

There is an indication of depletion in the ^{18}O composition of greywacke in the Crescent Spur Sandstone with increased depth from a $\delta^{18}O$ value of +13.2 per mil near the surface (M.L. 1200 m) to +10.0 per mil at a depth of 525 m M.L. (Table A6.1; Fig. 7.7). Although the initial composition of the greywackes may have varied, the depletion in ^{18}O composition may reflect a thermal metamorphic aureole to granite at greater depth (*c.f.* Taylor, 1974). A similar but more pronounced decrease in $\delta^{18}O$ toward the granite-sediment contact beneath the Renison mine is thought to be due to thermal metamorphism at progressively increasing temperatures (Patterson, 1979). However, the situation at Cleveland is complicated by the recently discovered altered quartz porphyry dyke, and the lowest (and deepest) $\delta^{18}O$ value (48315) may reflect proximity to this dyke rather than to granite.

Intrusive basalt/dolerite dyke

The basalt/dolerite dyke which intrudes the host volcano-sedimentary sequence has $\delta^{18}O$ values of +10.9 per mil where it occurs unaltered in the Deep Creek Volcanics and +17.7 per mil where it is completely altered in the sulphide lenses (Table A6.1; Figs. 7.6, 7.7). This marked increase of 6.8 mil probably reflects the occurrence of siderite, which is a major mineral in the altered dyke (*e.g.* $\delta^{18}O$ of

Stage II siderite is +16.6 per mil).

ISOTOPIC COMPOSITION OF THE HYDROTHERMAL FLUID

The oxygen isotopic composition of hydrothermal fluids associated with the various paragenetic stages can be calculated from the isotopic composition of hydrothermal minerals and from temperatures of formation derived from fluid inclusion data.

Quartz-water (1) and dolomite-water (2) oxygen isotope fractionation as a function of temperature can be expressed as:

$$1000 \ln \alpha = 3.57 (10^6 T^{-2}) - 2.71 \quad (1)$$

(Taylor, 1974)

$$1000 \ln \alpha = 3.06 (10^6 T^{-2}) - 3.24 \quad (2)$$

(Matthews and Katz, 1977)

Although there are several quartz-water fractionation curves, Taylor's (1974) calibration is used as a reasonable approximation. Whatever the quartz-water fractionation curve used, at any temperature, there is only about a 1 per mil variation in calculated $\delta^{18}O$ values of water in the hydrothermal fluid in equilibrium with quartz.

Using equations (1) and (2) and the measured $\delta^{18}O$ values for Stage I and Stage II quartz and Stage IV dolomite, and using temperatures derived from fluid inclusions, $\delta^{18}O$ values of water in the hydrothermal fluid are obtained (Fig. 7.8). In Stage I, the $\delta^{18}O$ values of quartz range from +11.7 to +12.6 per mil (mean +12.3 per mil) and the estimated temperature (pressure corrected) from fluid inclusion data is about 480°C. This gives a $\delta^{18}O$ value for the water in the hydrothermal fluid of +8.1 to +9.0 per mil (mean +8.7 per mil). In Stage II, quartz in the sulphide lenses has $\delta^{18}O$ values of +13.5 and +13.4 per mil, at an estimated temperature (pressure corrected) of about 500°C, which gives a $\delta^{18}O$ value of +10.2 or +10.1 per mil for water in the hydrothermal fluid (Fig. 7.8).

Dolomite in Stage IV has $\delta^{18}O$ values ranging from +14.9 to +16.2

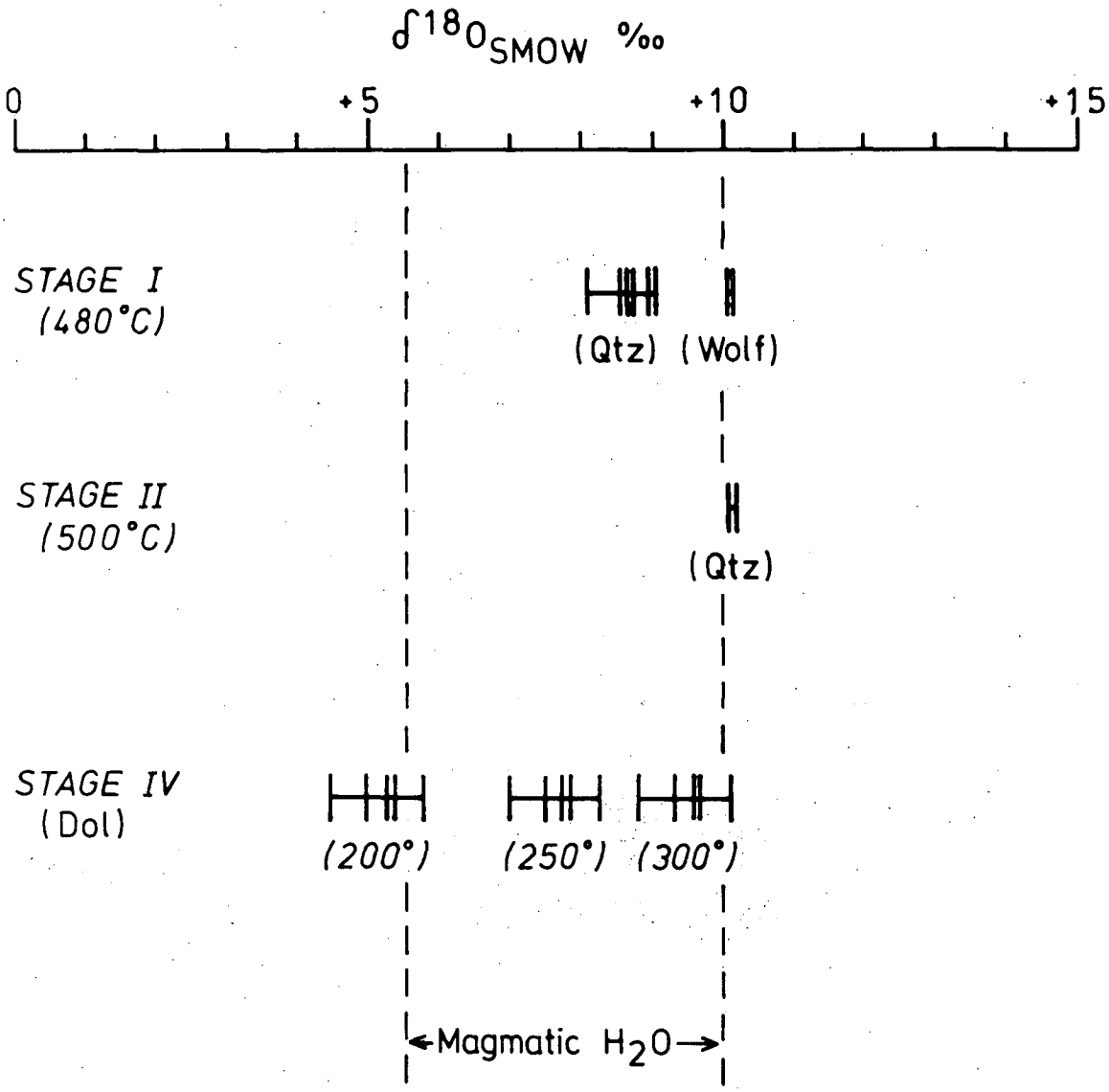

FIG. 7.8 Calculated oxygen isotopic composition of water coexisting with hydrothermal quartz (stages I and II) and dolomite (stage IV), at the temperatures indicated (see text for mineral-water fractionation data). Range of magmatic water is from Taylor (1979). The calculated $\delta^{18}O$ value of water coexisting with stage I wolframite is based on an empirical fractionation curve of Landis and Rye (1974).

per mil (mean of +15.6 per mil). The temperature of formation (pressure corrected) of Stage IV dolomite is estimated at about 300°C, which together with the $\delta^{18}O$ values of dolomite gives a $\delta^{18}O$ value of +8.8 to +10.1 per mil (mean +9.5 per mil) for water in the late stage hydrothermal fluid.

In addition to the quartz-water and dolomite-water fractionations used above, Landis and Rye (1974) have calculated the following wolframite-water fractionation expression:

$$1000 \ln \alpha = 3.0 \ (10^6 T^{-2}) - 9.9 \qquad (3)$$

This empirical fractionation curve, combined with the $\delta^{18}O$ values of wolframite (+5.5 to +5.6 per mil) and the estimated temperature of 480°C for Stage I, gives a $\delta^{18}O$ value of +10.1 or +10.2 per mil for water in the hydrothermal fluid. This compares favourably with the values of +8.1 to +9.0 per mil for Stage I fluid, derived from quartz-water fractionation.

The $\delta^{18}O$ value of water of cassiterite-forming fluids cannot be calculated until experimental data are available for cassiterite-water fractionation. However, Kelly and Rye (1979) report that preliminary data suggest that at 300°C ^{18}O fractionation between cassiterite and water is quite small (*i.e.* close to zero), and at higher temperatures is most likely negative. This is consistent with empirical quartz-cassiterite fractionation data produced by Borshchevskiy *et al*, (1979), and from which is derived the following cassiterite-water fractionation expression:

$$1000 \ln \alpha = 0.328 \ (10^6 T^{-2}) - 1.52 \qquad (4)$$

This empirical fractionation curve, combined with the $\delta^{18}O$ values of cassiterite and an estimated temperature of 500°C for Stage II mineralisation, gives $\delta^{18}O$ values of +6.3 and +7.6 per mil for co-existing water in the hydrothermal fluid, which is 3.5-4.0 per mil lower than values obtained from Stage II quartz.

The calculated oxygen isotopic compositions of the hydrothermal fluid have assumed the aqueous phase to be pure water, whereas the Cleveland hydrothermal fluid has an estimated salinity equivalent to a 10% NaCl solution. Truesdell (1974) has demonstrated a salinity effect on the ^{18}O fractionation between CO_2 and H_2O at elevated temperatures, requiring a small positive correction to the calculated water composition derived from mineral-water fractionation. However, in view of the imprecision in the above calculations (*e.g.* inexactness of temperature estimate, selection of quartz-water fractionation) this correction may be neglected (Taylor, 1979).

The $\delta^{18}O$ values of water in the hydrothermal fluid, calculated from quartz and dolomite in Stages I, II and IV, fall within the range +8.1 to +10.2 per mil, and thus are within the range of 'magmatic water' (Taylor, 1974, 1979). The limited variation in the $\delta^{18}O$ values of the water throughout the mineralisation episode indicates that there has been very little, if any, mixing of the hydrothermal fluid with meteoric or connate water, particularly during the waning stages of the mineralisation episode. It is not until the temperature of Stage IV mineralisation falls below 250°C that there is a significant decrease in $\delta^{18}O$ of the fluid (Fig. 7.8).

The hydrogen isotopic composition of water in the hydrothermal fluid is estimated from fluid collected from fluid inclusions contained in two samples of hydrothermal minerals (Appendix 6). A sample of Stage I quartz (104428) has a δD value of -57.5 per mil, and fluid from a sample of Stage IV fluorite (104319) has a value of -74.9 per mil. Both determinations are within the range of 'magmatic water' (Taylor, 1974, 1979), but the difference of almost 23 per mil between the two samples needs explanation. Assuming that the water sampled is repres-

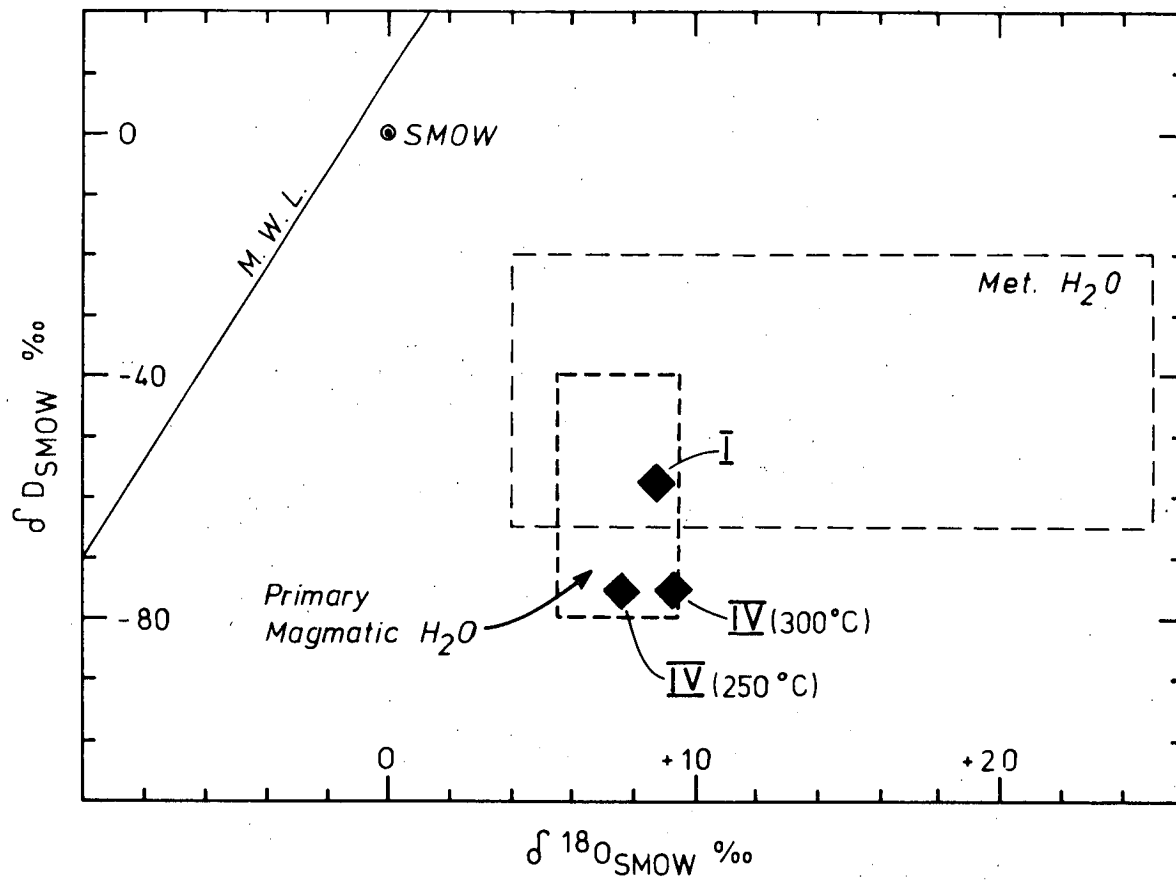

FIG. 7.9 Determined oxygen and hydrogen isotopic composition of hydrothermal fluid for stages I and IV (temperatures indicated). Fields for 'metamorphic water' (300° - 600°C) and 'primary magmatic water' are from Taylor (1979). M.W.L. = meteoric water line.

entative of the primary hydrothermal fluid, then the difference may be due to an influx of meteoric water during either the early or final stages of the mineralisation episode, this meteoric water being heavier or lighter than magmatic water depending on the latitude and altitude at the time of ore formation. Alternatively, it may be due to post-mineralisation 'contamination' by meteoric water occurring as secondary inclusions in the Stage IV fluorite. The fluid inclusion and oxygen isotope data do not support mixing of a 'magmatic' hydrothermal fluid with meteoric water at any time during ore formation. Palaeolatitude data of McElhinny and Embleton (1974) indicate that the position of Tasmania was probably tropical/equatorial during the Late Devonian-Early Carboniferous when the Cleveland deposit most likely formed, and that Tasmania then underwent a rapid movement towards the south pole in the Middle Carboniferous. With increasing latitude (and altitude) there is a systematic decrease in δD values of meteoric water (*e.g.* Taylor, 1979). Thus 'contamination' of the Stage IV fluorite by formation of secondary fluid inclusions containing meteoric water lighter than magmatic water could well have occurred at high palaeo-latitudes after ore formation.

The values of δD and $\delta^{18}O$ calculated for the Stage I and Stage IV hydrothermal fluid are plotted in Figure 7.9, together with the field of 'primary magmatic water' (after Taylor, 1979). Salinity corrections have not been applied to the data. It is apparent that the isotopic composition of both Stage I and Stage IV waters are consistent with derivation from a magmatic aqueous phase, the only variation being in δD values as explained above.

8. ENVIRONMENT AND CONDITIONS OF MINERALISATION AT CLEVELAND

The data accumulated in the preceding chapters are here combined in establishing the geological environment and manner of formation of the sulphide lenses. The temperature, composition and origin of the hydrothermal fluid is defined, and is then combined with data on mineral parageneses, stability fields of ore minerals, etc. to estimate physiochemical conditions of ore deposition.

GEOLOGICAL ENVIRONMENT AND MODE OF ORE FORMATION

The host Eocambrian-Cambrian succession of spilitic, tholeiitic basalt, mafic tuffs, argillite, chert and limestone (Deep Creek Volcanics and Hall Formation) overlain by interbedded turbiditic greywacke and argillite (Crescent Spur Sandstone) accumulated in an enclosed(?), subsiding, shallow marine environment during initial development of the Dundas Trough, probably in a crustal extension or rift setting. Sedimentation and burial continued through the Cambrian to Early Devonian, but was terminated by the mid-Devonian Tabberabberan orogeny which involved at least two phases of folding and faulting, followed by emplacement of Late Devonian, post-tectonic granitoids (*e.g.* Meredith Granite). The earliest phase of folding resulted in a major, north-east trending anticlinal structure, with an axial surface to the south-east of Cleveland. The mine sequence was dissected by several reverse faults (*e.g.* Nadir and Ratchet faults) feathering off a steeper, south-east dipping reverse fault (EN fault) which forms a structural boundary between the Deep Creek Volcanics and the Hall Formation. The age of the faulting is uncertain, though most movement occurred prior to mineralisation. The faulting may be associated with the first phase of Tabberabberan deformation, or it may reflect an up-thrown block associated with granite emplacement.

The sulphide lenses are essentially post-deformation (Cox and Glasson, 1971). The only evidence of later deformation is post-Stage II, pre-Stage IV movement on the reverse faults, local preferred orientation of pyrrhotite (Falvey, 1966; Ransom and Hunt, 1975), and local fracturing and brecciation of Stage II arsenopyrite and sphalerite. The relationships between major deformation, mineralisation and granite emplacement thus allow the granite and the ore to be approximately coeval. Geological evidence (stratigraphic reconstruction, granite composition) and fluid inclusion data indicate a confining pressure of about 150 MPa, corresponding to a depth of 5-6 km (lithostatic pressure) at the inferred time of ore deposition (Late Devonian-Early Carboniferous).

The development of Cleveland ore (sulphide lenses) is dependent upon the presence of the reverse faults, as they provided a plumbing system for ascending hydrothermal solutions. Mineralised sections of the low-angle, reverse faults contain abundant cassiterite, quartz and other silicates and sulphides, similar to early formed mineralisation in the sulphide lenses. Potassic alteration in the Deep Creek Volcanics is most intense adjacent to, and parallels the steep, south-east dipping EN fault, indicating it probably served as a major feeder channel. In the upper levels of the mine, alteration of the Henrys Volcanic Member decreases away from the reverse faults.

The sulphide lenses probably formed by replacement of limestone adjacent to irregular veins and fractures. These veins are rarely preserved in the sulphide lenses as their occurrence is masked by later recrystallisation, but where observed they commonly contain coarse-grained cassiterite (*e.g.* 104334). Similar veins with adjacent quartz-tourmaline-chlorite alteration occur in limestone and clastic sediments at the northern end of the mine. Compositional banding or lamination in mineralised units within the sulphide lenses parallels

bedding in adjacent argillite chert and tuff and probably reflects variation in composition of limestone preserved during replacement. On a larger scale, syn-sedimentary slump folds are preserved within some thick mineralised units. It is unlikely that the lamination in the ore is due to diffusion processes such as the various mechanisms proposed for development of 'wrigglite'-type textures (*e.g.* Kwak and Askins, 1981*a*), though wrigglite textures have been observed at Mt Bischoff (Kwak and Askins, 1981*b*).

The genetic relationship between the sulphide lenses (Stage II) and the topazised quartz porphyry dyke and penecontemporaneous W-Mo-Bi-Sn stockwork vein mineralisation (Stage I) has not been fully resolved. The sulphide lenses are clearly later than the Stage I veins. The concentric high-grade tin zone apparently centred on the porphyry dyke (Fig. 4.6) suggests a genetic relationship between the mineralised porphyry and cassiterite mineralisation in the sulphide lenses. The Stage II hydrothermal fluids, however, most likely ascended through fractures tapping a source to the south-east of the deposit, whereas the Stage I veins and porphyry dyke are confined to the footwall, to the north-west of the sulphide lenses (Fig. 4.5). The low-grade tin zone in the centre of the sulphide lenses, adjacent to the nose of the stockwork zone, may reflect metamorphism of the host rocks during emplacement of the porphyry which could have rendered the limestone in this area less receptive to alteration by later hydrothermal fluids.

TEMPERATURE, COMPOSITION AND ORIGIN OF THE HYDROTHERMAL FLUID

For a confining pressure of 150 MPa at the time of ore formation, fluid inclusion homogenisation temperature data indicate that the temperature of the hydrothermal fluid during formation of the sulphide lenses (Stage II) was within the range 420° to 550°C (pressure corrected) with a mode at about 500°C. Sulphur isotopic fractionation for a single

sphalerite-galena pair from a vein marginal to the deposit indicates a temperature of 537°C (± 30°C), but this is too high and probably results from slight differences in sphalerite and galena paragenesis. The temperature of the Stage II hydrothermal fluid is therefore considered to be 500°C (± 50°C). Fluid inclusion data indicate temperatures within the range 400° to 520°C (pressure corrected) for the Stage I hydrothermal fluid, with a mode at about 480°C (± 30°C). During the final stages of the mineralisaton episode (Stage IV), the fluid temperature decreased to less than 400°C with most fluid inclusion homogenisation temperature data indicating a pressure corrected fluid temperature of 290°-330°C (mean 300°C).

The absence of salt crystals in fluid inclusions at room temperature clearly places an upper limit of about 26.5% NaCl (Hass, 1976) on the salinity of the ore fluid. Fluid inclusion freezing data indicate a range in salinity of 8 to 14% NaCl (*i.e.* 1.5-2.8 molal NaCl solution) for the Stage II fluid, with a mode of about 10.5% NaCl (2.0 m). For Stage I mineralisation, the fluid has a similar range of 9 to 13% NaCl (1.7-2.5 m) but for Stage IV fluid the range is much broader, (7 to 15% NaCl) with a single fluid inclusion with a maximum of 19.5% NaCl. The mode of Stage IV salinity data is about 9.5% NaCl (*i.e.* 1.8 m). Thus the hydrothermal fluid as preserved in fluid inclusions, was low to moderately saline, with a range in salinity of 7 to 14% NaCl (1.3-2.8 m) and an overall mode of 10% NaCl, equivalent to a 1.9 molal NaCl solution. Fluids of similar salinity have been described as predominant at Mt Bischoff (Groves and Solomon, 1969; Groves *et al.*, 1972), at the Renison tin mine (Patterson *et al.*, 1981) and at numerous other tin-tungsten deposits (*e.g.* Cornwall, Czechoslovakia, Finland, Japan: *e.g.* Haapala and Kinnunen, 1982).

Carbon dioxide is a major component of the ore-forming fluids of some tin-tungsten deposits (*e.g.* Little, 1960), but is relatively minor in others (*e.g.* Kelly and Turneaure, 1970; Grant *et al.*, 1980). It has not been observed in fluid inclusions at Renison Bell (Collins, 1972; Patterson *et al.*, 1981) and is rare at Mt Bischoff (Groves and Solomon, 1969).

At Cleveland, carbon dioxide is a ubiquitous, though rare to minor, component of the Stage I and II fluids, but has not been observed in fluid inclusions in Stage IV fluorite. The primary hydrothermal fluid is probably best represented by fluid inclusions in Stage I quartz and fluorite. The fluid from which these veins formed is unlikely to have passed through carbonate rock, and thus any CO_2 in these inclusions is of a primary nature. The Stage I veins contain only a minor quantity of CO_2-bearing type 3 inclusions, and most are in the deepest of the specimens (Fig. 6.2; Table A5.1). Carbon dioxide has not been detected in type 1 inclusions indicating that CO_2 pressures are low. The isolated occurrence of CO_2-bearing inclusions in the Stage I minerals may be explained by either 'boiling' (or effervescence) of the fluid with concentration of the CO_2 into a volatile phase, or occasional injection of a fluid enriched in CO_2. Because there is no evidence to indicate boiling of the fluid (*e.g.* absence of highly saline inclusions, coexisting liquid and gaseous inclusions), the second alternative seems most likely.

CO_2-bearing type 3 inclusions are relatively common in Stage II quartz and fluorite from the sulphide lenses. It is unlikely that the CO_2-rich fluid in Stage II was derived from 'boiling' of a primary fluid enriched in CO_2. Firstly, there is no evidence for a primary fluid in which CO_2 is a major component (other than type 3 inclusions). Carbon dioxide(?) has been detected rarely in type 1

inclusions (Table A5.1). If 'boiling' of a fluid enriched in CO_2 had occurred at the inferred temperature and pressure of ore formation, then by reference to the CO_2-H_2O-NaCl system (*e.g.* Fig 6.5), two immiscible fluids would form: an (H_2O + NaCl) - CO_2 fluid with 10 - 20 mole per cent CO_2 (equivalent to type 3 inclusions) and a CO_2-(H_2O + NaCl) fluid with in excess of 50 mole per cent CO_2. However, there have been no fluid inclusions observed in Stage II minerals with more than about 15 mole per cent CO_2. Secondly, if 'boiling' did occur, then the salinity of the aqueous liquid phase of a boiled fluid would (depending on vapour loss) be greater than the original fluid, and at least a few high salinity inclusion fluids would be observed, but the only relatively saline inclusion fluid is in Stage IV fluorite (Figs. 6.4 through 6.6).

The most plausible explanation for the origin of type 3 inclusions occurring in Stage II mineralisation is that most of the CO_2 is derived from dissolution of the host limestone. Carbon isotope data indicate that there is also a magmatic component and/or CO_2 from dissolution of calcite in the Whyte River complex. CO_2 liberated by local dissolution of calcite would be absorbed by the hydrothermal fluid. The low salinity of type 3 inclusions (relative to type 1) is consistent with the salting-out effect on CO_2 solubility (Ellis and Golding, 1963). At the estimated pressure of ore formation (150 MPa) about 20 mole per cent CO_2 is soluble in a 6% NaCl solution (Takenouchi and Kennedy, 1965; Gehrig *et al.*, 1979). Therefore, type 1 inclusions with homogenisation temperatures less than 310°C (400° - 450°C pressure corrected) and associated type 3 inclusions probably represent an early fluid involved in the initial dissolution of the host limestone. The high homogenisation temperature (> 320°C; or > 450°C pressure corrected) type 1 inclusions represent slightly later, cassiterite-bearing Stage II hydrothermal fluid.

Despite the variation in fluid temperature and complications imposed by dissolution of limestone, the salinity of the hydrothermal fluid remained constant throughout the mineralisation episode, decreasing only slightly during Stage IV. The ^{18}O composition of the water in the hydrothermal fluid also remained constant throughout the mineralisation episode, with calculated $\delta^{18}O$ (and δD) values within the range of magmatic water.

Sulphide $\delta^{34}S$ values also are limited, with an extreme range of -0.2 to +5.5 per mil for the entire mineralisation episode (Stage V excluded), and a narrower range of -0.2 to +3.9 per mil for the main cassiterite-bearing Stage II mineralisation. The mineral assemblages and the inferred depositional conditions (temperature, fO_2, fS_2, pH) for mineralisation Stages I and II indicate a reduced fluid in which H_2S is the dominant sulphur species (*i.e.* $\delta^{34}S_{H_2S} = \delta^{34}S_{\Sigma S}$), and under such conditions $\delta^{34}S_{H_2S}$ is relatively insensitive to slight variation in fO_2 and pH (*e.g.* Ohmoto and Rye, 1979). At 500°C, pyrrhotite is enriched in ^{34}S by 0.2 per mil relative to H_2S (Ohmoto and Rye, 1979). In the sulphide lenses, pyrrhotite has a narrow range of 1.6 to 3.9 per mil and a mean value of 2.5 per mil indicating a mean $\delta^{34}S_{\Sigma S}$ value of 2.3 per mil for the main tin-bearing fluids. Total sulphur $\delta^{34}S$ values close to zero per mil indicate a magmatic or igneous source for the sulphur (Rye and Ohmoto, 1974; Ohmoto and Rye, 1979). The variation in sulphide $\delta^{34}S$ values (*e.g.* the slightly lower and higher $\delta^{34}S$ values in Stage II veins and in Stage III, respectively) probably reflect lower temperatures and/or small changes in fluid sulphur composition.

The consistency in salinity and isotopic composition of the hydrothermal fluid throughout the mineralisation episode indicates a magmatic origin and that there was little or no mixing of the fluid with meteoric water or seawater.

The nearest possible source of magmatic fluid is the Meredith Granite which crops out 4 km to the south and east of the Cleveland deposit (Fig. 3.1). The intensely altered (topazised) quartz porphyry dyke (?) intruding the footwall Crescent Spur Sandstone probably is a protrusion of the Meredith Granite which most likely extends northwards at a relatively shallow depth to below the Cleveland deposit. The cassiterite, wolframite, molybdenite-bearing Stage I mineralisation clearly is associated with the alteration of the porphyry. A similar association occurs at Mt Bischoff, where dolomite has been replaced by cassiterite-bearing massive pyrrhotite adjacent to altered (topazised) cassiterite-bearing quartz-feldspar porphyry dykes (Groves *et al.*, 1972; Solomon, 1980). Hence at both Cleveland and Mt Bischoff there is a definite association between tin-bearing massive sulphide mineralisation and granitic rock.

CONDITIONS OF ORE DEPOSITION AT CLEVELAND

Information on fluid temperature, salinity and CO_2 content can be combined with additional data from the mineralogy to estimate the fugacities of oxygen and sulphur during ore deposition. Quantitative estimates of other physicochemical parameters (*e.g.* pH, ΣS) is hampered by the high temperatures of formation of the Cleveland deposit, as this requires extrapolation of available thermochemical data well beyond accepted temperature limits, thereby introducing large uncertainties in such calculations. Details of thermodynamic data used to plot mineral stability fields on an fO_2 - fS_2 diagram are given in Table 8.1. In the preceding chapters, pressure has been expressed in SI units (*i.e.* pascals), but convention requires that fugacities be here expressed in atmospheres (it is sufficient to consider 1 atm = 10^5 Pa). Calculations involving thermodynamic data require temperatures to be

expressed in Kelvin, but it is convenient to continue to express temperatures in Celsius.

Although the estimated pressure during ore formation is 150 MPa (1500 atm), no pressure correction has been applied to the equilibrium constant, *K*. In equilibrium reactions involving solid phases, the effect of pressure on *K* may be expressed as (*e.g.* Anderson, 1977);

$$\ln K_{P_2} = \ln K_{P_1} - \frac{\Delta Vs}{RT}(P_2 - P_1) \qquad (1)$$

$$\text{or} \quad \Delta \log K_{(P_2 - P_1)} = \frac{-\Delta Vs}{2.303RT}(P_2 - P_1) \qquad (2)$$

where ΔVs is the difference in molar volume between product and reactant solid phases only in a particular reaction, and P_1 is the standard state pressure (*i.e.* 1 atm). In reactions for which molar volume data are available, the volume change is small (*i.e.* $\Delta Vs < 1$ cal/atm) resulting in negligible pressure corrections to log *K*, particularly in comparison to estimation of temperature. For example, the magnetite-pyrrhotite buffer is an important stability field boundary at Cleveland, and for the reaction:

$$3FeS + 2O_2 = Fe_3O_4 + \frac{3}{2}S_2, \qquad (3)$$

$$\Delta Vs = -0.24$$

resulting in a positive pressure correction to log *K* of 0.1, or less than 0.3% (500°C, 150MPa). The same magnitude variation in log *K* will result from a temperature variation of only 2°C, yet the inferred errors in estimated temperatures are ±30°C for Stage I, and ±50°C for Stage II. Similar magnitude variations in log *K* due to pressure, apply to reactions for which ΔVs can be calculated, and it is assumed that the pressure correction is similarly negligible for all other reactions.

	Reaction	Log K 480°C	500°C
1.	$FeS_2 = FeS + 1/2\ S_2$	- 2.8*	- 2.5*
2.	$3FeS_2 + 2O_2 = Fe_3O_4 + 3S_2$	28.4	28.0
3.	$2FeS_2 + 3/2\ O_2 = Fe_2O_3 + 2S_2$	22.7	22.3
4.	$3FeS + 2O_2 = Fe_3O_4 + 3/2\ S_2$	37.1	36.0
5.	$6Fe_2O_3 = 4Fe_3O_4 + O_2$	- 19.5	- 18.6
6.	$4FeS_2 + Cu_5FeS_4 = 5CuFeS_2 + S_2$	- 2.1*	- 1.7*
7.	$H_2S_{(aq)} + 1/2\ O_2 = H_2O_{(l)} + 1/2\ S_2$		9.2*
8.	$4/3\ Bi_{(l)} + S_2 = 2/3\ Bi_2S_3$	6.8	6.4
9.	$2FeAs_2 + 2FeS + S_2 = 4FeAsS$	8.1	7.6
10.	$Mo + S_2 = MoS_2$	16.9	16.2
11.	$Mo + O_2 = MoO_2$	31.2	30.1
12.	$4SnS + S_2 = 2Sn_2S_3$	5.8	5.4
13.	$2Sn_2S_3 + S_2 = 4SnS_2$	4.7	4.3
14.	$SnO_2 + 1/2\ S_2 = SnS + O_2$	- 22.4	- 21.7
15.	$SnO_2 + 2CuFeS_2 + S_2 = Cu_2FeSnS_4 + FeS_2 + O_2$		- 15.6*

TABLE 8.1 Equilibrium constants for the reactions used in constructing Figures 8.1 and 8.3.

Sources of thermodynamic data: 1-7, Ripley and Ohmoto (1977); 8-9, calculated from Barton and Skinner (1979); 10 and 11, calculated from Holland (1965); 12-13, calculated from Vaughan and Craig (1978); 14-15, calculated from Patterson *et al.* (1981).

* extrapolated.

The fugacities of oxygen and sulphur during Stage I mineralisation

As pyrrhotite is the stable iron sulphide, and microscopic textures indicate it is contemporaneous with vein development, sulphur fugacities must be below the pyrite-pyrrhotite boundary, corresponding at 480°C to a maximum sulphur fugacity of $10^{-5.5}$ atm. Arsenopyrite is a minor component of Stage I veins, which indicates a minimum sulphur fugacity of $10^{-8.1}$ atm at 480°C (Fig. 8.1). Sulphur fugacity is further refined by the co-existence of native bismuth and bismuthinite, intergrown with wolframite and molybdenite. This limits the sulphur fugacity to the bismuth-bismuthinite boundary which at 480°C has an fS_2 value of $10^{-6.8}$ atm.

As pyrrhotite is the dominant iron sulphide/oxide mineral in Stage I veins, oxygen fugacities must be below the pyrite-pyrrhotite-magnetite triple point, corresponding at 480°C to a maximum oxygen fugacity of $10^{-22.7}$ atm. Since sulphur fugacity is tied to the bismuth-bismuthinite boundary, oxygen fugacity must be lower than the intersection of this boundary and the pyrrhotite-magnetite boundary. At 480°C, this corresponds to a maximum oxygen fugacity of $10^{-23.7}$ atm. Oxygen fugacities may also be estimated from the relevant boundaries of mineral phases in the Sn-O-S system (Fig. 8.1), in particular, the lower limit of cassiterite stability. As cassiterite is the stable tin mineral in Stage I mineralisation, oxygen fugacities must be higher than the cassiterite-tin sulphides boundaries. Since sulphur fugacity is tied to the bismuth-bismuthinite boundary, oxygen fugacities must be above the intersection of this boundary and the cassiterite-herzenbergite boundary, corresponding at 480°C to a minimum oxygen fugacity of $10^{-25.8}$ atm.

Further constraints on oxygen fugacities may be imposed by the composition of gaseous phases (particularly CO_2, CH_4) in fluid inclusions (Ohmoto, 1970; Patterson *et al.*, 1981). Microthermometric data and an analysis of fluid from a specimen of Stage I quartz

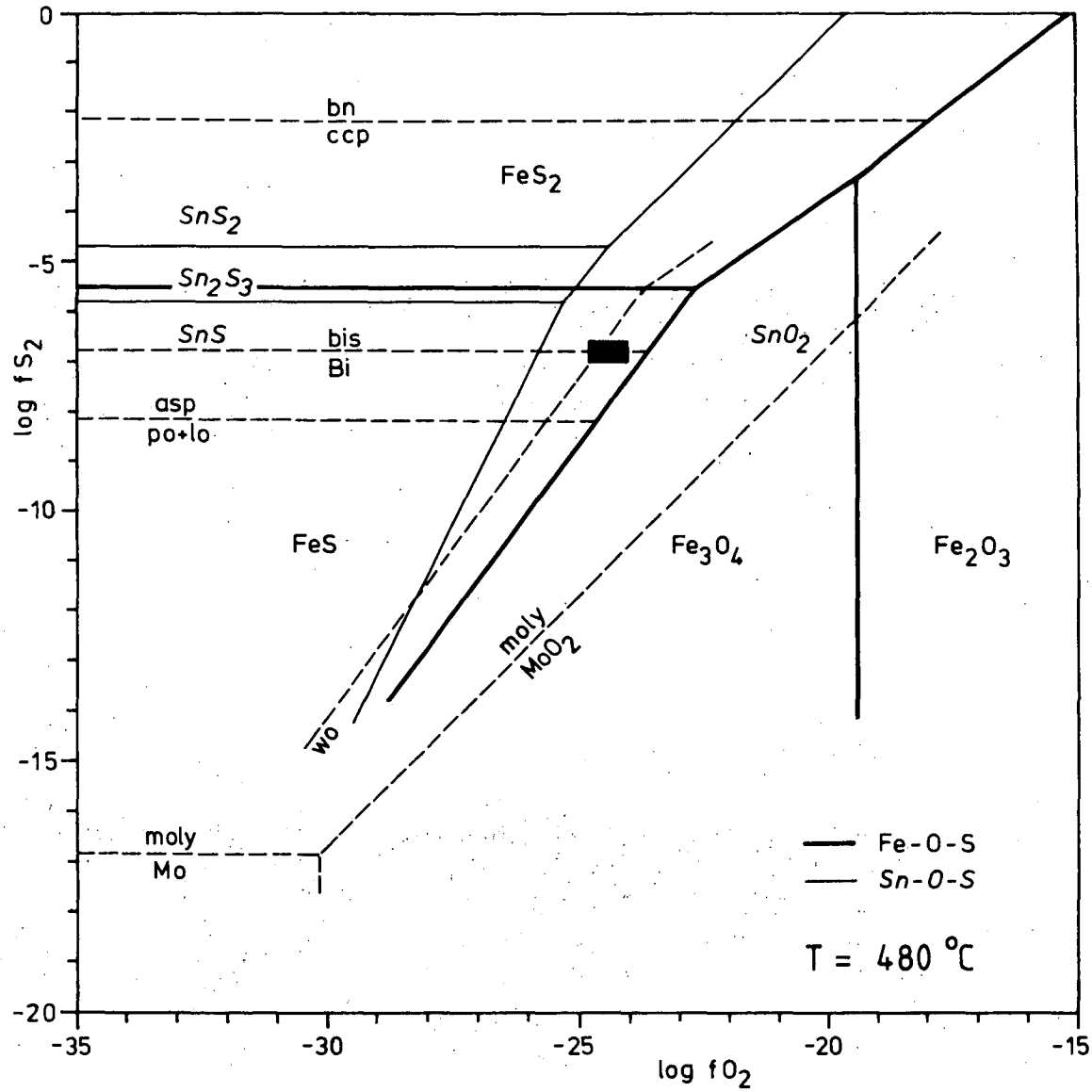

FIG. 8.1 Log fS_2-log fO_2 diagram at 480°C, showing depositional conditions for Stage I mineralisation (black box). Stability field boundaries are based on data in Table 8.1. Dashed line labelled 'wo' is for the reaction: ferberite = pyrrhotite + tungstenite (Hsu, 1976) plotted relative to solid buffer assemblages; ferberite being the stable phase at higher fO_2 or lower fS_2. Abbreviations: asp = arsenopyrite, bis = bismuthinite, bn = bornite, ccp = chalcopyrite, lo = loellingite, moly = molybdenite, po = pyrrhotite, wo = wolframite.

indicate that carbon dioxide is the dominant non-aqueous (and non-saline) component of Stage I inclusion fluids. Although the effect of pressure is significant below 100 MPa (Ohmoto, 1970), the CO_2-CH_4 boundaries at 100 MPa and 200 MPa are not significantly different (Patterson *et al.*, 1981). As CO_2 is the dominant gas phase, oxygen fugacities above $10^{-25.3}$ atm are indicated (Fig. 8.2). However, the CO_2:CH_4 molal ratio is probably greater than 10, which indicates a minimum oxygen fugacity of $10^{-24.8}$ atm at 480°C (Patterson, 1979).

In summary, it is inferred that the Stage I wolframite-molybdenite vein mineralisation formed at 480°C at low fS_2 ($10^{-6.8}$ atm) and low fO_2 ($10^{-23.7}$ to $10^{-24.8}$ atm). These fugacity conditions are plotted on Figure 8.1, relative to the mineral assemblages from which they have been derived. Thermodynamic data for the Mo-O-S system indicate that the inferred depositional conditions are well within the molybdenite stability field (Fig. 8.1). Experimental thermodynamic data on stability relations of wolframite (Hsu, 1976) indicate that the inferred conditions are well within the ferberite field in an Fe-W-O system (Fig. 8.2). Stability relations in an Fe(Mn)-W-O-S system are less precisely known, but available data indicate that the inferred fugacity conditions probably are close to the ferberite-(pyrrhotite + tungstenite) boundary (Hsu, 1976; Fig. 8.1).

Conditions of formation of cassiterite-bearing Stage II mineralisation

As pyrrhotite is the stable iron sulphide, and microscopic textures indicate it is contemporaneous with most cassiterite, silicates and fluorite deposition in the sulphide lenses, then sulphur fugacities must be below the pyrite-pyrrhotite boundary, corresponding at 500°C to a maximum sulphur fugacity of $10^{-5.0}$ atm. Native bismuth occurs in trace amounts in the sulphide lenses, but its exact paragenetic position within Stage II is uncertain, though it is probably contemporaneous with silicates, pyrrhotite, magnetite and cassiterite. This indicates sulphur fugacities below the bismuth-bismuthinite boundary

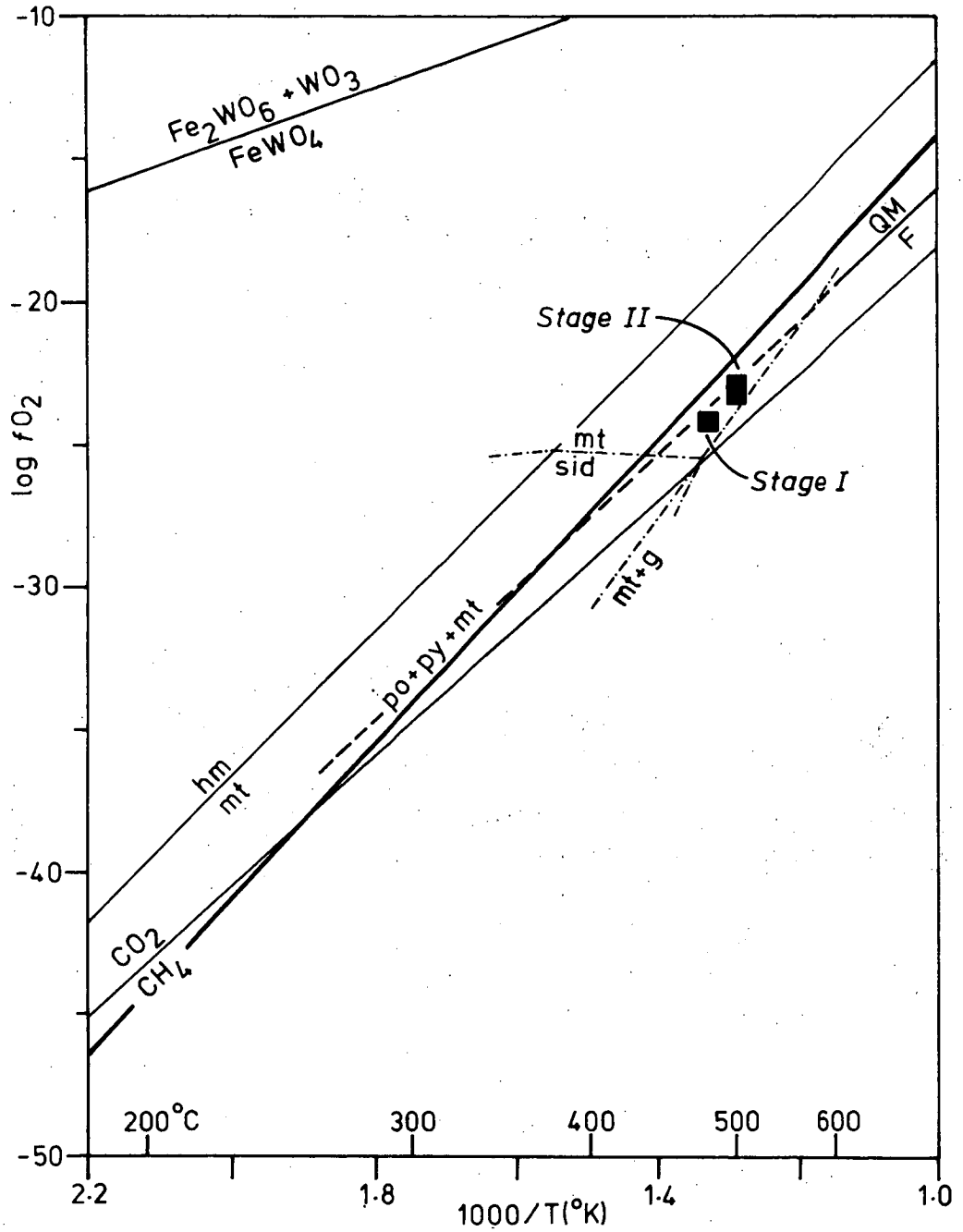

FIG. 8.2 Log fO_2-T diagram of various iron bearing buffer assemblages and carbon species (all at about 100 MPa) showing inferred fO_2 and T for Stages I and II (black boxes). Mineral equilibria represented are: magnetite + hematite (hm/mt), fayalite + magnetite + quartz (QM/F) (after Chou, 1978), pyrrhotite + pyrite + magnetite (po + py + mt). The CO_2/CH_4 boundary is after Patterson *et al.* (1981) and the ferberite boundary is from Hsu (1976). Dash-dot lines are stability fields for magnetite (mt), siderite (sid) and magnetite + graphite in the Fe-C-O system (French, 1971).

and a maximum fS_2 of $10^{-6.4}$ atm at 500°C.

The occurrence and composition of arsenopyrite may be used to estimate sulphur fugacities, but at Cleveland, arsenopyrite generally occurs at the extremities of the sulphide lenses and in veins surrounding the deposit where conditions of formation may be significantly different to the main part of the sulphide lenses. As loellingite has not been detected (Appendix 4) then minimum sulphur fugacities above the arsenopyrite-(loellingite + pyrrhotite) boundary are indicated, corresponding at 500°C to a minimum sulphur fugacity of $10^{-7.6}$ atm. Compositions of arsenopyrite may be used to calculate sulphur fugacity, using the experimental data of Kretschmar and Scott (1976). Stage II arsenopyrites have a wide compositional range between 31.8 and 34.6 at% As, but most of the variation is due to veins in the wall rocks (Table 4.1). Arsenopyrite in the Nadir fault has a narrow range with 33.6 and 34.6 at% As, corresponding at 500°C to fS_2 values of 10^{-5} and $10^{-6.2}$ atm, respectively. These values are at variance with other estimates of sulphur fugacities and may be due to higher fS_2 (or lower temperature) in the reverse faults. Arsenopyrite in veins in the wall rocks has a range of 31.8 to 34.0 at% As and define a temperature-fS_2 space, most of which is below the inferred conditions of formation of the sulphide lenses and indicate a decrease in temperature and/or sulphur fugacity away from the main part of the deposit. Arsenopyrite at the northern margin of the sulphide lenses contains 32.7 - 32.9 at% As indicating a maximum temperature of 450° - 480°C, depending on the pyrite-pyrrhotite boundary (*cf.* Kretschmar and Scott, 1976; Ripley and Ohmoto, 1977). Stage III arsenopyrites have a narrow compositional range of 32.5 to 33.3 at% As, which also are consistent with lower temperatures and/or sulphur fugacities during later stages of mineralisation.

As pyrrhotite is the dominant iron mineral in the upper ore, oxygen fugacities must be below the pyrite-pyrrhotite-magnetite triple point, corresponding at 500°C to a maximum oxygen fugacity of $10^{-21.7}$ atm. As sulphur fugacities are bracketed by the bismuth-bismuthinite and arsenopyrite-(loellingite + pyrrhotite) boundaries, then oxygen fugacities must be below the intersection of these lines with the pyrrhotite-magnetite boundary (*i.e.* below $10^{-22.8}$ to $10^{-23.6}$ atm, respectively). However, in deep intersections of the lower ore, magnetite and pyrrhotite were deposited contemporaneously, and in some sections magnetite is the dominant iron mineral, indicating that oxygen fugacities were confined to the pyrrhotite-magnetite buffer and possibly were a little higher, but probably not beyond the field of chalcopyrite (Fig. 8.3).

As cassiterite is the dominant tin mineral and is contemporaneous with silicates, pyrrhotite, magnetite, etc. then oxygen fugacities must have been higher than the cassiterite-herzenbergite boundary (Fig. 8.3). Fluid inclusion data indicate that carbon dioxide is the dominant volatite component of Stage II fluids, though most of the CO_2 apparently is derived from dissolution of limestone. Isotopic and salinity data indicate that Stage I and II fluids have a similar origin, and thus an assumed similar CO_2-CH_4 content, with a CO_2-CH_4 molal ratio greater than 1, corresponding at 500°C to a minimum oxygen fugacity of $10^{-24.4}$ atm (possibly a little higher) (Patterson *et al.*, 1981; Fig. 8.2). The apparent absence of siderite (and graphite) in magnetite-rich sections of the lower ore places a lower limit on oxygen fugacities (Fig. 8.2), corresponding at 500°C to a minimum fO_2 value of $10^{-23.3}$ atm (French, 1971).

The occurrence of hematite as an 'accidental' mineral in fluid inclusions in an assemblage dominated by pyrrhotite (and pyrrhotite + magnetite) is clearly anomalous. The hematite flakes were probably

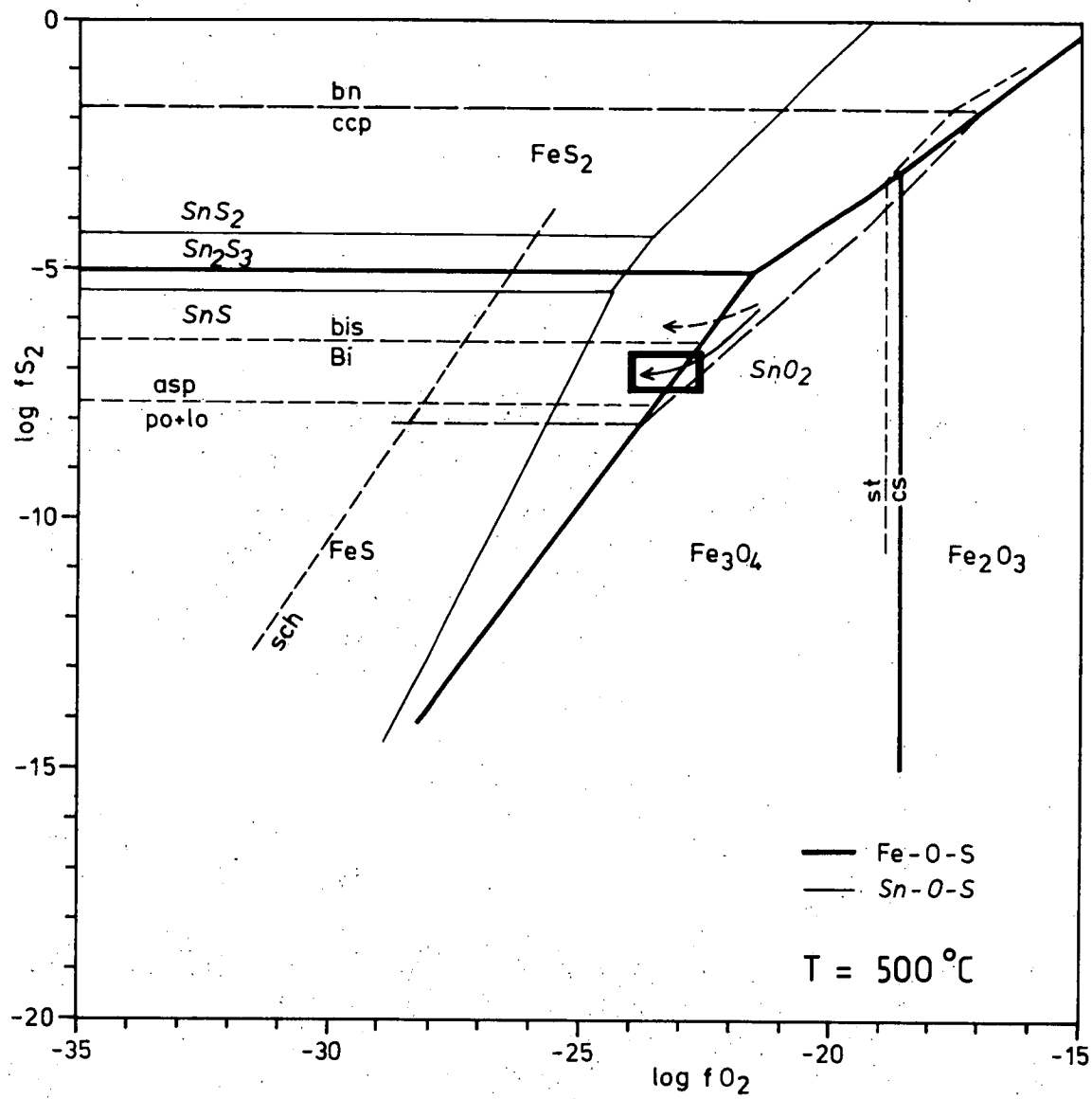

FIG. 8.3 Log fS_2-log fO_2 diagram at 500°C, showing depositional conditions for Stage II mineralisation (thick lined box). Stability field boundaries are based on data in Table 8.1. Dashed line labelled 'sch' is for the reaction: scheelite + quartz = tungstenite + wollastonite (Hsu, 1977) plotted relative to solid buffer assemblages; scheelite being the stable phase at higher fO_2 and lower fS_2. The stability field of chalcopyrite (long dash lines) is based on topological extension from the chalcopyrite + bornite + pyrite equilibrium. Arrow into the box indicates decrease in fO_2 (and fS_2(?)) in the sulphide lenses with decreased depth; dashed arrow is a possible path in the reverse faults. Abbreviations: asp = arsenopyrite, bis = bismuthinite, bn = bornite, ccp = chalcopyrite, cs = cassiterite (+ Cu, Fe sulphide), lo = loellingite, po = pyrrhotite, sch = scheelite, st = stannite (+ Fe sulphide/oxide).

transported in the fluid, thus indicating considerably higher oxygen fugacities and/or higher temperatures at greater depth, in the fluid source. This substantiates an apparent increase in fO_2 and/or higher temperatures with increased depth as reflected in changes in iron mineralogy from pyrrhotite in the upper ore to pyrrhotite + magnetite in the lower ore. If fO_2 varied, then it is likely that there was concomitant variation in fS_2 and a possible fO_2-fS_2 path, confined to the field of chalcopyrite stability, is shown in Figure 8.3 with fugacities decreasing with decrease in depth. Relatively rapid fluid movement through fractures may explain the higher sulphur fugacities in the Nadir fault (dashed path, Fig. 8.3).

Available experimental thermodynamic data on stability relations of scheelite (Hsu, 1977) indicate that the inferred fugacities are within the field of scheelite stability (Fig. 8.3). The occurrence of scheelite (in place of wolframite) in the sulphide lenses is consistent with a general association of scheelite and skarns (*e.g.* Rose and Burt, 1979). At Cleveland, scheelite occurs only in deep sections of the sulphide lenses in association with other minerals typical of skarn assemblages, such as magnetite, hornblende and danalite and possibly results from high calcium activities due to dissolution of limestone. However, the apparent absence of scheelite and abundance of fluorite in the upper ore indicates tungsten mineralogy is more complex, and that relative fluorine activities may also be important (Rose and Burt, 1979).

The presence of sericite as a trace to minor component of the sulphide lenses and its relative abundance at the expense of feldspar in the alteration halo in the Deep Creek Volcanics indicates a low pH fluid (Montoya and Hemley, 1975) at least 1 - 2 pH units below neutral. At pH conditions below neutral, pyrrhotite occurs only

where H_2S is the predominant aqueous sulphur species (*e.g.* Ripley and Ohmoto, 1977), thus allowing estimation of the total sulphur content of the ore fluid (where H_2S is predominant, $mH_2S = m\Sigma S$), using the reaction:

$$H_2S_{(aq)} + \tfrac{1}{2}O_2 = H_2O_{(l)} + \tfrac{1}{2}S_2 \qquad (5)$$

for which

$$\log aH_2S = \tfrac{1}{2}\log fS_2 - \tfrac{1}{2}\log fO_2 - \log K \qquad (6)$$

or $$\log mH_2S = \tfrac{1}{2}\log fS_2 - \tfrac{1}{2}\log fO_2 - \log K + \log \gamma H_2S \qquad (7)$$

where γH_2S is the activity coefficient of H_2S.

For the inferred oxygen and sulphur fugacities, and extrapolation of $\log K$ to 500°C, aH_2S equals 10^{-1}, corresponding to about 0.1 m ΣS. This represents a maximum ΣS value, as the occurrence of pyrrhotite + magnetite in the lower ore and low pH indicates a lower total sulphur content.

In summary, the cassiterite bearing sulphide lenses formed at 500°C at low fS_2 ($10^{-6.5}$ to $10^{-7.5}$ atm) and low fO_2 ($10^{-22.5}$ to 10^{-24} atm) with oxygen fugacities at the lower end of the fO_2 range at shallower depths. The inferred fugacity limits are plotted in Figure 8.3, in relation to the mineral assemblages from which they have been derived. Fugacity conditions of mineralisation in veins in the host rocks and of final stages of Stage II mineralisation have not been determined due to lack of temperature data, but the absence of pyrite and magnetite and presence of pyrrhotite indicates lower oxygen and sulphur fugacities at lower temperatures, and probably at similar relative positions in log fO_2 - log fS_2 space as for the sulphide lenses.

Depositional relationships of tin and copper minerals

Cassiterite, chalcopyrite and stannite occur throughout the sulphide lenses. Cassiterite commonly occurs alone, particularly in sulphide-poor, silicate and fluorite enriched assemblages. Stannite and chalcopyrite, and stannite alone, also occur without evidence of the prior existence of cassiterite, but commonly in association with pyrrhotite. Cassiterite occurring in sulphide (dominantly pyrrhotite) enriched assemblages commonly shows evidence of corrosion by, and development of a reaction rim or veinlets of stannite.

The relationships of tin-bearing minerals in Sn-Fe-Cu-O-S systems are shown in log fS_2 - log fO_2 diagrams, such as the isothermal (500°C) section in Figure 8.3. In a copper-free Sn-O-S system, the relevant boundaries are between cassiterite and various simple tin sulphides (herzenbergite, ottemanite and berndtite). At the temperature and inferred fS_2 - fO_2 conditions at Cleveland, cassiterite is the stable tin mineral, the simple tin sulphides requiring either lower oxygen fugacities or much higher sulphur fugacities. In a system containing a copper-iron sulphide, the relevant boundaries are those between cassiterite + copper-iron sulphide and stannite + iron sulphide, and the simple tin sulphides are absent (Patterson *et al.*, 1981).

The stability fields of pyrrhotite and cassiterite show decreasing overlap and eventual non-existence at progressively higher temperatures (*cf.* Fig. 8.3 with Figure 16 of Patterson *et al.*, 1981). Coexisting pyrrhotite + chalcopyrite + cassiterite assemblages are unlikely to form at temperatures above about 400°C, giving way to pyrrhotite + stannite + copper-iron sulphide at higher temperatures, (Patterson *et al.*, 1981). However, at Cleveland, the inferred depositional conditions are well within the stannite stability field (Fig. 8.3), but cassiterite is the dominant tin mineral. Microscopic textures indicate

that cassiterite intergrown with, or occurring as inclusions in silicate minerals (*e.g.* quartz, tourmaline, amphibole) generally shows no reaction with stannite, whereas cassiterite intergrown with pyrrhotite commonly shows replacement by stannite, and associated pyrrhotite too is replaced marginally by stannite and chalcopyrite.

Thus, it is inferred that the initial fluid was enriched in tin and depleted in copper, and that cassiterite was the only tin mineral deposited. Later fluids were enriched in copper (and probably depleted in tin), and under the inferred oxygen and sulphur fugacity conditions would have been in disequilibrium with cassiterite (and pyrrhotite). The later fluids reacted with and replaced accessible cassiterite with stannite, and pyrrhotite with chalcopyrite and stannite. Cassiterite inaccessible to later fluids (*i.e.* enclosed by unreactive silicate minerals) remained unaffected. Reaction between later fluids and cassiterite would have continued until the temperature dropped to below about 400°C, at which point the assemblage pyrrhotite + cassiterite would again have been stable.

The inferred depositional relationships between cassiterite and chalcopyrite + stannite has interesting implications for the source of the copper. The origin of most metals, sulphur, fluorine, boron, etc. is readily explained by their concentration in a magmatic aqueous phase during crystallisation of granitic magma, and migration through fractures until precipitated in a suitable host rock at appropriate conditions. However, Cleveland ore contains a comparatively substantial amount of copper (about 0.25%) as chalcopyrite and stannite, relative to trace-minor amounts at Renison and Mt Bischoff (Patterson *et al.*, 1981; Groves *et al.*, 1972). Mineragraphic textures and thermodynamic calculations confirm that copper (as $CuCl^{+}$) was an insignificant component of the main stanniferous hydrothermal fluids but was sufficiently enriched in later Stage II fluids to be saturated in respect of chalcopyrite

and stannite at the prevailing temperature, fO_2 and pH of the fluid. Copper in later fluids may have a primary magmatic origin, or alternatively, it may have been leached from spilitic basalt in the Deep Creek Volcanics and Henrys Volcanic Member which contains up to 400 g/t Cu. The only other cassiterite-sulphide deposit with a high copper content (chalcopyrite + stannite) is at Queen Hill, Zeehan (Lutley, 1975), and this too is in a sequence dominated by spilitic basalt. In the alteration halo in the Deep Creek Volcanics, there is an apparent, albeit tentative, inverse relationship between tin and copper as most altered basalt enriched in tin, is depleted in copper. Thus, the association of spilitic basalt, high copper (and stannite) content of ore, and tin enrichment/copper depletion in wall rocks is consistent with leaching of copper from basaltic rock by fluids undersaturated in copper.

Generalised conditions of Stage II mineralisation

The inferred depositional conditions of low fO_2, lowfS_2, low pH and reduced sulphur are consistent with evolution of aqueous fluid from peraluminous (S-type) granitic magma (Holland, 1972; Burnham and Ohmoto, 1980). During cooling, the relatively low oxygen fugacities may have been controlled by CO_2-CH_4 reaction, with an fO_2-T path close to the CO_2/CH_4 = 1 line (Burnham and Ohmoto, 1980; Patterson *et al.*, 1981; Fig. 8.3) During migration of the hydrothermal solution from granitic magma to a suitable host rock (*i.e.* limestone), the relatively low fO_2 and low pH may have been maintained by reaction with basaltic rock in the Deep Creek Volcanics, with fO_2 controlled by solid buffer assemblages such as quartz + magnetite + fayalite and nickel + nickel oxide (Patterson, 1979; Fig. 8.3).

A major depositional control is believed to be an increase in pH of an initially acidic solution caused by decarbonation reactions in the host limestone, such as:

$$CaCO_3 + 2HCl \rightarrow CaCl_2 + CO_2 + H_2O \quad (8)$$

Consumption of HCl would be sufficient to cause precipitation of sulphides (replacement of carbonate) by reactions such as:

$$MCl_2 + H_2S \rightarrow MS + 2HCl \quad (9)$$

provided metal (M) concentrations (as chlorides) were adequate. Other likely depositional processes include a decrease in temperate and an increase in oxygen fugacity. The relative lack of iron sulphides in Stage I veins compared to the sulphide lenses may be due to persistency of low pH and low fO_2 in temperature regimes still above iron sulphide saturation (Solomon, 1981).

Concomitant with the above reactions, copious amounts of CO_2 would have been evolved, causing locally high CO_2 pressures. This may account for early precipitation of siderite which requires high carbon dioxide fugacities at the inferred conditions (*cf.* Holland, 1959, 1965). The apparent absence of carbon dioxide inclusions however, indicates that most of the CO_2 evolved was dissolved in the aqueous phase, thus giving rise to type 3 CO_2-enriched aqueous inclusions. The lack of carbon dioxide inclusions also indicates large volumes of magmatic aqueous fluids as low fluid volumes may have become saturated in carbon dioxide with consequent possible trapping of a CO_2-rich phase.

9. GENESIS OF THE DEPOSIT

The origin of the Cleveland deposit has long been considered as epigenetic replacement of favourable horizons within the host volcano-sedimentary succession. Early workers (*e.g.* Reid, 1923) suggested chert and tuff were replaced, but later workers (*e.g.* Cox, 1968; Cox and Glasson, 1971), suggested beds of dolomite were replaced, mainly by analogy with the Mt Bischoff deposit.

The possibility of a syngenetic or volcanogenic origin has also been considered previously (*e.g.* Cox and Glasson, 1971; Palmer, 1976), but has recently been revived by Hutchinson (1979, 1980) and supported by Plimer (1980). Lehmann and Schneider (1981) have suggested that the stratabound character and association with spilite-type volcanism are inconsistent with an epigenetic interpretation. Solomon (1980) has argued against a syngenetic origin, highlighting the general association of tin and tin-tungsten mineralisation with granitoids, particularly the relationships between massive pyrrhotite mineralisation and quartz-feldspar porphyry dykes at Mt Bischoff and Renison Bell; and also the contrasting stratigraphic position and environments of accumulation of the host rocks at Cleveland, Mt Bischoff and Renison (see also Chapter 3). Patterson *et al.* (1981) have pointed out several features of the Renison ore bodies that indicate a syngenetic origin to be incorrect (*cf.* Hutchinson, 1982 and Patterson, 1982).

The evidence accumulated in this study also supports an epigenetic origin for the Cleveland deposit. For example: (1) the sulphide lenses occur within a near-vertical Eocambrian-Cambrian sequence that was folded prior to emplacement of the Late Devonian Meredith Granite, but the sulphide lenses exhibit no major deformation; (2) the host rocks are intruded by a basalt-

dolerite dyke associated with the Deep Creek volcanism, this dyke has been altered only where it intersects the sulphide lenses; (3) the Foleys zone quartz-wolframite-molybdenite stockwork vein system in the footwall Crescent Spur Sandstone (stratigraphically the youngest rock) is earlier than the mineralisation in the sulphide lenses and is associated with alteration of a quartz porphyry intrusive; (4) the limestone stratigraphically equivalent to the sulphide lenses is not anomalous in tin or copper, and is penetrated by the same quartz-sulphide veins as occur in the hanging wall and footwall rocks; (5) the hanging wall Deep Creek Volcanics contains a potassic alteration halo (defined by increasing alteration of pyroxene by actinolite, increasing K_2O, Rb, Sn and Zn, and decreasing Na_2O approaching the sulphide lenses) which parallels a major pre-ore(?) fault (EN fault); (6) alteration and bleaching of argillite and tuff interbedded with the limestone/mineralisation transgresses the bedding; (7) potassic alteration of spilitic basalt is prevalent in the Henrys Volcanic Member near the stratigraphic top of the Hall Formation, and has mildly affected basaltic rock in the Whyte River Complex, 250 m north-west of the sulphide lenses; (8) isotopic data indicate a magmatic origin for the ore fluids, and that there was no mixing with meteoric or oceanic waters; and (9) the lower levels of the sulphide lenses contain minerals (*e.g.* danalite, hornblende) typical of skarn mineralisation.

The association with subaqueous spilitic basalt appears only to be coincidental. The host rocks accumulated in a shallow marine environment, and the limestone was probably deposited during a period of quiesence between the volcanism and later turbiditic sedimentation. The basalt is altered with increasing intensity near the sulphide lenses but there is no evidence of the elements defining this alteration halo being concentrated in limestone stratigraphically equivalent to the sulphide lenses. The occurrence of spilitic basalt, however, is

fortuitous as it may have assisted migration of metals in solution, from a granitic source to shallower depths, by maintaining an original relatively low oxygen fugacity by reaction between the ore fluid and basalt (Patterson, 1979; Patterson *et al.*, 1981).

The stratiform nature of the sulphide lenses reflects original bedding in the host rocks. As the limestone is interbedded with relatively impervious argillite, chert and fine grained tuff, then it is only to be expected that the replacement mineralisation should take on the same form as the host rock.

The sequence of events and preferred model of mineralisation at Cleveland is as follows:

(1) An Eocambrian-Early Cambrian succession of spilitic basalt, mafic lapilli and vitric tuff, argillite, chert and limestone (Deep Creek Volcanics and Hall Formation) overlain by a sequence of turbiditic micaceous greywacke and argillite (Crescent Spur Sandstone) accumulated in a shallow marine environment. The high-titania, tholeiitic basalt reacted with seawater causing an enrichment in ^{18}O of +3.3 per mil relative to unaltered basaltic rock.

(2) Basalt-dolerite dykes and sills intruded, and later tectonic(?) emplacement of lenticular masses of serpentinised, low-titania basalt-dolerite-gabbro and ultramafic rock also of probable early Cambrian age, occurred.

(3) Folding of the host rocks took place during a period of deformation in the Early-late Middle Devonian resulting in a steep north-west dipping (and facing), north-east trending sequence, weakened by fractures, and locally overturned by reverse faulting.

(4) The Late Devonian-Early Carboniferous Meredith Granite, a high-level, late tectonic, peraluminous (S-type) granitic pluton was emplaced into the Early Palaeozoic rock, and an associated quartz porphyry dyke intruded the footwall Crescent Spur Sandstone.

(5). During a late phase of crystallisation of the Meredith Granite pluton, a magmatic aqueous phase emitted from the granite ascended into the early Cambrian succession through fractures and joints developed during Tabberabberan deformation and/or granite emplacement. Migration of this magmatic aqueous phase into the quartz porphyry dyke caused topazitic alteration of the porphyry and deposited wolframite, molybdenite, bismuth, bismuthinite and cassiterite in the altered porphyry and in a stockwork of veins penetrating both the porphyry and the Crescent Spur Sandstone. Fluid temperatures during this stage were about 480°C, with a low CO_2 content and salinity of about 1.9 m NaCl, and at low fO_2 and low fS_2.

(6) Ascent of the magmatic aqueous phase via the reverse faults (*e.g.* EN, Nadir and Ratchet faults in the upper ore) followed. The low-moderately saline (about 2.0 m NaCl) solution of initially low CO_2 content is inferred to have been acidic and at relatively low oxygen and sulphur fugacities at a temperature of about 500°C. Reaction with limestone in the Hall Formation caused an increase in pH and consequent precipitation of silicates, sulphides (predominantly arsenopyrite and pyrrhotite), fluorite, cassiterite and other oxides in the sulphide lenses and in faults in conjunction with decrease in temperature and probable increase in oxygen fugacity. The hydrothermal fluid reacted with basalt in the hanging wall Deep Creek Volcanics (and Henrys Volcanic Member) imparting a potassic alteration halo to the deposit. The main phase of mineralisation was followed by ascent of copper-enriched fluid which reacted with early-formed cassiterite and pyrrhotite and deposited stannite in the sulphide lenses and precipitated base-metal sulphides predominantly in veins surrounding the deposit, at temperatures probably in the range 350° to 450+°C. Extensive hypogene alteration of pyrrhotite,

carbonates etc. in Stages I and II occurred subsequent to Stage II mineralisation, but its exact paragenetic position is uncertain.

(7) Renewed movement on reverse faults preceded deposition of minor stage III quartz-arsenopyrite-stannite mineralisation from solutions of similar composition to Stage II.

(8) Passing of the magmatic aqueous phase continued with fluorite, quartz and carbonate precipitated in veins and vugs from waters at temperatures near 300°C and about 1.8 m NaCl.

(9) The final recognised product of the hydrothermal system is pyrite coating minerals in vugs and open veins and on joint surfaces.

(10) Subsequent uplift and erosion exposed the deposit.

Genesis of the Cleveland deposit is consistent with the genesis of many hydrothermal tin deposits, particularly other cassiterite-sulphide deposits in western Tasmania, and also with tin-tungsten veins and skarns, as reviewed in Chapter 1. It is spatially associated with a peraluminous (S-type) granitoid (Meredith Granite), and the footwall rocks have been intruded by a quartz porphyry dyke. Topazitic alteration of this dyke is similar to alteration of quartz-orthoclase porphyry dykes at Mt Bischoff which have isotopic ages the same as the Meredith Granite (McDougall and Leggo, 1965; Brooks, 1966).

The mineralogy of the Stage I quartz + fluorite + wolframite + molybdenite + bismuth + bismuthinite stockwork vein mineralisation is similar to many hydrothermal vein tungsten deposits, particularly the sub-volcanic porphyry W-Mo-Bi-Sn deposit at Mt Pleasant (Dagger, 1972; Parrish and Tully, 1978). The sulphide lenses have a mineralogy similar to other cassiterite-sulphide replacement deposits (*i.e.* Renison and Mt Bischoff), though less iron sulphide, but at depth the mineral assemblage is more typical of skarns in the contact zones of

granitic plutons. This transition from an iron sulphide dominant assemblage typical of the cassiterite-sulphide replacement bodies to iron sulphide/oxide + calc-silicates ± scheelite assemblages may be the only link between the two types of deposit. Mineralogical zoning at Cleveland is similar to many tin-tungsten deposits, with a central(?) W-Mo-Bi zone passing into a tin dominant zone and an outer and later base-metal sulphides zone. Tourmalinisation of wall rocks commonly is associated with tin mineralisation (*e.g.* Taylor, 1979) but at Cleveland there is also a potassic alteration halo in the hanging wall mafic volcanics.

The temperature of formation (about 500°C) is within the range of most tin deposits (300° - 550°C) but is higher than at Renison (300° - 350°C, Patterson *et al.*, 1981) and higher than much of Mt Bischoff (300° - 450°C) where the highest estimated temperature (580°C) is based on only one sample (Groves *et al.*, 1972). The estimated temperature of the lower ore may be too low, as many skarns range up to 600+°C, and most likely will increase with increased depth and hence closer proximity to granitic rock. Boiling of the hydrothermal fluid did not occur, probably due to the depth of formation and consequent high fluid pressures.

The salinity, and oxygen and sulphur isotopic composition of the hydrothermal fluid was relatively constant, and indicate a magmatic source throughout the mineralisation episode. This consistency probably reflects the depth of formation as high-level, hydrothermal tin deposits generally show a decrease in salinity with decreased fluid temperature during the later stages of mineralisation (*e.g.* Bolivia : Grant *et al.*, 1980), and decrease in ^{18}O composition of the hydrothermal fluid due to influx of meteoric water (*e.g.* Renison : Patterson *et al.*, 1981). The relatively low oxygen and sulphur fugacities and low pH are similar to conditions of formation of lower temperature cassiterite-bearing

stages at Renison (Patterson *et al.*, 1981) and some skarn deposits (*e.g.* Fujigatani : Sato, 1980). At low pH, low fO_2 and high temperatures, stannous chloride and fluoride (SnF^+) are the main tin species in solution (Patterson *et al.*, 1981, Eadington and Giblin, 1979). At Cleveland, the pH of the solution would have increased upon encountering limestone with subsequent precipitation of tin as cassiterite. Tin may also be precipitated by cooling the solution and by dilution of the hydrothermal fluid (with consequent changes in pH and/or fO_2), but these processes are unlikely to have been major controls on ore deposition at Cleveland.

In conclusion, the Cleveland cassiterite-sulphide deposit originated from the metasomatic replacement of limestone by tin-bearing, low to moderately saline acidic solutions of initially low CO_2 content derived from a granitic source related to the Meredith Granite.

REFERENCES

Abbotts, I.L., 1981, Masirah (Oman) Ophiolite sheeted dykes and pillow lavas : geochemical evidence for the former ocean ridge environment : Lithos, 14:283-294.

Anderson, G.M., 1977, Fugacity, activity, and the equilibrium constant in Greenwood, H.J. (ed.) Application of thermodynamics to petrology and ore deposits : Mineral.Assoc. Canada, Short Course Handbook, 2:17-37.

Banks, M.R., 1973, General geology in The lake country in Tasmania : Roy.Soc.Tasm., Hobart.

Barsukov, V.L., 1958, Recent developments in the geochemistry of tin, in Symposium on geochemical exploration : Proc. Int. Geol. Congr., 20th, 29-41.

Barsukov, V.L., Durasova, N.A., 1966, Metal content and metallogenetic specialisation of intrusive rocks in the regions of sulphide-cassiterite deposits (Miao-Chang and Sikhote-Alin) : Geochem. Internat., 3:97-107.

Barsukov, V.L., Sushchevskaya, T.M., 1973, Evolution of composition of hydrothermal solutions in the formation of tin-ore deposits : Geochem. Internat., 10:363-375.

Barton, P.B., Skinner, B.J., 1979, Sulfide mineral stabilities in Barnes, H.L. (ed.) Geochemistry of hydrothermal ore deposits, 2nd ed. : Wiley, New York, 278-403.

Berger, W.H., 1974, Deep sea sedimentation in Burk, C.A., Drake, C.L. (eds.) The geology of continental margins : Springer, New York, 213-241.

Blissett, A.H., 1962, Zeehan : Explan. Rep. Geol. Surv. Tasm., 1 mile geol. map series K/55-5-50.

Blissett, A.H., Gulline, A.B., 1961, Tin mineralisation near Mt Razorback, Dundas : Tech. Rep. Dep. Mines Tasm., 5:136-161.

Blockley, J.G., 1980, The tin deposits of Western Australia : West Australia Geol. Surv. Min. Res. Bull. 12.

Borshchevskiy, Yu. A., Borisova, S.L., Pavloskiy, A.B., Marshukova, N.K., 1979, Oxygen-isotope features of cassiterites from tin-ore deposits of Central Asia : Internat. Geol. Rev., 21:937-944.

Both, R.A., Rafter, T.A., Solomon, M., Jensen, M.L., 1969, Sulfur isotopes and zoning of the Zeehan mineral field : Econ. Geol., 64:618-628.

Both, R.A., Williams, K.L., 1968, Mineralogical zoning in the lead-zinc ores of the Zeehan field, Tasmania : J. Geol. Soc. Aust. 15:121-137 and 217-243.

Bottinga, Y., Javoy, M., 1975, Oxygen isotope partitioning among minerals in igneous and metamorphic rocks : Rev. Geophys. Space Phys., 13:401-418.

Bowden, P., 1982, Magmatic evolution in the Nigerian Younger Granite province in Evans, A.M., (ed.), Metallization associated with acid magmatism : Wiley, New York, 51-61.

Branch, C.D., 1968, Evolution of the Middle Proterozoic Chandabooka Caldera, Gawler Range acid volcano-plutonic province, South Australia : J. Geol. Soc. Aust., 25:199-216.

Brooks, C., 1966, The rubidium-strontium ages of some Tasmanian igneous rocks : J. Geol. Soc. Aust., 13:457-469.

Brooks, C., Compston, W., 1965, The age and initial Sr^{87}/Sr^{86} of the Heemskirk Granite, western Tasmania : J. geophys. Res., 70:6249-6262.

Brown, A.V., 1980, Some aspects of the geology of the Mt Lindsay-Dundas areas, western Tasmania : Unpub. Rep. Dep. Mines Tasm. 1980/42.

Brown, A.V., Rubenach, M.J., Varne, R., 1980, Geological environment, petrology and tectonic significance of the Tasmanian Cambrian ophiolitic and ultramafic complexes, in Panayiotou, A. (ed.) Ophiolites : Proceedings, International Ophiolite Symposium, Cyprus, 1979, 649-659.

Brown, A.V., Waldron, H.M., 1982, Preliminary review of Eocambrian-Cambrian basaltic associations and tectonic setting within western and north-western Tasmania : Unpub. Rep. Dep. Mines Tasm. 1982/10.

Burnham, C.W., Ohmoto, H., 1980, Late-stage processes of felsic magmatism in Ishihara, S., Takenouchi, S. (eds.) Granitic magmatism and related mineralization : Mining Geology Special Issue, No. 8 (Soc. Mining Geologists Japan), Tokyo, 1-11.

Burruss, R.C., 1981*a*, Analysis of phase equilibria in C-O-H-S fluid inclusions in Hollister, L.S., Crawford, M.L. (eds.) Fluid inclusions : applications to petrology : Mineral. Assoc. Canada, Short Course Handbook, 6:39-74.

Burruss, R.C., 1981*b*, Analysis of fluid inclusions : phase equilibria at constant volume : Am. Jour. Sci., 281:1104-1126.

Burt, D.M., 1978, Tin silicate-borate-oxide equilibria in skarns and greisens - the system $CaO-SnO_2-SiO_2-H_2O-B_2O_3-CO_2-F_2O_{-1}$: Econ. Geol. 73:269-282.

Canavan, F., 1973, Notes on the terms 'stratiform', 'stratabound' and 'stratigraphic control' as applied to mineral deposits : J. geol. Soc. Aust., 19:543-546.

Cann, J.R., 1969, Spilites from the Carlsberg Ridge, Indian Ocean : J. Petrology, 10:1-19.

Cann, J.R., 1970, Rb, Sr, Y, Zr and Nb in some ocean floor basalt rocks : Earth Planet. Sci. Lett., 10:7-11.

Carey, S.W., 1945, Geological report on Mt Cleveland tin mine : unpub. Rep. Dep. Mines Tasm., 1945:18-22.

Carpenter, L.G., Garrett, D.E., 1959, Tungsten in Searles Lake : Mining Engineering, 10:301-303.

Casadevall, T., Rye, R.O., 1980, The Tungsten Queen deposit, Hamme District, Vance County, North Carolina. A stable isotope study of a metamorphosed quartz-huebnerite vein : Econ. Geol., 75:523-537.

Chappell, B.W., White, A.J.R., 1974, Two contrasting granite types : Pacific Geol., 8:173-174.

Charoy, B., Weisbrod, A., 1975, Caractéristiques de la phase fluide associeé à la genese des gisements d'etain d'Abbaretz et de La Villeder (Bretagne Meridionale) : Mineral. Deposita, 10:89-99.

Chou, I-M., 1978, Calibration of oxygen buffers at elevated P and T using the hydrogen fugacity sensor : Am. Mineralogist, 63:690-703.

Claringbull, G.F., Hey, M.H., 1955, Stannite and isostannite : Mineralogical Abstracts, 13:31.

Clarke, D.B., 1981, The mineralogy of peraluminous granites : a review : Canad. Mineralogist, 19:3-17.

Coleman, R.G., 1977, Ophiolites : Springer-Verlag, Berlin-Heidelberg, 229p.

Coleman, R.J., 1975, The Savage River magnetite deposits in Knight, C.L. (ed.) Economic geology of Australia and Papua New Guinea, I, Metals : Melbourne, Aust. Inst. Min. Metall. Mon. 5:598-604.

Collins, P.L.F., 1972, The Geology and mineralisation of the South Renison Bell area, and the cassiterite-sulphide mineralisation of the Renison tin mine, Renison Bell : Unpub. Hon. thesis, Univ. of Tasmania.

Collins, P.L.F., 1978, The geology and mineralisation of north-west Tasmania, in Green, D.C., Williams, P.R. (eds.), Geology and mineralisation of N.W. Tasmania : Geol. Soc. Aust., Tasm. Div., Hobart, 2-8.

Collins, P.L.F., 1979*a*, Gas hydrates in CO_2-bearing fluid inclusions and the use of freezing data for estimation of salinity : Econ.Geol., 74:1435-1444.

Collins, P.L.F., 1979*b*, Metallic minerals in Jennings, I.B., Geological atlas 1 mile series. Sheet 37 (8115S). Sheffield : Explan. Rep. geol. Surv. Tasm.

Collins, P.L.F., 1981, The geology and genesis of the Cleveland tin deposit, western Tasmania : fluid inclusion and stable isotope studies : Econ. Geol., 76:365-392.

Collins, P.L.F., Gulline, A.B., Williams, E., 1981*a*, Geological atlas 1 mile series. Sheet 44 (8014N). Mackintosh : Explan. Rep. Dep. Mines Tasm.

Collins, P.L.F., Wyatt, B.W., Yeates, A.N., 1981*b*, A gamma-ray spectrometer and magnetic susceptibility survey of Tasmanian granitoids : Unpub. Rep. Dep. Mines Tasm. 1981/41.

Corbett, K.D., 1979, Stratigraphy, correlation and evolution of the Mt Read Volcanics in the Queenstown, Jukes-Darwin and Mt Sedgwick areas : Tasm. Geol. Surv. Bull. 58.

Corbett, K.D., 1981, Stratigraphy and mineralization in the Mt Read Volcanics, western Tasmania : Econ. Geol., 76: 209-230.

Corbett, K.D., Banks, M.R., Jago, J.B., 1972, Plate tectonics and the lower Palaezoic of Tasmania : Nature, 240:9-11.

Corbett, K.D., Brown, A.V., 1976, Queenstown : Explan. Rep. geol. Surv. Tasm., geol. atlas 1:250 000 series, Sheet No. SK-55/5.

Corbett, K.D., Green, G.R., Williams, P.R., 1977, The geology of central western Tasmania, in Banks, M.R., Kirkpatrick, J.B. (eds.) Landscape and Man : Roy. Soc. Tasm., Hobart.

Corbett, K.D., Reid, K.O., Corbett, E.B., Green, G.R., Wells, K., Sheppard, N.W., 1974, The Mt Read Volcanics and Cambro-Ordovician relationships at Queenstown, Tasmania : J. Geol. Soc. Aust., 21:173-186.

Cox, R., 1968*a*, The economic geology of the Cleveland and Magnet mines, Tasmania : Unpub. Ph.D. thesis, Univ. of Sydney.

Cox, R., 1968*b*, The use of comparative sampling methods at Cleveland mine, Tasmania : Proc. Australas. Inst. Mining Metall. 266:17-30.

Cox, R., 1968*c*, Assessment of tin ores in situ at Cleveland mine, Tasmania, with a portable radioisotope X-ray fluorescence analyser : Trans. Instn. Mining Metall., 77:B109-B116.

Cox, R., 1975, Magnet silver-lead-zinc orebody in Knight, C.L. (ed.) Economic geology of Australia and Papua New Guinea, I. Metals : Australas. Inst. Min. Metall, Mon 5:628-631.

Cox, R., Glasson, K.R., 1967, The geology and mineralisation of Cleveland mine in The geology of western Tasmania - a Symposium : Hobart, Univ. Tasm., Geol. Dept., Nov. 1967.

Cox, R., Glasson, K.R., 1971, Economic geology of the Cleveland mine, Tasmania : Econ. Geol., 66:861-878.

Cox, S.F., 1981, The stratigraphic and structural setting of the Mt Lyell volcanic-hosted sulfide deposits : Econ. Geol., 76: 231-245.

Crawford, M.L., 1981, Phase equilibria in aqueous fluid inclusions in Hollister, L.S., Crawford, M.L. (eds.), Fluid inclusions : applications to petrology : Mineral. Assoc. Canada, Short course handbook, 6:75-100.

Creenaune, P., 1980, The volcanics of the Heazlewood River Complex : Unpub. Hon. thesis, Univ. of Tasmania.

Crook, K.A.W., 1980, Tectonic implications of some field relations of the Adelaidean Cooee Dolerite, Tasmania : J. Geol. Soc. Aust., 26:353-362.

Dagger, G.W., 1972, Genesis of the Mount Pleasant tungsten-molybdenum-bismuth deposit, New Brunswick, Canada : Trans. Instn. Min. Metall., 81:B73-B102.

Danielson, M.J., 1975, King Island scheelite deposits in Knight, C.L. (ed.) Economic geology of Australia and Papua New Guinea, I. Metals : Australasian Inst. Mining Metall., Mon. 5, Melbourne, 592-598.

Davy, R., 1972, Geochemical prospecting for tin : Amdel Bull. 14:33-52.

Deer, W.A., Howie, R.A., Zussman, J., 1966, An introduction to the rock-forming minerals : Longmans, London, 528 p.

Department of Mines, 1970, Catalogue of the minerals of Tasmania : Rec. Geol. Surv. Tasm.

Duggan, N.T., 1980, The Que River deposit - a zinc-lead-copper occurrence in western Tasmania in Williams, E., et al. (eds.) Australian Geological Convention, 4th, Hobart, Jan. 1980, Programmes and Abstracts : Geol. Soc. Aust., 50.

Durasova, N.A., 1967, Some problems of the geochemistry of tin : Geochem Int., 4:671-681.

Eadington, P.J., Giblin, A., 1979, Alteration minerals and the precipitation of tin in granitic rocks : CSIRO Inst. Earth Resources, Tech. Comm. 68.

Edwards, A.B., 1951, Some occurrences of stannite in Australia : Proc. Aus. Inst. Mining Metall. 160-161:5-59.

Ellis, A.J., Golding, R.M., 1963, The solubility of calcite in sodium chloride solutions at high temperatures : Am. J. Sci., 261:259-267.

Elliston, J.N., 1954, Geology of the Dundas district, Tasmania : Pap. Proc. Roy. Soc. Tasm., 88:161-183.

Everard, G.B., 1964, Mount Cleveland mine, prospect : Tech. Rep. Dep. Mines Tasm., 8:128-133.

Falvey, D., 1966, The interpretation of geophysical surveys at Cleveland mine, Tasmania : Unpub. Hon. thesis, Univ. of Sydney.

Farrand, M., 1963, The relationship of mineralization to cherts in the Dundas Series at Mount Cleveland, near Waratah, western Tasmania : C.S.I.R.O. Mineragraphic Invest. Rep. 876.

Finucane, K.F., Blake, F., 1933, Report on the upper Wilson River and Mt Ramsay districts : Unpub. Rep. Dep. Mines Tasm., 1933:85-87.

Flinter, B.H., Hesp, W.R., Rigby, D., 1972, Selected geochemical, mineralogical and petrological features of granitoids of the New England Complex, Australia and their relation to Sn, W, Mo and Cu mineralization : Econ. Geol., 67:1241-1262.

Foden, J., 1973, The geochemistry of spilites from the Cambrian of western Tasmania : Unpub. Hon. thesis, Univ. of Tasmania.

Foose, M.P., Slack, J.F., Casadevall, T., 1980, Textural and structural evidence for a predeformation hydrothermal origin of the Tungsten Queen deposit, Hamme District, North Caroline : Econ. Geol., 75:515-522.

Ford, R.J., 1981, Platinum group minerals in Tasmania : Econ. Geol., 76:498-504.

Forester, R.W., Taylor, H.P., 1976, ^{18}O-depleted igneous rocks from the Tertiary complex of the Isle of Mull, Scotland : Earth Planet. Sci. Lett, 32:11-17.

French, B.M., 1971, Stability relations of siderite ($FeCO_3$) in the system Fe-C-O : Am Jour. Sci., 271:37-78.

Garlick, G.D., 1969, The stable isotopes of oxygen, in Wedepohl, K.K. (ed.) Handbook of geochemistry, vol. II/1, sec. 80 : Heidelberg, Springer-Verlag.

Garlick, G.D., Dymond, J.R., 1970, Oxygen isotope exchange between volcanic materials and ocean water : Geol. Soc. Am. Bull. 81:2137-2142.

Gee, R.D., 1967, The Proterozoic rocks of the Rocky Cape Geanticline in The geology of western Tasmania - a symposium : Dept. of Geology, Univ. Tasmania, Hobart.

Gee, R.D., 1979, Geological atlas 1 mile series. Zone 7 sheet 28 (8015N). Burnie : Explan. Rep. Geol. Surv. Tasm.

Gee, R.D., Marshall, B., Burns, K.L., 1970, The metamorphic and structural sequence in the Precambrian of the Cradle Mountain area, Tasmania : Rep. Geol. Surv. Tasm. 11.

Gehrig, M., Lentz, H., Franck, E.U., 1979, Thermodynamic properties of water-carbon dioxide-sodium chloride mixtures at high temperatures and pressures, in Timmerhaus, K.D., Barber, M.S. (eds.) High pressure science and technology, 6th AIRAPT Conference : New York, Plenum, 1:539-542.

Glasson, K.R., Hopwood, T., 1962, Geological report, Mt Cleveland mine, Waratah district, Tasmania : Unpub. Rep. Aberfoyle Tin Development Partnership.

Gotman, Y.D., Rub, M.G., 1960, Comparative characteristics of the tin-bearing granitoids of different ages of the south Primor'ye and certain other tin-bearing areas : Sovietskaia Geologiia, 1960 (2):48-56.

Grant, J.N., Halls, C., Sheppard, S.M.F., Avila, W., 1980, Evolution of the porphyry tin deposits of Bolivia, in Ishihara, S., Takenouchi, S. (eds.) Granitic magmatism and related mineralization : Mining Geology Special Issue, No. 8 (Soc. Mining Geologists Japan), Tokyo, 151-173.

Green, G.R., Solomon, M., Walshe, J.L., 1981, The formation of the volcanic-hosted massive sulfide ore deposit at Rosebery, Tasmania : Econ. Geol., 76:304-338.

Groves, D.I., 1966, The geology of the Heazlewood-Godkin area : Tech. Rep. Dep. Mines Tasm., 10:26-40.

Groves, D.I., 1968, The cassiterite-sulphide deposits of western Tasmania : Unpub. Ph.D. thesis, Univ. of Tasmania.

Groves, D.I., 1971, Regional significance of the Don Hill fault zone of Mt Bischoff, Tasmania : Tech. Rep. Dep. Mines Tasm., 14:7-15.

Groves, D.I., 1972*a*, The geochemical evolution of tin-bearing granites in the Blue Tier Batholith, Tasmania : Econ. Geol., 67:445-457.

Groves, D.I., 1972*b*, The zoned mineral deposits of the Scamander-St Helens district : Bull. geol. Surv. Tasm., 53.

Groves, D.I., 1977, The geology, geochemistry and mineralisation of the Blue Tier Batholith : Bull. geol. Surv. Tasm., 55:7-116.

Groves, D.I., Martin, E.L., Murchie, H., Wellington, H.K., 1972, A century of tin mining at Mt Bischoff, 1871-1971 : Bull. geol. Surv. Tasm., 54.

Groves, D.I., Solomon, M., 1964, The geology of the Mt Bischoff district : Pap. Proc. R. Soc. Tasm., 98:1-22.

Groves, D.I., Solomon, M., 1969, Fluid inclusion studies at Mt Bischoff, Tasmania : Inst. Mining Metallurgy Trans., 78:B1-B11.

Groves, D.I., Solomon, M., Rafter, T.A., 1970, Sulfur isotope fractionation and fluid inclusion studies at the Rex Hill mine, Tasmania : Econ. Geol., 65:459-469.

Groves, D.I., Taylor, R.G., 1973, Greisenization and mineralization at Anchor tin mine, north east Tasmania : Trans. Instn. Min. Metall., 82:B135-B146.

Haapala, I., Kinnunen, K., 1979, Fluid inclusions in cassiterite and beryl in greisen veins in the Eurajoki Stock, southwestern Finland : Econ. Geol., 74:1231-1238.

Haapala, I., Kinnunen, K., 1982, Fluid inclusion evidence on the genesis of tin deposits in Evans, A.M. (ed.), Metallization associated with acid magmatism (v.6) : Wiley, New York, 101-109.

Halley, S., 1982, A fluid inclusion study of the Lutwyche vein system, Rossarden : Unpubl. Hon. thesis, Univ. of Tasmania.

Hamaguchi, H., Kuroda, R., 1969, Tin : Abundance in rock-forming minerals (I), tin minerals (II), phase equilibria (III), in Wedepohl, KH. (ed.) Handbook of geochemistry II-4. 50-D-1 - 50-D-7. Springer-Verlag : Berlin.

Haas, J.L., 1971, The effect of salinity on the maximum thermal gradient of a hydrothermal system at hydrostatic pressure : Econ. Geol., 66:940-946.

Haas, J.L., 1976, Physical properties of the coexisting phases and thermochemical properties of the H_2O component in boiling NaCl solutions : Bull. U.S. geol. Surv., 1421-A, 73p.

Heaton, T.H.E., Sheppard, S.M.F., 1977, Hydrogen and oxygen isotope evidence for sea-water-hydrothermal alteration and ore deposition, Troodos complex, Cyprus : in Volcanic processes in ore genesis (inst. Min. Metall. and Geol. Soc. London, London), 42-57.

Hellsten, K.J., 1979, The emplacement and geometry of the mineralised quartz veins of the Rossarden-Storeys Creek area, Tasmania : Unpub. Hon. thesis, Monash Univ.

Hendel, E.M., Hollister, L.S., 1981, An empirical solvus for CO_2-H_2O-2.6 wt% salt " Geochim. et Cosmochim Acta, 45:225-228.

Henderson, Q.J., 1937, Geological features controlling the future of the Cleveland mine, vicinity of Waratah : Unpub. Rep. Dep. Mines Tasm., 1937:20-27.

Henderson, Q.J., 1943, Interview River wolfram deposits : Unpub. Rep. Dep. Mines Tasm., 1943:146-151.

Higgins, N.C., 1980, Genesis of the Grey River tungsten prospect : Unpub. Ph.D. thesis, Memorial Univ., Newfoundland.

Higgins, N.C., Solomon, M., Varne, R., in prep., The genesis of the granitoids of the Blue Tier Batholith, N.E. Tasmania.

Hine, R., Williams, I.S., Chappell, B.W., White, A.J.R., 1978, Contrasts between I- and S-type granitoids of the Kosciusko Batholith : J. Geol. Soc. Aust., 25:219-234.

Holl, R., Maucher, A., Westenberger, H., 1972, Synsedimentary-diagenetic ore fabrics in the strata- and time-bound scheelite deposits of Kleinarital and Felbertal in the eastern Alps : Mineral. Deposita, 7:217-226.

Holland, H.D., 1959, Some applications of thermochemical data to problems of ore deposits. I Stability relations among the oxides, sulphides, sulphates, and carbonates of ore and gangue minerals : Econ. Geol., 54:184-233.

Holland, H.D., 1965, Some applications of thermochemical data to problems of ore deposits. II Mineral assemblages and the composition of ore-forming fluids : Econ. Geol., 60:1101-1166.

Holland, H.D., 1972, Granites, solutions, and base metal deposits : Econ. Geol., 67:281-301.

Horsnail, R.F., 1979, The geology of tungsten : Proceedings of the first international tungsten symposium, Stockholm, September 5-7, 1979, 18-31.

Hosking, K.F.G., 1968, The relationship between primary deposits and granitic ricks, in A technical conference on tin : In. Tin Council, London, 1:267-311.

Hosking, K.F.G., 1970, Aspects of the geology of the tin-fields of South-East Asia, in Tech. Conf. on Tin, 2nd : Int. Tin Council, London, 1:39-79.

Hosking, K.F.G., 1970, The primary tin deposits of South-East Asia : Minerals, Sci. Eng., 1:24-50.

Hosking, K.F.G., 1973, Primary mineral deposits, in Gobett, D.J., Hutchinson, C.S. (eds.) Geology of the Malay Peninsula : Wiley-Interscience, New York, 335-390.

Hsieh, C.Y., 1963, A study of the tin deposits of China : Scientia Sinica 12:373-390.

Hsu, L.C., 1976, The stability relations of the wolframite series : Amer. Mineral., 61:944-955.

Hsu, L.C., 1977, Effects of oxygen and sulfur fugacities on the scheelite-tungstenite and powellite-molybdenite stability relations : Econ. Geol., 72:664-670.

Hudson, J.D., 1977, Stable isotopes and limestone lithification : J. Geol. Soc. London, 133:637-660.

Hughes, T.D., 1953, The Mount Cleveland mine : Unpub. Rep. Dep. Mines., 1953:61-71.

Hughes, T.D., 1954, The Mount Cleveland mine - supplementary report : Unpub. Rep. Dep. Mines Tasm., 1954:82-85.

Hunter, D.R., 1976, Some enigmas of the Bushveld complex : Econ. Geol., 71:229-248.

Hutchinson, R.W., 1979, Evidence of exhalative origin for Tasmanian tin deposits : CIM Bull., 72:90-104.

Hutchinson, R.W., 1980, Evidence of exhalative origin for Tasmanian tin deposits : Author's reply to discussion : CIM Bull., 73:167-168.

Hutchinson, R.W., 1982, Geologic setting and genesis of cassiterite-sulfide mineralization at Renison Bell, western Tasmania - A discussion : Econ. Geol., 77:199-206.

Irvine, T.N., Baragar, W.R.A., 1971, A guide to the chemical classification of the common volcanic rocks : Can. J. Earth Sci., 8:523-548.

Itsikson, M.I., 1960, The distribution of tin ore deposits within folded zones : Int. Geol. Review, 2:397-417.

Jack, R., Groves, D.I., 1965, Geology of the Mt Meredith-Yellowband Creek area : Tech. Rep. Dep. Mines Tasm., 9:26-36.

Jago, J.B., 1979, Tasmanian Cambrian biostratigraphy - a preliminary report : J. Geol. Soc. Aust., 26:223-230.

Jago, J.B., Reid, K.O., Quilty, P.G., Green, G.R., Dailey, B., 1972, Fossiliferous Cambrian limestone from within the Mt Read Volcanics, Mt Lyell mine area, Tasmania : J. Geol. Soc. Aust., 19:379-382.

Jessup, A., 1970, Geological report on mineral zoning in the Cleveland ore deposit : Unpub. Rep. Cleveland Tin N.L.

Keith, M.L., Weber, J.N., 1964, Carbon and oxygen isotopic composition of selected limestones and fossils : Geochim et Cosmochim. Acta, 28:1787-1816.

Kelly, W.C., Rye, R.O., 1979, Geologic, fluid inclusion, and stable isotope studies of the tin-tungsten deposits of Panasqueira, Portugal : Econ. Geol., 74:1721-1822.

Kelly, W.C., Turneaure, F.S., 1970, Mineralogy, paragenesis and geothermometry of the tin and tungsten deposits of the eastern Andes, Bolivia : Econ. Geol., 65:609-680.

Keunecke, O., Tate, K.H., 1954, Geophysical survey at Mt Cleveland mine, Waratah, Tasmania : Bureau Min. Res. Aust. Rec. 1954/7.

Kingsbury, C.J.R., 1965, Cassiterite and wolframite veins of Aberfoyle and Story's Creek in McAndrew, J. (ed.), Geology of Australian Ore Deposits : Publs. 8th Commonwealth Mining Metall. Cong., Melbourne, 1:506-511.

Klominsky, J., 1972, The Heemskirk Granite massif, western Tasmania - a study of chemical variability in plutonic rocks : Unpub. Ph.D. thesis, Univ. Tasmania, Hobart.

Klominsky, J., Groves, D.I., 1970, The contrast in granitic rock types associated with tin and gold mineralization in Tasmania : Proc. Aust. Inst. Min. Metall., 234:71-77.

Kloosterman, J.B., 1970, A two-fold analogy between the Nigerian and Amazonian tin provinces, in A second technical conference on tin : Int. Tin Council, Bangkok, 1:195-221.

Kretschmar, U., Scott, S.D., 1976, Phase relations involving arsenopyrite in the system Fe-As-S and their application : Can. Mineral. 14:364-386.

Kwak, T.A.P., Askins, P.W., 1981*a*, Geology and genesis of the F-Sn-W (-Be-Zn) skarn (wrigglite) at Moina, Tasmania : Econ. Geol., 76:439-467.

Kwak, T.A.P., Askins, P.W. 1981*b*, The nomenclature of carbonate replacement deposits with emphasis on Sn-F(-Be-Zn) 'wrigglite' skarns : J. Geol. Soc. Aust., 28:123-136.

Kwak, T.A.P., Tan, T.H., 1981, The geochemistry of zoning in skarn minerals at the King Island (Dolphin) mine : Econ. Geol., 76:468-497.

Kuys, K.J., 1981, Geology and mineralisation of the Oakleigh Creek mine : Unpub. Hon. thesis, Univ. Tasmania.

Landis, G.P., Rye, R.O., 1974, Geologic, fluid inclusion and stable isotope studies of the Pasto Bueno tungsten-base metal ore deposit, northern Peru : Econ. Geol., 69:1025-1059.

Leaman, D.E., Richardson, R.G., Shirley, J.E., 1980, Tasmania - the gravity field and its interpretation : Unpub. Rep. Dep. Mines Tasm., 1980/36.

Lehmann, B., Schneider, H.-J., 1981, Strata-bound tin deposits in Wolf, K.H. (ed.), Handbook of Strata-bound and Stratiform Ore Deposits : Elsevier, Amsterdam, 10:743-771.

Levinson, A.A., 1974, Introduction to exploration geochemistry : Applied Publishing, Calgary.

Little, W.M., 1960, Inclusions in cassiterite and associated minerals : Econ. Geol., 55:485-509.

Lutley, W.M. 1975, Cassiterite-sulphide mineralization at Queen Hill, Zeehan, western Tasmania : Unpub. M.Sc. thesis, Univ. Adelaide.

MacDonald, G.A., Katsura, T., 1964, Chemical composition of Hawaiian lavas : J. Petrol., 5:82-133.

Magak'yan, I.G., 1968, Ore deposits-tin : Int. Geol. REview, 10:108-121.

Manning, D.A.C., 1981, The effect of Fluorine on liquidus phase relationships in the system Qz-Ab-Or with excess water at 1 kb : Contrib. Min. Pet., 76:206-215.

Manson, W.St.C., Liddy, J., James, P.L., 1963, Composite samples from Mt Cleveland for vanning tests : Tech. Rep. Dep. Mines Tasm., 8:158-179.

Mason, A.A.C., 1965, Tin ore deposits of Mount Cleveland in Geology of Australian ore deposits, 2nd ed. : Pub. 8th Comm. Min. Metall. Congr., Melbourne, 503-505.

Materikov, M.P., 1977, Deposits of tin, in Smirnov, V.I. (ed.) Ore deposits of the U.S.S.R. : Pitman, London, 3:229-294.

Matthews, A., Katz, A., 1977, Oxygen isotope fractionation during the dolomitization of calcium carbonate : Geochim. et Cosmochim. Acta, 41:1431-1438.

Maucher, A., 1976, The strata-bound cinnabar-stibnite-scheelite deposits in Wolf, K.H. (ed.), Handbook of strata-bound and stratiform ore deposits : Elsevier, Amsterdam, 7:477-503.

McClenaghan, M.P., Turner, N.J., Baillie, P.W., Brown, A.V., Williams, P.R., Moore, W.R., 1982, Geology of the Ringarooma-Boobyalla area : Bull. geol. Surv. Tasm., 61.

McClenaghan, M.P., Williams, P.R., 1982, Distribution and characterisation of granitoid intrusions in the Blue Tier area : Pap. geol. Surv. Tasm., 4.

McDougall, I., Leggo, P.J., 1965, Isotopic age determinations on granitic rocks from Tasmania : J. Geol. Aoc. Aust. 12:295-332.

McElhinny, M.W., Embleton, B.J.J., 1974, Australian palaeomagnetism and the Phanerozoic plate tectonics of eastern Gondwanaland : Tectonophysics, 22:1-29.

Miyashiro, A., 1975, Classification, characteristics, and origin of ophiolites : J. Geology, 83:249-281.

Möller, P., Parekh, P.P., Schneider, H.-J., 1976, The application of Tb/Ca-Tb/La abundance ratios to problems of fluorspar genesis : Mineral. Deposita, 11:111-116.

Montoya, J.W., Hemley, J.J., 1975, Activity relations and stabilities in alkali feldspar and mica alteration reactions : Econ. Geol., 70:577-583.

Moon, K.J., 1983, The genesis of the Sangdong tungsten skarn deposit : Unpub. Ph.D. thesis, Univ. of Tasmania.

Moore, J.G., 1975, Mechanism of formation of pillow lava : Amer. Sci., 63:269-277.

Moore, A., 1980, Scheelite mineralisation in metasomatic hornblende-phlogopite rocks, Tantalite Valley, S.W.A./Namibia in Williams, E., et al. (eds.) Aust. Geol. Convention, 4th, Hobart, Jan. 1980, Programme and Abstracts : Geol. Soc. Aust., 31.

Muehlenbachs, K., Clayton, R.N., 1972*a*, Oxygen isotope studies of fresh and weathered submarine basalts : Can. J. Earth Sci., 9:172-184.

Muehlenbachs, K., Clayton, R.N., 1972*b*, Oxygen isotope geochemistry of of submarine greenstones : Can. J. Earth Sci., 9:471-478.

Munhá, J., Kerrich, R., 1980, Sea water basalt interaction in spilites from the Iberian pyrite belt : Contrib. Min. Petrol., 73:191-200.

Nye, P.B., 1923, The silver-lead deposits of the Waratah district : Bull. Geol. Surv. Tasm., 33.

Ohmoto, H., 1970, Fluid inclusions and isotope study of the lead/zinc deposits at the Bluebell mine, British Columbia, Canada : Soc. Mining Geologists Japan, Spec. Issue 2:93-99.

Ohmoto, H., 1972, Systematics of sulfur and carbon isotopes in hydrothermal ore deposits : Econ. Geol., 67:551-578.

Ohmoto, H., Rye, R.O., 1979, Isotopes of sulfur and carbon in Barnes, H.L. (ed.) Geochemistry of Hydrothermal Ore Deposits, 2nd Ed. : Wiley, New York, 509-567.

Olade, M.A., 1980, Geochemical characteristics of tin-bearing and tin-barren granites, northern Nigeria : Econ. Geol., 75:71-82.

Olatunju, J.A., Cuff, C., Taylor, R.G., 1977, Aspects of granitoids from the West Herberton region of the Herberton-Mt Garnet tinfield : Aust. Geol. Convention, 2nd, Monash Univ., Abstracts, 41.

Palmer, K.G., 1976, The Cleveland tin deposit, in Solomon, M., Green, G.R. (eds.) Ore deposits of western Tasmania : In. Geol. Cong., 25th, Sydney, 1976, Excursion Guide 31AC:27-31.

Parrish, I.S., Tully, V.V., 1978, Porphyry tungsten zones at Mt Pleasant, N.B. : CIM Bull., 71:93-100.

Patterson, D.J., 1976, The Renison tin deposit, in Solomon, M., Green, G.R. (eds.) Ore deposits of western Tasmania : Int. Geol. Cong., 25th, Sydney, 1976, Excursion Guide 31Ac:36-41.

Patterson, D.J., 1979, Geology and mineralization at Renison Bell, western Tasmania : Unpub. Ph.D. thesis, Univ. of Tasmania.

Patterson, D.J., 1982, Geologic setting and genesis of cassiterite-sulfide mineralization at Renison Bell, western Tasmania - A reply : Econ. Geol., 77:203-206.

Patterson, D.J., Ohmoto, H., Solomon, M., 1981, Geologic setting and genesis of cassiterite-sulphide mineralization at Renison Bell, western Tasmania : Econ. Geol., 76:393-438.

Pearce, J.A., Cann, J.R., 1971, Ophiolite origin investigated by discriminant analysis using Ti, Zr and Y : Earth Planet. Sci. Lett., 12:339-349.

Pearce, J.A., Cann, J.R., 1973, Tectonic setting of basic volcanic rocks determined using trace element analysis : Earth Planet. Sci. Lett., 19:290-300.

Pearce, T.H., Gorman, B.E., Birkett, T.C., 1975, The TiO_2-K_2O-P_2O_5 diagram; a method of discriminating between oceanic and non-oceanic basalts : Earth Planet. Sci. Lett., 24:419-426.

Petrova, Z.I., Legeydo, V.A., 1965, Geochemistry of tin in the magmatic process : Geochem. Int., 2:301-307.

Pitcher, W.S., 1979, The nature, ascent and emplacement of granitic magmas : J. geol. Soc. London, 136:627-662.

Plimer, I.R., 1980, Exhalative Sn and W deposits associated with mafic volcanism as precursors to Sn and W deposits associated with granites : Mineral. Deposita, 15:275-289.

Potter, R.W., 1977, Pressure corrections for fluid-inclusion homogenization temperatures based on the volumetric properties of the system NaCl-H_2O : Jour. Research U.S. Geol. Survey, 5:603-607.

Potter, R.W., Clynne, M.A., Brown, D.L., 1978, Freezing point depression of aqueous sodium chloride solutions : Econ. Geol., 73:284-285.

Rafter, T.A., Solomon, M., 1967, Sulphur isotope and oxygen isotope studies of Tasmanian ore deposits, in The geology of western Tasmania - a symposium : Hobart, Univ. of Tasmania, Geology Dept.

Råheim, A., 1977, Petrology of the Strathgordon area, western Tasmania Si^{4+}-content of phengite mica as monitor of metamorphic grade : J. Geol. Soc. Aust., 24:329-338.

Ransom, D.M., 1972, Reinterpretation of the geology of Cleveland cassiterite-sulphide deposit in The Palaeozoic geology, structure and mineralisation of western Tasmania - a symposium : Geol. Soc. Aust. Tas. Div., 3-4.

Ransom, D.M., Hunt, F.L., 1975, The Cleveland tin mine, in Knights, C.L. (ed.) Economic geology of Australia and Papua-New Guinea. I. Metals : Aust. Inst. Min. Metall. Mon. 5:584-591.

Rattigan, J.H., 1963, Geochemical guides and techniques in exploration for tin : Proc. Australasian Inst. Min. Metall. 207:137-151.

Reid, A.M., 1923, The Mount Bischoff tin field : Bull. geol. Surv. Tasm. 34.

Ripley, E.M., Ohmoto, H., 1977, Mineralogic, sulfur isotope and fluid inclusion studies of the stratabound copper deposits at the Raul mine, Perua : Econ. Geol., 72:1017-1041.

Roedder, E., 1972, Composition of fluid inclusions : U.S. Geol. Surv. Prof. Paper 440JJ.

Roedder, E., 1976, Fluid-inclusion evidence on the genesis of ores in sedimentary and volcanic rocks, in Wolf, K.H. (ed.) Handbook of strata-bound and stratiform ore deposits, v. 2 : Elsevier, Amsterdam, 67-110.

Roedder, E., 1979, Fluid inclusions as samples of ore fluids, in Barnes, H.L. (ed.) Geochemistry of Hydrothermal Ore Deposits, 2nd Ed. : Wiley, New York, 684-737.

Roedder, E., 1981, Origin of fluid inclusions and changes that occur after trapping in Hollister, L.S., Crawford, M.L. (eds.), Fluid inclusions : applications to petrology : Mineral. Assoc. Canada, Short Course Handbook, 6:101-137.

Rose, A.W., Burt, D.M., 1979, Hydrothermal alteration in Barnes, H.L. (ed.) Geochemistry of hydrothermal ore deposits : Wiley, New York, 173-235.

Rubenach, M., 1973, The Tasmanian ultramafic-gabbro and ophiolite complexes : Unpub. Ph.D. thesis, Univ. Tasmania.

Rubenach, M., 1974, The origin and emplacement of the Serpentine Hill complex, western Tasmania : J. Geol. Soc. Aust., 21:91-106.

Rye, R.O., Ohmoto, H., 1974, Sulfur and carbon isotopes and ore genesis : A review : Econ. Geol., 69:826-842.

Sato, K., 1980, Tungsten skarn deposit of the Fujigatani mine, southwest, Japan : Econ. Geol., 75:1066-1082.

Schneider, H.-J., Möller, P., Parekh, P.P., 1975, Rare earth elements distribution in fluorites and carbonate sediments of the East-Alpine mid-Triassic sequences in the Nördliche Kalkalpen : Mineral. Deposita, 10:330-344.

Schneider, H.-J., Möller, P., Parekh, P.P., Zimmer, E., 1977, Fluorine contents in carbonate sequences and rare earths distribution in fluorites of Pb-Zn deposits in East-Alpine mid-Triassic : Mineral. Deposita, 12:22-36.

Schwarcz, H.P., 1969, The stable isotopes of carbon, in Wedepohl, K.H. (ed.) Handbook of Geochemistry, v. II/1, Sec. 6-B-I : Heidelberg, Springer-Verlag.

Scott, B., 1954, The metamorphism of the Cambrian basic volcanic rocks of Tasmania and its relationship to the geosynclinal environment : Pap. Proc. Roy. Soc. Tasm., 88:129-149.

Schleglov, A.D., Butkevich, T.V., 1977, Deposits of tungsten, in Smirnov, V.I. (ed.), Ore deposits of the U.S.S.R. : Pitman, London, 3:180-228.

Sheppard, S.M.F., 1977, The Cornubian batholith, S.W. England : deuterium/hydrogen and oxygen-18/oxygen-16 studies of kaolinite and other alteration minerals : J. Geol. Soc. London, 133: 573-591.

Shepherd, T.J., Beckinsale, R.D., Rundle, C.C., Durham, J., 1976, Genesis of Carrock Fell tungsten deposits, Cumbria : fluid inclusion and isotopic study : Trans. Inst. Mining Metall., 85:B63-B73.

Sheraton, J.W., Black, .L.P., 1973, Geochemistry of mineralized granitic rocks of northeast Queensland : J. Geochem. Explor., 2:331-348.

Sillitoe, R.H., Halls, C., Grant, J.N., 1975, Porphyry tin deposits in Bolivia : Econ. Geol., 70:913-927.

Smirnov, V.I., 1976, Geology of mineral deposits : MOscow, Mir. Pub., 520 p.

Solomon, M., 1964, The spilite-heratophyre association of west Tasmania and the ore deposits at Mt Lyell, Rosebery and Hercules : Unpub. Ph.D. thesis, Univ. of Tasmania.

Solomon, M., 1965, Geology and mineralization of Tasmania : Publ. 8th Commw. Min. Metall. Congr., 1:464-477.

Solomon, M., 1969, The origin of the pillow lavas and hyaloclastite breccias of King Island, Australia : J. geol. Soc. London, 124:153-169.

Solomon, M., 1977, Metallic mineral deposits of the Pieman-Gordon region and the likelihood of new discoveries, in Banks, M.R., Kirkpatrick, (eds.) Landscape and Man : Roy. Soc. Tasm. Hobart.

Solomon, M., 1980, Evidence of exhalative origin for Tasmanian tin deposits : Discussion : CIM Bull., 73:166-167.

Solomon, M., 1981, An introduction to the geology and metallic ore deposits of Tasmania : Econ. Geol., 76:194-208.

Solomon, M., Green, G.R., Reid, K.O., 1976, Geological history of western Tasmania in Solomon, M., Green, G.R. (eds.) Ore deposits of western Tasmania : Internat. Geol. Cong., 25th, Sydney, 1976, Excursion Guide 31AC, 1-12.

Solomon, M., Griffiths, J.R., 1974, Aspects of the early history of southern Tasman Orogenic Zone, in Denmead, A.K., Tweedale, G.W., Wilson, A.F. (eds.) The Tasman geosyncline - A symposium : Brisbane, Geol. Soc. Aust., Queensland Div., 19-44.

Solomon, M., Groves, D.I., Klominsky, J., 1972, Metallogenic provinces and districts in the Tasman Orogenic Zone of eastern Australia : Proc. Aust. Inst. Min. Metall., 242:9-24.

Sourirajan, S., Kennedy, G.C., 1962, The systen H_2O-NaCl at elevated temperatures and pressures : Am. Jour. Sci., 260:115-141.

Spooner, E.T.C., Beckinsale, R.D., Fyfe, W.S., Smewing, J.D., 1974, O^{18} enriched ophiolitic metabasic rocks from E. Liguria (Italy), Pindos (Greece), and Troodos (Cyprus) : Contr. Mineralogy Petrology, 47:41-62.

Spry, A.H., 1964, Precambrian rocks of Tasmania. Part IV, The Zeehan-Corinna area : Pap. Proc. Roy. Soc. Tasm., 98:23-48.

Spry, A.H., Banks, M.R. (eds.), 1962, The geology of Tasmania : J. Geol. Soc. Aust., 9.

Štemprok, M., 1963, Distribution of Sn-W-Mo formation deposits around granites in Štemprok, M. (ed.), Problems of post magmatic ore deposition : Geol. Surv. Czech., Prague, 1:69-72.

Štemprok, M., 1965, Genetic features of the deposits of tin, tungsten and molybdenum formation, in Štemprok, M. (ed.), Problems of post magmatic ore deposition : Geol. Surv. Czech, Prague, 2:472-481.

Stillwell, F.L. 1944*a*, Tin ore from the Cleveland mine, Waratah district, Tasmania : C.S.I.R.O. Mineragraphic Invest. Rep. 305.

Stillwell, F.L. 1944*b*, Sulphide concentrates from Cleveland tin ore : CSIRO Mineragraphic Invest. Rep. 309.

Stockley, J., 1972, The Meredith Granite : Unpub. Hon. thesis. Univ. Tasmania.

Takenouchi, S., Kennedy, G.C., 1965, The solubility of carbon dioxide in NaCl solutions at high temperatures and pressures : Am. Jour. Sci., 263:445-454.

Tan, T.H., Kwak, T.A.P., 1979, The measurement of the thermal history around the Grassy Granodiorite, King Island, Tasmania, by use of fluid inclusion data : J. Geol., 87:43-54.

Tauson, L.V., Koziov, V.P., Kuz'min, M., 1968, Geochemical criteria of potential ore-bearing in granite intrusions : Int. Geol. Congr. 23, Proc. 6:123-129.

Taylor, B.L., 1954, Progress report on the North Pieman mineral area : Unpubl. Rep. Dep. Mines Tasm. 1954:159-199.

Taylor, H.P., 1974, The application of oxygen and hydrogen isotope studies to problems of hydrothermal alteration and ore deposition : Econ. Geol., 69:843-883.

Taylor, H.P., 1979, Oxygen and hydrogen isotope relationships in hydrothermal mineral deposits in Barnes, H.L. (ed.) Geochemistry of Hydrothermal Ore Deposits, 2nd ed. : Wiley, New York, 236-277.

Taylor, H.P., Forester, R.W., 1971, Low-O^{18} igneous rocks from the intrusive complexes of Skye, Mull, and Ardnamurchan, western Scotland : J. Petrol., 12:465-497.

Taylor, R.G., 1979, Tin ore deposits : Elsevier, Amsterdam, 543 p.

Tischendorf, G., 1973, The metallogenetic basis of tin exploration in the Erzgebirge : Trans. Inst. Mining Metall. 82:B9-B24.

Tischendorf, G., 1977, Geochemical and petrographic characteristics of silicic magmatic rocks associated with rare-element mineralization in Štemprok, M., Burnol, L., Tischendorf, G. (eds.), Metallization associated with acid magmati-m, Vol. 2, 41-96.

Tödheide, K., Franck, E.U., 1963, Dask zweiphasengebiet und die kritische kurve im system kohlendioxid-wasser bis zu drucken von 3500 bar : Z. Physik. Chemie. N.F., 37:387-401.

Truesdell, A.H., 1974, Oxygen isotope activities and concentrations in aqueous salt solutions at elevated temperatures : consequences for isotope geochemistry : Earth Planet. Sci. Lett., 23:387-396.

Turneaure, F.S., 1971, The Bolivian tin-silver province : Econ. Geol., 66:215-225.

Vallance, T.G., 1974, Spilitic degradation of a tholeiitic basalt : J. Petrol. 15:79-96.

Vaughan, D.J., Craig, J.R., 1978, Mineral chemistry of metal sulphides : Cambridge Univ. Press, Cambridge, 493 p.

Veizer, J., Hoefs, J., 1976, The nature of oxygen-18/oxygen-16 and carbon-13/carbon-12 secular trends in sedimentary carbonate rocks : Geochim. et Cosmochim. Acta, 40:1387-1395.

Wade, M.L., Solomon, M., 1958, Geology of the Mt Lyell mines, Tasmania : Econ. Geol. 53:367-416.

Walshe, J.L., Solomon, M., 1981, An investigation into the environment of formation of the volcanic-hosted Mt Lyell copper deposits using geology, mineralogy, stable isotopes, and a six-component chlorite solid solution model : Econ. Geol., 76:246-284.

Ward, M.A., 1981, The geology of the granites at Renison Bell-Pine Hill : Unpub. Hons. thesis, Univ. of Tasmania.

Waterhouse, L.L., 1914, The Stanley River tinfield : Geol. Surv. Tasm. Bull. 15.

Webster, S.S., Skey, E.H., 1979, Geophysical and geochemical case history of the Que River deposit, Tasmania, Australia : Canad. Geol. Survey. Econ. Geol. Rept., 31:697-720.

Wells, K., 1978, Geology and mineralisation in the South Heemskirk tin field, west Tasmania : Unpub. M.Sc. thesis, James Cook Univ. of North Queensland.

White, A.J.R., Beams, S.D., Cramer, J.J., 1977, Granitoid types and mineralisation with special reference to tin in Nozawa, T., Yamada, H. (eds.), Plutonism in relation to volcanism and metamorphism, Proc. 7th CPPP Mtg., Toyama, 89-100.

Wilkins, R.W.T., Ewald, A., 1982, Ore-forming fluids of the Aberfoyle tin-tungsten deposit, Tasmania. J. geol. Soc. London 139:96-97.

Williams, E., 1978, Tasman Fold Belt System in Tasmania : Tectonophysics, 48:159-205.

Williams, E., 1979, Tasman Fold Belt System in Tasmania : Revd. ed. : Dep. Mines Tasm.

Williams, E., Solomon, M., Green, G.R., 1975, The geological setting of metalliferous ore deposits in Tasmania, in Knight, C.L. (ed.) Economic Geology of Australia and Papua New Guinea - Metals : Aust. Inst. Min. Metall. Monograph 5:567-581.

Williams, E., Turner, N.J., 1974, Burnie : Explan. Rep. geol. Surv. Tasm., geol. atlas 1:250 000 series, Sheet No. SK-55/3.

Williams, P.R., 1982, Structural geology of the Mt Bischoff Precambrian rocks - Unpub. Rep. Dep. Mines Tasm., 1982/11.

Winkler, H.G.F., 1979, Petrogenisis of metamorphic rocks : Springer-Verlag, New York, 3rd ed.

Wolf, D., Espozo, E., 1972, Zur geochemie bolivianischer Kassiterite : Zeitschr. Angew. Geologie, 18:459-468.

Yermakov, N.P., 1965, Research on the nature of mineral-forming solutions : Pergamon, London.

Yong Won, J., 1963, Geology and origin of Sang Dong tungsten mine, Republic of Korea : Econ. Geok., 58:1285-1300.

Ypma, J.M., Simons, J.H., 1970, Genetic aspects of the tin mineralisation at Durango, Mexico in Fox, W. (ed.), A second technical conference on tin : Int. Tin Council, London, 1:177-192.

APPENDIX 1

Clarification and definition of Cambrian stratigraphy in the Cleveland mine area

The stratigraphy of the Cambrian sequences in the Cleveland mine area has been generally recognised as consisting of three main stratigraphic units, each of which has been assigned a variety of descriptive terms and formation names by previous workers. In this appendix, the stratigraphy is clarified, and is defined according to the Australian Code of Stratigraphic Nomenclature (see *J.Geol.Soc.Aust. 11* (1), 1964, pp 165-171). Grid co-ordinates are given to the nearest 100m, within the 100km square CQ of the Australian Map Grid, Zone 55 (see also fig. 3.3).

Cox (1968) and Cox and Glasson (1971) defined the Crescent Spur Group to consist of the three main stratigraphic units defined below. However, Groves (1968) considered the sedimentary/volcanic sequence in the Cleveland area to be part of the Arthur River sequence, which is correlated with the Crimson Creek Formation (Groves *et al.*, 1972). Designation of the three main units as a Group is not considered to be warranted, and they are here considered as part of the Arthur River sequence.

Name of Unit: DEEP CREEK VOLCANICS

Derivation of Name: Deep Creek is the long-standing name of a tributary of the Whyte River, which it joins 2km south of Luina, near CQ645061, Arthur River 1:100 000 sheet (7915). The name of this small rivulet has been recently changed to Washington Creek, but the original name is retained in this validation of the stratigraphic nomenclature.

Synonmy: The term "Deep Creek Basic Volcanics Formation" (DCBVF) was used by Cox (1968) and Cox and Glasson (1971) for the mafic volcanic sequence cropping out south-east of the Cleveland mine, and the term

"Whyte Hill Basic Volcanics Formation" (WHBVF) was used by Cox (1968) for a similar but less extensive suite of mafic volcanics cropping out on Whyte Hill (CQ686078). Both of these formations coincide with, and are superseded by the Deep Creek Volcanics.

Other terms used previously to distinguish this mafic volcanic suite in the Cleveland mine area include the "lavas" (Hughes, 1953), the "Basic Volcanics Formation" (Glasson and Hopwood, 1962; Cox and Glasson, 1967), the "massive volcanics" (Mason, 1965), the "basic volcanic unit" (Ransom and Hunt, 1975) and the "Deep Creek basic volcanics" (Palmer, 1976).

Distribution: The unit is exposed over 10km^2 in the southeast portion of the Cleveland 1:50 000 sheet area (7915-II), on the high ground between Deep Creek (Washington Creek) and Falls Creek, and on Whyte Hill.

Type Section and Reference Sections: The type section is in Deep Creek between CQ650065 and CQ665072. Reference sections occur in Falls Creek to the south of the Cleveland mine, between CQ646054 and CQ652047; and a short section occurs on the summit of Whyte Hill (at CQ688079).

Lithology: Massive and locally pillowed spilitic basalt lava, with intercalated and interbedded fine-grained and lapilli tuff, volcaniclastic greywacke, red-chocolate brown argillite and minor red-grey-green chert.

Thickness: The thickness of the unit is not known, and any estimate may be exaggerated by faulting. South-east of the Cleveland mine it is probably in excess of 600m. The reference section in Falls Creek is approximately 350m in thickness.

Relationships and Boundary Criteria: The formation is conformably overlain by the Hall Formation to the west. To the east, the unit is faulted against a suite of serpentinised ultramafic-mafic rocks at Whyte Hill but further south, in Falls Creek, it is bounded by a turbiditic greywacke sequence similar to the Crescent Spur Sandstone.

The nature of this latter boundary is not known.

Age: Eocambrian(?)-Early Cambrian(?) by correlation. Fossils have not been found in this unit.

Name of Unit: HALL FORMATION

Derivation of Name: The unit derives its name from Hall's workings, which are the original main open cut and underground mine workings (on Hall's lode, lens A) on the south-east flank of Godkin Ridge, at CQ652069, Arthur River 1:100 000 Sheet (7915).

Synonymy: The term "Hall's Formation" (HF) was originally used by Cox (1968) and Cox and Glasson (1971) for a single repetitive unit up to 30m thick and containing a single "lode bed". Equivalent terms of "Lode Formation" (Glasson and Hopwood, 1962; Cox and Glasson, 1967) and "lode horizon" (Mason, 1965) also have been used for this unit. Ransom (1972) and Ransom and Hunt (1975) re-interpreted the structure at the mine and defined a "lode-bearing unit" 50-100m thick. This unit was later designated as "Hall's formation" by Palmer (1976). The Hall Formation also coincides with the "slate" of Hughes (1953).

Distribution: The unit is exposed over 3km^2 on Whyte Hill, on the southeast flank of Crescent Spur and on the east bank of the Whyte River south of Deep Creek, on the Cleveland 1:50 000 sheet area (7915-II). A fault-emplaced inlier occurs in the Deep Creek Volcanics east of the Cleveland mine.

Type Section and Reference Section: The type section is a sub-surface section at the Cleveland mine (CQ651067), exposed in underground workings (*e.g.*, mine section N) and in diamond drill core retained at the mine. Representative samples are held by the Tasmania Geological Survey and by the University of Tasmania. A reference section occurs on Whyte Hill on the Corinna Road between CQ683080 and CQ686080.

Lithology: Light to dark grey and purple shale and fine-grained tuff, with limestone, grey-green-red chert, greywacke, basic tuff and basalt. Within the unit at the Cleveland mine, there are eleven lenses of mineralisation, which are divided into two groups (Footwall lodes and handing Wall lodes) by a wedge of basalt known as Henrys Volcanic Member.

Thickness: 80-120m in the Cleveland mine area.

Relationships and Boundary Criteria: Conformably overlies the Deep Creek Volcanics to the east and south-east, and is conformably overlain to the west by the Crescent Spur Sandstone.

Age: Eocambrian(?)-Early Cambrian(?) by correlation with the Crimson Creek Formation (Blissett, 1962). Fossils have not been found in this unit.

Name of Unit: CRESCENT SPUR SANDSTONE

Derivation of Name: Crescent Spur is an old name for the crescent-shaped ridge, convex to the north, extending west from Whyte Hill then south-west to the Cleveland mine. The spur has been recently re-named Godkin Ridge and at its south-west end is now called Crescent Hill (Arthur River 1:100 000 sheet). However, the original and long-standing name "Crescent Spur" is retained in this validation of the stratigraphic nomenclature.

Synonymy: The term "Crescent Spur Mica Sandstone Formation" (CSMSF) was used by Cox (1968) and Cox and Glasson (1971); and the term "Luina Beds" was used by Rubenach (1973). Previously, this unit has been referred to as the "Micaceous Sandstone Formation" (Glasson and Hopwood, 1962; Cox and Glasson, 1967), "massive micaceous sandstone" (Mason, 1965), "Crescent Spur mica sandstone" (Palmer, 1976) and "mica sandstone unit" (Ransom and Hunt, 1975); and corresponds to the "tuffs" of Hughes (1953).

Distribution: The unit crops out over about 10km^2 on Godkin Ridge and in the Whyte River valley near its confluence with Falls Creek (Cleveland 1:50 000 sheet area, 7915-II). Probable correlates also crop out in the headwaters of Falls Creek, and west of the Whyte River valley at Luina.

Type Section: The type section is on the north flank of Godkin Ridge on the Corinna Road between CQ667085 and CQ683080.

Lithology: Grey, fine- to medium-grained micaceous greywacke and interbedded siltstone and mudstone, with thick units of red-brown argillite and minor grey banded chert, spilitic basalt and associated mafic tuff and volcaniclastic greywacke. The unit also contains sub-concordant and disconcordant intrusive bodies of dolerite/gabbro.

Thickness: The type section is in excess of 350m thick.

Relationships and Boundary Criteria: The formation conformably overlies the Hall Formation in the east, and in the west and south-west is faulted against the Whyte River Complex (Rubenach, 1973).

Age: Eocambrian(?)-Early Cambrian(?) by correlation with the Crimson Creek Formation (Blissett, 1962). Fossils have not been found in this unit.

Name of Unit: HENRYS VOLCANIC MEMBER

Derivation of Name and Synonymy: The unit derives its name from Henry's workings which are one of the original mine workings (on Henry's footwall lode) on the south-east flank of Crescent Hill at CQ682070, Arthur River 1:100 000 sheet (7915). The term Henry's basic volcanics was used by Palmer (1976).

Distribution: As lenses at the Cleveland mine, and on Whyte Hill at CQ683080.

Type Section and Reference Section: The type section is a subsurface section at the Cleveland mine (CQ651067), exposed in underground workings and in diamond drill core retained at the mine. Representative samples are held by the Tasmania Geological Survey and the University of Tasmania. A reference section occurs on Whyte Hill on the Corinna Road at CQ684080.

Lithology: Massive and locally pillowed spilitic basalt and mafic tuff.

Thickness: Lenses up to 50m thick.

Relationships: The unit occurs as lenses within the Hall Formation close to its stratigraphic top.

REFERENCES

Blissett, A.H., 1962, Zeehan: Explan.Rep.Geol.Surv.Tasm., 1 mile geol. map series K/55-5-50.

Cox, R., 1968, The economic geology of the Cleveland and Magnet mines, Tasmania : Unpub. Ph.D. thesis, Univ. of Sydney.

Cox, R., and Glasson, K.R., 1967, The geology and mineralisation of Cleveland mine, *in* The geology of western Tasmania - a symposium, Univ. of Tasmania, Hobart, Nov., 1967.

Cox, R., and Glasson, K.R., 1971, Economic geology of the Cleveland mine, Tasmania : Econ. Geol., *66*: 861-878.

Glasson, K.R., and Hopwood, T., 1962, Geological report, Mt Cleveland mine, Waratah district, Tasmania: Unpub.Rep. Aberfoyle Tin Development Partnership, Feb. 1962.

Groves, D.I., 1968, The cassiterite-sulphide deposits of western Tasmania: Unpub. Ph.D. thesis, Univ. of Tasmania.

Groves, D.I., Martin, E.L., Murchie, H., and Wellington, H.K., 1972, A century of tin mining at Mt Bischoff, 1871-1971: Bull.geol.Surv.Tasm., 54.

Groves, D.I., and Solomon, M., 1964, The geology of the Mt Bischoff district: Pap.Proc.R.Soc.Tasm., *98*: 1-22.

Hughes, T.D., 1953, The Mount Cleveland mine: Unpub.Rep.Dep.Mines Tasm., 1953: 61-71.

Mason, A.A.C., 1965, Tin ore deposits of Mount Cleveland, *in* McAndrew, J., ed., Geology of Australian Ore Deposits : Publs 8th Commonwealth Mining Metall. Cong., Melbourne, *1*: 503-505.

Palmer, K.G., 1976, The Cleveland tin deposit, *in* Solomon, M., and Green, G.R., eds., Ore deposits of Western Tasmania : Internat. Geol. Cong., 25th, Sydney, 1976, Excursion Guide 31AC, 27-31.

Ransom, D.M., 1972, Reinterpretation of the geology of Cleveland cassiterite-sulphide deposit, *in* The Palaeozoic geology, structure and mineralisation of western Tasmania - a symposium, Geol. Soc. Aust. (Tasmania), Hobart, Oct. 1972, 3-4.

Ransom, D.M., and Hunt, F.L., 1976, The Cleveland tin mine, *in* Knight, C.L., ed., Economic geology of Australia and Papua-New Guinea. I. Metals : Australasian Inst. Mining and Metallurgy, Mon. 5, 584-591.

Rubenach, M., 1973, The Tasmanian ultramafic-gabbro and ophiolite complexes : Unpub. Ph.D. thesis, Univ. of Tasmania.

APPENDIX 2

Analysis of Cambrian volcanic and mafic igneous rock, and limestone

Field sampling

Systematic surface sampling of mafic volcanic and mafic-ultramafic igneous rock and of limestone is virtually impossible due to the deep weathering profile and lack of outcrop. Hence, most samples have been taken from diamond drill core and road cuttings on Whyte Hill and in the Cleveland mine area. Sampling of the Deep Creek Volcanics and the Hall Formation was mainly confined to mine section Qa, for which mafic volcanic sampling points are shown in Figure 5.1. Samples of limestone equivalent to the sulphide lenses were collected from drill holes on mine section Wa, at the northern end of the deposit, and from drill hole intersections of the correlate of the Hall Formation located south-east of the mine. Details of all samples analysed are given either in Appendix 7 or in notes accompanying the Tables of results.

Mafic volcanic samples analysed are of massive lava (except 48306) and were selected for their freshness (unweathered) and their lack of vesicles and veins of all types which are usually filled with quartz, calcite, chlorite and sulphides. Joints were avoided wherever possible. The average grainsize of most samples is approximately 1 mm which requires a sample mass of about 1 kg (Edleman, 1962; Kleeman, 1967). At surface outcrops samples weighing between 1 - 2 kg were collected but this is not practical when sampling drill core because of different core diameters. When sampling drill core, some 200 - 300 mm of half-core was sampled, generally weighing 0.5 - 1 kg.

Sample preparation

The rock samples were broken up either with a hammer or in a core splitter, then crushed to less than 2 mm in a mechanical steel jaw crusher. This may lead to some contamination with Fe and Ni. From the finely crushed rock, a 40 - 50 g sample was taken, and this was ground to a powder in a Siebtecnik vibratory swing mill, using an agate vessel and grinding discs.

Analysis of major elements

All major element analyses of mafic volcanic rocks, mafic igneous rocks and limestone were carried out by the author with the exception of analyses with serial numbers commencing 78.... (e.g. 781316) which were analysed at the Department of Mines Assay Laboratories, Launceston, Tasmania. Analyses of all elements were carried out on a Philips vacuum X-ray fluorescence spectrometer at the University of Tasmania.

Fused glass discs were prepared from the rock powder for major element analysis (except Na) using the method of Norrish and Hutton (1969). Standards used were University of Tasmania 'standard rocks' TAS-DOL-1, TAS-UM-1 and TAS-GRANITE-1. Fused discs were prepared from powders of these standard rocks the same as for the rock samples. The same flux, prepared as in Norrish and Hutton (1969), was used for the preparation of fused glass discs of both rock samples and 'standard rocks'. The conditions of analysis are given in Table A2.1. Power was reduced to 30kV, 10mA for analysis of calcium in limestone.

Sodium was determined using boric acid backed tablets of rock powder as in trace element analysis.

The ignition loss was determined by calculating weight loss after drying the rock powder at 110°C for 24 hours (H_2O^-) and then heating in a furnace at 1000°C for two hours. The FeO content of volcanic and igneous rocks was determined by analysts at the Department of Mines Laboratories, using wet-chemical techniques.

Trace element analyses

The rocks were analysed for all trace elements on the X-ray spectrograph as pressed tablets of rock powders, backed and edged with boric acid (Norrish and Chappell, 1967). A minimum of 6 gm of rock powder was used to prepare the tablets for analysis to ensure an 'infinitely thick' sample, particularly for the analysis of Sn. The instrumental conditions of analysis are given in Table A2.2.

Artificial kaolin-based and specpure SiO_2 standards and blanks were used in all determinations. Mass absorption coefficients were calculated from the major element analysis of the same rock. Detection limits (D.L.) were calculated according to the expression:

$$\text{D.L.} = \frac{3}{m}\sqrt{\frac{Rb}{Tb}}$$

where m is counts per second per g/t of the standard, Rb is the background count rate and Tb is the background counting time. Limits of detection are given in Table A2.2.

Corrections have been made to Zr and Y analyses for SrK_β interference on the $ZrK\alpha_1$ line, and RbK_β interference on $YK\alpha_1$. Ba ($L\alpha_1$) and V ($K\alpha_1$) were checked for interference by Ti.

The accuracy of the trace element results was tested by analysing standard rocks with similar trace element values and comparing the results with the recommended values. These comparisons (Table A2.3) show that there is good agreement, and that most results are within 5% of the recommended values. Poor results have been obtained for Cr and V in standard rock BR and for Ba in ZGI-BM.

Analytical Results

The results of X-ray fluorescence spectrographic analysis of major elements (mass %) and trace elements (g/t) of spilitic basalt from the Deep Creek Volcanics and Henrys Volcanic Member are given in Table A2.4; a basalt/dolerite dyke in Table A2.6; basalt, dolerite and ultramafic rock from the Whyte River Complex in Table A2.7; limestone from the Hall Formation in Table A2.9; and Cambrian argillite and gabbro and Tertiary basalt in Table A2.10.

Several whole-rock analyses have been undertaken at the Department of Mines Laboratories, Launceston under the supervision of H.K. Wellington. These analyses have serial numbers 780998, 780999, 781001, 781002, 781003, 781005, 781006, 781011, 781012, 781013, 781299, 781316 and 781320. Spilitic basalt samples 781299 and 781316, and a sample of basalt/dolerite dyke (781320) were crushed and ground as described above, and rock powders submitted for analysis. Other samples were submitted as unbroken rock.

Additional analytical data for spilitic basalt in the Deep Creek Volcanics and Henrys Volcanic Member from Foden (1973) are listed in Table A2.5, and additional analyses of mafic rock from the Whyte River Complex in Table A2.7 (from Foden, 1973; Creenaune, 1980).

Niggli values and CIPW norms were calculated for mafic volcanic rock in the Deep Creek Volcanics, the Henrys Volcanic Member and the Whyte River Complex using CSIRO computer programme 'CPNORM'. Results are given in Table A2.8.

REFERENCES

Abbey, S., 1973, Studies in 'standard samples' of silicate rocks and minerals, Part 3. Extension and revision of 'usable values': Geol.Surv.Canada Paper 73-36.

Creenaune, P., 1980, The volcanics of the Heazlewood River Complex : Unpub.Hon. thesis, Univ. of Tasmania.

Edelman, N., 1962, Mathematics and geology : Geol.För.Stockh.Förh., *84* : 343-350.

Foden, J., 1973, The geochemistry of spilites from the Cambrian of western Tasmania : Unpub.Hon.thesis, Univ. of Tasmania.

Kleeman, A.W., 1967, Sampling error in the chemical analysis of rocks : J.geol.Soc.Aust. *14* : 43-47.

Norrish, K., Chappell, B.W., 1967, Physical Methods in Determinative Mineralogy (ed. J. Zussman), Chap. 4., Academic Press.

Norrish, K., Chappell, B.W., 1969, An accurate spectrographic method for the analysis of a wide range of geological samples : Geochim. Cosmochim Acta, *33* : 431-453.

TABLE A2.1 Instrument settings for X-ray fluorescence major element analysis.

Oxide	SiO_2	TiO_2	Al_2O_3	Fe_2O_3	MnO	MgO	CaO	Na_2O	K_2O	P_2O_5
Tube	Cr	Cr	Cr	Cr	Au	Cr	Cr	Cr	Cr	Cr
Tube voltage (kV)	50	50	50	50	50	50	50	50	50	50
Tube current (mA)	30	30	30	30	50	50	30	50	30	50
Crystal (1)	PE	LiF	PE	LiF	LiF	TlAP	LiF	TlAP	PE	GE
Collimator (2)	C	F	C	C	F	C	F	C	F	C
Angle ($^o2\theta$)	108.7	86.3	145.1	57.55	63.15	136.2	113.1	54.3	50.2	140.8
Count time (secs)	100	20	100	50	50	100	20	50	20	50

Gas-flow proportional counter

Vacuum throughout

(1) Lif = Lif_{200}

(2) Collimation: C = coarse, F = fine

TABLE A2.2 Instrument settings for analysis of trace elements by X-ray fluorescence spectrography and limits of detection.

ELEMENT	Ag	Ba	Cr	Cu	Nb	Ni	Pb
Tube	Au	Cr	Au	Au	Au	Au	Mo
Crystal (1)	LF1	LF1	LF1	LF1	LF2	LF1	LF2
Collimator	Fine	Fine	Fine	Fine	Fine	Fine	Fine
Tube voltage (kV)	60	50	50	50	60	50	60
Tube current (mA)	40	50	50	40	40	30	40
Peak ($^o2\theta$)	16.0	87.15	69.35	45.0	30.35	48.65	40.3
Background ($^o2\theta$)	16.6	±2.5	±1.0	44.0 46.5	±0.5	±1.0	±0.8
Counter (2)	S	F	F	F+S	S	F+S	S+F
Counting time :							
Peak (secs)	100	50	50	20	100	50	50
Bkg.(secs)	100	50	50	20	100	10	50
Interference (3)		Ti	VK_β				
Detection limit (g/t)	3	3	1	2	3	2	3

ELEMENT	Rb	Sn	Sr	V	Y	Zn	Zr
Tube	Mo	Au	Au	Cr	Mo	Au	Au
Crystal (1)	LF2	LF1	LF2	LF1	LF2	LF1	LF2
Collimator	Fine	Fine	Fine	Fine	Fine	Fine	Fine
Tube voltage (kV)	50	60	60	50	50	50	60
Tube current (mA)	30	40	40	50	30	30	40
Peak ($^o2\theta$)	37.85	14.0	35.75	76.94	33.75	41.75	32.0
Background ($^o2\theta$)	37.2 38.5	±0.5	35.05 36.45	76.0 78.0	±1.0	41.05 43.15	±1.0
Counter (2)	S	S	S	F	S	F+S	S
Counting time :							
Peak (secs)	20	100	20	50	20	20	20
Bkg.(secs)	20	100	20	50	20	20	20
Interference (3)				TiK_β	$\underline{RbK_\beta}$		$\underline{SrK_\beta}$
Detection limit (g/t)	3	2	3	3	3	1	3

(1) Crystal : LF1 = LiF_{200}, LF2 = LiF_{220}.

(2) Counter : F = gas flow counter, S = scintillation counter.

(3) Main interfering peaks underlined.

TABLE A2.3 Comparitive analysis of trace elements in standard rocks using X-ray fluorescence spectrography. All value are in g/t.

	AGV - 1		BCR - 1		BR		G - 2		ZGI - BM		GA		T - 1	
	Rec.	Det.	Rec.	Det.	Rec.	Det.	Rec.	Det.	Rec.	Det.	Rec.	Det.	Rec.	Det.
Ba	-	-	680	714	1050	1093	1850	1823	260	236	-	-	-	-
Cr	-	-	-	-	420	307	-	-	125	133	-	-	-	-
Cu	-	-	-	-	70	71	-	-	45	32	-	-	-	-
Nb	14-18	10	-	-	90	88	-	-	17	17	-	-	-	-
Ni	-	-	13	7	270	251	-	-	-	-	-	-	-	-
Pb	36	29	15	11	-	-	-	-	-	-	-	-	-	-
Rb	-	-	47	44	-	-	-	-	-	-	175	172	-	-
Sn	-	-	-	-	-	-	-	-	4.6	5	-	-	29(?)	23
Sr	660	658	330	344	1350	1335	480	463	-	-	-	-	-	-
V	-	-	410	396	240	282	34	19	180	187	-	-	-	-
Y	-	-	46	42	-	-	-	-	-	-	18(?)	18	-	-
Zr	220	218	185	193	240	248	300	286	-	-	-	-	-	-

Rec. = recommended "usable" value from Abbey (1973).

Det. = determined value this study.

TABLE A2.4 Major element and trace element analyses of spilitic basalt in the Deep Creek Volcanics and the Hall Formation.

Analysts: P.L.F. Collins; except 781002, 781011, 781012, 781299 and 781316, analysed by J. Furst and L.M. Hay, Department of Mines Laboratories, Launceston, Tasmania.

*S(m) = distance, in metres, of samples of the Deep Creek Volcanics from the nearest sulphide lens. HV = Henry's Volcanic Member.

Sample details:

For analyses with University of Tasmania numbers (e.g. 48302) details are given in Appendix 7.

For analyses with Department of Mines registered numbers (e.g. 781002) details are as follows:

Analysis No.	Description	Location.
781002	Spilitic basalt, Crescent Spur Sandstone, Corinna Road on Whyte Hill (78-425).	CQ674083
781011	Spilitic basalt, Deep Creek Volcanics, Deep Creek (78-446)	CQ664072
781012	Spilitic basalt, Deep Creek Volcanics, Deep Creek (78-447)	CQ664072
781299	Altered spilitic basalt, Deep Creek Volcanics (Qa section)	C88@242'
781316	Altered spilitic basalt, Deep Creek Volcanics (GD section).	C783@812'

	48305	48302	48306	48325	48326	48333
Major elements (mass%)						
SiO_2	47.09	45.35	49.05	47.17	49.28	47.81
TiO_2	2.49	2.56	1.59	1.57	1.67	3.76
Al_2O_3	13.10	13.29	13.40	13.53	14.07	12.64
Fe_2O_3	2.64	4.83	2.23	3.35	2.74	2.84
FeO	12.61	11.30	11.43	9.95	10.35	12.70
MnO	0.38	0.25	0.29	0.23	0.23	0.28
MgO	6.81	6.25	5.88	6.45	6.99	5.53
CaO	8.70	10.58	8.22	10.63	10.51	8.54
Na_2O	2.63	3.31	3.92	3.15	2.44	3.10
K_2O	0.23	0.20	0.28	0.61	0.48	0.46
P_2O_5	0.31	0.30	0.17	0.17	0.17	0.78
LOI/H_2O^+	2.67	2.30	4.05	2.35	1.82	2.42
TOTAL	99.66	100.49	100.51	99.16	100.75	100.86
Trace elements (g/t)						
Ag	<3	-	-	-	-	<3
Ba	35	121	108	147	141	89
Co	-	-	-	-	-	-
Cr	92	92	48	50	48	50
Cu	301	285	173	160	155	36
Nb	14	15	7	8	8	21
Ni	65	65	56	61	55	28
Pb	7	4	7	5	<3	3
Rb	11	7	38	28	42	48
Sr	311	620	141	362	230	209
Sn	<2	<2	<2	<2	<2	<2
V	317	415	473	395	467	449
Y	44	46	29	27	29	76
Zr	159	162	89	85	90	187
Zn	136	110	80	123	93	126
S(m)*	400	380	325	305	209	275

	48332	48331	48307	48317	48330
Major elements (mass%)					
SiO_2	49.80	50.09	48.3	50.33	46.3
TiO_2	1.73	1.69	1.6	2.47	3.6
Al_2O_3	14.47	14.07	13.9	12.83	12.8
Fe_2O_3	0.60	2.13	2.9	2.42	6.6
FeO	11.69	10.56	10.4	12.01	9.2
MnO	0.20	0.25	0.20	0.60	0.25
MgO	6.57	6.16	5.9	6.29	4.7
CaO	9.09	9.49	8.5	7.97	9.4
Na_2O	3.12	3.40	3.7	2.70	2.2
K_2O	0.94	0.85	0.65	0.83	1.1
P_2O_5	0.17	0.18	0.13	0.28	0.52
LOI/H_2O^+	2.50	1.85	3.1	2.03	3.5
H_2O^-			0.08		0.31
TOTAL	100.88	100.72	99.36	100.76	100.48
Trace elements (g/t)					
Ag	<3	-	-	-	-
Ba	252	266	322	87	321
Co	-	-	-	-	-
Cr	50	51	36	116	42
Cu	165	179	202	41	65
Nb	8	8	14	11	23
Ni	55	60	65	71	46
Pb	5	5	3	6	10
Rb	132	118	93	127	118
Sr	339	416	455	207	275
Sn	<2	<2	4	191	2
V	399	475	439	381	559
Y	30	31	30	34	57
Zr	95	88	107	147	200
Zn	102	120	146	286	164
S(m)*	185	140	130	85	80

	48290	48308	48309	48322	781316
Major elements (mass %)					
SiO_2	48.81	47.66	48.96	49.26	43.9
TiO_2	2.46	3.87	2.53	2.54	3.7
Al_2O_3	13.99	13.17	13.68	13.69	12.8
Fe_2O_3	2.02	2.94	1.83	2.22	2.8
FeO	11.61	11.56	11.68	11.71	13.7
MnO	0.37	0.29	0.38	0.43	0.65
MgO	6.76	5.51	6.38	6.17	5.9
CaO	8.73	8.10	9.11	9.31	7.9
Na_2O	1.11	3.14	2.00	1.09	1.2
K_2O	1.58	1.20	1.26	2.15	2.2
P_2O_5	0.28	0.74	0.29	0.29	0.64
Loss/H_2O^+	2.66	1.83	1.89	1.02	4.5
H_2O^-					0.12
TOTAL	100.38	100.01	99.99	99.88	100.01
Trace Elements (g/t)					
Ag	-	-	-	-	-
Ba	99	251	84	150	265
Co	-	-	-	-	-
Cr	123	60	123	113	54
Cu	99	26	207	73	161
Nb	10	20	10	10	24
Ni	76	42	77	72	49
Pb	<3	< 3	<3	6	<10
Rb	300	174	201	546	450
Sr	239	269	363	180	210
Sn	33	< 2	12	139	260
V	439	477	383	399	535
Y	30	72	34	32	24
Zr	135	184	142	139	80
Zn	31	164	293	237	172
S(m)*	70	70	50	40	40

	48289	48327	48323	48321	48334
Major elements (mass %)					
SiO_2	46.77	45.80	48.62	50.01	50.56
TiO_2	2.49	2.67	2.50	2.48	2.64
Al_2O_3	12.99	15.08	13.36	13.18	14.23
Fe_2O_3	2.67	2.22	2.03	1.83	1.52
FeO	12.35	12.03	11.77	12.19	11.06
MnO	0.92	0.54	0.36	0.46	0.51
MgO	6.20	7.27	6.27	6.28	5.75
CaO	8.86	8.39	9.99	9.28	8.82
Na_2O	0.89	1.30	1.27	1.00	2.09
K_2O	1.50	1.49	1.51	1.83	1.30
P_2O_5	0.30	0.31	0.29	0.29	0.29
Loss/H_2O^+	3.45	2.77	1.06	1.51	1.99
TOTAL	99.39	99.86	99.03	100.34	100.76
Trace elements (g/t)					
Ag	-	-	-	<3	-
Ba	178	175	122	113	142
Co	-	-	-	-	-
Cr	105	131	130	127	133
Cu	134	13	250	398	317
Nb	14	11	11	10	11
Ni	61	76	79	79	72
Pb	10	6	11	4	8
Rb	170	227	290	386	225
Sr	243	333	184	243	321
Sn	122	107	51	164	143
V	436	398	384	423	425
Y	41	32	32	32	39
Zr	154	151	144	141	148
Zn	583	287	229	257	268
S(m)*	40	35	30	25	15

	48329	781299	48316	48318	48319
Major elements (mass %)					
SiO_2	49.66	44.3	48.26	50.06	47.37
TiO_2	3.95	3.7	1.67	1.17	2.46
Al_2O_3	13.22	11.8	13.82	14.86	12.84
Fe_2O_3	1.55	2.5	2.21	1.82	2.63
FeO	16.28	14.4	11.27	10.07	13.34
MnO	0.69	0.79	0.48	0.55	0.80
MgO	5.45	5.3	5.63	6.10	6.12
CaO	1.75	7.5	9.23	8.37	7.87
Na_2O	0.03	0.38	0.85	1.35	0.95
K_2O	4.71	1.8	2.32	2.12	2.45
P_2O_5	0.82	0.52	0.18	0.14	0.31
Loss/H_2O^+	2.67	6.0	3.25	3.00	3.09
H_2O^-		0.10			
TOTAL	100.78	99.09	99.17	99.61	100.23
Trace elements (g/t)					
Ag	<3	-	<3	<3	-
Ba	442	163	131	132	482
Co	-	-	-	-	-
Cr	63	51	53	142	110
Cu	26	14	11	30	9
Nb	23	20	11	6	13
Ni	45	38	58	62	63
Pb	13	10	3	3	9
Rb	1116	340	609	381	393
Sr	16	108	125	207	208
Sn	582	346	320	240	221
V	-	598	452	312	456
Y	46	57	30	15	47
Zr	189	194	95	63	164
Zn	445	433	206	270	302
S(m)*	10	5	HV	HV	HV

	48320	48324	781011	781012	781002
Major elements (mass %)					
SiO_2	47.63	46.86	47.7	46.3	47.6
TiO_2	2.59	2.65	1.7	1.8	1.3
Al_2O_3	13.57	13.40	14.5	15.1	12.9
Fe_2O_3	2.68	2.05	5.2	4.6	5.2
FeO	13.13	13.48	7.5	8.4	7.7
MnO	0.67	0.72	0.17	0.23	0.21
MgO	5.97	6.64	6.0	6.3	8.5
CaO	8.42	8.99	9.3	9.1	5.6
Na_2O	2.69	0.45	3.9	3.7	3.4
K_2O	0.45	1.35	0.15	0.30	1.9
P_2O_5	0.34	0.35	0.31	0.29	0.22
Loss/H_2O^+	1.87	3.22	3.2	3.5	4.1
SO_3	-	-	0.02	0.03	0.01
TOTAL	100.01	100.66	99.65	99.65	98.64
Trace elements (g/t)					
Ag	-	-	-	-	-
Ba	120	258	62	90	231
Co	-	-	47	57	51
Cr	105	108	116	109	231
Cu	308	16	188	260	152
Nb	13	15	<5	13	< 5
Ni	67	62	103	93	113
Pb	7	14	<11	<11	<11
Rb	63	257	4	8	59
Sr	306	99	284	380	117
Sn	73	493	< 6	-	15
V	383	483	388	408	323
Y	46	47	30	3	33
Zr	158	161	115	26	108
Zn	453	321	110	146	117
S(m)*	HV	HV	-	-	HVW

TABLE A2.5 Major element and trace element analyses of spilitic basalt in the Deep Creek Volcanics and Henrys Volcanic Member from Foden (1973)

Sample details:

Sample localities are illustrated in Foden (1973, fig. 3). Analyses 41036-39 and 41042 are of basalt from the Deep Creek Volcanics, and analyses 41043 and 41045 are of basalt equivalent to the Henrys Volcanic Member.

The analyses indicate varying degrees of alteration of the spilitic basalt, as evidenced by their K_2O, Na_2O and Rb values (see Chapter 5), but the analytical data has not been used in establishing the alteration halo to the Cleveland mineralization as the exact sample locations are not known. However, it has been ascertained (J. Foden, pers. comm.) that specimen 41036 is from near 7 level adit (the main mine portal) and that 41037-39 are from drill core, but the diamond drill hole numbers and depths are not known. Specimen 41042 is of surface outcrop and, apart from 41045 (on Whyte Hill), is the most distant sample from the mine.

	41036	41037	41038	41039	41042	41043	41045
Major elements (mass %)							
SiO_2	45.93	46.79	49.05	47.30	50.11	50.55	48.40
TiO_2	3.84	2.35	1.68	1.76	1.83	1.40	1.59
Al_2O_3	12.57	13.09	13.25	13.25	14.12	14.08	13.56
Fe_2O_3	15.97*	2.16	13.70*	14.55*	14.84	14.08*	15.24
FeO	-	10.72	-	-	-	-	-
MnO	0.69	0.29	0.22	0.23	0.21	0.23	0.25
MgO	4.54	5.92	6.60	7.50	5.18	6.27	5.13
CaO	8.20	11.27	8.33	8.34	7.50	5.18	9.17
Na_2O	0.30	1.37	3.24	2.43	3.93	2.72	3.69
K_2O	3.49	1.41	0.38	0.38	0.08	1.08	0.84
P_2O_5	0.66	0.23	0.15	0.15	0.17	0.13	0.20
L.O.I.	2.75	4.41	2.62	3.72	2.41	3.66	2.34
TOTAL	98.93	100.01	99.22	99.61	100.38	99.38	100.41
Trace elements (g/t)							
Co	-	-	41	-	-	-	-
Cr	81	118	53	75	53	161	70
Ni	38	71	55	48	27	79	45
Rb	974	341	49	36	5	42	25
Sr	95	250	311	164	129	228	305
V	685	432	397	422	397	331	371
Y	62	28	38	36	37	36	43
Zr	220	167	116	124	138	71	115

* Total Fe as Fe_2O_3

TABLE A2.6 Major element and trace element analyses of porphyritic basalt/dolerite dyke intersecting the Deep Creek Volcanics and the Hall Formation.

Analysts: P.L.F. Collins; except 781320, analysed by J. Furst and L. M. Hay, Department of Mines Laboratories, Launceston, Tasmania.

* Basalt is the average of six unaltered spilitic basalts in the Deep Creek Volcanics (samples 48302, 48305, 48306, 48325, 48326, 48333) all in excess of 250 m from the sulphide lenses, from data in Table A2.4.

Analysis number 781320 is for specimen number 48339.

	781320	48328	48288	Basalt*
Major elements (mass %)				
SiO_2	41.7	44.30	31.32	47.62
TiO_2	2.2	2.35	2.40	2.27
Al_2O_3	12.7	14.27	15.84	13.34
Fe_2O_3	0.14	2.14	2.07	3.10
FeO	10.6	11.30	22.86	11.39
MnO	0.24	0.18	0.30	0.28
MgO	4.3	4.67	1.44	6.32
CaO	11.6	8.98	2.06	9.53
Na_2O	2.5	2.75	1.29	3.09
K_2O	1.2	1.38	1.25	0.38
P_2O_5	0.54	0.55	0.65	0.34
LOI	10.3	7.48	17.63	2.60
TOTAL	99.02	100.35	99.11	100.26
Trace elements (g/t)				
Ag	-	-	-	<3
Ba	460	1119	280	107
Cr	159	112	136	63
Cu	71	47	60	248
Nb	30	37	45	12
Ni	70	58	58	55
Pb	10	4	12	5
Rb	57	73	35	29
Sr	582	612	178	312
Sn	-	<2	<2	<2
V	276	313	594	419
Y	27	24	31	42
Zr	179	169	175	129
Zn	136	99	81	111

TABLE A2.7 Major element and trace element analyses of mafic igneous rocks in the Whyte River Complex

Analysts: 48335, 48336 by P.L.F. Collins.
41040, 41041 from Foden (1973, Table 8).
781003, 781005, 781013 by J. Furst and L.M. Hay, Department of Mines, Launceston, Tasmania.
60951 from Creenaune (1980, Table 9).

Sample details :

For analyses with Department of Mines registered numbers (e.g. 781003), details are as follows:

Analysis No.	Description.	Location.
781003	Serpentinised peridotite (78-429)	CQ657080
781005	Serpentinised peridotite (78-438)	CQ648079
781013	Serpentinised peridotite (78-455)	CQ645068

	48335	48336	41040	41041
Major elements (mass %)				
SiO_2	53.15	52.34	48.03	43.00
TiO_2	0.41	0.40	0.18	0.11
Al_2O_3	14.76	13.37	12.42	8.09
Fe_2O_3	1.21	1.21	7.89*	2.71
FeO	9.40	9.00	-	7.47
MnO	0.21	0.17	0.24	0.14
MgO	7.15	8.32	9.64	25.40
CaO	5.29	7.74	18.00	4.12
Na_2O	4.09	4.28	0.85	0.01
K_2O	0.33	0.40	0.01	0.03
P_2O_5	0.06	0.05	0.02	0.01
L.O.I.	3.48	2.62	3.74	10.05
TOTAL	99.54	99.90	101.02	101.14
Trace elements (g/t)				
Ba	85	84	-	-
Co	-	-	-	55
Cr	187	159	197	2415
Cu	48	17	-	-
Nb	<3	<3	-	-
Ni	75	70	81	1253
Pb	<3	<3	-	-
Rb	54	63	1	1
Sr	71	64	38	7
Sn	-	-	-	-
V	315	281	178	117
Y	16	16	14	8
Zr	15	17	10	4
Zn	80	44	-	-

* Total Fe as Fe_2O_3

	781003	781005	781013	60951
Major elements (mass %)				
SiO_2	40.3	39.0	38.8	55.19
TiO_2	0.07	0.11	0.07	0.25
Al_2O_3	6.0	5.8	4.9	13.57
Fe_2O_3	2.5	3.8	3.5	3.45
FeO	6.5	4.8	5.4	7.82
MnO	0.18	0.15	0.17	0.18
MgO	30.4	29.6	31.0	5.78
CaO	4.8	3.5	2.6	8.66
Na_2O	0.24	0.07	0.05	3.44
K_2O	< 0.01	< 0.01	<0.01	0.19
P_2O_5	0.05	0.14	0.09	0.02
L.O.I./H_2O^+	7.3	12.0	12.2	2.52
SO_3	0.05	0.03	0.02	-
CO_2	0.26	0.20	0.26	-
TOTAL	98.65	99.20	99.06	101.07
Trace elements (g/t)				
Ba	<40	< 40	<40	-
Co	101	94	92	-
Cr	2717	3208	3239	-
Cu	39	36	<5	-
Nb	5	<5	6	1
Ni	1120	1380	1550	41
Pb	<11	<11	<11	-
Rb	9	9	3	-
Sr	3	<2	<2	84
Sn	<6	<6	-	-
V	91	102	69	262
Y	2	5	5	-
Zr	<5	8	<5	8
Zn	85	64	72	-

TABLE A2.8 Niggli values and C.I.P.W norms for mafic volcanic rocks from the Cleveland mine area (Deep Creek Volcanics, Henrys Volcanic Member, Whyte River Complex). Data for the Deep Creek Volcanics and Henrys Volcanic Member are listed in the same order as analytical data in Table A2.4.

	DEEP CREEK VOLCANICS								
	48305	48302	48306	48325	48326	48333	48332	48331	48317
Niggli values									
al	18.1	17.4	19.2	18.3	19.1	18.1	20.2	19.7	18.4
Fm	53.8	50.1	49.5	47.5	48.9	51.7	48.0	47.0	53.1
c	21.8	25.1	21.5	26.3	25.9	22.3	23.2	24.1	20.8
alk	6.3	7.4	9.7	7.9	6.1	8.0	8.6	9.1	7.7
Si	110.1	100.3	119.9	108.6	113.1	116.4	118.4	118.9	122.9
ti	4.4	4.3	2.9	2.7	2.9	6.9	3.1	3.0	4.5
C.I.P.W. norms									
Quartz	-	-	-	-	-	0.7	-	-	1.8
Orthoclase	1.4	1.2	1.7	3.5	2.8	2.7	5.4	5.0	4.8
Albite	21.9	25.6	32.7	25.6	20.3	25.8	26.0	28.3	22.6
Anorthite	22.9	20.7	17.8	20.6	25.8	18.8	22.2	20.4	20.2
Nepheline	-	1.2	-	0.3	-	-	-	-	-
Corundum	-	-	-	-	-	-	-	-	-
Diopside	14.5	24.2	17.8	25.0	20.3	14.8	17.4	20.5	14.2
Hypersthene	22.3	-	8.1	-	20.0	21.2	8.6	7.2	25.4
Olivine	3.3	12.0	10.6	12.2	1.0	-	12.5	9.5	-
Magnetite	3.8	7.0	3.2	4.8	3.9	4.1	0.9	3.0	3.5
Ilmenite	4.7	4.8	3.0	2.9	3.1	7.0	3.2	3.2	4.7
Apatite	0.7	0.7	0.4	0.4	0.4	1.8	0.4	0.4	0.7

	DEEP CREEK VOLCANICS (continued)									
	48290	48308	48309	48322	48289	48327	48323	48321	48334	48329
Niggli values.										
al	20.0	19.1	19.4	19.5	18.6	20.6	18.8	18.9	20.9	21.6
fm	52.3	50.1	50.5	50.6	54.0	53.4	50.3	51.8	48.4	64.8
c	22.6	21.4	23.5	24.0	23.0	20.9	25.6	24.2	23.6	5.2
alk	5.0	9.4	6.6	5.8	4.4	5.1	5.3	5.2	7.1	8.4
si	118.2	117.7	117.8	118.7	113.4	106.3	116.5	121.4	126.1	137.4
ti	4.5	7.2	4.6	4.6	4.5	4.7	4.5	4.5	4.9	8.2
C.I.P.W. norms										
Qz	3.7	-	0.8	2.8	3.5	-	2.6	4.5	3.1	11.1
Or	9.3	7.0	7.3	12.6	8.7	8.7	8.8	10.6	7.6	27.3
Ab	9.3	26.3	16.7	9.1	7.4	10.9	10.7	8.3	17.4	0.3
An	28.4	18.0	24.3	26.0	26.6	30.5	26.0	25.8	25.2	3.3
Ne	-	-	-	-	-	-	-	-	-	-
Co	-	-	-	-	-	-	-	-	-	6.7
Di	10.5	14.0	15.1	14.8	12.3	7.1	17.5	14.7	13.3	-
Hy	27.6	16.3	24.3	24.0	26.8	26.6	23.0	25.4	22.9	36.1
Ol	-	2.3	-	-	-	3.2	-	-	-	-
Mt	2.9	4.2	2.6	3.2	3.8	3.2	2.9	2.6	2.2	2.2
Ilm	4.6	7.3	4.7	4.8	4.7	5.0	4.7	4.6	4.9	7.3
Ap	0.7	1.7	0.7	0.7	0.7	0.7	0.7	0.7	0.7	1.9

	HENRYS VOLCANIC MEMBER					WHYTE RIVER COMPLEX			
	48316	48318	48319	48320	48324	48335	48336	41040	41041
Niggli values									
al	20.3	22.1	18.3	18.9	18.6	22.8	18.9	15.2	8.8
fm	49.4	48.7	55.4	52.9	55.7	51.4	50.5	42.8	83.2
c	24.6	22.6	20.4	21.3	22.6	14.8	20.0	40.2	7.9
alk	5.7	6.7	6.0	6.8	3.0	11.0	10.6	1.7	0.1
si	119.8	126.0	114.4	112.5	110.2	139.4	125.9	100.1	77.2
ti	3.1	2.2	4.5	4.6	4.7	0.8	0.7	0.3	0.2
C.I.P.W.norms									
Qz	2.7	2.8	1.3	-	3.9	0.1	-	-	-
Or	13.6	12.5	14.4	2.6	7.9	1.9	2.4	0.1	0.2
Ab	7.2	11.3	8.0	22.3	3.7	34.3	35.8	7.2	0.1
An	27.0	28.1	23.3	23.2	30.1	20.7	15.8	30.0	20.2
Ne	-	-	-	-	-	-	-	-	-
Co	-	-	-	-	-	-	-	-	0.6
Di	14.5	10.1	11.2	13.0	9.6	4.0	17.8	47.3	-
Hy	23.6	26.1	29.0	23.3	32.0	31.4	7.9	7.2	42.9
Ol	-	-	-	2.4	-	-	13.8	1.1	22.1
Mt	3.2	2.6	3.8	3.8	2.9	1.7	1.7	3.4	3.9
Ilm	3.2	2.2	4.6	4.8	5.0	0.8	0.8	0.3	0.2
Ap	0.4	0.3	0.7	0.8	0.8	0.1	0.1	-	-

	DYKE	SPILITIC BASALT (from Foden, 1973)						
	48328	41036	41037	41038	41039	41042	41043	41045
Niggli values								
al	21.1	19.4	18.5	19.4	18.8	20.7	22.3	19.4
fm	45.7	51.1	47.2	50.2	53.6	49.7	53.9	46.8
c	24.2	22.9	28.9	22.0	21.4	20.0	14.9	23.8
alk	8.9	6.6	5.3	8.4	6.2	9.6	8.9	10.0
si	111.4	119.8	112.4	121.1	113.4	124.7	135.6	117.2
ti	4.4	7.5	4.2	3.1	3.2	3.4	2.8	2.9
C.I.P.W. norms								
Qz	-	6.8	0.8	1.1	1.6	1.5	6.0	-
Or	8.0	20.6	8.2	2.2	2.2	0.5	6.4	5.0
Ab	22.8	2.5	11.4	27.4	20.6	33.3	23.0	31.2
An	22.1	22.7	25.0	20.6	24.3	20.6	23.1	18.1
Ne	-	-	-	-	-	-	-	-
Co	-	-	-	-	-	-	-	-
Di	15.2	11.2	23.6	16.1	13.1	12.8	1.4	21.5
Hy	1.2	15.7	17.3	18.7	23.1	18.5	25.8	3.7
Ol	13.2	-	-	-	-	-	-	7.5
Mt	3.0	7.0	3.0	5.9	6.3	7.0	6.1	6.6
Ilm	4.4	7.3	4.4	3.2	3.3	3.5	2.7	3.0
Ap	1.3	1.6	0.5	0.4	0.4	0.4	0.3	0.5

TABLE A2.9 Major element and trace element analyses of limestone in the Hall Formation.

Analyst: P.L.F. Collins

$CaCO_3$ equiv. = equivalent calcite calculated from CaO content

Analyses are of limestone in the Hall Formation at the northern end of the Cleveland mine except 48355 and 48356 which are of limestone in the correlate of the Hall Formation within the Deep Creek Volcanics to the south-east of the mine (see fig. 3.3).

	48291	48293	48295	48296
Major elements (mass %)				
SiO_2	13.78	16.52	12.33	10.33
TiO_2	0.12	0.27	0.12	0.08
Al_2O_3	2.29	3.33	1.81	0.96
Fe_2O_3	2.30	3.85	2.30	0.80
MnO	0.64	0.45	0.47	0.46
MgO	1.68	1.49	1.31	0.96
CaO	43.57	41.58	45.46	47.61
Na_2O	0.00	0.00	0.00	0.00
K_2O	0.24	0.39	0.23	0.16
P_2O_5	0.22	0.27	0.19	0.24
LOI	35.25	30.70	36.13	37.62
TOTAL	100.09	98.84	100.35	99.21
$CaCO_3$ equiv	77.75	74.20	81.13	84.96
Trace elements (g/t)				
Ba	4	34	17	17
Cu	16	64	25	12
Ni	12	-	9	-
Pb	9	3	<3	<3
Rb	18		25	11
Sr	201	439	449	403
Sn	8	8	27	<2
Zn	64	117	146	16
Zr	18	33	19	27

	48298	48301	48355	48356
Major elements (mass %)				
SiO_2	14.84	42.24	27.24	20.86
TiO_2	0.20	0.37	0.50	0.36
Al_2O_3	2.71	6.59	6.43	4.46
Fe_2O_3	2.80	1.98	3.28	3.69
MnO	0.60	0.86	0.40	0.50
MgO	0.42	4.97	2.12	1.82
CaO	43.81	22.27	31.79	37.26
Na_2O	0.00	0.00	0.08	0.04
K_2O	0.48	1.21	1.50	1.02
P_2O_5	0.16	0.22	0.58	0.19
LOI	33.60	19.98	25.25	28.14
TOTAL	99.62	100.70	99.16	98.34
$CaCO_3$ equiv	78.18	39.74	56.73	66.49
Trace elements (g/t)				
Ba	43	127	106	
Cu	59	2	15	21
Ni	-	-	-	-
Pb	3	<3	<3	6
Rb	35	50	60	36
Sr	359	117	260	300
Sn	10	<2	<2	<2
Zn	291	127	39	39
Zr	23	69	41	29

TABLE A2.10 Major element and trace element analyses of Cambrian argillite and gabbro, and Tertiary basalt.

Analysts: J. Furst and L. M. Hay, Department of Mines Laboratories, Launceston, Tasmania.

Sample details :

Analysis No.	Description	AMG Co-ords
780998	Argillite, Magnet Creek (78-413)	CQ 704068
781001	Hornfelsed argillite, Butlers Road (78-419)	CQ 730073
780999	Gabbro, Arthur River (78-415)	CQ 711072
781006	Tertiary basalt, quarry, Corinna Road (78-440)	CQ 739061

	780998	781001	780999	781006
Major elements (mass %)				
SiO_2	59.4	51.7	49.7	46.6
TiO_2	2.3	2.2	0.43	1.6
Al_2O_3	12.7	15.6	15.3	13.9
Fe_2O_3	6.2	8.0	2.2	1.2
FeO	5.6	6.4	6.8	10.5
MnO	0.14	0.10	0.20	0.17
MgO	4.6	4.1	8.0	9.8
CaO	2.2	2.9	10.5	8.9
Na_2O	2.1	4.3	3.3	2.8
K_2O	2.2	1.9	0.45	0.64
P_2O_5	0.22	0.42	0.21	0.38
LOI/H_2O^+	1.8	1.3	2.5	2.8
SO_3	0.01	0.05	0.17	0.11
TOTAL	99.47	98.97	99.76	99.4
Trace elements (g/t)				
Ba	162	384	285	210
Co	43	36	57	69
Cr	289	110	366	294
Cu	7	22	53	60
Nb	43	21	<5	11
Ni	124	81	109	226
Pb	<11	35	126	<11
Rb	113	64	11	8
Sr	64	209	259	312
V	166	243	219	198
Y	46	51	20	18
Zr	405	279	40	114
Zn	101	158	538	124

APPENDIX 3

Meredith Granite analytical data

Samples of the Meredith Granite have been analysed for their major element and trace element composition to supplement previous geochemical investigations undertaken by Groves (1968) and Stockley (1972). The samples include quartz-feldspar porphyry from a dyke cropping out on Butlers Road and a mafic biotite-rich segregation within porphyritic adamellite, neither of which granitic rock type have been previously analysed.

All samples are from the north-trending lobe protruding from the north-eastern corner of the granitoid (fig. 4.1). Sample location details are given in Table A3.1 and Appendix 7. For equigranular granitic rock, 2 - 4 kg of sample was taken, and for porphyritic varieties in excess of 5 kg was taken and prepared for analysis. All analyses were carried out at the Department of Mines Analytical Laboratories, Launceston, under the supervision of H.K. Wellington, Chief Chemist and Metallurgist.

Results of analyses are listed in Table A3.1.

For comparison, additional analytical data for granitic rocks from the Meredith Granite, Heemskirk Granite and the porphyry dykes at Mt Bischoff are summarised in Table A3.2. All data in Table A3.2 are from Groves (1968) and Groves *et al.* (1972).

REFERENCES

Groves, D.I., 1968, The cassiterite-sulphide deposits of western Tasmania : Unpub. Ph.D. thesis, Univ. of Tasmania.

Groves, D.I., Martin, E.L., Murchie, H., and Wellington, H.K., 1972, A century of tin mining at Mt Bischoff, 1871-1971 : Bull.geol.Surv.Tasm., 54

Stockley, J., 1972, The Meredith Granite : Unpub. Hon. thesis, Univ.of Tasmania.

TABLE A3.1 Major element and trace element analyses of granitic rock from the Meredith Granite.

Analysts: J. Furst and L. M. Hay, Department of Mines Laboratories, Launceston, Tasmania.

Sample details:

Analysis No.	Description	A.M.G. CO-ords
781004	Equigranular, fine-grained biotite granite or microgranite (78-430)	CQ 717050
781007	Equigranular biotite granite (78-441)	CQ 728058
781008	Porphyritic biotite granite (78-442)	CQ 730058
781009	Porphyritic biotite granite, Wombat flat (78-443)	CQ 720040
781010	Mafic segregation in porphyritic granite, Wombat Flat (78-444)	CQ 720040
781000	Quartz-feldspar porphyry, Butlers Road (78-417)	CQ 725074

	781004	781007	781008	781009	781010	781000
Major elements (mass %)						
SiO_2	74.2	71.1	68.9	69.8	67.9	69.9
TiO_2	0.20	0.39	0.49	0.49	0.52	0.58
Al_2O_3	12.7	13.5	14.5	13.7	14.5	13.7
Fe_2O_3	0.06	0.30	0.50	0.73	0.70	0.61
FeO	1.2	1.9	2.6	2.3	2.8	2.6
MnO	0.02	0.05	0.05	0.06	0.06	0.06
MgO	0.35	0.66	0.81	0.81	1.1	0.99
CaO	0.62	1.5	1.9	2.2	2.4	1.1
Na_2O	2.9	2.9	3.2	3.0	3.3	3.0
K_2O	5.3	5.4	4.5	4.6	3.9	4.9
P_2O_5	0.06	0.22	0.30	0.31	0.22	0.14
LOI/H_2O^+	1.2	1.6	1.4	1.6	1.6	1.4
SO_3	0.03	<0.01	0.04	0.02	0.01	0.63
TOTAL	98.84	99.52	99.19	99.62	99.01	99.61
Trace elements (g/t)						
Ba	197	524	602	580	552	682
Co	<10	<10	14	<10	<10	<10
Cr	<10	13	<10	<10	14	17
Cu	6	<5	6	6	6	41
Li	27	59	56	47	56	47
Mo	11	8	10	11	14	6
Nb	18	19	19	17	22	13
Ni	12	<5	5	11	<5	6
Pb	<11	<11	<11	<11	<11	11
Rb	240	267	226	221	214	230
Sr	56	127	150	129	120	137
Sn	17	<6	10	<6	8	17
Th	31	31	30	34	30	35
U	13	12	<11	<11	<11	<11
V	11	16	35	35	43	39
W	14	<11	<11	<11	<11	17
Y	42	44	49	46	49	55
Zr	148	247	342	251	280	259
Zn	14	25	40	36	38	46

TABLE A3.2 Average analyses of granitic rock from the Meredith Granite, Heemskirk Granite and Mt. Bischoff porphyry. All data from Groves (1968) and Groves *et al* (1972).

1A,B Equigranular biotite adamellite, Meredith Granite (average of 3 analyses, range in column B).

2A,B Porphyritic biotite adamellite, Meredith Granite (average of 5 analyses, range in Column B).

3 Microgranite, Meredith Granite (average of 2 analyses).

4 Porphyritic granite/adamellite dyke, Meredith Granite.

5A,B Quartz - feldspar porphyry, Mt. Bischoff (average of 5 analyses, range in column B).

6 Red granite, Heemskirk Granite (average of 7 analyses).

7 White granite, Heemskirk Granite (average of 7 analyses).

Notes:

(1) Total iron as FeO where no separate value of Fe_2O_3 is reported.

(2) Loss on ignition includes H_2O^+.

(3) The number of trace element analyses averaged varies for each element and granitic rock type.

	1A	1B	2A	2B	3
SiO_2	72.2	70.0 -75.6	73.3	70.1 -74.8	74.35
TiO_2	0.36	0.06- 0.52	0.27	0.08- 0.70	0.13
Al_2O_3	14.10	13.0 -14.7	13.40	12.8 -15.2	13.50
Fe_2O_3					
FeO(1)	2.00	0.55- 3.00	2.07	1.3 - 3.2	2.03
MnO	0.02	0.00- 0.03	0.05	0.02- 0.13	0.02
MgO	0.85	0.45- 1.1	0.65	0.2 - 1.6	0.8
CaO	0.81	0.35- 1.10	0.76	0.33- 1.48	0.17
Na_2O	3.1	2.8 - 3.7	3.2	2.5 - 3.4	3.6
K_2O	4.7	4.2 - 5.2	4.8	4.5 - 5.4	4.15
P_2O_5	0.04	0.00- 0.10	0.04	0.00- 0.10	0.01
LOI(2)	0.79	0.71- 0.86	0.58	0.43- 9.84	0.70
H_2O^-	0.38	0.35- 0.42	0.18	0.13- 0.23	0.28
TOTAL	99.36		99.30		99.74
C.I.P.W. norms					
Quartz	31.5	28.8 -36.2	32.7	28.4 -34.5	35.3
Orthoclase	28.7	24.8 -30.7	28.6	26.6 -31.9	24.5
Albite	26.5	23.7 -31.3	25.4	21.1 -28.8	30.4
Anorthite	3.8	1.7 - 5.5	3.8	1.6 - 7.0	0.8
Corundum	2.4	1.8 - 2.8	2.0	1.3 - 3.0	2.9
Magnetite	0.5	0.0 - 1.5	0.25	0.0 - 1.25	0.9
Hypersthene	4.4	2.0 - 6.1	5.05	2.8 - 8.8	3.7
Ilmenite	0.7	0.1 - 1.0	0.6	0.2 - 1.3	0.25
Apatite	0.07	0.0 - 0.2	0.1	0.0 - 0.25	0.05
Trace elements (3)					
Ba	552	508 - 595	396	185 - 506	83
Cu	9	3 - 16	6	<3 - 13	4
Li	42	30 - 54	45	28 - 52	48
Ni	3?	<3 - 62?	5	<3 - 10	4
Pb	33	-	27	19 - 34	25
Rb	218	173 - 242	243	210 - 314	327
Sr	80	28 - 116	47	15 - 103	14
Sn	<3	<3	5	<3 - 13	4
Th	21	19 - 25	19	16 - 27	18
U	9	8 - 11	9	6 - 13	19
Zn	54	24 - 81	28	10 - 77	22

	4	5A	5B	6	7
SiO_2	74.9	75.3	73.6 -79.7	75.52	74.44
TiO_2	0.10	0.02	0.00- 0.06	0.19	0.21
Al_2O_3	12.2	14.25	13.5 -14.7	12.73	13.44
Fe_2O_3				0.61	0.20
FeO(1)	1.45	1.95	1.5 - 2.3	1.13	1.66
MnO	0.04	0.06	0.00- 0.12	0.04	0.05
MgO	0.01	0.6	0.6 - 0.65	0.25	0.18
CaO	0.46	0.20	0.01- 0.46	0.60	0.83
Na_2O	3.9	0.14	0.1 - 0.6	2.93	2.77
K_2O	4.6	4.9	2.7 - 6.0	5.23	5.00
P_2O_5	0.03	0.09	0.09	0.05	0.11
LOI(2)	0.37	1.62	1.35- 2.15	0.54	0.55
H_2O	0.15	0.23	0.12- 0.30	0.25	0.14
TOTAL	98.30	99.36		100.07	99.58
C.I.P.W. norms					
Quartz	32.4	52.3	45.6 -65.2	36.3	36.3
Orthoclase	27.2	28.8	16.0 -35.5	30.9	29.6
Albite	33.0	2.2	0.8 - 5.1	25.0	23.4
Anorthite	2.1	0.9	0.0 - 2.3	2.7	3.4
Corundum	0.0	8.2	6.5 - 9.6	1.3	2.2
Magnetite	0.0	0.2	0.0 - 0.9	0.9	0.3
Hypersthene	2.9	4.8	4.0 - 5.9	2.1	3.1
Ilmenite	0.2	0.02	0.0 - 0.1	0.25	0.4
Apatite	0.1	0.1	0.0 - 0.2	0.1	0.3
Trace elements(3)					
Ba	-	149	96 - 192	-	-
Cu	4	4	<3 - 6	-	-
Li	66	93	45 - 111	-	-
Ni	6	5	4 - 7	-	-
Pb	-	32	21 - 39	-	-
Rb	245	906	689 - 1250	358	399
Sr	12	3	<3 - 4	35	38
Sn	3	72	30 - 144	-	-
Th	18	11	7 - 20	49	24
U	3	13	10 - 22	12	18
Zn	15	122	67 - 184	-	-

APPENDIX 4

Mineralogical analytical techniques

Electron probe microanalysis

Micro-probe analysis of silicate, oxide and carbonate minerals in spilitic basalt, Deep Creek Volcanics, and of sulphides in ore was undertaken at the University of Tasmania using a JEOL JXA50 energy dispersive electron probe and scanning electron microscope, coupled to an energy dispersive analysis system (EDAX 7078) which was calibrated with either pure element standards or synthetic standards using a correction programme developed by Griffin (1979). Analyses were carried out on carbon coated polished sections at an accelerating voltage of 15 kV for silicates and 20 kV for sulphides.

Analytical data for minerals in spilitic basalt are listed in Table A4.1 (all un-normalised). Clinopyroxene and plagioclase generally are within 2% of a 100% total, but actinolite has anhydrous totals in excess of 100%. Sphene has consistent totals of 97.4 - 97.9% with the balance made up with water and/or fluorine. High iron and aluminium contents in the sphene are most likely due to substitution for titanium, which is low (*cf.* Deer *et al.*, 1966). Calcite analyses indicate pure calcite, with trace iron, magnesium and manganese. Chlorites have low anhydrous totals allowing for about 10% H_2O, except 40, 41 which were not used to compile Table 3.2. Chlorite in the groundmass has a brunsvigite composition, typical of spilite (Deer *et al.*, 1966). Analyses of magnetite(?) indicate titaniferous magnetite with quartz in solid solution(?), but the high calcium content is enigmatic.

Sulphides were analysed primarily to determine the composition of stannite and results are given in Table A4.2. All analyses have been normalised to 100% with the prenormalised total in brackets. In addition to pure element standards, the microprobe was also calibrated with a synthetic Cu_2SnS_3 standard kindly supplied by

Prof. G. Moh, Heidleberg University. Analyses of the standard are given in Table A4.2 (1 - 10). A dash (-) in Tables A4.1 and A4.2 indicates not detected (*i.e.* below about 0.1% oxide).

X-ray diffraction analysis of arsenopyrite

The atomic % arsenic in arsenopyrite was determined by measuring the d(131) spacing of arsenopyrites and then calculating the arsenic composition from the linear expression (Kretschmar and Scott, 1976):

$$\text{As (atomic \%)} = 866.67\ d(131) - 1381.12$$

Arsenopyrite d(131) spacings were measured using a Philips X-ray diffraction unit which generated Ni-filtered, CuK_α radiation, and an internal standard of reagent grade CaF_2 which was annealed at 700°C for 24 hours. A unit cell edge of 5.4626Å for CaF_2 was used, for which the d(311) line has been calculated to be 1.6469Å (Kretschmar and Scott, 1976). The arsenopyrite (131) and CaF_2 (311) peaks were scanned several times for each specimen at a scanning rate of ½°2θ/minute, using a different sample for each scan. Sufficient CaF_2 was added to make the intensity of the two peaks roughly equal. Interference from pyrite (311) and loellingite (031) and (221) lines was not detected.

The results are presented in Table A4.3. The variation in determination of atomic % arsenic is mainly due to poor peak definition but is within the precision range (± 0.45 at% As) used by Kretschmar (1973) in determining the expression.

X-ray diffraction analysis of wolframite

The composition of wolframite was determined by the X-ray diffraction method of Hsu (1976), in which the difference in °2θ between the d(200) peak of wolframite and the d(102) peak of quartz is proportional to mole % $MnWO_4$.

The wolframite d(200) spacing was measured using a Philips X-ray diffraction unit which generated Ni-filtered, CuK_α radiation and a sufficient quantity of natural quartz (specimen 104365) to make

the peaks approximately equal in intensity. The peaks were scanned at a rate of ¼°2θ/minute, and results are as follows (number of replicate scans averaged in brackets):

Specimen	Δ°2θ	mole % $MnWO_4$
104382 (4)	1.65	17
104432 (3)	1.60	11
104460 (4)	1.60	11

The results indicate wolframite in Stage I veins is the iron-rich variety, ferberite.

Trace element and REE analysis of fluorite

Trace element analysis (electron mciroprobe) and rare earth element (REE) analysis (neutron activation analysis) of five fluorite specimens from the Cleveland mine (Stages II and IV) have been kindly undertaken by Prof. H.-J. Schneider of the Freie Universität, Berlin. Sample preparation and neutron activation experimental procedures are described by Möller *et al.* (1974) and Schneider *et al.* (1975).

The results obtained are listed in Table A4.4. Two additional samples (104317, 104346) were analysed but these results have been rejected because of the presence of minor amounts of sphalerite(?) which causes problems in REE determination as the high activity of ^{65}Zn masks several γ-lines of interest (Schneider *et al.*, 1975). This problem was not encountered in the other five fluorites (H.-J. Schneider, *pers. comm.*).

REFERENCES

Deer, W.A., Howie, R.A., Zussman, J., 1966, An introduction to the rock-forming minerals : Longmans, London.

Griffin, B.J., 1979, Energy dispersive analysis system calibration and operation with Tas-sueds, and advanced interactive data reduction package : Univ. Tasmania, Geol. Dept. Pub.

Hsu, L.C., 1976, The stability relations of the wolframite series : American Mineralogist, *61* : 944-955.

Kretschmar, U., 1973, Phase relations involving arsenopyrite in the system Fe-As-S and their application : Unpub. Ph.D. thesis, Univ. Toronto.

Kretschmar, U., Scott, S.D., 1976, Phase relations involving arsenopyrite in the system Fe-As-S and their application : Canadian Mineralogist, *14* : 364-386.

Möller, P., Parekh, P.P., Schneider, H.-J., 1976, The application of Tb/Ca-Tb/La abundance ratios to problems of fluorspar genesis : Mineral. Deposita, *11* : 111-116.

Schneider, H.-J., Möller, P., Parekh, P.P., 1975, Rare earth elements distribution in fluorites and carbonate sediments of the East-Alpine mid-Triassic sequences in the Nördlicke Kalkalpen : Mineral. Deposita, *10* : 330-344.

TABLE A4.1 Microprobe analyses of silicate, carbonate and oxide minerals in spilitic basalt (Deep Creek Volcanics).

1-12 = clinopyroxene, 48299. C=centre, M=mid-way and R=rim of individual crystals (1, 5 and 10 only).

13-16 = clinopyroxene, 48307.

17-20 = plagioclase, 48299.

21-24 = plagioclase, 48307.

25-27 = actinolite, 48307. Analysis 25 is on the outer edge of clinopyroxene grain analysis 13, and 27 on the outer edge of 14.

28-31 = sphene, 48299.

32,33 = calcite in groundmass, 48299.

34-38 = chlorite in groundmass, 48299.

39 = chlorite in vesicle, 48299. E=edge and C=centre of vesicle.

40.41 = chlorite in vesicles, 48307.

42-45 = magnetite (?), 48299.

	IC.	IR.	2.	3.	4.	5C.	5R.	6.	7.	8.
Mass % oxide										
SiO_2	49.89	51.70	49.26	47.15	47.77	50.17	49.04	49.28	50.03	47.40
TiO_2	0.90	0.55	1.35	1.20	1.17	0.83	1.14	1.09	1.08	1.29
Al_2O_3	3.50	2.20	2.64	3.38	3.97	4.70	3.05	3.76	4.12	3.65
FeO	9.30	8.45	17.20	15.80	13.46	8.72	15.36	13.13	9.98	16.48
MnO	-	-	0.38	0.28	0.18	-	0.15	-	-	0.18
MgO	14.80	15.69	11.72	12.46	13.58	14.80	12.09	13.16	14.18	12.41
CaO	21.10	21.72	19.16	17.90	18.63	21.47	20.02	20.37	21.47	17.35
Na_2O	-	-	-	-	-	-	-	-	-	-
K_2O	-	-	-	-	-	-	-	-	-	-
Cr_2O_3	0.37	0.32	0.26	0.19	0.31	0.39	0.26	0.26	0.23	0.32
TOTAL	99.87	100.63	101.98	98.35	99.03	101.08	101.11	101.09	101.10	99.11
Atomic proportion										
O ions	6	6	6	6	6	6	6	6	6	6
Si	1.868	1.912	1.868	1.843	1.834	1.850	1.863	1.852	1.856	1.839
Ti	0.025	0.015	0.038	0.035	0.034	0.023	0.033	0.031	0.030	0.038
Al	0.154	0.096	0.118	0.156	0.179	0.204	0.137	0.167	0.180	0.167
Fe	0.291	0.262	0.545	0.516	0.432	o.269	0.488	0.413	0.310	0.535
Mn	-	-	0.012	0.009	0.006	-	0.005	-	-	0.006
Mg	0.827	0.865	0.662	0.726	0.777	0.814	0.685	0.737	0.784	0.718
Ca	0.847	0.860	0.779	0.750	0.766	0.848	0.815	0.820	0.853	0.722
Na	-	-	-	-	-	-	-	-	-	-
K	-	-	-	-	-	-	-	-	-	-
Cr	0.011	0.009	0.008	0.006	0.009	0.012	0.008	0.008	0.007	0.010
TOTAL	4.023	4.020	4.031	4.041	4.038	4.020	4.033	4.028	4.021	4.034

	9.	10C.	10M.	10R.	11.	12.	13.	14.	15.	16.
Mass % oxide										
SiO_2	48.34	49.15	49.31	47.50	50.05	48.29	52.41	49.91	49.95	50.12
TiO_2	1.42	0.80	0.64	1.16	1.04	1.18	1.15	1.22	0.80	0.55
Al_2O_3	3.44	4.38	2.91	3.26	4.04	2.89	2.78	2.70	2.04	0.87
FeO	14.91	9.07	8.98	14.43	12.79	16.58	14.92	13.77	17.21	21.11
MnO	-	-	-	0.19	-	0.25	-	0.28	0.39	0.81
MgO	11.73	15.04	14.73	11.67	14.43	11.37	12.60	12.75	11.47	10.40
CaO	19.83	20.33	21.21	19.93	19.23	18.96	19.52	18.39	17.35	15.34
Na_2O	-	-	-	-	-	-	-	0.62	0.53	0.51
K_2O	-	-	-	-	-	-	-	-	-	-
Cr_2O_3	0.25	0.22	0.37	0.22	0.20	0.32	0.28	0.39	0.26	0.29
TOTAL	99.94	99.00	98.12	98.35	101.78	99.83	103.67	98.78	98.47	101.02
Atomic proportion										
O ions	6	6	6	6	6	6	6	6	6	6
Si	1.854	1.851	1.880	1.854	1.855	1.867	1.918	1.896	1.922	1.956
Ti	0.041	0.023	0.018	0.034	0.029	0.034	0.032	0.035	0.023	0.016
Al	0.155	0.194	0.131	0.150	0.177	0.132	0.120	0.121	0.093	0.040
Fe	0.478	0.286	0.286	0.471	0.397	0.536	0.457	0.437	0.554	0.689
Mn	-	-	-	0.006	-	0.008	-	0.009	0.013	0.027
Mg	0.671	0.844	0.837	0.679	0.797	0.655	0.687	0.722	0.658	0.605
Ca	0.816	0.821	0.867	0.833	0.764	0.785	0.765	0.749	0.715	0.641
Na	-	-	-	-	-	-	-	0.046	0.039	0.039
K	-	-	-	-	-	-	-	-	-	-
Cr	0.008	0.006	0.011	0.007	0.006	0.010	0.008	0.012	0.008	0.009
TOTAL	4.023	4.025	4.030	4.034	4.025	4.028	3.987	4.027	4.025	4.023

	17.	18.	19.	20.	21.	22.	23.	24.	25.	26.
Mass % oxide										
SiO_2	51.42	52.66	52.59	52.76	70.36	68.41	67.68	67.75	52.05	49.59
TiO_2	0.12	0.77	0.10	0.15	0.12	-	0.15	0.13	1.32	0.25
Al_2O_3	28.52	24.41	27.94	27.84	21.14	20.41	20.75	20.52	3.21	6.22
FeO	0.99	2.75	1.03	1.30	0.48	0.33	0.28	0.26	14.02	24.97
MnO	-	-	-	-	-	-	-	-	0.23	0.30
MgO	0.22	1.18	0.18	0.28	-	-	-	-	13.10	7.46
CaO	12.52	10.66	11.77	12.10	1.06	0.81	1.26	0.88	19.87	11.91
Na_2O	4.52	5.33	5.23	5.12	10.42	9.73	9.53	10.10	0.58	0.75
K_2O	0.24	0.93	0.22	0.24	0.11	0.13	0.18	0.17	-	0.23
Cr_2O_3	0.19	0.13	0.29	0.20	0.16	0.18	0.15	0.19	0.29	0.31
TOTAL	98.72	98.82	99.37	100.02	103.86	98.34	95.91	96.46	104.69	101.99
Atomic proportion										
O ions	8	8	8	8	8	8	8	8	23	23
Si	2.381	2.463	2.417	2.414	2.960	2.978	2.952	2.957	7.236	7.273
Ti	0.004	0.027	0.003	0.005	0.004	-	0.005	0.004	0.138	0.028
Al	1.557	1.345	1.514	1.502	1.048	1.047	1.067	1.056	0.526	1.075
Fe	0.038	0.107	0.040	0.050	0.017	0.012	0.010	0.009	1.631	3.063
Mn	-	-	-	-	-	-	-	-	0.027	0.037
Mg	0.015	0.082	0.012	0.019	-	-	-	-	2.715	1.871
Ca	0.621	0.534	0.580	0.593	0.048	0.038	0.059	0.041	2.960	1.632
Na	0.406	0.483	0.466	0.455	0.850	0.822	0.806	0.855	0.156	0.215
K	0.014	0.055	0.013	0.014	0.006	0.007	0.010	0.009	-	0.043
Cr	0.007	0.005	0.011	0.007	0.005	0.006	0.005	0.007	0.032	0.036
TOTAL	5.044	5.103	5.055	5.060	4.937	4.910	4.914	4.939	15.421	15.272

	27.	28.	29.	30.	31.	32.	33.	34.	35.	36.
Mass % oxide										
SiO_2	47.19	31.34	31.40	32.11	30.67	0.31	0.76	26.99	28.45	26.49
TiO_2	0.25	29.40	29.28	28.29	30.88	-	-	0.11	-	0.09
Al_2O_3	8.18	4.26	4.33	5.14	3.92	-	0.29	17.34	17.66	17.59
FeO	25.77	4.45	4.43	4.50	2.57	0.39	1.13	36.13	36.05	37.09
MnO	-	-	-	-	-	-	-	0.40	0.42	0.46
MgO	6.53	-	-	-	-	-	-	8.33	8.02	9.14
CaO	11.64	27.93	28.02	27.43	29.45	60.76	56.08	0.53	0.68	0.29
Na_2O	1.12	-	-	-	-	-	-	-	-	-
K_2O	0.30	-	-	-	-	-	-	0.06	0.11	-
Cr_2O_3	0.29	-	-	-	-	-	-	0.23	0.16	0.21
TOTAL	101.27	97.37	97.47	97.89	97.31	61.46	58.26	90.11	91.53	91.39
Atomic proportion										
O ions	23	20	20	20	20	4	4	28	28	28
Si	7.020	4.234	4.236	4.309	4.134	0.019	0.048	5.874	6.056	5.712
Ti	0.028	2.986	2.971	2.855	3.130	-	-	0.017	-	0.015
Al	1.435	0.677	0.688	0.813	0.623	-	0.021	4.447	4.431	4.472
Fe	3.206	0.507	0.500	0.505	0.290	0.012	0.060	6.578	6.417	6.689
Mn	-	-	-	-	-	-	-	0.073	0.077	0.084
Mg	1.449	-	-	-	-	-	-	2.700	2.543	2.937
Ca	1.856	4.042	4.052	3.944	4.252	3.942	3.811	0.124	0.155	0.068
Na	0.323	-	-	-	-	-	-	-	-	-
K	0.057	-	-	-	-	-	-	0.018	0.030	-
Cr	0.034	-	-	-	-	-	-	0.038	0.027	0.036
TOTAL	15.407	12.446	12.447	12.426	12.429	3.973	3.940	19.869	19.734	20.014

	37.	38.	39E.	39C.	40.	41.	42.	43.	44.	45.
Mass % oxide										
SiO_2	26.02	26.17	26.30	25.98	30.61	28.92	27.87	8.85	7.97	6.62
TiO_2	0.13	0.11	-	-	-	-	7.60	13.45	13.82	13.71
Al_2O_3	16.74	16.72	18.70	18.01	21.58	20.43	9.94	1.09	2.81	2.68
FeO	36.00	35.74	36.87	35.75	34.75	34.28	42.98	65.24	67.10	67.45
MnO	0.59	0.40	0.57	0.43	0.27	0.23	-	-	-	-
MgO	7.48	8.10	8.55	8.17	12.92	12.35	2.10	-	-	-
CaO	0.64	0.46	0.33	0.27	0.13	0.17	7.23	7.57	5.27	4.37
Na_2O	-	-	-	-	0.86	-	2.68	-	-	-
K_2O	0.09	-	0.07	0.10	-	0.07	1.16	-	-	-
Cr_2O_3	0.18	0.18	0.15	0.13	0.16	0.26	0.16	0.17	0.15	0.18
TOTAL	87.86	87.86	91.54	88.85	101.29	96.69	101.72	96.38	97.13	95.00
Atomic proportion										
O ions	28	28	28	28	28	28	32	32	32	32
Si	5.848	5.859	5.651	5.739	5.748	5.714	6.603	2.755	2.463	2.122
Ti	0.022	0.017	-	-	-	-	1.355	3.152	3.209	3.302
Al	4.435	4.413	4.736	4.690	4.776	4.756	2.774	0.401	1.022	1.010
Fe	6.769	6.693	6.626	6.605	5.457	5.664	8.516	16.995	17.326	18.073
Mn	0.112	0.078	0.103	0.079	0.043	0.039	-	-	-	-
Mg	2.505	2.704	2.737	2.692	3.616	3.638	0.738	-	-	-
Ca	0.154	0.109	0.077	0.065	0.025	0.036	1.835	2.525	1.744	1.502
Na	-	-	-	-	0.314	-	1.228	-	-	-
K	0.024	-	0.021	0.027	-	0.018	0.352	-	-	-
Cr	0.032	0.032	0.025	0.023	0.024	0.041	0.031	0.042	0.038	0.046
TOTAL	19.903	19.904	19.976	19.920	20.003	19.906	23.431	25.870	25.802	26.055

TABLE A4.2 Microprobe analyses of sulphides, Cleveland Mine (specimen 104349). Data are also given for a copper-tin-sulphur standard.

	Cu	Fe	Sn	Zn	S	(Total)
Cu_2SnS_3 synthetic standard						
1.	37.14	-	35.18	-	27.59	(98.86)
2.	37.49	-	35.08	-	27.43	(97.93)
3.	37.28	-	35.15	-	27.58	(97.59)
4.	37.02	-	35.07	-	27.92	(98.51)
5.	37.03	-	34.96	-	28.02	(97.25)
6.	36.81	-	35.17	-	28.02	(98.35)
7.	37.17	-	34.99	-	27.84	(97.82)
8.	36.95	-	35.02	-	28.03	(99.42)
9.	36.85	-	35.55	-	27.51	(99.73)
10.(av)	37.08	-	35.13	-	27.77	-
Stannite						
11.	30.14	18.14	21.72	-	30.01	(102.19)
12.	31.04	14.76	23.26	-	30.94	(100.17)
13.	31.22	14.69	23.13	-	30.95	(97.86)
14.	29.66	14.26	25.93	-	30.15	(102.38)
15.	30.22	13.45	26.87	-	29.46	(102.73)
16.	30.20	13.23	26.77	-	29.80	(100.31)
17.	30.41	13.06	27.13	-	29.39	(101.57)
Pyrrhotite						
18.	0.32	61.02	-	0.88	37.77	(99.39)
19.	-	59.86	-	-	40.14	(101.99)
20.	-	60.67	-	-	39.33	(102.50)
21.	0.27	60.39	-	-	39.33	(100.48)
22.	0.18	60.53	-	-	39.29	(102.33)
23.	0.42	60.47	-	-	39.12	(101.15)
24.	0.41	60.22	-	-	39.38	(101.86)
Chalcopyrite						
25.	34.57	30.67	-	-	34.76	(104.23)
26.	34.62	30.49	-	-	34.88	(102.58)
27.	34.83	30.47	-	-	34.70	(104.67)
28.	34.74	30.58	-	-	34.70	(102.20)

TABLE A4.3 X-ray diffraction determination of arsenopyrite composition.

Sample No.	d_{131}	As(atomic %)		Mean
104366	1.6335	34.59	II	
	1.6335	34.59		34.59
	1.6311	32.51	III	
	1.6311	32.51		32.51
104368	1.6310	32.42		
	1.6311	32.51		
	1.6310	32.42		
	1.6321	33.37		
	1.6312	32.59		32.66
104368 (repeat)	1.6312	32.59		
	1.6312	32.59		32.59
104370	1.6315	32.85		
	1.6321	33.37		
	1.6318	33.11		
	1.6312	32.59		
	1.6312	32.69		32.90
104370 (repeat)	1.6308	32.25		
	1.6311	32.51		
	1.6321	33.37		32.71
104376	1.6319	33.20		
	1.6319	33.20		
	1.6321	33.37		
	1.6319	33.20		
	1.6325	33.72		33.34
104435	1.6328	33.98		
	1.6321	33.37		
	1.6335	34.59		33.98
104438	1.6321	33.37		
	1.6329	34.06		
	1.6321	33.37		
	1.6321	33.37		33.55

Sample No.	d_{131}	As(atomic %)	Mean
104449	1.6323	33.55	
	1.6315	32.85	
	1.6313	32.68	
	1.6318	33.11	
	1.6323	33.55	
	1.6315	32.85	33.10
104465	1.6301	31.64	
	1.6297	31.29	
	1.6289	30.60	
	1.6311	32.51	
	1.6314	32.77	31.76
104466	1.6332	34.32	
	1.6326	33.81	
	1.6327	33.89	
	1.6324	33.63	33.91
104469	1.6316	32.94	
	1.6321	33.37	
	1.6324	33.63	
	1.6321	33.37	33.32

TABLE A4.4. Trace element and rare earth element composition (g/t) of fluorite, Cleveland mine.

	1.	2.	3.	4.	5.
Ca (mass %)	47	50	38	49	49
La	2.54	0.16	2.88	7.01	4.59
Ce	8.33	1.33	6.96	17.93	12.84
Sm	4.53	0.77	2.12	9.25	4.34
Eu	1.37	0.19	0.86	2.49	1.19
Tb	2.18	0.77	0.43	5.48	1.01
Yb	8.91	10.93	0.85	28.31	2.98
Lu	1.10	1.44	0.11	3.53	0.35
ΣREE	28.96	15.59	14.21	74.00	27.30
Na	253.6	58.2	29.9	76.1	9.1
Sc	0.71	0.095	0.45	0.11	0.79
Cr	1.45	-	3.80	-	-
Fe	13493	1107	8106	3428	288
Co	5.26	1.67	0.40	0.20	0.28
Sr	-	-	156.1	34.2	47.6
Cs	0.18	0.050	0.27	-	0.40
Th	0.57	-	1.07	-	1.33
Atomic ratio:					
Tb/Ca ($\times 10^{-6}$)	1.08	0.380	0.212	2.70	0.498
Tb/La	0.759	4.21	0.131	0.683	0.192

Analyst : Neutron activation analysis by H. Seitz (HMI) for H-J. Schneider, Freie Universität, Berlin.

1, Fluorite in sulphide lens (Halls), 15L, Stage II.

2, Vein fluorite, 14L/15L decline (104308).

3, Fluorite in vug in sulphide lens (Halls), 14L, Stage II (104301).

4, Fluorite in sulphide lens (Halls), 15L, Stage II.

5, Vein fluorite, 15L, Stage IV (104319).

APPENDIX 5

Fluid inclusion microthermometry

Analytical technique

Specimens for fluid inclusion study were collected from underground development drives and cross-cuts, and from diamond drill core intersections of mineralisation both at depth and in areas previously mined out, and now inaccessible. Most underground specimens were collected when mine development was at 14, 15 and 16 levels. Details of specimen locations are given in Appendix 7.

Fluid inclusions were examined in thin (1 mm or less), doubly polished plates of ore/vein samples and of crystals. The plates were initially examined under the microscope for selection of suitable inclusions, and the plates were then broken into smaller chips that could be handled in the microthermometric apparatus.

Most heating, and all freezing measurements were made on a Chaixmeca cooling/heating stage (Poty *et al.*, 1976) mounted on a Leitz petrographic microscope at the University of Tasmania. The only modification made to the Chaixmeca apparatus has been to place a thin (170 μm thick) glass coverslip over the condenser lens, as a means of protecting the lens. Cooling experiments were undertaken using a 25X objective fitted with a plastic sleeve, and most heating experiments were conducted using a 40X objective and a thin (170 μm) glass coverslip window.

Prior to the availability of the Chaixmeca apparatus, a small number of heating measurements were made on a stage constructed at the University of Tasmania. The temperature of the heating chamber (and sample) in this stage was measured using either alumnel-chromel or iron-constanton thermocouples connected to a digital thermometer. The thermocouple was placed below and in contact with the sample being

heated, and the temperature readout of the digital thermometer was in divisions of 1°C.

All quantitative observations of phase transitions were performed in the heating cycle. The heating rate during freezing experiments (i.e. below 40°C) was regulated at 0.5 - 1°C/min., and for heating experiments was regulated at 1 - 2°C/min. Inclusions were also observed during the cooling cycle of freezing experiments (for detection of CO_2 and/or other gases in inclusions) and a few measurements of nucleation of solid phases and have been recorded. These measurements are however, semi-quantitative as the cooling rate could not be adequately controlled, and nucleation of solid phases requires supercooling and is dependent upon a variety of factors.

Calibration of microthermometric apparatus

The accuracy and precision of measurements of the temperatures of observed phase transitions is insured by calibration of the temperature read-out relative to known phase transitions (usually the melting point) in standard compounds. This is necessary because, in the Chaixmeca apparatus the Pt resistance element measures the temperature of the stage a few millimetres from the optic axis of the condenser lens on which the sample rests; and in the University of Tasmania stage the thermocouple measures the temperature of the stage below the sample, and not always in the exact same position. Other problems and errors encountered in calibration of microthermometric apparatus are discussed by Roedder (1976) and Hollister *et al*. (1981).

The initial calibration of the Chaixmeca apparatus in 1976, and the calibration of the University of Tasmania stage was undertaken jointly with Dr C.J. Eastoe, and a later check calibration of the Chaixmeca apparatus in 1978 was undertaken by the author (fig. A5.1).

The Chaixmeca apparatus was calibrated relative to the melting points of pure substances and Merck standards in air, at ambient pressure. The standards were either sandwiched between two glass coverslips or sealed in 1 mm outside diameter glass capillary tubes. Operating conditions were the same as those applying during routine operating conditions. Standards used for temperature calibration were toluene (melting point - 95°C), chloroform (- 63.5°C), carbon tetrachloride (- 22.99°C), de-ionised water (0°C), benzene (+ 5.5°C), Merck 9670 (+ 70°C), Merck 9700 (+ 100°C), Merck 9735 (+ 135°C), Merck 9780 (+ 180°C), Merck 9800 (+ 200°C), Merck 9847 (+ 247°C), sodium nitrate (+ 306.8°C) and potassium dichromate (+ 398°C). Measurements on toluene, chloroform and potassium dichromate were not entirely satisfactory. Attempts to freeze toluene were unsuccessful. Chloroform, of unknown purity, was difficult to freeze, and it was only twice successfully frozen. The purity of the potassium dichromate was also unknown (technical grade) and gave non-reproducible results over a relatively large temperature range (fig. A5.1 A, B).

Working calibration curves for the Chaixmeca apparatus, derived from measurements on standard compounds, and for different microscope objectives are given in Fig. A5.1, in which ΔT is the difference between the observed phase change (Tr) and the actual phase change of the standard. ΔT is added to the temperature of the observed phase change (melting, homogenisation) to obtain the actual temperature (e.g., $Th = Tr + \Delta T$, where Th is the temperature of homogenisation). The obvious features of the calibration curves are that the observed temperatures of cooling measurements (i.e. below about 40°C) are 0.2°C too low (fig. A5.1 A), and the reproducibility of these measurements is ± 0.1°C. The observed temperatures of heating experiments are too high, and the magnitude of the correction for the 40X objective increases from 0°C at 60°C, to 14°C at 500°C. Reproducibility of heating measurements increases from

±0.2°C at 60°C, to ±3°C at 500°C. Another feature is that calibration curves for heating experiments are markedly affected by the thickness of the window on top of the heating chamber (c.f. figs. A5.1 A and A5.1 B).

The Chaixmeca apparatus was re-calibrated about 18 months after commissioning of the equipment, to ascertain whether there was any instrumental drift during heating experiments. The check calibration, for a 40X objective, shows a slight negative shift in ΔT, increasing from 0°C at 60°C to 1°C at 500°C (fig. A5.1 C). Taking into consideration all of the problems encountered in calibration of the apparatus and the reproducibility of results, this negative shift is not considered significant. However, it does demonstrate the need for periodic re-calibration of the apparatus.

Calibration of the University of Tasmania heating stage and digital thermometer was undertaken in a manner similar to that described above for the Chaixmeca apparatus. For heating measurements, standard compounds (mannitol (melting point 168°C), sodium nitrate and potassium dichromate) were sealed in glass capillary tubes; and at low temperatures (below 60°C), the temperature readout was checked with a thermometer. In the temperature range 150° - 450°C, the temperature readout was consistently 10°C too high and the reproducibility ranged from ±3°C at 150°C, to ±6°C at 450°C. In the temperature range 15° - 40°C no correction was necessary and measurements are accurate to ±0.5°C. A check measurement on specimen 104307, inclusion number 5 gave Th, CO_2 L-V of 29°C with the University of Tasmania stage, and 29.2°C with the Chaixmeca apparatus.

FIG. A5.1 Working calibration curves for Chaixmeca microthermometric apparatus at the University of Tasmania.

A. 25X objective fitted with a plastic sleeve (below 40°C) and for 10X objective and thick (1.8 mm) window (calibrated October, 1976).

B. 40X objective and thin (170 μm) glass coverslip window (calibrated October, 1976).

C. Check calibration for 40X objective and glass coverslip window (calibrated May, 1978). The thick dashed line is the 1976 calibration (from B).

Tr is the temperature recorded on the Chaixmeca control unit, and ΔT is the difference between the temperature readout (Tr) and the actual temperature. Vertical lines indicate the range of measurements of phase transitions of pure standards, and the short horizontal bar indicates the mean value for each standard.

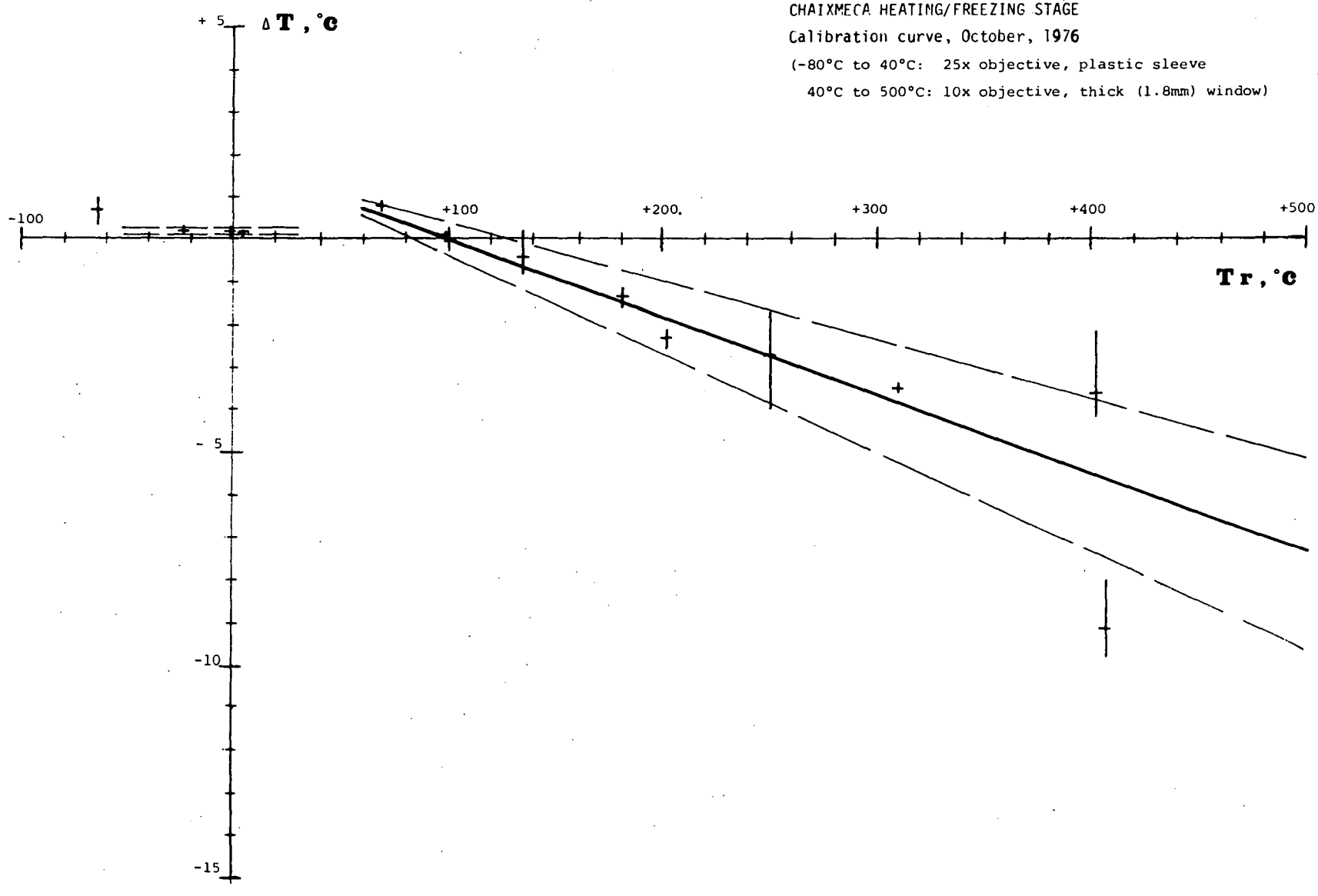
CHAIXMECA HEATING/FREEZING STAGE
Calibration curve, October, 1976
(-80°C to 40°C: 25x objective, plastic sleeve
40°C to 500°C: 10x objective, thick (1.8mm) window)
ΔT, °C
+ 5
- 5
-10
-15
-100
+100
+200
+300
+400
+500
Tr, °C

FIGURE A5.1A

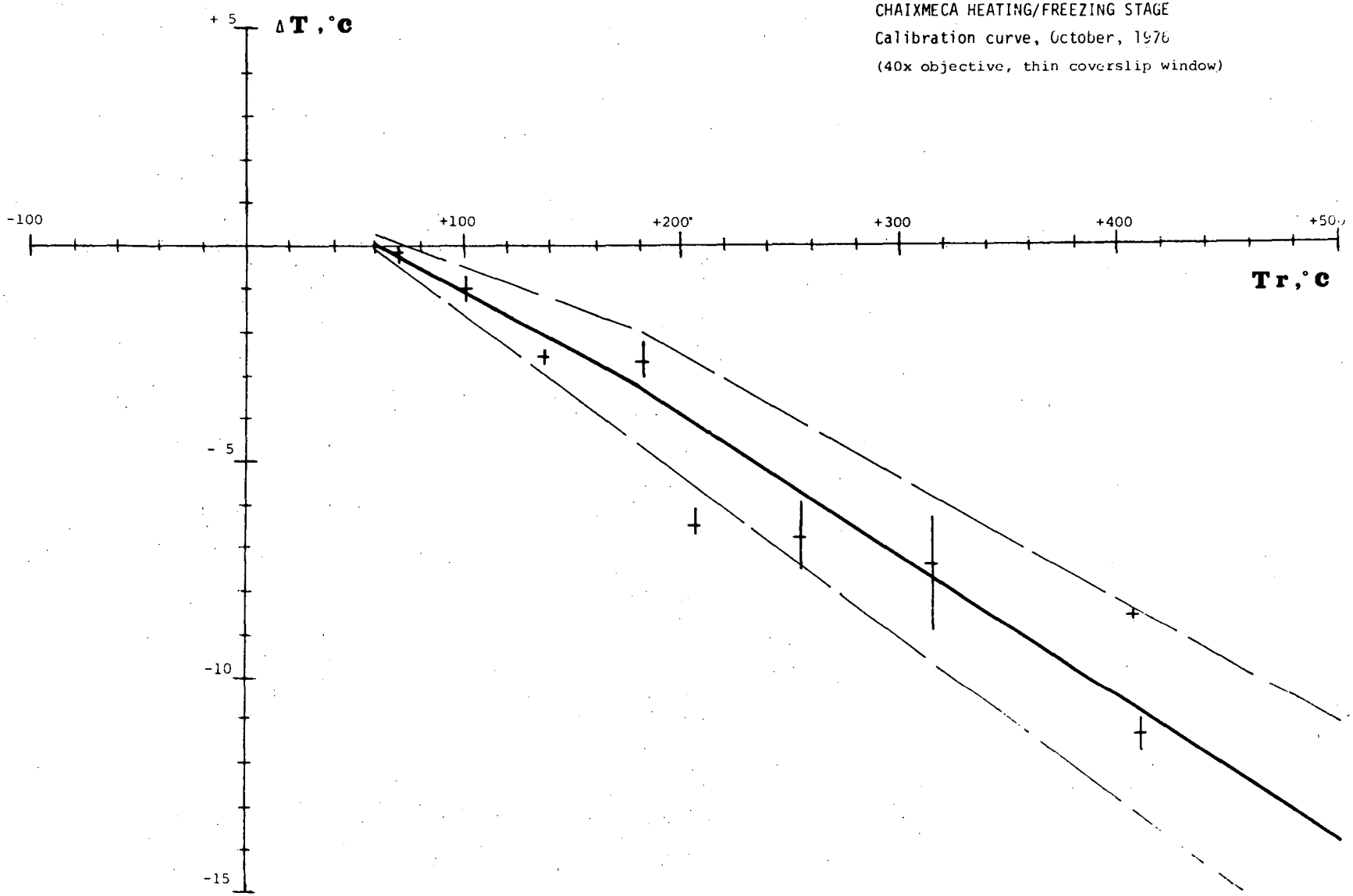
CHAIXMECA HEATING/FREEZING STAGE
Calibration curve, October, 1976
(40x objective, thin coverslip window)
ΔT, °C
+ 5
- 5
-10
-15
-100
+100
+200
+300
+400
+500
Tr, °C

FIGURE A5.1B

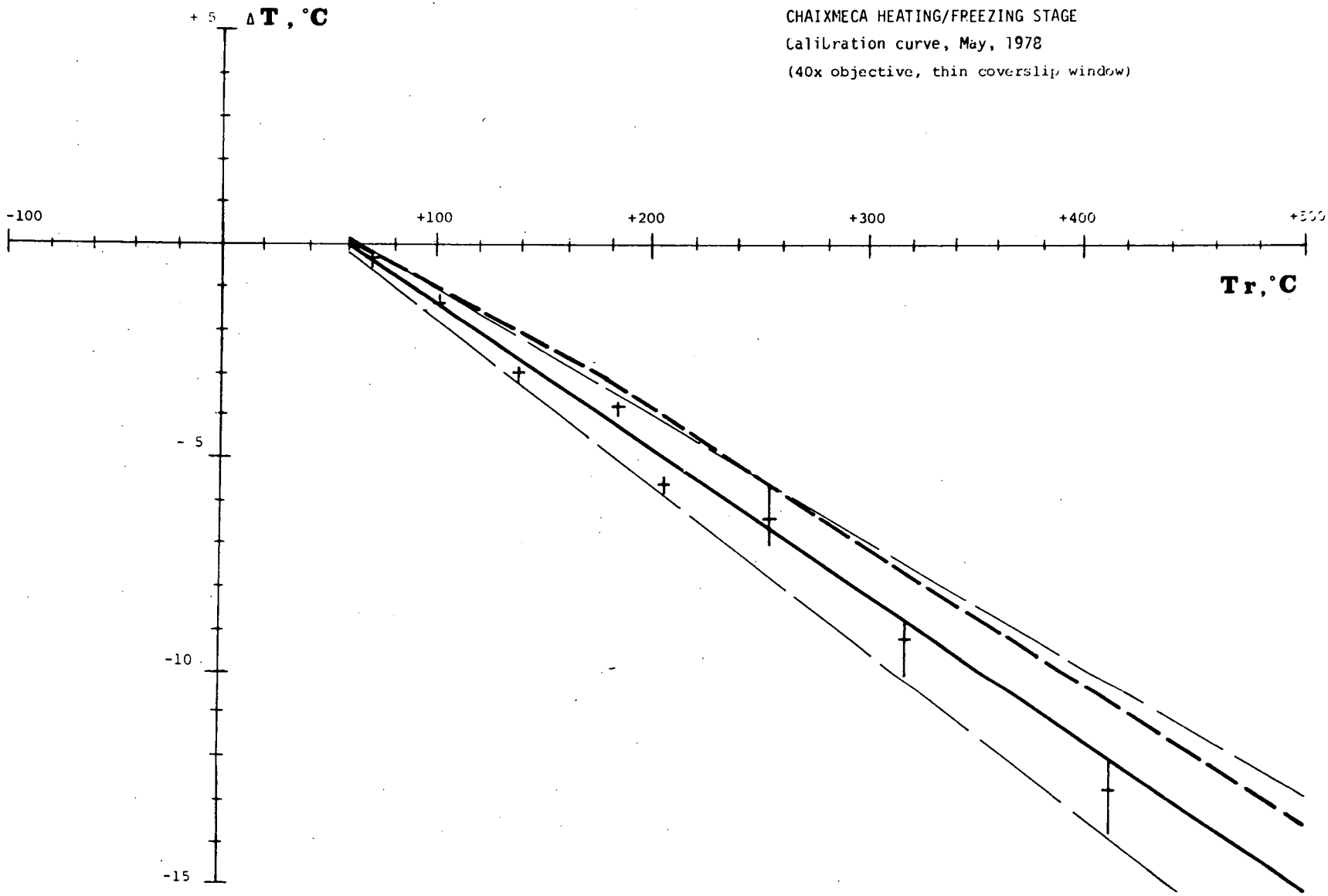
CHAIXMECA HEATING/FREEZING STAGE
Calibration curve, May, 1978
(40x objective, thin coverslip window)
ΔT, °C
+ 5
- 5
-10
-15
-100
+100
+200
+300
+400
Tr, °C

FIGURE A5.1C

Experimental observations

All of the data on individual inclusions gathered in this research are listed in Tables A5.1 and A5.2 The temperatures of observed phase transitions have been corrected for experimental error using the calibration curves in figure A5.1 A (cooling experiments) and figure A5.2B (heating experiments). Unless indicated otherwise, all inclusions are believed to be either primary or pseudosecondary.

The column headings and abbreviations used in Tables A5.1 and A5.2 are as follows:

Sample: Specimen number; the mineral examined in each chip, its occurrence and stage of mineralisation; grain number within large chips (e.g., gn. 1); and inclusion number. Fl = fluorite, Qtz = quartz, Apat. = apatite, Sid = siderite, xtal = crystal lining a vug.

Description:

Occur: Mode of occurrence of inclusions in a host mineral include: isol. = solitary inclusion; disper. = inclusions closely dispersed throughout a grain; group = small number of inclusions within a small, non-planar area of a single grain; plan. = planar array of inclusions; plan. S = planar array of secondary inclusions. Sets of inclusions in the same group, plan., or disper. arrangement are indicated by ditto (") after the first inclusion of that set.

Shape: Shape of each inclusion (see also Plate 6.1). Different shapes include: xtal. = euhedral negative crystal of the host mineral; facet. = faceted, subhedral negative crystal; wedge = wedge-shaped, faceted inclusion; ovoid = rounded, non-faceted inclusion; elong. = inclusion with one dimension significantly longer than the other; needle (or tube) = long tubular inclusion;

irreg. = highly irregular, non-faceted shape.

Tm, ice: Temperature of final melting of ice, and in parentheses, the equivalent mass % NaCl. ms = metastability.

Tm, hyd: Temperature of final melting of gas hydrate (presumably CO_2 hydrate), and in parentheses, the equivalent mass % NaCl (see Collins, 1979; Appendix 8).

Th, CO_2, L-V: Temperature of homogenisation (L to liquid, G to vapour) of the CO_2 phase. Cr = critical homogenisation.

A dash in columns Tm, hyd and $ThCO_2$, L-V, means a two-phase aqueous inclusion, with no evidence of the presence of CO_2.

Th, L-V: The final homogenisation temperature (L to liquid, G to vapour, Cr = critical homogenisation). Other abbreviations are: leaked = near-surface inclusion that leaked through a fracture developed during heating, prior to homogenisation; Dec. = decrepitated.

Comments: The most important comments are:

(i) the number and type of solid mineral phases (x or X) present in an inclusion (ax = anisotropic mineral, ix = isotropic mineral, ox = opaque mineral); small minerals occupying less than about 2 vol. % of an inclusion are designated by "x", and large accidental(?) trapped solids by "X".

(ii) Tn, hyd and Tn, ice are the temperature (°C) of nucleation of the fluid during freezing of gas hydrate and ice, respectively; accuracy of measurements is probably not better than ±5°C (see Collins, 1979; Appendix 8).

(iii) $TmCO_2$ is the temperature of final melting of the solid CO_2 phase.

(iv) observation or detection of a CO_2 liquid phase (CO_2L), a gas hydrate phase after ice melting (CO_2 hyd), and "double freezing" of the fluid (designated by d.n.).

(v) Vol. % L, CO_2 and G, CO_2 is the volume % of the CO_2 liquid phase and CO_2-rich gas phase at the temperature specified, and calculated by assuming areal ratios are proportional to volume ratios.

(vi) X_{CO_2} is the mole fraction of CO_2 in type 3 inclusions at 40°C, using the volumetric method of Burruss (1981).

(vii) comments on the chip or grain are indicated by an asterisk (*).

REFERENCES

Burruss, R.C., 1981, Analysis of phase equilibria in C-O-H-S fluid inclusions in Hollister, L.S., Crawford, M.L. (eds.), Fluid inclusions : applications to petrology : Mineral. Assoc. Canada, Short Course Handbook, 6:39-74.

Collins, P.L.F., 1979, Gas hydrates in CO_2-bearing fluid inclusions and the use of freezing data for estimation of salinity : Econ. Geol., 74:1435-1444.

Hollister, L.S., Crawford, M.L., Roedder, E., Burruss, R.C., Spooner, E.T.C., Touret, J., 1981, Practical aspects of microthermometry in Hollister, L.S., Crawford, M.L., (eds.), Fluid inclusions : applications to petroloty : Mineral. Assoc. Canada, Short Course Handbook, 6:278-304.

Poty, B., Leroy, J., Jachimowicz, L., 1976, Un novel appareil pour la mesure des temperatures sous le microscope : l'installation de microthermometrie Chaixmeca : Bull. Soc. Fr. Mineral. Cristallogry., 99:182-186.

Roedder, E., 1976, Fluid-inclusion evidence on the genesis of ores in sedimentary and volcanic rocks, Chapter 4, in Wolf, K.H., (ed.), Handbook of strata-bound and stratiform ore deposits, Amsterdam, Elsevier, 2:67-110.

TABLE A5.1 Fluid inclusion microthermometric data, using Chaixmeca cooling/heating apparatus.

Note:

1. Abbreviations are described in Appendix 5.
2. Below 35°C, temperature data are accurate to ±0.1°C, and the error increases to ±3°C at 500°C (see Appendix 5: Fig. A5.1 A,B).
3. All temperature data have been corrected for instrumental error using the calibration curves in Figure A5.1 and no further corrections are necessary.

SAMPLE.			DESCRIPTION. occur.	shape.	Tm,ice °C(%NaCl)	Tm,hyd °C(%NaCl)	$ThCO_2$,L-V °C	Th,L-V °C	COMMENTS.
104300.									
F1, II xtal	gn1	1.	plan	elong.	-8.3(12.1)	6.8(6.4)	26.3L	228.1L	3x;Tn,hyd-32.9; Tn,ice-48.6;$TmCO_2$-57.7; Vol %(@18°C)L,CO_2=8.9 G,CO_2=4.8; XCO_2=0.08.
		2.	"	facet.	-8.4(12.2)	7.1(5.8)	27.0L		2x;Tn,hyd-31.7;Tn,ice-47.3.
		3.	"	elong.	-8.4(12.2)	6.9(6.2)	26.1L		Tn,hyd-30.8;Tn,ice-47.9.
		4.	"	elong.	-8.5(12.4)	7.1(5.8)	27.9G		Tn,hyd-33.6;Tn,ice-53.2.
		5.	"	elong.	-8.3(12.1)	7.1(5.8)	27.3L		Tn,hyd-34;Tn,ice-49.9.
		6.	"	wedge	-8.4(12.2)	7.4(5.3)	27.1L		3x;Tn,hyd-31.7;Tn,ice-53.
		7.	"	wedge	-8.3(12.1)	7.3(5.4)	26.7L	229.1L	3x;Tn,hyd-30.2;Tn,ice-47.
		8.	"	elong.		7.3(5.4)	26.9L		2x;Tn,hyd-31.6;Tn,ice-41.1
	gn2	9.	plan.	elong.	-7.4(11.0)	7.5(5.1)	27.5G	253.9L	3x;Tn,hyd-28;Tn,ice-43.2.
		10.	"	elong.			?G	259.3L	d.n.
		11.	"	facet.	-7.4(11.0)	7.5(5.1)	27.2G	256.3L	2x;Tn,hyd-29.9;Tn,ice-41.6.
		12.	"	elong.	-7.4(11.0)	7.8(4.5)	25.3L	291.6L	2x;Tn,hyd-28.6;Tn,ice-43.2.
		13.	"	elong.	-7.4(11.0)		?G	260.2L	1x;Tn,hyd-28.1;Tn,ice-44.
		14.	plan.	elong.		-	-	239.1L	
		15.	"	ovoid		-	-	265.3L	
		16.	"	ovoid		-	-	242.4L	
		17.	"	ovoid		-	-	274.3L	
		18.	"	elong.		-	-	280.3L	
104301.									
F1, II xtal		1.	plan.	ovoid	-6.6(10.0)	-	-		1x.
		2.	"	ovoid	-6.6(10.0)	-	-	338.0L	2x.
		3.	"	elong.	-6.6(10.0)	-	-	340.1L	1x.
		4.	"	elong.	-6.7(10.2)	-	-	339.7L	1x.
		5.	"	facet.		-	-	339.5L	
		6.	"	irreg.		-	-	339.9L	
		7.	"	elong.	-6.8(10.3)	-	-	340.0L	
		8.	"	tube		-	-	339.8L	

SAMPLE.		DESCRIPTION. occur.	shape.	Tm,ice °C(%NaCl)	Tm,hyd °C(%NaCl)	$ThCO_2$,L-V °C	Th,L-V °C	COMMENTS.
Fl, II gnl	9.	group	facet.		-	-	301.8L	2ax, lox.
outer xtal	10.	"	facet.		-	-	304.8L	lax, lix, 3ox.
	11.	"	facet.		-	-	298.5L	lax, lix, lox.
	12.	plan.	irreg.	-6.4(9.8)	?6.2(7.5)	-	271.9L	lax.
	13.	"	ovoid	-5.5(8.6)	-	-	269.6L	2ix.
	14.	"	facet.		-	-	255.2L	2ax,lix.
gn2	15.	plan	xtal.		-	-	297.3L	3ax, 5ix.
	16.	"	wedge		-	-	308.8L	lox.
	17.	"	xtal.	-6.3(9.7)	-	-	311.1L	
	18.	"	facet.	-6.2(9.5)	-	-	314.9L	
	19.	"	irreg.	-6.0(9.3)	-	-	315.0L	lax, lix, lox.
	20.	"	xtal.		-	-	317.1L	2ox.
	21.	"	facet.		-	-	316.1L	lox.
	22.	"	elong.		-	-	313.2L	
	23.	plan.	ovoid		-	-	318.0L	
	24.	"	ovoid		-	-	317.3L	
Qtz, II	25.	group	xtal.	-7.0(10.5)	-	-	294.4L	
ore	26.	"	facet.	-7.0(10.5)	-	-	299.6L	
	27.	plan.S	facet.	-6.3(9.7)	-	-	211.1L	
	28.	group	ovoid.	-6.8(10.3)	-	-	312.7L	
	29.	"	elong.	-6.8(10.3)	-	-	298.8L	
	30.	plan.	facet.		-	-	306.1L	
	31.	"	facet.		-	-	310.7L	lx.
	32	"	facet.		-	-	312.9L	
	33.	isol.	xtal.		-	-	312.6L	
Fl, II gnl	34.	isol.	facet.	-5.8(8.0)	-	-	342.6L	2x;Tn,ice-43.
base xtal	35.	isol.	ovoid.		-	-	321.0L	
	36.	isol.	irreg.		-	-	342.9L	
	37.	isol.	facet.		-	-	343.7L	3x.
gn2	38.	isol.	wedge	-5.7(8.9)	-	-	333.3L	4x;Tn,ice-50 } Isol. pr.
	39.	isol.	facet.	-5.7(8.9)	-	-	326.2L	Tn,ice-50 }

SAMPLE.		DESCRIPTION. occur.	shape.	Tm,ice °C(%NaCl)	Tm,hyd °C(%NaCl)	$ThCO_2$,L-V °C	Th,L-V °C	COMMENTS.
	40.	isol.	elong.	-5.6(8.7)	-	-	316.82	4x;Tn,hyd(?)-35.6; Tn,ice-42.
	41.	isol.	facet.		-	-	330.1L	
Fl, II ore	42.	plan.	elong.	-6.4(9.8)			234.2L	2x;Tn,hyd-39.2; Tn,ice-45.4;CO_2L obs.
	43.	"	elong.	-6.1(9.4)			236.0L	3x;Tn,hyd/ice-38.3; CO_2hyd and CO_2L obs.
	44.	"	facet.	-5.2(8.2)	-	-	253.5L	2x;no CO_2L obs.
	45.	"	ovoid.	-5.2(8.2)	-	-	255.3L	no CO_2L obs.
	46.	"	ovoid.	-5.2(8.2)	-	-	254.2L	no CO_2L obs.
	47.	"	ovoid.	-6.1(9.4)	-	-	215.3L	no CO_2L obs.
	48.	"	facet.	-6.2(9.5)	-	-	213.4L	
	49.	"	facet.	-5.3(8.3)	-	-	254.8L	2x.
	50.	"	facet.	-6.4(9.8)		-		CO_2hyd obs. } adj. inclusions
	51.	"	facet.	-5.0(7.9)	-	-		no CO_2hyd }
	52.	"	ovoid.		-	-	258.3L	
Qtz, II gnl ore	53.	disper.	facet	-8.8(12.7)	-	-	281.1G	2x.
	54.	"	facet.	-9.0(12.9)	-	-	354.1L	
	55.	"	facet.		-	-	274.5L	bubble did not reappear.
	56.	"	wedge	-8.1(11.9)	-	-	331.9L	
	57.	"	facet.		-	-	323.1L	
	58.	"	elong.		-	-	343.8L	
	59.	"	ovoid		-	-	352.1L	
	60.	"	elong.		-	-	353.4L	
	61.	"	facet.	-8.6(12.5)	-	-	361.9L	
	62.	"	elong.	-8.8(12.7)	-	-	347.5L	
	63.	"	ovoid.		-	-	343.9L	
	64.	"	facet.		-	-	345.4L	
	65.	'	irreg.		-	-	351.7L	
gn2	66.	isol.	xtal.	-8.3(12.1)	-	-	337.9L	}
	67.	isol.	facet.		-	-	314.6L	1x } isol. pr.

SAMPLE.		DESCRIPTION occur.	shape.	Tm,ice °C(%NaCl)	Tm,hyd °C(%NaCl)	ThCO$_2$,L-V °C	Th,L-V °C	COMMENTS.
	68.	isol.	xtal.	-8.2(12.0)	-	-	324.9L	
	69.	isol.	xtal.		-	-	324.9L	
	70.	group	facet.		-	-	312.7L	
	71.	"	facet.	-9.2(13.2)	-	-	351.8L	
	72.	"	facet.		-	-	345.1L	
	73.	plan.S.	ovoid		-	-	278.2L	
	74.	"	irreg.		-	-	274.7L	
104307.								
F1, IV	1.	isol.	xtal.	-0.7(1.2)	-	-	241.2L	perpendicular to bands.
	2.	isol.	wedge	-5.9(9.2)				parallel to bands.
	3.	isol.	irreg.	-5.9(9.2)			188.9L	
	4.	isol.	wedge.	-0.4(0.7)	-	-	136.1L	
F1, II gnl	5.	group	wedge	-7.3(10.9)	8.0(4.1)	29.4G	295.6L	lax,lix,lox;Tn,hyd-33.1; Tn,ice-44.6;Tm,CO_2-59.5; Vol %(@ 22°C)L,CO_2=18.7 G,CO_2=17.2; XCO_2= 0.1.
	6.	"	ovoid		-	-	280.2L	No CO_2L/hyd detected } adj.
	7.	"	elong.				300.5L	CO_2L obs } to 5.
	8.	group	elong.	-8.7(12.6)			303.2L	CO_2L obs.
	9.	"	wedge	-8.1(11.9)	7.6(4.9)	27.2G	300.2L	3x;Tn,hyd-31.3;Tn,ice-47.3.
	10.	"	elong		-	-	300.6L	No CO_2L/hyd detected.
	11.	"	ovoid		-	-	303.3L	No CO_2L/hyd detected.
	12.	"	ovoid		-	-	299.3L	
	13.	"	elong.		-	-	296.2L	
	14.	"	elong.		-	-	302.4L	
	15.	"	wedge		-	-	299.1L	
	16.	"	ovoid		-	-	305.8L	
	17.	group	elong.				298.9L	CO_2L obs.
	18.	"	ovoid				299.2L	CO_2L obs.
	19.	"	facet	-12.5(16.6)	6.6(6.8)	27.8	302.9L	
	20.	"	facet		-	-	299.9L	
	21.	"	facet		-	-	298.3L	
	22.	"	ovoid		-	-	304.8L	

SAMPLE.		DESCRIPTION. occur.	shape.	Tm,ice °C(%NaCl)	Tm,hyd °C(%NaCl)	ThCO$_2$,L-V °C	Th,L-V °C	COMMENTS.
	23.	"	facet.				305.3L	CO_2L obs.
	24.	"	elong.				303.2L	CO_2L obs.
	25.	"	elong.		-	-	302.9L	
	26.	"	facet.		-	-	303.3L	
	27.	"	facet.		-	-	302.9L	
	28.	"	elong		-	-	294.8L	
	29.	"	facet.		-	-	296.1L	
	30.	"	wedge	-13.5(17.5)	7.2(5.6)	G	305.9L	CO_2L obs.
	31.	"	elong.	-8.6(12.5)	7.9(4.3)	29.5G	302.6L	Tn,hyd-35.0;Tn,ice-54.2;
gn2	32.	plan.S	ovoid		-	-	190.5L	
	33.	"	elong.		-	-	206.4L	
	34.	"	facet.	-7.8(11.5)	-	-	207.5L	
	35.	"	elong.	-7.9(11.7)	-	-	207.8L	
	36.	"	elong.		-	-	206.0L	
	37.	"	elong.		-	-	207.8L	
	38.	"	facet.		-	-	206.9L	
	39.	"	ovoid		-	-	208.7L	
	40.	"	elong.		-	-	208.7L	
	41.	"		-7.8(11.5)	-	-		
Fl, IV	42.	isol.	elong	-5.8(9.0)	-	-	leaked	* Inclusions 42-56 all
	43.	isol.	elong.	-5.9(9.1)	-	-	164.6L	assoc. with colour growth
	44.	isol.	elong.	-5.2(8.2)	-	-	175.8L	bands in fl, all faceted
	45.	isol.	elong.		-	-	197.0L	as irreg. rhombs,
	46.	isol.	wedge	-6.2(9.5)	-	-	186.8L	tetrahedra etc.
	47.	isol.	facet.	-6.5(9.9)	-	-	233.0L	
	48.	isol.	facet.	-6.0(9.3)	-	-	203.4L	
	49.	isol.	wedge	-5.9(9.1)	-	-	170.8L	
	50.	isol.	elong.	-7.8(11.5)	-	-	197.4L	
	51.	isol.	wedge	-5.8(9.0)	-	-	209.6	
	52.	isol.	elong.	-5.1(8.0)	-	-	254.1L	
	53.	isol.	irreg.	-5.4(8.5)	-	-	224.5L	

SAMPLE.		DESCRIPTION. occur.	shape.	Tm,ice °C(%NaCl)	Tm,hyd °C(%NaCl)	$ThCO_2$,L-V °C	Th,L-V °C	COMMENTS.
	54.	isol.	irreg.		-	-	191.2L	
	55.	isol.	wedge	-5.3(8.3)	-	-	192.5L	
	56.	isol.	elong.	-5.0(7.9)	-	-	197.0L	
104308.								
Fl,vein	1.	isol.	facet.	-4.9(7.8)	-	-	149.3L	lix, lox.
	2.	group	facet.		-	-	202.8L	
	3.	"	facet.		-	-	255.8L	
	4.	isol.	ovoid		-	-	286.2L	
104320.								
Fl,vein,II	1.	isol.	irreg.		-	-	305.2L	
	2.	isol.	irreg.		-	-	311.3L	
	3.	isol.	facet.		-	-	343.5L	
	4.	isol.	facet.		-	-	331.0L	
	5.	isol.	ovoid		-	-	357.5L	
	6.	isol.	facet.	-5.6(8.7)	-	-	322.4L	
	7.	isol.	irreg.		-	-	321.0L	
	8.	isol.	wedge	-6.8(10.3)	-	-	334.9L	
	9.	isol.	irreg.		-	-	318.0L	
	10.	isol.	irreg.		-	-	352.8L	
Qtz, II.gn2	11.	group	xtal.	-7.2(10.8)	-	-	329.7L	
vein.	12.	"	xtal.	-7.2(10.8)	-	-	353.3L	
	13.	plan.	elong.	-10.6(14.7)			212.3L	d.n.
	14.	"	elong.	-9.9(13.9)			235.5L	d.n.
	15.		elong.	-9.1(13.1)	-	-	214.9L	
	16.	"	ovoid	-10.8(14.9)	-	-	246.4L	
	17.	"	facet.	-10.7(14.8)			252.2L	d.n.
	18.	"	elong.	-8.7(12.8)	-	-	209.6L	
104321.								
Fl, II	1.	isol.	elong.	-6.3(9.7)	-	-	239.7L	
	2.	group	irreg.			28.0Cr	199.2G	
	3.	"	elong.			27.7Cr?	170.0G	

SAMPLE.		DESCRIPTION. occur.	shape.	Tm,ice °C(%NaCl)	Tm,hyd °C(%NaCl)	ThCO$_2$,L-V °C	Th,L-V °C	COMMENTS.
	4.	isol.	irreg.		-	-	235.6L	
	5.	isol.	irreg.	-6.4(9.8)	-	-	217.4L	1x.
	6.	isol.	irreg.		-	-	177.6L	adj. to fracture.
	7.	isol.	irreg.	-6.6(10.0)	-	-	208.6L	
Qtz, II	8.	isol.	facet.	-8.7(12.6)	-	-	321.2L	
	9.	isol.	xtal.	-8.4(12.2)	-	-	292.4L	2x.
	10.	isol.	facet.	-8.4(12.2)	-	-	348.9L	
Fl, II	11.	isol.	irreg.	-8.0(11.8)	-	-	308.3L	
	12.	isol.	facet.		-	-	336.0L	
	13.	plan.	irreg.		-	-	305.9L	
	14.	group	ovoid		-	-	313.3L	1x.
	15.	"	ovoid		-	-	353.6L	
104345.								
Fl, II	1.	group	irreg.	-8.2(12.0)	-	-	201.8L	Tm, unknown at -5.3°C.
	2.	"	ovoid	-8.5(12.4)	-	-	256.0L	
	3.	"	facet.	-8.0(11.8)	-	-	237.0L	3x.
	4.	'	facet.	-8.3(12.1)	-	-	232.8	10x.
	5.	"	facet.		-	-	253.1L	
	6.	'	irreg.		-	-	258.1L	
	7.	"	irreg.	-8.5(12.4)	-	-	263.1L	1x.
	8.	'	irreg.		-	-	275.1L	
	9.	"	irreg.	-5.6(8.7)	-	-	316.5L	
Fl, II	gn1 10.	"	ovoid	-9.2(13.2)	-	-	297.8L	
	11.	"	ovoid		-	-	290.9L	
	12.	"	irreg.		-	-	298.1L	
	13.	"	elong.		-	-	283.0L	
	14.	"	elong.				244.9L	CO_2L obs.
	15.	"	facet.		-	-	310.2L	
	16.	"	ovoid		-	-	310.0L	
	17,	'	ovoid		-	-	312.8	
	gn2 18.	group	ovoid		-	-	236.6L	

SAMPLE.			DESCRIPTION. occur.	shape.	Tm,ice °C(%NaCl)	Tm,hyd °C(%NaCl)	ThCO$_2$L-V °C	Th,L-V °C	COMMENTS.
		19.	"	ovoid	-7.1(10.7)	-	-	303.1L	
		20.	"	elong.		-	-	249.9L	
		21.	"	facet.	-7.2(10.8)	-	-	298.2L	
		22.	"	irreg.		-	-	213.8L	
		23.	"	irreg.		-	-	244.1L	
		24.	"	ovoid	-7.1(10.7)	-	-	299.7L	
		25.	"	wedge		-	-	281.8L	
		26.	group	facet.		-	-	270.8L	
		27.	"	irreg.		-	-	278.7L	
	gn3	29.	group	facet.		-	-	314.1L	
		30.	"	elong.		-	-	273.8L	
		31.	"	wedge		-	-	272.5L	
		32.	"	ovoid		-	-	293.9L	
Fl, II	gn1	33.	isol.	ovoid	-6.8(10.3)	-	-	326.5L	
		34.	isol.	facet.	-6.6(10.0)	-	-	303.5L	
	gn2	35.	isol.	irreg.		-	-	281.5L	
		36.	isol.	ovoid		-	-	295.2L	
Fl, II	gn1	37.	isol.	facet.		-	-	374.5L	1x.
		38.	group	elong.		-	-	375.9L	
		39.	"	elong.		-	-	324.6L	
		40.	isol.	xtal.		-	-	349.6L	
		41.	group	facet.		-	-	350.1L	
		42.	"	facet.	-9.5(13.5)	-	-	364.3L	
		43.	isol.	facet.	-9.3(13.3)	-	-	365.4L	
		44.	isol.	irreg.	-7.2(10.8)	-	-	343.9L	
		45.	isol.	ovoid	-7.5(11.2)	-	-	346.1L	
		46.	isol.	xtal.	-7.4(11.1)	-	-	327.8L	
		47.	isol.	facet.		-	-	365.9L	
		48.	isol.	facet		-	-	396.5L	
	gn2	49.	isol.	irreg.		-	-	348.6L	
		50.	isol.	ovoid		-	-	349.1L	

SAMPLE.		DESCRIPTION. Occur.	shape.	Tm,ice °C(%NaCl)	Tm,hyd °C(%NaCl)	ThCO$_2$,L-V °C	Th,L-V °C	COMMENTS.
	51.	isol.	facet.	-8.2(12.0)	-	-	353.1	
	52.	isol.	facet.		-	-	358.7	
Qtz, II	53.	isol.	facet.	-8.0(11.8)	-	-	343.1	
	54.	isol.	facet.		-	-	313.0	
Fl, II?	55.	plan.	irreg.	-8.5(12.4)	7.4(5.3)	28.5Cr	264.7L	Tn,hyd-28.8;Tn,ice-45.9.
	56.	"	elong.	-10.0(14.1)	7.1(5.8)	28.4Cr	207.1G	Tn,hyd-35.4:Tn,ice-43.0.
	57.	"	irreg.	-8.6(12.5)	7.4(5.3)	28.9G	267.4L	Tn,hyd-35.3;Tn,ice-45.0.
	58.	"	elong.	-9.2(13.2)	7.4(5.3)	26.8G	177.2G	Tn,hyd-33.3;Tn,ice-43.2.
	59.	"	ovoid				287.2L	
	60.	"	elong.			26.8L		
	61.	"	elong.			28.7G	207.1G	
	62.	"	irreg.			27.9L	207.1G	
	63.	plan.	irreg.				274.4L	CO_2L obs.
	64.	"	irreg.				301.7L	CO_2L obs.
	65.	"	ovoid		-	-	280.1L	
	66.	"	elong.				285.5L	CO_2L obs.
	67.	"	elong.				284.4L	CO_2L
	68.	"	ovoid				278.9L	CO_2L
	69.	"	facet.		-	-	288.5L	
	70.	"	facet.		-	-	283.7L	
Fl, II	71.	plan.S	facet.	-7.7(11.4)	-	-	220.9L	
	72.	"	elong.	-7.7(11.4)	-	-	195.7L	
	73.	"	facet.	-7.8(11.5)	-	-	205.4L	
	74.	"	facet.	-8.7(12.6)	-	-	191.6L	
	75.	"	facet.	-8.0(11.8)	-	-	172.3L	
	76.	"	elong.		-	-	144.8L	
	77.	"	elong.		-	-	150.1L	
	78.	"	elong.		-	-	164.8L	
	79.	"	facet.		-	-	190.6L	
	80.	"	facet.		-	-	210.7L	
	81.	"	elong.		-	-	201.4L	

SAMPLE.		DESCRIPTION. occur.	shape.	Tm,ice °C(%NaCl)	Tm,hyd °C(%NaCl)	ThCO$_2$,L-V °C	Th,L-V °C	COMMENTS.
	82.	"	irreg.		-	-	252.9L	
	83.	"	elong.		-	-	218.4L	
	84.	"	facet.		-	-	181.2L	
	85.	"	facet.		-	-	227.4L	
	86.	"	facet.		-	-	238.3L	
	87.	"	ovoid		-	-	196.3L	
	88.	"	irreg.		-	-	194.9L	
Qtz, II	89.	isol.	facet.	-6.4(9.8)	-	-	329.7L	
	90.	isol.	elong.		-	-	322.3L	
	91.	plan.	xtal.	-9.2(13.2)			280.6L	d.n.?
	92.	"	ovoid	-9.1(13.1)			292.9L	d.n.?
	93.	"	ovoid	-10.0(14.1)			293.9L	d.n.?
	94,	"	ovoid	-9.1(13.1)			293.9L	d.n.?
	95.	"	facet.		-	-	291.6L	
	96.	"	facet.	-9.1(13.1)	-	-	281.7L	
	97.	"	facet.	-8.6(12.5)			278.8L	CO_2L (?)
	98.	"	elong.		-	-	282.7L	
	99.	"	elong.		-	-	296.2L	
	100.	"	facet.		-	-	298.7L	
Qtz,II gnl	101	isol.	facet.		-	-	298.1L	
	102	plan.S	irreg.		-	-	205.2L	
	103	"	elong.		-	-	234.6L	
	104.	"	facet.		-	-	246.8L	
	105.	"	facet.	-6.9(10.4)	-	-	224.8L	
	106.	"	irreg.		-	-	245.6L	
	107.	"	ovoid	-6.9(10.4)	-	-	246.5l	
	108.	"	ovoid		-	-	259.4L	
	109.	"	elong.		-	-	258.5L	
	110.	"	facet.		-	-	241.0L	
	111.	"	facet.		-	-	223.5L	
	112.	"	facet.		-	-	232.6L	

SAMPLE.			DESCRIPTION occur.	shape.	Tm,ice °C(%NaCl)	Tm,hyd °C(%NaCl)	$ThCO_2$,L-V °C	Th,L-V °C	COMMENTS.
		113.	"	ovoid	-6.9(10.4)	-	-	238.7L	
		114.	"	ovoid		-	-	251.9L	
		115.	"	elong.		-	-	224.5L	
		116.	"	elong.		-	-	201.2L	
	gn2	117.	plan.S	ovoid		-	-	258.4L	
		118.	"	ovoid		-	-	260.4L	
		119.	"	ovoid		-	-	259.5L	
		120.	"	facet		-	-	257.0L	
		121.	"	facet.		-	-	251.3L	
		122.		elong.	-6.6(10.0)	-	-	240.1L	
		123.	"	elong.	-6.6(10.0)	-	-	250.4L	
		124.	"	facet.	-6.7(10.2)	-	-	248.0L	
		125.	"	facet.		-	-	245.2L	lx.
		126.	"	elong.	-6.7(10.2)	-	-	251.5L	
		127.	"	ovoid	-6.7(10.2)	-	-	251.1L	
		128.	"	facet.		-	-	225.6L	
		129.	"	elong.		-	-	229.9L	
104346.									
Qtz, II		1.	isol.	facet.	-8.5(12.4)	-	-	329.7L	
		2.	isol.	xtal.	-8.6(12.5)	-	-	326.4L	
		3.	isol.	ovoid		-	-	329.0L	
		4.	isol.	elong.		-	-	338.9L	
		5.	isol.	ovoid		-	-	340.9L	
		6.	isol.	xtal.		-	-	348.1L	
		7.	isol.	xtal.		-	-	344.8L	
Qtz, II		8.	group	ovoid		-	-	300.8L	
		9.	"	elong.		-	-	305.9L	
Fl,II	gn1	10.	isol.	sol.X	-8.5(12.4)	-	-	203.1L	
	gn2	11.	isol.	sol.X		-	-	283.7L	
		12.	isol.	sol.X		-	-	332.7L	lax.
		13.	isol.	facet		-	-	299.3L	

SAMPLE.			DESCRIPTION. occur.	shape.	Tm,ice °C(%NaCl)	Tm,hyd °C(%NaCl)	$ThCO_2$,L-V °C	Th,L-V °C	COMMENTS.
		14.	isol.	sol.X		-	-	324.7L	lax.
		15.	isol.	sol.X		-	-	254.6L	laX.
		16.	isol.	sol.X		-	-	267.9L	2X.
		17.	isol.	sol.X		-	-	278.9L	2X.
Qtz,II		18.	group	elong.		-	-	314.6L	
		19.	"	facet.		-	-	315.8L	
		20.	"	ovoid		-	-	296.1L	
		21.	"	facet.		-	-	323.5L	
		22.	"	ovoid		-	-	302.9L	
		23.	"	irreg.		-	-	329.2L	
		24.	"	irreg.		-	-	298.4L	
		25.	group	ovoid		-	-	324.6L	
		26.	"	ovoid		-	-	328.4L	
104351.									
Fl,IV.	gn1	1.	isol.	facet.		-	-	140.1L	
xtal.		2.	isol.	xtal.	-7.0(10.5)	-	-	171.5L	
		3.	isol.	facet.		-	-	173.8L	
		4.	isol.	xtal.		-	-	155.3L	
	gn2	5.	isol.	xtal.	-5.2(8.2)	-	-	171.2L	
		6.	isol.	wedge	-4.3(6.2)	-	-	171.2L	
		7.	isol.	wedge	-5.3(8.3)	-	-	172.3L	
		8.	isol.	xtal.	-5.6(8.7)	-	-	171.5L	
		9.	isol.	facet.	-5.7(8.8)	-	-		
	gn3	10.	isol.	facet.	-6.1(9.4)	-	-	171.8L	
		11.	isol.	facet.	-6.1(9.4)	-	-	172.5L	
		12.	isol.	facet.	-6.2(9.5)	-	-	173.4L	tetrahedron shape.
		13.	isol.	facet.	-6.0(9.3)	-	-	177.1L	
		14.	isol.	xtal.	-6.5(9.9)	-	-	172.2L	
	gn4	15.	isol.	irreg.		-	-	171.2L	
		16.	isol.	xtal.		-	-	172.5L	
		17.	isol.	facet.		-	-	175.3L	lx.

SAMPLE.			DESCRIPTION occur.	shape.	Tm,ice °C(%NaCl)	Tm,hyd °C(%NaCl)	$ThCO_2$,L-V °C	Th,L-V °C	COMMENTS.
		18.	isol.	facet.		-	-	169.7L	tetrahedron shape.
	gn5	19.	isol.	wedge	-5.3(8.3)	-	-	163.9L	
Qtz,II	gn1	20.	groupS	ovoid	-9.7(13.7)	-	-	190.9L	
ore		21.	"	ovoid	-9.7(13.7)	-	-	187.4L	
		22.	isol.	facet.	-9.9(14.0)	-	-	372.3L	
	gn2	23.	isol.	facet.		-	-	328G.	
		24.	isol.	facet.		-	-	341.3L	
		25.	isol.	ovoid		-	-	341.2L	
		26.	isol.	facet.		-	-	339.4L	
		27.	isol.	facet.		-	-	346.6L	
Qtz,II		28.	isol.	xtal.		7.0(6.0)	-	321.5L	Tn,hyd -36?
ore		29.	isol.	xtal.		-	-	324.5L	
		30.	isol.	irreg.		-	-	289.2L	
		31.	isol.	ovoid	-8.7(12.6)	-	-		
F1, II		32.	plan.S	facet.		-	-	144.0L	
ore		33.	"	facet.	-4.7(7.5)	-	-	161.8L	
		34.	"	facet.		-	-	164.6L	
		35.	isol.	irreg.	-8.1(11.9)	-	-	320.7L	
104379.									
F1, II	gn1	1.	plan.	facet.		-	-	256.8L	
		2.	"	facet.		-	-	247.1L	
		3.	"	facet.		-	-	244.5L	
		4.	"	ovoid		-	-	257.2L	
		5.	"	facet.		-	-	263.0L	
		6.	plan.	elong.		-	-	286.8L	
		7.	"	ovoid.		-	-	294.8L	
		8.	"	ovoid		-	-	292.4L	
		9.	"	ovoid		-	-	296.0L	
	gn2	10.	group	ovoid	-6.4(9.8)	-	-	280.4L	lox.
		11.	"	facet.	-6.4(9.8)	-	-	299.9L	
		12.	"	facet.	-6.5(9.9)	-	-	325.4L	
		13.	"	facet.	-6.2(9.5)	-	-	295.1L	

SAMPLE.			DESCRIPTION. occur.	shape.	Tm,ice °C(%NaCl)	Tm,hyd °C(%NaCl)	$ThCO_2$,L-V °C	Th,L-V °C	COMMENTS.
		14.	"	facet.		-	-	305.4L	
		15.	"	ovoid		-	-	330.1L	
		16.	"	facet.		-	-	296.8L	
		17.	"	ovoid.		-	-	332.9L	
		18.	isol.	irreg.	-6.6(10.0)	-	-	261.9L	lox, lax.
		19.	"	elong.	-6.4(9.8)	-	-	296.5L	
		20.	isol.	ovoid.		-	-	284.7L	
		21.	isol.	facet.		-	-	311.1L	
		22.	isol.	ovoid	-6.2(9.5)	-	-	306.2L	
		23.	isol.	ovoid		-	-	287.4L	
		24.	isol.	ovoid	-6.2(9.5)	-	-	282.3L	
		25.	isol.	facet.		-	-	326.1L	
		26.	isol.	facet.		-	-	253.5L	
104380.									
Qtz, I		1.	isol.	facet.		-	-	288.7L	
Fl, I	gn1	2.	isol.	ovoid		-	-	298.3L	2ox.
		3.	isol.	ovoid		-	-	299.5L	2ox.
		4.	isol.	facet.		-	-	312.5L	
		5.	isol.	facet.		-	-	267.1L	2x.
		6.	plan.S	elong.		-	-	226.9L	
		7.	"	irreg.		-	-	240.3L	
		8.	"	elong.		-	-	250.5L	
		9.	"	elong.		-	-	246.3L	
Fl, I	gn1	10.	isol.	xtal.		-	-	299.8L	
		11.	isol.	facet.	-8.4(12.3)	-	-	310.9L	
	gn2	12.	group	facet.	-8.6(12.5)	-	-	319.0L	
		13.	"	facet.	-8.4(12.3)	-	-	333.0L	
		14.	"	ovoid.	-8.7(12.6)	-	-	319.5L	2x.
		15.	"	ovoid		-	-	302.4L	4x; leaked on freezing.
		16.	group	ovoid		-	-	303.3L	
		17.	"	ovoid		-	-	333.5L	

SAMPLE.			DESCRIPTION. occur.	shape.	Tm,ice °C(%NaCl)	Tm,hyd °C(%NaCl)	$ThCO_2$,L-V °C	Th,L-V °C	COMMENTS.
		18.	"	facet.		-	-	308.3L	1x.
		19.	isol.	facet.	-9.2(13.2)	-	-	295.3L	2x.
104381.									
Fl, I	gn1	1.	isol.	ovoid	-6.8(10.3)	-	-	333.4L	
		2.	isol.	ovoid		-	-	340.6L	
		3.	isol.	ovoid		-	-	341.2L	
		4.	isol.	facet.		-	-	332.9L	
		5.	isol.	facet.		-	-	328.3L	
		6.	isol.	ovoid		-	-	329.4L	
		7.	isol.	facet.		-	-	322.0L	
		8.	isol.	facet.		-	-	333.5L	
		9.	isol.	facet.	-6.4(9.8)	-	-	342.5L	
	gn2	10.	group	facet.	-7.1(10.6)	-	-	342.6L	
		11.	"	facet.		-	-	343.5L	
		12.	"	facet.		-	-	339.7L	
		13.	"	elong.		-	-	320.9L	
		14.	"	facet.		-	-	344.1L	
		15.	plan.	facet.		-	-	227.1L	
		16.	"	ovoid		-	-	213.1L	
		17.	"	ovoid		-	-	261.2L	
Qtz. I		18.	isol.	elong.		-	-	347.8L	
		19.	isol.	facet.		-	-	357.4L	
104382.									
Fl, I		1.	isol.	facet.	-7.3(10.9)	-	-	300.9L	* Fl gn adjacent to wolframite blade.
		2.	isol.	elong.		-	-	238.6L	
		3.	isol.	facet.	-8.4(12.2)	-	-	326.5L	
		4.	isol.	facet.	-7.6(11.3)	-	-	301.2L	
		5.	isol.	elong.		-	-	270.5L	
		6.	plan.	facet.		-	-	312.3L	
		7.	"	facet.		-	-	333.9L	
		8.	"	elong.		-	-	335.5L	

SAMPLE.		DESCRIPTION. occur.	shape.	Tm,ice °C(%NaCl)	Tm,hyd °C(%NaCl)	$ThCO_2$,L-V °C	Th,L-V °C	COMMENTS.
	9.	"	ovoid		-	-	342.4L	
	10.	isol.	facet.	-7.4(11.0)	-	-	313.9L	
	11.	isol.	facet.		-	-	335.9L	
	12.	isol.	irreg.		-	-	306.7L	
	13.	isol.	facet.	-7.8(11.5)	-	-	322.3L	
	14.	isol.	elong.	-8.3(12.1)	-	-	304.7L	
	15.	isol.	facet.	-7.6(11.3)	-	-	313.9L	
	16.	group	ovoid		-	-	293.1L	
	17.	"	ovoid		-	-	292.0L	
	18.	group	irreg.		-	-	305.7	
	19.	"	facet.		-	-	331.1	
	20.	isol.	facet.	-7.5(11.2)	-	-	302.1	large; no d.n.
	21.	isol.	facet.	-7.4(11.0)	-	-	285.5L	
	22.	isol.	facet.	-7.0(10.5)	-	-	246.3L	
	23.	isol.	facet.		-	-	315.6L	
Qtz, I	24.	isol.	facet.		-	-	251.8L	
	25.	isol.	facet.		-	-	342.8L	
	26	isol.	facet.	-8.1(11.9)	-	-	334.8L	
	27.	isol.	elong.	-8.7(12.6)	-	-	339.9L	
	28.	group	facet.		-	-	230.0G	
	29.	"	elong.		-	-	334.9L	
	30.	"	facet.		-	-	280.6L	
	31.	"	elong.	-9.1(13.1)	-	-	336.4L	
	32.	"	facet.		-	-	354.8L	
	33.	"	elong.		-	-	297.1L	
	34.	isol.	elong.	-7.4(11.0)	-	-	313.7L	
104388.								
F1, II	1.	group	facet.		-	-	238.3L	lix.
	2.	"	facet.		-	-	126.9L	lax; laX, green, high relief, rhomb.

SAMPLE.		DESCRIPTION. occur.	shape.	Tm,ice °C(%NaCl)	Tm,hyd °C(%NaCl)	$ThCO_2$,L-V °C	Th,L-V °C	COMMENTS.
	3.	"	xtal.		-	-	126.6L	laX.green,high relief, rhomb;At319.2°C bubble reappeared with Th,L-V 324.2 G.
	4.	"	xtal.		-	-	134.6L	2ax; loX
	5.	"	facet.		-	-	137.0L	laX,green, high relief, rhomb.
	6.	"	irreg.		-	-	137.4L	laX,green, high relief.
Fl, II	7.	group	xtal.		-	-	123.3L	laX.
	8.	"	facet.		-	-	147.9L	laX.
	9.	"	facet.		-	-	147.1L	
	10.	isol.	irreg.	-5.6(8.7)	-	-	255.9L	laX,green, high relief; liX, rhomb.
Qtz, II	11.	isol.	facet.		-	-	176.2L	laX,green, high relief; liX,cube?; liX; liX, low relief, cubic.
	12.	isol.	facet.		-	-	209.8L	lx, lX.
Fl, II	13.	group	facet.		-	-	225.3L	2X.
	14.	"	irreg.		-	-	191.0L	1X.
	15.	"	irreg.		-	-	199.6L	laX,green, high relief, cubic.
	16.	group	irreg.	-4.5(7.2)	-	-	204.0L	laX; 2iX, low relief.
	17.	"	irreg.	-4.4(7.0)	-	-		lox; laX,green,high relief.
	18.	"	facet.		-	-	218.5L	2X.
104395.								
Qtz, II gnl	1.	isol.	facet.		-	-	361.4L	Inclusions 1-16 all very small (5-10 μm).
	2.	isol.	ovoid		-	-	359.0L	
	3.	isol.	ovoid		-	-	415.2Cr	
	4.	isol.	facet.		-	-	365.9L	
	5.	plan.	ovoid		-	-	286.4L	
	6.	"	facet.		-	-	284.4G	

SAMPLE.		DESCRIPTION. occur.	shape.	Tm,ice °C(%NaCl)	Tm,hyd °C(%NaCl)	$ThCO_2$,L-V °C	Th,L-V °C	COMMENTS.
	7.	group	irreg.		-	-	337.8L	
	8.	"			-	-	323.6L	
	9.	isol.	facet.		-	-	373.9L	
	10.	isol.	facet.		-	-	395.8Cr	
	11.	group	facet.		-	-	365.1L	
	12.	"	ovoid		-	-	361.7L	
	13.	"	facet.		-	-	410.6Cr	
gn2	14.	group	facet.		-	-	323.7L	
	15.	"	facet.		-	-	331.4L	
	16.	"	facet.		-	-	362.0L	
Sid, IV?	17.	isol.	xtal.	-9.2(13.2)	-	-	221.4L	* Sid in interstices of quartz I
	18.	isol.	xtal.	-6.9(10.4)	-	-	143.1L	
	19.	isol.	xtal.		-	-	222.1L	
	20.	isol.	xtal.		-	-	155.2L	
	21.	isol.	xtal.		-	-	214.4L	
104396.								
F1, II	1.	isol.	irreg.		-	-	254.7L	
	2.	isol.	facet.		-	-	276.9L	1X.
	3.	isol.	facet.		-	-	299.4L	
	4.	isol.	ovoid		-	-	317.0L	
	5.	plan.	facet.	-7.0(10.5)	-	-	281.7L	
	6.	plan.	elong.	-5.9(9.2)	-	-	309.8L	
	7.	"	ovoid		-	-	300.1L	
	8.	plan.	facet.		-	-	317.0L	1x, red flake (hematite?)
	9.	"	ovoid		-	-	349.3L	
	10.	"	ovoid		-	-	358.3L	
	11.	"	elong.		-	-	353.7L	
	12.	"	ovoid		-	-	348.9L	
	13.	isol.	facet.		-	-	297.2L	
	14.	isol.	ovoid		-	-	358.7L	
F1, II	15.	group	irreg.	-6.3(9.7)	8.1(3.9)	25.9L	leaked	lax; lix; lox.

SAMPLE.			DESCRIPTION. occur.	shape.	Tm,ice °C(%NaCl)	Tm,hyd °C(%NaCl)	ThCO$_2$,L-V °C	Th,L-V °C	COMMENTS.
Qtz, II		16.	group	irreg.	-7.6(11.3)	7.6(4.9)	27.9L	?150G	lox; Tn, hyd 34.5; Tn, ice 43.8.
Fl, II		17.	isol.	irreg.	-5.5(8.6)			240.9L	Thin rim CO$_2$L.
		18.	group	irreg.			28.1L	leaked	lax, lix.
		19.	"	irreg.	-6.9(10.4)	8.3(3.5)	27.3Cr	leaked	lx; Tn, hyd -37.5: Tn, ice -51.6.
104397.									
Fl, II		1.	isol.	xtal.	-6.9(10.4)	-	-	354.4L	
		2.	isol.	xtal.	-6.8(10.3)	-	-	354.9L	
Qtz, II		3.	group	sol.X		-	-	264.2L	2X.
		4.	"	sol.X		-	-	227.9L	1X.
		5.	group	irreg.		-	-	340.4L	1X.
		6.	"	irreg.		-	-	347.9L	1X.
Fl, II	gn1	7.	isol.	irreg.	-8.0(11.8)		27.1Cr	?160G	Rare.
		8.	isol.	irreg.	-8.7(12.6)	-	-	leaked	No CO$_2$L obs; no d.n.
		9.	group	facet.	-7.3(10.9)	-	-	297.8L	
		10.	"	ovoid		-	-	368.4L	1x.
		11.	"	ovoid		-	-	334.7L	
		12.	"	facet.		-	-	354.7L	
		13.	"	irreg.		-	-	361.6L	
		14.	"	elong.		-	-	330.7L	2x.
		15.	"	facet.		-	-	359.6L	
		16.	"	ovoid		-	-	358.4L	1x.
		17.	isol.	facet.	-6.3(9.7)	-	-	347.0L	
		18.	isol.	ovoid	-6.1(9.4)	-	-	352.4L	
		19.	isol.	ovoid	-6.8(10.3)	-	-		} Chip shattered on heating.
		20.	isol.	ovoid	-6.9(10.4)	-	-		}
	gn2	21.	isol.	facet.	-7.6(11.3)	-	-	340.4L	1x.
		22.	isol.	facet.		-	-	344.3L	
	gn3	23.	isol.	ovoid	-5.7(8.9)	-	-	341.3L	1x.
		24.	isol.	sol.X	-5.0(7.9)	-	-	344.9L	1x.

SAMPLE.		DESCRIPTION. occur.	shape.	Tm,ice °C(%NaCl)	Tm,hyd °C(%NaCl)	ThCO$_2$L-V °C	Th,L-V °C	COMMENTS.
	25.	isol.	ovoid	-6.4(9.8)	-	-	301.1L	1x.
	26.	isol.	irreg.		-	-	347.7L	several x.
F1, II	gn1 27.	plan.	ovoid		-	-	338.7L	
	28.	"	ovoid		-	-	349.0L	
	29.	"	ovoid		-	-	352.6L	
	30.	"	facet.		-	-	351.2L	
	31.	"	facet.		-	-	349.4L	
	32.	plan.	ovoid		-	-	348.8L	
	33.	"	facet.		-	-	351.9L	
	34.	"	facet.		-	-	354.8L	
	35.	"	ovoid		-	-	346.9L	
	36.	"	ovoid		-	-	354.1L	
	37.	isol.	ovoid		-	-	339.2L	
	38.	isol.	ovoid		-	-	341.0L	
	39.	plan.	facet.		-	-	342.3L	
	40.	"	facet.		-	-	345.0L	
	41.	plan.	ovoid		-	-	342.0L	
	42.	"	ovoid		-	-	348.1L	
	43.	"	ovoid		-	-	341.8L	
	44.	"	ovoid		-	-	350.7L	
	45.	"	ovoid		-	-	347.4L	
	gn2 46.	isol.	facet.		-	-	317.6L	
	47.	isol.	facet.		-	-	333.4L	
	gn3 48.	isol.	sol.X		-	-	198.7L	1x.
	49.	isol.S	irreg.		-	-	203.8L	
	50.	isol.S	irreg.		-	-	228.4L	
	51.	plan.	ovoid		-	-	342.8L	
	52.	"	facet.		-	-	318.9L	
	53.	"	ovoid		-	-	292.9L	
	54.	"	facet.		-	-	347.9L	several x.
	55.	"	ovoid		-	-	357.2L	

SAMPLE.		DESCRIPTION. occur.	shape.	Tm,ice °C(%NaCl)	Tm,hyd °C(%NaCl)	ThCO$_2$,L-V °C	Th,L-V °C	COMMENTS.
	56.	"	ovoid		-	-	352.5L	
	57.	"	ovoid		-	-	369.3L	
	58.	"	ovoid		-	-	367.4L	pierced by tourmaline needle.
	59.	"	ovoid		-	-	371.3L	
	60.	"	ovoid		-	-	364.4L	
104399.								
	1.	group	irreg.			24.8L	384.4L	Th, L-V rapid.
	2.	"	irreg.			26.2L	?193G	
	3.	"	irreg.			22.5L	?164G	
104401.								
Fl, II	1.	group	ovoid.		-	-	199.1L	lox.
lode	2.	"	facet.		-	-	267.9L	
	3.	"	sol.X		-	-	265.4L	
Fl.	4.	group	ovoid		-	-	317.8L	
veinlet	5.	"	facet.		-	-	352.1L	
	6.	"	facet.		-	-	317.8L	
Fl, II	7.	group	ovoid		-	-	306.7L	
lode	8.	"	ovoid		-	-	301.4L	
	9.	"	ovoid		-	-	314.2L	
	10.	"	elong.		-	-	256.8L	
	11.	"	ovoid		-	-	259.3L	
	12.	"	facet.		-	-	323.6L	
	13.	"	ovoid		-	-	322.6L	
104402.								
Fl, II	gnl 1.	isol.	facet.	-7.5(11.2)	-	-	374.0L	lox.
	2.	plan.S	irreg.		-	-	138.2L	
	3.	isol.	facet.	-7.9(11.7)	-	-	310.3L	
	4.	isol.	ovoid	-7.0(10.5)	-	-	318.8L	
	5.	isol.	facet.	-6.5(9.9)			307.3L	Hydrate obs?
	6.	isol.	facet.	-6.6(10.0)			287.4L	Hydrate obs?

SAMPLE.	DESCRIPTION. occur.	shape.	Tm,ice °C(%NaCl)	Tm,hyd °C(%NaCl)	$ThCO_2$,L-V °C	Th,L-V °C	COMMENTS.
gn2 7.	isol.	elong.	-6.8(10.3)	8.9(2.3)		290.5L	Tn,hyd -32.5:Tn,ice,-36.9: No CO_2L.
gn3 8.	isol.	irreg.		-	-	278.3L	
9.	plan.	ovoid		-	-	328.1L	
10.	"	ovoid		-	-	323.6L	
11.	"	ovoid		-	-	343.6L	
12.	"	elong.		-	-	333.2L	
13.	plan.S	irreg.		-	-	264.9L	
14.	"	irreg.		-	-	267.1L	
15.	plan.	ovoid		-	-	338.4L	
16.	"	ovoid		-	-	341.9L	
17.	"	ovoid		-	-	344.6L	
18.	"	ovoid		-	-	346.7L	
gn4 19.	isol.	elong.		-	-	304.6L	
20.	group	facet.		-	-	231.7L	
21.	"	ovoid		-	-	235.2L	
22.	"	irreg.				338.7L	CO_2L phase obs?
23.	"	irreg.		-	-	305.9L	
gn5 24.	isol.	irreg.	-6.7(10.2)			283.1L	Tn,hyd -32.8;Tn,ice -44.1.
25.	isol.	xtal.				283.1L	Hydrate obs; d.n.
26.	isol.	irreg.		-	-	283.1L	
27.	isol.	xtal.	-6.6(10.0)			328.4L	d.n.
28.	isol.	elong.		-	-	290.1L	
gn6 29.	isol.	facet.		-	-	252.2L	
30.	isol.	ovoid		-	-	323.5L	
31.	isol.	elong.		-	-	308.9L	
gn7 32.	isol.	irreg.		-	-	286.1L	adjacent to plan.S.
33.	plan.	elong.		-	-	254.0L	
34.	group	facet.	-5.6(8.7)	-	-	335.3L	
35.	"	ovoid	-6.1(9.4)	-	-	312.2L	
36.	isol.	irreg.		-	-	251.1L	2x.

SAMPLE.			DESCRIPTION. occur.	shape.	Tm,ice °C(%NaCl)	Tm,hyd °C(%NaCl)	ThCO$_2$,L-V °C	Th,L-V °C	COMMENTS.
	gn8	37.	isol.	irreg.	-7.9(11.7)	7.9(4.3)	28.4G	212.3L	lax; lix; Tn,hyd -31.9; Tn,ice -47.4.
		38.	isol.	irreg.				286.4	CO$_2$L; Th, L-V rapid.
		39.	isol.	ovoid	-5.9(9.2)	-	-	325.7L	
		40.	isol.	ovoid		-	-	327.2L	
104413. F1, II	gn1	1.	group	irreg.		-	-	294.6L	
		2.	"	xtal.	-9.7(13.7)			293.6L	d.n.
		3.	"	irreg.		-	-	290.8L	
		4.	"	facet.	-10.3(14.4)	-	-	300.8L	
		5.	isol.	irreg.	-7.8(11.5)			299.4L	d.n.; lx, red flake (hematite?)
		6.	group	irreg.	-7.5(11.2)			287.0L	d.n.
		7.	"	ovoid	-7.9(11.7)			295.4L	d.n.
		8.	"	irreg.	-8.0(11.8)			262.6L	d.n.
	gn2	9.	isol.	facet.		-	-	308.3L	
		10.	isol.	irreg.		-	-	261.7L	CO$_2$L
		11.	group	facet.	-9.0(12.9)	-	-	322.2L	
		12.	"	facet.	-7.6(11.3)	-	-	322.5L	
		13.	"	facet.	-9.0(12.9)			290.5L	d.n.
		14.	"	ovoid	-8.5(12.4)	7.2(5.6)		256.4L	lox; lx; Tm,hyd -34.9: Tm,ice -56.2.
		15.	"	facet.		-	-	273.1L	lox; 2x.
		16.	"	irreg.		-	-	267.6L	lax; lox.
		17.	"	facet.		-	-	316.8L	
		18.	"	irreg.		-	-	281.7L	
		19.	"	facet.		-	-	317.3L	
	gn3	20.	plan.	ovoid		-	-	327.0L	
		21.	"	irreg.		-	-	268.2L	CO$_2$L?
		22.	"	irreg.		-	-	263.0L	CO$_2$L?
		23.	"	facet.		6.7(6.5)		289.1L	lax; lox; Tm hyd -40.0: Tm, ice -53.7: No CO$_2$L.

SAMPLE.		DESCRIPTION. occur.	shape.	Tm,ice °C(%NaCl)	Tm,hyd °C(%NaCl)	ThCO$_2$L-V °C	Th,L-V °C	COMMENTS.
	24.	"	ovoid	-9.3(13.3)			292.4L	Tm,hyd -40.0; Tm,ice -58.8; NoCO$_2$L.
	25.	"	irreg.		-	-	313.5L	
	26.	group	irreg.		-	-	317.3L	
	27.	"	facet.		-	-	334.5L	
104419.								
F1, II	1.	plan.	irreg.	-7.2(10.8)	-	-	128.9L	2ax; laX.
ore	2.	"	elong.	-7.4(11.0)	-	-	149.5L	lax; lox; laX.
	3.	"	elong.		-	-	138.3L	
	4.	"	elong.	-7.4(11.0)	-	-	166.9L	laX.
	5.	"	irreg.	-7.5(11.1)	-	-	133.0L	laX; liX.
	6.	"	irreg.	-7.3(10.9)	-	-	123.7L	laX; liX.
	7.	"	irreg.	-7.2(10.8)	-	-	139.6L	laX; liX.
	8.	"	elong.	-7.1(10.7)	-	-	123.7L	lox; laX, liX.
	9.	"	irreg.		-	-	131.6L	liX.
	10.	"	irreg.		-	-	141.0L	liX.
	11.	"	facet.		-	-	175.4L	liX.
F1, IV?	12.	plan.	facet.		-	-	137.7L	
vein.	13.	isol.	irreg.		-	-	140.2L	
	14.	plan.	irreg.		-	-	193.5L	laX.
104422.								
F1, II	1.	group	irreg.			24.8L	?150G	
	2.	"	irreg.			25.7L	267.3L	
	3.	"	irreg.		7.7(4.7)	31.0L	275.2L	Tm,hyd -43.3;Tm,ice -54.2.
	4.	"	irreg.			24.5L	252Dec.	lx.
	5.	group	ovoid		-	-	308.7L	
	6.	"	ovoid		-	-	291.9L	
	7.	"	ovoid		-	-	318.5L	
	8.	"	facet.		-	-	319.4L	
	9.	isol.	elong.		-	-	287.9L	
	10.	isol.	facet.		-	-	320.4L	
	11.	isol.	irreg.		7.8(4.6)	31.1Cr	284.2L	Tm,hyd -37.5;Tm,ice -54.0.

SAMPLE.		DESCRIPTION. occur.	shape.	Tm,ice °C(%NaCl)	Tm,hyd °C(%NaCl)	ThCO$_2$,L-V °C	Th,L-V °C	COMMENTS.
	12.	isol.	irreg.				243.4L	
	13.	isol.	irreg.				263.5L	
104423.								
F1, II	1.	group	irreg.	-6.3(9.7)	8.1(3.9)	25.4L		2x; lax,prismatic; Tm,hyd -30;Tm,ice -43.1; Vol % (at 20°C) L,CO_2=15 G, CO_2=7; XCO_2=0.11.
	2.	"	irreg.	-6.2(9.5)	8.7(2.7)	24.1L		1x; Tm,hyd -31.5; Tm, ice -42.5.
	3.	"	irreg.	-6.0(9.3)	8.8(2.5)	26.4L		Tm, hyd -30.6;Tm,ice -36; Vol % (at 23°C) L,CO_2=11.3; G,CO_2=3.0; XCO_2= 0.08
	4.	"	irreg.	-6.2(9.5)	9.0(2.1)	25.6L		
	5.	"	irreg.	-6.7(10.2)	9.1(2.0)	25.3L		Tm,hyd -37.5; Tm ice -35.
	6.	plan.	irreg.	-6.2(9.5)	7.8(4.6)			CO_2L.
	7.	"	facet.	-7.1(10.6)	8.7(2.7)			2x; Tm,hyd -30.2; Tm,ice -39.4.
	8.	"	facet.	-6.7(10.2)				Tm,hyd -30.4; Tm,ice -49.7.
	9.	"	irreg.		9.2(1.8)			Tm,hyd -31.5;Tm,ice -38.9.
F1, II	10.	group	facet.			28.3L	247.8L	
	11.	"	facet.	-7.3(10.9)		27.0L	?180G	
	12.	"	facet.	-6.2(9.5)			?177G	CO_2L.
	13.	"	ovoid			27.9L	244.5L	
	14.	"	irreg.			24.6L	?170G	
	15.	"	ovoid			24.3L	?170G	CO_2 hyd. detected.
	16.	"	irreg.			28.8L	254.3L	CO_2 hyd. detected.
	17.	"	elong.			25.8L	243.8L	CO_2 hyd. detected.
	18.	"	ovoid	-7.9(11.6)		24.0L	242.6L	
	19.	"	irreg.			23.0L		
F1, II gnl	20.	group	xtal.	-6.6(10.1)	8.8(2.5)	27.9L	249.2L	Tm,hyd -30.2;Tm,ice -49.0.
	21.	"	elong.	-6.9(10.4)	8.6(3.0)	27.6L	245.8L	Tm,hyd -33.2;Tm,ice -46.4.

SAMPLE.		DESCRIPTION. occur.	shape.	Tm,ice °C(%NaCl)	Tm,hyd °C(%NaCl)	$ThCO_2$,L-V °C	Th,L-V °C	COMMENTS.
	22.	"	facet.	-7.5(11.2)	8.5(3.2)	28.2L	248.5L	Tm,hyd -34.7; Tm,ice -42.7.
	23.	"	ovoid			28.7L	248.3L	Tm,hyd/ice -34.7.
	24.	"	facet.	-7.3(10.9)	8.6(3.0)	27.8L	245.5L	Tm,hyd -33.9;Tm, ice -49.8.
	25.	"	facet.	-7.4(11.0)	8.6(3.0)	28.4L	248.9L	Tm,hyd -34.5;Tm,ice -48.3
	26.	"	ovoid			29.4L	247.9L	Tm,hyd -33.5;Tm,ice -47.6.
	27.	"	irreg.			29.7L	252.2L	Tm,hyd -33.5;Tm,ice -46.6.
	28.	"	elong.	-6.4(9.8)	8.6(3.0)	28.7L	251.2L	Tm,hyd -32.3;Tm,ice -48.7.
gn2	29.	plan.	facet.		-	-	249.5L	
	30.	"	facet.		-	-	264.6L	
	31.	"	elong.		-	-	271.7L	
	32.	"	facet.		-	-	285.5L	
	33.	"	ovoid		-	-	306.6L	
	34.	"	ovoid		-	-	298.3L	
	35.	"	facet.		-	-	322.8L	
	36.	"	ovoid		-	-	324.6L	
	37.	"	xtal.		-	-	296.9L	
	38.	"	facet.		-	-	308.9L	
	39.	"	xtal.		-	-	299.9L	
Apat. II	40.	isol.	ovoid		-	-	286L	* solid grain included in fluorite.
F1, II	41.	isol.	facet.	-7.6(11.3)	-	-	295.6L	* Same grain as contains opatite grain (incl.40).
F1, II	42.	isol.	sol.X	-5.9(9.1)	-	-	191.2L	
	43.	isol.	elong.	-9.2(13.2)	8.0(4.1)	30.3Cr	258.0L	lax; lox; Tm,hyd -35.5; Tm,ice -51.5.
	44.	isol.	facet.	-8.4(12.2)	8.0(4.1)	29.8L	247.7L	2ox; Tm,hyd -35.1; Tm,ice -51.4.
	45.	isol.	facet.			29.8G	246.7L	
	46.	isol.			-	-	254.9L	
F1, II	47.	isol.	ovoid		-	-	304.9L	
	48.	isol.	irreg.		-	-	303.4L	

SAMPLE.			DESCRIPTION. Occur.	shape.	Tm,ice °C(%NaCl)	Tm,hyd °C(%NaCl)	$ThCO_2$,L-V °C	Th,L-V °C	COMMENTS.
Apat., II		49.	group	facet.		-	-	321.2L	* Solid grain in fluorite
		50.	"	facet.		-	-	311.7L	containing inclusions
									47 and 48.
104427.									
Fl, I	gnl	1.	group	irreg.		-	-	185.9L	
		2.	"	ovoid		-	-	234.7L	
		3.	"	facet.		-	-	262.8L	1x.
		4.	"	facet.		-	-	261.9L	
		5.	"	facet.		-	-	297.3L	
		6.	"	ovoid		-	-	321.6L	
	gn2	7.	isol.	facet.		-	-	294.0L	
		8.	isol.	ovoid		-	-	326.3L	
	gn3	9.	group	facet.		-	-	283.7L	
		10.	"	ovoid		-	-	318.7L	
		11.	"	ovoid		-	-	304.9L	
		12.	"	ovoid		-	-	304.5L	
		13.	"	ovoid		-	-	325.2L	
		14.	"	ovoid		-	-	326.8L	
	gn4	15.	plan.S	elong.			28.9Cr	?210G	Th rapid just before
		16.	"	irreg.			29.4Cr	?115G	homog. to G.
		17.	"	irreg.			27.2L	?188G	
		18.	"	irreg.				210.5L	
		19.	"	elong.			27.0L	190.4L	
		20.	isol.	irreg.		-	-	263.0L	
		21.	isol.	sol.X		-	-	298.7L	
		22.	isol.	elong.		-	-	295.8L	
		23.	iaol.	irreg.		-	-	275.9	
		24.	isol.	xtal.		-	-	276.3	
Qtz		25.	isol.	elong.		-	-	285.5	* Adjacent to wolframite
									blade.
104429.									
Fl, IV	gnl	1.	isol.	wedge	-4.7(7.5)	-	-	132.2L	

SAMPLE.			DESCRIPTION. occur.	shape.	Tm,ice °C(%NaCl)	Tm,hyd °C(%NaCl)	$ThCO_2$,L-V °C	Th,L-V °C	COMMENTS.
		2.	isol.	needle	ms.	-	-	133.2L	
		3.	isol.	facet.	ms.	-	-	119.1L	
		4.	isol.	facet.	ms.	-	-	145.9L	
		5.	isol.	needle	ms.	-	-	176.2L	
	gn2	6.	isol.	irreg.	ms.	-	-	133.4L	
		7.	group	needle	ms.	-	-	124.4L	
		8.	"	irreg.	-5.2(8.2)	-	-	136.3L	
104430.									
F1, IV		1.	isol.	irreg.	ms.	-	-	127.7L	
		2.	isol.	facet.		-	-	137.7L	
		3.	isol.	irreg.		-	-	166.3L	
		4.	isol.	wedge	-15.8(19.5)	-	-	190.7L	
		5.	isol.	wedge.	ms.	-	-	134.3L	
		6.	isol.	facet.		-	-	126.6L	
		7.	isol.	facet.	ms.	-	-	137.1L	
104431.									
F1, IV	gn1	1.	isol.	facet.	-10.1(14.2)	-	-	165.0L	
		2.	group	needle	-9.6(13.6)	-	-	189.4L	
		3.	"	facet.	-10.1(14.2)	-	-	167.0L	
		4.	isol.	needle	-10.1(14.2)	-	-	183.5L	
		5.	isol.	irreg.	-5.3(8.3)	-	-	158.5L	
	gn2	6.	isol.	irreg.	-7.2(10.8)	-	-	160.9L	
		7.	isol.	elong.	-4.7(7.5)	-	-	159.3L	
		8.	isol.	irreg.	-7.2(10.8)	-	-	162.1L	
		9.	isol.	facet.		-	-	161.3L	
		10.	isol.	needle	-4.8(7.6)	-	-	164.6L	
		11.	isol.	irreg.		-	-	158.2L	1x.
F1, IV		12.	isol.	xtal.	-4.7(7.5)	-	-	151.6L	
		13.	isol.	irreg.		-	-	151.4L	
104448.									
F1, IV	?gn1	1.	isol.	ovoid	-8.4(12.2)	-	-	138.3L	1ox.
		2.	isol.	irreg.	-8.1(11.9)	-	-		2ax; 1ox.

SAMPLE.			DESCRIPTION. occur.	shape.	Tm,ice °C(%NaCl)	Tm,hyd °C(%NaCl)	$ThCO_2$,L-V °C	Th,L-V °C	COMMENTS.
		3.	isol.	elong.	-7.6(11.3)	-	-	200.9L	lax.
	gn2	4.	plan.	needle		-	-	121.3L	
		5.	"	needle		-	-	128.1L	
		6.	"	needle		-	-	127.8L	
104450.									
F1, II	gn1	1.	group	elong.		-	-	298.7L	
		2.	"	elong.		-	-	266.4L	1x.
		3.	"	irreg.		-	-	286.5L	
		4.	isol.	ovoid		-	-	321.4L	2X.
		5.	isol.	ovoid		-	-	330.2L	1X.
		6.	isol.	ovoid		-	-	320.7L	2X.
		7.	isol.	ovoid		-	-	323.5L	3X.
		8.	isol.	ovoid		-	-	333.0L	
	gn2	9.	isol.	irreg.		-	-	337.0L	1x.
		10.	isol.	irreg.		-	-	343.0L	1x.
		11.	isol.	elong.		-	-	328.4L	2X.
104455.									
F1, I		1.	disper.	facet.		-	-	293.0L	
		2.	"	facet.		-	-	251.0L	
		3.	"	xtal.		-	-	226.7L	
		4.	"	ovoid		-	-	270.3L	
		5.	"	irreg.		-	-	274.9L	
		6.	"	facet.		-	-	287.3L	
		7.	"	elong.		-	-	291.6L	
		8.	"	ovoid		-	-	311.7L	
		9.	group	ovoid		-	-	327.6L	
		10.	"	xtal.		-	-	319.6L	
		11.	"	elong.		-	-	321.4L	
F1, I	gn1	12.	plan.	irreg.		-	-	302.9L	
		13.	"	ovoid		-	-	339.5L	
		14.	"	irreg.		-	-	334.8L	partially necked inclusion.

SAMPLE.		DESCRIPTION. occur.	shape.	Tm,ice °C(%NaCl)	Tm,hyd °C(%NaCl)	ThCO$_2$,L-V °C	Th,L-V °C	COMMENTS.
	15.	"	ovoid		-	-	328.8L	
	16.	"	ovoid		-	-	324.8L	
	17.	"	facet.		-	-	337.9L	
	18.	"	facet.		-	-	324.5L	
	19.	"	irreg.		-	-	337.6L	
	20.	"	facet.		-	-	336.6L	
	21.	"	facet.		-	-	334.8L	
	22.	"	irreg.		-	-	330.2L	
	23.	isol.	facet.		-	-	332.8L	
gn2	24.	group	ovoid		-	-	309.3L	
	25.	"	ovoid		-	-	309.9L	
	26.	"	ovoid		-	-	315.3L	
	27.	"	irreg.		-	-	371.8L	
Fl, I	28.	plan.	ovoid			31.1Cr	295.4Cr	Vol % (at 20°C)L,CO_2=16.3 G,CO_2=48.6: XCO_2=0.3.
	29.	"	ovoid				298.7L	
	30.	"	ovoid		8.9(2.3)	31.0G	303.4L	Tm,hyd -31.6;Tm,ice -40.9; Tm CO_2 -60.5.
	31.	"	ovoid				311.3L	
	32.	"	ovoid				297.6Cr	
	33.	"	facet.			30.9Cr	301.9L	
	34.	"	ovoid			30.8G	296.9L	
	35.	"	facet.				294.7L	
	36.	"	ovoid				300.1L	
	37.	"	elong.			31.1L	296.1L	
Fl, I	38.	group	facet.		-	-	298.7L	
	39.	"	facet.		-	-	176.1L	
	40.	"	facet.		-	-	316.3L	
	41.	"	irreg.		-	-	287.5L	
	42.	"	facet.		-	-	241.6L	
	43.	"	ovoid		-	-	255.1L	

SAMPLE.		DESCRIPTION. occur.	shape.	Tm,ice °C(%NaCl)	Tm,hyd °C(%NaCl)	$ThCO_2$,L-V °C	Th,L-V °C	COMMENTS.
Fl, I	44.	isol.	facet.		-	-	297.9L	
	45.	plan.	facet.		-	-	306.2L	lox.
	46.	"	ovoid		-	-	275.8L	
	47.	"	irreg.		-	-	287.3L	lax; lix; lox.
	48.	isol.	facet.		-	-	265.0L	
	49.	isol.	facet.		-	-	285.9L	lax; lix.
	50.	group	irreg.		-	-	263.6L	
	51.	"	irreg.		-	-	274.1L	
	52.	"	ovoid		-	-	314.4L	
	53.	"	irreg.		-	-	284.7L	
Fl, I	54.	disper.	xtal.	-7.2(10.8)	-	-	351.3L	
	55.	"	facet.	-6.1(9.4)	-	-	345.3L	
	56.	"	facet.	-6.8(10.3)	-	-	313.3L	
	57.	"	ovoid	-5.7(8.9)	-	-	333.8L	lx.
	58.	"	ovoid		-	-	333.8L	
	59.	"	facet.	-5.9(9.2)	-	-	319.7L	
Fl, I	60.	group	elong.	-5.4(8.5)	8.7(2.7)		278.1L	d.n.; no $CO_2$2 phase; lax; lx, red flake(hematite)
	61.	"	ovoid	-5.1(8.0)	-	-	296.7L	2ax; lox.
	62.	"	irreg.	-5.3(8.3)	-	-	304.8L	2x.
	63.	isol.	facet.	-5.0(7.9)	-	-	289.6L	lix; lox.

TABLE A5.2 Fluid inclusion homogenization temperature data, using the University of Tasmania heating stage.

Note:

1. Abbreviations are described in Appendix 5.
2. Th, L-V is accurate to $\pm 3^{o}C$ at $150^{o}C$ and increases to $\pm 6^{o}C$ at $450^{o}C$; Th CO_2, L-V is accurate to $\pm 0,5^{o}C$.
3. All inclusions are two-phase aqueous inclusions (some with minute daughter (?) minerals) except where indicated otherwise.
4. A few freezing measurements were obtained using the Chaixmeca appartus at the University of Tasmania.
5. All temperature data have been corrected for instrumental error using experimentally determined calibration factors (Appendix 5).

SAMPLE.		DESCRIPTION. Occur.	Shape.	Th, L-V °C	COMMENTS.
104301					
Fl, II gnl xtal	1.	isol.	facet	290L	
	2.	plan	ovoid	257L	
	3.	"	ovoid	256L	
	4.	"	ovoid	256L	
	5.	"	elong.	251L	
	6.	"	ovoid	263L	
	7.	"	elong.	261L	
	8.	"	elong.	263L	
	9.	"	ovoid	261L	
gn2	10.	isol.	irreg.	276L	
	11.	isol.	facet.	305L	
	12.	isol.	facet.	296L	
	13.	plan.S	ovoid	232L	
	14.	"	elong.	239L	
	15.	"	ovoid	260L	
	16.	"	elong.	236L	
	17.	"	ovoid	234L	
gn3	18.	isol.	ovoid	291L	2ax; lox,cubic; Tm,ice @ -5.0(7.9% NaCl).
	19.	plan.S	ovoid		Tm, ice @-1.3 (2.2% NaCl).
	20.	"	ovoid		Tm, ice @-1.6 (2.6% NaCl).
gn4	21.	group	ovoid	333L	
	22.	"	irreg.	320L	
	23.	"	irreg.	330L	
	24.	"	elong.	324L	
	25.	"	ovoid	330L	
	26.	"	ovoid	331L	
	27.	"	ovoid	333L	
gn5	28.	plan.S	elong.	257L	
	29.	"	elong.	250L	
	30.		elong.	247L	
	31.	"	ovoid	239L	
	32.	"	ovoid	311L	
	33.	"	facet	236L	

SAMPLE.		DESCRIPTION. Occur.	Shape.	Th_{δ}L-V °C	COMMENTS.
	34.	"	facet	231L	
gn.6	35.	plan.S	ovoid	323L	
	36.	"	ovoid	312L	
	37.	"	ovoid	263L	
	38.	"	elong.	264L	
	39.	"	elong.	265L	
	40.	"	irreg.	267L	
	41.	"	irreg.	255L	
	42.	"	elong.	250L	
	43.	"	irreg.	261L	
	44.	"	irreg.	250L	
	45.	"	irreg.	258L	
	46.	plan.S	ovoid	167L	
	47.	"	elong.	169L	
gn7	48.	plan.S	elong.	261L	
	49.	"	elong.	269L	
	50.	"	elong.	254L	
	51.	"	elong.	254L	
	52.	isol.	xtal.	344L	Tm, ice @-6.5 (9.9% NaCl).
	53.	isol.	facet.	330L	
Fl, II	54.	group	facet.	310L	
outer xtal.	55.	"	facet.	319L	
	56.	plan.	ovoid	326L	
104307					
Fl, II	1.	plan.S?	ovoid	236L	
	2.	"	irreg.	221L	
	3.	"	ovoid	228L	
	4.	"	ovoid	231L	
	5.	"	ovoid	228L	
	6.	"	irreg.	231L	
	7.	"	elong.	225L	
	8.	"	elong.	223L	
	9.	"	irreg.	230L	
	10.	"	irreg.	219L	
	11.	"	ovoid	222L	
	12.	"	ovoid	214L	

SAMPLE.		DESCRIPTION. Occur.	Shape.	Th, L-V °C	COMMENTS.
F1, IV	13.	isol.	facet.	240L	
	14.	isol.	facet.	162L	
	15.	group	facet.	214L	
	16.	"	facet.	268L	
	17.	"	facet.	129L	
F1, II	18.	plan.S?		200L	
	19.	"		202L	
	20.	"		208L	
	21.	"		212L	
	22.	"		217L	
	23.	"		226L	
	24.	"		233L	
	25.	plan.		284L	
	26.	"		286L	
	27.	"		291L	
	28.	"		290L	
	29.	"		292L	
	30.	"		293L	
	31.	"		293L	
F1, IV	32.	plan.	facet.	136L	
	33.	"	facet.	125L	
	34.	"	facet.	139L	
	35.	plan.S.	irreg.	175L	
	36.	"	irreg.	188L	
104357.					
	1.	isol.	ovoid	324L	
	2.	isol.	facet.	307L	
	3.	isol.	irreg.	298L	
104359.					
F1. gnl	1.	plan.	irreg	134L	lax; 1 green hexag.plate (biotite ?).
	2.	isol.	irreg.	150L	2x.
	3.	isol.	irreg.	149L	Tm, ice @-7.3 (11.2% NaCl).
	4.	group	irreg.	140L	
	5.	"	facet	137L	
	6.	"	irreg.	133L	

SAMPLE.		DESCRIPTION. Occur.	Shape.	Th,L-V °C	COMMENTS.
	7.	plan.	elong.	145L	
	8.	isol.	irreg.	141L	
gn2	9.	plan.	irreg.	182G	CO_2L.
	10.	"	elong.	189L	CO_2L.
	11.	"	facet	197L	CO_2L.
	12.	"	facet.	192L	CO_2L.
	13.	"	irreg.	180G	CO_2L
	14.	"	irreg.	218L	CO_2L
	15.	isol.	facet.	233L	CO_2L
gn3	16.	plan.	facet.	220G	Th CO_2,L-V @ 28 (L); Th, L-V instant.
	17.	"	facet.	220G	Th CO_2,L-V @ 25 (L); Th, L-V instant.
	18.	"	facet.	237L	Th CO_2,L-V @ 27 (L)
	19.	"	irreg.	238L	CO_2L
	20.	"	elong.	238L	CO_2L
	21.	"	irreg.	?200G	Th CO_2,L-V @ 26 (L); Th, L-V repid.
	22.	"	irreg.	?200G	Th CO_2,L-V @ 27 (L); Th, L-V rapid.
	23.	"	irreg.	?200G	Th CO_2,L-V @ 26 (L); Th, L-V rapid.
	24.	"	irreg.	?200G	Th CO_2,L-V @ 27 (L); Th, L-V rapid.
	25.	"	ovoid	236L	CO_2L
	26	"	ovoid	237L	CO_2L
	27	"	ovoid	252L	CO_2L
	28.	"	irreg.	?175G	Th CO_2,L-V @ 24 (L); Th, L-V rapid.
	29.	"	elong.	?175G	Th CO_2,L-V @ 25 (L); Th, L-V rapid.
	30.	"	elong.	?175G	Th CO_2,L-V @ 24 (L); Th, L-V rapid.
	31.	"	irreg.	?158G	Th CO_2,L-V @ 25 (L); Th, L-V rapid.
	32.	"	irreg.	?158G	Th CO_2,L-V @ 23 (L); Th, L-V rapid.
	33.	"	irreg.	?158G	Th CO_2,L-V @ 25 (L); Th, L-V rapid.
	34.	"	irreg.	?158G	Th CO_2,L-V @ 26 (L); Th, L-V rapid.

SAMPLE.		DESCRIPTION. Occur.	Shape.	Th,L-V °C	COMMENTS.
	35.	"	irreg.	235L	Th CO_2,L-V @ 27 (L) }
	36.	"	elong.	225L	Th CO_2,L-V @ 27 (L) } #
					# Repeat determination Th CO_2,L-V after cooling gave consistent results.
	37.	plan	irreg.	241L	CO_2L.
	38.	"	irreg.	253L	CO_2L.
	39.	"	elong.	238L	CO_2L.
	40.	"	irreg.	277L	CO_2L.
	41.	"	irreg.	286L	CO_2L.
	42.	"	irreg.	279L	CO_2L.
	43.	"	elong.	285L	CO_2L.
gn4	44.	isol.	facet.	233L	Tm,ice @ -6.5(9.9% NaCl).
	45.	isol.	xtal.	288L	Tm,ice @ -6.8(10.3%NaCl).
	46.	isol.	irreg.	171L	3ax.
104413.					
F1, II gn1	1.	plan.	ovoid	218L	
	2.	"	ovoid	220L	
	3.	"	facet.	213L	
	4.	"	ovoid	222L	
	5.	"	elong.	292L	
	6.	isol.	facet.	>298L	Leaked just prior to Th.
gn2	7.	plan.S	facet.	213L	
	8.	"	elong	212L	
	9.	"	elong.	224L	
	10.	"	irreg.	239L	
	11.	plan.	ovoid	285L	
	12.	"	ovoid	291L	
	13.	isol.	facet.	275L	
104422.					
F1, II	1.	plan.		279L	
	2.	"		284L	
	3.	"		285L	
	4.	"		288L	
	5.	"		289L	
	6.	"		295L	
	7.	"		294L	

SAMPLE.		DESCRIPTION. Occur.	Shape.	Th,L-V °C	COMMENTS.
	8.	"		298L	
	9.	"		302L	
	10.	"		302L	
	11.	"		304L	
	12.	"		306L	
	13.	plan.S	ovoid	191L	
	14.	"	ovoid	193L	
	15.	"	irreg.	227L	
	16.	group		311L	
	17.	"		313L	
	18.	plan.	elong.	233L	
	19.	"	facet.	305L	
	20.	"	ovoid	300L	
	21.	group	ovoid	291L	
	22.	"	ovoid	276L	
	23.	"	ovoid	310L	
	24.	"	ovoid	312L	
	25.	"	ovoid	313L	
	26.		ovoid	313L	
104423.					
F1, II	1.	isol.	irreg.	?123G	Th CO_2,L-V @ 24 (L)
	2.	isol.	irreg.	?157G	Th CO_2,L-V @ 27 (L)
	3.	isol.	irreg.	?125G	Th CO_2,L-V @ 27 (L)
	4.	group	ovoid	250L	Adjacent to inclusion 3, No CO_2
	5.	"	elong.	248L	
	6.	"	ovoid	250L	
F1, II	7.	plan.	elong.	279L	
	8.	"	irreg.	257L	
	9.	"	ovoid	276L	
	10.	"	ovoid	315L	
	11.	"	ovoid	310L	
	12.	"	ovoid	313L	
	13.	"	facet	310L	
104429.					
F1, IV	1.	isol	xtal.	158L	

SAMPLE.		DESCRIPTION. Occur.	Shape.	Th,L-V °C	COMMENTS.
104430.					
F1, IV	1.	plan.S?	irreg.	162L	
	2.	"	irreg.	183L	
	3.	"	irreg.	200L	
	4.	"	irreg.	171L	
104431.					
F1,IV gn1	1.	plan.S?		162L	
	2.	"		162L	
	3.	"		162L	
	4.	"		164L	
	5.	"		165L	
	6.	"		166L	
gn2	7.	isol.	elong.	165L	
	8.	plan.	irreg.	179L	
	9.	isol.	irreg.	178L	
	10.	group	irreg.	174L	
	11.	"	irreg.	178L	
	12.	"	irreg.	179L	

APPENDIX 6

Stable isotope experimental methods

Stable isotope analyses of hydrothermal mineral phases and of the host rocks at the Cleveland mine were performed at the Institute of Nuclear Sciences, D.S.I.R., Lower Hutt, New Zealand.

All analyses were made by the author, except for sulphur isotopic analyses of sulphide samples 104316, 104421, 104463, 104467, 104468 and 104469, and hydrogen isotope analyses of fluid inclusion waters which were kindly undertaken by Dr B.W. Robinson and his technical staff.

Oxide minerals and silicate host rocks

Quartz, wolframite and cassiterite were hand picked from selected specimens from the various stages of mineralisation and analysed by extraction of oxygen with bromine pentafluoride and quantitative conversion to CO_2 as outlined by Clayton and Mayeda (1963), prior to mass spectrometric analysis.

Samples of the host rocks and ore were crushed and quartered several times, and a small split taken and stored. The sample was then ground to a powder immediately prior to reaction with BrF_5.

Oxygen yields of 100 ± 5% were obtained for all rock and mineral samples. The reproducibility of the $\delta^{18}O$ values for individual reaction tubes was better than ± 0.2 per mil, but since five different reaction tubes were used for the extraction, the overall reproducibility of the $\delta^{18}O$ values is ± 0.4 per mil.

The oxygen isotopic data of the country rocks are given in Table A6.1, and the oxide minerals in Table A6.2. All of the oxygen isotope anlayses are relative to the standard NBS 28 (Friedman and Gleason, 1973) with an assigned $\delta^{18}O$ value of + 9.8 per mil.

Sulphide minerals

Sulphide phases were hand picked from specimens from each stage of the mineralisation episode and at various localities within each stage.

Pyrrhotite, pyrite, chalcopyrite, arsenopyrite, marcasite, stannite and molybdenite were combusted directly and quantitatively to SO_2 by reaction with an excess of Cu_2O in a vacuum at 1000°C (Robinson and Kusakabe, 1975). Sphalerite and galena were converted to Ag_2S by an acid evolution method which involved reaction of the sulphide with warm conc. HCl (1:1 v/v) and passing the H_2S gas evolved through a slightly acidic (HNO_3) 0.1N $AgNO_3$ solution. The Ag_2S produced was cleaned with a slightly alkaline (NH_4OH) solution, dried and weighed (to check for complete reaction), and was then reacted with excess Cu_2O in a vacuum at 800°C.

For pure sulphide samples, yields of 95-100% SO_2 were obtained. However, because of its perfect cleavage molybdenite remained relatively coarse when crushed, and incomplete combustion occurred. This was overcome by grinding a mixture of molybdenite and clean quartz prior to mixing the sample with Cu_2O.

The SO_2 liberated was analysed by mass spectrometric techniques similar to those described by Hulston and Shilton (1958). The overall reproducibility of results, for the whole experimental procedure is ± 0.2 per mil.

All sulphur isotopic data are relative to the standard Canon Diablo Troilite (C.D.T.), and the results are given in Table A6.2.

Carbonate rocks and minerals

Carbonate mineral samples were hand picked, and limestone samples were crushed and quartered several times to obtain a uniform sample. A small split was taken and stored, and ground to powder immediately prior to analysis.

CO_2 was evolved by a phosphoric acid method, modified from McCrea (1950). Reaction times were 2 - 4 days for calcite, dolomite and limestone, and three weeks for siderite.

The $\delta^{18}O$ and $\delta^{13}C$ values for calcite, dolomite and limestone have a reproducibility of ± 0.2 per mil, but yields from siderite were low and reproducibility here is probably not better than ± 0.5 per mil. Kinetic fractionation factors used for correcting $\delta^{18}O$ values are the same as for Blattner and Cooper (1974).

All carbon and oxygen isotopic analyses are relative to the standard Te Kuiti Limestone with an assigned $\delta^{18}O$ value of + 26.06 per mil and $\delta^{13}C_{PDB}$ value of - 1.67 per mil. The results are given in Table A6.3. Te Kuiti Limestone data are from Craig (1957).

Inclusion fluids

Fluid was collected from fluid inclusions in one sample of stage I quartz (104428) and one sample of stage IV fluorite (104319). The samples were initially cleaned with hydrochloric acid and in an electrolytic cleaning cell, then outgassed in a sealed stainless steel tube under vacuum at 150°C. The tube was then crushed and the resulting fluid collected in an evacuated system.

Fluid extraction and collection, and mass spectrometry were undertaken by Dr B.W. Robinson and his technical staff. Yields from the two samples were sufficient to avoid any memory effect of atmospheric contamination (B.W. Robinson, *pers. comm.*).

The results are as follows:

Sample number:-	104428	104319
Mineral:-	Quartz	Fluorite
Sample mass (g):-	50	56
Fluid mass (mg):-	14.7	19.8
δD_{SMOW} (per mil):-	- 57.5	- 74.9

The quartz sample (104428) had a relatively high CO_2 pressure, but there was insufficient CO_2 for isotopic analysis. Carbon dioxide (?) was just detected in the fluorite sample (104319). Neither sample had a high non-condensible component.

REFERENCES

Blattner, P., and Cooper, A.F., 1974, Carbon and oxygen isotopic composition of carbonatite dikes and metamorphic country rock of the Haast Schist Terrain, New Zealand: Contr. Mineralogy Petrology, *44*: 17-27.

Clayton, R.N., and Mayeda, T.K., 1963, The use of bromine pentafluoride in the extraction of oxygen from oxides and silicates for isotopic analysis : Geochim. et Cosmochim. Acta, *27*: 43-52.

Craig, H., 1957, Isotopic standards for carbon and oxygen and correction factors for mass-spectrometric analysis of carbon dioxide : Geochim. et Cosmochim. Acta, *12*: 133-149.

Friedman, I., and Gleason, J.D., 1973, A new silicate intercomparison standard for ^{18}O analysis : Earth Planet.Sci.Lett., *18*: 124.

Hulston, J.R., and Shilton, W.B., 1958, Sulphur isotopic variations in nature. Part 4 - Measurements of sulphur isotopic ratio by mass spectrometry : New Zealand Jour.Sci., *1*: 91-102.

McCrea, J.M., 1950, On the isotopic chemistry of carbonates and a palaeo-temperature scale : J.Chem.Phys., *18*: 849-857.

Robinson, B.R., and Kusakabe, M., 1975, Quantitative preparation of sulfur dioxide, for $^{34}S/^{32}S$ analyses, from sulphides by combustion with cuprous oxide : Analyt. Chem., *47*: 1179-1181.

TABLE A6.1 Whole-rock oxygen isotopic composition of the host rocks, Cleveland mine.

Specimen number	Description	Distance* to ore(m)	Depth* (m.M.L.)	$\delta^{18}O_{SMOW}$ (per mil)
	Deep Creek Volcanics			
48299	Spilitic basalt	400	1435	+ 8.7
48302	Spilitic basalt	380	1390	+10.0
48309	Altered spilitic basalt	50	1150	+10.3
48317	Altered spilitic basalt	85	815	+ 9.8
48321	Altered spilitic basalt	2		+ 9.5
48327	Altered spilitic basalt	35	1230	+ 9.3
48329	Altered spilitic basalt	10	1285	+ 9.9
48330	Altered spilitic basalt	85	1300	+10.1
781299	Altered spilitic basalt	5	1320	+10.0
	Hall Formation			
48313	Greywacke	20	910	+12.0
48316	Altered spilitic basalt	10(HV)	1050	+10.2
48345	Chocolate-brown shale	0	1220(14L)	+13.1
48346	White, bleached shale/chert	0	1220(14L)	+13.7

Specimen number	Description	Distance* to ore(m)	Depth* (m,M.L.)	$\delta^{18}O_{SMOW}$ (per mil)
	Crescent Spur Sandstone			
48315	Greywacke	≥190	525	+10.0
48337	Greywacke	15	800	+11.8
48338	Greywacke	≥130	650	+12.0
48340	Greywacke	≥200	860	+12.0
48341	Greywacke	≥150	1200	+13.2
48342	Greywacke	120	940	+11.1
48343	Greywacke	10	1020	+12.3
	Intrusive rock			
48339	Basalt/dolerite dyke	≥150	1130	+10.9
48288	Altered basalt/ dolerite dyke	0	1220(14L)	+17.7

Analyst: P. L. F. Collins.

* Distance to ore, is distance of the specimen to the nearest sulphide lens. Depth is relative to the mine level (M.L.) for which 1000m is equivalent to sea level. Specimen locations are illustrated in figures 5.1 and 7.7.

HV = Henrys Volcanic Member.

TABLE A6.2 Oxygen and sulphur isotopic composition of hydrothermal minerals from the Cleveland Mine .

Specimen number	Description	Stage	Mineral	(+)$\delta^{18}O_{SMOW}$ per mil	$\delta^{34}S_{CDT}$ per mil
104378	Vein	I	Mo		+ 5.5
104382	Vein	I	Qz	+12.6	
			Wo	+ 5.5	
104428	Vein	I	Qz	+11.7	
104432	Vein	I	Qz	+12.6	
			Wo	+ 5.5	
			Mo		+ 4.3
104440	Vein	I	Qz	+12.2	
104458	Vein	I	Mo		+ 3.7
104460	Vein	I	Qz	+12.3	
			Wo	+ 5.6	
104462	Vein	I	Qz	+12.3	
104365	Vein in fault (Nadir Fault)	II	Qz	+14.4	
104366	Vein in fault (Nadir Fault)	II	Qz	+14.4	
104367	Vein in fault (Nadir Fault)	II	Po		+ 2.4
			Cp		+ 2.5
104368	Vein in fault (Nadir Fault)	II	Qz	+14.9	
			Cs	+ 5.3	
		III	Asp		+ 3.0
			St		+ 3.2
104301	Ore (Halls lenses, north)	II	Qz	+13.5	
	Vug in sulphide lens.	IV(?)	QZ	+14.3	
104305	Ore (Halls lenses, north)	II	Po		+ 3.7
104316*	Ore (Halls lenses, north)	II	Po		+ 1.9
			Cp		+ 2.5
104324	Ore (Halls lenses, north)	II	Po		+ 2.6
			Cpp		+ 2.3
			Sp		+ 2.6
104326	Ore (Halls lenses, north)	II	Po		+ 2.3

Specimen number	Description	Stage	Mineral(+)	$\delta^{18}O_{SMOW}$ per mil	$\delta^{34}S_{CDT}$ per mil
104329	Ore (Halls lenses, north)	II	Po		+ 2.7
104345	Ore (Halls lenses, north)	II	Po		+ 2.5
104363*	Ore (Halls lenses, north)	II	Po		+ 2.6
			Sp		+ 2.7
104330	Ore (Halls lens, south)	II	Po		+ 2.2
104331	Ore (Halls lens, south)	II	Po		+ 3.2
104332	Ore (Halls lens, south)	II	Qz	+13.4	
			Po		+ 2.3
104442	Ore (Halls lens, south)	II	Sp		+ 1.5
104321	Vein (Halls lens, south)	II	Qz	+15.4	
			Cp		+ 1.8
104348	Vein (Halls lens, south)	II	Qz	+13.4	
104336	Ore (Khaki lode)	II	Po		+ 2.9
104338	Ore (Khaki lode)	II	Po		+ 1.8
			Cp		+ 3.3
104341	Ore (Khaki lode)	II	Po		+ 2.1
			Cp		+ 2.0
		?	Mar.		+ 2.7
104369	Ore (Khaki lode)	II	Cs	+ 6.6	
104464	Ore (Khaki lode)	II	Sp		+ 2.2
104373	Ore (Halls lenses, lower ore)	II	Po		+ 2.4
104374	Ore (Halls lenses, lower ore)	II	WR	+ 9.6	
104376	Ore (Halls lenses, lower ore)	II	Po		+ 1.6
	Vein in sulphide lens	III	Asp		+ 4.4
104387	Ore (Halls lenses, lower ore)	II	Po		+ 2.3

Specimen number	Description	Stage	Mineral(+)	$\delta^{18}O_{SMOW}$ per mil	$\delta^{34}S_{CDT}$ per mil
104390	Ore (Halls lenses, lower ore)	II	WR	+ 8.0	
104415	Ore (Halls lenses, lower ore)	II	Po		+ 3.1
104417	Ore (Halls lenses, lower ore)	II	Po		+ 3.9
104421*	Ore (Halls lenses, lower ore)	II	Po		+ 2.2
104423	Ore (Halls lenses, lower ore)	II	Po		+ 2.6
104425	Ore (Halls lenses, lower ore)	II	Po		+ 2.4
104450	Ore (Halls lenses, lower ore)	II	Po		+ 2.4
104370	Vein,Hall Formation (northern end)	II	Asp		+ 3.3
104372	Vein,Hall Formation (northern end)	II	Po		+ 2.1
			Cp		+ 2.4
			Sp		+ 2.2
104463	Vein, Deep Creek Volcanics	II	Qz	+14.2	
			Sp		+ 1.7
104461	Vein, Deep Creek Volcanics	II	Qz	+14.0	
			Po		+ 0.5
			Cp		+ 1.4
			Sp		+ 1.6
104465	Vein, Deep Creek Volcanics	II	Qz	+15.7	
			Sp		+ 1.9
			Asp		+ 2.7
104466	Vein, Deep Creek Volcanics	II	Qz	+15.7	
104467*	Vein, Deep Creek Volcanics	II	Sp		+ 1.6
			Py		+ 0.7
104444	Vein, Crescent Spur Sandstone	II	Po		+ 1.9
			Sp		+ 1.6
			Gn		+ 0.5

Specimen number	Description	Stage	Mineral(+)	$\delta^{18}O_{SMOW}$ per mil	$\delta^{34}S_{CDT}$ per mil.
104468*	Vein, Crescent Spur Sandstone	II	Po		+ 1.5
			Cp		+ 1.7
			Sp		+ 0.9
			Mar.		+ 1.2
104469*	Vein, Crescent Spur Sandstone	II	Po		+ 1.5
			Cp		+ 0.2
			Sp		- 0.2
			Asp		+ 2.6
104470	Washington Hay Mine	II(?)	Gn		+ 5.9
		?	Py		+11.8
104361	Lining vug, coating dolomite	V	Py		+22.1

Analysts: P.L.F. Collins

*Analysed by Dr. B.W. Robinson and Miss I. Smolnicki.

+ Mineral symbols:

Asp	= arsenopyrite,	Cp	= chalcopyrite,
Cs	= cassiterite,	Gn	= galena,
Mar	= marcasite,	Mo	= molydenite,
Py	= pyrite,	Qz	= quartz,
Sp	= sphalerite,	St	= stannite,
Wo	= wolframite,	WR	= whole rock.

TABLE A6.3 Oxygen and carbon isotopic composition of carbonate rocks and minerals from the Cleveland Mine.

Specimen number	Description*	Mineral	$\delta^{18}O_{SMOW}$ per mil	$\delta^{13}C_{PDB}$ per mil
48335	Limestone (HF)	Calcite	+ 13.7	- 1.5
48291	Limestone (HF)	Calcite	+ 13.0	- 2.3
48293	Limestone (HF)	Calcite	+ 13.2	- 1.7
48298	Limestone (HF)	Calcite	+ 12.1	- 2.1
104369	Ore, Stage II	Siderite	+ 16.7	- 7.0
104442	Ore, Stage II	Siderite	+ 16.6	- 5.1
104365	Vein, Stage IV	Dolomite	+ 14.9	- 2.5
104368	Vein, Stage IV	Dolomite	+ 15.7	- 2.8
104361	Vein, Stage IV	Dolomite	+ 15.4	- 2.4
104364	Vein, Stage IV	Dolomite	+ 15.7	- 3.0
104347	Vug, Stage IV	Dolomite	+ 16.2	- 2.7
104301	Vug, Stage IV (?)	Calcite	+ 11.2	- 1.8
A	Serpentinite (WRC)	Calcite	+ 12.4	- 9.8
B	Serpentinite (WRC)	Calcite	+ 12.5	-10.3

Analyst: P.L.F. Collins, except specimens A and B, analysed by R.N. Wooley.

* HF = Hall Formation, WRC = Whyte River Complex.

Specimen A: DDH C1499 @ 91m, serpentinised ultramafic rock with calcite stringer veins.

Specimen B: DDH c1499 @ 129m, as above.

APPENDIX 7

Rock and ore specimen catalogue

All specimens used during this investigation and referred to in the thesis are catalogued either at the Geology Department, University of Tasmania or at the Geological Survey, Tasmania Department of Mines.

Specimens with numbers 48284 to 48356 are rock specimens, and 104300 to 104470 are ore specimens catalogued at the University of Tasmania. All other specimen numbers (e.g. 78-430, 80-56) refer to the Geological Survey catalogue. Some specimens catalogued at the University of Tasmania which were prepared by and initially entered in the Geological Survey collection, have the relevant catalogue number given at the end of the specimen description.

Abbreviations used to describe the type of specimen, and any preparation, are as follows:

R	=	hand specimen
T	=	thin section
Pt	=	polished thin section
Ps	=	polished section
D	=	X-ray disc
P	=	X-ray tablet
C	=	crushed and/or powdered specimen
F	=	polished chip for fluid inclusion studies
I	=	isotope analysis (and specimen)

Specimen locations are given as follows:

(i) Surface specimens are located to the nearest 10 m in the 100 km square CQ of the Australian Metric Grid, Zone SK-55 (e.g., CQ84519273).

(ii) Underground specimens are located to the nearest 1 m by mine level (L) or decline (D) and mine grid co-ordinates (eastings, northings) (e.g., 14L; 11003, 15598 or 14/15D; 10790, 15455).

(iii) Diamond drill core specimens are located by drill hole number and depth (either in metres or feet) (e.g., C800 @ 108.5 m). The depth only is given for samples with consecutive numbers from the same drill hole.

Following the specimen description, the name of the stratigraphic unit is given in parentheses, abbreviated as follows:

DCV = Deep Creek Volcanics

HF = Hall Formation

CSS = Crescent Spur Sandstone

WRC = Whyte River Complex

MG = Meredith Granite

For ore specimens, the relevant stage of the mineralisation episode is also indicated.

ROCK SPECIMENS - UNIVERSITY OF TASMANIA.

Cat.No.	Prep'n.	Location.	Description.
48284	RT	14L;11003,15598	Chert (with veins) (HF)
48285	RT	14L;11007,15609	Argillite (HF)
48286	RT	14L;11008,15608	Argillite (HF)
48287	RT	14L;11008,15608	Tuff and argillite (HF)
48288	RTCDPI	14L;10678,15219	Altered basalt dolerite dyke.
48289	RTCDP	Qa adit portal	Altered spilitic basalt(DCV)
48290	RTCDP	3L adit portal	as above
48291	RPtDPI	C735 @ 1266'	Limestone (HF)
48292	RPt	@ 1316'	Calcareous argillite (HF)
48293	RPtDPI	@ 1396'	Limestone (HF)
48294	RPt	@ 1409'	as above
48295	RPtDP	@ 1425.5'	as above
48296	RPtDP	@ 1429'	Stylolitic limestone (HF)
48297	RT	@ 1458'	Chert,argillite and tuff (HF)
48298	RPtDPI	@ 1483'	Limestone (HF)
48299	RPtCI	@ 155'	Spilitic basalt (DCV)
48300	RTC	@ 536'	as above
48301	RPtDP	C752 @ 786'	Limestone and red shale (HF)
48302	RTCDPI	C800 @ 108.5m	Spilitic basalt (DCV)
48303	RPt	@ 688.4m	as above
48304	RT	C881 @ 144'	Litho-vitric tuff (DCV)
48305	RTCDP	@ 207'	Spilitic basalt (DCV)
48306	RTDP	@ 504'	Autobrecciated spilitic basalt (DCV).
48307	RPtCDP	@ 1142'	Spilitic basalt (DCV)
48308	RPtCDP	@ 1328'	as above
48309	RTCDPI	@ 1411'	as above
48310	RT	@ 1464.5'	Lapilli tuff (DCV)
48311	RT	@ 1467'	Lapilli/vitric tuff (DCV)
48312	RPt	C953 @ 766'	Limestone (HF)
48313	RTI	C969 @ 1983.5'	Micaceous greywacke (HF)
48314	RT	@ 2393'	as above
48315	RTI	@ 1047.8m	Micaceous greywacke with veinlets and alteration (CSS)
48316	RTCDPI	C254 @ 1036'	Altered spilitic basalt (HVM)
48317	RTCDPI	@ 2029'	Altered spilitic basalt (DCV)
48318	RTCDP	C630 @ 24.5m	Altered porphyritic spilitic basalt (HVM)
48319	RTDP	C474 @ 126.5m	Altered spilitic basalt (HVM)
48320	RTCDP	C118 @ 92'	as above.
48321	RTCDPI	C856 @ 1718'	Altered spilitic basalt (DCV)
48322	RTCDP	C845 @ 1665'	as above
48323	RTCDP	C800 @ 527m	Altered porphyritic spilitic basalt (DCV)
48324	RTCDP	C36 @ 188'	Altered spilitic basalt (HVM)
48325	RTCDP	C735 @ 90'	Spilitic basalt (DCV)
48326	RTCDP	C953 @ 626'	as above
48327	RTCDPI	C645 @ 71m	Altered spilitic basalt (DCV)
48328	RTCDP	C274 @ 948.5'	Vesicular basalt/dolerite dyke (76-672)
48329	RTCDPI	C474 @ 197	Altered spilitic basalt)DCV) (76-674)
48330	RTDPI	C581 @ 9.5m	as above (76-675)

Cat.No.	Prep'n.	Location.	Description.
48331	RTCDP	C581 @ 69m	Spilitic basalt (DCV) (76-676)
48332	RTCDP	@ 114m	as above (76-677)
48333	RTCDP	C881 @ 710'	as above (76-678)
48334	RTCDP	@ 1569'	Altered spilitic basalt (DCV)
48335	RTDP	C994 @ 444'	Altered spilitic basalt (WRC)
48336	RTDP	@ 496"	as above
48337	RI	C969 @ 2365'	Greywacke (CSS)
48338	RI	@ 937m	Greywacke (CSS)
48339	RTCI	C1135 @ 352m	Basalt/dolerite dyke (77-617)
48340	RI	C1165 @ 623m	Greywacke (CSS)
48341	RI	C402 @ 750'	Greywacke (CSS)
48342	RI	C600 @ 2100'	Greywacke (CSS)
48343	RI	@ 1737'	Greywacke (CSS)
48344	R	CQ65030646	Weathered limestone (HF)
48345	RI	14L;10993,15595	Chocolate-brown shale (HF)
48346	RI	14L;10996,15594	Light-grey, altered (bleached) shale/chert (HF)
48347	RT		Quartz-feldspar porphyry dyke, Butlers Rd (78-417)
48348	RT	C969 @ 2343.5'	Micaceous greywacke (CSS)
48349	RT	@ 2396.5'	as above
48350	RT	@ 849.15m	as above
48351	RT	@ 908.6m	Micaceous greywacke (CSS) with veins
48352	RPt	25/26D;10815,15347	Altered quartz porphyry
48353	RPt	25/26D;10812,15344	Altered quartz porphyry
48354	RPt	25/26D;10820,15344	Altered quartz porphyry
48355	RDPI	C953 @ 773'	Limestone (HF)
48356	RDP	C580 @ 400'	Limestone (HF)

ORE SPECIMENS - UNIVERSITY OF TASMANIA.

Cat.No.	Prep'n.	Location.	Description.
104300	RF	13L;10848,15449	Fluorite, quartz,tourmaline vein.
104301	RFI	14L;10965,15535	Halls;vug lined with fluorite, quartz, calcite (II) in sulphide ore (II).
104302	RPt	24L;11300,15535	Halls;massive ore with scheelite (II).
104303	RPt	14L;10993,15593	Halls;banded sulphide ore (II)
104304	RPt	14L;10992,15597	Halls;banded sulphide ore (II)
104305	RPtI	14L;10992,15597	Halls;py-po-ccp vein in ore (II)
104306	RPt	14L;10994,15597	Halls;banded sulphide ore (II)
104307	RF	14L;10780,15380	Fluorite,quartz,chlorite vein.
104308	RF	14/15D;10790,15455	Quartz,chlorite,tourmaline, fluorite,cassiterite vein.
104309	RPt	14L;11000,15597	Halls;massive ore (II).
104310	RPs	14L;10999,15598	Halls;massive ore (po-ccp-sp) (II).
104311	RPs	14L;10998,15598	Halls;massive ore with cassiterite (II).
104312	RPt	14L;10997,15602	Halls;banded sulphide ore (II).
104313	R	14L;10998,15601	Halls;banded ore (II)
104314	RPt	14L;11000,15603	Halls;banded ore (II) with tuff bed (HF).
104315	RPt	8L;10682,15417	Khaki;massive ore (II).
104316	RPsI	14L;11012,15607	Halls;massive ore (II) with qtz-po-ccp vein.
104317	RPt	10L;10582,15290	Khaki;qtz-fl-asp vein (II) in greywacke (CSS?).
104318	RF	13/14D;10720,15464	Quartz,carbonate,fluorite vein.
104319	RFI	15/16D;10806,15472	Fluorite vein (IV).
104320	RF	15/16D;10808,15475	Fluorite vein (IV) and "low grade" ore (II).
104321	RFI	14L;10706,15268	Quartz,chlorite,fluorite, pyrrhotite,chalcopyrite vein (II).
104322	RPt	14L;10892,15448	Halls; banded ore (II).
104323	RPt	12L;10978,15592	Halls;massive ore (II).
104324	RPtI	13L;10992,15604	Halls;banded sulphide ore (II)
104325	RPt	11L;10962,15592	Halls;massive ore (II)
104326	RPtI	11L;10936,15530	Halls;massive pyrrhotite ore (II).
104327	RPt	13L;10942,15534	Halls;massive ore (II).
104328	RPt	13L;10924,15504	Halls;massive ore (II).
104329	RPtI	13L;10910,15494	Halls;massive ore (II) with fluorite veins.
104330	RPtI	10L;10712,15308	Halls,(B south); massive ore (II).
104331	RI	10L;10718,15314	as above.
104332	RPtI	10L;10772,15408	Halls;massive quartz, sulphide ore (II), low grade zone.
104333	RPt	10L;10736,15406	Halls(B south);banded ore (II) low grade zone, and qtz-fl-wolf-cass vein (I).

Cat.No.	Prep'n.	Location.	Description.
104334	RPt	10L;10692,15422	Khaki;banded ore (II).
104335	RPt	10L;10608,15308	Khaki;massive ore (II).
104336	RI	7L;10712,15514	Khaki;massive quartz, sulphide ore(II).
104337	R	7L;10654,15386	Khaki;massive ore (II).
104338	RI	7L;10678,15444	Khaki;massive sulphide ore(II).
104339	R	8L;10658,15390	Khaki;fluorite vein in tourmaline ore (II).
104340	RPt	9L;10698,15422	Khaki;massive ore (II).
104341	RPtI	9L;10714,15438	Khaki; massive ore (II).
104342	RPs	14L;10706,15249	Halls (B south); massive ore with marcasite (II).
104343	RPs	15L;10933,15474	Halls; banded ore (II).
104344	RPs	15L;10935,15473	Halls; massive ore (II).
104345	RFI	15L;10936,15470	Halls; massive sulphide ore with coarse fluorite (II).
104346	RF	15L;10936,15470	Halls; massive ore (II).
104347	RI	15L;10920,15462	Halls;qtz-fl-tour-chl in chert (II).
104348	RI	14L;10677,15210	Halls (B south); tour-fl-qtz-chl-po-ccp-carb vein.
104349	RPs	15L;10935,15477	Halls;massive ore (II).
104350	RPs	15L;10935,15477	Halls;massive ore (II).
104351	RF	15/16D;10828,15485	Fluorite crystals in vug(IV)
104352	RPt	14L;10666,15202	Halls (B south);massive sphalerite ore (II).
104353	RPt	14L;10669,15200	Halls (B south);massive ore (II).
104354	RPt	14L;10670,15199	Halls (B south);massive tourmaline ore (II).
104355	RPs	15L;10945,15488	Halls; massive ore (II).
104356	RPsPt	15L;10951,15491	Halls; banded and massive pyrrhotite ore (II).
104357	RPtF	15L;10998,15583	Halls;massive ore with cassiterite (II).
104358	RPt	15L;10991,15580	Halls; massive ore with fluorite,cassiterite (II).
104359	RPtF	10L;10606,15300	Mar-fl-ccp-py-qtz vein, in massive sulphide ore (II).
104360	R	16LD;10925,15480	Tour-qtz-chl-fl-sulphide vein.
104361	RIF	16L;10971,15523	Nadir fault;fluorite, carbonate vein (IV) with pyrite coating (V).
104362	RPs	14L;10977,15607	Halls;massive pyrrhotite ore (II).
104363	RI	15L;11038,15602	Halls;massive ore with sp, asp (II).
104364	RI	15L;11038,15600	Perserverance fault; carbonate, fluorite, quartz vein (IV).
104365	RI	16L;10991,15562	Nadir fault, quartz vein(II).
104366	RI	16L;11014,15574	Nadir fault; quartz vein(II).
104367	RI	16L;10993,15568	Nadir fault; quartz vein with pyrrhotite (II).

Cat.No.	Prep'n.	Location.	Description.
104368	RPtI	16L;10986,15547	Nadir fault;cassiterite, tourmaline in quartz vein(II) and qtz-asp-stan in vug(III).
104369	RI	10L;10705,15417	Khaki;banded ore(II) with quartz,fluorite,wolframite vein (I).
104370	RIPs	C735 @ 1463'	Po-ccp-sp-asp ore/vein (II) (77-599)
104371	RPs	@ 1467'	Sp-po-ccp ore/vein (II) (77-600).
104372	RIPs	C752 @ 1213'	Qtz-sp-ccp-po-py vein (77-611).
104373	RI	C800 @ 588.4m	Halls;massive ore (II).
104374	RI	@ 600.3m	Halls;massive ore (II).
104375	RPt	@ 609.3m	Halls;massive ore with "spinifex" texture (II).
104376	RI	@ 648.5m	Halls;massive ore (II), quartz,arsenopyrite vein(III).
104377	R	C261 @ 973.5'	Qtz-carb-fl-chl-tourm vein with molybdenite selvedge(I).
104378	RI	@ 980'	as above.
104379	RF	@ 1360.5'	Fluorite-tourm-qtz vein.
104380	RF	@ 1406'	Quartz,fluorite vein (I) in greywacke.
104381	RF	@ 1652.5'	Quartz fluorite vein (Wolf-molyb.) (I).
104382	RFI	@ 1661.3'	Quartz, fluorite,wolframite vein (I).
104383	RPt	C881 @ 1069'	Lithic tuff with qtz-sp-ccp veining.
104384	RPs	@ 1237.5'	Qtz-sp vein.
104385	RPs	@ 1334'	Qtz-sp vein.
104386	RPs	@ 1367.5'	Sp-ccp-qtz vein.
104387	RI	@ 1706'	Halls (?); massive ore (II).
104388	RF	@ 1855.5'	Halls(?); massive ore with coarse fluorite (II).
104389	RPt	@ 1861'	Halls (?);massive ore (II).
104390	RI	@ 1878'	as above.
104391	RPt	@ 1942'	Henrys (?)lower ore; massive ore (II).
104392	RPs	C402 @ 532'	Qtz-sp-ccp-asp vein (77-585).
104393	RPs	C1165 @ 504.7m	Po-py-sp-ccp-asp vein (77-592).
104394	RPs	C1155 @ 535m	Qtz-sp-asp-ccp vein (77-596).
104395	RF	C261 @ 419'	Quartz,fluorite (II)in chert.
104396	RF	C261 @ 488'	Halls (?);massive ore (II).
104397	RF	@ 494'	Halls (?); massive ore with coarse fluorite (II).
104398	RF	@ 511'	Quartz, fluorite rich ore (II).
104399	RF	@ 608'	Halls (?); massive ore (II).
104400	RF	@ 1529'	Quartz, fluorite vein.
104401	RF	@ 1738'	Halls (?); massive ore with coarse fluorite (II).
104402	RF	@ 1750.5'	Halls (?); fluorite, quartz in chert.
104403	RPs	C969 @ 1484'	Qtz-sp-ccp vein (II) in basalt (DCV)

Cat.No.	Prep'n.	Location.	Description.
104404	RPt	C969 @ 1853.5'	Halls (?) lower; banded ore (II).
104405	RPt	@ 1855'	Halls (?) lower; banded sulphide ore (II).
104406	RPt	@ 2095'	Halls (?) lower; massive ore (II).
104407	RPt	@ 2098'	Halls (?)lower; banded sulphide ore (II).
104408	RPt	@ 2104.5'	Halls (?) lower;massive ore (II).
104409	RPt	@ 2110'	Halls (?) lower; thinly banded ore (II).
104410	RPt	@ 2115'	Halls (?) lower;massive ore (II).
104411	RPt	@ 2122.5'	as above.
104412	R	@ 2127'	as above.
104413	RF	@ 2134'	Halls (?) lower;massive ore with coarse fluorite (II).
104414	RPt	@ 2137'	Halls (?) lower; banded sulphide ore (II).
104415	RPtI	@ 2141'	Halls (?) lower; massive sulphide ore (II).
104416	R	@ 2151.5'	as above.
104417	RPtI	@ 2160'	Halls (?) lower; massive ore (II) with "thumbprint" texture.
104418	R	@ 2166'	Halls (?) lower; massive ore (II).
104419	RF	C1008 @ 2205'	Halls (?) lower; fluorite in massive ore (II) and fluorite veins (IV).
104420	RF	@ 1876'	Halls (?) lower; banded ore (II) with coarse fluorite.
104421	RI	@ 1888.5'	Halls (?) lower; massive ore with coarse fluorite and pyrrhotite.
104422	RF	C969 @ 2163'	Halls (?) lower; massive ore with coarse fluorite vein (II).
104423	RIF	@ 2185'	Halls (?) lower; massive ore with coarse fluorite (II).
104424	RPt	@ 2231'	Halls (?) lower;massive ore (II).
104425	RPtI	@ 2242'	Halls (?) lower; banded ore (II) and sulphide vein.
104426	R	@ 792.2m	Qtz-fl vein in shale.
104427	RF	@ 936.5m	Qtz-fl-wolf vein (I) in greywacke (CSS).
104428	RI	@ 957.5m	Qtz-fl-wolf-molyb vein (I).
104429	RF	@ 1015.9m	Fluorite vein (IV)
104430	RF	@ 1028.7m	as above.
104431	RF	@ 1030.5m	as above.
104432	RPsI	@ 1043.9m	Qtz-wolf-molyb. vein (I)
104433	RPs	C768 @ 1082'	Qtz-po-ccp vein in basalt (77-604).
104434	RPs	@ 1514'	Qtz-sp-ccp-po vein in greywacke (77-605).

Cat.No.	Prep'n.	Location.	Description.
104435	RPs	C783 @ 221.5'	Qtz-sp-asp vein(II) (77-606).
104436	RPs	@ 1554'	Qtz-wolf-molyb-bis vein (I) (76-607).
104437	RPs	@ 1630	Qtz-wolf-molyb-bis vein (I) (76-608).
104438	RPs	16L;11014,15574	Qtz-cass-ccp-asp-po vein (II) (77-615) Nadir fault.
104439	RF	C783 @ 1129'	Fl-qtz-wolf-molyb vein (I).
104440	RIF	@ 1194'	Qtz-fl vein (I).
104441	RPs	C146 @ 9'	Halls; massive ore with oolitic structure (II) (77-609).
104442	RI	C658 @ 679'	Halls (?) south; massive sphalerite siderite ore (II).
104443	R	@ 747.5'	as above.
104444	RIPs	C349 @ 399.5'	Qtz-po-sp-ccp-gn vein (II) (77-588).
104445	R	@ 1235.5'	Khaki (?); massive ore with fluorite.
104446	R	C600 @ 1666.5'	Halls (?);massive ore (II).
104447	R	@ 1685.5'	as above.
104448	RF	@ 1801'	Qtz-fl vein (IV) in tourmalinised greywacke.
104449	R	15L;11038,15602	Quartz, carbonate, fluorite, sp, asp, ccp vein (III).
104450	RFI	C969 @ 2103'	Halls (?) lower; massive ore with coarse fluorite (II).
104451	RPs	@ 2169'	Magnetite; pyrrhotite banded ore (II).
104452	RPs	@ 2201'	as above.
104453	RPs	C349 @ 803'	Sp-po-ccp-asp vein (II) (77-589)
104454	RF	C969 @ 1037.4m	Fluorite vein (IV) cutting qtz-wolf-molyb vein (I).
104455	RF	@ 1038.2m	Qtz-wolf-molyb vein (I).
104456	RPt	111;10904,15498	Halls; massive ore (II).
104457	R	C969 @ 1028.6m	Fluorite vein (IV).
104458	RI	C1008 @ 2334'	Qtz-wolf-molyb vein (I).
104459	RPs	@ 1811'	Halls (?); banded magnetite ore (II) (77-602).
104460	RI	C261 @ 980'	Qtz-wolf-molyb vein (I).
104461	RIPs	C1008 @ 1489'	Qtz-po-sp-ccp vein (II) (77-603).
104462	RI	C783 @ 998'	Qtz-wolf vein (I).
104463	RIPs	C580 @ 658'	Qtz-sp-asp vein (II)(77-598).
104464	RI	C1130 @ 289.5'	Khaki;sphalerite rich ore (II).
104465	RIPs	C1155 @ 135m	Qtz-asp-sp-ccp vein (II) (77-595).
104466	RIPs	C1165 @ 105m	Qtz-sp-asp-ccp-gn vein (II). (77-590).
104467	RIPs	@ 124.4m	Qtz-asp-ccp-sp vein (II) (77-591).
104468	RIPs	C402 @ 541'	Sp-ccp-po-mar-qtz vein (II). (77-586).
104469	RI	@ 887'	Sp-po-ccp vein (II).
104470	RPtI	Washington Hay Mine	Galena, sphalerite, siderite veins.

SPECIMENS CATALOGUED AT THE GEOLOGICAL SURVEY.

Specimens catalogued at the Geological Survey and used during the investigation have serial numbers 76-668 to 76-679, 77-585 to 77-616 (ore and veins), 77-617 to 77-639, 78-413 to 78-458, 78-771 to 78-776 a nd 81-22 to 81-72. Details of those specimens referred to in the thesis are given below.

Cat.No.	Prep'n.	Location.	Description.
77-620	RT	C1023 @ 277.4m	Volcaniclastic conglomerate and argillite (DCV)
77-622	RT	@ 278.5m	Volcaniclastic conglomerate (DCV)
77-629	RT	C1155 @ 219.6m	Volcaniclastic conglomerate and tuffaceous siltstone (DCV)
77-634	RT	C1165 @ 243.3m	Lithic tuff (DCV)
78-413	RT	CQ 704068	Argillite
78-415	RT	CQ 711072	Gabbro
78-417	RT	CQ 725074	Quartz-feldspar porphyry (MG)
78-419	RT	CQ 730073	Hornfelsed argillite
78-425	RT	CQ 674083	Spilitic basalt
78-429	RT	CQ 657080	Serpentinised peridotite (WRC)
78-430	RT	CQ 717050	Fine grained biotite granite/ microgranite (MG)
78-432	RT	CQ 690074	Carbonate veins in sheared serpentinite
78-434	RT	CQ 689073	Porphyritic basalt, serpentinised.
78-436	RT	CQ 667062	Serpentinite
78-437	RT	CQ 686072	Olivine (?) basalt, serpentinised
78-438	RT	CQ 648079	Serpentinised peridotite (WRC)
78-440	RT	CQ 739061	Olivine basalt (Tertiary)
78-441	RT	CQ 728058	Equigranular biotite granite (MG)
78-442	RT	CQ 730058	Porphyritic biotite granite (MG)
78-443	RT	CQ 720040	as above
78-444	RT	CQ 720040	Mafic segregation in porphyritic biotite granite(MG)
78-446	RT	CQ 664072	Spilitic basalt (DCV)
78-447	RT	CQ 664072	as above
78-455	RT	CQ 645068	Serpentinised peridotite (WRC)
78-771	RT	CQ 64750705	Red argillite with reduction spots (DCV)
81-22	RT	CQ 66650849	Porphyritic spilitic basalt(WRC)
81-23	RT	CQ 66230829	Gabbro (altered), (WRC)
81-27	RT	CQ 68760799	Vesicular basalt (DCV)
81-29	RT	CQ 64750531	Chert with thin tuff bands(DCV)
81-31	RT	CQ 64890505	Sub-porphyritic spilitic basalt (DCV)
81-32	RT	CQ 68620794	Volcaniclastic greywacke (DCV)

Cat.No.	Prep'n.	Location.	Description.
81-33	RT	CQ 68440802	Greywacke (HF)
81-34	RT	CQ 68640795	Volcaniclastic greywacke(DCV)
81-36	RT	CQ 68370800	Spilitic basalt (HVM)
81-37	RT	CQ 68340799	Autobrecciated spilitic basalt (HVM)
81-38	RT	CQ 68130822	Basalt (CSS)
81-39	RT	CQ 68020834	Greywacke (CSS)
81-45	RT	CQ 67450829	Spilitic basalt (CSS)
81-46	RT	CQ 67400829	Litho-vitric tuff (CSS)
81-47	RT	CQ 67400829	Interbedded litho-vitric tuff and red/brown argillite (CSS)
81-48	RT	CQ 67210836	Litho-vitric tuff (CSS)
81-49	RT	CQ 67200834	as above
81-50	RT	CQ 67190833	Volcaniclastic greywacke (CSS)
81-51	RT	CQ 67180833	as above
81-52	RT	CQ 67280835	Litho-vitric tuff (CSS)
81-53	RT	CQ 67380830	as above
81-54	RT	CQ 68070829	Dolerite/gabbro
81-55	RT	CQ 68000835	as above
81-56	RT	CQ 67710811	as above
81-57	RT	CQ 67330831	Basalt/dolerite
81-58	RT	CQ 67350832	as above
81-59	RT	CQ 67250837	as above
81-67	RT	C 969 @ 908.6m	Tourmalinised greywacke (CSS)
81-68	RT	@ 1014.6m	Greywacke with vein and alteration (CSS)
81-69	RT	@ 1033.75m	as above
81-70	RT	@ 824.2m	Altered greywacke (CSS)
81-71	RT	@ 826.9m	Tourmalinised greywacke (CSS)
81-72	RT	@ 849.8m	Greywacke (CSS)

These articles have been removed for copyright or proprietary reasons.

Collins, P. L. F., 1979, Gas hydrates in CO2-bearing fluid inclusions and the use of freezing data for estimation of salinity, Economic geology, 74, 1435-1444

Collins, P. L. F., 1981, The geology and genesis of the Cleveland tin deposit, western Tasmania : fluid inclusion and stable isotope studies, Economic geology, 76, 365-392